

Digital Spectral Analysis

To my children : Guillaume, Aurélien, Anastasia, Virginia, Enrica

Digital Spectral Analysis

parametric, non-parametric and advanced methods

Edited by
Francis Castanié



First published 2011 in Great Britain and the United States by ISTE Ltd and John Wiley & Sons, Inc.

Apart from any fair dealing for the purposes of research or private study, or criticism or review, as permitted under the Copyright, Designs and Patents Act 1988, this publication may only be reproduced, stored or transmitted, in any form or by any means, with the prior permission in writing of the publishers, or in the case of reprographic reproduction in accordance with the terms and licenses issued by the CLA. Enquiries concerning reproduction outside these terms should be sent to the publishers at the undermentioned address:

ISTE Ltd
27-37 St George's Road
London SW19 4EU
UK
www.iste.co.uk

John Wiley & Sons, Inc.
111 River Street
Hoboken, NJ 07030
USA
www.wiley.com

© ISTE Ltd 2011

The rights of Francis Castanié to be identified as the authors of this work have been asserted by him in accordance with the Copyright, Designs and Patents Act 1988.

Library of Congress Cataloging-in-Publication Data

Digital spectral analysis : parametric, non-parametric, and advanced methods / edited by Francis Castanié.
p. cm.
Includes bibliographical references and index.
ISBN 978-1-84821-277-0
1. Spectral theory (Mathematics) 2. Signal processing--Digital techniques--Mathematics. 3. Spectrum analysis. I. Castanié, Francis.
QA280.D543 2011
621.382'2--dc23
2011012246

British Library Cataloguing-in-Publication Data
A CIP record for this book is available from the British Library
ISBN 978-1-84821-277-0

Printed and bound in Great Britain by CPI Antony Rowe, Chippenham and Eastbourne.



Table of Contents

Preface	xiii
PART 1. TOOLS AND SPECTRAL ANALYSIS	1
Chapter 1. Fundamentals	3
Francis CASTANIÉ	
1.1. Classes of signals	3
1.1.1. Deterministic signals	3
1.1.2. Random signals	6
1.2. Representations of signals	9
1.2.1. Representations of deterministic signals	9
1.2.2. Representations of random signals	13
1.3. Spectral analysis: position of the problem	20
1.4. Bibliography	21
Chapter 2. Digital Signal Processing	23
Éric LE CARPENTIER	
2.1. Introduction	23
2.2. Transform properties	24
2.2.1. Some useful functions and series	24
2.2.2. Fourier transform	29
2.2.3. Fundamental properties	33
2.2.4. Convolution sum	34
2.2.5. Energy conservation (Parseval's theorem)	36
2.2.6. Other properties	38
2.2.7. Examples	39
2.2.8. Sampling	41
2.2.9. Practical calculation, FFT	46

2.3. Windows	49
2.4. Examples of application	57
2.4.1. LTI systems identification.	57
2.4.2. Monitoring spectral lines	61
2.4.3. Spectral analysis of the coefficient of tide fluctuation	62
2.5. Bibliography	64
Chapter 3. Introduction to Estimation Theory with Application in Spectral Analysis	67
Olivier BESSON and André FERRARI	
3.1. Introduction	67
3.1.1. Problem statement	68
3.1.2. Cramér-Rao lower bound	69
3.1.3. Sequence of estimators.	74
3.1.4. Maximum likelihood estimation	77
3.2. Covariance-based estimation	86
3.2.1. Estimation of the autocorrelation functions of time series	87
3.2.2. Analysis of estimators based on $\hat{c}_{xx}(m)$	91
3.2.3. The case of multi-dimensional observations	93
3.3. Performance assessment of some spectral estimators	95
3.3.1. Periodogram analysis	95
3.3.2. Estimation of AR model parameters.	97
3.3.3. Estimation of a noisy cisoid by MUSIC	101
3.3.4. Conclusion	102
3.4. Bibliography	102
Chapter 4. Time-Series Models	105
Francis CASTANIÉ	
4.1. Introduction	105
4.2. Linear models	107
4.2.1. Stationary linear models	108
4.2.2. Properties	110
4.2.3. Non-stationary linear models	114
4.3. Exponential models	117
4.3.1. Deterministic model	117
4.3.2. Noisy deterministic model	119
4.3.3. Models of random stationary signals	119
4.4. Nonlinear models	120
4.5. Bibliography	121

PART 2. NON-PARAMETRIC METHODS	123
Chapter 5. Non-Parametric Methods	125
Éric LE CARPENTIER	
5.1. Introduction	125
5.2. Estimation of the power spectral density	130
5.2.1. Filter bank method	130
5.2.2. Periodogram method	132
5.2.3. Periodogram variants	136
5.3. Generalization to higher-order spectra	141
5.4. Bibliography	142
PART 3. PARAMETRIC METHODS	143
Chapter 6. Spectral Analysis by Parametric Modeling	145
Corinne MAILHES and Francis CASTANIÉ	
6.1. Which kind of parametric models?	145
6.2. AR modeling	146
6.2.1. AR modeling as a spectral estimator	146
6.2.2. Estimation of AR parameters	146
6.3. ARMA modeling	154
6.3.1. ARMA modeling as a spectral estimator	154
6.3.2. Estimation of ARMA parameters	154
6.4. Prony modeling	156
6.4.1. Prony model as a spectral estimator	156
6.4.2. Estimation of Prony parameters	156
6.5. Order selection criteria	158
6.6. Examples of spectral analysis using parametric modeling	162
6.7. Bibliography	166
Chapter 7. Minimum Variance	169
Nadine MARTIN	
7.1. Principle of the MV method	174
7.2. Properties of the MV estimator	177
7.2.1. Expressions of the MV filter	177
7.2.2. Probability density of the MV estimator	182
7.2.3. Frequency resolution of the MV estimator	186
7.3. Link with the Fourier estimators	188
7.4. Link with a maximum likelihood estimator	190
7.5. Lagunas methods: normalized MV and generalized MV	192
7.5.1. Principle of the normalized MV	192

viii Digital Spectral Analysis

7.5.2. Spectral refinement of the NMV estimator	194
7.5.3. Convergence of the NMV estimator	195
7.5.4. Generalized MV estimator	198
7.6. A new estimator: the CAPNORM estimator	200
7.7. Bibliography	204
Chapter 8. Subspace-Based Estimators and Application to Partially Known Signal Subspaces	207
Sylvie MARCOS and Remy BOYER	
8.1. Model, concept of subspace, definition of high resolution	207
8.1.1. Model of signals	207
8.1.2. Concept of subspaces	208
8.1.3. Definition of high resolution	209
8.1.4. Connection with spatial analysis or array processing	210
8.2. MUSIC	211
8.2.1. Principle of the MUSIC method	211
8.2.2. Pseudo-spectral version of MUSIC	213
8.2.3. Polynomial version of MUSIC	214
8.3. Determination criteria of the number of complex sine waves	216
8.3.1. AIC criterion (Akaike information criterion)	216
8.3.2. Minimum description length criterion	216
8.4. The MinNorm method	217
8.5. “Linear” subspace methods	219
8.5.1. The linear methods	219
8.5.2. The propagator method	219
8.6. The ESPRIT method	223
8.7. Illustration of the subspace-based methods performance	226
8.8. Adaptive research of subspaces	229
8.9. Integrating <i>a priori</i> known frequencies into the MUSIC criterion	233
8.9.1. A spectral approach: The Prior-MUSIC algorithm	233
8.9.2. A polynomial-based rooting approach: The projected companion matrix-MUSIC algorithm	237
8.10. Bibliography	243
PART 4. ADVANCED CONCEPTS	251
Chapter 9. Multidimensional Harmonic Retrieval: Exact, Asymptotic, and Modified Cramér-Rao Bounds	253
Remy BOYER	
9.1. Introduction	253
9.2. CanDecomp/Parafac decomposition of the multidimensional harmonic model	255

9.3. CRB for the multidimensional harmonic model	257
9.3.1. Deterministic CRB	257
9.3.2. Deterministic asymptotic CRB for the M-order harmonic model of dimension P	258
9.3.3. Asymptotic CRB for a constant amount of data	261
9.4. Modified CRB for the multidimensional harmonic model	266
9.4.1. Definition of the modified CRB for $T = 1$	266
9.4.2. Modified CRB in the case of a large number of samples	267
9.4.3. Generalization to time-varying initial phase	268
9.4.4. Analysis of the MACRB	269
9.4.5. Numerical illustrations	271
9.5. Conclusion	272
9.6. Appendices	273
9.6.1. Appendix A: ACRB for the MD-harmonic model of dimension P	273
9.6.2. Appendix B: Exact CRB for the first-order harmonic model of dimension P	276
9.6.3. Appendix C: ACRB for the MD-harmonic model with multiple snapshots	278
9.6.4. Appendix D: Application to the bistatic MIMO radar with widely separated arrays	279
9.7. Bibliography	284
Chapter 10. Introduction to Spectral Analysis of Non-Stationary Random Signals	287
Corinne MAILHES and Francis CASTANIÉ	
10.1. Evolutive spectra	288
10.1.1. Definition of the “evolutive spectrum”	288
10.1.2. Evolutive spectrum properties	289
10.2. Non-parametric spectral estimation	290
10.3. Parametric spectral estimation	291
10.3.1. Local stationary postulate	292
10.3.2. Elimination of a stationary condition	293
10.3.3. Application to spectral analysis	296
10.4. Bibliography	297
Chapter 11. Spectral Analysis of Non-uniformly Sampled Signals	301
Arnaud RIVOIRA and Gilles FLEURY	
11.1. Applicative context	301
11.2. Theoretical framework	302
11.2.1. Signal model	302
11.2.2. Sampling process	302

x Digital Spectral Analysis

11.3. Generation of a randomly sampled stochastic process	302
11.3.1. Objective	302
11.3.2. Generation of the sampling times.	302
11.3.3. CARMA processes	303
11.4. Spectral analysis using undated samples	305
11.4.1. Non-parametric estimation.	305
11.4.2. Parametric estimation.	307
11.5. Spectral analysis using dated samples	309
11.5.1. Masry's work	309
11.5.2. Slotting technique.	310
11.5.3. IRINCORREL: A consistent spectral estimator	311
11.6. Perspectives	314
11.7. Bibliography	315

Chapter 12. Space–Time Adaptive Processing 317
Laurent SAVY and François LE CHEVALIER

12.1. STAP, spectral analysis, and radar signal processing	319
12.1.1. Generalities.	319
12.1.2. Radar configuration with side antenna	320
12.1.3. Radar configuration with forward antenna	324
12.2. Space–time processing as a spectral estimation problem	327
12.2.1. Overview of space–time processing	327
12.2.2. Processing in additive white noise	328
12.2.3. Processing in additive colored noise	330
12.3. STAP architectures	334
12.3.1. Generalities and notations	334
12.3.2. Pre-Doppler STAP	335
12.3.3. Post-Doppler STAP.	344
12.4. Relative advantages of pre-Doppler and post-Doppler STAP	354
12.4.1. Estimation of adaptive filtering coefficients	354
12.4.2. Exclusion of target signal from training data	356
12.4.3. Clutter heterogeneity	356
12.4.4. Computing load	357
12.4.5. Angular position estimation	357
12.4.6. Anti-jamming and STAP compatibility	358
12.5. Conclusion	358
12.6. Bibliography	359
12.7. Glossary	360

Chapter 13. Particle Filtering and Tracking of Varying Sinusoids 361
David BONACCI

13.1. Particle filtering	361
------------------------------------	-----

Table of Contents xi

13.1.1. Generalities	362
13.1.2. Strategies for efficient particle filtering	365
13.2. Application to spectral analysis	370
13.2.1. Observation model	370
13.2.2. State vector	371
13.2.3. State evolution model	372
13.2.4. Simulation results	373
13.3. Bibliography	375
List of Authors	377
Index	379

Preface

The oldest concept dealt with in signal processing is the concept of frequency, and its operational consequence, the constant quest of frequency contents of a signal. This concept is obviously linked to the fascination for sine functions, deriving from the 19th Century discovery of the “magic” property of the sine functions, or more precisely complex exponentials: it is the only function set able to cross what we call today “linear invariant systems” without going out of this set, i.e. the output of such a system remains in the same class as the input. The distribution of qualifying quantities, such as power or energy of a signal over frequency, the so-called spectrum, is probably one of the most studied topics in signal processing. The concept of frequency itself is not limited to time-related functions, but is much more general: in particular image processing deals with space frequency concept related to geometrical length units, etc.

We can, with good reason, wonder on the pertinence of the importance given to spectral approaches. From a fundamental viewpoint, they relate to the Fourier transformation, projection of signals, on the set of special periodic functions, which include complex exponential functions. By generalizing this concept, the basis of signal vector space can be made much wider (Hadamard, Walsh, etc.), while maintaining the essential characteristics of the Fourier basis. In fact, the projection operator induced by the spectral representations measures the “similarity” between the projected quantity and a particular basis: they have henceforth no more – and no less – relevance than this.

The predominance of this approach in signal processing is not only based on this reasonable (but dry) mathematical description, but probably has its origins in the fact that the concept of frequency is in fact a perception through various human “sensors”: the system of vision, which perceives two concepts of frequency (time-dependent for colored perception, and spatial via optical concepts of separating

power or resolution) and hearing, which no doubt is at the historical origin of the perceptual concept of frequency – Pythagoras and the “Music of the Spheres” and probably other proprioceptive sensors (all those who suffer from seasickness have a direct physical experience of the frequency sensitivity).

Whatever the reasons may be, spectral descriptors are the most commonly used in signal processing; realizing this, the measurement of these descriptors is therefore a major issue. This is the reason for the existence of this book, dedicated to this measurement that is classically christened as *spectral analysis*. The term *digital* refers to today’s most widely spread technical means to implement the proposed methods of the analysis.

It is not essential that we must devote ourselves to a tedious hermeneutic to understand spectral analysis through countless books that have dealt with the subject (we will consult with interest the historical analysis of this field given in [MAR 87]). If we devote ourselves to this exercise in erudition concerning the cultural level, we realize that the theoretical approaches of current spectral analysis were structured from the late 1950s; these approaches have the specific nature of being controlled by the availability of technical tools that allow the analysis to be performed. It must kept in mind that the first spectral analyzers used optical analyzers (spectrographs), then at the end of this archaeological phase – which is generally associated with the name of Isaac Newton – spectral analysis got organized around analog electronic technologies. We will not be surprised indeed that the theoretical tools were centered on concepts of selective filtering, and sustained by the theory of time-continuous signals (see [BEN 71]). At this time, the criteria qualifying the spectral analysis methods were formulated: frequency resolution or separating power, variance of estimators, etc. They are still in use today, and easy to assess in a typical linear filtering context.

The change to digital processing tools was first done by transposition of earlier analog approaches, adapting the time axis to discrete time signals. Second, a simultaneous increase in the power of processing tools and algorithms opened the field up to more and more intensive digital methods. But beyond the mere availability of more comfortable digital tools, the existence of such methods freed the imagination, by allowing the use of descriptors derived from the domain of parametric modeling. This has its origin in a field of statistics known as analysis of chronological series (see [BOX 70]), the so-called time series, which was successfully applied by G. Yule (1927) for the determination of periodicities of the number of sun spots; but it is actually the present availability of sufficiently powerful digital methods, from the mid-1970s, which led the community of signal processing to consider parametric modeling as a tool for spectral analysis, with its own characteristics, including the possibilities to obtain “super resolutions” and/or to process signals of very short duration. We will see that characterizing these

estimators with the same criteria as estimators from the analog world is not an easy task – the mere quantitative assessment of the frequency resolution or spectral variances becomes a complicated problem.

Part 1 brings together the *processing tools* that contribute to spectral analysis. Chapter 1 lists the basics of the *signal theory* needed to read the following parts of the book; the informed reader could obviously skip this. Next, digital signal processing, the theory of estimation, and parametric modeling of time series are presented.

The “classical” methods, known nowadays as *non-parametric methods*, form part of the second part. The privative appearing in the qualification of “non-parametric” must not be seen as a sign of belittling these methods – they are the most used in industrial spectral analysis.

Part 3 obviously deals with parametric methods, studying first the methods based on models of time series, Capon's methods and its variants, and then the estimators based on the concepts of sub-spaces.

The fourth and final part is devoted to advanced concepts. It provides an opening to parametric spectral analysis of non-stationary signals, a subject with great potential, which is tackled in greater depth in another book of the IC2 series [HLA 05] of space-time processing and proposes an inroad in most recent particle filtering-based methods.

Francis CASTANIÉ
May 2011

Bibliography

- [BEN 71] BENDAT J.S., PIERSOL A.G., *Random Data: Analysis and Measurement Procedures*, Wiley Intersciences, 1971.
- [BOX 70] BOX G., JENKINS G., *Time Series Analysis, Forecasting and Control*, Holden-Day, San Francisco, 1970.
- [HLA 05] HLAWATSCH F., AUGER F., *Temps-fréquence: Concepts et Outils*, Hermès Science, Paris, 2005.
- [HLA 08] HLAWATSCH F., AUGER F. (eds), *Time-frequency Analysis: Concepts and Methods*, ISTE Ltd, London and John Wiley & Sons, New York, 2008.
- [MAR 87] MARPLE S., *Digital Spectral Analysis with Applications*, Prentice Hall, Englewood Cliffs, NJ, 1987.

PART 1

Tools and Spectral Analysis

Chapter 1

Fundamentals

1.1. Classes of signals

Every signal-processing tool is designed to be adapted to one or more signal classes and presents a degraded or even deceptive performance if applied outside this group of classes. Spectral analysis too does not escape this problem, and the various tools and methods for spectral analysis will be more or less adapted, depending on the class of signals to which they are applied.

We see that the choice of classifying properties is fundamental, because the definition of classes itself will affect the design of processing tools.

Traditionally, the first classifying property is the deterministic or non-deterministic nature of the signal.

1.1.1. *Deterministic signals*

The definitions of determinism are varied, but the simplest is the one that consists of calling any signal that is reproducible in the mathematical sense of the term as a deterministic signal, i.e. any new experiment for the generation of a continuous time signal $x(t)$ (or discrete time $x(k)$) produces a mathematically identical signal. Another subtler definition, resulting from the theory of random signals, is based on the exactly predictive nature of $x(t)$ $t \geq t_0$ from the moment that it is known for $t < t_0$ (singular term of the Wold decomposition, e.g. see Chapter 4 and [LAC 00]). Here, we discuss only the definition based on the reproducibility of $x(t)$,

Chapter written by Francis CASTANIÉ.

4 Digital Spectral Analysis

as it induces a specific strategy on the processing tools: as all information of the signal is contained in the function itself, any bijective transformation of $x(t)$ will also contain all this information. Representations may thus be imagined, which, without loss of information, will demonstrate the characteristics of the signal better than the direct representation of the function $x(t)$ itself.

The deterministic signals are usually separated into classes, representing integral properties of $x(t)$, strongly linked to some quantities known by physicists.

Finite energy signals verify the integral properties in equations [1.1] and [1.2] with continuous or discrete time:

$$E = \int_R |x(t)|^2 dt < \infty \quad [1.1]$$

$$E = \sum_{k=-\infty}^{+\infty} |x(k)|^2 < \infty \quad [1.2]$$

We recognize the membership of $x(t)$ to standard function spaces (noted as L_2 or l_2), as well as the fact that this integral, to within some dimensional constant (an impedance in general), represents the energy E of the signal.

Signals of *finite average power* verify:

$$P = \lim_{T \rightarrow \infty} \frac{1}{T} \int_{-T/2}^{+T/2} |x(t)|^2 dt < \infty \quad [1.3]$$

$$P = \lim_{N \rightarrow \infty} \frac{1}{2N+1} \sum_{k=-N}^{+N} |x(k)|^2 < \infty \quad [1.4]$$

If we accept the idea that the sums of equation [1.1] or [1.2] represent “energies”, those of equation [1.3] or [1.4] then represent powers.

It is clear that these integral properties correspond to mathematical characteristics whose morphological behavior along the time axis is very different: the finite energy signals will be in practice “pulse-shaped”, or “transient” signals such that $|x(t)| \rightarrow 0$ for $|t| \rightarrow \infty$. This asymptotic behavior is not at all necessary to ensure the convergence of the sums, and yet all practical finite energy signals verify it. For example, the signal below is of finite energy:

$$\begin{aligned} x(t) &= A e^{-at} \cos(2\pi ft + \theta) & t \geq 0 \\ &= 0 & t < 0 \end{aligned}$$

(This type of damped exponential oscillatory waveform is a fundamental signal in the analysis of linear systems that are invariant by translation.)

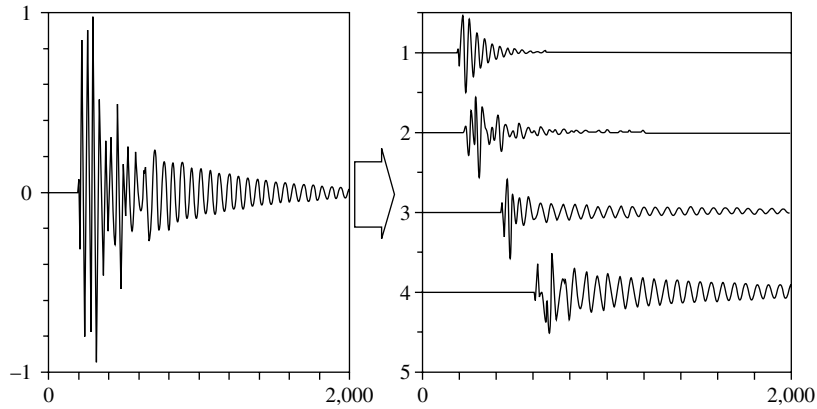


Figure 1.1. Electromagnetic interference signal and its decomposition

On the more complex example of Figure 1.1, we see a finite energy signal of the form:

$$x(t) = \sum_{i=1}^4 x_i(t - t_i)$$

where the four components $x_i(t)$ start at staggered times (t_i) . Its shape, even though complex, is supposed to reflect a perfectly reproducible physical experiment.

Finite power signals will be, in practice, *permanent* signals, i.e. not canceling at infinity. For example:

$$\begin{aligned} x(t) &= A(t) \sin(\psi(t)) \quad t \in \mathbb{R} \\ |A(t)| &< \infty \end{aligned} \tag{1.5}$$

An example is given in Figure 1.2. It is clear that there is obviously a start and an end, but its mathematical model cannot take this unknown data into account, and it is relevant to represent it by an equation of the type [1.5]. This type of signal, modulated in amplitude and angle, is fundamental in telecommunications.

6 Digital Spectral Analysis

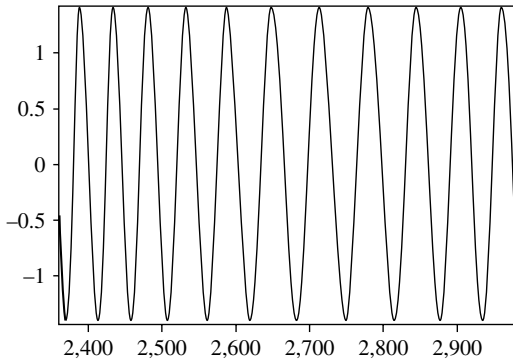


Figure 1.2. Frequency-modulated sine curve

1.1.2. Random signals

The deterministic models of signals described in the previous section are absolutely unrealistic, in the sense that they do not take into account any inaccuracy, or irreproducibility, even if partial. To model the uncertainty on the signals, several approaches are possible today, but the one that was historically adopted at the origin of the signal theory is a probabilistic approach.

In this approach, the signal is regarded as resulting from a drawing in a probability space. The observation $x_j(t)$ (j th outcome or “realization”) is one of the results of the random event, but is no longer *the* signal: the latter is now constituted by all the possible outcomes $x(t, \omega)$. The information of the signal is no longer contained in one of the realizations $x_j(t)$, but in the probability laws that govern $x(t, \omega)$. Understanding this fact is essential: it is not relevant, in this approach, to look for representations of the signal in the form of transformations on one of the outcomes that could well demonstrate the properties sought; here, we must “go back” as far as possible to the probability laws of $x(t, \omega)$, from the observation of one (or a finite number) of the outcomes, generally over a finite time interval. How, from the data $\{x_j(t) | j = 1, \dots, K, t \in [t_0, t_1]\}$, we can go back to the laws of $x(t, \omega)$ is the subject of the estimation theory (see Chapter 3).

Figure 1.3 shows some outcomes of a same physical signal (Doppler echo signal from a 38 GHz traffic radar carried by a motor car). Every realization contains the same relevant information: same vehicle speed, same pavement surface, same trajectory, etc. However, there is no reproducibility of outcomes, and there are fairly large morphological differences between them. At the very most, we cannot avoid noticing that they have a “family likeness”. The probabilistic description is nothing

but one of the approaches that helps account for this “family likeness”, i.e. by the membership of the signal to a well-defined probability space.

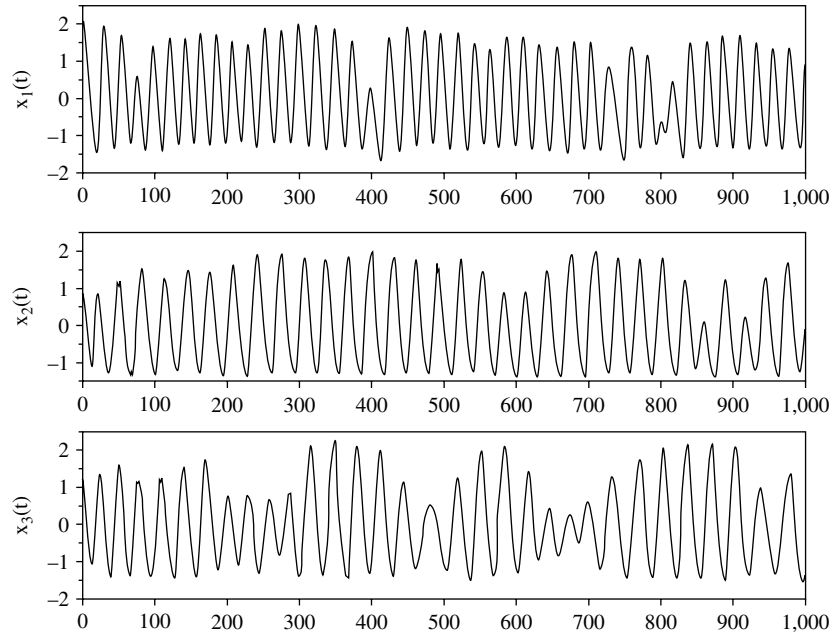


Figure 1.3. Example of three outcomes of an actual random signal

The laws are probability sets

$$P[x(t_1) \in D_1, x(t_2) \in D_2, \dots, x(t_n) \in D_n] = L(D_1, D_2, \dots, D_n, t_1, t_2, \dots, t_n) \quad [1.6]$$

whose most well-known examples are the probability densities in which $D_i = [x_i, x_i + dx_i]$.

$$P[\dots] = p(x_1, \dots, x_n, t_1, \dots, t_n) dx_1, \dots, dx_n \quad [1.7]$$

and the distribution functions, with $D_i =]-\infty, x_i]$:

$$P[\dots] = F(x_1, \dots, x_n, t_1, \dots, t_n) \quad [1.8]$$

8 Digital Spectral Analysis

The set of these three laws fully characterizes the random signal, but a partial characterization can be obtained via the moments of order M of the signal, defined (when these exist) by:

$$\begin{aligned} E\left(x(t_1)^{k_1} \dots x(t_n)^{k_n}\right) &= \int \dots \int_{\Re^n} x_1^{k_1} \dots x_n^{k_n} p(x_1, \dots, x_n, t_1, \dots, t_n) dx_1, \dots, dx_n \\ &= \int \dots \int_{\Re^n} x_1^{k_1} \dots x_n^{k_n} dF(x_1, \dots, x_n, t_1, \dots, t_n) \end{aligned} \quad [1.9]$$

with $M = \sum_i k_i$

It can be shown that these moments are linked in a simple way to the Taylor series expansion of the characteristic function of the n -tuple $\{x_1(t_1), \dots, x_n(t_n)\}$ defined by:

$$\begin{aligned} \phi(u_1, \dots, u_n) &= \phi(\mathbf{u}) \triangleq E\left(\exp(j\mathbf{u}^T \mathbf{x})\right) \\ \mathbf{u} &= |u_1 \dots u_n|^T, \mathbf{x} = |x_1 \dots x_n|^T \end{aligned} \quad [1.10]$$

We see that the laws and the moments have a dependence on the considered points $\{t_1, \dots, t_n\}$ of the time axis. The separation of random signals into classes very often refers to the nature of this dependence: if a signal has one of its characteristics invariant by translation, or in other words, independent of the time origin, we will call the signal stationary for this particular characteristic. We will thus speak of *stationarity in law* if:

$$p(x_1, \dots, x_n, t_1, \dots, t_n) = p(x_1, \dots, x_n, t_1 + t_0, \dots, t_n + t_0)$$

and of *stationarity for the moment of order M* if:

$$E\left(x(t_1)^{k_1} \dots x(t_n)^{k_n}\right) = E\left(x(t_1 + t_0)^{k_1} \dots x(t_n + t_0)^{k_n}\right)$$

The interval t_0 for which this type of equality is verified holds various stationarity classes:

- *local* stationarity if this is true only for $t_0 \in [T_0, T_1]$,
- *asymptotic* stationarity if this is verified only when $t_0 \rightarrow \infty$, etc.

We will refer to [LAC 00] for a detailed study of these properties.

Another type of time dependence is defined when the considered characteristics recur *periodically* on the time axis: we then speak of *cyclostationarity*. For example, if:

$$E\left(x(t_1)^{k_1} \dots x(t_n)^{k_n}\right) = E\left(x(t_1 + T)^{k_1} \dots x(t_n + T)^{k_n}\right) \forall (t_1, \dots, t_n)$$

the signal will be called cyclostationary for the moment of order M (see [GAR 89]).

1.2. Representations of signals

The various classes of signals defined above can be represented in many ways, i.e. forming of the information present in the signal, which does not have any initial motive other than to highlight certain characteristics of the signal. These representations may be complete, if they carry all the information of the signal, and partial otherwise.

1.2.1. Representations of deterministic signals

1.2.1.1. Complete representations

As the postulate of the deterministic signal is that any information that affects it is contained in the function $x(t)$ itself, it is clear that any bijective transformation applied to $x(t)$ will preserve this information.

From a general viewpoint, such a transformation may be written with the help of integral transformations on the signal, such as:

$$R(u_1, \dots, u_m) = H \left[\int \dots \int G[x(t_1), \dots, x(t_n)] \cdot \psi(t_1, \dots, t_n, u_1, \dots, u_m) \dots dt_1 \dots dt_n \right] [1.11]$$

where the operators $H [.]$ and $G [.]$ are not necessarily linear. The kernel $\psi(t, f) = e^{-j2\pi ft}$ has a fundamental role to play in the characteristics that we wish to display. This transformation will not necessarily retain the dimensions, and in general, we will use representations such as $m \geq n$. We will expect it to be invertible (i.e. there exists an exact inverse transformation), and that it helps highlight certain properties of the signal better than the function $x(t)$ itself. It must also be understood that the demonstration of a characteristic of the signal may considerably mask other characteristics: the choice of $H [.]$, $G [.]$, and $\psi(.)$ governs the choice of what will be highlighted in $x(t)$. In the case of discrete time signals, discrete expressions of the same general form exist.

10 Digital Spectral Analysis

The very general formula of equation [1.11] fortunately reduces to very simple elements in most cases.

Here are some of the most widespread examples: orthogonal transformations, linear time–frequency representations, timescale representations, and quadratic time–frequency representations.

Orthogonal transformations

This is the special case where $m = n = 1$, $H[x] = G[x] = x$, and $\psi(t, u)$ is a set of orthogonal functions. The undethronable Fourier transform is the most well known with $\psi(t, f) = e^{-j2\pi ft}$. We may once again recall its definition here:

$$\hat{x}(f) = \text{FT}(x(t)) = \int_{\mathfrak{R}} x(t) e^{-j2\pi ft} dt \text{ with } f \in \mathfrak{R} \quad [1.12]$$

and its discrete version for a signal vector $\mathbf{x} = [x(0) \dots x(N-1)]^T$ of length N :

$$\hat{x}(l) = \text{DFT}(x(k)) = \sum_{k=0}^{N-1} x(k) e^{-j2\pi \frac{kl}{N}} \text{ with } l \in [0, N-1] \quad [1.13]$$

If we bear in mind that the inner product appearing in equation [1.12] or [1.13] is a measure of likelihood between $x(t)$ and $e^{-j2\pi ft}$, we immediately see that the choice of this function set $\psi(t, f)$ is not innocent: we are looking to highlight complex sine curves in $x(t)$.

If we are looking to demonstrate the presence of other components in the signal, we will select another set $\psi(t, u)$. The most well-known examples are those where we look to find components with binary or ternary values. We will then use functions such as Hadamard–Walsh or Haar (see [AHM 75]).

Linear time–frequency representations

This is the special case where $H[x] = G[x] = x$ and $\psi(t, \tau, f) = w(t - \tau) e^{-j2\pi ft}$, leading to an expression of the type:

$$R(\tau, t) = \int x(t) w(t - \tau) e^{-j2\pi ft} dt \quad [1.14]$$

Timescale (or wavelet) representations

This is the special case where $H[x] = G[x] = x$ and $\psi(t, \tau, a) = \psi_M^*\left(\frac{t-\tau}{a}\right)$, which gives:

$$R(\tau, a) = \int x(t) \psi_M^*\left(\frac{t-\tau}{a}\right) dt \quad [1.15]$$

where $\psi_M(t)$ is the parent wavelet. The aim of this representation is to look for the parent wavelet in $x(t)$, translated and expanded by the factors τ and a , respectively.

Quadratic time-frequency representations

In this case, $G[.]$ is a quadratic operator, and $H[.] = x$. The most important example is the Wigner–Ville transformation:

$$R(t, f) = \int x\left(t + \frac{\tau}{2}\right) x\left(t - \frac{\tau}{2}\right)^* e^{-j2\pi f \tau} d\tau \quad [1.16]$$

which is invertible if at least one point of $x(t)$ is known.

The detailed study of these three types of representations is the central theme of another book of the same series (see [HLA 05]).

Representations with various more complex combinations of $H[x]$, $G[x]$, and $\psi_M(.)$ can be found in [OPP 75] and [NIK 93], from among abundant literature.

1.2.1.2. Partial representations

In many applications, we are not interested in the entire information present in the signal, but only in a part of it. The most common example is that of energy representations, where only the quantities linked to the energy or power are considered.

The energy or power spectral density

If we are interested in the frequency energy distribution (we will call it “spectral”), we are led to consider the following quantity:

$$S_x(f) = |\text{FT}(x(t))|^2 = |\bar{x}(f)|^2 \triangleq \text{ESD}(x(t)) \quad [1.17]$$

12 Digital Spectral Analysis

for continuous time signals, and:

$$S_x(l) = |\text{DFT}(x(k))|^2 = |\hat{x}(l)|^2 \triangleq \text{ESD}(x(k)) \quad [1.18]$$

for discrete time signals.

These representations do not allow the signal to be reconstructed, as the phase of the transform is lost. We will call them energy spectral densities (ESD). But the main reason for interest in these partial representations is that they show the energy distribution along a non-time axis (here the frequency). In fact, Parseval's theorem states:

$$E = \int_R |x(t)|^2 dt = \int_R |\hat{x}(f)|^2 df \quad [1.19]$$

and $|\hat{x}(f)|^2$ represents the energy distribution in f , just as $|x(t)|^2$, therefore, represents its distribution over t .

For discrete time signals, Parseval's theorem is expressed a little differently:

$$E = \sum_{k=0}^{N-1} |x(k)|^2 = \frac{1}{N} \sum_{l=0}^{N-1} |\hat{x}(l)|^2$$

but the interpretation is the same.

The quantities $S_x(f)$ or $S_x(l)$ defined above have an inverse Fourier transform, which can easily be shown as being expressed by:

$$\text{IFT}(S_x(f)) = \int_R x(t) x^*(t-\tau) dt \triangleq \gamma_{xx}(\tau) \quad [1.20]$$

This function is known as the autocorrelation function of $x(t)$. We see that the ESD of $x(t)$ could have axiomatically been defined as follows:

$$S_x(f) = \text{ESD}(x(t)) \triangleq \text{FT}(\gamma_{xx}(\tau)) \quad [1.21]$$

When we are interested in *finite power* signals, their Fourier transform exists in terms of distributions. This generally prohibits the definition of the square of the

modulus, and thus the power spectral density (PSD) as by equation [1.17] or [1.18]. It is, however, always possible to define the autocorrelation function by:

$$\gamma_{xx}(\tau) \triangleq \lim_{T \rightarrow \infty} \frac{1}{T} \int_{-T/2}^{+T/2} x(t) x^*(t - \tau) dt \quad [1.22]$$

Its Fourier transform is used to define the PSD by:

$$S_x(f) = \text{PSD}(x(t)) \triangleq \text{FT}(\gamma_{xx}(\tau)) \quad [1.23]$$

This function gives the frequency distribution of the power, such that its sum along the axis f once again gives the total power:

$$\int_{\Re} S_x(f) df = \gamma_{xx}(0) = P \quad [1.24]$$

All these are greatly detailed, e.g. in [DUV 91], and taken up in section 2.2 of this book.

The reader will easily understand that the previously mentioned definitions of energy (or power) spectral densities are based on the Fourier transform, only for the isometry represented by equation [1.19]. We can thus easily generalize these concepts through other orthogonal transforms (Hadamard–Walsh, Haar, etc.) that have the same property of preserving the inner product. The axis along which the ESD will give the energy distribution will no longer be a frequency axis, but an axis corresponding to the subscripting of the family of orthogonal functions retained (see [HAR 69]).

1.2.2. Representations of random signals

1.2.2.1. General approach

As specified in section 1.1.2, the complete knowledge of the information present in the signal requires the knowledge of the probability laws. This occurs in practice only when we have a theoretical model establishing the law, and only its parameters remain to be determined: this is a problem that, therefore, deals with the theory of parametric estimation (see Chapter 3).

Except for this slightly ideal case, the representations of random signals will only be partial. Among these representations, the moments and cumulants are the

most used (if not the only ones). We will talk of *knowledge of the order K* of the signal if all moments up to the K order are known, i.e. the set of:

$$E\left(x(t_1)^{k_1} \dots x(t_n)^{k_n}\right) \text{ for } M = 1, 2, \dots, K$$

with $M = \sum_i k_i$

Each moment is a function of n variables, and it is obvious that for a high value of K , the representation will be very complex. The practical ambitions are largely limited, and we practically limit ourselves to $K = 2$, and in a few cases to $K = 3$ or 4. For a definition and presentation of cumulants, refer to [LAC 97] and [NIK 93].

1.2.2.2. Second-order representations

The most important case is that of the second-order representation, which reduces to:

$$\begin{aligned} m_x(t) &= E(x(t)) \\ \gamma_{xx}(t_1, t_2) &= E(x(t_1)x^*(t_2)) \end{aligned} \quad [1.25]$$

We see that this representation requires the use of a single variable (the average), and a function with two variables (the autocorrelation function).

In the case where we can additionally make the stationary hypothesis, this reduces to a constant and a function with one variable:

$$\begin{aligned} m_x &= E(x(t)) \\ \gamma_{xx}(\tau) &= E(x(t)x^*(t-\tau)) \end{aligned} \quad [1.26]$$

Considering the complexity of representations as the order increases, we can presume that a limitation to such low orders is only for the sake of simplicity: it would therefore be troublesome if the sacrifice made for the sake of simplicity is too great, and that the essence of the signal information is lost in this limitation.

There exists a very important class of random processes for which the knowledge of the second-order is complete: this is the class of Gaussian signals, for which all laws are fully determined, for all orders, if we know the quantities given by equation [1.25] (or equation [1.26]) *stricto sensu* for all $(t, t_1, t_2) \in \mathbb{R}^3$. We will refer to [LAC 00] for a detailed representation of these signals. But for the essence, their abundance among actual signals results from asymptotic theorems

on linear mixtures of laws that are (almost) arbitrary, which have an inevitable attraction for the Gaussian law.

In addition, other classes of signals enjoy the same parsimony of complete representations: certain nonlinear transformations of Gaussian signals (such as those found in telecommunications), compound random processes, invariant spherical processes, etc.

Even if the second-order representation remains partial, it is of great interest as it is consistent with an “energy” representation of random signals, very close to the one described in section 1.2.1.2.

In fact, the ergodic theorem (see [DUV 91, LAC 00]) tells us that, in the field of application of this theorem, there is an identity between the mathematical expectation operator $E[\cdot]$ and that of the time average $\lim_{T \rightarrow \infty} \frac{1}{T} \int_{-T/2}^{+T/2} dt$ applied to any characterization $x_j(t)$. For example, the first-order ergodicity can be used to write:

$$E[x(t)] = \lim_{T \rightarrow \infty} \frac{1}{T} \int_{-T/2}^{+T/2} x_j(t) dt \triangleq \langle x_j(t) \rangle \forall j \quad [1.27]$$

The stochastic average and the time average – which is known as the *direct current* (DC) for electrical quantities – are therefore, in this case, confounded.

The second-order ergodicity is highly revealing; in fact:

$$E[|x(t)|^2] = \lim_{T \rightarrow \infty} \frac{1}{T} \int_{-T/2}^{+T/2} |x_j(t)|^2 dt = \langle |x_j(t)|^2 \rangle = P \quad [1.28]$$

In the time average appearing in the second member, we recognize the average power of the j th realization (which is independent of j in this case). The Bochner–Khintchine theorem allows us to make the link between the second-order moment (autocorrelation function) and the PSD (in terms of stationarity random signals):

$$\begin{aligned} \gamma_{xx}(\tau) &\triangleq E(x(t)x^*(t-\tau)) \\ S_{xx}(f) &\triangleq \text{FT}(\gamma_{xx}(\tau)) \end{aligned} \quad [1.29]$$

and from there, we find the form similar to equation [1.23]:

16 Digital Spectral Analysis

$$\begin{aligned}\gamma_{xx}(0) &= \int_{\Re} S_x(f) df = P \\ \gamma_{xx}(0) &= E \left[|x(t)|^2 \right] = \lim_{T \rightarrow \infty} \frac{1}{T} \int_{-T/2}^{+T/2} |x_j(t)|^2 dt = \left\langle |x_j(t)|^2 \right\rangle = P\end{aligned}$$

The power figuring in the right-hand term of this equation corresponds to the usual definition of power using a time average. The PSD as defined for the stationarity and ergodic random processes is therefore identical to the PSD as defined by finite power signals, applied to any realization of the signal.

We must, however, note that this similarity does not apply as soon as we leave the stationary and ergodic framework: the loss of one of the two properties prohibits the two definitions of the PSD, with only equation [1.29] remaining valid. This type of divergence is discussed in Chapter 9.

Very complete theoretical results were established for the spectral density classes. This set of properties results essentially from the fact that the *class of correlation functions* and that of *characteristic functions* (from probability calculus) are confounded (differing by a multiplicative constant). This highly significant result helps take advantage of all historical work on characteristic functions. One of the essential consequences is that the nature of this mathematical object is well worked out; in particular, a very general decomposition helps affirm that for any second-order stationarity signal [LAC 00]:

$$S_{xx}(f) = S_1(f) + S_2(f) + S_3(f) \quad [1.30]$$

where the three components have well-established properties:

The component $S_1(f)$ is the “continuous” part of the PSD. This name is not strictly correct: it is only the derivative of a continuous increasing function in the wide sense. It can thus have discontinuities, asymptotes, etc., but on a set of zero measure. The summability of $S_1(f)$ generally ensures “pleasant” behavior for $|f| \rightarrow \infty$, that is to say, $S_1(\infty) = 0$ (although this is not a necessary condition).

The component $S_2(f)$ is the derivative of a non-decreasing step function. Its compact expression is therefore:

$$S_2(f) = \sum_i A_i \delta(f - f_i) \quad [1.31]$$

where each $A_i \delta(f - f_i)$ is a monochromatic component (known as “line”) of power $A_i \geq 0$ and frequency f_i . The summability of $S_2(f)$ therefore ensures that of the series

$\{A_i\}$, i.e. $P_2 = \sum_i A_i < \infty$. The term P_2 represents the total power of periodic components of the signal. We say that $S_2(f)$ is a *line spectrum*.

The special case where a sub-set of the series $\{f_i\}$ consists of rational numbers between mutually rational values corresponds to a *periodic component* in the random signal. This type of component deserves a special development, as it is not intuitively evident that a signal can be random and stationarity as well as periodic at the same time.

However, if we define the periodicity as in the mean square sense of a signal $x(t)$ with:

$$E\left(\left|x(t) - x(t + mT)\right|^2\right) = 0 \quad \forall m \in \mathbb{Z} \quad [1.32]$$

with T representing the period of the random signal $x(t)$, this can be broken down into a Fourier series with *random coefficients*:

$$C_k = \frac{1}{T} \int_{-T/2}^{+T/2} x(t) e^{-j2\pi k \frac{t}{T}} dt \quad [1.33]$$

The random variables $\{C_k\}$ have the following striking properties:

$$\begin{aligned} E(C_k) &= 0 \text{ for } k \neq 0 \\ E(C_k^* C_m) &= 0 \text{ for } k \neq m \\ E(|C_k|^2) &= A_k \end{aligned} \quad [1.34]$$

where the power A_k is associated with the line at frequency $f_k = k/T$ appearing in equation [1.31].

Note that there exists a line for $f = 0$ (by convention, we note it as $f_0 = 0$), which is linked to what is commonly known as the “DC component”, as it is easy to show that:

$$A_0 = |E(x(t))|^2 \quad [1.35]$$

where the average $E(x(t))$ is identical to the continuous component of electronics engineers, if the signal is ergodic (see equation [1.27]).

The term $S_3(f)$ is known as singular and is, generally, absent in physical signals.

18 Digital Spectral Analysis

The previous properties are very important to understand what kind of object we will be confronted with when we will perform a second-order spectral analysis on stationary signals. Figure 1.4 summarizes the properties of these PSDs.

The main role of the autocorrelation function and its Fourier transform, the PSD, is largely justified by the regularity of their behavior in the invariant linear transformations. We must briefly recall here that if two random signals are linked by an invariant linear filtering operation of kernel $h(t)$ (continuous time) or $h(k)$ (discrete time), a kernel that is also its impulse response, we can write it in the convoluted form:

$$y(t) = x \otimes h(t) = \int_{\Re} x(u)h(t-u)du$$

$$y(k) = x \otimes h(k) = \sum_{m=-\infty}^{+\infty} x(m)h(k-m) \quad [1.36]$$

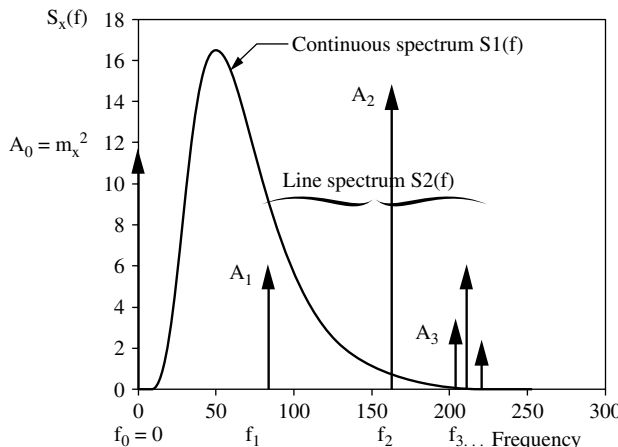


Figure 1.4. Morphology of PSDs in the stationarity case

The Wiener–Lee (or Blanc–Lapierre) theorems can be used to write:

$$S_{yx}(f) = S_x(f) \cdot \bar{h}(f) \xrightarrow{\text{FT}} \gamma_{yx}(\tau) = \gamma_{xx} \otimes h(\tau)$$

$$S_{yy}(f) = S_{xx}(f) |\bar{h}(f)|^2 \xrightarrow{\text{FT}} \gamma_{yy}(\tau) = \gamma_{xx} \otimes h \otimes h^-(\tau) \quad [1.37]$$

where the input–output intercorrelation appears:

$$\gamma_{yx}(\tau) = E(y(t)x^*(t-\tau)) \quad [1.38]$$

1.2.2.3. Higher-order representations

We are moving away (timidly) from this second-order representation for the last few years, because, as has just been explained, it is consistent with a representation of *power* characteristics of the signal. In these representations, the concepts of phase are lost, and the *non-Gaussian* nature of the signals is not clearly demonstrated. These two aspects are among the main motivations to increase the order of representations, leading to *higher-order* representations (means greater than 2). We will refer to [LAC 97] and [NIK 93] on these fundamental points. What is important for this book is to note that spectral representations are an essential tool for estimation in this field of *higher-order statistics* (HOS).

If we limit this short presentation to null mean, real and stationarity signals of the considered order, the cumulants of the third and fourth order have the following expression, versus the moments:

$$\begin{aligned} C_{xxx}(\tau_1, \tau_2) &= E_{xxx}(\tau_1, \tau_2) = E(x(t)x(t-\tau_1)x(t-\tau_2)) \\ C_{xxxx}(\tau_1, \tau_2, \tau_3) &= E_{xxxx}(\tau_1, \tau_2, \tau_3) \\ &\quad - \gamma_{xx}(\tau_1)\gamma_{xx}(\tau_2 - \tau_3) \\ &\quad - \gamma_{xx}(\tau_2)\gamma_{xx}(\tau_1 - \tau_3) \\ &\quad - \gamma_{xx}(\tau_3)\gamma_{xx}(\tau_1 - \tau_2) \end{aligned} \quad [1.39]$$

Using these quantities, we define *multi spectra* by multidimensional Fourier transform of cumulants:

$$S_{xxx\dots x}(f_1, \dots, f_{n-1}) = \text{FT}\left(C_{xxx\dots x}(\tau_1, \dots, \tau_{n-1})\right) \quad [1.40]$$

These quantities represent a generalization of PSDs, in the sense that the invariant linear processing (of input $x(t)$ and output $y(t)$) has the advantage of simple formulations. For example, a generalization of Wiener–Lee equations is given by:

$$\begin{aligned} S_{yy\dots y}(f_1, \dots, f_{n-1}) &= S_{xxx\dots x}(f_1, \dots, f_{n-1})\hat{h}(f_1)\dots\hat{h}(f_{n-1}) \\ &\quad \cdot \hat{h}(f_1 + f_2 + \dots + f_{n-1}) \end{aligned} \quad [1.41]$$

The *multispectral analysis* is one of the methods that allows the estimation of HOS. We will, however, note that we do not have results in the form of multispectra as general and elegant as those that are given on p. 14 for the PSDs.

1.3. Spectral analysis: position of the problem

In the previous two sections, we have seen that the characteristics that carry the information in a signal can be extremely diverse. Changing to a transformed domain is a common practice, as in this domain the information “relevant” to the signal (or deemed to be so) is more visible than in the signal itself. In addition, a certain number of processes can be written more clearly in the transformed domain. This is the case with invariant linear processes, whose expression is very compact in the frequency domain.

We are entitled to wonder about the relevance of this omnipresence of the Fourier transform, and its almost systematic use: sclerosis linked to professional habits or deserved success.

One of the reasons for the success of the kernel $e^{-j2\pi ft}$ (or its equivalent with f complex, the Laplace transform) is that this family of special functions is one of the eigenfunctions of invariant linear systems. When we analyze such systems, it is legitimate to project (break down) the signals on this basis, the linearity of the system ensuring individual processing of each component. Fundamentally, this property is at the root of spectral equations that are as useful as the Wiener–Lee relations.

Outside the invariant linear framework, the Fourier transform with the exponential kernel is not justified as much, and other kernels may be better suited: the linear transforms on Gallois fields in base 2 justify the use of binary kernel transforms, the search for polynomial modulation laws requires higher-order Wigner–Ville representations, the highlighting of translations and time dilations induces wavelet representations, etc.

The following chapters deal almost exclusively with the exponential kernel, but the informed reader could easily generalize most of the concepts and results to other kernels, by rather simple transpositions of concepts of frequency resolution, estimation variance, bias-variance trade-off, etc.

However, the importance of the exponential kernel for applications is practically a fact of life, the other representations sharing a small portion of applications. This justifies the bias of the current book, which is to center the discussion on *spectral analysis with the Fourier kernel*, rather than making a presentation with a more general class of kernels $\psi(t, u)$ and to deduce from this the properties of Fourier analysis: as a result, the book loses elegance, but no doubt gains clarity and pedagogy.

In addition, the majority of chapters is devoted to second-order spectral analysis, for the same reasons of extent of the fields of application. However, the extension to multispectra is quite obvious, and the books already listed show that multispectral analysis borrows everything from second-order analysis.

In the very large set of spectral analysis methods, we discern *non-parametric* methods, the subject of Chapter 5, which make very few hypotheses on the signal: these hypotheses are essentially the existence of Fourier transforms of the analyzed quantities (the signal itself in the deterministic context, second-order moments in random context), and most often the stationarity (strict or local) of moments in random context.

Parametric methods, the subject of Chapters 4 and 6, are based on a more restrictive *a priori* assumption: we suppose that we know a behavioral model of the signal, general model that will be adjusted to the physical signal using a set of parameters. This approach is summarized in Chapter 4. The relevant spectral quantities can be expressed in terms of this set of parameters, which helps the following strategy: we implement parameter estimators, which are used to establish in a second-step spectral estimators, thus as by-products of the initial parametric estimation.

A very special case is that of signals made up of a *finite set of sinusoidal functions*, which are deterministic or random, possibly polluted by a random additive phenomenon. This very special framework received great attention from the signal and image processing community, as it helps model a large set of practical situations. We have devoted a large amount of space to it (see sections 4.3 and 6.2.3, and Chapter 8).

The tools necessary for the understanding of developments of Parts 2 and 3 are summarized in the following chapters of this first part.

1.4. Bibliography

- [AHM 75] AHMED N., RAO K.R., *Orthogonal Transform for Digital Signal Processing*, Springer-Verlag, 1975.
- [DUV 91] DUVAUT P., *Traitemen du signal*, Hermès, Paris, 1991.
- [GAR 89] GARDNER W., *Introduction to Random Processes*, McGraw-Hill, 1989.
- [HAR 69] HARMUTH H.F., *Transmission of Information by Orthogonal Functions*, Springer-Verlag, 1969.
- [HLA 05] HLAWATSCH F., AUGER F. (eds), *Time-Frequency Analysis*, ISTE Ltd, London, John Wiley & Sons, New York, 2008.

22 Digital Spectral Analysis

- [LAC 97] LACOUME J.L., AMBLARD P.O., COMON P., *Statistiques d'ordre supérieur pour le traitement du signal*, Masson, 1997.
- [LAC 00] LACAZE B., *Processus aléatoires pour les communications numériques*, Hermès, Paris, 2000.
- [NIK 93] NIKIAS C., PETROPULU A., *Higher-Order Spectra Analysis*, Prentice Hall, 1993.
- [OPP 75] OPPENHEIM A., SCHAFFER R., *Digital Signal Processing*, Prentice Hall, 1975.

Chapter 2

Digital Signal Processing

2.1. Introduction

A continuous time-deterministic signal $x(t)$, $t \in \mathfrak{R}$ is by definition a function of \mathfrak{R} in C :

$$\begin{aligned}x &: \mathfrak{R} \rightarrow C \\t &\mapsto x(t)\end{aligned}$$

where the variable t is the time. In short, we often talk about a continuous signal, even if the considered signal is not continuous in the usual mathematical sense. For example, we can state displacement, speed, and acceleration signals in mechanics, voltage and current signals in electricity, biomedical signals (electrocardiogram, electroencephalogram, electromyogram, etc.), temperature signals, etc.

A discrete time-deterministic signal $x(k)$, $k \in Z$ is, by definition, a *series* of complex numbers:

$$x = (x(k))_{k \in Z}$$

In short, we often refer to discrete signals. As an example of a discrete time signal, we can state the sunset time according to the day. Generally, the considered signals, whether they are continuous or discrete, have real values, but the generalization given here of complex signals poses no theoretical problem.

Chapter written by Éric LE CARPENTIER.

24 Digital Spectral Analysis

The spectral analysis of deterministic signals consists of a decomposition based on simpler signals (e.g. sine curves), similar to the way a point is marked in space using its three coordinates. It is thus necessary to define an inner product, which is used to measure the projection of a signal on a basic element.

Let x and y be two signals; their inner product $\langle x, y \rangle$ is defined continuously and discretely respectively by:

$$\langle x, y \rangle = \int_{-\infty}^{+\infty} x(t) y^*(t) dt \quad \langle x, y \rangle = \sum_{k=-\infty}^{+\infty} x(k) y^*(k) \quad [2.1]$$

The energy of a signal x is defined by the inner product $\langle x, x \rangle$. The set of signals (with continuous or discrete time) with finite energy, along with the inner product defined above, constitutes a vector space. Very often, the basic elements selected (such as the exponential basis of the Fourier transform) do not verify the finite energy property. A rigorous mathematical processing requires the knowledge of the theory of distributions; we will be content here with an intuitive introduction.

In the case of periodic signals with a known continuous period T or discrete period N , the inner product has the following form:

$$\langle x, y \rangle = \frac{1}{T} \int_0^T x(t) y^*(t) dt \quad \langle x, y \rangle = \frac{1}{N} \sum_{k=0}^{N-1} x(k) y^*(k) \quad [2.2]$$

Thus, the inner product $\langle x, x \rangle$ is the power of the periodic signal. The set of periodic signals (with continuous or discrete time) with finite power, along with the inner product defined above, constitute a vector space.

These concepts are dealt with in greater detail in section 2.2.2, particularly in the case of the Fourier transform, in honor of the French mathematician J.B. Fourier (1768–1830), which consists in taking cisoid functions as basis vectors. We will present beforehand some functions and series required for the development of this transform.

2.2. Transform properties

2.2.1. Some useful functions and series

The *unit constant* 1_{\Re} is a function that is always equal to 1; for all t :

$$1_{\Re}(t) = 1 \quad [2.3]$$

The *continuous time cisoid* of amplitude $a > 0$, frequency $f \in \mathfrak{R}$ and initial phase $\phi \in \mathfrak{R}$ is defined by:

$$t \mapsto a e^{j(2\pi f t + \phi)} \quad [2.4]$$

The *unit step* U is the zero function for the negative instants, and unit for the positive instants. It thus has a discontinuity at 0. The value at 0 is not important. However, we will adopt the following convention: if a signal x has a discontinuity at t_0 , then $x(t_0)$ is equal to the arithmetic mean of the left $x(t_0 -) = \lim_{t \uparrow t_0} x(t)$ and right limits $x(t_0 +) = \lim_{t \downarrow t_0} x(t)$. With this convention we thus obtain:

$$u(t) = \begin{cases} 0 & \text{if } t < 0 \\ \frac{1}{2} & \text{if } t = 0 \\ 1 & \text{if } t > 0 \end{cases} \quad [2.5]$$

The *rectangular window* $l_{t_0 t_1}$ for all t , is defined by:

$$l_{t_0, t_1}(t) = \begin{cases} 1 & \text{if } t_0 < t < t_1 \\ \frac{1}{2} & \text{if } t = t_0 \text{ or } t = t_1 \\ 0 & \text{otherwise} \end{cases} \quad [2.6]$$

To define the *Dirac delta function* rigorously, knowledge about the mathematical theory of distributions is required. We will be content here with an intuitive introduction. The Dirac delta function δ can be defined as the limit of the function with unit integral $\frac{1}{2T} l_{-T, T}$ when $T \geq 0$. We thus obtain:

$$\begin{cases} \delta(t) = 0 & \text{if } t \neq 0 \\ \delta(0) = +\infty \end{cases} \quad \text{with the condition } \int_{-\infty}^{+\infty} \delta(t) dt = 1 \quad [2.7]$$

If we integrate the Dirac delta function, we immediately observe that for all t :

$$\int_{-\infty}^t \delta(u) du = U(t) \quad [2.8]$$

The Dirac delta function can be considered as the derivative of the unit step:

$$\delta = \frac{dU}{dt} = \dot{U} \quad [2.9]$$

26 Digital Spectral Analysis

If we multiply the Dirac delta function δ by a number a , we obtain the Dirac delta function $a\delta$ of weight a ($a\delta(t) = 0$ if $t \neq 0$, $a\delta(0) = \infty$, $\int_{-\infty}^{+\infty} a\delta(t)dt = a$).

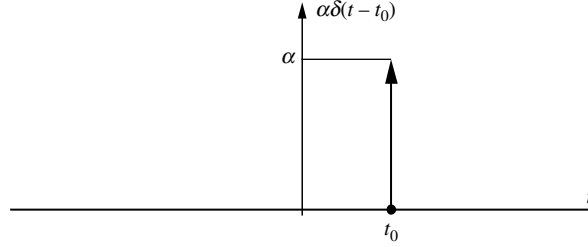


Figure 2.1. Weighted Dirac delta function at t_0

The weighted Dirac delta function at t_0 , i.e. $t \mapsto a\delta(t-t_0)$, is generally represented by an arrow centered on t_0 of height proportional to a (Figure 2.1).

The Dirac delta function thus helps generalize the concept of derivative to the signals presenting points of discontinuity, for which the derivative is not defined in the usual sense and at these points is equal to a pulse whose weight is equal to the jump in the discontinuity. The Dirac delta function verifies the following property; for all signals x , and all t_0 :

$$\int_{-\infty}^{+\infty} x(t) \delta(t-t_0) dt = x(t_0) \quad [2.10]$$

This property is quite natural in the case where the function x is continuous at t_0 . We will accept that it remains exact if the convention on the value of a signal at these points of discontinuity is respected. It can be generalized to the ℓ th derivative $\delta^{(\ell)}$ of the Dirac delta function; by induction, integrating by parts we obtain for all $\ell \geq 0$ and all t :

$$\int_{-\infty}^{+\infty} x(t) \delta^{(\ell)}(t-t_0) dt = (-1)^\ell x^{(\ell)}(t_0) \quad [2.11]$$

Moreover, time scaling leads to the following property; for all t , and for all non-zero real numbers, α :

$$\delta(\alpha t) = \frac{1}{|\alpha|} \delta(t) \quad [2.12]$$

Finally, we will accept that the Dirac delta function can also be expressed by the following integral formulation:

$$\delta(t) = \int_{-\infty}^{+\infty} e^{j2\pi f t} df \quad [2.13]$$

The *Dirac comb* of period T , Ξ_T is a periodized version of Dirac delta functions, defined for all t by:

$$\Xi_T(t) = \sum_{k=-\infty}^{+\infty} \delta(t - kT) \quad [2.14]$$

We will accept the following formulation in the form of a series; for all t :

$$\Xi_T(t) = \frac{1}{T} \sum_{\ell=-\infty}^{+\infty} e^{j2\pi \frac{\ell}{T} t} \quad [2.15]$$

The *sine cardinal* is defined for all t by:

$$\text{sinc}(t) = \begin{cases} \frac{\sin(t)}{t} & \text{if } t \neq 0 \\ 1 & \text{if } t = 0 \end{cases} \quad [2.16]$$

The value at 0 is obtained by continuity extension. This function (Figure 2.2) becomes zero for all t multiples of $-n$, except 0.

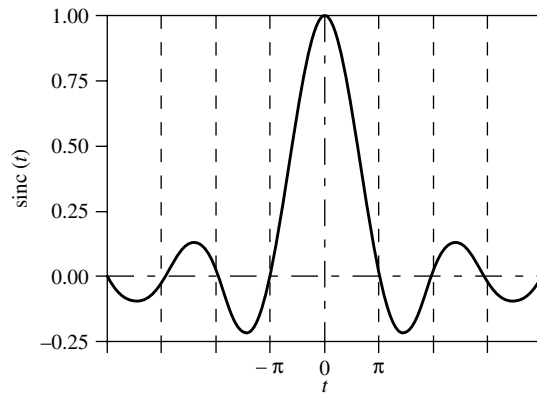


Figure 2.2. Sine cardinal sinc

The *Dirichlet function* (or Dirichlet's kernel, or periodic sinc function) diric_N , parameterized by the integer $N \geq 1$, is defined for all t by:

$$\text{diric}_N(t) = \begin{cases} \frac{\sin(\pi t N)}{N \sin(\pi t)} & \text{if } t \notin \mathbb{Z} \\ (-1)^t (N-1) & \text{if } t \in \mathbb{Z} \end{cases} \quad [2.17]$$

The value at the integer abscissa is obtained by continuity extension; it is always equal to 1 if N is odd, $(-1)^*$ if N is even. The Dirichlet's function is even and periodic with period 1 if N is odd; it is even, periodic with period 2 and symmetrical in relation to the point $\left(\frac{1}{2}, 0\right)$ if N is even (Figure 2.3). Thus, in all cases, its absolute value is even and periodic with period 1. It is 0 for all non-integer t multiple of $\frac{1}{N}$. The arch of this function centered on 0 is called the main lobe, the others are secondary lobes. The main lobe gets narrower and the secondary lobes' amplitude gets smaller as N increases.

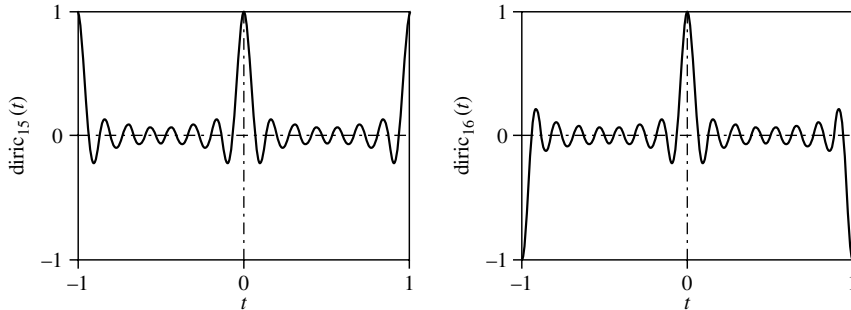


Figure 2.3. Dirichlet functions diric_{15} and diric_{16}

The *unit series* 1_Z is the series equal to 1; for all k :

$$1_Z(k) = 1 \quad [2.18]$$

The *discrete time cisoid* of amplitude a , frequency v , and initial phase ϕ is defined by:

$$\left(a e^{j(2\pi v k + \phi)} \right)_{k \in \mathbb{Z}} \quad [2.19]$$

We immediately notice that the frequency of the cisoid is defined modulo 1.

The *rectangular window* $1_{k_0, k_1}$ is defined for all k by:

$$1_{k_0, k_1}(k) = \begin{cases} 1 & \text{if } k_0 \leq k \leq k_1 \\ 0 & \text{otherwise} \end{cases}$$

The Kronecker δ sequence is defined for all k by:

$$\begin{cases} \delta(k) = 0 & \text{if } k \neq 0 \\ \delta(0) = 1 & \end{cases} \quad [2.20]$$

following property; for all signals x , and for all k_0 :

$$\sum_{k=-\infty}^{+\infty} x(k) \delta(k - k_0) = x(k_0) \quad [2.21]$$

Finally, it can be expressed by the following integral formulation:

$$\delta(k) = \int_{-\frac{1}{2}}^{+\frac{1}{2}} e^{j2\pi v k} dv \quad [2.22]$$

The unit comb of period N , Ξ_N is a periodized version of the Kronecker sequence, defined for all k by:

$$\Xi_N(k) = \sum_{\ell=-\infty}^{+\infty} \delta(k - \ell N) \quad [2.23]$$

The unit comb can also be expressed in the following manner; for all k :

$$\Xi_N(k) = \frac{1}{N} \sum_{\ell=0}^{N-1} e^{j2\pi \frac{\ell}{N} k} \quad [2.24]$$

2.2.2. Fourier transform

The Fourier transform $\hat{x}(f)$ of a continuous time signal $x(t)$ is a complex value function of the form $\hat{x}: f \mapsto \hat{x}(f)$ with a real variable, defined for all f by:

30 Digital Spectral Analysis

$$\hat{x}(f) = \int_{-\infty}^{+\infty} x(t) e^{-j2\pi f t} dt \quad [2.25]$$

At the outset let us note that if the variable t is consistent in relation to time, then the variable f is consistent in relation to a frequency. We will accept that the Fourier transform of a signal is defined (i.e. the above integral converges) if the signal is of finite energy.

The Fourier transform does not lead to any loss of information. In fact, knowing $\hat{x}(f)$, we can recreate $x(t)$ from the following inversion formula; for all t :

$$x(t) = \int_{-\infty}^{+\infty} \hat{x}(f) e^{j2\pi f t} df \quad [2.26]$$

We demonstrate this theorem by directly calculating the above integral and using equations [2.10] and [2.13]:

$$\begin{aligned} \int_{-\infty}^{+\infty} \hat{x}(f) e^{j2\pi f t} df &= \int_{-\infty}^{+\infty} \int_{-\infty}^{+\infty} x(u) e^{j2\pi f u} du e^{j2\pi f t} df \\ &= \int_{-\infty}^{+\infty} x(u) \left[\int_{-\infty}^{+\infty} e^{j2\pi f(t-u)} df \right] du \\ &= \int_{-\infty}^{+\infty} x(u) \delta(t-u) du \\ &= x(t) \end{aligned}$$

which concludes the demonstration.

For a periodic continuous time signal of period T , the Fourier transform $\hat{x}(f)$ is a series of pulses with $\frac{1}{T}$ spacing whose weight can be calculated using its Fourier series decomposition $\hat{x}(\ell)$:

$$\hat{x}(f) = \sum_{\ell=-\infty}^{+\infty} \hat{x}(\ell) \delta\left(f - \frac{\ell}{T}\right) \quad [2.27]$$

with:

$$\hat{x}(\ell) = \frac{1}{T} \int_0^T x(t) e^{-j2\pi \frac{\ell}{T} t} dt \quad [2.28]$$

The inverse transform can be written as:

$$x(t) = \sum_{\ell=-\infty}^{+\infty} \hat{x}(\ell) e^{j2\pi \frac{\ell}{T} t} \quad [2.29]$$

To demonstrate this property, let us calculate the Fourier transform $\hat{x}(f)$; for all f :

$$\hat{x}(f) = \int_{-\infty}^{+\infty} x(t) e^{-j2\pi f t} dt = \sum_{\ell=-\infty}^{+\infty} \int_{\ell T}^{(\ell+1)T} x(t) e^{-j2\pi f t} dt$$

Thus, by changing the variable $u = t - \ell T$:

$$\begin{aligned} \hat{x}(f) &= \sum_{\ell=-\infty}^{+\infty} \int_0^T x(u) e^{-j2\pi f(u+\ell T)} du \\ &= \left(\sum_{\ell=-\infty}^{+\infty} e^{-j2\pi f \ell T} \right) \left(\int_0^T x(u) e^{-j2\pi f u} du \right) \end{aligned}$$

We find in the left-hand term, the Dirac comb $\Xi_{1/T}$. Thus:

$$\begin{aligned} \hat{x}(f) &= \frac{1}{T} \Xi_{1/T}(f) \int_0^T x(u) e^{-j2\pi f u} du \\ &= \frac{1}{T} \left(\sum_{\ell=-\infty}^{+\infty} \delta\left(f - \frac{\ell}{T}\right) \right) \left(\int_0^T x(u) e^{-j2\pi f u} du \right) \\ &= \sum_{\ell=-\infty}^{+\infty} \left(\frac{1}{T} \int_0^T x(u) \delta\left(f - \frac{\ell}{T}\right) e^{-j2\pi f u} du \right) \end{aligned}$$

For all f and for all ℓ , $\delta\left(f - \frac{\ell}{T}\right) e^{-j2\pi f u} = \delta\left(f - \frac{\ell}{T}\right) e^{-j2\pi \frac{\ell}{T} u}$. Therefore:

32 Digital Spectral Analysis

$$\hat{x}(f) = \sum_{\ell=-\infty}^{+\infty} \left(\frac{1}{T} \int_0^T x(u) e^{-j2\pi \frac{\ell}{T} u} du \right) \delta\left(f - \frac{\ell}{T}\right) = \sum_{\ell=-\infty}^{+\infty} \hat{x}(\ell) \delta\left(f - \frac{\ell}{T}\right)$$

By the inverse Fourier transform, we obtain equation [2.29], which concludes the demonstration.

The Fourier transform $\hat{x}(v)$ of a discrete time signal $x(k)$ is a function of the form:

$$\begin{aligned} \hat{x} : \Re &\rightarrow C \\ v &\mapsto \hat{x}(v) \end{aligned}$$

defined for all v by:

$$\hat{x}(v) = \sum_{k=-\infty}^{+\infty} x(k) e^{-j2\pi v k} \quad [2.30]$$

We will accept that the Fourier transform of a discrete time signal is defined (i.e. the series mentioned above converges) if the signal is of finite energy. It is periodic with period 1.

The Fourier transform of discrete time signals can be linked to the Fourier transform of continuous time signals in the following way. Let x_1 be the continuous time signal obtained from x in the following manner, where T is a positive real number:

$$x_1(t) = T \sum_{k=-\infty}^{+\infty} x(k) \delta(t - kT)$$

x_1 is thus zero everywhere except at instants kT multiples of the period T where it has a pulse of weight $T x(k)$. Using equation [2.10] we easily obtain that the Fourier transform $\hat{x}(v)$ of a discrete time signal $x(k)$ is none other than the Fourier transform $\hat{x}_1(f)$ of a continuous time signal $x_1(t)$, with a change in scale and rounded to a factor, the result being independent of T ; for all v :

$$\hat{x}(v) = \frac{1}{T} \hat{x}_1\left(\frac{v}{T}\right) \quad [2.31]$$

The Fourier transform does not result in any loss of information. In fact, knowing $\hat{x}(v)$, we can recreate $x(k)$ from the following inversion formula (obtained from a demonstration similar to the continuous case); for all values k :

$$x(k) = \int_{-\frac{1}{2}}^{+\frac{1}{2}} \hat{x}(v) e^{j2\pi v k} dv \quad [2.32]$$

For a periodic discrete time signal of period N , the Fourier transform $\hat{x}(v)$ is a series of comb pulses with $\frac{1}{N}$ spacing whose weight can be calculated using its decomposition into the discrete Fourier transform $\hat{x}(\ell)$:

$$\hat{x}(v) = \sum_{\ell=0}^{N-1} \hat{x}(\ell) \Xi_1\left(v - \frac{\ell}{N}\right) \quad [2.33]$$

with:

$$\hat{x}(\ell) = \frac{1}{N} \sum_{k=0}^{N-1} x(k) e^{-j2\pi \frac{\ell k}{N}} \quad [2.34]$$

The inverse transform can be written as:

$$x(k) = \sum_{\ell=0}^{N-1} \hat{x}(\ell) e^{j2\pi \frac{\ell k}{N}} \quad [2.35]$$

2.2.3. Fundamental properties

Examination of equations [2.26, 2.29, 2.32 and 2.35] shows that the different forms of the Fourier transform help break down the signal in the form of a sum of cisoids. A discrete time signal has a periodic transform. Inversely, a periodic signal is broken down into a discrete (countable) set of cisoids. The modulus of the transform provides information on the amplitude of these cisoids and is called the amplitude spectrum. The phase provides information on the initial phase of these cisoids and is called the phase spectrum.

The Fourier transform verifies the linearity property: let x and y be two signals and let a be a complex number. Then:

$$\begin{cases} \widehat{x+y} = \hat{x} + \hat{y} \\ \widehat{ax} = a\hat{x} \end{cases} \quad [2.36]$$

The Fourier transform of the conjugate signal x^* is the Fourier transform of the returned signal x and conjugated. The Fourier transform of the returned signal x^- is the Fourier transform of the returned signal x .

$$\widehat{x^*} = (\hat{x})^{-*} \quad [2.37]$$

$$\widehat{x^-} = \hat{x}^- \quad [2.38]$$

We can deduce the properties of symmetry of the transform of particular signals represented in Table 2.1.

Signal		Transform
Real number	$x = x^*$	Even real part Odd imaginary part
Imaginary	$x = x^*$	Odd real part Even imaginary part
Even	$x = x^-$	Even
Odd	$x = x^-$	Odd
Even real parts Odd imaginary part	$x = x^*$	Real
Odd real parts Even imaginary part	$x = -x^*$	Imaginary

Table 2.1. Symmetry of the Fourier transform

2.2.4. Convolution sum

A particular operation between functions or series is the convolution sum \otimes . Let $x(t)$ and $y(t)$ be two functions with a real variable; their convolution sum $x \otimes y(t)$ is defined for all t by:

$$x \otimes y(t) = \int_{-\infty}^{+\infty} x(\tau)y(t-\tau)d\tau \quad [2.39]$$

Similarly, let $x(k)$ and $y(k)$ be two series; their convolution sum $x \otimes y(k)$ is defined for all k by:

$$x \otimes y(k) = \sum_{m=-\infty}^{+\infty} x(m)y(k-m) \quad [2.40]$$

When two functions $x(t)$ and $y(t)$ are periodic, of similar period T (or if they are both of finite support $[0, T]$), we can also define their circular convolution sum $x \otimes y(t)$, which is a periodic function of period T such that, for all values of t :

$$x \otimes y(t) = \frac{1}{T} \int_0^T x(\tau)y((t-\tau) \bmod T) d\tau \quad [2.41]$$

Similarly, for two periodic series $x(k)$ and $y(h)$ with the same period N (or if they are both of finite support $\{0, \dots, N-1\}$), their circular convolution sum $x \otimes y(k)$ is periodic of period N , and defined for all values of n by:

$$x \otimes y(k) = \frac{1}{N} \sum_{m=0}^{N-1} x(m)y((k-m) \bmod N) \quad [2.42]$$

The convolution sum and the circular convolution sum verify the commutative and associative properties and the identity element is:

$$\begin{cases} \delta(t) & \text{for the functions} \\ \delta(k) & \text{for the series} \\ T \Xi_T(t) & \text{for the functions of period } T \\ N \Xi_N(k) & \text{for the series of period } N \end{cases} \quad [2.43]$$

In addition, by noting $x_{t_0}(t)$ the delayed function $x(t)$ by t_0 ($x_{t_0}(t) \triangleq x(t-t_0)$) we can easily show:

$$\begin{cases} x_{t_0} \otimes y(t) = x \otimes y_{t_0}(t) & \text{for the functions} \\ x_{k_0} \otimes y(k) = x \otimes y_{k_0}(k) & \text{for the series} \\ x_{t_0} \otimes y(\ell) = x \otimes y_{t_0}(\ell) & \text{for the functions of period } T \\ x_{k_0} \otimes y(\ell) = x \otimes y_{k_0}(\ell) & \text{for the series of period } N \end{cases} \quad [2.44]$$

In particular, the convolution of a function or a series with the delayed identity element delays it by the same amount.

36 Digital Spectral Analysis

We can easily verify that the Fourier transform of a convolution sum or circular convolution sum is the product of transforms:

$$\begin{cases} \widehat{x \otimes y}(f) = \hat{x}(f)\hat{y}(f) & \text{Fourier transform (continuous time)} \\ \widehat{x \otimes y}(v) = \hat{x}(v)\hat{y}(v) & \text{Fourier transform (discrete time)} \\ \widehat{x \otimes y}(\ell) = \hat{x}(\ell)\hat{y}(\ell) & \text{Fourier series (period } T \text{)} \\ \widehat{x \otimes y}(\ell) = \hat{x}(\ell)\hat{y}(\ell) & \text{Discrete Fourier transform (period } N \text{)} \end{cases} \quad [2.45]$$

Inversely, the transform of a product is a convolution sum:

$$\begin{cases} \widehat{xy}(f) = \hat{x} \otimes \hat{y}(f) & \text{Fourier transform (continuous time)} \\ \widehat{xy}(v) = \hat{x} \otimes \hat{y}(v) & \text{Fourier transform (discrete time)} \\ \widehat{xy}(\ell) = \hat{x} \otimes \hat{y}(\ell) & \text{Fourier series (period } T \text{)} \\ \widehat{xy}(\ell) = N \hat{x} \otimes \hat{y}(\ell) & \text{Discrete Fourier transform (period } N \text{)} \end{cases} \quad [2.46]$$

2.2.5. Energy conservation (Parseval's theorem)

The energy of a continuous time signal $x(t)$ or a discrete time signal $x(k)$ can be calculated by integrating the square of the Fourier transform modulus $\hat{x}(v)$ or its transform in standardized frequency $\hat{x}(v)$:

$$\langle x, x \rangle = \langle \hat{x}, \hat{x} \rangle \quad [2.47]$$

The function or the series $|\hat{x}|^2$ is known as the energy spectrum, or energy spectral density of a signal x , because its integral (or its summation) gives the energy of the signal x .

The power of a periodic signal of continuous period T , or discrete period N , can be calculated by the summation of the square of the decomposition modulus in the Fourier series or discrete Fourier transform. For the Fourier series, this is written as:

$$\langle x, x \rangle = \langle \hat{x}, \hat{x} \rangle \quad [2.48]$$

and for the discrete Fourier transform as:

$$\langle x, x \rangle = N \langle \hat{x}, \hat{x} \rangle \quad [2.49]$$

To sum up, by recalling the definition of the inner product, Parseval's theorem can be written as:

$$\text{-- Continuous time signals: } \int_{-\infty}^{+\infty} |x(t)|^2 dt = \int_{-\infty}^{+\infty} |\hat{x}(f)|^2 df$$

$$\text{-- T-periodic signals: } \frac{1}{T} \sum_0^T |x(t)|^2 dt = \sum_{\ell=-\infty}^{+\infty} |\hat{x}(\ell)|^2$$

$$\text{-- Discrete time signals: } \sum_{k=-\infty}^{+\infty} |x(k)|^2 = \int_{-\frac{1}{2}}^{+\frac{1}{2}} |\hat{x}(v)|^2 dv$$

$$\text{-- N-periodic signals: } \frac{1}{N} \sum_{k=0}^{N-1} |x(k)|^2 = \sum_{\ell=0}^{N-1} |\hat{x}(\ell)|^2$$

Let us demonstrate this property in the case of continuous time signals. Let x^- be the returned signal x (for all values of t , $x^-(t) = x(-t)$). By combining equations [2.37] and [2.38], we obtain:

$$\widehat{x^-}^*(f) = [\hat{x}(f)]^*$$

Thus:

$$\widehat{x \otimes x^-}^*(f) = \hat{x}(f) \widehat{x^-}^*(f) = \hat{x}(f) [\hat{x}(f)]^* = [\hat{x}(f)]^2$$

by inverse Fourier transform calculated at $t = 0$:

$$x \otimes x^-^*(0) = \int_{-\infty}^{+\infty} |\hat{x}(f)|^2 df$$

Moreover:

$$x \otimes x^-^*(0) = \int_{-\infty}^{+\infty} x(t) x^-^*(0-t) dt = \int_{-\infty}^{+\infty} x(t) x^*(t) dt = \int_{-\infty}^{+\infty} |x(t)|^2 dt$$

which concludes the demonstration.

2.2.6. Other properties

Modulation – The product of a continuous time signal $x(t)$ by a complex cisoid of frequency f_0 offsets the Fourier transform by f_0 :

$$y(t) = x(t)e^{j2\pi f_0 t} \quad \hat{y}(f) = \hat{x}(f - f_0) \quad [2.50]$$

The product of a discrete time signal $x(t)$ by a complex cisoid of frequency v_0 offsets the Fourier transform by v_0 :

$$y(k) = x(k)e^{j2\pi v_0 k} \quad \hat{y}(v) = \hat{x}(v - v_0) \quad [2.51]$$

This property is used in telecommunication systems by modulating the amplitude, f_0 being the frequency of the carrier sine wave.

Time shifting – Shifting a continuous time signal $x(t)$ by a time t_0 (if $t_0 > 0$, it consists of a lag; if $t_0 < 0$, it consists of a lead) means multiplying the Fourier transform by the cisoid of “frequency” t_0 :

$$y(t) = x(t - t_0) \quad \hat{y}(f) = e^{j2\pi f t_0} \hat{x}(f) \quad [2.52]$$

Shifting the discrete time signal $x(k)$ by a time $k_0 \in Z$ means multiplying the Fourier transform b the cisoid of “frequency” k_0 :

$$y(k) = x(k - k_0) \quad \hat{y}(v) = e^{j2\pi v k_0} \hat{x}(v) \quad [2.53]$$

Derivative – Let $x(t)$ be a continuous time signal of derivative $\dot{x}(t) = \frac{dx}{dt}(t)$. Then, for all values of f :

$$\hat{\dot{x}}(f) = j2\pi f \hat{x}(f) \quad [2.54]$$

For a T -periodic signal, whose derivative is also T -periodic, the decomposition into Fourier series of the derivative signal can be written as:

$$\hat{\dot{x}}(\ell) = j2\pi \frac{\ell}{T} \hat{x}(\ell) \quad [2.55]$$

Time scaling – The time-dependent expansion by a factor $a \in \Re$ of a continuous time signal leads to a frequency contraction by a factor $\frac{1}{a}$:

$$y(t) = x(at) \quad \hat{y}(f) = \frac{1}{|a|} \hat{x}\left(\frac{f}{a}\right) \quad [2.56]$$

For a discrete time signal, the equivalent property must be used with greater care. Let $a \in Z$ and let x be a zero discrete time signal for all the non-multiple instants of a . Consider the signal y obtained from the signal x by the time scaling by the factor a ; then, the Fourier transform of y is obtained by the contraction of x :

$$y(k) = x(ak) \quad \hat{y}(v) = \hat{x}\left(\frac{v}{a}\right) \quad [2.57]$$

2.2.7. Examples

Dirac delta function

From equation [2.10], we immediately obtain:

$$\hat{\delta}(f) = 1_{\Re}(f) \quad [2.58]$$

Continuous time rectangular window

The Fourier transform of the continuous time rectangular window $1_{[-T/2, T/2]}$ is the sine cardinal function:

$$\hat{1}_{[-T/2, T/2]}(f) = T \operatorname{sinc}(\pi T f) \quad [2.59]$$

Sine cardinal

The Fourier transform of the sinus cardinal is the rectangular window:

$$\widehat{\operatorname{sinc}}(f) = \pi 1_{[-\frac{1}{2\pi}, \frac{1}{2\pi}]}(f) \quad [2.60]$$

Unit constant

It is not of finite energy, but nevertheless has a Fourier transform, in terms of the theory of distributions, which is the Dirac delta function:

$$\hat{1}_{\Re}(f) = \delta(f) \quad [2.61]$$

This result can be easily obtained by exchanging the role of the variables t and f in equation [2.13].

Continuous time cisoid

We have the following transformation:

$$x(t) = e^{j2\pi f_0 t} \quad \hat{x}(f) = \delta(f - f_0)$$

This means that the Fourier transform of the cisoid of frequency f_0 is a pulse centered on f_0 . By using the linearity of the Fourier transform, we easily obtain the Fourier transform of a real sine wave, whatever its initial phase; particularly:

$$x(t) = \cos(2\pi f_0 t) \quad \hat{x}(f) = \frac{1}{2} [\delta(f - f_0) + \delta(f + f_0)] \quad [2.62]$$

$$x(t) = \sin(2\pi f_0 t) \quad \hat{x}(f) = \frac{-j}{2} [\delta(f - f_0) - \delta(f + f_0)] \quad [2.63]$$

Dirac comb

The Fourier transform of the Dirac comb is a Dirac comb:

$$\hat{\Xi}_T(f) = \frac{1}{T} \Xi_{1/T}(f) \quad [2.64]$$

This result is immediately obtained from equation [2.15] and the linearity of the Fourier transform.

Kronecker sequence

From equation [2.21], we immediately obtain:

$$\hat{\delta}(v) = 1_{\Re}(v) \quad [2.65]$$

Discrete time rectangular window

The Fourier transform of the gateway $1_{0,N-1}$ is expressed according to Dirichlet's kernel (equation [2.17]):

$$\hat{1}_{0,N-1}(v) = N e^{-j\pi(N-1)v} \text{diric}_N(v) \quad [2.66]$$

It is equal to N for all integer values of the abscissa.

Unit series

The Fourier transform of the constant series $l_z(k)$ is the Dirac comb Ξ_1 :

$$\hat{l}_z(v) = \Xi_1(v) \quad [2.67]$$

This result is obtained using equation [2.15].

Discrete time cisoid

We have the following transformation:

$$x(k) = e^{j2\pi v_0 k} \quad \hat{x}(f) = \Xi_1(v - v_0) \quad [2.68]$$

This means that the Fourier transform of the cisoid of frequency v_0 is a comb centered on v_0 . Using the linearity of the Fourier transform, we obtain the Fourier transform of real sine waves.

Unit comb

The Fourier transform of the unit comb is a Dirac comb:

$$\hat{\Xi}_N(v) = \frac{1}{N} \Xi_{\frac{1}{N}}(v) \quad [2.69]$$

This result is obtained using equation [2.24].

2.2.8. Sampling

In the majority of applications, the signal studied is a continuous time signal. The spectral analysis, using a digital calculator, requires the sampling of this signal to obtain a discrete time signal. This sampling must be done in a suitable way, so as not to lose too much information. We will develop later the Shannon condition, a mathematical condition which makes it possible to understand the concept of suitable sampling and its practical implications.

Consider a continuous time signal $x(t)$, sampled at the period T_c , and considered continuous at sampling instants; we thus obtain the discrete time signal $x_e(k)$; for all values of k :

$$x_e(k) = x(kT_c)$$

Knowing the sampled signal $x_e(k)$, is it possible to recreate the original signal $x(t)$? In the spectral domain, it is equivalent to asking the following question: Knowing $\hat{x}_e(v)$, can we recreate $\hat{x}(f)$? Let us recall the expression of these two Fourier transforms; for all values of f :

$$\hat{x}(f) = \int_{-\infty}^{+\infty} x(t) e^{-j2\pi f t} dt$$

And for all values of v :

$$\hat{x}_e(v) = \sum_{k=-\infty}^{+\infty} x_e(k) e^{-j2\pi v k}$$

We note that if we bring the integral close to the definition of \hat{x} by the rectangle approximation, we obtain for all values of f :

$$\begin{aligned} \hat{x}(f) &\approx T_c \sum_{k=-\infty}^{+\infty} x(kT_c) e^{-j2\pi f n T_c} \\ &\approx T_c \hat{x}_e(f T_c) \end{aligned}$$

We see that sampling leads to a loss of information. However, under certain conditions, we can exactly recreate the continuous signal from the sampled signal and show that the relation mentioned above is not an approximate one. Consider $x_i(t)$ as a continuous time signal obtained from the sampled signal $x_e(k)$ by:

$$x_i(t) = T \sum_{k=-\infty}^{+\infty} x_e(k) \delta(t - kT_c)$$

By keeping in mind the definition of the Dirac comb Ξ , we obtain:

$$x_i(t) = T_c x(t) \Xi_{T_c}(t) \quad [2.70]$$

Thus, by the Fourier transform, using equations [2.31, 2.70, 2.46, and 2.64] successively, we have for all values of f :

$$\begin{aligned} \hat{x}_e(f T_c) &= \frac{1}{T_c} \hat{x}_i(f) \\ &= \widehat{x \Xi_{T_c}}(f) = \hat{x} \otimes \widehat{\Xi}_{T_c}(f) \\ &= \frac{1}{T_c} \left(\hat{x} \otimes \Xi_{\frac{1}{T_c}} \right)(f) \end{aligned}$$

Then, using the definition of the convolution sum [2.39], the definition of the Dirac comb [2.14] and equation [2.10], we obtain:

$$\begin{aligned}\hat{x}_e(fT_c) &= \frac{1}{T_c} \int_{-\infty}^{+\infty} \hat{x}(g) \Xi_{\frac{1}{T_c}}(f-g) dg \\ &= \frac{1}{T_c} \int_{-\infty}^{+\infty} \hat{x}(g) \sum_{k=-\infty}^{+\infty} \delta\left(f-g-\frac{k}{T_c}\right) dg \\ &= \frac{1}{T_c} \sum_{k=-\infty}^{+\infty} \int_{-\infty}^{+\infty} \hat{x}(g) \delta\left(f-g-\frac{k}{T_c}\right) dg \\ &= \frac{1}{T_c} \sum_{k=-\infty}^{+\infty} \hat{x}\left(f-\frac{k}{T_c}\right)\end{aligned}$$

This means that the Fourier transform of the sampled signal approximated to the factor T_c is the sum of the Fourier transform of the continuous time signal and its translated versions by a multiple of $\frac{1}{T_c}$. We obtain a periodic function of period $\frac{k}{T_c}$; we call this phenomenon the periodization of the spectrum.

For example, let us observe what happens when the Fourier transform of a continuous signal $\hat{x}(f)$ is of finite support $\{f \mid |f| < f_{\max}\}$ and has the shape of Figure 2.4(a). If $f_{\max} < \frac{1}{2T_c}$, the shifted copies of the spectrum lead to Figure 2.4(b). The spectrum of the sampled signal is thus represented in Figure 2.4(c). We see that if $f_{\max} > \frac{1}{2T_c}$, the spectrum is not distorted. However, if $f_{\max} > \frac{1}{2T_c}$, the shifted copies of the spectrum lead to Figure 2.4(d). The spectrum of the sampled signal is thus represented in Figure 2.4(e). Thus, if $f_{\max} > \frac{1}{2T_c}$, we notice a distortion of the spectrum close to the Nyquist frequency $\frac{1}{2T_c}$. This phenomenon is called spectrum aliasing. We can thus conclude that if a continuous signal $x(t)$ of period T_c is sampled such that the Fourier transform $x(f)$ is zero outside the interval $\left[-\frac{1}{2T_c}, \frac{1}{2T_c}\right]$ (this condition is called the Shannon condition), then for all $f \in \left[-\frac{1}{2T_c}, \frac{1}{2T_c}\right]$ we have:

$$\hat{x}(f) = T_c \hat{x}_e(fT_c) \quad [2.71]$$

44 Digital Spectral Analysis

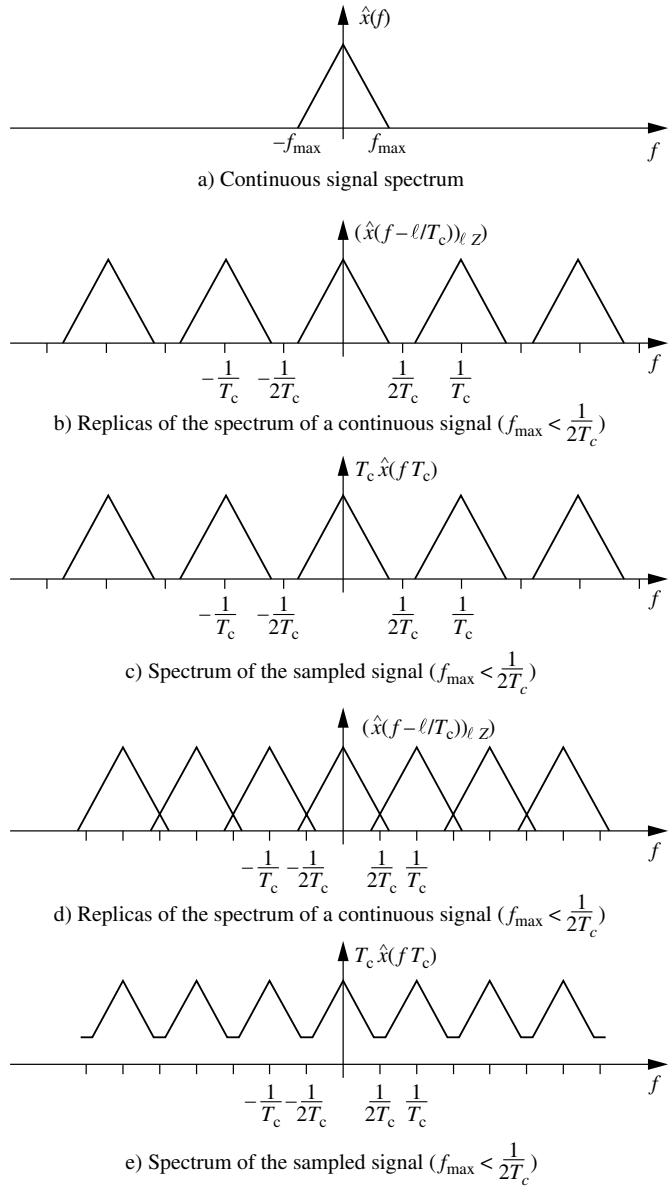


Figure 2.4. Periodization and spectral aliasing

By the inverse Fourier transform, we can recreate the continuous time signal x by the following integral formulation; for all values of t :

$$\begin{aligned} x(t) &= \int_{-\frac{1}{2T_c}}^{+\frac{1}{2T_c}} \hat{x}(f) e^{j2\pi f t} df \\ &= T_c \int_{-\frac{1}{2T_c}}^{+\frac{1}{2T_c}} \hat{x}_e(fT_c) e^{j2\pi f t} df \\ &= \int_{-\frac{1}{2}}^{+\frac{1}{2}} \hat{x}_e(v) e^{j2\pi \frac{v}{T_c} t} dv \end{aligned} \quad [2.72]$$

Moreover, equation [2.71] can be written more concisely; if the Shannon condition is verified, then for all values of f :

$$\hat{x}(f) = \hat{x}_e(fT_c) T_c \text{sinc}_{-\frac{1}{2T_c}, \frac{1}{2T_c}}(f) \quad [2.73]$$

By using the Fourier transform definition, the delay theorem and equation [2.60], we obtain the reconstruction of the continuous time signal $x(t)$ by the formulation in the form of the following series; for all values of t :

$$x(t) = \sum_{k \in Z} x_e(k) \text{sinc}\left[\pi\left(\frac{t}{T_c} - k\right)\right] \quad [2.74]$$

To visualize these concepts, let us consider a real sine wave of 70 Hz, sampled at 65 Hz (Figure 2.5(a)). The sampled signal is thus a sine wave of 5 Hz frequency. In fact, the spectrum of amplitude of the continuous time sine wave is even, and consists of two pulses at 70 Hz and -70 Hz (Figure 2.5(b)). To sample correctly, at least two sampling points per period of the continuous time sine wave are necessary. After sampling, we obtain the spectrum as in Figure 2.5(c), which has a peak at 5 Hz.

The spectral aliasing phenomenon also explains why the wheel of a vehicle being filmed seems to rotate slowly in the other direction or even seems stationary when the images are sampled at 24 Hz (25 Hz on television). The spectral aliasing can also be found, e.g. in the tuning of the ignition point of a spark ignition engine motor through a stroboscope.

Generally, one must be careful when a continuous time signal is sampled, so that the Shannon condition is fulfilled, at the risk of seeing the low frequencies generated

46 Digital Spectral Analysis

by the aliasing of high frequencies of the continuous time signal in the sampled signal. In practice, before any sampling, the signal observed must be filtered by a low-pass analog filter, known as *anti-aliasing*, whose cut-off frequency is 2.5 to 5 time less than the sampling frequency.

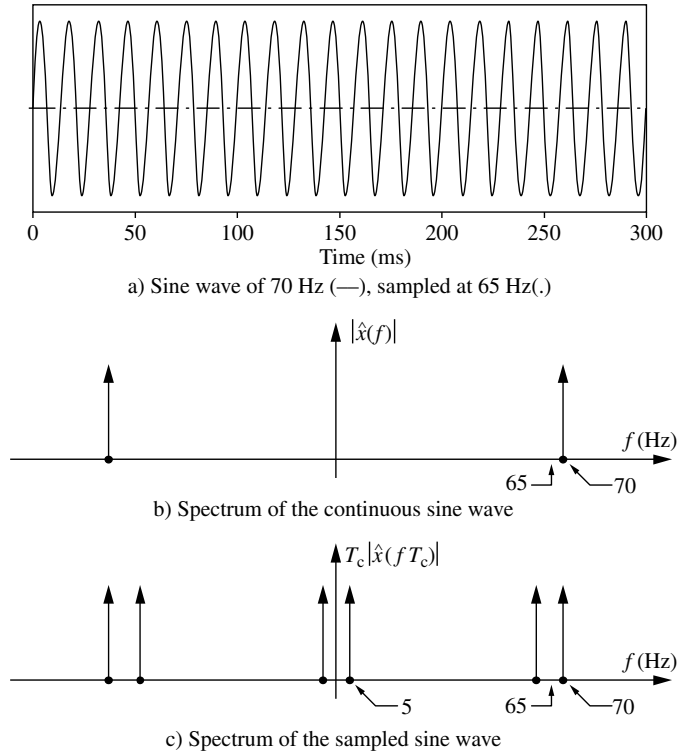


Figure 2.5. Sine wave and spectral folding

2.2.9. Practical calculation, FFT

In practice, we record a signal $x = (x(k))_{k \in \mathbb{Z}}$, which has a N finite number of points, i.e. $(x(k))_{0 \leq k \leq N-1}$. It is thus tempting to approach the Fourier transform \hat{x} , i.e.:

$$\hat{x}(v) = \sum_{k=-\infty}^{+\infty} x(k) e^{-j2\pi v k}$$

by the finite sum:

$$X(v) = \sum_{k=0}^{N-1} x(k) e^{-j2\pi v k}$$

This amounts to approaching x by the Fourier transform of the signal x multiplied by the rectangular window $1_{0,N-1}$ i.e. $\widehat{x1_{0,N-1}}$. We will see the effects and inconveniences of this truncation in section 2.3.

To come back to the calculation of a finite series, it is necessary to sample the frequency axis $[0,1[$, e.g. by using regular sampling of M points in this interval:

$$v \in \left\{ \frac{m}{M}, 0 \leq m \leq M-1 \right\} \quad [2.75]$$

Thus we have, for all values of $m \in \{0, \dots, M-1\}$, by noting $X_e(m) = X(\frac{m}{M})$:

$$X_e(m) = \sum_{k=0}^{N-1} x(k) e^{-j2\pi \frac{mk}{M}} \quad [2.76]$$

If $M = N$, we recognize, to the multiplicative factor $\frac{1}{N}$, the operator of the discrete Fourier transform. If $M > N$, we recognize the operator of the discrete transform applied to the series $(x(k))_{0 \leq k \leq N-1}$ completed by $M - N$ zeros (this addition of zeros is known as *zero padding*).

Implicitly, this approximate calculation amounts to periodizing the signal: we calculate the discrete Fourier transform of the N -periodic signal whose one period is the interval of N points available, possibly extended by $M - N$ zeros.

This calculation, which is performed using $M(M - 1)$ additions and M^2 multiplications, i.e. $O(M^2)$ operations, can become very cumbersome for a large M . The FFT algorithms help reduce this calculation complexity, if M is not a prime number. The most widely used algorithm known as Cooley–Tukey in base 2 can reduce this number of calculations to $O(M \log_2 M)$ operations and this is only in the case where M is a power of 2. It is based on the following time-dependent decimation principle. Let X_{even} (respectively X_{odd}) be the transform of the series

of $\frac{M}{2}$ even index points (respectively with odd index) extracted from the series x (to which we have added $M - N$ zeros):

$$X_{\text{even}}(m) = \sum_{k=0}^{\frac{M}{2}-1} x(2k) e^{-j2\pi \frac{m k}{M/2}}$$

$$X_{\text{odd}}(m) = \sum_{k=0}^{\frac{M}{2}-1} x(2k+1) e^{-j2\pi \frac{m k}{M/2}}$$

We thus easily obtain for all values of $m \in \{0, \dots, M-1\}$, by drawing options from the periodicity of period $\frac{M}{2}$ of X_{even} and X_{odd} :

$$X_e(m) = X_{\text{even}}(m) + e^{-j2\pi \frac{m}{M}} X_{\text{odd}}(m) \quad [2.77]$$

This calculation consists of an addition and a multiplication, for fixed m . The calculation of the complete series $(X_e(m))_{0 \leq m \leq M-1}$ thus consists of M additions and M multiplications. The discrete Fourier transform of order M is thus calculated in function of 2 discrete Fourier transforms of order $\frac{M}{2}$ using M additions and M multiplications. By iterating the process, we notice that these 2 discrete Fourier transforms of order $\frac{M}{2}$ are calculated in function of 4 discrete Fourier transforms of order $\frac{M}{4}$ using $2 \times \frac{M}{2}$ additions and $2 \times \frac{M}{2}$ multiplications, i.e. M additions and M multiplications. This process can be iterated $\log_2 M$ times, until the calculation of M discrete Fourier transforms of the first order, which requires no operations. Finally, this calculation thus requires $M \log_2 M$ additions and $M \log_2 M$ multiplications.

If the fact that M is a power of 2 seems very restrictive, it is possible to develop the FFT algorithms in the case where M can be factorized in the form of a product of integer numbers $M = M_1 M_2, \dots, M_p$. Thus we are talking of algorithms in a multiple base, which require $O(M(M_1 + \dots + M_p))$ operations [BRI 74].

These fast algorithms require the calculation of the discrete Fourier transform in its entirety. It is often preferable to return to a direct calculation if we only need to calculate this transform in low frequencies known *a priori*.

2.3. Windows

Consider a continuous time signal $x(t)$ with an unlimited support which we recorded during the time interval $[0, T]$. Thus it is natural to approximate its Fourier transform $\hat{x}(f)$, i.e.:

$$\hat{x}(f) = \int_{-\infty}^{+\infty} x(t) e^{-j2\pi f t} dt$$

by the finite integral:

$$\int_0^T x(t) e^{-j2\pi f t} dt$$

This amounts to approximating $\hat{x}(f)$ by the Fourier transform of the signal $x(t)$ multiplied by the rectangular window $1_{0,T}(t)$. Let us observe $\widehat{x1}_{0,T}(f)$ the result of this approximation in the case where the signal $x(t)$ is a cisoid of frequency f_0 , amplitude a and initial phase ϕ :

$$x(t) = a e^{j(2\pi f_0 t + \phi)} \quad \hat{x}(v) = a e^{j\phi} \delta(v - f_0)$$

The product is transformed by the Fourier transform into a convolution sum. This convolution along with the Dirac delta function shifted to F_0 thus shifts the Fourier transform of the window to f_0 . We thus obtain:

$$\widehat{x1}_{0,T}(f) = a e^{j\phi} \widehat{1}_{0,T}(f - f_0)$$

Thus, in the place of the expected pulse at f_0 , we observe the sine cardinal centered on v_0 (see Figure 2.6).

This spectral “leakage” exists even if the signal processed is not a sine wave. In particular, if the signal consists of two sine waves of very different amplitudes, the secondary lobes coming from the sine wave of large amplitude can mask the main lobe coming from the other sine wave. A solution consists in balancing the signal observed using a smoother truncation window, whose Fourier transform is such that the amplitude of the secondary lobes is much smaller compared to the amplitude of the main lobe, than in the case of the rectangular window. We will thus approximate the Fourier transform $x(f)$ of the signal $x(t)$ by $\widehat{xw}_{0,T}(f)$ where $w_{0,T}(t)$ is the zero signal outside the interval $[0, T]$.

50 Digital Spectral Analysis

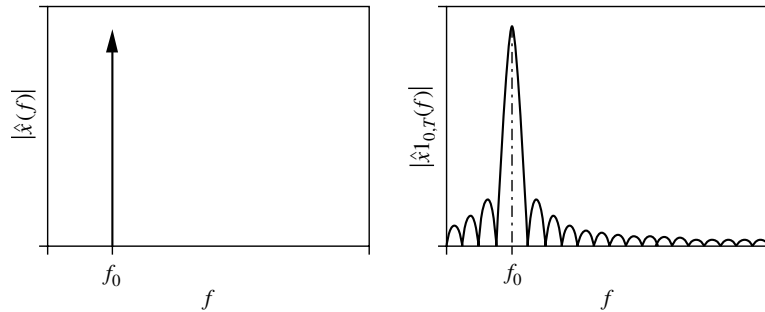


Figure 2.6. Fourier transform of a sine wave before and after truncation

Many truncation windows exist in the literature, all symmetrical in relation to the $t = \frac{T}{2}$ axis. Table 2.2 represents the common windows and Table 2.3 their Fourier transform. Usually this transform is represented in decibels, by plotting the frequency response in decibels that is 10 times the logarithm in base 10 of the spectral energy density, or 20 times the logarithm in base 10 of the spectral amplitude density:

$$W_{\text{dB}}(f) = 10 \log_{10} |\hat{w}_{0,T}(f)|^2 = 20 \log_{10} |\hat{w}_{0,T}(f)| \quad [2.78]$$

	$W_{0,T}(t)$ ($0 \leq t \leq T$)
Rectangular	1
Hamming	$0.54 - 0.46 \cos(2\pi \frac{t}{T})$
Hanning	$0.50 - 0.50 \cos(2\pi \frac{t}{T})$
Blackman	$0.42 - 0.50 \cos(2\pi \frac{t}{T}) + 0.08 \cos(4\pi \frac{t}{T})$
Bartlett	$1 - \left \frac{2t}{T} - 1 \right $

Table 2.2. Continuous time truncation windows

	$\hat{w}_{0,T}(f)$
Rectangular	$e^{-j \pi f T} T \operatorname{sinc}(\pi f T)$
Hamming	$e^{-j \pi f T} T \{0.54 \operatorname{sinc}(\pi f T) + 0.23 \operatorname{sinc}(\pi f T + \pi) + 0.23 \operatorname{sinc}(\pi f T - \pi)\}$
Hanning	$e^{-j \pi f T} T \{0.50 \operatorname{sinc}(\pi f T) + 0.25 \operatorname{sinc}(\pi f T + \pi) + 0.25 \operatorname{sinc}(\pi f T - \pi)\}$
Blackman	$e^{-j \pi f T} T \{0.42 \operatorname{sinc}(\pi f T) + 0.25 \operatorname{sinc}(\pi f T + \pi) + 0.25 \operatorname{sinc}(\pi f T - \pi) + 0.04 \operatorname{sinc}(\pi f T + 2\pi) + 0.04 \operatorname{sinc}(\pi f T - 2\pi)\}$
Bartlett	$e^{-j \pi f T} \frac{T}{2}$

Table 2.3. Transform of continuous time truncation windows

The first characteristic of a truncation window is the width of the main lobe. This width can be measured by the -3 dB bandwidth, i.e. $B_{-3\text{dB}}(T)$, that is to say the frequency interval for which the Fourier transform module $|\hat{w}_{0,N-1}(f)|$ is greater than its maximum value \hat{w}_0 divided by $\sqrt{2}$ (or, similarly, the interval for which the spectral energy density is greater than half its maximum value). The modulus of the Fourier transform of a window with real values is even. This interval is thus $\left[-\frac{B_{-3\text{dB}}(T)}{2}, \frac{B_{-3\text{dB}}(T)}{2}\right]$. The equation to be solved to obtain this bandwidth is thus:

$$\left| \hat{w}_{0,T} \left(\frac{B_{-3\text{dB}}(T)}{2} \right) \right| = \frac{\hat{w}_{0,T}(0)}{\sqrt{2}} \quad [2.79]$$

That is to say in decibels:

$$W_{\text{dB}} \left(\frac{B_{-3\text{dB}}(T)}{2} \right) = W_{\text{dB}}(0) - 3 \quad [2.80]$$

52 Digital Spectral Analysis

According to the scale change theorem, a time-dependent expansion of a factor $a > 0$ can be translated by a frequential contraction of a factor $\frac{1}{a}$. Thus, we can standardize this bandwidth in the following way:

$$\dot{B}_{-3\text{dB}} = T B_{-3\text{dB}}(T) \quad [2.81]$$

This reduced bandwidth is independent of the amplitude and the length T of the window support, and it depends only on its shape.

Another measurement of the width of the main lobe is the equivalent noise bandwidth $B_{\text{en}}(T)$ of the bandwidth. It is the bandwidth of the window whose spectral energy density is rectangular, having the same integral and same maximum value $\hat{w}_{0,T}^2(0)$ as the density of the window considered (the spectral energy density of a real positive function is always maximum for the zero frequency). We immediately obtain the expression of this bandwidth, in the frequential and time-dependent fields (by using Parseval's theorem):

$$\begin{aligned} B_{\text{en}}(T) &= \frac{\int_{-\infty}^{+\infty} |\hat{w}_{0,T}(f)|^2 df}{\hat{w}_{0,T}^2(0)} \\ &= \frac{\int_0^T w_{0,T}^2(t) dt}{\left(\int_0^T w_{0,T}(t) dt\right)^2} \end{aligned}$$

Here too we can define the reduced bandwidth independent of T :

$$B_{\text{en}} = T B_{\text{en}}(T) \quad [2.82]$$

The second characteristic of a window is the amplitude of the secondary lobes in relation to the amplitude of the main lobe. A natural measurement is the amplitude of the strongest secondary lobe brought to the amplitude of the main lobe. Consider f_{\max} as the abscissa of the maximum of the strongest secondary lobe:

$$f_{\max} = \max \left\{ f \neq 0 \mid \frac{d|\hat{w}_{0,T}|}{df}(f) = 0 \right\} \quad [2.83]$$

The amplitude of the strongest secondary lobe brought to the amplitude of the main lobe is thus:

$$\frac{|\hat{w}_{0,T}(f_{\max})|}{\hat{w}_{0,T}(0)} \quad [2.84]$$

This quantity is independent of T . We generally express it in decibels, i.e.:

$$20 \log_{10} \left(\frac{|\hat{w}_{0,T}(f_{\max})|}{\hat{w}_{0,T}(0)} \right) = W_{\text{dB}}(f_{\max}) - W_{\text{dB}}(0) \quad [2.85]$$

Generally, the amplitude of the lobes reduces as the frequency increases. In the plane $(\log f, W_{\text{dB}}(f))$, the maxima of the lobes pass through a straight line whose slope can be measured in dB/octave, increase in the value of the ordinate of this line when the frequency is multiplied by 2. This slope measures the “speed” of suppression of the secondary lobes when the frequency increases.

A third characteristic is the positivity of the transform of even windows. In Table 2.3, the Fourier transform of the even window $w_{T,T}(t)$ is obtained according to the transform of $w_{0,T}(t)$ by multiplying this transform by the $e^{j\pi f t}$ function (according to the delay theorem). We immediately notice that the Bartlett window verifies the positivity property.

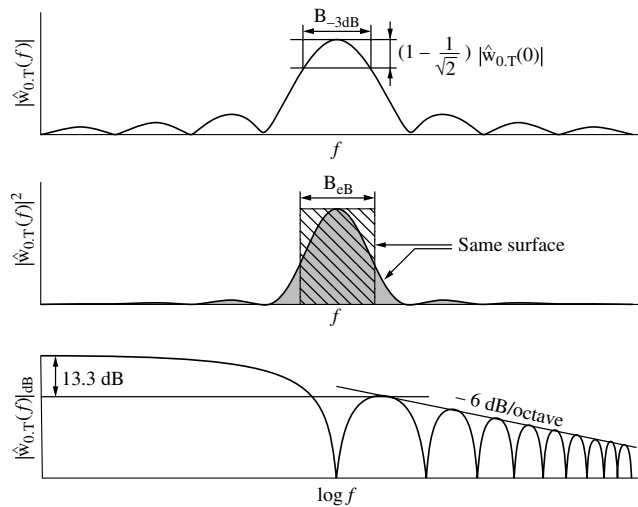


Figure 2.7. Graphical representation of indices (rectangular window)

Figure 2.7 graphically represents these indices in the case of the rectangular window. Table 2.4 gives the value of these different indices for various windows. Qualitatively speaking, selecting a window representing weak secondary lobes (in order to detect a sine wave of weak power) at the value of a large main lobe (and thus has a loss in resolution: adding the main lobes of two sine waves of similar frequency will give only a single lobe).

	Band at -3 dB	Band Equivalent to Noise	Stronger Secondary Lobes	Decreasing Secondary Lobes
Rectangular	0.89	1.00	-13.3 dB	-6 dB/octave
Hamming	1.30	1.36	-43.0 dB	-6 dB/octave
Hanning	1.44	1.50	-31.5 dB	-18 dB/octave
Blackman	1.68	1.73	-58.0 dB	-18 dB/octave
Bartlett	1.28	1.33	-26.5 dB	-12 dB/octave

Table 2.4. Characteristics of continuous time windows

For digital processing, we record a signal $x(k)$, $k \in \mathbb{Z}$ with only a finite number of points N , i.e. $x(k)$, $0 < k < N - 1$. We approximate the Fourier transform \hat{x} , i.e.:

$$\hat{x}(\nu) = \sum_{k=-\infty}^{+\infty} x(k) e^{-j2\pi \nu k}$$

by a finite sum: $\sum_{k=0}^{N-1} x(k) e^{-j2\pi \nu k}$

This amounts to approximating \hat{x} by the Fourier transform of the signal x multiplied by the gateway $xl_{0,N-1}$, i.e. $\widehat{x1}_{0,N-1}$. Let us observe the results of this approximation in the case where the signal x is a cisoid of frequency ν_0 , of amplitude a and initial phase ϕ :

$$x(k) = a e^{j(2\pi \nu_0 k + \phi)} \quad \hat{x}(\nu) = a e^{j\phi} \Xi_1(\nu - \nu_0)$$

The product is transformed by the Fourier transform into a circular convolution sum. This convolution with the comb shifted to ν_0 thus shift the Fourier transform of the window to ν_0 . We thus obtain:

$$\widehat{x1}_{0,N-1}(\nu) = a e^{j\phi} \widehat{1}_{0,N-1}(\nu - \nu_0)$$

Therefore, in the place of the expected pulse at v_0 , we observe Dirichlet's kernel centered on v_0 , and thus a spectral "leakage", as in the case of continuous time signals, is obtained. The discrete time windows designed to correct this phenomenon generally result from the sampling of the continuous time windows (Table 2.5). Figures 2.8 and 2.9 provide the shape of these windows as well as their frequency response in dB, for $N = 32$.

	$w_N(k) (0 \leq k \leq N - 1)$
Rectangular	1
Hamming	$0.54 - 0.46 \cos\left(2\pi \frac{\kappa}{N-1}\right)$
Hanning	$0.50 - 0.50 \cos\left(2\pi \frac{\kappa}{N-1}\right)$
Blackman	$0.42 - 0.50 \cos\left(2\pi \frac{\kappa}{N-1}\right) + 0.08 \cos\left(4\pi \frac{\kappa}{N-1}\right)$
Bartlett	$1 - \left \frac{2\kappa}{N-1} - 1 \right $

Table 2.5. Discrete time windows

We can measure the characteristics of these windows in a manner similar to the case of the continuous windows. The definition of the bandwidth at -3 dB $B_{-3\text{dB}}(N)$ becomes:

$$\left| \hat{w}_{0,N-1} \left(\frac{B_{-3\text{dB}}(N)}{2} \right) \right| = \frac{\hat{w}_{0,N-1}(0)}{\sqrt{2}} \quad [2.86]$$

and its reduced version becomes:

$$\dot{B}_{-3\text{dB}} = NB_{-3\text{dB}}(N) \quad [2.87]$$

The equivalent noise bandwidth B_{en} , in its reduced form, becomes:

$$\begin{aligned} \dot{B}_{\text{en}} &= N \frac{\int_{-\frac{1}{2}}^{+\frac{1}{2}} |\hat{w}_{0,N-1}(v)|^2 dv}{\hat{w}_{0,N-1}^2(0)} \\ &= N \frac{\sum_{k=0}^{N-1} w_{0,T}^2(k)}{\left(\sum_{k=0}^{N-1} w_{0,N-1}(k) \right)^2} \end{aligned}$$

56 Digital Spectral Analysis

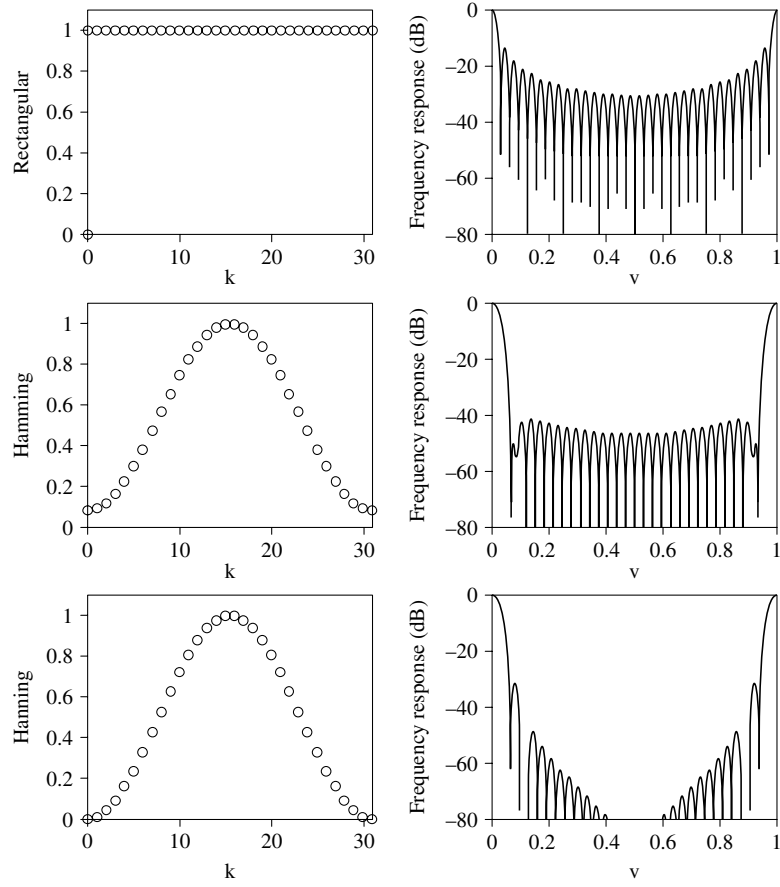


Figure 2.8. Rectangular, Hamming, and Hanning windows and their frequency response (in dB)

The amplitude of the secondary lobe is defined in the same way as in continuous. However, these indices that are independent of the length T of the continuous window depend on N in discrete. By considering the discrete time windows as a sampling to the period $\frac{T}{N}$ of the corresponding continuous time window, we can consider the spectral aliasing phenomenon as negligible for quite large N ; the indices defined in discrete thus tend toward their equivalent in continuous time for quite a large N . Thus, Table 2.4 remains valid in discrete time, for quite large values of N (and for lobes sufficiently spaced out of the reduced frequency 1/2 for the decreasing index of secondary lobes).

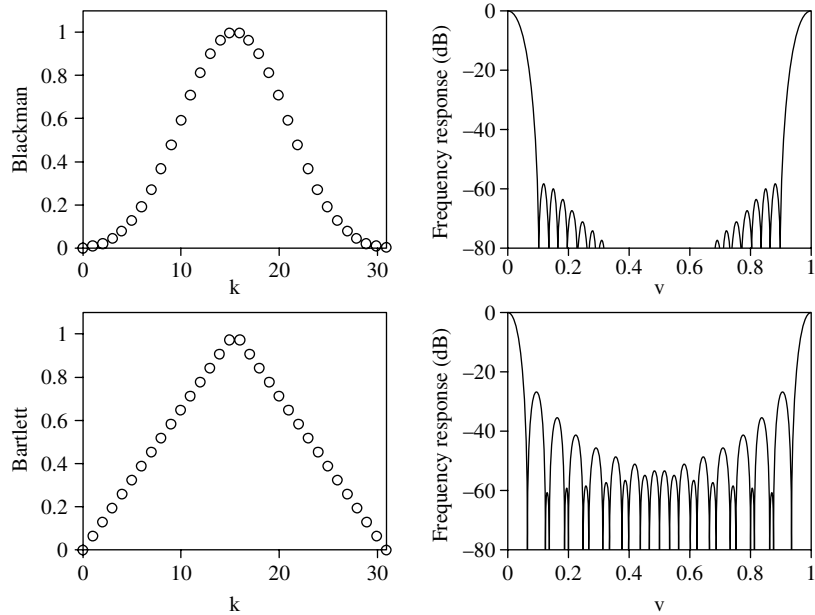


Figure 2.9. Blackman and Bartlett windows and their frequency response (in dB)

The definition of discrete time windows often varies in a subtle way, particularly for the windows becoming zero at 0 and $N-1$, such as the Hanning window. We thus lose the information brought by the first and last points. We can correct this oversight by expanding the window to take them into account and increase the resolution by a factor $\frac{N+2}{N}$. For example, the Hanning window is written in some books as:

$$w_{0,N-1}(k) = 0.50 \cos\left(2\pi \frac{k+1}{N+1}\right)$$

2.4. Examples of application

2.4.1. LTI systems identification

The Fourier transform is of particular practical interest for the representation of dynamic systems. A system consists of a cause–effect relationship between a batch of input signals and a batch of output signals, indicated by the diagram in Figure 2.10.

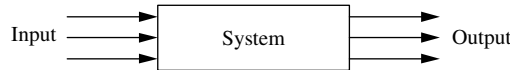


Figure 2.10. Symbolic representation of a system

For example, when we take a bath, we use a system with two inputs (angular position of hot and cold water taps) and two outputs (flow rate and water temperature).

Here, we will limit ourselves to single input and single output systems. Consider a system S of input u and output y ; we will provisionally note the cause–effect relation linking the signals y and u in the form:

$$y = S(u)$$

We call the *impulse response* of a system S the Dirac delta function response $S(\delta)$ for continuous time systems, or the Kronecker sequence response $S(\delta)$ for the discrete time systems.

A system S is said to verify the *superposition* principle, or *additivity* principle, if the response to the sum of two inputs is the sum of the responses to each input, whatever the signals u and v may be:

$$S(u + v) = S(u) + S(v)$$

A system S is said to verify the *homogeneity* principle if the responses to two proportional inputs are proportional with the same proportionality coefficient, whatever the signal u and the complex number a may be:

$$S(au) = a S(u)$$

A system is said to be *linear* if it verifies the superposition and homogeneity principles.

A system is *time invariant* if a time delay at the input leads to the same time delay at the output. By denoting y_τ as the signal y delayed by τ ($y_\tau(t) = y(t - \tau)$) time, we have, whatever the signals u and y and the real number τ may be:

if

$$y = S(u)$$

then

$$y_\tau = S(u_\tau)$$

A linear time invariant system will be indicated with an abbreviated form known as “LTI system”.

Numerous physical systems can be considered as linear and invariant over time (particularly, the systems governed by linear differential equations with constant coefficients). The mathematical representation of such systems is well standardized and can be easily interpreted. An LTI system is completely characterized by its pulse response because this is sufficient to calculate the response of the system at any input.

Consider h as the pulse response of the system S :

$$h = S(\delta)$$

Then, the response of the system to an ordinary excitation u is the convolution sum between h and u :

$$S(u) = h \otimes u$$

Let us show this property for a continuous time system, the demonstration in discrete time is analogous, h being the pulse response of the system; we can thus write:

$$t \mapsto h(t) \text{ is the response at } t \mapsto \delta(t)$$

Then, from the time-dependent invariance property, for all values of τ :

$$t \mapsto h(t - \tau) \text{ is the response at } t \mapsto \delta(t - \tau)$$

From the homogeneity property, for all values of r and all signals u :

$$t \mapsto u(\tau)h(t - \tau)d\tau \text{ is the response at } t \mapsto u(\tau)\delta(t - \tau)d\tau$$

From the superposition property, we have, for all signals u :

$$t \mapsto \int_{-\infty}^{+\infty} u(\tau)h(t - \tau)d\tau \text{ is the response at } t \mapsto \int_{-\infty}^{+\infty} u(\tau)\delta(t - \tau)d\tau$$

which can be written more concisely by recalling the definition of the convolution sum [2.39] and equation [2.10]:

$$t \mapsto h \otimes u(t) \text{ is the response at } t \mapsto u(t) \text{ which completes the demonstration.}$$

60 Digital Spectral Analysis

Using the Fourier transform, we immediately note that the Fourier transform of the output y of the system is equal to the product of the Fourier transform of the pulse response h and the Fourier transform of the input u .

$$\hat{y} = \hat{h} \hat{u} \quad [2.88]$$

The Fourier transform of the pulse response is known as the transfer function, or harmonic response, or frequency response.

Consider a continuous time LTI system, of pulse response $h(t)$, excited by a cisoid $u(t)$ of amplitude a , frequency f_0 , and initial phase ϕ ; for all values of t :

$$u(t) = a e^{j(2\pi f_0 t + \phi)}$$

Using the Fourier transform, we have, for all values of f :

$$\hat{u}(f) = a e^{j\phi} \delta(f - f_0)$$

Thus, the Fourier transform of the response y is:

$$\begin{aligned} \hat{y}(f) &= \hat{h}(f) \hat{u}(f) \\ &= a \hat{h}(f) e^{j\phi} \delta(f - f_0) \\ &= a \hat{h}(f_0) e^{j\phi} \delta(f - f_0) \end{aligned}$$

Using the inverse Fourier transform, we have, for all values of t :

$$\begin{aligned} y(t) &= a \hat{h}(f_0) e^{j\phi} e^{j2\pi f_0 t} \\ &= a |\hat{h}(f_0)| e^{j[2\pi f_0 t + \phi + \arg(\hat{h}(f_0))]} \end{aligned}$$

This therefore signifies that the response of an LTI system with pulse response $h(t)$ at a sinusoidal input of frequency f_0 is a sine wave of the same frequency, whose amplitude is multiplied by $|\hat{h}(f_0)|$ and phase shifted by $\arg(\hat{h}(f_0))$. Similar reasoning can be used for the discrete time signals $|\hat{h}(f_0)|$.

The harmonic response is a necessary and sufficient tool for the characterization of LTI systems. It is useful to represent it for real systems (i.e. whose input and output have real values) by one of following three methods:

- 1) The Bode plot, plotted using $|\hat{h}(f)|$ and $\arg(\hat{h}(f))$ according to $\log(f)$;
- 2) The Nyquist plot, plotted in the complex plane of $\Im(\hat{h}(f))$ according to $\Re(\hat{h}(f))$, graduated in function of the frequency;
- 3) The Nichols' plot, plotted in $|\hat{h}(f)|$ is expressed in dB according to $\arg\left(\left|\hat{h}(f)\right|_{\text{dB}} = 20 \log_{10} |\hat{h}(f)|\right)$ graduated in function of the frequency.

The Nichols and Nyquist plots are of great interest to control engineers, because they help deduce system performance after servo-control, particularly the stability in a closed loop.

These plots can be obtained point by point using a sine wave generator and other adequate measuring instruments (alternating current voltmeter, phase-meter). Another solution consists in calculating from beforehand the Fourier transform of these signals using a recording of the input u and output y of the system and applying the formula for $\hat{u}(f) \neq 0$:

$$\hat{h}(f) = \frac{\hat{y}(f)}{\hat{u}(f)}$$

In practice, these Fourier transforms can be obtained only approximately, by spectral analysis on a sampled recording. The transfer function thus obtained is called “empirical estimator of the transfer function” [LJU 87], which is nothing but the ratio of the discrete Fourier transform of an output signal with the input signal. If there exist frequencies for which $u(f) = 0$, we can use adjustment techniques [IDI 08].

2.4.2. Monitoring spectral lines

The Fourier transform, as defined in section 2.2, is a tool suitable for the spectral analysis of sine wave signals. This concept will be discussed in detail in Chapter 5, dedicated to the spectral analysis of random stationary signals. However, the calculation of a Fourier transform of a signal modulated in frequency is of limited interest, because it does not demonstrate the time-dependent variation of the spectral content. We present here a preliminary approach to the time-frequency analysis: the sliding Fourier transform helps carry out a spectral analysis close to an instant and whose principle is as follows.

Given a continuous time signal $x(t)$, the sliding Fourier transform according to the time t and the frequency f can be expressed by:

$$R(t, f) = \int_{-\infty}^{+\infty} x(\tau) w(\tau - t) e^{-j2\pi f \tau} d\tau \quad [2.89]$$

where $w(t)$ is a finite support even real window. The window $w(\tau - t)$ is thus centered on the analysis instant t . At fixed t_0 , the transform $R(t_0, f)$ is nothing but the Fourier transform of the signal $x(t)$ truncated on an interval centered on t_0 , and can be considered as a measurement of resemblance between the truncated signal and the sine wave $e^{j2\pi f \tau}$. Inversely, $R(t_0, f)$ can be considered as a measurement of resemblance between the signal $x(t)$ and the sine wave $e^{j2\pi f \tau}$ truncated on the interval centered on t_0 .

The window $w(t)$ can be rectangular, or smoothed (section 2.3), to reduce the spectral dilution phenomenon, at the cost of a deterioration in the resolution. We notice here the time-frequency duality principle: monitoring a sliding frequency requires a short support window, to ensure a proper time-dependent location, whereas a proper spectral location requires a long support window. The choice of this parameter is thus subjective and depends on the processed signal (slow or fast sliding of the frequency) as well as on the aim in mind (good time dependent or spectral localization).

For a discrete time signal, the sliding Fourier transform can be written as:

$$R(k, v) = \sum_{n=-\infty}^{+\infty} x(n) w(n - k) e^{-j2\pi nv} \quad [2.90]$$

As an example, Figure 2.11 represents a signal of statoric current measured on one phase of an induction motor, sampled at 10 ms, as well as the modulus of the corresponding sliding Fourier transform $|R(t, f)|$, calculated using a Hanning window of 40 points.

2.4.3. Spectral analysis of the coefficient of tide fluctuation

In France, it is useful to measure the fluctuation m of the tide (difference in height of the water during high tide and low tide) using the coefficient of tide fluctuation c , independent of the geographical point considered and defined by:

$$c = \frac{m}{u} \times 100$$

where u is a unit of height that depends on the geographical point (e.g. 6.10 m at Brest). This coefficient is theoretically between 20 and 120. This coefficient is shown in Figure 2.12 during the year 2001 according to the time of high tides at Mont-Saint-Michel (counted in days starting from January 1, 0.00 hours), and the corresponding tide fluctuation coefficient.

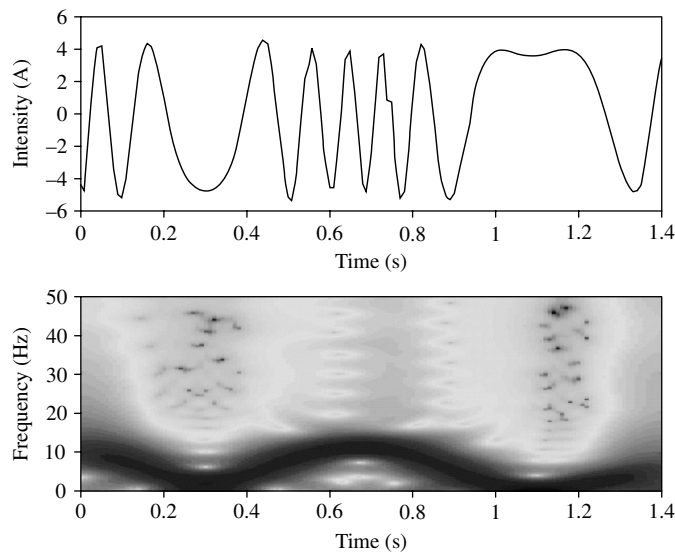


Figure 2.11. Sliding Fourier transform of statoric current of an asynchronous machine

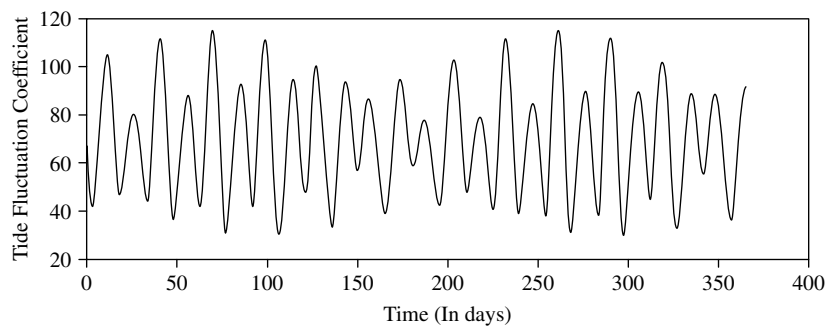


Figure 2.12. Tide fluctuation coefficient according to time for high tides

The duration between two consecutive high tides is not constant. To simplify, between two high tides, we will count the slope of the regression line of the time of

high tide according to the high tide index, and we will consider this value as the sampling period for the tide fluctuation coefficient. We obtain:

$$T_c = 12.42 \text{ hours} = 0.517 \text{ days}$$

In Figure 2.13 is represented the Fourier transform, calculated using a FFT on 4,096 points, of the weighted tide fluctuation coefficient by a Blackman's window.

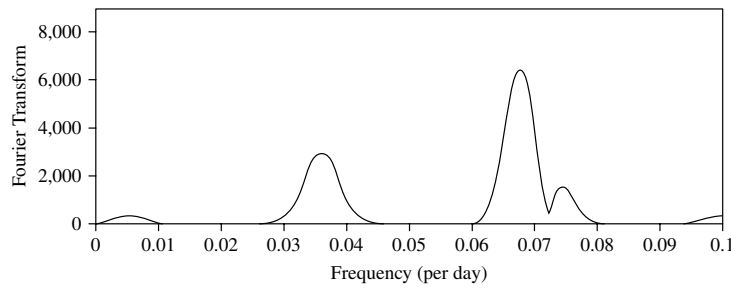


Figure 2.13. Fourier transform of the weighted tide fluctuation coefficient using a Blackman window

We clearly see a peak for the frequency 3.63 day^{-1} , i.e. a period of 27.53 days, which can be interpreted as the lunar month. We also see a peak for a frequency which is approximately double, i.e. a period of half a lunar month; in a qualitative way, the spring tides come when we have the following two types of alignments: earth–moon–sun, or moon–earth–sun, which explains the half lunar month. We will leave it to the astronomers to interpret this spectral decomposition further.

2.5. Bibliography

- [BEL 00] BELLANGER M., *Digital Processing of Signals: Theory and Practice*, Wiley, 2000.
- [BRI 74] BRIGHAM E., *The Fast Fourier Transform*, Prentice Hall, 1974.
- [HAR 78] HARRIS J., “On the use of windows for harmonic analysis with the discrete Fourier transform”, *Proceedings of the IEEE*, vol. 66, no. 1, pp. 51–84, January 1978.
- [IDI 08] IDIER J. (ed.), *Bayesian Approach to Inverse Problems*, ISTE Ltd, London, John Wiley & Sons, New York, 2008.
- [KWA 91] KWAKERNAAK H., SIVAN R., *Modem Signals and Systems*, Prentice Hall, 1991.
- [LJU 87] LJUNG L., *System Identification: Theory for the User*, Prentice Hall, 1987.
- [LJU 99] LJUNG L., *System Identification - Theory For the User*, Prentice Hall, 1999.
- [MAR 87] MARPLE S. JR., *Digital Spectral Analysis with Applications*, Prentice Hall, 1987.

[MAX 96] MAX J., LACOUME J., *Méthodes et techniques de traitement du signal et applications aux mesures physiques, Volume 1: principes généraux et méthodes classiques*, 5th edition, Masson, 1996.

[OPP 75] OPPENHEIM A., SCHAEFER R., *Digital Signal Processing*, Prentice Hall, 1975.

[POR 97] PORAT B., *A Course in Digital Signal Processing*, Wiley, 1996.

Chapter 3

Introduction to Estimation Theory with Application in Spectral Analysis

3.1. Introduction

Spectral analysis entails analyzing a signal in the frequency domain, from the observation of this signal over a time-limited interval. Therefore, central to all methods presented in this book is the problem of estimating the parameters that describe the power spectral density (PSD) of the signal. In this chapter, we provide a brief tour of estimation with a view to answer the following questions. How can I formulate an estimation problem? How can I obtain estimates and assess their performance? Are there systematic approaches or, at least, generic approaches to obtain estimates? Of course, this short chapter cannot answer in detail all these questions. Therefore, we give only the main results, followed by illustrative examples that are directly related to spectral analysis. The theory of estimation is documented at length in many books; we recommend particularly references [AND 71, TRE 71, SÖD 89, BRO 91, SCH 91, KAY 93, POR 94] for further reading. In the first part of this chapter, we consider a rather general framework for estimation, which encompasses most of the problems tackled in the body of this book. Some more specific analyses are presented next.

Chapter written by Olivier BESSON and André FERRARI.

3.1.1. Problem statement

In what follows, we consider that N samples $\{x(n)\}_{n=0}^{N-1}$ of the signal are available and stacked into the vector $\mathbf{x} \in \mathbb{R}^{N \times 1}$:

$$\mathbf{x} = \begin{bmatrix} x(0) \\ x(1) \\ \vdots \\ x(N-1) \end{bmatrix}$$

The vector \mathbf{x} is considered as random; for example, it can correspond to the sampling of a random process such as speech, or can be written as the combination of a deterministic signal and a random additive noise, a model commonly used in radar.

The natural description of \mathbf{x} is given by the probability density function (pdf), $p(\mathbf{x}; \boldsymbol{\theta})$, which is **parametrized** by a vector $\boldsymbol{\theta} = [\theta_1, \theta_2, \dots, \theta_p]^T$, that we want to estimate. Since we have a family of different pdfs for \mathbf{x} , which depend on $\boldsymbol{\theta}$, it is then possible to infer $\boldsymbol{\theta}$ from \mathbf{x} . Thus, we consider an estimator $\hat{\boldsymbol{\theta}}$ of $\boldsymbol{\theta}$ from \mathbf{x} , namely

$$\hat{\boldsymbol{\theta}} = \mathbf{f}(\mathbf{x}) \quad [3.1]$$

$\hat{\boldsymbol{\theta}}$ being a function of \mathbf{x} is thus a random vector itself and would be fully characterized by its own pdf. However, one is generally interested by the following quantities that are easier to obtain:

The bias gives the *average error* and is defined as:

$$\text{b}(\hat{\boldsymbol{\theta}}) = \mathbb{E}\{\hat{\boldsymbol{\theta}}\} - \boldsymbol{\theta} \quad [3.2]$$

It is desirable to have unbiased estimators, that is to say estimators which provide, on average, the exact value of $\boldsymbol{\theta}$.

The covariance matrix quantifies the dispersion around the mean value and is defined as:

$$\mathbf{C}(\hat{\boldsymbol{\theta}}) = \mathbb{E}\left\{\left[\hat{\boldsymbol{\theta}} - \mathbb{E}\{\hat{\boldsymbol{\theta}}\}\right]\left[\hat{\boldsymbol{\theta}} - \mathbb{E}\{\hat{\boldsymbol{\theta}}\}\right]^T\right\} \quad [3.3]$$

The diagonal elements of the covariance matrix correspond to the respective variances of the different elements of $\hat{\boldsymbol{\theta}}$, i.e. $C(k, k) = \text{var}(\hat{\theta}(k))$. The off-diagonal elements give the correlation between the estimates of two distinct components. Obviously, the smaller the variance, the better the estimation.

REMARK 3.1.– Another important criterion is the mean square error (mse) on the estimation of a scalar parameter θ , whose definition is given by:

$$\begin{aligned}\text{mse}(\hat{\theta}) &= \mathbb{E}\left\{\left(\hat{\theta} - \theta\right)^2\right\} \\ &= b^2(\hat{\theta}) + \text{var}(\hat{\theta})\end{aligned}$$

This last equation shows that both the bias and the variance contribute to the mse, and generally reducing one term without caution will tend to increase the other. Consequently, two approaches can be investigated: either the bias is constrained to be zero and the variance is to be minimized, or a trade-off between bias and variance is allowed and the mse is to be minimized. \square

3.1.2. Cramér-Rao lower bound

Herein we consider unbiased estimators with possibly minimum variance. This naturally leads to the following question: is there an estimator whose variance is uniformly (i.e. whatever the value of θ) smaller than the variance of all other estimators? Before answering this question, an important point is the existence of a lower bound for the covariance matrix; we are thus led to the concept of Cramér-Rao bounds (CRBs) whose definition is given below.

THEOREM 3.1.– (Cramér-Rao bound). *If the pdf $p(\mathbf{x}; \theta)$ satisfies the following regularity condition¹:*

$$\mathbb{E}\left\{\frac{\partial \ln p(\mathbf{x}; \theta)}{\partial \theta}\right\} = 0 \quad \forall \theta$$

then, whatever the unbiased estimator $\hat{\theta}$, its covariance matrix verifies²

$$\mathbf{C}(\hat{\theta}) \geq \mathbf{F}^{-1}(\theta)$$

where $\mathbf{F}(\theta)$ is the Fisher information matrix (FIM) given by:

$$\begin{aligned}\mathbf{F}(\theta) &= -\mathbb{E}\left\{\frac{\partial^2 \ln p(\mathbf{x}; \theta)}{\partial \theta \partial \theta^T}\right\} \\ &= \mathbb{E}\left\{\frac{\partial \ln p(\mathbf{x}; \theta)}{\partial \theta} \frac{\partial \ln p(\mathbf{x}; \theta)}{\partial \theta^T}\right\}\end{aligned}\tag{3.4}$$

¹ This condition is verified in most cases, except in the case where the domain where the pdf is not zero depends on θ .

² In what follows, the notation $\mathbf{A} \geq \mathbf{B}$ for two symmetric matrices \mathbf{A} and \mathbf{B} mean that $\forall z$, $z^T(\mathbf{A} - \mathbf{B})z \geq 0$.

and the derivative is evaluated at the true parameter θ . Furthermore, one can find an estimator, which reaches the bound, i.e. $C(\hat{\theta}) = F^{-1}(\theta)$, if the derivative of the log-likelihood function can be factored as

$$\frac{\partial \ln p(x; \theta)}{\partial \theta} = A(\theta) [g(x) - \theta] \quad [3.5]$$

where the vector $g(x)$ is a function of x only, and $A(\theta)$ depends on θ only. In this case,

$$\hat{\theta} = g(x) \quad [3.6]$$

is a minimum variance unbiased (MVU) estimator and its covariance matrix is $A^{-1}(\theta) = F^{-1}(\theta)$. This estimator is said to be efficient.

The previous theorem is quite powerful as it indicates that, under a “generally verified” regularity condition, there exists a lower bound for the covariance matrix of any unbiased estimator. Furthermore, it provides a necessary and sufficient condition for the existence of an efficient estimator (thus with minimum variance). Nevertheless, it is quite unusual that this factorization condition is fulfilled and most often the CRB is not reached, except asymptotically, that is to say when the number of observations tends toward infinity.

COROLLARY 3.1.– Suppose we want to estimate $\beta = f(\theta)$ from x , then the CRB for estimation of β is given by:

$$\frac{\partial \beta}{\partial \theta^T} F^{-1}(\theta) \frac{\partial \beta^T}{\partial \theta}$$

where $\partial \beta / \partial \theta^T$ is the Jacobian matrix whose (k, ℓ) element is $\partial \beta_k / \partial \theta_\ell$. If $\hat{\theta}$ is an efficient estimator and the transformation $f(\theta)$ is linear, then $\hat{\beta} = f(\hat{\theta})$ is also efficient. However, if the transformation is nonlinear, the efficiency is generally not retained. \square

To illustrate the use of the previous theorem, we now consider the case of Gaussian signals:

$$x \sim \mathcal{N}(s(\theta), R(\theta))$$

whose pdf is:

$$p(x; \theta) = \frac{1}{(2\pi)^{N/2} |R(\theta)|^{1/2}} \exp \left\{ -\frac{1}{2} [x - s(\theta)]^T R^{-1}(\theta) [x - s(\theta)] \right\}$$

where $|R(\theta)|$ stands for the determinant of the matrix $R(\theta)$, $s(\theta)$ the mean (which possibly corresponds to a useful deterministic signal) and $R(\theta)$ the covariance matrix.

A straightforward use of Theorem 3.1 leads to the following expression:

$$\begin{aligned} [\mathbf{F}(\boldsymbol{\theta})]_{k\ell} &= \left[\frac{\partial \mathbf{s}(\boldsymbol{\theta})}{\partial \theta_k} \right]^T \mathbf{R}^{-1}(\boldsymbol{\theta}) \left[\frac{\partial \mathbf{s}(\boldsymbol{\theta})}{\partial \theta_\ell} \right] \\ &\quad + \frac{1}{2} \text{Tr} \left\{ \mathbf{R}^{-1}(\boldsymbol{\theta}) \frac{\partial \mathbf{R}(\boldsymbol{\theta})}{\partial \theta_k} \mathbf{R}^{-1}(\boldsymbol{\theta}) \frac{\partial \mathbf{R}(\boldsymbol{\theta})}{\partial \theta_\ell} \right\} \end{aligned} \quad [3.7]$$

where $\text{Tr}\{\mathbf{A}\} = \sum_{k=1}^N \mathbf{A}(k, k)$ denotes the trace of matrix \mathbf{A} . We now consider the two following cases.

Case 3.1. The signal is the sum of a useful deterministic signal $\mathbf{s}(\boldsymbol{\theta})$ and a noise whose covariance matrix $\mathbf{R}(\boldsymbol{\theta}) = \mathbf{R}$ does not depend on $\boldsymbol{\theta}$.

The previous formula simplifies to:

$$\mathbf{F}(\boldsymbol{\theta}) = \frac{\partial \mathbf{s}^T(\boldsymbol{\theta})}{\partial \boldsymbol{\theta}} \mathbf{R}^{-1} \frac{\partial \mathbf{s}(\boldsymbol{\theta})}{\partial \boldsymbol{\theta}^T}$$

since the covariance matrix does not depend on $\boldsymbol{\theta}$. Let us focus on the *existence* of an efficient estimator. Differentiation of the log-likelihood gives:

$$\frac{\partial \ln p(\mathbf{x}; \boldsymbol{\theta})}{\partial \boldsymbol{\theta}} = \frac{\partial \mathbf{s}^T(\boldsymbol{\theta})}{\partial \boldsymbol{\theta}} \mathbf{R}^{-1} \mathbf{x} - \frac{\partial \mathbf{s}^T(\boldsymbol{\theta})}{\partial \boldsymbol{\theta}} \mathbf{R}^{-1} \mathbf{s}(\boldsymbol{\theta})$$

The condition for the existence of an efficient estimator may be written as:

$$\begin{aligned} \frac{\partial \ln p(\mathbf{x}; \boldsymbol{\theta})}{\partial \boldsymbol{\theta}} &= \mathbf{F}(\boldsymbol{\theta}) [\mathbf{g}(\mathbf{x}) - \boldsymbol{\theta}] \Rightarrow \\ \frac{\partial \mathbf{s}^T(\boldsymbol{\theta})}{\partial \boldsymbol{\theta}} \mathbf{R}^{-1} \frac{\partial \mathbf{s}(\boldsymbol{\theta})}{\partial \boldsymbol{\theta}^T} \boldsymbol{\theta} &= \frac{\partial \mathbf{s}^T(\boldsymbol{\theta})}{\partial \boldsymbol{\theta}} \mathbf{R}^{-1} \mathbf{s}(\boldsymbol{\theta}) \Rightarrow \\ \frac{\partial \mathbf{s}(\boldsymbol{\theta})}{\partial \boldsymbol{\theta}^T} \boldsymbol{\theta} &= \mathbf{s}(\boldsymbol{\theta}) \end{aligned}$$

In fact, the latter equation holds only if $\mathbf{s}(\boldsymbol{\theta})$ is a linear function of $\boldsymbol{\theta}$ [MAD 00]. Therefore, unless the data \mathbf{x} obeys a linear model, i.e. $\mathbf{x} = \mathbf{H}\boldsymbol{\theta} + \mathbf{w}$, where \mathbf{w} is a white Gaussian noise, there does not exist an efficient estimator, at least for finite N .

The following example addresses a practically important case where no efficient estimator can be found, still the CRB can be derived.

EXAMPLE 3.1.– Let us consider the case of a noisy complex sinusoid:

$$x(n) = A e^{j(2\pi n f + \varphi)} + b(n)$$

where $b(n)$ are independent, complex-valued zero-mean Gaussian distributed random variables³ with variance $\mathbb{E}\{|b(n)|^2\} = \sigma^2$. The vector containing the unknown parameters is here $\boldsymbol{\theta} = [A, \omega, \varphi, \sigma^2]^T$ with $\omega = 2\pi f$. The equation [3.7] for the FIM for a real Gaussian vector can be extended to the case of complex-valued vectors as [KAY 93, p. 525]

$$\begin{aligned} [\mathbf{F}(\boldsymbol{\theta})]_{k\ell} &= 2\text{Re} \left\{ \left[\frac{\partial \mathbf{s}(\boldsymbol{\theta})}{\partial \theta_k} \right]^H \mathbf{R}^{-1}(\boldsymbol{\theta}) \left[\frac{\partial \mathbf{s}(\boldsymbol{\theta})}{\partial \theta_\ell} \right] \right\} \\ &\quad + \text{Tr} \left\{ \mathbf{R}^{-1}(\boldsymbol{\theta}) \frac{\partial \mathbf{R}(\boldsymbol{\theta})}{\partial \theta_k} \mathbf{R}^{-1}(\boldsymbol{\theta}) \frac{\partial \mathbf{R}(\boldsymbol{\theta})}{\partial \theta_\ell} \right\} \end{aligned} \quad [3.8]$$

Using the previous equation with $\mathbf{s}(\boldsymbol{\theta}) = Ae^{j\varphi}[1, e^{j\omega}, e^{j2\omega}, \dots, e^{j(N-1)\omega}]^T$ and $\mathbf{R}(\boldsymbol{\theta}) = \sigma^2 \mathbf{I}$ leads to

$$\mathbf{F}(\boldsymbol{\theta}) = \frac{2}{\sigma^2} \begin{pmatrix} N & 0 & 0 & 0 \\ 0 & A^2 Q & A^2 P & 0 \\ 0 & A^2 P & N A^2 & 0 \\ 0 & 0 & 0 & \frac{N}{2\sigma^2} \end{pmatrix}$$

where $P = \sum_{n=0}^{N-1} n$ and $Q = \sum_{n=0}^{N-1} n^2$. Observe that the FIM is block-diagonal, which indicates that, somehow, estimation of the noise power is decoupled from that of the parameters of the exponential signal. Inverting $\mathbf{F}(\boldsymbol{\theta})$ gives [RIF 74]:

$$\begin{aligned} \text{var}(\hat{A}) &\geq \frac{\sigma^2}{2N} \\ \text{var}(\hat{\omega}) &\geq \frac{6\sigma^2}{A^2 N(N^2 - 1)} \end{aligned}$$

³ Herein a complex random variable $x = x_R + jx_I$ is said to be complex Gaussian distributed $x \sim \mathcal{N}_c(\mu = \mu_R + j\mu_I, \sigma^2)$ if its real part x_R and imaginary part x_I are independent and distributed as $x_R \sim \mathcal{N}(\mu_R, \sigma^2/2)$, $x_I \sim \mathcal{N}(\mu_I, \sigma^2/2)$, i.e. they are independent Gaussian distributed random variables with variance $\sigma^2/2$. This definition can be extended to the case of complex-valued random vectors, see [KAY 93, Ch. 15] for a brief and clear exposure. Briefly stated, a random vector $\mathbf{x} \in \mathbb{C}^N$ is said to have a complex multivariate Gaussian distribution $\mathbf{x} \sim \mathcal{N}_c(\boldsymbol{\mu}, \mathbf{R})$ with mean $\boldsymbol{\mu}$ and covariance matrix $\mathbf{R} = \mathbb{E}\{(\mathbf{x} - \boldsymbol{\mu})(\mathbf{x} - \boldsymbol{\mu})^H\}$ if its pdf can be written as $p(\mathbf{x}; \boldsymbol{\mu}, \mathbf{R}) = \pi^{-N} |\mathbf{R}|^{-1} \exp\left\{-(\mathbf{x} - \boldsymbol{\mu})^H \mathbf{R}^{-1} (\mathbf{x} - \boldsymbol{\mu})\right\}$. In what precedes the superscript H stands for the conjugate transpose.

$$\begin{aligned}\text{var}(\hat{\varphi}) &\geq \frac{\sigma^2(2N-1)}{A^2N(N+1)} \\ \text{var}(\hat{\sigma}^2) &\geq \frac{\sigma^4}{N}\end{aligned}$$

Notice that the CRB for estimation of A and φ is of the order N^{-1} while the CRB for estimation of ω is inversely proportional to N^3 . Note also that $CRB(\omega)$ is inversely proportional to the signal-to-noise ratio (SNR) A^2/σ^2 .

Case 3.2. The signal is a random process with zero mean $[s(\theta) \equiv 0]$ and covariance matrix $\mathbf{R}(\theta)$. The FIM is obtained from the derivatives of the covariance matrix:

$$[\mathbf{F}(\theta)]_{k\ell} = \frac{1}{2} \text{Tr} \left\{ \mathbf{R}^{-1}(\theta) \frac{\partial \mathbf{R}(\theta)}{\partial \theta_k} \mathbf{R}^{-1}(\theta) \frac{\partial \mathbf{R}(\theta)}{\partial \theta_\ell} \right\}$$

The attempt to obtain a factorization as in equation [3.5] rapidly leads to implicit equations that cannot be solved in most cases, so that it becomes practically impossible to derive an efficient estimator. Nevertheless, the expression of the FIM can sometimes result in simple formulas that provide insight into the best achievable performance, as shown in the following example.

EXAMPLE 3.2.- We try here to calculate the CRB for a Gaussian autoregressive (AR) process of order p , for which the unknown parameter vector may be written $\theta = [\sigma^2, a_1, \dots, a_p]^T$. Friedlander and Porat [FRI 89] proved, using the previous expression, that the FIM could be written in this case as:

$$\mathbf{F}(\theta) = \bar{\mathbf{F}}(\theta) + (N-p) \begin{pmatrix} (2\sigma^4)^{-1} & 0 \\ 0 & \mathbf{R}_p \end{pmatrix}$$

where $\bar{\mathbf{F}}(\theta)$ is a matrix that does not depend on N and where, for $k, \ell = 1, \dots, p$, $\mathbf{R}_p(k, \ell) = \gamma_{xx}(k-\ell)$ with $\gamma_{xx}(\cdot)$ the correlation function of the process. Therefore, when $N \rightarrow \infty$, $\bar{\mathbf{F}}(\theta)$ becomes negligible compared to the second term and we can write:

$$\mathbf{C}(\theta) \geq \frac{1}{N} \begin{pmatrix} 2\sigma^4 & 0 \\ 0 & \mathbf{R}_p^{-1} \end{pmatrix}$$

Before concluding this section, we present an interesting result due to Whittle, which expresses the normalized asymptotic FIM under mild assumptions. Let us consider a stationary Gaussian random process of zero mean and PSD $S_x(f)$. Then [DZH 86, POR 94],

$$\begin{aligned}[\mathbf{F}_0]_{k,\ell} &\triangleq \lim_{N \rightarrow \infty} N^{-1} [\mathbf{F}(\theta)]_{k,\ell} \\ &= \frac{1}{2} \int_{-1/2}^{1/2} \frac{1}{S_x^2(f)} \frac{\partial S_x(f)}{\partial \theta_k} \frac{\partial S_x(f)}{\partial \theta_\ell} df\end{aligned}\tag{3.9}$$

This formula allows, in particular, to obtain extremely simple expressions in the case of ARMA process, see [FRI 84a, FRI 84b].

3.1.3. Sequence of estimators

The theoretical elements that have just been given are related to random vectors with fixed dimension N . However, in most cases we rarely know how to carry out a statistical analysis of $\hat{\theta}$ for finite N , and derivation of explicit expressions of the bias and variance of the estimator requires the hypothesis of a large number of samples [STO 98]. Hence one is naturally led to study the asymptotic behavior of a sequence of random variables, namely the sequence of estimates $\hat{\theta}$ when N varies. Prior to that we need to define the types of convergences considered.

Let ξ_N be a sequence of random variables and a_N a series of strictly positive real numbers.

DEFINITION 3.1.– ξ_N is said to converge in probability to 0 if, $\forall \delta > 0$,

$$\lim_{N \rightarrow \infty} P\{|\xi_N| \geq \delta\} = 0$$

We thus use the notation $\xi_N = o_p(1)$.

DEFINITION 3.2.– ξ_N is said to be bounded in probability if $\forall \epsilon > 0$, $\exists \delta > 0$ such that

$$P\{|\xi_N| \geq \delta\} < \epsilon, \forall N$$

We thus use the notation $\xi_N = O_p(1)$.

Accordingly, we define:

$$\xi_N = o_p(a_N) \Leftrightarrow a_N^{-1}\xi_N = o_p(1)$$

$$\xi_N = O_p(a_N) \Leftrightarrow a_N^{-1}\xi_N = O_p(1)$$

We now define three types of convergences.

Convergence in probability ξ_N is said to converge in probability to the random variable ξ if:

$$\xi_N - \xi = o_p(1)$$

Convergence in distribution Let $F_{\xi_N}(\cdot)$ be the cumulative distribution function of ξ_N . Then ξ_N converges in distribution to the random variable ξ if

$$\lim_{N \rightarrow \infty} F_{\xi_N}(x) = F_\xi(x)$$

for every x such that the cumulative distribution function of ξ , $F_\xi(x)$, is continuous.⁴

Mean square convergence ξ_N converges in mean square toward ξ if

$$\lim_{N \rightarrow \infty} \mathbb{E} \left\{ (\xi_N - \xi)^2 \right\} = 0$$

RESULT 3.1.— The mean square convergence implies the convergence in probability, which itself implies the convergence in distribution.

Let us apply these definitions to a sequence of estimates. For the sake of notational convenience we temporarily denote it as $\hat{\theta}_N$ to emphasize its dependence with respect to N .

DEFINITION 3.3.— $\hat{\theta}_N$ is said asymptotically unbiased if:

$$\lim_{N \rightarrow \infty} \mathbb{E} \left\{ \hat{\theta}_N - \boldsymbol{\theta} \right\} = \mathbf{0}$$

Another important property is *consistency*.

DEFINITION 3.4.— The estimator $\hat{\theta}_N$ is said weakly consistent if:

$$\lim_{N \rightarrow \infty} P \left\{ \left\| \hat{\theta}_N - \boldsymbol{\theta} \right\| < \delta \right\} = 1 \quad \forall \delta$$

DEFINITION 3.5.— The estimator $\hat{\theta}_N$ is said to be consistent in mean square if:

$$\lim_{N \rightarrow \infty} \mathbb{E} \left\{ (\hat{\theta}_N - \boldsymbol{\theta}) (\hat{\theta}_N - \boldsymbol{\theta})^T \right\} = \mathbf{0}$$

Clearly, if one can tolerate an mse for finite N , the asymptotic mse should be zero; otherwise, even with an infinite number of samples, one could not recover the true parameter.

Definition 3.5 is generally stronger. We refer the reader to [POR 94, Ch. 3], [BRO 91, Ch. 6] for further details on the convergences of estimator sequences and

⁴ In the case ξ is Gaussian distributed with mean μ_ξ and variance σ_ξ^2 , we will denote $\xi_N \xrightarrow{as} \mathcal{N}(\mu_\xi, \sigma_\xi^2)$.

associated properties. One of the key points of a sequence of estimators is the speed at which the estimation errors decrease. Since they usually go to zero, it is natural to scale $\hat{\theta}_N - \theta$ by an increasing monotonic function of N , $d(N)$ such that, for example, $d(N)(\hat{\theta}_N - \theta) = O_p(1)$. For instance, in Example 3.2, $d(N)$ would be \sqrt{N} . Note that here we implicitly consider that all components of $\hat{\theta}_N$ converge at the same speed. If this is not so, we need to consider the asymptotic distribution $D(N)(\hat{\theta}_N - \theta)$ where $D(N) = \text{diag}(d_1(N), d_2(N), \dots, d_p(N))$.

Ideally, we would like to establish the convergence in distribution of $d(N)(\hat{\theta}_N - \theta)$ toward a random vector ζ with known distribution, as this would fully characterize the asymptotic behavior of $d(N)(\hat{\theta}_N - \theta)$. For instance, if ζ is a random Gaussian vector with zero mean and covariance matrix Γ , $\hat{\theta}_N$ is said to be asymptotically Gaussian distributed and Γ is referred to as the asymptotically normalized covariance matrix of $\hat{\theta}_N$.

In practice, however, we usually establish an expression for:

$$\Sigma(\theta) \triangleq \lim_{N \rightarrow \infty} d^2(N) E \left\{ (\hat{\theta}_N - \theta) (\hat{\theta}_N - \theta)^T \right\}$$

as it is generally simpler to obtain, see the examples in the next sections.

In the same way as we defined the FIM with fixed N , we can study the limit:

$$\mathbf{F}_0(\theta) \triangleq \lim_{N \rightarrow \infty} d^{-2}(N) \mathbf{F}(\theta)$$

which is known as the normalized information matrix. Thus, an estimator is said to be asymptotically efficient when:

$$\Sigma(\theta) = \mathbf{F}_0^{-1}(\theta)$$

Most of the estimators considered in this book will be mean square convergent with a decrease of the order of $d(N) = \sqrt{N}$, that is to say that their “variance decreases as $1/N$ ”.

REMARK 3.2.– The framework presented here for the theoretical analysis of estimators is that of stationary processes for which the analysis is generally carried out with a number of samples tending toward infinity. It may be noted that this technique is not applicable in numerous cases, for example, for deterministic signals of finite energy buried in additive noise. In such a case, the analysis is carried out assuming that the SNR tends toward infinity, [KAY 93, Ch. 9], [ERI 93], [TRE 85]. We will further examine this issue in Example 3.5.

3.1.4. Maximum likelihood estimation

As we saw in Theorem 3.1, the condition for the existence of an efficient estimator is relatively difficult to verify. The usual alternative in this case is to look for asymptotically efficient estimators. Within this category, the chief systematic approach is the maximum likelihood estimator (MLE). The principle is very simple: it consists of finding the parameter θ that maximizes the likelihood function $\theta \rightarrow p(\mathbf{x}; \theta)$; the MLE is the vector of parameters that make the observed data as likely as possible, that is to say

$$\hat{\theta}^{ML} = \arg \max_{\theta} p(\mathbf{x}; \theta)$$

In practice, we generally prefer maximizing the logarithm of the likelihood function⁵ $\mathcal{L}(\mathbf{x}; \theta) = \ln p(\mathbf{x}; \theta)$. The MLE enjoys a number of desirable properties that are listed now.

THEOREM 3.2.– (Efficiency). *If an efficient estimator exists, then the maximum likelihood procedure will produce it.*

Theorem 3.2 follows directly from Theorem 3.1. Indeed, since $\hat{\theta}^{ML}$ is a maximizer of the likelihood function, or equivalently the log-likelihood function, the derivative of the latter should be zero at $\theta = \hat{\theta}^{ML}$. However, an efficient estimator exists if and only if the derivative of the log-likelihood function can be factored as in equation [3.5] in which $\mathbf{A}(\theta) = \mathbf{F}(\theta)$ is the FIM. Therefore, observing that the FIM is positive definite, the MLE of θ is necessarily $\mathbf{g}(\mathbf{x})$, i.e. the efficient estimator. Note that $\mathbf{g}(\mathbf{x})$ will effectively maximize the log-likelihood function since the second-order derivative of the latter at $\theta = \mathbf{g}(\mathbf{x})$ is $-\mathbf{F}(\theta)$ and is therefore negative definite. Theorem 3.2 ensures that the MLE will achieve the CRB if an efficient estimator exists. This is for instance the case with the widely used linear model $\mathbf{x} = \mathbf{H}\theta + \mathbf{b}$ where \mathbf{b} is a Gaussian distributed random vector with known covariance matrix.

THEOREM 3.3.– (Asymptotic properties). *If $p(\mathbf{x}; \theta)$ satisfies some “regularity” conditions, then the MLE is consistent, asymptotically (as $N \rightarrow \infty$) Gaussian distributed and its normalized asymptotic covariance matrix is $\mathbf{F}_0^{-1}(\theta)$.*

The previous theorem shows that the ML estimator is asymptotically optimal. For example, in the case where $d(N) = \sqrt{N}$, it means that

$$\sqrt{N} (\hat{\theta}^{ML} - \theta) \xrightarrow{as} \mathcal{N}(\mathbf{0}, \mathbf{F}_0^{-1}(\theta))$$

⁵ Herein, the log-likelihood will be given up to an additive constant, the latter being irrelevant in the maximization.

This property suggests that the ML can only be outperformed in finite samples. However, in most cases, its variance for finite N will not depart significantly from the CRB, except in very small sample support.⁶

THEOREM 3.4.–(Invariance). *Let $\beta = f(\theta) \in \mathbb{R}^q$ for some function $f(\cdot): \mathbb{R}^p \rightarrow \mathbb{R}^q$. Then the MLE of β is given by:*

$$\hat{\beta}^{ML} = f(\hat{\theta}^{ML})$$

If $f(\cdot)$ is not an invertible function, $\hat{\beta}^{ML}$ is obtained as:

$$\hat{\beta}^{ML} = \arg \max_{\beta} \bar{p}(\mathbf{x}; \beta)$$

$$\bar{p}(\mathbf{x}; \beta) = \max_{\theta; \beta=f(\theta)} p(\mathbf{x}; \theta)$$

Theorem 3.4 enables one to obtain the MLE of any function of θ . This property is particularly helpful when estimation of θ turns out to be very difficult while estimating $\beta = f(\theta)$ is easier to implement in practice.

To summarize, the MLE constitutes a chief systematic approach as it possesses optimality properties, at least for large N . In principle, it can always be implemented as it entails solving a maximization problem, for which efficient mathematical tools exist. However, it might be computationally intensive to solve the maximization problem. In addition, the log-likelihood function may exhibit local extrema, which could prevent from obtaining the true ML solution. The ML approach is however used in a large number of classical problems. For instance, it can be used in the case of deterministic signals buried in Gaussian noise with known covariance matrix, i.e. $\mathbf{x} \sim \mathcal{N}(\mathbf{s}(\theta), \mathbf{R})$. In such a case, the log-likelihood function is simply:

$$\mathcal{L}(\mathbf{x}; \theta) = -\frac{1}{2} [\mathbf{x} - \mathbf{s}(\theta)]^T \mathbf{R}^{-1} [\mathbf{x} - \mathbf{s}(\theta)]$$

and the ML approach amounts to solving a nonlinear least-squares problem, namely:

$$\begin{aligned} \hat{\theta}^{ML} &= \arg \min_{\theta} [\mathbf{x} - \mathbf{s}(\theta)]^T \mathbf{R}^{-1} [\mathbf{x} - \mathbf{s}(\theta)] \\ &= \arg \min_{\theta} \left\| \mathbf{R}^{-1/2} [\mathbf{x} - \mathbf{s}(\theta)] \right\|^2 \end{aligned}$$

⁶ In the previous theorem we investigate the asymptotic properties of the MLE for large N . As was alluded to in the CRB section, this approach may not be relevant, e.g. for finite energy deterministic signals embedded in noise, for which “asymptotic” should be understood in terms of SNR. In such a case, the “asymptotic” properties of the MLE still prevail. However, for low SNR, the MLE may depart from the CRB: in fact, it is customary to observe a “threshold” effect [KAY 93], i.e. the variance of the MLE remains close to the CRB until some SNR threshold where its variance is much worse than the CRB.

The MLE consists of fitting, in the best least-squares sense, the data \boldsymbol{x} and the model $\boldsymbol{s}(\boldsymbol{\theta})$, after whitening. In contrast, when the noise covariance matrix is unknown and depends on $\boldsymbol{\theta}$, i.e. when $\boldsymbol{x} \sim \mathcal{N}(\boldsymbol{s}(\boldsymbol{\theta}), \boldsymbol{R}(\boldsymbol{\theta}))$, implementing the MLE is considerably more complicated, which constitutes a limitation in practice. For example, for linear AR or ARMA models, the exact pdf of the signal has a complicated expression [SÖD 89, Ch. 7], which prevents from using the ML approach. In such a case, one is led either to use an approximated expression for the log-likelihood function (see next remark) or to turn to estimators based on the correlation function.

REMARK 3.3.– In the case of a Gaussian process, it is possible to show that the log-likelihood function can be *approximated* by:

$$\mathcal{L}_w(\boldsymbol{x}; \boldsymbol{\theta}) = - \sum_{n=1}^{(N-1)/2} \ln S_x(f_n, \boldsymbol{\theta}) - \sum_{n=1}^{(N-1)/2} \frac{I(f_n)}{S_x(f_n, \boldsymbol{\theta})} \quad [3.10]$$

where $f_n = n/N$ and:

$$I(f) = \frac{1}{N} \left| \sum_{n=0}^{N-1} x(n) e^{-j2\pi n f} \right|^2$$

is the **periodogram** of the signal \boldsymbol{x} . The expression in equation [3.10] is the discrete version of what is referred to as the Whittle log-likelihood function [WHI 62]. Convergence analysis for estimator based on maximizing $\mathcal{L}_w(\boldsymbol{x}; \boldsymbol{\theta})$ has been extensively studied. It is interesting to note that, under quite standard assumptions, this likelihood function can be interpreted as the asymptotic distribution of the periodogram, which will be derived in section 3.3.1. This formula is particularly important in spectral analysis problems when only a model for the PSD $S_x(f, \boldsymbol{\theta})$ is available.

We now illustrate the ML approach in two cases.

EXAMPLE 3.3.– *Frequency estimation for a complex exponential signal in additive noise.* Let us first consider a practically relevant problem in spectral analysis, namely that of estimating the frequency f of an exponential signal in white noise:

$$x(n) = A e^{j(2\pi n f + \varphi)} + b(n) \quad n = 0, \dots, N-1$$

This is a typical problem, for instance, in radar where, depending on the type of waveform used, f can provide information about the range or the speed of a target. We assume herein that the amplitude A and phase φ are unknown deterministic quantities. As for the additive noise, we assume that the samples $b(n)$ are independent and identically distributed as complex Gaussian with zero-mean and variance σ^2 , so that

the pdf of the vector $\mathbf{b} = [b(0), b(1), \dots, b(N-1)]^T$ is given by:

$$p(\mathbf{b}; \sigma^2) = (\pi\sigma^2)^{-N} \exp\left\{-\sigma^{-2}\mathbf{b}^H\mathbf{b}\right\}$$

where the superscript H stands for Hermitian, i.e. conjugate transpose. We consider the case where σ^2 is unknown so that the parameter vector to be estimated here is $\boldsymbol{\theta} = [\omega, A, \varphi, \sigma^2]^T$ where $\omega = 2\pi f$. For notational convenience, we define $\tilde{A} = Ae^{j\varphi}$ and let $\mathbf{a}(\omega) = [1, e^{j\omega}, \dots, e^{j(N-1)\omega}]^T$, so that the vector of received samples can be compactly written as:

$$\mathbf{x} = \tilde{A}\mathbf{a}(\omega) + \mathbf{b}$$

Since the deterministic part of the model, namely $\tilde{A}\mathbf{a}(\omega)$, is not linear with respect to (w.r.t.) ω , there does not exist an efficient estimator, at least for finite N . It is thus natural to resort to the ML estimator. Toward this end, note that the log-likelihood function is here:

$$\mathcal{L}(\mathbf{x}; \boldsymbol{\theta}) = -N \ln \pi - N \ln \sigma^2 - \sigma^{-2} (\mathbf{x} - \tilde{A}\mathbf{a}(\omega))^H (\mathbf{x} - \tilde{A}\mathbf{a}(\omega))$$

To obtain the MLE, we will not maximize $\mathcal{L}(\mathbf{x}; \boldsymbol{\theta})$ w.r.t. all components of $\boldsymbol{\theta}$ simultaneously. Rather, the maximization will be conducted successively since, as will become clear shortly, maximizing w.r.t. one component of $\boldsymbol{\theta}$, keeping the others fixed, results in closed-form expressions. More precisely, we first maximize w.r.t. σ^2 , assuming that ω and \tilde{A} are fixed: as will be shown the maximizing argument is simple to obtain. Plugging back in the log-likelihood function, we are thus left with maximizing a function that depends only on ω and \tilde{A} . The latter can be maximized explicitly w.r.t. \tilde{A} , leaving a maximization problem w.r.t. ω only. Let us now apply this procedure. It is straightforward to show that:

$$\frac{\partial \mathcal{L}(\mathbf{x}; \boldsymbol{\theta})}{\partial \sigma^2} = -\frac{N}{\sigma^2} + \frac{\|\mathbf{x} - \tilde{A}\mathbf{a}(\omega)\|^2}{\sigma^4}$$

so that, for any ω and \tilde{A} , the maximum of $\mathcal{L}(\mathbf{x}; \boldsymbol{\theta})$ w.r.t. σ^2 is obtained for:

$$\sigma^2 = N^{-1} \|\mathbf{x} - \tilde{A}\mathbf{a}(\omega)\|^2$$

and is given by:

$$\max_{\sigma^2} \mathcal{L}(\mathbf{x}; \boldsymbol{\theta}) = \text{const.} - N \ln \|\mathbf{x} - \tilde{A}\mathbf{a}(\omega)\|^2$$

Therefore, we are left with the problem of minimizing, w.r.t. ω and \tilde{A} , the function:

$$\begin{aligned} g(\omega, \tilde{A}) &= \left\| \mathbf{x} - \tilde{A}\mathbf{a}(\omega) \right\|^2 \\ &= \mathbf{x}^H \mathbf{x} - \tilde{A} \mathbf{x}^H \mathbf{a}(\omega) - \tilde{A}^* \mathbf{a}^H(\omega) \mathbf{x} + \left| \tilde{A} \right|^2 \mathbf{a}^H(\omega) \mathbf{a}(\omega) \\ &= \mathbf{a}^H(\omega) \mathbf{a}(\omega) \left| \tilde{A} - \frac{\mathbf{a}^H(\omega) \mathbf{x}}{\mathbf{a}^H(\omega) \mathbf{a}(\omega)} \right|^2 + \mathbf{x}^H \mathbf{x} - \frac{|\mathbf{a}^H(\omega) \mathbf{x}|^2}{\mathbf{a}^H(\omega) \mathbf{a}(\omega)} \end{aligned}$$

Clearly, for a fixed ω , the minimum of $g(\omega, \tilde{A})$ is achieved for:

$$\begin{aligned} \tilde{A} &= \frac{\mathbf{a}^H(\omega) \mathbf{x}}{\mathbf{a}^H(\omega) \mathbf{a}(\omega)} \\ &= \frac{1}{N} \sum_{n=0}^{N-1} x(n) e^{-jn\omega} \end{aligned}$$

and is given by:

$$h(\omega) = \mathbf{x}^H \mathbf{x} - \frac{|\mathbf{a}^H(\omega) \mathbf{x}|^2}{\mathbf{a}^H(\omega) \mathbf{a}(\omega)}$$

It follows that the MLE of ω consists of minimizing $h(\omega)$ or equivalently in maximizing:

$$\begin{aligned} I(\omega) &= \frac{|\mathbf{a}^H(\omega) \mathbf{x}|^2}{\mathbf{a}^H(\omega) \mathbf{a}(\omega)} \\ &= \frac{1}{N} \left| \sum_{n=0}^{N-1} x(n) e^{-jn\omega} \right|^2 \end{aligned}$$

The latter function is recognized as the **periodogram**: it corresponds in fact to the (properly normalized) squared modulus of the Fourier transform of the signal. It emerges here as the MLE of a particular kind of process but can also serve as an estimate of the PSD for any random process. We will study the statistical analysis of the periodogram later.

EXAMPLE 3.4.– Frequency estimation for a complex exponential signal in multiplicative noise. We consider here a problem, slightly different from the previous problem, where the signal of interest, namely an exponential signal, now undergoes random amplitude variations. This kind of problem is relevant, e.g. in radar systems with fluctuating targets whose radar cross section varies with time. More specifically, we assume that the received data can be modeled as

$$x(n) = a(n) e^{j(2\pi n f + \varphi)} \quad n = 0, \dots, N-1$$

where $a(n)$ is a random, zero-mean complex-valued Gaussian process, whose covariance function is given by:

$$c_{aa}(m) = \mathbb{E} \{a^*(n)a(n+m)\} = P_a \rho_a^{|m|}$$

where $\rho_a \in \mathbb{R}$ and $0 < \rho_a < 1$. The covariance sequence of $a(n)$ is thus exponentially decaying (as would be the case if $a(n)$ was an AR process of order 1): the closer ρ_a to 0, the faster $c_{aa}(m)$ goes to zero. The parameter vector to be estimated here is $\theta = [\omega, P_a, \rho_a]^T$ where $\omega = 2\pi f$. ω is the parameter of most interest while P_a and ρ_a can be considered as nuisance parameters. Therefore, in the sequel we focus on estimation of ω . From the assumptions made, the vector $\mathbf{x} = [x(0), x(1), \dots, x(N-1)]^T$ has a Gaussian distribution, with mean $\mathbf{0}$ and a covariance matrix equal to $\mathbf{R} = P_a \Phi \mathbf{R}_a \Phi^H$ where:

$$\Phi = \text{diag} \left(1, e^{j\omega}, \dots, e^{j(N-1)\omega} \right)$$

$$\mathbf{R}_a = \begin{pmatrix} 1 & \rho_a & \rho_a^2 & \cdots & \rho_a^{N-1} \\ \rho_a & 1 & \rho_a & \cdots & \vdots \\ \rho_a^2 & \ddots & \ddots & \ddots & \rho_a^2 \\ \vdots & \ddots & \ddots & \ddots & \rho_a \\ \rho_a^{N-1} & \cdots & \rho_a^2 & \rho_a & 1 \end{pmatrix}$$

The log-likelihood function then takes the following form:

$$\begin{aligned} \mathcal{L}(\mathbf{x}; \theta) &= -N \ln \pi - \ln |\mathbf{R}| - \mathbf{x}^H \mathbf{R}^{-1} \mathbf{x} \\ &= -N \ln \pi - N \ln P_a - \ln |\mathbf{R}_a| - P_a^{-1} \mathbf{x}^H \Phi \mathbf{R}_a^{-1} \Phi^H \mathbf{x} \end{aligned}$$

where we used the fact that $\Phi^H \Phi = \mathbf{I}$. For the sake of convenience, let $\mathbf{y} = \Phi^H \mathbf{x}$. Differentiating $\mathcal{L}(\mathbf{x}; \theta)$ w.r.t. P_a and equating the result to zero, it follows that the value of P_a , which maximizes the log-likelihood function, is:

$$P_a = N^{-1} \mathbf{y}^H \mathbf{R}_a^{-1} \mathbf{y}$$

so that we are left with the problem of maximizing:

$$g(\omega, \rho_a) = -N \ln (\mathbf{y}^H \mathbf{R}_a^{-1} \mathbf{y}) - \ln |\mathbf{R}_a|$$

w.r.t. ω and ρ_a . The matrix \mathbf{R}_a has a special structure, namely Toeplitz, and hence possesses some special properties. More precisely, it is known that

$$|\mathbf{R}_a| = (1 - \rho_a^2)^{N-1} \text{ and:}$$

$$\mathbf{R}_a^{-1} = \frac{1}{(1 - \rho_a^2)} \begin{pmatrix} 1 & -\rho_a & 0 & \cdots & 0 \\ -\rho_a & 1 + \rho_a^2 & -\rho_a & \ddots & \vdots \\ 0 & \ddots & \ddots & \ddots & 0 \\ \vdots & \ddots & \ddots & 1 + \rho_a^2 & -\rho_a \\ 0 & \cdots & 0 & -\rho_a & 1 \end{pmatrix}$$

Using the above result, it ensues that:

$$\begin{aligned} \mathbf{y}^H \mathbf{R}_a^{-1} \mathbf{y} &= (1 - \rho_a^2)^{-1} \left[|x(0)|^2 + |x(N-1)|^2 + (1 + \rho_a^2) \sum_{n=1}^{N-2} |x(n)|^2 \right. \\ &\quad \left. - \rho_a e^{-j\omega} \sum_{n=0}^{N-1} x^*(n)x(n+1) - \rho_a e^{j\omega} \sum_{n=0}^{N-1} x(n)x^*(n+1) \right] \\ &= (1 - \rho_a^2)^{-1} [\alpha + \beta (1 + \rho_a^2) - \gamma \rho_a e^{-j\omega} - \gamma^* \rho_a e^{j\omega}] \end{aligned}$$

with obvious definitions for α , β , and γ . Observing the function $g(\omega, \rho_a)$, we notice that only the term $\mathbf{y}^H \mathbf{R}_a^{-1} \mathbf{y}$ depends on ω . Therefore, to maximize $g(\omega, \rho_a)$ w.r.t. ω we need to maximize only $\gamma \rho_a e^{-j\omega} + \gamma^* \rho_a e^{j\omega} = 2\rho_a \operatorname{Re}\{\gamma e^{-j\omega}\}$. Clearly, the solution is given by:

$$\hat{\omega}^{ML} = \operatorname{angle}(\gamma) = \operatorname{angle} \left(\sum_{n=1}^{N-1} x^*(n)x(n+1) \right) \quad [3.11]$$

It is instructive to note that the maximum likelihood estimate of ω is nothing but the phase of the usual estimate of $c_{xx}(m) = \mathbb{E}\{x^*(n)x(n+m)\}$, for $m = 1$. This makes sense since $c_{xx}(m) = P_a \rho_a^{|m|} e^{jm\omega}$ and hence the phase of $c_{xx}(1)$ is ω . We observe that despite the apparent complexity of the log-likelihood function, the maximization problem leads to a simple and closed-form expression for the ML estimate of ω . To complete the derivation, this value of ω should be reported in $g(\omega, \rho_a)$, leaving a maximization problem w.r.t. ρ_a only. We do not pursue this route here, instead we show how to obtain the CRB for estimation of ω . Clearly, the log-likelihood function can be written as:

$$\begin{aligned} \mathcal{L}(\mathbf{x}; \boldsymbol{\theta}) &= -N \ln \pi - N \ln P_a - (N-1) \ln (1 - \rho_a^2) \\ &\quad - P_a^{-1} (1 - \rho_a^2)^{-1} [\alpha + \beta (1 + \rho_a^2) - \gamma \rho_a e^{-j\omega} - \gamma^* \rho_a e^{j\omega}] \end{aligned}$$

Differentiating the previous equation w.r.t. ω leads to:

$$\frac{\partial \mathcal{L}(\mathbf{x}; \boldsymbol{\theta})}{\partial \omega} = -\frac{\rho_a}{P_a (1 - \rho_a^2)} [j\gamma e^{-j\omega} - j\gamma^* e^{j\omega}]$$

An important observation to make is that:

$$\mathbb{E}\{\gamma\} = (N-1)c_{xx}(1) = (N-1)P_a\rho_a e^{j\omega}$$

which implies that $\mathbb{E}\{j\gamma e^{-j\omega} - j\gamma^* e^{j\omega}\} = 0$. It follows that:

$$\begin{aligned}\mathbb{E}\left\{\frac{\partial^2 \mathcal{L}(\mathbf{x}; \boldsymbol{\theta})}{\partial \omega \partial P_a}\right\} &= \frac{\partial}{\partial P_a} \left(-\frac{\rho_a}{P_a(1-\rho_a^2)}\right) \mathbb{E}\{j\gamma e^{-j\omega} - j\gamma^* e^{j\omega}\} = 0 \\ \mathbb{E}\left\{\frac{\partial^2 \mathcal{L}(\mathbf{x}; \boldsymbol{\theta})}{\partial \omega \partial \rho_a}\right\} &= \frac{\partial}{\partial \rho_a} \left(-\frac{\rho_a}{P_a(1-\rho_a^2)}\right) \mathbb{E}\{j\gamma e^{-j\omega} - j\gamma^* e^{j\omega}\} = 0\end{aligned}$$

and hence the FIM is *block-diagonal*, i.e.

$$\mathbf{F}(\boldsymbol{\theta}) = \begin{pmatrix} F_{11} & 0 & 0 \\ 0 & F_{22} & F_{23} \\ 0 & F_{32} & F_{33} \end{pmatrix}$$

Consequently, the CRB for estimation of ω is simply the inverse of F_{11} . The latter is obtained as:

$$\begin{aligned}F_{11} &= \mathbb{E}\left\{-\frac{\partial^2 \mathcal{L}(\mathbf{x}; \boldsymbol{\theta})}{\partial \omega^2}\right\} \\ &= \frac{\rho_a}{P_a(1-\rho_a^2)} \mathbb{E}\{\gamma e^{-i\omega} + \gamma^* e^{i\omega}\} \\ &= \frac{2\rho_a^2(N-1)}{1-\rho_a^2}\end{aligned}$$

and finally, the CRB for estimation of ω is given by:

$$CRB(\omega) = \frac{1-\rho_a^2}{2\rho_a^2(N-1)}$$

As could be expected, the closer ρ_a to 1, i.e. the “closer” $x(n)$ to a constant-amplitude exponential signal, the smaller the CRB. In contrast, when $\rho_a \rightarrow 0$, the correlation function $c_{aa}(m)$ tends to that of a white noise, and the CRB goes to infinity, meaning that the frequency is no longer identifiable.

EXAMPLE 3.5.– Frequency estimation for a damped exponential signal. This final example is a variation on Example 3.3 where the exponential signal is now damped, namely:

$$x(n) = A\rho^n e^{j(2\pi n f + \varphi)} + b(n)$$

where $\rho \in]0, 1[$. The main difference with Example 3.3 is that the signal is now of *finite energy* and hence the usual “asymptotic” theory of the MLE should thus

be revisited, as explained now. We begin with the CRB for estimation of the vector $\boldsymbol{\theta} = [A, \rho, \omega, \varphi, \sigma^2]^T$ of the unknown parameters, where again $\omega = 2\pi f$. For the sake of notational convenience, let $\boldsymbol{\theta}_s = [A, \rho, \omega, \varphi]^T$. Using equation [3.8] for the FIM, with $\mathbf{R}(\boldsymbol{\theta}) = \sigma^2 \mathbf{I}$ and $\mathbf{s}(\boldsymbol{\theta}) = Ae^{j\varphi} [1, \rho e^{j\omega}, \rho^2 e^{j2\omega}, \dots, \rho^{N-1} e^{j(N-1)\omega}]^T$ leads to:

$$\mathbf{F}(\boldsymbol{\theta}) = \frac{2}{\sigma^2} \begin{pmatrix} P & A\rho^{-1}Q & 0 & 0 & 0 \\ A\rho^{-1}Q & A^2\rho^{-2}R & 0 & 0 & 0 \\ 0 & 0 & A^2R & A^2Q & 0 \\ 0 & 0 & A^2Q & A^2P & 0 \\ 0 & 0 & 0 & 0 & \frac{N}{2\sigma^2} \end{pmatrix}$$

where $P = \sum_{n=0}^{N-1} \rho^{2n}$, $Q = \sum_{n=0}^{N-1} n\rho^{2n}$ and $R = \sum_{n=0}^{N-1} n^2\rho^{2n}$. The block-diagonal structure of the FIM simplifies its inversion (indeed only the diagonal blocks need to be inverted) and the upper-left 4×4 block of the CRB takes the following form:

$$\mathbf{CRB}(\boldsymbol{\theta}_s) = \frac{\sigma^2}{2A^2(PR - Q^2)} \begin{pmatrix} A^2R & -A\rho Q & 0 & 0 \\ -A\rho Q & \rho^2P & 0 & 0 \\ 0 & 0 & P & -Q \\ 0 & 0 & -Q & R \end{pmatrix}$$

Using algebraic expressions for P, Q , and R (we skip the details for the sake of simplicity), it can be shown that:

$$\begin{aligned} CRB(\omega) &= \frac{\sigma^2}{2A^2} \frac{(1 - \rho^{2N})(1 - \rho^2)^3}{\rho^2 [\rho^{4N} - N^2\rho^{2N+2} + 2(N^2 - 1)\rho^{2N} - N^2\rho^{2N-2} + 1]} \\ &\xrightarrow[N \rightarrow \infty]{} \frac{\sigma^2}{2A^2} \frac{(1 - \rho^2)^3}{\rho^2} \end{aligned}$$

which shows that the CRB does not go to zero as the number of samples goes to infinity. However, this makes sense. Since the signal of interest has finite energy, collecting additional samples is useless as only noise will be present. Therefore, no additional information about the parameters of interest is made available and the CRB does not decrease. In this case, the asymptotic theory of the MLE, as $N \rightarrow \infty$ is meaningless, and asymptotic should be understood here in terms of the SNR, or equivalently the noise power. Indeed, as $\sigma^2 \rightarrow 0$, the CRB goes to 0.

The MLE can be obtained following the lines of Example 3.3, namely the log-likelihood function is successively maximized with respect to σ^2 , $\tilde{A} = Ae^{j\varphi}$, leaving a 2D maximization problem w.r.t. ρ and ω . More precisely, the MLE of the latter is obtained by maximizing:

$$f(\omega, \rho) = \frac{\left| \sum_{n=0}^{N-1} x(n)\rho^n e^{-jn\omega} \right|^2}{\sum_{n=0}^{N-1} \rho^{2n}}$$

In contrast to the constant-amplitude case, the MLE does not boil down to a 1D maximization problem, since maximization of $f(\omega, \rho)$ w.r.t. ρ only does not result in a closed-form expression. Therefore, some optimization algorithms must be used. Observe that the MLE will be asymptotically efficient, i.e. it will approach the CRB as $\sigma^2 \rightarrow 0$.

A computationally less demanding and widely spread alternative is to resort to the so-called linear prediction or Prony's method. Indeed, the signal of interest $s(n) = A\rho^n e^{j(2\pi n f + \varphi)}$ obeys a simple prediction equation, namely:

$$s(n) - \rho e^{j\omega} s(n-1) = 0$$

Therefore, one is naturally led to consider minimizing the prediction error, i.e. obtaining ρ and ω as:

$$\hat{\omega}, \hat{\rho} = \arg \min_{\omega, \rho} \sum_{n=1}^{N-1} |x(n) - \rho e^{j\omega} x(n-1)|^2$$

The solution is easily obtained as:

$$\hat{\rho} e^{j\hat{\omega}} = \frac{\sum_{n=1}^{N-1} x^*(n-1)x(n)}{\sum_{n=1}^{N-1} x^*(n-1)x(n-1)}$$

The method of linear prediction can be extended to the case of multiple damped exponential signals and is closely related to AR modeling, see Chapter 6 for further details.

3.2. Covariance-based estimation

Most spectral analysis methods rely, implicitly or explicitly, on the second-order moments of the signal. In other words, the first step of a spectral analysis procedure consists of estimating the correlation function of the signal. Consequently, the performance of any spectral analysis estimator will depend on the performance in estimating the correlation function (the next section will be devoted to this relation). In this section, we first briefly review and assess the performance of correlation estimates in the case of a random stationary process for which N samples $\{x(n)\}_{n=0}^{N-1}$ are observed. As was explained earlier, analysis of the correlation estimates for finite N is nearly intractable, and hence only asymptotic analyses, i.e. as N goes to infinity, will be presented. We will successively investigate the case of stationary processes with continuous spectra, and then turn to the case of line spectra. The second part of this section will outline the main mathematical results used to "transfer" the asymptotic properties of the estimated correlations to the estimated spectral analysis parameters. The last part of this section will deal with the problem of estimating the covariance matrix of a random multi-dimensional observation vector, a problem that naturally arises when the data are received on an array of sensors.

3.2.1. Estimation of the autocorrelation functions of time series

We first define the two following hypotheses.

HYPOTHESIS 3.1.– The covariances are absolutely summable, that is to say:

$$\sum_{m=-\infty}^{\infty} |c_{xx}(m)| \leq C_0 < \infty$$

HYPOTHESIS 3.2.– The fourth-order cumulants verify:

$$\sum_{n=-\infty}^{\infty} |\text{cum}(n+k, n, \ell)| \leq K_0 < \infty$$

where:

$$\begin{aligned} \text{cum}(k, m, \ell) = & E\{x(n)x(n+k)x(n+m)x(n+\ell)\} - c_{xx}(k-m)c_{xx}(\ell) \\ & - c_{xx}(k-\ell)c_{xx}(m) - c_{xx}(k)c_{xx}(m-\ell) \end{aligned}$$

Let

$$\begin{aligned} \mu &= E\{x(n)\} \\ \gamma_{xx}(m) &= E\{x(n)(x(n+m)\} \\ c_{xx}(m) &= E\{(x(n)-\mu)(x(n+m)-\mu)\} \\ &= \gamma_{xx}(m) - \mu^2 \end{aligned}$$

be the mean, the correlation function, and the covariance function of this signal. The usual estimator of the mean is:

$$\hat{\mu} = \frac{1}{N} \sum_{n=0}^{N-1} x(n) \quad [3.12]$$

This estimator is obviously unbiased:

$$E\{\hat{\mu}\} = \frac{1}{N} \sum_{n=0}^{N-1} E\{x(n)\} = \mu$$

Let us now study its variance:

$$\begin{aligned}\text{var}(\hat{\mu}) &= \mathbb{E}\{\hat{\mu}^2\} - \mu^2 \\ &= \frac{1}{N^2} \sum_{k=0}^{N-1} \sum_{n=0}^{N-1} \mathbb{E}\{x(k)x(n)\} - \mu^2 \\ &= \frac{1}{N^2} \sum_{k=0}^{N-1} \sum_{n=0}^{N-1} c_{xx}(n-k) \\ &= \frac{1}{N} \sum_{m=-(N-1)}^{N-1} \left(1 - \frac{|m|}{N}\right) c_{xx}(m)\end{aligned}$$

The previous formula is exact, whatever the number of samples N . Let us now study the limit of this variance when N tends toward infinity. Using Hypothesis 3.1, we can show that [POR 94, section 4.2]:

$$\lim_{N \rightarrow \infty} N\text{var}(\hat{\mu}) = \sum_{m=-\infty}^{\infty} c_{xx}(m) \quad [3.13]$$

which proves that $\hat{\mu}$ is a consistent (in mean square) estimator of μ .

REMARK 3.4.— The previous derivation establishes the mean square consistency of the estimator of the mean and provides an expression of $\lim_{N \rightarrow \infty} N\text{var}(\hat{\mu})$ under a non-restrictive hypothesis. Moreover, if $x(n) - \mu$ is a linear process, that is to say if:

$$x(n) - \mu = \sum_{k=0}^{\infty} \gamma_k e(n-k)$$

where $e(n)$ is a sequence of random variables independent identically distributed with zero mean and variance σ_e^2 , with $\sum_{k=-\infty}^{\infty} |\gamma_k| < \infty$ and $\sum_{k=-\infty}^{\infty} \gamma_k \neq 0$, then [BRO 91, Theorem 7.1.2]:

$$\sqrt{N}(\hat{\mu} - \mu) \xrightarrow{as} \mathcal{N}\left(0, \sum_{m=-\infty}^{\infty} c_{xx}(m)\right)$$

which adds to equation [3.13] the asymptotic Gaussian distribution of $\hat{\mu} - \mu$.

Once the mean has been estimated, we can subtract it from the measurements to obtain a new signal $x(n) - \hat{\mu}$. In what follows, without losing generality, we will suppose that the process has zero mean. The asymptotic results presented later are not affected by this hypothesis [POR 94]. The two natural estimators of the covariance

(or correlation) function are:

$$\bar{c}_{xx}(m) = \frac{1}{N-m} \sum_{n=0}^{N-m-1} x(n)x(n+m) \quad [3.14]$$

$$\hat{c}_{xx}(m) = \frac{1}{N} \sum_{n=0}^{N-m-1} x(n)x(n+m) \quad [3.15]$$

The mean of each of these estimators is calculated as follows:

$$\mathbb{E}\{\bar{c}_{xx}(m)\} = \frac{1}{N-m} \sum_{n=0}^{N-m-1} \mathbb{E}\{x(n)x(n+m)\} = c_{xx}(m) \quad [3.16]$$

$$\mathbb{E}\{\hat{c}_{xx}(m)\} = \frac{1}{N} \sum_{n=0}^{N-m-1} \mathbb{E}\{x(n)x(n+m)\} = \left(1 - \frac{m}{N}\right) c_{xx}(m) \quad [3.17]$$

As a result, $\bar{c}_{xx}(m)$ is an unbiased estimator, whereas the bias of $\hat{c}_{xx}(m)$ is $\frac{m}{N}c_{xx}(m)$. However, $\hat{c}_{xx}(m)$ is an asymptotically unbiased estimator of the covariance function. Let us now study the variances and covariances of these estimations. We focus on $\hat{c}_{xx}(m)$. We have:

$$\begin{aligned} \mathbb{E}\{\hat{c}_{xx}(m)\hat{c}_{xx}(\ell)\} &= \frac{1}{N^2} \sum_{n=0}^{N-m-1} \sum_{k=0}^{N-\ell-1} \mathbb{E}\{x(n)x(n+m)x(k)x(k+\ell)\} \\ &= \frac{1}{N^2} \sum_{n=0}^{N-m-1} \sum_{k=0}^{N-\ell-1} \{c_{xx}(m)c_{xx}(\ell) \\ &\quad + c_{xx}(n-k)c_{xx}(n+m-k-\ell) \\ &\quad + c_{xx}(k-m-n)c_{xx}(k+\ell-n) \\ &\quad + \text{cum}(m, k-n, k+\ell-n)\} \\ &= \left(1 - \frac{m}{N}\right) \left(1 - \frac{\ell}{N}\right) c_{xx}(m)c_{xx}(\ell) \\ &\quad + \frac{1}{N^2} \sum_{n=0}^{N-m-1} \sum_{k=0}^{N-\ell-1} c_{xx}(n-k)c_{xx}(n+m-k-\ell) \\ &\quad + \frac{1}{N^2} \sum_{n=0}^{N-m-1} \sum_{k=0}^{N-\ell-1} c_{xx}(k-m-n)c_{xx}(k+\ell-n) \\ &\quad + \frac{1}{N^2} \sum_{n=0}^{N-m-1} \sum_{k=0}^{N-\ell-1} \text{cum}(m, k-n, k+\ell-n) \end{aligned}$$

so that

$$\begin{aligned} \text{cov}(\hat{c}_{xx}(m), \hat{c}_{xx}(\ell)) &= \frac{1}{N^2} \sum_{n=0}^{N-m-1} \sum_{k=0}^{N-\ell-1} c_{xx}(n-k)c_{xx}(n+m-k-\ell) \\ &\quad + c_{xx}(k-m-n)c_{xx}(k+\ell-n) \\ &\quad + \text{cum}(m, k-n, k+\ell-n) \end{aligned} \quad [3.18]$$

The previous formula uses only the fact that the considered signal is stationary. If, moreover, we set Hypothesis 3.2, then we can prove the following theorem [POR 94, section 4.2].

THEOREM 3.5.– (Bartlett). *Under absolute summability hypotheses of the covariances and cumulants, we have:*

$$\begin{aligned} \lim_{N \rightarrow \infty} N \text{cov}(\hat{c}_{xx}(m), \hat{c}_{xx}(\ell)) &= \sum_{n=-\infty}^{\infty} c_{xx}(n)c_{xx}(n+m-\ell) \\ &\quad + c_{xx}(n+m)c_{xx}(n-\ell) \\ &\quad + \text{cum}(n+m, n, \ell) \end{aligned} \quad [3.19]$$

This theorem is known as Bartlett's formula. We note that if the process is Gaussian, the fourth-order cumulants are zero. Similarly to the mean, the signal linearity will allow to achieve asymptotic Gaussianity of the covariances. Let $\hat{\mathbf{c}} = [\hat{c}_{xx}(0), \hat{c}_{xx}(1), \dots, \hat{c}_{xx}(M)]^T$ be the estimated vector of covariances $\mathbf{c} = [c_{xx}(0), c_{xx}(1), \dots, c_{xx}(M)]^T$ constructed from [3.15].

RESULT 3.2.– If the process is linear, $\sqrt{N}(\hat{\mathbf{c}} - \mathbf{c}) \xrightarrow{as} \mathcal{N}(\mathbf{0}, \Sigma)$ where the elements of the covariance matrix Σ are computed using Bartlett's formula; see [BRO 91, p. 228]. This result can also be applied if we assume that the process is Gaussian [POR 94, p. 105].

EXAMPLE 3.6.– Covariance estimation of a Gaussian moving average process. Let us assume that $x(n)$ is an moving average process of order q (see Chapter 6 for further details):

$$x(n) = \sum_{k=0}^q b_k e(n-k) \quad [3.20]$$

where $e(n)$ is a sequence of Gaussian random variables independent with zero mean and variance σ_e^2 . Straightforward computations show that, for $m \geq 0$:

$$c_{xx}(m) = \begin{cases} \sum_{\ell=0}^{q-m} b_\ell b_{\ell+m} & m \leq q \\ 0 & m > q \end{cases} \quad [3.21]$$

Application of Bartlett's formula for $0 \leq m \leq q$, $0 \leq \ell \leq q$ and $m \geq \ell$ gives:

$$\Sigma_{m,\ell} = \sum_{n=-q}^{q-(m-\ell)} c_{xx}(n)c_{xx}(n+m-\ell) + \sum_{n=\ell-q}^{q-m} c_{xx}(n+m)c_{xx}(n-\ell) \quad [3.22]$$

where the expressions of $c_{xx}(n)$ as a function of the true parameters are given by equation [3.21].

The results given until now concern only random wide-sense stationary processes (and possibly linear processes). Similar results can be proved for other classes of signals, particularly sine wave signals, which are commonly used in spectral analysis. Let us consider the following signal:

$$x(n) = \sum_{k=1}^p A_k \sin(2\pi n f_k + \phi_k) + b(n) = s(n) + b(n) \quad [3.23]$$

where $\{\phi_k\}$ are assumed to be independent and uniformly distributed over $[0, 2\pi[$ and $b(n)$ is a sequence of random variables independent and identically distributed, with zero mean and variance σ^2 . The covariance function is then:

$$c_{xx}(m) = \frac{1}{2} \sum_{k=1}^p A_k^2 \cos(2\pi m f_k) + \sigma^2 \delta(m) = c_{ss}(m) + \sigma^2 \delta(m) \quad [3.24]$$

for which Hypothesis 3.1 clearly does not apply. One can thus show that (see [STO 89a]):

RESULT 3.3.- If $x(n)$ is given by (3.23), then $\sqrt{N}(\hat{c} - c) \xrightarrow{as} \mathcal{N}(\mathbf{0}, \Sigma)$ where the elements (m, ℓ) of Σ are:

$$\begin{aligned} \Sigma(m, \ell) &= 2\sigma^2 [c_{ss}(\ell + m) + c_{ss}(\ell - m)] \\ &\quad + \sigma^4 \delta(\ell - m) + [\mathbb{E}\{b^4(n)\} - 2\sigma^4] \delta(\ell) \delta(m) \end{aligned} \quad [3.25]$$

Finally, we would like to mention that very general theoretical results, as they concern signals that are a combination of deterministic and random components (stationary or non-stationary), were published by Dandawaté and Giannakis [DAN 95]. This last article makes it possible to include a very large class of signals and provides analytical expressions of asymptotic distributions of moment estimates. Finally, the reader is invited to read [DAN 95, LAC 97] for the analysis of estimator of higher-order moments.

3.2.2. Analysis of estimators based on $\hat{c}_{xx}(m)$

The theoretical results of previous sections are the basis from which we can analyze the statistical performance of a large number of estimators used in spectral

analysis. In fact, a majority of spectral analysis techniques are based on the use of a set of estimated covariance lags $\{\hat{c}_{xx}(m)\}_{m=0}^M$ or, in other words, the estimator may be written:

$$\hat{\theta}_N = \mathbf{g}(\hat{\mathbf{c}}) \quad [3.26]$$

We note that the vector $\hat{\mathbf{c}}$ considered here consists of estimates of the covariance function. Nevertheless, the approach recommended below can easily be generalized in the case where, for example, $\hat{\mathbf{c}}$ contains estimates of moments of higher order, as soon as we know the asymptotic properties of the vector $\hat{\mathbf{c}}$. Generally, there are two cases:

- 1) either the function \mathbf{g} is sufficiently simple (e.g. linear) and we can carry out the statistical analysis rather straightforwardly;
- 2) or the function \mathbf{g} is a more complex function. Nevertheless, it is generally continuous and differentiable (at least in a neighborhood of \mathbf{c}) and the convergence of $\hat{\mathbf{c}}$ toward \mathbf{c} allows the use of probabilistic Taylor series expansions.

Before describing the approach in detail, some results related to the asymptotic theory may be recalled; see [BRO 91, Ch. 6], [POR 94, Appendix C].

RESULT 3.4.- Let ξ_N be a sequence of random vectors of dimension p such that $\xi_N - \xi = O_p(a_N)$ and $\lim_{N \rightarrow \infty} a_N = 0$. If g is a function of \mathbb{R}^p in \mathbb{R} such that the derivatives $\partial g / \partial \xi$ are continuous in a neighborhood of ξ , then:

$$g(\xi_N) = g(\xi) + \left[\frac{\partial g}{\partial \xi} \right]^T (\xi_N - \xi) + o_p(a_N)$$

RESULT 3.5.- Consider ξ_N and ζ_N two sequences of random vectors of dimension p such that $\xi_N - \zeta_N = o_p(1)$. Assume that ξ_N converges in distribution to ξ . Then ζ_N converges also in distribution toward the random vector ξ .

Using the two previous results, we can then obtain (see [BRO 91, Ch. 6]) the following result.

RESULT 3.6.- Let ξ_N be a sequence of random vectors of dimension p such that $a_N^{-1} (\xi_N - \xi) \stackrel{as}{\sim} \mathcal{N}(\mathbf{0}, \Sigma)$ and $\lim_{N \rightarrow \infty} a_N = 0$. Consider

$$\mathbf{g}(\mathbf{x}) = [g_1(\mathbf{x}), g_2(\mathbf{x}), \dots, g_q(\mathbf{x})]^T$$

a function of \mathbb{R}^p in \mathbb{R}^q , continuous and differentiable in a neighbourhood of ξ . Let $\mathbf{D} = \partial \mathbf{g} / \partial \mathbf{x}^T$ be the $q \times p$ matrix of partial derivatives, evaluated at ξ and assume that all the diagonal elements of $\mathbf{D} \Sigma \mathbf{D}^T$ are non-zero. Then:

$$a_N^{-1} (\mathbf{g}(\xi_N) - \mathbf{g}(\xi)) \stackrel{as}{\sim} \mathcal{N}(\mathbf{0}, \mathbf{D} \Sigma \mathbf{D}^T)$$

As an illustrative example, let us consider that $\xi_N = \hat{c}$ with a view to analyze the asymptotic behavior of $\hat{\theta}_N$ in equation [3.26]. Application of results 3.2 and 3.6 with $\xi = c$ and $a_N^{-1} = \sqrt{N}$ leads immediately to:

$$\sqrt{N}(\hat{\theta}_N - \theta) \xrightarrow{as} \mathcal{N}(\mathbf{0}, \mathbf{D}\Sigma\mathbf{D}^T)$$

where the elements of the covariance matrix Σ are computed using Bartlett's formula. Results 3.4–3.6 help analyze the performance of a large class of estimators based on \hat{c} . We will apply this procedure in section 3.3 for two specific cases:

- 1) estimation of parameters of an AR model;
- 2) estimation of the frequency of a noisy sinusoidal signal.

The previous results also apply directly to the analysis of estimators of the PSD. In fact, as described in Chapter 6, many parametric spectral analysis techniques consist of estimating a vector of parameters θ and using $\hat{\theta}_N$ in the expression of the PSD $S_x(f, \theta)$:

$$\hat{S}_x(f, \theta)_N \triangleq S_x(f, \hat{\theta}_N)$$

If $\hat{\theta}_N$ is an estimator of θ such that $a_N^{-1}(\hat{\theta}_N - \theta) \xrightarrow{as} \mathcal{N}(\mathbf{0}, \Sigma)$ and $\lim_{N \rightarrow \infty} a_N = 0$, then Result 3.6 implies that:

$$a_N^{-1}(\hat{S}_x(f, \theta)_N - S_x(f, \theta)) \xrightarrow{as} \mathcal{N}(\mathbf{0}, \mathbf{d}^T(f, \theta)\Sigma\mathbf{d}(f, \theta))$$

where $\mathbf{d}(f, \theta) = \partial S_x(f, \theta)/\partial \theta$. Using similar reasoning and Corollary 3.1, Friedlander and Porat suggest in [FRI 84b] to use $\mathbf{d}^T(f, \theta)\mathbf{F}^{-1}(\theta)\mathbf{d}(f, \theta)$, where the Fisher matrix is obtained from Whittle's equation [3.9], as a lower bound on the variance of $\hat{S}_x(f, \theta)_N$:

$$\text{var}(\hat{S}_x(f, \theta)_N) \geq \frac{2}{N} \mathbf{d}^T(f, \theta) \left\{ \int_{-1/2}^{1/2} \frac{\mathbf{d}(f, \theta)\mathbf{d}(f, \theta)^T}{S_x^2(f, \theta)} df \right\}^{-1} \mathbf{d}(f, \theta)$$

3.2.3. The case of multi-dimensional observations

We now consider the case where, at time instant n , the data are collected simultaneously on an array of M sensors, so that the available observation vector is $\mathbf{x}(n) = [x_1(n), x_2(n), \dots, x_M(n)]^T$. $x_m(n)$ corresponds to the output of sensor number m at time instant n . Let us assume that N snapshots $\{\mathbf{x}(n)\}_{n=1}^N$ are available and gathered in the following $M \times N$ matrix:

$$\mathbf{X} = [\mathbf{x}(1), \mathbf{x}(2), \dots, \mathbf{x}(N)]$$

An ubiquitous task in array processing is to estimate the covariance matrix $\mathbf{R} = \mathbb{E}\{\mathbf{x}(n)\mathbf{x}^T(n)\}$ from \mathbf{X} . For the sake of simplicity in this chapter, we assume that the snapshots $\mathbf{x}(n)$ are independent and identically distributed: more precisely, they are assumed to be zero-mean, Gaussian distributed, with covariance matrix \mathbf{R} . Under this hypothesis, the joint distribution of the snapshots is given by:

$$\begin{aligned} p(\mathbf{X}; \mathbf{R}) &= \prod_{n=1}^N p(\mathbf{x}(n); \mathbf{R}) \\ &= \prod_{n=1}^N (2\pi)^{-M/2} |\mathbf{R}|^{-1/2} \exp\left\{-\frac{1}{2}\mathbf{x}^T(n)\mathbf{R}^{-1}\mathbf{x}(n)\right\} \\ &= (2\pi)^{-MN/2} |\mathbf{R}|^{-N/2} \text{etr}\left\{-\frac{1}{2}\mathbf{R}^{-1}\mathbf{S}\right\} \end{aligned}$$

where $\text{etr}\{\cdot\}$ stands for the exponential of the trace of the matrix between braces and:

$$\mathbf{S} = \sum_{n=1}^N \mathbf{x}(n)\mathbf{x}^T(n) = \mathbf{X}\mathbf{X}^T$$

To estimate \mathbf{R} , we consider a maximum likelihood approach. Assuming that $N \geq M$, the matrix \mathbf{S} is positive definite with probability 1 [MUI 82], so that it admits a unique positive-definite square root $\mathbf{S}^{1/2}$. Let $\mathbf{S}^{1/2}\mathbf{R}^{-1}\mathbf{S}^{1/2} = \mathbf{U}\Lambda\mathbf{U}^T$ denote the eigenvalue decomposition of $\mathbf{S}^{1/2}\mathbf{R}^{-1}\mathbf{S}^{1/2}$ where \mathbf{U} is the orthonormal matrix of its eigenvectors, i.e. $\mathbf{U}^T\mathbf{U} = \mathbf{I}$, and $\Lambda = \text{diag}\{\lambda_1, \lambda_2, \dots, \lambda_M\}$ stands for the diagonal matrix of its positive eigenvalues. The log-likelihood function can thus be rewritten as:

$$\begin{aligned} \mathcal{L}(\mathbf{X}; \mathbf{R}) &= \text{const.} - \frac{N}{2} \ln |\mathbf{R}| - \frac{1}{2} \text{Tr}\{\mathbf{R}^{-1}\mathbf{S}\} \\ &= \text{const.} + \frac{N}{2} \ln |\mathbf{S}^{1/2}\mathbf{R}^{-1}\mathbf{S}^{1/2}| - \frac{N}{2} \ln |\mathbf{S}| - \frac{1}{2} \text{Tr}\{\mathbf{S}^{1/2}\mathbf{R}^{-1}\mathbf{S}^{1/2}\} \\ &= \text{const.} + \frac{N}{2} \ln |\Lambda| - \frac{N}{2} \ln |\mathbf{S}| - \frac{1}{2} \text{Tr}\{\Lambda\} \\ &= \text{const.} - \frac{N}{2} \ln |\mathbf{S}| + \frac{1}{2} \sum_{m=1}^M (N \ln \lambda_m - \lambda_m) \end{aligned}$$

The function $f(\lambda) = N \ln \lambda - \lambda$ has a unique maximum in \mathbb{R}^+ , which is achieved for $\lambda = N$. It follows that the log-likelihood is maximum for $\Lambda = N\mathbf{I}$, which implies that $\mathbf{S}^{1/2}\mathbf{R}^{-1}\mathbf{S}^{1/2} = N\mathbf{I}$, and therefore the MLE of \mathbf{R} is given by:

$$\hat{\mathbf{R}}^{ML} = \frac{1}{N}\mathbf{S}$$

which is referred to as the sample covariance matrix. Note that the estimate is positive definite, as is required for a covariance matrix. The random matrix \mathbf{S} is known to follow a Wishart distribution [MUI 82], i.e. the joint distribution of its elements is given by:

$$p(\mathbf{S}) = \frac{|\mathbf{S}|^{(N-M-1)/2}}{2^{MN/2} \Gamma_M(\frac{N}{2}) |\mathbf{R}|^{N/2}} \text{etr} \left\{ -\frac{1}{2} \mathbf{R}^{-1} \mathbf{S} \right\}$$

where $\Gamma_M(\nu) = \pi^{\frac{M(M-1)}{4}} \prod_{k=1}^M \Gamma((\nu-k+1)/2)$. The previous distribution provides a complete statistical characterization of \mathbf{S} , and hence of the MLE of \mathbf{R} . In particular, it implies that [TAG 94]:

$$\begin{aligned} \mathbb{E} \left\{ \hat{\mathbf{R}}^{ML} \right\} &= \mathbf{R} \\ \mathbb{E} \left\{ (\hat{\mathbf{R}}_{k,\ell}^{ML} - \mathbf{R}_{k,\ell}) (\hat{\mathbf{R}}_{p,q}^{ML} - \mathbf{R}_{p,q}) \right\} &= \frac{1}{N} [\mathbf{R}_{k,q} \mathbf{R}_{p,\ell} + \mathbf{R}_{k,p} \mathbf{R}_{\ell,q}] \end{aligned}$$

which shows that $\hat{\mathbf{R}}^{ML}$ is an unbiased and consistent estimator of \mathbf{R} . In many applications, in particular in space-time adaptive processing for radar described in Chapter 12 of this book, it is desired to design a filter \mathbf{w} such that the output power is minimized while a constant gain is guaranteed for a given signal of interest \mathbf{v} . In such a case, the optimal filter is proportional to $\mathbf{S}^{-1}\mathbf{v}$, and therefore its performance, such as the output SNR, will be directly related to the statistics of \mathbf{S}^{-1} . Under the stated assumptions, it is well known, see [MUI 82], that \mathbf{S}^{-1} follows an inverse Wishart distribution, i.e. its distribution is given by:

$$p(\mathbf{S}^{-1}) = \frac{|\mathbf{S}|^{(N+M+1)/2}}{2^{MN/2} \Gamma_M(\frac{N}{2}) |\mathbf{R}|^{N/2}} \text{etr} \left\{ -\frac{1}{2} \mathbf{S}^{-1} \mathbf{R} \right\}$$

The inverse Wishart distribution of \mathbf{S}^{-1} allows us to analyze the SNR loss at the output of the filter $\mathbf{S}^{-1}\mathbf{v}$ with respect to the SNR at the output of the optimal (clairvoyant) filter $\mathbf{R}^{-1}\mathbf{v}$, see [REE 74, KHA 87].

3.3. Performance assessment of some spectral estimators

3.3.1. Periodogram analysis

The periodogram is a natural estimation tool for the PSD. Let us recall that its expression is:

$$\begin{aligned} I(f) &= \frac{1}{N} \left| \sum_{n=0}^{N-1} x(n) e^{-j2\pi n f} \right|^2 \\ &= \sum_{m=-(N-1)}^{N-1} \hat{\gamma}_{xx}(m) e^{-j2\pi m f} \end{aligned} \tag{3.27}$$

where:

$$\hat{\gamma}_{xx}(m) = \frac{1}{N} \sum_{n=0}^{N-m-1} x(n)x(n+m)$$

is the biased estimator of the autocorrelation function. The objective of this section is to derive the asymptotic properties of $I(f)$ for a real-valued signal. First, let us calculate the estimator bias. The periodogram mean can directly be written as:

$$\begin{aligned} \mathbb{E}\{I(f)\} &= \sum_{m=-(N-1)}^{N-1} \left(1 - \frac{|m|}{N}\right) \gamma_{xx}(m) e^{-j2\pi mf} \\ &= \int_{-1/2}^{1/2} S_x(\nu) W(f - \nu) d\nu \end{aligned}$$

where $W(f) = \frac{1}{N} \left[\frac{\sin(\pi f N)}{\sin(\pi f)} \right]^2$ is the Fourier transform of the triangular window. As a result, the periodogram is a biased estimator of the PSD. Nevertheless, if Hypothesis 3.1 is verified, which is always the case for a linear process, then:

$$\lim_{N \rightarrow \infty} \mathbb{E}\{I(f)\} = S_x(f) \quad [3.28]$$

The periodogram is thus an asymptotically unbiased estimator of the PSD. Moreover, we can establish [POR 94] that:

$$\sum_{m=-\infty}^{\infty} |m| |\gamma_{xx}(m)| < \infty \Rightarrow \mathbb{E}\{I(f)\} = S_x(f) + O(1/N)$$

Let us now study the asymptotic distribution of the periodogram. This development is generally done under the hypothesis that the process $x(n)$ is linear [PRI 94, POR 94] or that the cumulants of $x(n)$ are absolutely summable [BRI 81].

HYPOTHESIS 3.3.– The cumulants are absolutely summable, i.e.:

$$\forall k, \sum_{u_1, \dots, u_{k-1} = -\infty}^{+\infty} |\text{cum}(u_1, \dots, u_{k-1})| < \infty$$

Let us emphasize that it is possible under this hypothesis to define the multi-spectrum of order k , [LAC 97]:

$$S_x(f_1, \dots, f_{k-1}) = \sum_{u_1, \dots, u_{k-1} = -\infty}^{+\infty} \text{cum}(u_1, \dots, u_{k-1}) e^{-j2\pi \sum_{\ell=1}^{k-1} u_\ell f_\ell}$$

The first step consists of calculating the asymptotic properties of the discrete Fourier transform:

$$\mathbf{d}(f) = \frac{1}{\sqrt{N}} \sum_{n=1}^N x(n)e^{-j2\pi n f}$$

RESULT 3.7.— Let $k(N)$ be an integer such that $f_k(N) \triangleq k(N)/N \rightarrow f_k$ for $k = 1, \dots, K$ when $N \rightarrow \infty$. If $f_k(N) \pm f_\ell(N) \not\equiv 0 \pmod{1}$, then $d(f_k(N))$, $k = 1, \dots, K$ are asymptotically independent and distributed according to a complex Gaussian distribution with variance $S_x(f_k)$:

$$\mathbf{d}(f_k(N)) \xrightarrow{as} \mathcal{N}_c(0, S_x(f_k))$$

A proof of this result can be found in [BRI 81]. The cumulants of the Fourier transform tend toward those of a complex process, which is jointly Gaussian and independent at the same time. Once the asymptotic distribution of the Fourier transform is obtained, that of the periodogram is obtained directly by noting that:

$$I(f) = \operatorname{Re}\{\mathbf{d}(f)\}^2 + \operatorname{Im}\{\mathbf{d}(f)\}^2$$

RESULT 3.8.— Under the same hypotheses as used previously, if $f_k(N) \pm f_\ell(N) \not\equiv 0 \pmod{1}$, the $I(f_k(N))$ are asymptotically independent $S_x(f_k) \times \chi_2^2/2$ variates, where χ_2^2 stands for a chi-square distributed variable with 2 degrees of freedom.

If $U \sim \chi_2^2$, then $E\{U\} = 2$ and $\operatorname{var}(U) = 4$, and hence:

- as seen above $I(f_k(N))$ is an asymptotically unbiased estimator of the PSD;
- $\operatorname{var}(I(f_k(N)))$ tends toward $S_x(f_k)^2$, which shows that *the periodogram is not a consistent estimator of the PSD*.

This result proves that the periodogram is a poor estimator of the PSD. However, one can take advantage of the asymptotic independence of the periodogram at different frequencies to reduce its variance. This is the principle of numerous methods that construct an asymptotically consistent estimator of the PSD by local averaging of the periodogram [BRI 81].

3.3.2. Estimation of AR model parameters

In this section, we illustrate how the above theory can be used to assess the performance of conventional estimators of the parameters of an autoregressive model.

Let us assume that $x(n)$ is an AR process of order p (see Chapter 6 for further details) whose PSD can be written as:

$$S_x(f) = \frac{\sigma^2}{|A(f)|^2}$$

$$A(f) = 1 + \sum_{k=1}^p a_k e^{-j2\pi kf}$$

Our interest lies in estimating the parameter vector $\mathbf{a} = [a_1, a_2, \dots, a_p]^T$. Accordingly, we are interested in the poles of the model, i.e. the roots of the polynomial (with $a_0 = 1$ by definition)

$$A(z) = \sum_{k=0}^p a_k z^{-k}$$

$$= \prod_{k=1}^q (1 - \rho_k e^{j\omega_k} z^{-1})(1 - \rho_k e^{-j\omega_k} z^{-1})$$

where, for the sake of simplicity, we have assumed that p is even and that the roots of $A(z)$ occur in complex-conjugate pairs. The parameters ρ_k and ω_k are instrumental in shaping the PSD of the process. Briefly stated, for ρ_k close to 1, one can observe sharp peaks in the PSD located at $\omega = \omega_k$. Let $\boldsymbol{\omega} = [\omega_1, \dots, \omega_q]^T$ and let us denote $\hat{\mathbf{a}} = [\hat{a}_1, \hat{a}_2, \dots, \hat{a}_p]^T$ an estimate of \mathbf{a} . Let $\hat{z}_k = \hat{\rho}_k e^{j\hat{\omega}_k}$ denote the roots of the polynomial $\hat{A}(z) = 1 + \sum_{k=1}^p \hat{a}_k z^{-k}$ and let us define $\hat{\boldsymbol{\omega}} = [\hat{\omega}_1, \dots, \hat{\omega}_q]^T$. In the sequel, we are interested in deriving the asymptotic covariance matrix of $\sqrt{N}(\hat{\mathbf{a}} - \mathbf{a})$ and that of $\sqrt{N}(\hat{\boldsymbol{\omega}} - \boldsymbol{\omega})$. Toward this end, the first step is to relate the errors $\sqrt{N}(\hat{\mathbf{a}} - \mathbf{a})$ to $\sqrt{N}(\hat{\mathbf{c}} - \mathbf{c})$ where $\hat{\mathbf{c}} = [\hat{c}_{xx}(0), \hat{c}_{xx}(1), \dots, \hat{c}_{xx}(M)]^T$ and $\mathbf{c} = [c_{xx}(0), c_{xx}(1), \dots, c_{xx}(M)]^T$. Since the statistics of $\sqrt{N}(\hat{\mathbf{c}} - \mathbf{c})$ are known from Bartlett's formula, the results of the previous section will be used to find the asymptotic covariance matrix of $\sqrt{N}(\hat{\mathbf{a}} - \mathbf{a})$. Next, the function $\hat{\boldsymbol{\omega}} = \mathbf{g}(\hat{\mathbf{a}})$ being continuous and differentiable, a Taylor series expansion will be used to relate $\sqrt{N}(\hat{\mathbf{a}} - \mathbf{a})$ to $\sqrt{N}(\hat{\boldsymbol{\omega}} - \boldsymbol{\omega})$, leading to the asymptotic covariance matrix of the frequencies. Let us start with the usual estimate of \mathbf{a} , see Chapter 6:

$$\hat{\mathbf{a}} = -\hat{\mathbf{R}}_p^{-1} \hat{\mathbf{r}} \quad [3.29]$$

with:

$$\hat{\mathbf{R}}_p = \begin{pmatrix} \hat{c}_{xx}(0) & \hat{c}_{xx}(-1) & \cdots & \cdots & \hat{c}_{xx}(-p+1) \\ \hat{c}_{xx}(1) & \hat{c}_{xx}(0) & \cdots & \cdots & \hat{c}_{xx}(-p+2) \\ \vdots & \vdots & \ddots & & \vdots \\ \vdots & \vdots & & \ddots & \vdots \\ \hat{c}_{xx}(p-1) & \hat{c}_{xx}(p-2) & \cdots & \cdots & \hat{c}_{xx}(0) \end{pmatrix}$$

$$\hat{\mathbf{r}} = \begin{pmatrix} \hat{c}_{xx}(1) \\ \hat{c}_{xx}(2) \\ \vdots \\ \hat{c}_{xx}(p) \end{pmatrix}.$$

Then, using Results 3.6 and 3.2, it follows that:

$$\sqrt{N}(\hat{\mathbf{a}} - \mathbf{a}) \xrightarrow{as} \mathcal{N}\left(\mathbf{0}, \frac{\partial \mathbf{a}}{\partial \mathbf{c}^T} \Sigma \frac{\partial \mathbf{a}^T}{\partial \mathbf{c}}\right)$$

The matrix of partial derivatives $\partial \mathbf{a} / \partial \mathbf{c}^T$ can be easily calculated using the Yule–Walker equations

$$c_{xx}(m) = - \sum_{k=1}^p a_k c_{xx}(m-k) + \sigma^2 \delta(m)$$

see [POR 94]. The previous derivation used directly Result 3.6, which is very general. Alternatively, one might look for a specific derivation, which depends on the problem at hand. For instance, in our case, one could write:

$$\begin{aligned} \sqrt{N}(\hat{\mathbf{a}} - \mathbf{a}) &= -\sqrt{N} \hat{\mathbf{R}}_p^{-1} (\hat{\mathbf{r}} + \hat{\mathbf{R}}_p \mathbf{a}) \\ &= -\hat{\mathbf{R}}_p^{-1} \left\{ \sqrt{N} \left[(\hat{\mathbf{r}} - \mathbf{r}) + (\hat{\mathbf{R}}_p - \mathbf{R}_p) \mathbf{a} \right] \right\} \\ &= -\mathbf{R}_p^{-1} \left\{ \sqrt{N} \left[(\hat{\mathbf{r}} - \mathbf{r}) + (\hat{\mathbf{R}}_p - \mathbf{R}_p) \mathbf{a} \right] \right\} + o_p(1) \\ &= -\mathbf{R}_p^{-1} \sqrt{N} \boldsymbol{\epsilon} + o_p(1) \end{aligned} \quad [3.30]$$

However, the vector $\sqrt{N} \boldsymbol{\epsilon}$ is asymptotically Gaussian distributed with mean $\mathbf{0}$ and a covariance matrix \mathbf{S} whose (k, ℓ) element is

$$\mathbf{S}(k, \ell) = \sum_{i=0}^p \sum_{j=0}^p a_i a_j \sigma_{k-i, \ell-j}$$

where $\sigma_{k,\ell} = \lim_{N \rightarrow \infty} N \text{cov}(\hat{c}_{xx}(k), \hat{c}_{xx}(\ell))$, and an expression for $\sigma_{k,\ell}$ is given in Theorem 3.5. Hence, using equation [3.30] along with Result 3.5, one can conclude that:

$$\sqrt{N}(\hat{\mathbf{a}} - \mathbf{a}) \xrightarrow{as} \mathcal{N}(\mathbf{0}, \mathbf{R}_p^{-1} \mathbf{S} \mathbf{R}_p^{-1})$$

In the case of a Gaussian process, and using the Yule–Walker equations, it can be proved that:

$$\mathbf{S}(k, \ell) = \sigma^2 c_{xx}(k - \ell)$$

so that $\mathbf{S} = \sigma^2 \mathbf{R}_p$ and finally:

$$\sqrt{N}(\hat{\mathbf{a}} - \mathbf{a}) \xrightarrow{as} \mathcal{N}(\mathbf{0}, \sigma^2 \mathbf{R}_p^{-1})$$

From Example 3.2 we know that the normalized asymptotic FIM is indeed $\sigma^2 \mathbf{R}_p^{-1}$, which shows that $\hat{\mathbf{a}}$ is asymptotically optimal for a Gaussian AR process. Let us turn now to the analysis of $\sqrt{N}(\hat{\boldsymbol{\omega}} - \boldsymbol{\omega})$. The basic idea is to use a Taylor series expansion of $(\hat{\boldsymbol{\omega}} - \boldsymbol{\omega}) = \mathbf{g}(\hat{\mathbf{a}}) - \mathbf{g}(\mathbf{a})$ to relate the two errors. Proceeding this way, it can be shown (see [STO 89b] for full details) that:

$$\sqrt{N}(\hat{\boldsymbol{\omega}} - \boldsymbol{\omega}) = \mathbf{F}\mathbf{G} \left\{ \sqrt{N}(\hat{\mathbf{a}} - \mathbf{a}) \right\} + o_p(1)$$

with:

$$\mathbf{F} = \begin{pmatrix} \frac{\beta_1}{\alpha_1^2 + \beta_1^2} & 0 & \frac{-\alpha_1}{\alpha_1^2 + \beta_1^2} & 0 \\ \ddots & \ddots & \ddots & \ddots \\ 0 & \frac{\beta_q}{\alpha_q^2 + \beta_q^2} & 0 & \frac{-\alpha_q}{\alpha_q^2 + \beta_q^2} \end{pmatrix}$$

$$\mathbf{G} = \begin{pmatrix} \mathbf{h}_1^T \\ \vdots \\ \mathbf{h}_q^T \\ \mathbf{g}_1^T \\ \vdots \\ \mathbf{g}_q^T \end{pmatrix}$$

and, for $k = 1, \dots, q$

$$\begin{aligned} \alpha_k &= [\rho_k^{-2} \cos(\omega_k) \ 2\rho_k^{-3} \cos(2\omega_k) \ \cdots \ p \rho_k^{-p-1} \cos(p\omega_k)] \mathbf{a} \\ \beta_k &= [\rho_k^{-2} \sin(\omega_k) \ 2\rho_k^{-3} \sin(2\omega_k) \ \cdots \ p \rho_k^{-p-1} \sin(p\omega_k)] \mathbf{a} \\ \mathbf{g}_k &= [\rho_k^{-2} \sin(\omega_k) \ \rho_k^{-3} \sin(2\omega_k) \ \cdots \ \rho_k^{-p-1} \sin(p\omega_k)]^T \\ \mathbf{h}_k &= [\rho_k^{-2} \cos(\omega_k) \ \rho_k^{-3} \cos(2\omega_k) \ \cdots \ \rho_k^{-p-1} \cos(p\omega_k)]^T \end{aligned}$$

Consequently, we end up with the following asymptotic distribution:

$$\sqrt{N}(\hat{\omega} - \omega) \xrightarrow{as} \mathcal{N}\left(\mathbf{0}, \mathbf{FGR}_p^{-1} \mathbf{S} \mathbf{R}_p^{-1} \mathbf{G}^T \mathbf{F}^T\right)$$

3.3.3. Estimation of a noisy cisoid by MUSIC

Many estimators, for example, the MLE, are obtained by minimization of a function, that is to say:

$$\hat{\theta}_N = \arg \min_{\theta} J_N(\theta)$$

where the criterion $J_N(\theta)$ depends directly either on the data or on the estimated correlation function. In general, the approach to derive the performances of the estimator consists of expanding the derivative of the criteria into a Taylor series and using the asymptotic arguments presented earlier. This is the case of the MUSIC algorithm presented in Chapter 8 for which the frequencies are determined as the arguments that minimize the square norm of the projection of $\mathbf{a}(\omega)$ on the estimated noise subspace $\hat{\mathbf{V}}_b$:

$$J_N(\omega) = \frac{1}{2} |\hat{\Pi}_b^H \mathbf{a}(\omega)|^2, \quad \hat{\Pi}_b = \hat{\mathbf{V}}_b \hat{\mathbf{V}}_b^H \quad [3.31]$$

In what follows, we provide the main steps for analysis of MUSIC in the single component case:

$$x(n) = A e^{j\omega_0 n} + b(n)$$

For a general derivation the reader is referred, for example, to [STO 91]. Let $\hat{\omega}$ be the minimizer of equation [3.31]. The convergence of $\hat{\omega}$ toward ω_0 allows us to use a Taylor expansion of $J'_N(\hat{\omega})$ near ω_0 :

$$0 = J'_N(\omega_0) + J''_N(\omega_0)(\hat{\omega} - \omega_0) + \dots$$

Under a first-order assumption, the error on the estimation of ω_0 is approximately:

$$\hat{\omega} - \omega_0 \simeq -J'_N(\omega_0)/J''_N(\omega_0) \quad [3.32]$$

where:

$$\begin{aligned} J'_N(\omega_0) &= \operatorname{Re} \left\{ \mathbf{a}(\omega)^H \hat{\Pi}_b \mathbf{d}(\omega) \right\} \\ J''_N(\omega_0) &= \operatorname{Re} \left\{ \mathbf{a}(\omega)^H \hat{\Pi}_b \mathbf{d}'(\omega) + \mathbf{d}(\omega)^H \hat{\Pi}_b \mathbf{d}(\omega) \right\} \end{aligned}$$

The first- and second-order derivatives of $J_N(\omega)$ at $\omega = \omega_0$ can be simplified using the perturbation analysis of projection operators presented in [KRI 96]:

$$\hat{\Pi}_b = \Pi_b + \delta \Pi_b + \dots$$

– Convergence of projection $\hat{\Pi}_b$ toward Π_b allows one to write:

$$\begin{aligned} J''_N(\omega_0) &\simeq \operatorname{Re} \{ \mathbf{a}(\omega)^H \Pi_b \mathbf{d}'(\omega) + \mathbf{d}(\omega)^H \Pi_b \mathbf{d}(\omega) \} \\ &= \operatorname{Re} \{ \mathbf{d}(\omega)^H \Pi_b \mathbf{d}(\omega) \} = 2\operatorname{Re} \left\{ \mathbf{d}(\omega)^H (\mathbf{I} - \mathbf{V}_s \mathbf{V}_s^H) \mathbf{d}(\omega) \right\} \quad [3.33] \\ &= M(M^2 - 1)/12 \end{aligned}$$

– Retaining only the first term in projector expansion we have:

$$J'_N(\omega_0) \simeq \operatorname{Re} \{ \mathbf{a}(\omega)^H \delta \Pi_b \mathbf{d}(\omega) \} \quad [3.34]$$

with:

$$\delta \Pi_b = -\Pi_s(\hat{\mathbf{R}} - \mathbf{R})S^\# - S^\# \Delta(\hat{\mathbf{R}} - \mathbf{R})\Pi_s, \quad S = |A|^2 \mathbf{a}(\omega) \mathbf{a}(\omega)^H$$

and $S^\#$ is the pseudo-inverse of S .

By substituting equations [3.34] and [3.33] in [3.32] we obtain an expression of the error on $\hat{\omega}$ as a function of $\hat{\mathbf{R}} - \mathbf{R}$. Consequently, this derivation leads to an expression of the variance of $\hat{\omega}$ as a function of the variance of $\hat{\mathbf{R}}$. Then, asymptotic arguments such as the ones in Results 3.4–3.6 help complete the calculation of the asymptotic variance of $\hat{\omega}$, see [STO 91] for a detailed analysis.

3.3.4. Conclusion

In this chapter, we studied the techniques to carry out the statistical analysis of estimators commonly used in spectral analysis. The approach generally consists of relating the estimation errors on the parameters θ to the estimation errors on the moments of the signal and use the asymptotic arguments based on Taylor expansions. If this approach does not cover all the possible cases, it provides answers to a large number of problems of spectral analysis. The books mentioned in the bibliography contain helpful information on how to tackle other possible cases.

3.4. Bibliography

- [AND 71] ANDERSON T.W., *The Statistical Analysis of Time Series*, John Wiley, New York, 1971.
- [BRI 81] BRILLINGER D.R., *Time Series: Data Analysis and Theory*, McGraw-Hill, 1981.
- [BRO 91] BROCKWELL P.J., DAVIS R.A., *Time Series: Theory and Methods*, Springer Series in Statistics, Springer-Verlag, Berlin, 2nd edition, 1991.

- [DAN 95] DANDAWATÉ A.D., GIANNAKIS G.B., “Asymptotic theory of k th-order cyclic moment and cumulant statistics”, *IEEE Transactions on Information Theory*, vol. 41, no. 1, pp. 216–232, January 1995.
- [DZH 86] DZHAPARIDZE K., *Parameter Estimation and Hypothesis Testing in Spectral Analysis of Stationary Time Series*, Springer-Verlag, New York, 1986.
- [ERI 93] ERIKSSON A., STOICA P., SÖDERSTRÖM T., “Second-order properties of MUSIC and ESPRIT estimates of sinusoidal frequencies in high SNR scenarios”, *IEE Proceedings F Radar and Signal Processing*, vol. 140, no. 4, pp. 266–272, August 1993.
- [FRI 84a] FRIEDLANDER B., “On the computation of the Cramer-Rao bound for ARMA parameter estimation”, *IEEE Transactions on Acoustics, Speech and Signal Processing*, vol. 32, no. 4, pp. 721–727, August 1984.
- [FRI 84b] FRIEDLANDER B., PORAT B., “A general lower bound for parametric spectrum estimation”, *IEEE Transactions on Acoustics, Speech and Signal Processing*, vol. 32, no. 4, pp. 728–733, August 1984.
- [FRI 89] FRIEDLANDER B., PORAT B., “The exact Cramer-Rao bound for Gaussian autoregressive processes”, *IEEE Transactions on Aerospace and Electronic Systems*, vol. 25, no. 1, pp. 3–8, January 1989.
- [KAY 93] KAY S.M., *Fundamentals of Statistical Signal Processing: Estimation Theory*, Prentice Hall, Englewood Cliffs, NJ, 1993.
- [KHA 87] KHATRI C.G., RAO C.R., “Effects of estimated noise covariance matrix in optimal signal detection”, *IEEE Transactions on Acoustics, Speech and Signal Processing*, vol. 35, no. 5, pp. 671–679, May 1987.
- [KRI 96] KRIM H., FORSTER P., “Projections on unstructured subspaces”, *IEEE Transactions on Signal Processing*, vol. 44, no. 10, pp. 2634–2637, October 1996.
- [LAC 97] LACOUME J.-L., AMBLARD P.-O., COMON P., *Statistiques d'Ordre Supérieur pour le Traitement du Signal*, Masson, Paris, 1997.
- [MAD 00] MADSEN A.H., “On the existence of efficient estimators”, *IEEE Transactions on Signal Processing*, vol. 48, no. 11, pp. 3028–3031, November 2000.
- [MUI 82] MUIRHEAD R.J., *Aspects of Multivariate Statistical Theory*, John Wiley, Hoboken, NJ, 1982.
- [POR 94] PORAT B., *Digital Processing of Random Signals: Theory & Methods*, Prentice Hall, Englewood Cliffs, NJ, 1994.
- [PRI 94] PRIESTLEY M.B., *Spectral Analysis and Time Series*, Monographs and Textbooks, Academic Press, 8th edition, 1994.
- [REE 74] REED I.S., MALLETT J.D., BRENNAN L.E., “Rapid convergence rate in adaptive arrays”, *IEEE Transactions on Aerospace and Electronic Systems*, vol. 10, no. 6, pp. 853–863, November 1974.
- [RIF 74] RIFE D.C., BOORSTYN R.R., “Single-tone parameter estimation from discrete-time observations”, *IEEE Transactions on Information Theory*, vol. 20, no. 5, pp. 591–598, September 1974.

- [SCH 91] SCHARF L.L., *Statistical Signal Processing: Detection, Estimation and Time Series Analysis*, Addison Wesley, Reading, MA, 1991.
- [SÖD 89] SÖDERSTRÖM T., STOICA P., *System Identification*, Prentice Hall International, London, UK, 1989.
- [STO 89a] STOICA P., SÖDERSTRÖM T., TI F.N., “Overdetermined Yule–Walker estimation of the frequencies of multiple sinusoids: accuracy aspects”, *Signal Processing*, vol. 16, no. 2, pp. 155–174, February 1989.
- [STO 89b] STOICA P., SÖDERSTRÖM T., TI F.N., “Asymptotic properties of the high-order Yule–Walker estimates of sinusoidal frequencies”, *IEEE Transactions on Acoustics, Speech and Signal Processing*, vol. 37, no. 11, pp. 1721–1734, November 1989.
- [STO 91] STOICA P., SÖDERSTRÖM T., “Statistical analysis of MUSIC and subspace rotation estimates of sinusoidal frequencies”, *IEEE Transactions on Signal Processing*, vol. 39, no. 8, pp. 1836–1847, August 1991.
- [STO 98] STOICA P., “Asymptomania?”, *IEEE Signal Processing Magazine*, vol. 15, no. 1, pp. 16, January 1998.
- [TAG 94] TAGUE J.A., CALDWELL C.I., “Expectations of useful complex Wishart forms”, *Multidimensional Systems and Signal Processing*, vol. 5, pp. 263–279, 1994.
- [TRE 71] VAN TREES H.L., *Detection, Estimation and Modulation Theory*, John Wiley, New York, 1971.
- [TRE 85] TRETTER S.A., “Estimating the frequency of a noisy sinusoid by linear regression”, *IEEE Transactions on Information Theory*, vol. 31, no. 6, pp. 832–835, November 1985.
- [WHI 62] WHITTLE P., “Gaussian estimation in stationary time series”, *Bulletin of the International Statistical Institute*, vol. 39, pp. 105–129, 1962.

Chapter 4

Time-Series Models

4.1. Introduction

The time series $x(k)$, during the processing of a signal, generally comes from the periodic sampling of a continuous time signal $x(t)$, that is to say:

$$x(k) \triangleq x(t)|_{t=kT_c}$$

The main idea of the models of such a series is to suggest a dynamic equation, which takes into account the time dependence variation of $x(k)$ most often in terms of its past $\{x(k-1), x(k-2), \dots, x(-\infty)\}$. This equation can take into account any future values of $m > k$, but the processing real time constraints can be limited to causal dynamic equations:

$$x(k) = F[x(k-1), x(k-2), \dots, x(-\infty)] \quad [4.1]$$

The operator $F[\cdot]$ can be of a varied nature – linear, nonlinear, finite or non-finite dimension, etc.

The practical use of such dynamic equations is to obtain compact expression (thus $F[\cdot]$ in finite dimension) equipped with a set of parameters θ , which help adapt

Chapter written by Francis CASTANIÉ.

this model. $F[x(k-1), x(k-2), \dots, x(-\infty), \theta]$ has a certain variety of each actual signal. The effectiveness of a model will be measured on the one hand in a range of signal classes of which it can model the variation with considerable accuracy, and on the other hand on the number of characteristics of the signal that it can model.

If equation [4.1] represents no physical reality (which will practically always be the case), the adjustment of the model to a physical signal can only be done in the case of a precise criterion of accuracy applied to a characteristic of the signal, which is also precise and limited. We will see later in this section that if a model is fitted to respect the characteristics at the M -order of the signal (e.g. moments), it will not adjust itself to characteristics of a different order or laws, etc.

Thus, the choice of a model is very important and never easy: it affects the actual success of methods, which result from its use.

As part of the current book, the model must also provide a relation between the parameters θ and the spectral properties to be measured. If, e.g. we are interested in the power spectral density (PSD) $S_x(f)$ of $x(t)$, the model retained $F[x(k-1), x(k-2), \dots, x(-\infty), \theta]$ must satisfy the relation:

$$\theta \Rightarrow S_x(f, \theta) \quad [4.2]$$

All estimators $\hat{\theta}$ of θ can thus provide a corresponding estimator of $S_x(f)$ from a relation of the type:

$$\hat{S}_x(f) \triangleq \hat{S}_x(f, \hat{\theta}) \quad [4.3]$$

This approach must be verified for all the spectral characteristics of interest: stationary or non-stationary PSD and energy spectral density (ESD), multispectra, etc.

The fundamental problem that such an approach poses in the context of spectral analysis is to evaluate how the estimation errors on $\hat{\theta}$ will affect $\hat{S}_x(f)$. The tools present in section 3.4 make it possible to tackle it as a particular case of an estimator function, and by a limited expansion to evaluate the bias, variance, covariances, etc. of $\hat{S}_x(f)$ from the equivalent characteristics of $\hat{\theta}$. The application to the model known as *autoregressive* given in section 3.4.1 is a paradigm of this type of problem.

From among the models, the most classical models are strongly linked to “system” representation of the signal: the signal observed $x(k)$ is conceptually

represented as the output of a system, fed by an input $u(k)$. We select an input as neutral as possible, which is described by a restricted number of parameters, the largest number of parameters possible being carried by the transfer function such as the one represented in Figure 4.1.

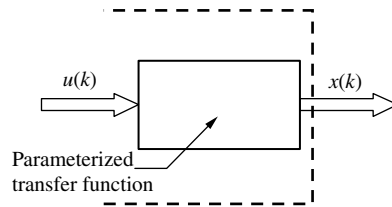


Figure 4.1. Modeling “system” approach

This approach was historically decisive for signal processing, then for images: all identification tools, essentially developed by the control engineer, and to a lesser degree in numerical analysis where it can be used to solve the main problem, which is that of estimation of parameters of the model that help adjust $x(k)$ to the physical signal. The difference (and additional difficulty) with the problem of identification of the systems is that the virtual input $u(k)$ is not physically accessible. Thus, we will have to base ourselves only on the observation of $x(k)$ to build the estimators. The hypotheses, which we will make on the transfer function of the system, will help classify the models: we will discuss the linear or nonlinear, stationary or non-stationary models, etc. according to the corresponding properties of the system. As for the inputs, they will be selected for their “neutrality”, that is to say they would limit the class $x(k)$ generated as much as possible: the most current would be the null mean white noise, but we will also find excitations derived from a series of periodic pulses (such as voice models), from a finite set of pulses (multi-pulse models), or even a single pulse, etc.

4.2. Linear models

When the system shown in Figure 4.1 is linear, the very large set of results on this class of systems can be used: this is a very strong motive to accept the limitation to this particular case and we will discover that it will provide a class of very efficient models. The system could be invariant by translation or otherwise. In the first case, it could lead to models of stationary signals, if $u(k)$ itself is stationary; in the second case, we would have access to non-stationary models otherwise known as “evolutionary”.

4.2.1. Stationary linear models

If we suppose that the system shown in Figure 4.1 is invariant and linear, with an impulse response $\{h(k)\}$, and thus of transmittance in z :

$$\check{h}(z) \triangleq ZT(h(k)) \quad [4.4]$$

we know that the input–output relation may be written as:

$$x(k) = u \otimes h(k) = \sum_{m=-\infty}^{+\infty} u(m)h(m-k) \quad [4.5]$$

which may be reduced to:

$$x(k) = \sum_{m=-\infty}^k u(m)h(m-k) = \sum_{m=0}^{+\infty} h(m)u(m-k) \quad [4.6]$$

if we limit ourselves to the causal models.

The system is rigorously defined by an infinity of parameters $\{h(k)\}$, except if we further reduce to finite impulse response (FIR) systems [BEL 89, NAJ 02]. This limited case known as moving average (MA) models will be tackled later.

To help have a more general system, but which is however defined by a *finite* number of parameters, to this day only one solution is known to us: the system is described by a linear recurrence of finite order, with constant coefficients:

$$x(k) = -\sum_{n=1}^p a_n x(k-n) + \sum_{n=0}^q b_n u(k-n) \quad [4.7]$$

This corresponds to a transmittance, which is a rational fraction:

$$\check{h}(z) = \frac{\sum_{n=0}^q b_n z^{-n}}{\sum_{n=0}^p a_n z^{-n}} \quad a_0 = 1 \quad [4.8]$$

The parameter vector θ_h of the system is in this case:

$$\theta_h^T = |a_1 \cdots a_p \ b_0 \cdots b_q|$$

with $\dim(\theta_h) = p + q + 1$.

This consists of an infinite impulse response (IIR) filter, according to the usual system theory terminology. The link between this parameter vector of finite length and the impulse response of infinite length $\{h(k)\}$ appearing in equation [4.5] is visible when we expand into a series:

$$\check{h}(z) = \frac{\sum_{n=0}^q b_n z^{-n}}{\sum_{n=0}^p a_n z^{-n}} = \sum_{n=0}^{+\infty} h(n) z^{-n} \quad [4.9]$$

which will not be reduced to a polynomial except for a trivial case when the numerator is divisible by the denominator.

The particular case of FIR mentioned earlier is only the one where $a_n = 0$ for $n \neq 0$. In this case, the transmittance can be written in the form of a polynomial:

$$\check{h}(z) = \sum_{n=0}^q b_n z^{-n} = \sum_{n=0}^q h(n) z^{-n} \quad [4.10]$$

We note that if the input $u(k)$ is considered inaccessible (it is a virtual input), but some of its probabilistic characteristics are known, we can perhaps calculate some probabilistic characteristics of $x(k)$, considering that we know how the said characteristics propagate through an invariant linear system. The simplest case is when we are only interested in the second-order characteristics (Wiener–Lee relations; [KAY 88, MAR 87]), which may be written in discrete time as:

$$\begin{aligned} S_x(z) &= S_u(z) \check{h}(z) \check{h}^*(\frac{1}{z^*}) \text{ for } z \in \mathbb{C} \\ S_x(e^{i2\pi\nu}) &= S_u(e^{i2\pi\nu}) \left| \check{h}(e^{i2\pi\nu}) \right|^2 \text{ for } z = e^{i2\pi\nu} \end{aligned} \quad [4.11]$$

It is no doubt compelling to take for $S_u(z)$, the simplest PSD possible:

$$S_u(z) = C^{te} = \sigma^2$$

that is to say for $u(k) = n(k)$ a *zero mean white noise*. In this case, the PSD can be written as:

$$S_x(e^{i2\pi\nu}) = \sigma^2 |\tilde{h}(e^{i2\pi\nu})|^2 \quad [4.12]$$

which we can write to demonstrate the role of the parameter vector:

$$S_x(e^{i2\pi\nu}, \theta_h) = \sigma^2 |\tilde{h}(e^{i2\pi\nu}, \theta_h)|^2 \quad [4.13]$$

The complete parameter vector, including the single scalar parameter of the input is thus:

$$\theta = \left| \sigma^2 \theta_h^T \right|^T = \left| \sigma^2 a_1 \cdots a_p b_0 \cdots b_q \right|^T \quad [4.14]$$

This type of model of a recursive system of finite order excited by a stationary and null mean white noise is strictly speaking (see [BOX 70]) a model known as ARMA (for AutoRegressive with Adjusted Mean), noted as ARMA (p,q). However, we will find the name ARMA more widely accepted in literature, once the system complies with equation [4.7] for an input, which is not necessarily a white noise. The case of the FIR system is noted as MA, the recursion terms (or autoregressive) having disappeared.

We can clearly see in equation [4.13] the role that the free parameters θ play: they help conform to PSD of $x(k)$, in the particular framework of rational spectra (in fact rational trigonometric spectra). It is also clear that if we imagine an estimation method of θ , which helps adjust the PSD of a model to that of a physical signal (which will be dealt with in Chapter 6), this will not imply anything (in all generality) as for the adjustment of other characteristics, such as higher statistics, laws, etc.

4.2.2. Properties

4.2.2.1. Stationarity

We can show [BOX 70, KAY 88] that the stationarity of $x(k)$ is only linked to the stability of the linear system (it is understood that the excitation $\eta(k)$ is itself stationary): all stable systems will lead to a stationary model. Thus the stationary condition is equivalent to the stability condition, which implies that the $\{a_n\}$ in:

$$\check{h}(z) = \frac{\sum_{n=0}^q b_n z^{-n}}{\sum_{n=0}^p a_n z^{-n}} = \frac{B(z)}{A(z)}$$

written under polar form:

$$\{a_n\} \Rightarrow A(z) = \sum_{n=0}^p a_n z^{-n} = \prod_{n=1}^p (1 - p_n z^{-1}) \Rightarrow \{p_n\}$$

are such that:

$$|p_n| < 1 \quad \forall n \quad [4.15]$$

4.2.2.2. Moments and spectra

If we limit ourselves to zero mean signals, the general theorems given in Chapter 1 on the multispectra make it possible to obtain the general relation [NIK 93]:

$$S_{xx \dots x}(v_1, \dots, v_{n-1}) = S_{nn \dots n}(v_1, \dots, v_{n-1}) \cdot H(v_1, \dots, v_{n-1}) \quad [4.16]$$

with:

$$H(v_1, \dots, v_{n-1}) = \check{h}(\exp(i2\pi v_1)) \dots \check{h}(\exp(i2\pi v_{n-1})) \check{h}^*(\exp(i2\pi[v_1 + \dots + v_{n-1}]))$$

If we consider the whiteness of the excitation $n(k)$ at the considered order:

$$S_{nn \dots n}(v_1, \dots, v_{n-1}) = C_{nn \dots n}(0, \dots, 0) \quad \forall v_1, \dots, v_{n-1}$$

we obtain an expression, which generalizes equation [4.12] to all orders. This helps obtain useful spectral relations for this book. However, the equation for generating the signal $x(k)$ of equation [4.7] helps write a direct fundamental relation on the moments.

To start with, let us consider the autocorrelation function of $x(k)$, $\gamma_{xx}(m)$. It is easy to directly show [KAY 88] from equation [4.7] that:

$$\begin{aligned}
\gamma_{xx}(m) &= E(x(k)x^*(k-m)) \\
&= \sum_{n=1}^p a_n \gamma_{xx}(m-n) + \sigma^2 \sum_{n=m}^q b_n h^*(m-n) \quad 0 \leq m \leq q \\
&= \sum_{n=1}^p a_n \gamma_{xx}(m-n) \quad m \geq q+1
\end{aligned} \tag{4.17}$$

The last line of this equation has many applications: it shows that if we consider the correlation function $\gamma_{xx}(m)$ only for $m \geq q+1$, the recurrence (identical to the recursive part of the equation of the signal itself) establishes a very simple link between the correlation and the AR $\{a_k\}$ parameters. In the form of a matrix, for $m = K, K+1, \dots, K+p-1$ ($\forall K \geq q+1$) it may be written as:

$$\mathbf{R}\mathbf{a} = -\mathbf{r} \tag{4.18}$$

with:

$$\mathbf{R} = \begin{vmatrix} \gamma_{xx}(K-1) & \cdots & \gamma_{xx}(K-p) \\ \gamma_{xx}(K) & \cdots & \gamma_{xx}(K-p+1) \\ \vdots & \ddots & \vdots \\ \gamma_{xx}(K+p-2) & \cdots & \gamma_{xx}(K-1) \end{vmatrix}$$

and:

$$\mathbf{r} = \begin{vmatrix} \gamma_{xx}(K) \\ \gamma_{xx}(K+1) \\ \vdots \\ \gamma_{xx}(K+p-1) \end{vmatrix}$$

This allows us to know a if we know a sufficient interval of $\gamma_{xx}(m)$, by inverting equation [4.18] under regularity conditions of \mathbf{R} : it will be the Yule–Walker relation, which is the key to most of the estimators with AR parameters (section 6.2):

$$\mathbf{a} = -\mathbf{R}^{-1}\mathbf{r} \tag{4.19}$$

We will note that the matrix to be inverted has a very particular structure known as Toeplitz:

$$[\mathbf{R}]_{ij} = \gamma_{xx}(K - 1 + i - j)$$

and, as a result, rapid inversion algorithms exist [BOX 70, KAY 88].

System of linear equations, rapid algorithms: all the components were assembled in this equation to create a historical success!

The relations between the MA $\{b_n\}$ parameters and the correlation function cannot be directly used from equation [4.17]: this relation shows a combination between these parameters and the coefficients of the impulse response, which is in itself a nonlinear combination of $\{b_n\}$ and $\{a_n\}$. Section 6.2 suggests methods for resolutions, which are essentially nonlinear.

In the case of the pure AR(p) model, which is particularly important for the applications (that is to say with $b_0 = 1, b_1 = \dots = b_q = 0$), we can select $K = 1$ in the Yule–Walker equations: the matrix \mathbf{R} is the most symmetrical.

4.2.2.3. Relation with Wold's decomposition

For example, it is shown in [LAC 00], that *all* second-order stationary random processes, with some conditions of regularity, may be written in the form:

$$x(k) = \sum_{n=0}^{\infty} c_n \xi(k-n) + v(k) \quad [4.20]$$

where the series of $\{\xi(n)\}$ is a series of non-correlated variables (noted as *innovations*), the series of coefficients $\{c_n\}$ is determined by projection techniques, and the term “singular” $v(k)$ has the special feature of being exactly predictable from its past.

This extremely general decomposition is Wold's decomposition.

The singular term $v(k)$ represents a *deterministic* signal (it is one of the definitions, among many, of the determinism of signals). If we exclude it from the model, the rest of the decomposition is similar to equation [4.5]: the series $\{\xi(n)\}$ is a white noise series, and the coefficients $\{c_n\}$ play the role of pulse response coefficients. Can we say that any stationary random signal (which has a Wold's decomposition) is an ARMA signal?

This is often found in literature, but is wrong: if we limit equation [4.20] in the case of $v(k) = 0 \forall k$, we obtain a common convolution equation:

$$x(k) = c \otimes \xi(k)$$

and if ZT $\check{\xi}(z)$ of $\xi(k)$ exists, it plays the role of a transmittance. The fundamental difference with the transmittance $\check{h}(z)$ defining the ARMA model is that $\check{\xi}(z)$ is not, generally, a rational fraction.

There are many examples of non-rational PSD signals in physics: spectra of turbulence signals, signals with long dependence and a fractal nature, etc. [ABR 02].

However, we see that the ARMA models will be powerful approximants of stationary signals, at least in their spectral characteristics, because the theory of rational approximation states that we can always approximate a function $\xi(z)$ as closely as we want, under relatively large convergence constraints, by a rational fraction of sufficient p and q degrees. This supports the common practical approach, which is to approximate the PSD of a physical signal by a series of the ARMA (p, q) models of increasing orders, until some fidelity criterion on the PSD of the model is satisfied (see Chapter 6).

4.2.3. Non-stationary linear models

The general way of writing a non-stationary linear model is as follows:

$$x(k) = \sum_l h(l, k) u(l) \quad [4.21]$$

where the pulse response $h(l, k)$ is not reduced to a kernel with 1 dimension $h(l - k)$ as in the translation invariant case.

If we reduce the class of the models we are interested in to non-correlated excitations ($u(l) = n(l)$ is a white noise of power σ^2), we obtain a simple relation on the correlation functions:

$$\begin{aligned} R_{xx}(k, m) &= E[x(k)x^*(m)] = \sigma^2 \left\{ \sum_l h(l, k) h^*(l, m) \right\} \\ &= \sigma^2 H(k, m) = \sigma^2 \check{H}(k, k - m) \end{aligned}$$

The first question is to decide a definition of an “*evolutive spectrum*”, because, as mentioned in section 1.2.2, the beautiful uniqueness of the definition of PSD does

not exist outside the stationary framework: Chapter 9 of this book gives an introduction to this problem and a complete study can be found in another book of the same treatise [HLA 05]. Whatever this definition may be, it is based on a two-dimensional Fourier transform of $H(k, m)$ or on one of its versions, such that $\tilde{H}(k, k - m)$.

The non-stationary linear models must therefore present systems with pulse responses having two variables, equipped with a vector of parameter θ , which helps, as in the stationary case, to adjust them to the spectral characteristics of physical signals.

There are several approaches to destationarize the system, which is at the heart of the model:

- 1) We can select an unstable system: to destabilize the system is to generate a non-stationary model.
- 2) We can use inputs that are non-stationary.
- 3) The parametric system in itself can be selected as *varying*, that is to say it is no more limited to being a translation system.

And, of course, the combination of the three possibilities.

The first solution has limited possibilities: in fact, to destabilize the model, we cannot push one or more poles outside or on the unit circle.

A pole outside the unit circle results in an exponential instability, which is very “explosive” for most applications. The poles that are exactly on the unit circle can lead to purely periodic or polynomial instabilities: they are the root of the ARIMA models which are introduced in [BOX 70] (see Chapter 6 and [HLA 05]).

The non-stationary inputs change the problem: how can this non-stationarity be easily described and parameterized? The *multi-pulse* models are one of the pragmatic approaches to this problem (see a brief introduction in section 9.3.2).

A more attractive “system” approach consists of using linear filters with time variable parameters: in equation [4.7], the parameters $\{a_n, b_n\}$ become time functions k . What follows is a possible way of writing:

$$x(k) = - \sum_{n=1}^p a_n(k-n)x(k-n) + \sum_{n=0}^q b_n(k-n)u(k-n) \quad [4.22]$$

If the excitation $u(k)$ is a centered stationary white noise $n(k)$, some properties of the ARMA models of the previous paragraph can be generalized, which will be presented in section 6.1. These models are known as *evolutionary ARMA*.

A main problem still needs to be resolved: the parameterization. The time-varying filter and all its characteristics, such as the impulse response, are known if we know function sets $\{a_n(k), b_n(k)\}$. Thus, a suitable parameterization of these families needs to be found, which can be either deterministic or random. If we limit ourselves to the case of deterministic functions, the standard approach consists of projecting them on a finite set of functions. If we select a set of base functions $\{f_m(k)\}$, the projection may be written as:

$$a_n(k) = \sum_{m=1}^M a_{nm} f_m(k) \quad [4.23]$$

$$b_n(k) = \sum_{m=1}^M b_{nm} f_m(k)$$

and the global parameter vector of the model is now:

$$\theta = [a_{11} a_{12} \cdots a_{1M} a_{21} a_{22} \cdots a_{2M} \cdots a_{pM}]^T \quad [4.24]$$

One of the key properties of these models is the extension of the Yule–Walker theorem, applied to the following vectors:

$$\mathbf{x}(k) = \begin{bmatrix} f_1(k)x(k) \\ \vdots \\ f_M(k)x(k) \end{bmatrix} \text{ and } \mathbf{u}(k) = \begin{bmatrix} f_1(k)u(k) \\ \vdots \\ f_M(k)u(k) \end{bmatrix}$$

and:

$$\mathbf{a}_n = \begin{bmatrix} a_{n0} \\ \vdots \\ a_{nM} \end{bmatrix} \text{ and } \mathbf{b}_n = \begin{bmatrix} b_{n0} \\ \vdots \\ b_{nM} \end{bmatrix}$$

which leads to the following way of writing a dynamic model:

$$x(k) = -\sum_{n=1}^p \mathbf{a}_n^T \mathbf{x}(k-n) + \sum_{n=0}^q \mathbf{b}_n^T \mathbf{u}(k-n) \quad [4.25]$$

This equation helps write an expression of the Yule–Walker type:

$$\begin{aligned} E & \left[\begin{pmatrix} x(k-1) \\ \vdots \\ x(k-p) \end{pmatrix} \left(x^T(k-1) \cdots x^T(k-p) \right) \theta \right] \\ & = -E \left[\begin{pmatrix} x(k-1) \\ \vdots \\ x(k-p) \end{pmatrix} x(k) \right] \end{aligned}$$

which is also a basic tool with which we define estimators of parameter vector θ from equation [4.24].

4.3. Exponential models

A class of models with special focus on signal processing: these are the complex exponential base decompositions.

The main reason is the property that these functions are eigenfunctions of invariant linear systems. The exponential models are historically created by Prony (1795), and were unearthed and revived in the 1970s by Kumaresan and Tufts [KUM 82, KAY 88, MAR 87]. They can be broken down into deterministic, noisy deterministic, and random models.

4.3.1. Deterministic model

Supposing we can write a (deterministic) signal in the form of:

$$x(k) = \begin{cases} \sum_{m=1}^p B_m z_m^k & \text{for } k \geq 0 \\ 0 & \text{for } k < 0 \end{cases} \quad [4.26]$$

The parameters of this model belong to two families:

1) The “poles” $\{z_m\}$, which carry the frequency f_m and damping α_m information:

$$z_m = e^{-\alpha_m} e^{-j2\pi f_m}$$

2) The “complex amplitudes” $\{B_m\}$, which carry the amplitude A_m and phase information ϕ_m :

$$B_m = A_m e^{j\phi_m}$$

We can show that the deterministic signal of equation [4.26] verifies a recursion:

$$x(k) = - \sum_{n=1}^p a_n x(k-n) \quad \text{for } k \geq p \quad [4.27]$$

where the coefficients $\{a_n\}$ are linked to the only poles $\{z_m\}$ in the following manner:

$$\begin{aligned} \bar{a}(z) &\triangleq \sum_{n=0}^p a_n z^{-n} = \prod_{m=1}^p (1 - z_m z^{-1}) \\ &\text{with } a_0 = 1 \end{aligned} \quad [4.28]$$

We see that finding the poles $\{z_m\}$ by knowing the signal is relatively easy, in two steps:

1) From equation [4.27], a group of p values of $x(k)$ help express a linear system whose vector $\mathbf{a} = [a_1 \dots a_p]^T$ is the solution:

$$\mathbf{a} = -\mathbf{X}^{-1} \mathbf{x}_p$$

$$\mathbf{X} = \begin{pmatrix} x(p-1) & \cdots & x(0) \\ \vdots & \ddots & \vdots \\ x(2p-2) & \cdots & x(p-1) \end{pmatrix} \quad \text{and} \quad \mathbf{x}_p = \begin{pmatrix} x(p) \\ \vdots \\ x(2p-1) \end{pmatrix} \quad [4.29]$$

2) The expression of the polynomial $\bar{a}(z)$ of equation [4.28] and the solution (numerical) of its roots help obtain the $\{z_m\}$:

$$\mathbf{a} \Rightarrow \bar{a}(z) = 0 \Rightarrow \{z_m\} \quad [4.30]$$

The resolution of complex amplitudes associated to each pole leads to a simple linear problem (the model of equation [4.26] is linear in $\{B_m\}$ if the $\{z_m\}$ is known):

$$\mathbf{B} = \mathbf{V}^{-1} \mathbf{x}_0 \quad [4.31]$$

with $\mathbf{V} = [z_m^k]$ and $\mathbf{x}_0 = [x(0) \dots x(p-1)]^T$.

It can be noted that if we limit some poles to being of unit modulus $|z_m| = 1$, this makes it possible to include the sine waves studied (that is to say undamped) in the model. Such a customization is important for numerous applications, and is closer to the methods presented in Chapter 8. Such a model is known as *harmonic Prony*.

4.3.2. Noisy deterministic model

If we now consider a noisy model:

$$\begin{aligned} x(k) &= \sum_{m=1}^p B_m z_m^k + n(k) k \geq 0 \\ &= s(k) + n(k) \end{aligned}$$

then the previous approach, however, can no longer be applied. But it is legitimate to look for an estimator $\hat{s}(k)$ of $s(k)$. For this, we will use the same steps used previously, but the exact resolutions of linear systems appearing in equations [4.29] and [4.31] will be implemented on the overdetermined systems, in the least-squares sense so as to minimize the influence of the noise term $n(k)$.

From this estimator $s(k)$:

$$\hat{s}(k) \triangleq \sum_{m=1}^p \hat{B}_m \hat{z}_m^k$$

will follow a (deterministic) spectral estimator, because:

$$\bar{s}(z) = \sum_{m=1}^p \frac{\hat{B}_m}{\left(1 - \hat{z}_m z^{-1}\right)}$$

The relation required from equation [4.2] is thus established.

4.3.3. Models of random stationary signals

It is not efficient to apply the approach mentioned above to the implementations of stationary random signals, because the morphology of the model itself is not suitable: a set of decreasing exponentials will be designed for the signals of

“transient” form, but unsuitable for the implementation of “permanent” signals. Similarly, the increasing exponentials will not be suitable.

However, the moments or cumulants are deterministic functions, which are made up of decreasing or almost periodic terms: a family of complex exponentials is well suited for this situation.

For example, for a second-order analysis, any estimator of the correlation function can be written as:

$$\hat{\gamma}_{xx}(k) = \gamma_{xx}(k) + \varepsilon(k)$$

where $\varepsilon(k)$ is the estimation error (see section 3.2 for its statistical properties), $\gamma_{xx}(\tau)$ has a hermitian symmetry $\gamma_{xx}(-k) = \gamma_{xx}^*(k)$, and thus a one-sided model of the following type may be used:

$$\gamma_{xx}(k) = \sum_{m=1}^p B_m z_m^k \quad k \geq 0$$

completed by symmetry, to gain access to the expression of the PSD (using a bilateral z transform of $\gamma_{xx}(k)$):

$$S_{xx}(z) = \sum_{m=1}^p B_m \frac{1 - z_m^2}{(1 - z_m z^{-1})(1 - z_m z)} \quad [4.32]$$

4.4. Nonlinear models

There is a strong interest for this class of models, which help express a very large morphological variability for the signals, much greater than the linear or exponential models. The basic principle remains the same, with a finite dynamic equation:

$$x(k) = F[x(k-1), x(k-2), \dots, x(k-P), u(k), \dots, u(k-Q), \theta]$$

excited by a neutral deterministic or random input.

The models can be characterized by the sub-classes of operators $F[.]$ used, and their relation to the properties of the model. The predictive qualities of these models are mainly the objective of their study.

For this book, these models present a major difficulty: we generally do not know the relation between the operator $F[.]$, the parameters of the model θ , and the spectral characteristics (PSD, etc.). Thus, to date, they are not tools for spectral analysis.

An inquisitive or avid reader can consult the references [PRI 91] and mainly [TON 90].

4.5. Bibliography

- [ABR 02] ABRY P., GONÇALVES P., LEVY-VEHEL J., *Lois d'échelle, fractales et ondelettes*, IC2 series, vol. 2, Hermès Sciences, Paris, 2002.
- [BEL 89] BELLANGER M., *Signal Analysis and Adaptive Digital Filtering*, Masson, 1989.
- [BOX 70] BOX G., JENKINS G., *Time Series Analysis, Forecasting and Control*, Holden-Day, San Francisco, 1970.
- [HLA 05] HLAWATSCH F., AUGER F. (eds), *Time-Frequency Analysis*, ISTE Ltd, London, John Wiley & Sons, New York, 2008.
- [KAY 88] KAY S.M., *Modem Spectral Estimation: Theory and Applications*, Prentice Hall, Englewood Cliffs, NJ, 1988.
- [KUM 82] KUMARESAN R., TUFTS D., “Estimating the parameters of exponentially damped sinusoids and pole-zero modeling in noise”, *IEEE Transactions on Acoustics Speech and Signal Processing*, vol. 30, no. 6, pp. 833–840, December 1982.
- [LAC 00] LACAZE B., *Processus aléatoires pour les communications numériques*, Hermès Science, Paris, 2000.
- [MAR 87] MARPLE S., *Digital Spectral Analysis with Applications*, Prentice Hall, Englewood Cliffs, NJ, 1987.
- [NAJ 02] NAJIM M., *Traitements numériques des signaux*, Hermès Science, Paris, 2002.
- [NIK 93] NIKIAS C., PETROPULU A., *Higher-Order Spectra Analysis*, Prentice Hall, 1993.
- [PRI 91] PRIESTLEY M., *Non-linear and Non-stationary Time Series Analysis*, Academic Press, 1991.
- [TON 90] TONG H., *Non-linear Time Series*, Oxford Science Publications, 1990.

PART 2

Non-Parametric Methods

Chapter 5

Non-Parametric Methods

5.1. Introduction

A random discrete time signal $\mathbf{x}(k), k \in Z$ is stationary in the wide sense if its mean m_x and its autocorrelation function $r_{xx}(\kappa)$ defined by:

$$\begin{cases} m_x = E(\mathbf{x}(k)) \\ r_{xx}(\kappa) = E((\mathbf{x}(k) - m_x)^*(\mathbf{x}(k + \kappa) - m_x)) \end{cases} \quad \forall \kappa \in Z \quad [5.1]$$

are independent of the index k , that is to say, independent of the time origin. $\sigma_x^2 = r_{xx}(0)$ is the variance of the considered signal. $\frac{r_{xx}(\kappa)}{\sigma_x^2}$ is the correlation coefficient between the signal at time k and the signal at time $k + \kappa$. Usually we limit ourselves only to the average and the autocorrelation function to characterize a random stationary signal, even though this second-order characterization is very incomplete [NIK 93].

Chapter written by Éric LE CARPENTIER.

Practically, we have only one realization $x(k), k \in Z$ of a random signal $\mathbf{x}(k)$, for which we can define its time average $\langle x(k) \rangle$:

$$\langle x(k) \rangle = \lim_{N \rightarrow \infty} \frac{1}{2N+1} \sum_{k=-N}^N x(k) \quad [5.2]$$

The random signal $\mathbf{x}(k)$ is known as ergodic for the mean if the mean m_x is equal to the time average of any realization $x(k)$ of this random signal:

$$E(x(k)) = \langle x(k) \rangle \text{ ergodicity for the mean} \quad [5.3]$$

Subsequently, we suppose that the random signal $\mathbf{x}(k)$ is ergodic for the mean and, to simplify, of zero mean.

The random signal $\mathbf{x}(k)$ is ergodic for the autocorrelation if the autocorrelation function $r_{xx}(\kappa)$ is equal to the time average $\langle x^*(k)x(k+\kappa) \rangle$ calculated from any characterization $x(k)$ of this random signal:

$$E(x^*(k)x(k+\kappa)) = \langle x^*(k)x(k+\kappa) \rangle \quad \forall \kappa \in Z \quad [5.4]$$

ergodicity for the autocorrelation.

This time average being defined for all values of κ by:

$$\langle x^*(k)x(k+\kappa) \rangle = \lim_{N \rightarrow \infty} \frac{1}{2N+1} \sum_{k=-N}^N x^*(k)x(k+\kappa) \quad [5.5]$$

The simplest example of an ergodic stationary random signal for the autocorrelation is the cisoid $ae^{j(2\pi\nu_0 k + \phi)}$, $k \in Z$ with initial phase ϕ uniformly distributed between 0 and 2π , of the autocorrelation function $a^2 e^{j2\pi\nu_0 k}$, $\kappa \in Z$. However, the ergodicity is lost if the amplitude is also random. In practice, the ergodicity can rarely be rigorously verified. Generally, it is a hypothesis necessary to deduce the second-order static characteristics of the random signal considered from a single realization.

Under the ergodic hypothesis, the variance σ_x^2 of the signal considered is equal to the power $\langle |x(k)|^2 \rangle$ of all the characterizations x :

$$\sigma_x^2 = \langle |x(k)|^2 \rangle = \lim_{N \rightarrow \infty} \frac{1}{2N+1} \sum_{k=-N}^N |x(k)|^2 \quad [5.6]$$

That is to say, the energy of the signal x multiplied by the truncation window $1_{[-N,N]}$ is equal to 1 over the interval $\{-N, \dots, N\}$ and zero outside, divided by the length of this interval, when $N \rightarrow +\infty$. From Parseval's theorem, we obtain:

$$\begin{aligned}\sigma_x^2 &= \lim_{N \rightarrow \infty} \frac{1}{2N+1} \int_{-\frac{1}{2}}^{+\frac{1}{2}} |\widehat{x1}_{[-N,N]}(\nu)|^2 d\nu \\ &= \int_{-1/2}^{+1/2} \left\{ \lim_{N \rightarrow \infty} \frac{1}{2N+1} |\widehat{x1}_{[-N,N]}(\nu)|^2 \right\} d\nu\end{aligned}\quad [5.7]$$

Thus, from equation [5.7], we have broken down the power of the signal on the frequency axis using the $\nu \mapsto \lim_{N \rightarrow \infty} \frac{1}{2N+1} |\widehat{x1}_{[-N,N]}(\nu)|^2$ function. In many books, the spectral density of the power of a random signal is defined by this function. In spite of the ergodic hypothesis, we can show that this function depends on the characterization considered. Here, we will define the power spectral density (or power spectrum) S_{xx} as the overall average of this function:

$$S_{xx}(\nu) = \lim_{N \rightarrow \infty} E\left(\frac{1}{2N+1} |\widehat{x1}_{[-N,N]}(\nu)|^2\right) \quad [5.8]$$

$$= \lim_{N \rightarrow \infty} E\left(\frac{1}{2N+1} \left| \sum_{k=-N}^N x(k) e^{-j 2\pi \nu k} \right|^2\right) \quad [5.9]$$

Thus, we have two characterizations of a stationary random signal in the wide sense, ergodic for the autocorrelation. Wiener–Khinchine theorem makes it possible to show the equivalence of these two characterizations. Under the hypothesis the series $(\kappa r_{zz}(\kappa))$ is summable, i.e.:

$$\sum_{\kappa=-\infty}^{+\infty} |\kappa r_{zz}(\kappa)| < \infty \quad [5.10]$$

Thus, the power spectral density is the Fourier transform of the autocorrelation function: the two characterizations defined earlier coincide:

$$S_{xx}(\nu) = \hat{r}_{xx}(\nu) \quad [5.11]$$

$$= \sum_{\kappa=-\infty}^{+\infty} r_{xx}(\kappa) e^{-j 2\pi \nu \kappa} \quad [5.12]$$

This theorem can be demonstrated in the following manner: by expanding expression [5.9], we obtain:

$$S_{xx}(\nu) = \lim_{N \rightarrow \infty} E\left(\frac{1}{2N+1} \sum_{n=-N}^N \sum_{k=-N}^N x(n)x^*(k)e^{-j 2\pi \nu (n-k)} \right)$$

From the linearity of the mathematical expectation operator and using the definition of the autocorrelation function:

$$S_{xx}(\nu) = \lim_{N \rightarrow \infty} \frac{1}{2N+1} \sum_{n=-N}^N \sum_{k=-N}^N r_{xx}(n-k)e^{-j 2\pi \nu (n-k)}$$

By changing the variable $\kappa = n - k$, the cardinal of the set $\{(n, k) \mid \kappa = n - k \text{ and } |n| \leq N \text{ and } |k| \leq N\}$ is $2N + 1 - |\kappa|$:

$$S_{xx}(\nu) = \lim_{N \rightarrow \infty} \frac{1}{2N+1} \sum_{\kappa=-2N}^{2N} (2N+1-|\kappa|) r_{xx}(\kappa) e^{-j 2\pi \nu \kappa}$$

Finally we obtain:

$$\begin{aligned} S_{xx}(\nu) &= \lim_{N \rightarrow \infty} \sum_{\kappa=-2N}^{2N} \left(1 - \frac{|\kappa|}{2N+1} \right) r_{xx}(\kappa) e^{-j 2\pi \nu \kappa} \\ &= \hat{r}_{xx}(\nu) - \lim_{N \rightarrow \infty} \frac{1}{2N+1} \sum_{\kappa=-2N}^{2N} |\kappa| r_{xx}(\kappa) e^{-j 2\pi \nu \kappa} \end{aligned}$$

Under hypothesis [5.10], the second term mentioned above disappears, and we obtain equation [5.12].

These considerations can be taken up succinctly for continuous time signals. A random discrete time signal $x(t)$, $t \in \mathfrak{R}$ is said to be stationary in the wide sense if its average m_x and its autocorrelation function $r_{xx}(\tau)$ defined by:

$$\begin{cases} m_x = E(x(t)) \\ r_{xx}(\tau) = E((x(t) - m_x)^*(x(t + \tau) - m_x)) \end{cases} \quad \forall \tau \in \mathfrak{R} \quad [5.13]$$

are independent of the time t .

For a characterization $x(t)$, $t \in \mathfrak{R}$ of a random signal $\mathbf{x}(t)$, the time average $\langle x(t) \rangle$ is defined by:

$$\langle x(t) \rangle = \lim_{T \rightarrow \infty} \frac{1}{2T} \int_{-T}^T x(t) dt \quad [5.14]$$

The ergodicity for the mean can be written as:

$$E(x(t)) = \langle x(t) \rangle \quad [5.15]$$

Subsequently, we will suppose that the random signal $x(t)$ is ergodic for the mean and, to simplify, of zero mean.

The random signal $x(t)$ is ergodic for the autocorrelation if:

$$E(x^*(t)x(t+\tau)) = \langle x^*(t)x(t+\tau) \rangle \quad \forall \tau \in \Re \quad [5.16]$$

This time average is defined for all values of τ by:

$$\langle x^*(t)x(t+\tau) \rangle = \lim_{T \rightarrow \infty} \frac{1}{2T} \int_{-T}^T x^*(t)x(t+\tau) dt \quad [5.17]$$

The power spectral density S_{xx} can then be expressed by:

$$S_{xx}(f) = \lim_{T \rightarrow \infty} E\left(\frac{1}{2T} \left| \widehat{x}_{1-T,T}(f) \right|^2\right) \quad [5.18]$$

$$= \lim_{T \rightarrow \infty} E\left(\frac{1}{2T} \left| \int_{-T}^T x(t) e^{-j 2\pi f t} dt \right|^2\right) \quad [5.19]$$

If the function $(\tau r_{xx}(\tau))$ is summable, i.e.:

$$\int_{-\infty}^{+\infty} |\tau r_{xx}(\tau)| d\tau < \infty \quad [5.20]$$

then the power spectral density is the Fourier transform of the autocorrelation function:

$$S_{xx}(f) = \hat{r}_{xx}(f) \quad [5.21]$$

$$= \int_{-\infty}^{+\infty} r_{xx}(\tau) e^{-j 2\pi f \tau} d\tau \quad [5.22]$$

In both cases (continuous and discrete), we can show that if a linear system invariant over time of pulse response h is excited by a stationary random signal of the autocorrelation function r_{xx} and spectrum S_{xx} , the autocorrelation function r_{yy} and the spectrum S_{yy} of the filter signal $y = h \otimes x$ can be expressed by:

$$r_{yy} = h^{-*} \otimes h \otimes r_{xx} \quad [5.23]$$

$$S_{yy} = |h|^2 S_{xx} \quad [5.24]$$

5.2. Estimation of the power spectral density

Under the hypothesis of a continuous or discrete time random signal \mathbf{x} ergodic for the autocorrelation verifying hypothesis [5.10], and using a recording of finite length $x(t), 0 \leq t \leq T$ or $x(k), 0 \leq k \leq N - 1$ of a realization x , we attempt to obtain an estimator of power spectral density S_{xx} , where we can obtain the static characteristics (bias, variance, correlation) as well as the resolution, that is to say the capacity of the estimator to separate the spectral contributions of two narrow band components, e.g. two cisoids.

The filter bank method (see section 5.2.1), used in analog spectrum analyzers, is more naturally used in the analysis of continuous time signals. The periodogram method (see section 5.2.2) and its variants (see section 5.2.3) are used for the analysis of discrete time signals, and are generally calculated using the fast Fourier transform (FFT) algorithms.

5.2.1. Filter bank method

The power spectral density describes the distribution of power along the frequency axis. Thus, to estimate this density, it is natural to filter the signal observed $x(t)$ by a band-pass filter bank of impulse response h_ℓ whose center frequencies f_ℓ are distributed along the frequency axis. Thus, the power P_ℓ of ℓ^e filter signal $y_\ell = h_\ell \otimes x$ equals:

$$P_\ell = \int_{-\infty}^{+\infty} S_{y_\ell y_\ell}(f) df \quad [5.25]$$

$$= \int_{-\infty}^{+\infty} |\hat{h}_\ell(f)|^2 S_{xx}(f) df \quad [5.26]$$

If the power spectral density S_{xx} does not vary much in the bandwidth of the ℓ^e filter, then:

$$P_\ell \approx S_{xx}(f_\ell) \int_{-\infty}^{+\infty} |\hat{h}_\ell(f)|^2 df \quad [5.27]$$

Thus, the power of the output filter ℓ^e , normalized by the energy of the pulse response of this filter, restores the power spectral density in the center frequency, in the case where this density does not vary much in the bandwidth.

In practice, the frequencies of interest are uniformly distributed along the frequency axis:

$$f_\ell = \ell f_1 \quad [5.28]$$

and the filters are obtained by spectral offset of the center low-pass filter on the zero frequency:

$$\hat{h}_\ell(f) = \hat{h}_0(f - f_\ell) \quad [5.29]$$

This condition being fulfilled, the output power y_ℓ , while considering in addition that the transfer function module of the low-pass filter of pulse response h_0 has an even module, can be written as:

$$P_\ell = \int_{-\infty}^{+\infty} |\hat{h}_0(f_\ell - f)|^2 S_{xx}(f) df \quad [5.30]$$

$$= \left(S_{xx} \otimes |\hat{h}_0|^2 \right)(f) \quad [5.31]$$

To ensure that there is no loss of data, we set a filter bank with perfect reconstruction ($x(t) = \sum_\ell y_\ell(t)$), which leads to the following condition:

$$\sum_\ell \hat{h}_\ell(f) = 1 \quad [5.32]$$

or, something less restrictive, that $x(t)$ and $\sum_\ell y_\ell(t)$ have the same power spectral density, such as the condition:

$$\sum_\ell |\hat{h}_\ell(f)|^2 = 1 \quad [5.33]$$

This last condition is more or less fulfilled if the frequential step $f_{\ell+1} - f_\ell = f_1$ is equal to the bandwidth a-3 dB of the filters (interval length $\left\{ f \mid |\hat{h}_0(f)| > \frac{\hat{h}(0)}{\sqrt{2}} \right\}$).

From this analysis, we obtain an estimator of power spectral density using a realization $x(t)$, $0 \leq t \leq T$ from the following sequence of operations:

– *Filtering.* The signal $x(t)$, $0 \leq t \leq T$ is filtered by the bank; we obtain the filter signals $y_\ell(t)$, $0 \leq t \leq T$;

– *Quadrature*. We calculate the instantaneous power of these filter signals, i.e. $|y_\ell(t)|^2$, $0 \leq t \leq T$;

– *Integration*. The power of each filter signal is estimated, without bias, by time averaging the instantaneous power:

$$\bar{P}_\ell = \frac{1}{T} \int_0^T |y_\ell(t)|^2 dt \quad [5.34]$$

– *Normalization*. The estimation of the spectral density is obtained by standardizing the estimated power by the energy of the pulse response of the filters: $E_h = \int_{-\infty}^{+\infty} |\hat{h}_0(f)|^2 df = \int_{-\infty}^{+\infty} h_0^2(t) dt$

$$\bar{S}_{xx}(f_\ell) = \frac{\bar{P}_\ell}{E_h} \quad [5.35]$$

This estimator is approximately without bias when the spectral density S_{xx} does not vary much in a frequential sampling step. For a sine wave $a e^{j(2\pi f_s t + \phi)}$ where ϕ is an initial phase uniformly distributed between 0 and 2π , the spectrum is equal to $a^2 \delta(f - f_s)$; we obtain from equation [5.31] the average value of the spectrum:

$$E(\bar{S}_{xx}(f_\ell)) = a^2 \frac{|\hat{h}_0(f_\ell - f_s)|^2}{E_h}$$

The pulse of the exact spectrum leaks to the adjacent analysis frequencies; this phenomenon is more prominent when the frequential sampling step is large. In a signal made up of narrow and large band components, the spectral contribution of the narrow band components can be masked by the spectral contribution of large band components, and all the more when the center frequency of these narrow band components is farther from an analysis frequency.

5.2.2. Periodogram method

Starting from expression [5.9], it is usual to suggest the following estimator of the power spectral density known as periodogram from a recording of N points:

$$I_{xx}(\nu) = \frac{1}{N} |\widehat{x l_{0,N-1}}(\nu)|^2 \quad [5.36]$$

$$= \frac{1}{N} \left| \sum_{k=0}^{N-1} x(k) e^{-j 2\pi \nu k} \right|^2 \quad [5.37]$$

where $1_{0,N-1}$ is the rectangular window equal to 1 over the interval $\{0, \dots, N-1\}$ and zero outside. In relation to the initial definition of the power spectral density, we have lost the mathematical expectation operator, as well as transition to the limit.

From expression [5.11], it is also natural to suggest the following estimator:

$$I'_{xx}(\nu) = \sum_{\kappa=-N+1}^{N-1} \bar{r}_{xx}(\kappa) e^{-j 2\pi \nu \kappa} \quad [5.38]$$

where \bar{r}_{xx} is a preliminary estimation of the autocorrelation function; the natural estimator of the autocorrelation function is defined by:

$$\bar{r}_{xx}(\kappa) = \begin{cases} \frac{1}{N-\kappa} \sum_{k=0}^{N-\kappa-1} x^*(k) x(k+\kappa) & \text{if } 0 \leq \kappa \leq N-1 \\ \frac{1}{N+\kappa} \sum_{k=-\kappa}^{N-1} x^*(k) x(k+\kappa) & \text{if } -(N-1) \leq \kappa \leq 0 \\ 0 & \text{otherwise} \end{cases} \quad [5.39]$$

We can easily check that this estimator is non-biased over the interval $|\kappa| \leq N-1$. However, we generally prefer using a biased estimator of the autocorrelation function defined by:

$$\bar{r}_{xx}(\kappa) = \begin{cases} \frac{1}{N} \sum_{k=0}^{N-\kappa-1} x^*(k) x(k+\kappa) & \text{if } 0 \leq \kappa \leq N-1 \\ \frac{1}{N} \sum_{k=-\kappa}^{N-1} x^*(k) x(k+\kappa) & \text{if } -(N-1) \leq \kappa \leq 0 \\ 0 & \text{otherwise} \end{cases} \quad [5.40]$$

The average value of this estimator may be written as:

$$E(\bar{r}_{xx}(\kappa)) = B_{-N,N}(\kappa) r_{xx}(\kappa) \quad [5.41]$$

where $B_{-N,N}$ is the even Bartlett window, i.e.:

$$B_{-N,N}(\kappa) = \begin{cases} 1 - \frac{|\kappa|}{N} & \text{if } |\kappa| \leq N-1 \\ 0 & \text{otherwise} \end{cases} \quad [5.42]$$

This estimator, though having a bias, guarantees that the estimation of the Toeplitz Hermitian autocorrelation matrix $\left[\bar{r}_{xx}(\ell-k) \right]_{\substack{1 \leq \ell \leq N \\ 1 \leq k \leq N}}$ is semi-definite positive.

It is easy to show that if the biased estimator of the autocorrelation function is used, then the periodogram and the estimator I'_{xx} are equal.

$$I_{xx} = I'_{xx} \quad [5.43]$$

From equations [5.38] and [5.41], we can immediately deduce that the average value of the periodogram is equal to the circular convolution of the exact spectral density and the Fourier transform of the Bartlett window $B_{-N,N}$.

$$E(I_{xx}) = S_{xx} \otimes \hat{B}_{-N,N} \quad [5.44]$$

where $B_{-N,N}$ can be expressed by (this result is easily obtained by considering $B_{-N,N}$ as the convolution integral of $(1_{0,N-1}(k))_{k \in \mathbb{Z}}$ and $(1_{0,N-1}(-k))_{k \in \mathbb{Z}}$ divided by N):

$$\hat{B}_{-N,N}(\nu) = N \left(\frac{\sin(\pi\nu N)}{N \sin(\pi\nu)} \right)^2 \quad [5.45]$$

This function has a unit integral over a period (by applying Parseval's theorem), and tends toward infinity when N tends toward infinity at integer abscissa. Thus, it tends toward the Dirac comb Ξ_1 of period 1, which is the identity element for the circular convolution integral. Thus, the periodogram is asymptotically unbiased:

$$\lim_{N \rightarrow \infty} E(I_{xx}) = S_{xx} \quad [5.46]$$

For finite N , the convolution of the real spectrum with Bartlett's window can result in a spectral leakage phenomenon. For example, for a cisoid of amplitude a , the frequency ν_0 , of uniformly distributed initial phase between 0 and 2π , the periodogram obtained can be written as $a^2 \hat{B}_{-N,N}(\nu - \nu_0)$. For an addition of two cisoids, the average value of the periodogram obtained is the sum of the contributions of each cisoid. If these two cisoids are of largely different powers, the secondary lobes of Bartlett's window centered on the frequency of the sine wave of high power, that much higher as N is smaller, can mask the main lobe of Bartlett's window centered on the frequency of the sine wave of low power. Thus, the periodogram is less sensitive.

To calculate and draw the periodogram, the frequency axis must be calibrated $[0, 1[$ e.g. using a regular calibration of M points on this interval (with $M \geq N$):

$$\nu \in \left\{ \frac{\ell}{M}, 0 \leq \ell \leq M-1 \right\} \quad [5.47]$$

Thus, we have, for all $\ell \in \{0, \dots, M-1\}$:

$$I_{xx}\left(\frac{\ell}{M}\right) = \frac{1}{N} \left| \sum_{k=0}^{N-1} x(k) e^{-j 2\pi \frac{\ell k}{M}} \right|^2 \quad [5.48]$$

By adding $M - N$ zeros to the series of N available points (*zero-padding*), and by choosing for M a power of 2, we calculate this estimator using FFT algorithms (see Chapter 2).

This aspect provides other interpretations of the periodogram. Let us consider the series of M points (i.e. $(x(0), \dots, x(N-1))$) completed by $M - N$ zeros) contain a period of a periodic signal x_p of period M . This periodic signal can be broken down into a sum of M cisoids of frequencies $\frac{\ell}{M}$, ℓ varying from 0 to $N-1$, of amplitude $|\hat{x}_p(\ell)|$ and initial phase $\arg(\hat{x}_p(\ell))$:

$$x_p(k) = \sum_{\ell=0}^{M-1} \hat{x}_p(\ell) e^{j 2\pi \frac{\ell k}{M}} \quad [5.49]$$

where \hat{x}_p is the discrete Fourier transform of the series x_p , i.e.:

$$\hat{x}_p(\ell) = \frac{1}{M} \sum_{k=0}^{N-1} x(k) e^{-j 2\pi \frac{\ell k}{M}} \quad [5.50]$$

$I_{xx}\left(\frac{\ell}{M}\right)$ is thus to the multiplicative factor $\frac{M^2}{N}$ the power of the sine wave ℓ^e present in this decomposition, that is to say, to the factor $\frac{M}{N}$, the average power spectral density of the signal x_p in the interval of a frequency magnitude $\frac{1}{M}$ centered on $\frac{\ell}{M}$:

$$I_{xx}\left(\frac{\ell}{M}\right) = \frac{M}{N} M |\hat{x}_p(\ell)|^2 \quad [5.51]$$

It is to be noted that the *zero-padding* technique introduces a redundancy in the periodogram. In fact, knowing only its value for multiple frequencies of $\frac{1}{N}$, we can recreate the estimator of the autocorrelation function from the inverse Fourier transform and, from this estimator, calculate the periodogram at any frequency by the direct Fourier transform. The value of the periodogram at $\frac{\ell}{N}$ frequencies with $0 \leq \ell \leq N - 1$ is sufficient. As a result, it is natural to measure the resolution of the periodogram by $\frac{1}{N}$, which is the frequency sampling value of this minimum representation.

The variance of the periodogram is approximately equal to the value of the power spectral density and does not decrease with the length N of the recording (see section 3.3). The periodogram variants, which will be developed in the next section, will reduce this variance. As a result, this procedure leads to a deterioration of the resolution power. This resolution/variance compromise, considered as important before obtaining the spectral parametric estimation, is the main disadvantage of standard methods of spectral analysis.

5.2.3. Periodogram variants

The average periodogram or Bartlett's periodogram consists of splitting the signal of N points into K sections of length $\frac{N}{K}$, to calculate the periodogram on each segment, and then to average the periodograms obtained:

$$\bar{S}_{xx} = \frac{1}{K} \sum_{k=1}^K I_k \quad [5.52]$$

where I_k is the periodogram of the k th segment. If we neglect the dependence between the various segments, we obtain a reduction in the variance by a factor $\frac{1}{K}$ at the cost of a deterioration in the resolution, by $\frac{K}{N}$.

The modified periodogram consists of calculating the periodogram on the signal available $(x(k))_{0 \leq k \leq N-1}$ multiplied by a real truncation window $(w(k))_{k \in \mathbb{Z}}$ zero outside the interval $\{0, \dots, N-1\}$ (see Chapter 2), so as to reduce the spectral leakage and the variance:

$$\bar{S}_{xx} = \frac{1}{NU} \sum_{k=1}^N x(k) w(k) e^{-j 2\pi \nu k} \quad [5.53]$$

where U is a standardization factor designed to ensure that the modified periodogram is asymptotically without bias. From equations [5.37, 5.38], and [5.43], the following formula can be written:

$$\bar{S}_{xx} = \frac{1}{U} \sum_{\kappa=-(N-1)}^{N-1} \bar{r}_{xx}(\kappa) e^{-j 2\pi \nu \kappa} \quad [5.54]$$

where \bar{r}_{xx} can be expressed by:

$$\bar{r}_{xx}(\kappa) = \begin{cases} \frac{1}{N} \sum_{k=0}^{N-\kappa-1} x^*(k) w(k) x(k+\kappa) w(k+\kappa) & \text{if } 0 \leq \kappa \leq N-1 \\ \frac{1}{N} \sum_{k=-\kappa}^{N-1} x^*(k) w(k) x(k+\kappa) w(k+\kappa) & \text{if } -(N-1) \leq \kappa \leq 0 \\ 0 & \text{otherwise} \end{cases} \quad [5.55]$$

We immediately obtain by considering $w^-(k) = w(-k)$:

$$E(\bar{r}_{xx}(\kappa)) = r_{xx}(\kappa) \left(\frac{1}{N} w * w^- \right)(\kappa) \quad [5.56]$$

From the Fourier transform, we obtain:

$$E(\bar{S}_{xx}) = S_{xx} \otimes \left(\frac{1}{NU} |\hat{w}|^2 \right) \quad [5.57]$$

If the function $\frac{1}{NU} |\hat{w}|^2$ is of unit integral over a period, it tends toward the Dirac comb Ξ_1 and the estimator is asymptotically unbiased. By applying Parseval's theorem, this integral is equal to $\frac{1}{NU} \sum_{k=0}^{N-1} w^2(k)$. Thus, the normalization factor U is equal to:

$$U = \frac{1}{N} \sum_{k=0}^{N-1} w^2(k) \quad [5.58]$$

This procedure is also accompanied by a loss in resolution, the main lobe of the Fourier transform of all the windows being larger than the rectangular window.

The Welsh periodogram combines the average periodogram and the modified periodogram. We split the signal with N points available into K sections overlapping L points, calculate the modified periodogram on each segment, and then average the modified periodograms obtained. The deterioration in the resolution is much less and the variance is lower than for $L = 0$; however, the variance does not decrease any further in $\frac{1}{K}$, the different segments are correlated. On a Gaussian sequence, with a Hanning window, we can show that the variance is minimum for $L \approx 0.65K$. Usually $L \approx 0.5K$.

The correlogram, or *windowed periodogram*, consists of a prior estimation of an autocorrelation function using equation [5.38], by applying a real even truncation window w zero outside the interval $\{-(L-1), \dots, (L-1)\}$ ($L < N$) and the Fourier transform W :

$$\bar{S}_{xx}(\nu) = \sum_{\kappa=-(L-1)}^{L-1} \bar{r}_{xx}(\kappa) w(\kappa) e^{-j 2\pi \nu \kappa} \quad [5.59]$$

It is necessary that $w(0) = 1$, so that the power spectral density obtained once again gives the variance $\bar{r}_{xx}(0)$. From the inverse Fourier transform, we obtain:

$$\bar{S}_{xx} = I_{xx} \otimes W \quad [5.60]$$

The windowed periodogram can be considered as a smoothing of the periodogram, which reduces the oscillations caused by the secondary lobes of Bartlett's window and present in the periodogram. If the exact calculation of the variance of the windowed periodogram is difficult, an approximate calculation shows that this variance is approximately multiplied, in relation to the non-windowed periodogram, by the coefficient between 0 and 1 defined by:

$$\frac{1}{N} \sum_{\kappa=-(L-1)}^{L-1} w^2(\kappa)$$

To ensure a positive estimation, it is sufficient to consider a positive Fourier transform truncation window. As a result, Bartlett's window is often used.

Blackman and Tuckey, the sources of the method, recommend $L \approx \frac{N}{10}$.

For example, let us consider a 128-point data sequence of a sum of a sine wave of amplitude 100, frequency 100 Hz, a sine wave of amplitude 100, frequency 109 Hz, a sine wave of amplitude 7, frequency 200 Hz, and a white noise of variance 25 (Figure 5.1).

In the standard periodogram (Figure 5.2(a)), we mainly observe the lobes of Dirichlet's kernel centered on the frequencies of two predominant sine waves,

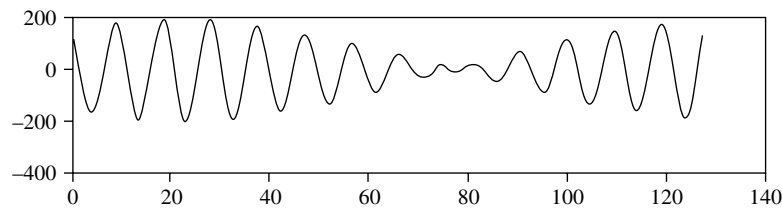


Figure 5.1. Signal

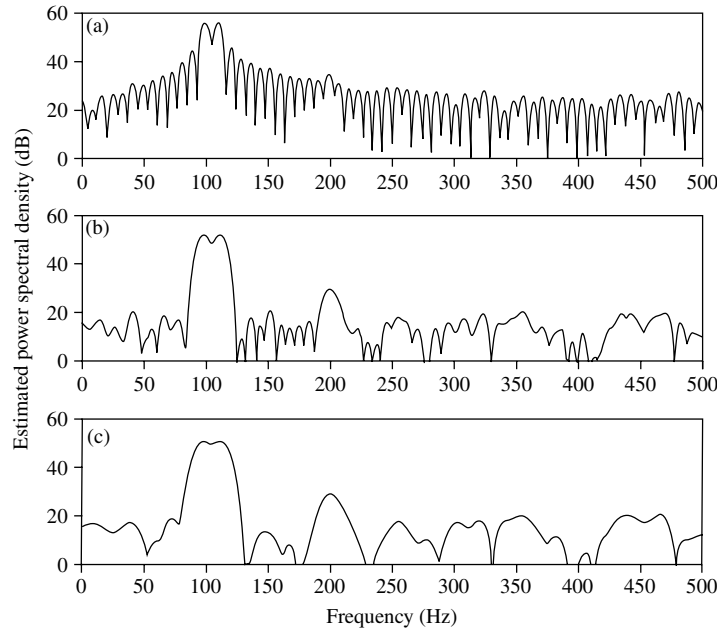


Figure 5.2. Estimated power spectral density: (a) from the periodogram; (b) from the modified periodogram (Hamming's window); (c) from the modified periodogram (Blackman's window)

which mask the spectral contribution of the sine wave of weak amplitude. The use of Hamming's window for the modified periodogram (Figure 5.2(b)) reduces the amplitude of the secondary lobes (at the cost of the enlargement of the main lobe, the two predominant sine waves are less apart) and makes it possible to view the contribution of the third sine wave. With a Blackman's window (Figure 5.2(c)), with a larger bandwidth, but with weaker secondary lobes, these two effects are even more prominent. The averaging effect of Bartlett's or Welsh's periodogram on 3 segments of 64 points is overlapped by 32 points (Figure 5.3), reducing the variance, thus the oscillations of the spectrum in the zones describing the bandwidth contributions of white noise, but from the enlargement of the main lobe, the two dominant sine waves cannot be distinguished any more; it is with Bartlett's window that we faithfully find the bandwidth contribution of the white noise, close to 14 dB (Figure 5.2(c)).

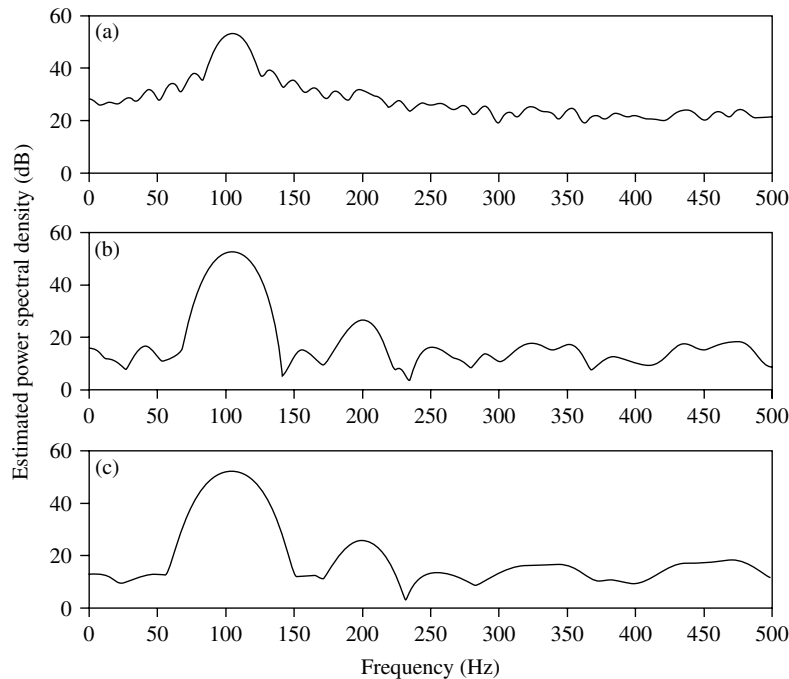


Figure 5.3. Estimated power spectral density (Hamming's window of 64 samples, covering 32 samples): (a) from Bartlett's periodogram; (b) from Welsh's periodogram (Hamming's window); (c) from Welsh's periodogram (Blackman's window)

5.3. Generalization to higher-order spectra

Consider \mathbf{x} as an ergodic and centered stationary random signal. The moment M_n of order n is defined in the following manner; for all values of $\kappa = [\kappa_1 \dots \kappa_{n-1}]^T \in Z_{n-1}$ (also see section 1.2.2.3):

$$M_n(\kappa) = E\left(\mathbf{x}(k) \prod_{i=1}^{n-1} \mathbf{x}(k + \kappa_i)\right) \quad [5.61]$$

The multispectrum S_n of order n is the multidimensional Fourier transform of the moment of order n : for all values of $\nu = [\nu_1 \dots \nu_{n-1}]^T \in \Re^{n-1}$:

$$S_n(\nu) = \sum_{\kappa \in Z^n} M_n(\kappa) e^{j2\pi \nu^T \kappa} \quad [5.62]$$

From a recording of finite length $(x(k))_{0 \leq k \leq N-1}$ of characterization x of a random signal \mathbf{x} , the spectrum S_n can be estimated from the natural estimator:

$$\bar{S}_n(\nu) = \sum_{\kappa \in Z^n} \bar{M}_n(\kappa) e^{j2\pi \nu^T \kappa} \quad [5.63]$$

where \bar{M}_n is a biased estimator of the moment of order n :

$$\bar{M}_n(\kappa) = \frac{1}{N} \sum_k x(k) \prod_{i=1}^{n-1} \mathbf{x}(k + \kappa_i) \quad [5.64]$$

The summation occurring for all values of k between 0 and $N - 1$ and such that for all values of I , $k + k_i$ is between 0 and $N - 1$. This method (which is indirect because it passes from the estimation of the moment) is similar to the correlogram of the second order. In practice, to reduce the variance of this estimator, we will consider the estimated moment as a multidimensional truncation window w_{n-1} , defined by the product of a standard one-dimensional window w :

$$w_{n-1}(\kappa) = \prod_{i=1}^{n-1} w(\kappa_i) \quad [5.65]$$

The other method (which is direct because it operates directly on the data), called periodogram of higher order, is defined in the following manner:

$$\bar{S}_n(\nu) = \frac{1}{N} X * \left(\sum_{i=1}^{n-1} \nu_i \right) \prod_{i=1}^{n-1} X(\nu_i) \quad [5.66]$$

where $X(\nu_i) = \sum_{k=0}^{N-1} x(k) e^{-j 2\pi \nu_i k}$. As it is of the second order, it is useful to carry out an average of the periodograms from different sections of the original signal, and to weight the different sections by a truncation window – Welsh's procedure [NIK 93].

5.4. Bibliography

- [KAY 81] KAY S., MARPLE S., “Spectrum analysis: a modern perspective”, *IEEE Proceedings*, vol. 69, no. 11, pp. 1380–1418, 1981.
- [MAR 87] MARPLE S., Jr., *Digital Spectral Analysis with Applications*, Prentice Hall, 1987.
- [MAX 96] MAX J., LACOUME J., *Méthodes et techniques de traitement du signal et applications aux mesures physiques. Vol. 1: principes généraux et méthodes classiques*, Masson, 1996.
- [NIK 93] NIKIAS C., PETROPULU A., *Higher-Order Spectra Analysis*, Prentice Hall, 1993.
- [OPP 75] OPPENHEIM A., SCHAEFER R., *Digital Signal Processing*, Prentice Hall, 1975.
- [POR 94] PORAT B., *Digital Processing of Random Signals*, Prentice Hall, 1994.

PART 3

Parametric Methods

Chapter 6

Spectral Analysis by Parametric Modeling

When dealing with spectral analysis, Fourier-based methods are the first and basic answer. However, these methods suffer from well-known problems, especially when the observation window of the signal to be analyzed is short, leading to a small amount of signal samples in the presence of a low signal-to-noise ratio (SNR). When faced with these experimental conditions, parametric modeling can be a good alternative for spectral analysis. For that, it is necessary to understand the various existing models, their properties, the estimation methods for their parameters, and the various possible implementations.

In this chapter, we present the various parametric models of stationary processes. Chapter 4 already gave an introduction to this chapter by presenting the models of the time series. The aim of this chapter is to go through these models by tackling their parameter estimation problem as well as their implementation form, with a view to spectral analysis.

6.1. Which kind of parametric models?

In this chapter, two kinds of stationary parametric models are discussed as an alternative to Fourier-based methods for spectral analysis:

- ARMA models, with a particular focus on AR models;
- Prony models.

Chapter written by Corinne MAILHES and Francis CASTANIÉ.

The “geometrical” methods based on the decomposition of a signal sub-space and of a noise sub-space (MUSIC, ESPRIT, etc.), specific to sinusoidal signals, are presented in Chapter 8.

These two models (ARMA and Prony) are presented in Chapter 4 (ARMA models are presented in section 4.2 and Prony model in section 4.3) but to make the reading of this chapter easier, some reminders will be given at the beginning of each section.

6.2. AR modeling

6.2.1. AR modeling as a spectral estimator

Autoregressive modeling (AR) is certainly the most popular analysis in parametric spectral analysis. The AR model of order p of a signal $x(k)$ is given by:

$$x(k) = -\sum_{n=1}^p a_n x(k-n) + u(k) \quad [6.1]$$

in which $u(k)$ represents a zero mean stationary white noise.

Looking for the “best” AR model that fits a given signal $x(k)$ is equivalent to estimating the AR coefficients a_n $n = 1, \dots, p$ and the noise variance σ_u^2 which minimize some specific error criterion between the model and the signal (usually a least square one). The problem of AR parameter estimation will be discussed in the following paragraph. Anyway, once AR parameters are estimated, AR modeling can be used for spectral estimation. Considering that [6.1] can be viewed as a modeling of the signal $x(k)$ as the output of an all-pole filter excited by the white noise sequence $u(k)$, the AR spectral estimator is of the form:

$$S_{AR}(f) = \frac{\sigma_u^2}{\left|1 + \sum_{n=1}^p a_n e^{-i2\pi f n}\right|^2} \quad [6.2]$$

6.2.2. Estimation of AR parameters

Let us consider a signal $x(k)$, $k = 0, \dots, N - 1$, which has to be modeled using [6.1]. Classical methods for estimating autoregressive coefficients consist of minimizing the Linear Prediction Error (LPE) in the mean square sense. By considering the recursion equation [6.1], a linear predictor of the signal can be

built in both forward and backward directions. The forward predictor $\hat{x}(k)$ of $x(k)$ is defined by:

$$\hat{x}(k) = -\sum_{n=1}^p a_n x(k-n) \quad [6.3]$$

The forward linear prediction error is then defined by:

$$e(k) = x(k) - \hat{x}(k) = x(k) + \sum_{n=1}^p a_n x(k-n) \quad [6.4]$$

and the error of backward linear prediction by:

$$b(k) = x(k-p-1) + \sum_{n=1}^p a_{p+1-n} x(k-n) \quad [6.5]$$

The parameters $\text{AR}\{a_n\}_{n=1,p}$ are estimated so that they minimize the following quadratic criterion:

$$\min_{a_n} \left\{ \sigma_e^2 = \sum_{k=p}^{N-1} |e(k)|^2 \right\} \quad [6.6]$$

and/or the equivalent backward criterion $\min_{a_n} \{\sigma_b^2\}$.

If the signal of interest is an AR model and can be written as [6.1] with an order p_1 , it can be shown [KAY 88] that the coefficients minimizing such criteria are good estimators of the coefficients $\{a_n\}$ of [6.1] if the order of the chosen model p is equal to p_1 .

The solution of this least-squares problem is expressed in the following way:

$$\hat{\mathbf{a}} = -(\mathbf{X}^H \mathbf{X})^{-1} \mathbf{X}^H \mathbf{x} \quad \text{with } \hat{\mathbf{a}} = \begin{bmatrix} \hat{a}_1 \\ \vdots \\ \hat{a}_p \end{bmatrix} \quad [6.7]$$

Depending on the chosen minimization window the matrices and the vectors \mathbf{X} and \mathbf{x} are defined in different ways. In the case where:

$$\mathbf{X} = \mathbf{X}_1 = \begin{bmatrix} x(p-1) & \cdots & x(0) \\ \vdots & \ddots & \vdots \\ x(N-2) & \cdots & x(N-p-1) \end{bmatrix} \quad \mathbf{x} = \mathbf{x}_1 = \begin{bmatrix} x(p) \\ \vdots \\ x(N-1) \end{bmatrix} \quad [6.8]$$

this estimation method is improperly called the *covariance method* because the matrix $\mathbf{X}_1^H \mathbf{X}_1$ and the vector $\mathbf{X}_1^H \mathbf{x}_1$ are estimations of covariances with one normalizing coefficient. Morf has given an order recursive algorithm making it possible to calculate this solution without explicit inversion of the matrix [KAY 88, MOR 77].

By adopting a least-squares solution, which minimizes the forward [6.6] and backward sum of the prediction errors, we choose:

$$\mathbf{X} = \mathbf{X}_2 = \begin{bmatrix} x^*(N-p) & \cdots & x^*(N-1) \\ \vdots & \ddots & \vdots \\ x^*(p) & \cdots & x^*(1) \\ x(p-1) & \cdots & x(0) \\ \vdots & \ddots & \vdots \\ x(N-2) & \cdots & x(N-p-1) \end{bmatrix} \quad [6.9]$$

$$\mathbf{x} = \mathbf{x}_2 = \begin{bmatrix} x^*(N-p-1) \\ \vdots \\ x^*(0) \\ x(p) \\ \vdots \\ x(N-1) \end{bmatrix}$$

This is the *modified covariance method* and it is generally more efficient than the covariance method. Sometimes it is also called the maximum entropy method [LAN 80] because it is a particular case when the noise is Gaussian. Burg developed an order recursive algorithm making it possible to obtain the reflection coefficients that minimize the sum of the forward and backward prediction errors, which makes it possible to deduce the *AR* parameters [BUR 75] via the Levinson–Durbin recursion. The advantage of this algorithm is that the estimated poles are always inside or on the unit circle. Its main disadvantages are a spectral line splitting in the case of a signal made up of a noisy sinusoid with a strong SNR and sensitivity at the initial phase [SWI 80, WIL 93]. This sensitivity at the phase can be simply highlighted by considering the particular case of the following signal:

$$x(k) = \cos(2\pi fk + \phi) + u(k)$$

In this case, the AR parameters are estimated using:

$$\hat{\mathbf{a}} = \begin{bmatrix} \hat{a}_1 \\ \hat{a}_2 \end{bmatrix} = - \begin{bmatrix} x(1) & x(0) \\ x(2) & x(1) \end{bmatrix}^{-1} \begin{bmatrix} x(2) \\ x(3) \end{bmatrix} \quad [6.10]$$

The sensitivity of the solution $\hat{\mathbf{a}}$ is evaluated through the conditioning κ of the system [6.10] [GOL 89]:

$$\kappa = \frac{\lambda_{\max}}{\lambda_{\min}} \quad [6.11]$$

where λ_{\max} and λ_{\min} are the eigenvalues of the following matrix:

$$\begin{aligned} & \begin{bmatrix} \cos(2\pi f + \phi) & \cos(\phi) \\ \cos(4\pi fn + \phi) & \cos(2\pi f + \phi) \end{bmatrix} \\ & \Rightarrow \begin{cases} \lambda_{\max} = \cos(2\pi f + \phi) + \sqrt{\cos(\phi)\cos(4\pi f + \phi)} \\ \lambda_{\min} = \cos(2\pi f + \phi) - \sqrt{\cos(\phi)\cos(4\pi f + \phi)} \end{cases} \quad [6.12] \end{aligned}$$

The difference between these two eigenvalues impacts on the extent of the errors in $\hat{\mathbf{a}}$. It is evident that when $\phi = \frac{\pi}{2}$, the eigenvalues are identical and the errors in $\hat{\mathbf{a}}$ are minimal. When the estimation of the AR parameters is realized in the least-squares sense, the sensitivity at the initial phases of the sinusoids diminishes but it can remain important if the number of samples is small.

But the estimation of the AR parameters of an AR model of order p can also be done starting from:

$$\gamma_{xx}(m) = E[x(k)x^*(k-m)] = - \sum_{n=1}^p a_n \gamma_{xx}(m-n) + \sigma_u^2 \delta(m) \quad [6.13]$$

which we call *Yule–Walker* equations that were already mentioned in Chapter 4. This result shows that the autocorrelation of $x(k)$ satisfies the same recursion as the signal. A large number of estimation methods solves the Yule–Walker equations by replacing the theoretic autocorrelation $\gamma_{xx}(m)$ by an estimation $\hat{\gamma}_{xx}(m)$:

$$\hat{\mathbf{a}} = - \underbrace{\begin{bmatrix} \hat{\gamma}_{xx}(0) & \hat{\gamma}_{xx}^*(1) & \cdots & \hat{\gamma}_{xx}^*(p-1) \\ \hat{\gamma}_{xx}(1) & \hat{\gamma}_{xx}(0) & \cdots & \hat{\gamma}_{xx}^*(p) \\ \vdots & \ddots & \ddots & \vdots \\ \hat{\gamma}_{xx}(p-1) & \cdots & \cdots & \hat{\gamma}_{xx}(0) \end{bmatrix}}_{\hat{\mathbf{R}}_x^{-1}}^{-1} \underbrace{\begin{bmatrix} \hat{\gamma}_{xx}(1) \\ \hat{\gamma}_{xx}(2) \\ \vdots \\ \hat{\gamma}_{xx}(p) \end{bmatrix}}_{\hat{\mathbf{r}}_x} \quad [6.14]$$

It is the *autocorrelation method* and $\hat{\mathbf{R}}_x$ is the (estimated) autocorrelation matrix. When $\hat{\gamma}_{xx}(m)$ is the biased estimator of the correlation, the poles are always inside the unit circle, which is not the case with the unbiased estimator which gives, however, a better estimation. The Levinson–Durbin algorithm [LEV 47] provides an order recursive solution of system [6.14] in $O(p^2)$ computational burden. To reduce the noise influence and to obtain a better estimation, the system [6.14] can use a larger number of equations ($>> p$) and be solved in the least-squares sense (LS) or in the total least-squares sense (TLS) [VAN 91]. These methods are called LSYW and TLSYW (see [DUC 98]):

$$\begin{aligned} \text{LSYW} \quad \hat{\mathbf{a}} &= -\left(\hat{\mathbf{R}}_x^H \hat{\mathbf{R}}_x\right)^{-1} \hat{\mathbf{R}}_x^H \hat{\mathbf{r}}_x \\ \text{TLSYW} \quad \hat{\mathbf{a}} &= -\left(\hat{\mathbf{R}}_x^H \hat{\mathbf{R}}_x - \sigma_{\min}^2 \mathbf{I}\right)^{-1} \hat{\mathbf{R}}_x^H \hat{\mathbf{r}}_x \\ \hat{\mathbf{R}}_x &= \begin{bmatrix} \hat{\gamma}_{xx}(0) & \cdots & \hat{\gamma}_{xx}^*(p-1) \\ \vdots & \ddots & \vdots \\ \hat{\gamma}_{xx}(N_0-1) & \cdots & \hat{\gamma}_{xx}(N_0-p) \end{bmatrix} \quad \hat{\mathbf{r}}_x = \begin{bmatrix} \hat{\gamma}_{xx}(1) \\ \vdots \\ \hat{\gamma}_{xx}(N_0) \end{bmatrix} \end{aligned} \quad [6.15]$$

where σ_{\min} is the smaller singular value of the matrix $[\hat{\mathbf{R}}_x \hat{\mathbf{r}}_x]$, \mathbf{I} the identity matrix, and N_0 the number of equations. The value of N_0 should be at most of the order of $\frac{N}{2}$ when the unbiased estimator of the correlation is used so as not to make correlations with a strong variance intervene.

The TLS solution is more efficient than the LS method because it minimizes the errors in $\hat{\mathbf{r}}_x$ and in $\hat{\mathbf{R}}_x$ at the same time, but it presents a disadvantage which we will encounter later. It is generally better to envisage a calculation of the LS and TLS solutions via the singular value decomposition (SVD) of the matrix $\hat{\mathbf{R}}_x$:

$$\hat{\mathbf{R}}_x = \hat{\mathbf{U}}_p \hat{\Sigma}_p \hat{\mathbf{V}}_p^H \quad \text{with } \hat{\Sigma}_p = \text{diag}(\hat{\sigma}_1, \dots, \hat{\sigma}_p) \text{ and } \hat{\sigma}_k \geq \hat{\sigma}_{k+1}$$

This is particularly interesting in the case of an ill-conditioned system because the SVD proves a greater numeric stability. The LS and TLS solutions calculated by the SVD are:

$$\begin{aligned} \text{LSYW} \quad \hat{\mathbf{a}} &= -\hat{\mathbf{V}}_p \left(\hat{\Sigma}_p \right)^{-1} \hat{\mathbf{U}}_p^H \hat{\mathbf{r}}_x \quad \left(\hat{\Sigma}_p \right)^{-1} = \text{diag} \left(\frac{1}{\hat{\sigma}_1}, \dots, \frac{1}{\hat{\sigma}_p} \right) \\ \text{TLSYW} \quad \begin{bmatrix} \hat{\mathbf{a}} \\ 1 \end{bmatrix} &= \frac{\mathbf{v}_{p+1}}{\mathbf{v}_{p+1}(p+1)} \end{aligned} \quad [6.16]$$

where \mathbf{v}_{p+1} is the eigenvector associated with the smallest eigenvalue of the matrix $\left[\hat{\mathbf{R}}_x \hat{\mathbf{r}}_x \right]^H \left[\hat{\mathbf{R}}_x \hat{\mathbf{r}}_x \right]$, i.e. the $(p+1)$ th column vector of the matrix $\hat{\mathbf{V}}_{p+1}$ so that $\left[\hat{\mathbf{R}}_x \hat{\mathbf{r}}_x \right] = \hat{\mathbf{U}}_{p+1} \hat{\Sigma}_{p+1} \hat{\mathbf{V}}_{p+1}^H$.

There exists an extension of the Levinson–Durbin algorithm for solving LSYW, it is what we call the least-squares *lattice* [MAK 77, PRO 92]. The interest of this algorithm is that it is time and order recursive, which makes it possible to implement parameter estimation adaptive procedures.

We can very easily notice that these methods are biased because the correlation at 0th lag makes the power of the white noise σ_u^2 intervene. The approached value of this bias for [6.14] is:

$$\begin{aligned} \hat{\mathbf{a}} &= -\left(\hat{\mathbf{R}}_{x-u} + \sigma_u^2 I \right)^{-1} \hat{\mathbf{r}}_{x-u} \\ \hat{\mathbf{a}} &\approx \mathbf{a} + \sigma_u^2 \hat{\mathbf{R}}_{x-u}^{-2} \hat{\mathbf{r}}_{x-u} = \mathbf{a} - \sigma_u^2 \hat{\mathbf{R}}_{x-u}^{-1} \mathbf{a} \end{aligned} \quad [6.17]$$

where $x - u$ is the noiseless signal. Certain methods [KAY 80, SAK 79] exploit this relation in order to try to eliminate this bias, but these require an estimation of σ_u^2 . The simplest solution for obtaining a non-biased estimation of the *AR* parameters consists of not making the zero lag correlation intervene in the estimation:

$$\hat{\mathbf{a}} = -\begin{bmatrix} \hat{\gamma}_{xx}(p) & \cdots & \hat{\gamma}_{xx}(1) \\ \vdots & \ddots & \vdots \\ \hat{\gamma}_{xx}(2p-1) & \cdots & \hat{\gamma}_{xx}(p) \end{bmatrix}^{-1} \begin{bmatrix} \hat{\gamma}_{xx}(p+1) \\ \vdots \\ \hat{\gamma}_{xx}(2p) \end{bmatrix} \quad [6.18]$$

That is called the modified Yule–Walker method (MYW). When we solve this system in the classic or total least-squares sense, we call these methods LSMYW

and TLSMYW [STO 92]. When the signal $x(k)$ is really an AR(p), these estimators are asymptotically unbiased ($N \rightarrow \infty$). However, if $x(k)$ is made up of a sum of sinusoids and white noise, the MYW estimators are also asymptotically unbiased [GIN 85].

The case of a colored noise slightly modifies the MYW estimators. The hypothesis that the noise $u(k)$ is a moving average process (MA) of order q is the most common:

$$u(k) = \sum_{n=0}^q b_n \varepsilon(k-n) \quad [6.19]$$

where $\varepsilon(n)$ is a zero mean Gaussian white noise. In this case, the correlation $\gamma_{xx}(m)$ of $u(k)$ is null when $m > q$. Thus, an estimator of the AR parameters of the signal $x(n)$ which can be viewed as an ARMA (p, q) because of the colored noise in [6.1] is:

$$\hat{\mathbf{a}} = - \begin{bmatrix} \hat{\gamma}_{xx}(p+q) & \cdots & \hat{\gamma}_{xx}(q+1) \\ \vdots & \ddots & \vdots \\ \hat{\gamma}_{xx}(2p+q-1) & \cdots & \hat{\gamma}_{xx}(p+q) \end{bmatrix}^{-1} \begin{bmatrix} \hat{\gamma}_{xx}(p+q+1) \\ \vdots \\ \hat{\gamma}_{xx}(2p+q) \end{bmatrix} \quad [6.20]$$

Of course, identifying the noise structure in practice is far from being an easy task and very often we satisfy ourselves with the whiteness hypothesis.

These methods suppose that the order p is known. In practice it is not necessarily simple to determine it (we will see the methods further), but it should not be underestimated in order not to forget to estimate all the signal poles. When it is overestimated, besides the signal poles, poles linked to the noise also appear; they are more or less damped but in any case they are generally more damped than the signal poles (if the SNR is not too weak). This makes it possible to distinguish between the signal poles and the noise poles. The LSMYW method of an overestimated order is called high-order Yule–Walker method (HOYW). An order overestimation presents the advantage of improving the signal poles estimation. The LSMYW method is relatively efficient to distinguish between the signal and the noise poles, on the contrary the TLSMYW method has the disadvantage of attracting the poles (including those of the noise) on the unit circle making the distinction very difficult. We will show this phenomenon with one example, we consider $N = 100$ samples of a signal made up of sinusoids of frequencies 0.2 and 0.3 and of a white noise such as SNR = 10 dB. The poles are estimated by the LSMYW and TLSMYW methods with a number of equations $N/2$ and an order $p = 10$. Figure 6.1 represents the plot of the poles estimated in the complex plane for a signal realization.

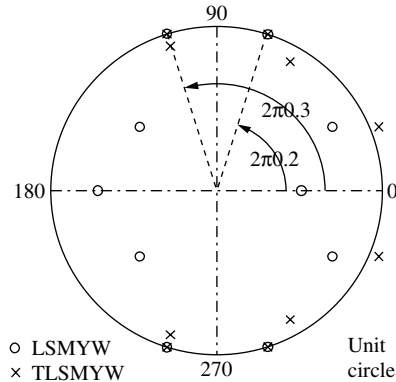


Figure 6.1. Influence of the order overestimation for the LSMYW and TLSMYW methods

We notice that the poles linked to the noise of the LSMYW method are clearly damped in relation to those obtained with TLSMYW which sometimes fall outside the unit circle. When the order is overestimated, the TLSMYW method should be avoided. However, for a correct order, the estimation by TLSMYW is better than that of LSMYW.

Up to now, the LSMYW method is one of the most efficient of those that we have described [CHA 82, STO 89]. Söderström and Stoica [SÖD 93] have given the asymptotic performances of this method in the case of a noisy exponential (white noise) of circular frequency $\omega = 2\pi f$ and amplitude A :

$$\text{Var}(\hat{\omega}) = \lim_{N \rightarrow \infty} E[(\hat{\omega} - \omega)^2] = \frac{1}{N} \frac{\sigma_u^4}{A^4} \frac{2(2p+1)}{3p(p+1)N_0^2} \quad [6.21]$$

where p represents the order and $N_0 \geq p$ the number of equations. This expression can be compared to the asymptotic Cramer–Rao bound of the circular frequency ω (see Chapter 3):

$$\text{CRB}(\omega) = \frac{6\sigma_u^2}{A^2 N^3} \quad [6.22]$$

The expressions obtained in [6.21] and [6.22] do not obviously show that the variance of HOYW [6.21] remains above the Cramer–Rao bound, as it has to be. However, this is the case. The frequency estimation variance [6.21] approaches the bound [6.22] only asymptotically. Söderström and Stoica [SÖD 91] compare this method to the Root-MUSIC and ESPRIT methods (see Chapter 8) in terms of

precision and computational burden. HOYW makes a good compromise between these two aspects.

6.3. ARMA modeling

6.3.1. ARMA modeling as a spectral estimator

As most of the processes can be well approximated by a linear rational model, the ARMA model (p, q) is an interesting general model. It is described by a finite order linear recursion with constant coefficients:

$$x(k) = -\sum_{n=1}^p a_n x(k-n) + \sum_{n=0}^q b_n u(k-n) \quad [6.23]$$

in which $u(k)$ represents a zero mean stationary white noise.

The coefficients a_n correspond to the AR part of the model, while the coefficients b_n determine the MA part. Obviously, an AR model of order p is a special case of an ARMA model $(p, 0)$.

ARMA modeling provides thus a spectral estimation of the signal $x(n)$.

6.3.2. Estimation of ARMA parameters

The estimation of ARMA parameters [KAY 88, MAR 87] is made in two steps: first, we estimate the AR parameters and then the MA parameters. This sub-optimal solution leads to a considerable reduction of the computational complexity with respect to the optimal solution that would consist of estimating the AR and MA parameters. The estimation can be efficiently performed in two steps. Starting from equation [6.23], we show that the autocorrelation function of an ARMA process itself follows a recursion of the AR type but starting from the lag $q + 1$ (see Chapter 4, equation [4.17]):

$$\gamma_{xx}(m) = -\sum_{n=1}^p a_x \gamma_{xx}(m-n) \text{ for } m > q \quad [6.24]$$

The estimation of the AR parameters is done as before by taking these MYW equations into account (starting from the rank $q + 1$) (see equation [6.20]).

The estimation of the MA parameters is done first by filtering the process by the inverse AR filter, using the AR estimated parameters so that we come back to an MA of order q , according to the principle in Figure 6.2.

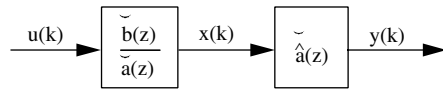


Figure 6.2. Principle of the estimation of MA parameters in an ARMA

If the inverse AR filter is supposed perfectly known, we obtain (by using equation [6.23]):

$$y(k) = x(k) + \sum_{n=1}^p a_n x(k-n) = \sum_{n=0}^q b_n u(k-n) \quad [6.25]$$

and the filtered process $y(k)$ is a pure $MA(q)$. Thus, we simply come back to a problem of estimation of MA parameters. This model $MA(q)$ can theoretically be modeled by an infinite order AR by writing:

$$\bar{b}(z) = \frac{1}{\bar{c}(z)} \text{ with } \bar{c}(z) = \sum_{n=0}^{+\infty} c_n z^{-n} \quad [6.26]$$

We obtain a relation between the MA coefficients and the coefficients of the equivalent AR model:

$$c_k = - \sum_{n=1}^q b_n c_{k-n} + \delta(k)$$

$\delta(k)$ standing for the Kronecker symbol ($\delta(0) = 1$ and $\delta(k) = 0$, for any $k \neq 0$).

In practice, we choose to estimate an AR model of high-order M such as $M \gg q$. Using the AR parameters estimated this way, we obtain a set of equations in the form:

$$\varepsilon(k) = \hat{c}_k + \sum_{n=1}^q b_n \hat{c}_{k-n} \quad [6.27]$$

Ideally, $\varepsilon(k)$ should be null everywhere except for $k = 0$ where it should be equal to 1. As the order of the estimated AR is not infinite, it is nothing of the sort and the estimation of the MA parameters should be done by minimizing a quadratic criterion of the form:

$$\sum_k |\varepsilon(k)|^2$$

The index k takes values on an interval, which is linked to the used estimation methods. Indeed, equation [6.27] can be viewed as an AR model of order q where the \hat{c}_k 's play the role of the signal, the b_n 's the AR coefficients, and $\varepsilon(k)$ the additive noise. Taking this into consideration, various AR estimation techniques can be applied with, as particular cases: $k = 0, \dots, M + q$ corresponding to the method of autocorrelations and $k = q, \dots, M$ corresponding to the covariance method.

6.4. Prony modeling

6.4.1. Prony model as a spectral estimator

To have a more physical description of the signal, in terms of frequency, amplitude, phase, and damping, the Prony model can also be envisaged. This model consists of describing the signal as a sum of p complex exponentials. This model is thus *a priori* deterministic, contrary to the ARMA and AR models. Thus, it makes it possible to model deterministic signals or moments (e.g. autocorrelation functions) by:

$$x(k) = \sum_{m=1}^p B_m z_m^k \quad [6.28]$$

Such a model allows to define a spectral estimator of the modeled signal $x(k)$. Two different estimators can be proposed, depending on the modeling window. If it is assumed that this model is valid only for $k \geq 0$ and that $x(k) = 0$ for $k < 0$, the Prony spectral estimator is:

$$S_{xx}(z) = \sum_{m=1}^p B_m \frac{1 - z_m^2}{(1 - z_m z^{-1})(1 - z_m z)} \quad [6.29]$$

However, when using this model on correlation functions, it would be of interest to provide another hypothesis for $k < 0$ than the null one.

6.4.2. Estimation of Prony parameters

The classic estimation method of the Prony model parameters is based on the recursion expression of a sum of exponentials:

$$x(k) = \sum_{n=1}^p B_n z_n^k = - \sum_{n=1}^p a_n x(k-1) \text{ for } k \geq p \quad [6.30]$$

which leads to:

$$x(k) = \sum_{n=1}^p a_n x(k-n) + \sum_{n=0}^p a_n u(k-n) \quad p \leq k \leq N-1 \quad (a_0 = 1) \quad [6.31]$$

We find the well-known equivalence between a sum of p noisy exponentials and the ARMA (p, p) model for which the AR and MA coefficients are identical. The poles z_n are deduced from the polynomial roots:

$$\bar{a}(z) = \sum_{n=0}^p a_n z^{-n} = \prod_{n=1}^p (1 - z^{-1} z_n) \quad [6.32]$$

The classic estimation method of the AR parameters in the estimation procedure of the Prony model parameters consists of minimizing the quadratic error:

$$e = \min_{a_n} \sum_{k=p}^{N-1} \left| x(k) + \sum_{n=1}^p a_n x(k-n) \right|^2 \quad [6.33]$$

which, in a matrix form, is written as:

$$\begin{aligned} & \min_{a_n} \left\| \begin{bmatrix} x(p-1) & \cdots & x(0) \\ \vdots & \ddots & \vdots \\ x(N-1) & \cdots & x(N-p) \end{bmatrix} \begin{bmatrix} a_1 \\ \vdots \\ a_p \end{bmatrix} + \begin{bmatrix} x(p) \\ \vdots \\ x(N) \end{bmatrix} \right\|^2 \\ & \min_{\mathbf{a}} \|\mathbf{X}\mathbf{a} + \mathbf{x}\|^2 \end{aligned} \quad [6.34]$$

and leads to the least-squares solution \mathbf{a}_{LS} :

$$\mathbf{a}_{LS} = -(\mathbf{X}^H \mathbf{X})^{-1} \mathbf{X}^H \mathbf{x} \quad [6.35]$$

This method is sometimes called *LS-Prony*. When the system is solved in the total least-squares sense, we speak of *TLS-Prony*. We will note that the matrix $\mathbf{X}^H \mathbf{X}$ is the estimation of the covariance matrix, with one multiplying factor ($\frac{1}{N-p}$). This method is thus identical to the covariance method for the estimation of the *AR* coefficients and of the signal poles. This method can be slightly changed in the case of $\frac{p}{2}$ undamped real sinusoids to force the estimated poles to be of unit module:

$$\min_{a_n} \left\| \begin{bmatrix} x^*(N-p+1) & \cdots & x^*(N) \\ \vdots & \ddots & \vdots \\ x^*(1) & \cdots & x^*(p) \\ x(p-1) & \cdots & x(0) \\ \vdots & \ddots & \vdots \\ x(N-1) & \cdots & x(N-p) \end{bmatrix} \begin{bmatrix} a_1 \\ \vdots \\ a_{\frac{p}{2}-1} \\ a_{\frac{p}{2}} \\ a_{\frac{p}{2}-1} \\ \vdots \\ a_1 \\ 1 \end{bmatrix} + \begin{bmatrix} x^*(N-p) \\ \vdots \\ x^*(0) \\ x(p) \\ \vdots \\ x(N) \end{bmatrix} \right\|^2 \quad [6.36]$$

We speak then of the *harmonic Prony* method. Other estimation methods of the *AR* parameters, implementing the correlation, can be used, e.g. *LSYW* and *LSMYW*.

Once the poles are estimated (\hat{z}_n), the complex amplitudes are obtained by solving the Vandermonde system:

$$\begin{bmatrix} 1 & 1 & \cdots & 1 \\ \hat{z}_1 & \hat{z}_2 & \cdots & \hat{z}_p \\ \hat{z}_1^2 & \hat{z}_2^2 & \cdots & \hat{z}_p^2 \\ \vdots & \vdots & \ddots & \vdots \\ \hat{z}_1^{M-1} & \hat{z}_2^{M-1} & \cdots & \hat{z}_p^{M-1} \end{bmatrix} \begin{bmatrix} B_1 \\ \vdots \\ B_p \end{bmatrix} \approx \begin{bmatrix} x(0) \\ x(1) \\ x(2) \\ \vdots \\ x(M-1) \end{bmatrix} \quad [6.37]$$

$$\hat{\mathbf{V}}\mathbf{B} \approx \mathbf{x}$$

Solutions in the least-squares sense and in the total least-squares sense can be envisaged. It was shown in [DUC 97] that the total least-squares solution is less efficient in terms of bias than that of the classic least-squares. However, the number of equations M of the Vandermonde system can be chosen in an optimal manner, as detailed in [DUC 95].

6.5. Order selection criteria

Choosing a model system is a problem which is as important as the choice of the model itself. Selecting too small an order means smoothing the obtained spectrum, while choosing too large an order introduces secondary spurious peaks.

There is a large number of order selection criteria which are for most cases based on the statistic properties of the signal (maximum likelihood estimation: MLE).

Others, simpler and less efficient, are based on the comparison of the eigenvalues of the correlation matrix to some threshold correlation matrix [KON 88].

A large number of order selection criteria uses the prediction error power decrease when the order increases. When the theoretic order is reached, this power remains constant. However, a criterion based only on the prediction error power shape does not make it possible to take the estimated spectrum variance increase into account when the order is overestimated. That is why the criteria integrate these two phenomena. One of the first criteria proposed by Akaike [AKA 70] was the *FPE* (final prediction error): the estimated error corresponds to the value that minimizes:

$$FPE(k) = \frac{N+k}{N-k} \hat{\rho}_k \quad [6.38]$$

where:

$$\hat{\rho}_k = \hat{\gamma}_{xx}(0) + \sum_{l=1}^k \hat{a}_l \hat{\gamma}_{xx}(l) \quad [6.39]$$

is the power of the prediction error that decreases with k while the term $\frac{N+k}{N-k}$ increases with k (to take the estimated spectrum variance augmentation into account when k increases). The AR parameters are estimated through Yule–Walker equations with the biased estimator of the correlation. The most well-known criterion proposed by Akaike is the *AIC* (Akaike information criterion) [AKA 74]:

$$AIC(k) = N \ln(\hat{\rho}_k) + 2k \quad [6.40]$$

This criterion is more general than *FPE* and it can be applied to determine the order of an MA part of an ARMA model. Asymptotically ($N \rightarrow \infty$) *FPE* and *AIC* are equivalent, but for a small number of samples *AIC* is better. It was proved that *AIC* is inconsistent and it tends to overestimate the order [KAS 80]. Rissanen [RIS 83] proposed to modify *AIC* by replacing the term $2k$ by a term, which increases more rapidly (depending on N). This criterion is named *MDL* (minimum description length):

$$MDL(k) = N \ln(\hat{\rho}_k) + k \ln(N) \quad [6.41]$$

This criterion is consistent and gives better results than *AIC* [WAX 85].

It would be tedious to present all the criteria that were developed; for more information on this, see the following references: [BRO 85, BUR 85, FUC 88, PUK 88, YIN 87, WAX 88].

Wax and Kailath [WAX 85] expressed the *AIC* and *MDL* criteria depending on the eigenvalues of the autocorrelation matrix \hat{R}_X :

$$AIC(k) = N(p-k) \ln \left(\frac{\left(\prod_{t=k+1}^p \hat{\lambda}_t \right)^{\frac{1}{p-k}}}{\frac{1}{p-k} \sum_{t=k+1}^p \hat{\lambda}_t} \right) + k(2p-k) \quad k=1, \dots, p-1 \quad [6.42]$$

$$MDL(k) = N(p-k) \ln \left(\frac{\left(\prod_{t=k+1}^p \hat{\lambda}_t \right)^{\frac{1}{p-k}}}{\frac{1}{p-k} \sum_{t=k+1}^p \hat{\lambda}_t} \right) + \frac{1}{2} k(2p-k) \ln(N) \quad [6.43]$$

where $\hat{\lambda}_t$ are the ordered eigenvalues ($\hat{\lambda}_t \geq \hat{\lambda}_{t+1}$) of the squared correlation matrix \hat{R}_x with p rows and p columns. It is possible to define these criteria according to the singular values $\hat{\sigma}_t$ of the extended non-squared correlation matrix \hat{R}_x with M rows and p columns ($M > p$) by replacing $\hat{\lambda}_t$ by $\hat{\sigma}_t^2$ in the expressions [6.42] and [6.43] [HAY 89].

The increase in the number of rows of the matrix \hat{R}_x improves the order estimation performances. We have compared the two expressions [6.41] and [6.43] of the *MDL* criterion in the following example. We consider $N = 100$ samples of a signal made up of two sinusoids of identical amplitudes of frequencies 0.1 and 0.2 embedded in an additional white noise. The dimension of the matrix \hat{R}_x is (30×30) . The simulations were carried out for SNRs of 10 dB and 0 dB and are presented in Figures 6.3 and 6.4.

Let us consider first Figure 6.3 where $\text{SNR} = 10$ dB. The dimension of the sub-space signal is 4 because the signal has two sinusoids. The criterion [6.43] (top curve) reaches its minimum for $k = 4$. However, the criterion [6.41] (bottom curve) is minimum when $k = 8$. These results illustrate the efficiency of the criterion defined starting from the eigenvalues of the autocorrelation matrix and the mediocre performances of the criterion defined starting from the prediction error power.

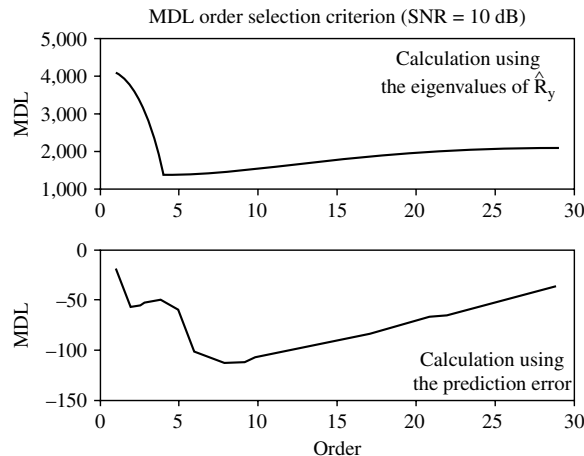


Figure 6.3. Comparison of the MDL criteria [6.43] and [6.41] for $\text{SNR} = 10 \text{ dB}$

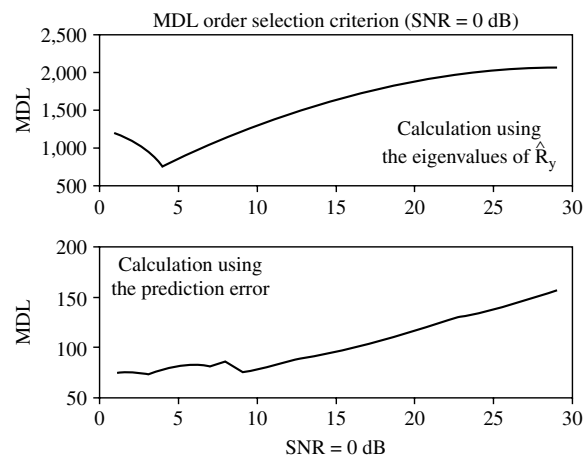


Figure 6.4. Comparison of the MDL criteria [6.43] and [6.41] for $\text{SNR} = 0 \text{ dB}$

Now, let us consider the case of the same signal but with a $\text{SNR} = 0 \text{ dB}$ (Figure 6.4). For a weaker SNR, the criterion [6.41] (bottom curve) is inefficient while the criterion [6.43] (top curve) gives a correct result.

These simulations have highlighted the efficiency of the *MDL* criterion [6.43] and, in a more general manner, the efficiency of the criteria built starting from the eigenvalues of the autocorrelation matrix $\hat{\mathbf{R}}_x$.

In the case of a Prony model, the model order corresponds to the number of searched exponential components, which evidently reduces to an order determination problem of AR model. All the preceding criteria are applicable.

In the case of an ARMA model, selecting the models p and q of the respective AR and MA parts is not a simple problem. Few published works tackle this problem, excepting the very simple cases. The *AIC* criterion is one of the most used in the form:

$$\text{AIC}(p,q) = N \ln(\hat{\rho}_{pq}) + 2(p+q)$$

where $\hat{\rho}_{pq}$ represents the estimated power of the entrance noise of the ARMA model. As in the case of the AR model, the minimum of this function with two variables provides the couple (p, q) of the AR and MA orders to be taken into account.

6.6. Examples of spectral analysis using parametric modeling

In the case of a signal made up of a sinusoid and an additive white noise, we take interest in the AR model spectrum evolution, according to the SNR, for a fixed AR order. Various results can be found in the literature, depending on the hypotheses taken for the modeled signal. For an example, we can mention [LAC 84] which provides the equivalent bandwidth expression for a pure sinusoid with additive white noise, modeled by an AR model of order p :

$$\Delta f_p = \frac{6}{\pi p(p+1)\beta}$$

β being the SNR. Figure 6.5 makes it possible to highlight that the bandwidth at -3dB of the spectrum lobe depends on the SNR: the weaker the SNR is, the more the lobe enlarges. The AR spectral resolution is affected by the noise presence.

In the case of a noisy sinusoidal signal, Figure 6.6 plots the evolution of the AR spectrum according to the order of the chosen model, for a previously fixed SNR. The larger the order is, the better the spectral resolution (inversely related to the width of the “peaks”). But if the chosen order is too big, false (or spurious) “peaks” appear.

The effect of the order choice is again illustrated on the case of a signal made up of three sinusoids in white noise. The minimal order necessary for the estimation of these three sinusoids is of 6. Of course, the presence of the additive white noise

makes it necessary to choose a higher order. Figure 6.7 presents the AR spectrum evolution, while the chosen order is below 6: if we could see that like an animated cartoon, we would see the successive lines “push” according to the chosen order. Below, we have represented the periodogram, which makes it possible to appreciate the smoothing produced by the AR spectral analysis.

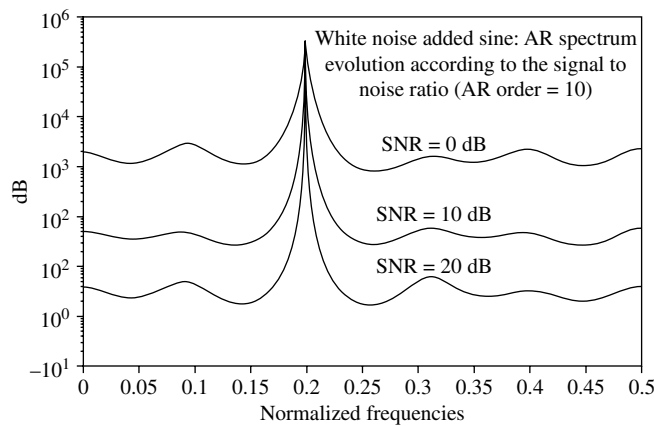


Figure 6.5. Evolution of the AR spectrum according to the SNR in the case of a noisy sinusoid

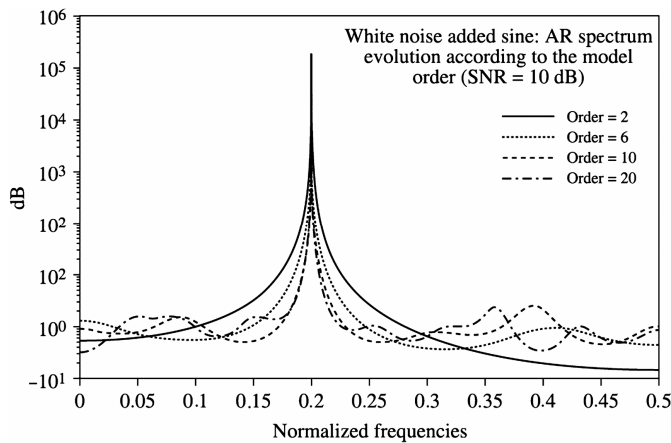


Figure 6.6. AR spectrum evolution according to the order of the chosen model in the case of a noisy sinusoid

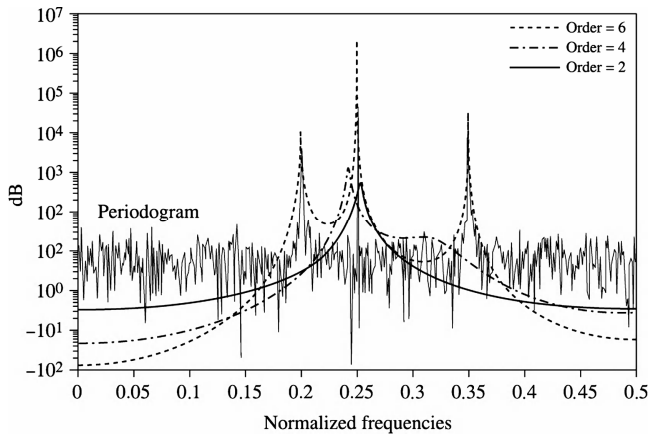


Figure 6.7. AR spectrum evolution (compared to the periodogram) according to the order chosen for a signal made up of 3 sinusoids in white noise

Figure 6.8 presents the AR spectrum evolution on the same signal made up of three sinusoids in white noise when the chosen order is superior to 6. The three lines are better and better estimated but at the order 50, the AR modeling makes two false “peaks” appear, which are actually noise peaks.

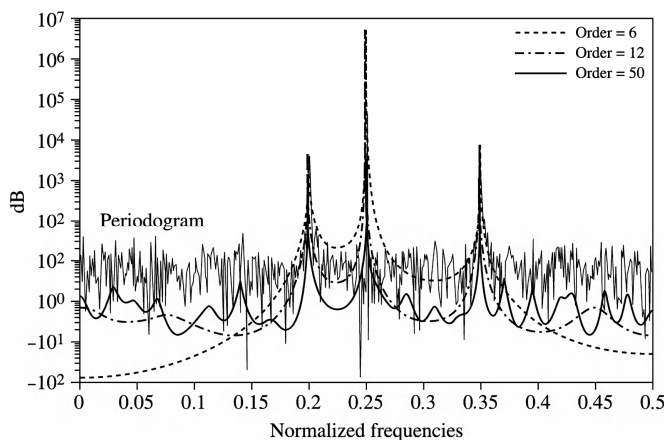


Figure 6.8. AR spectrum evolution (compared to the periodogram) according to the order (from 6 to 50) chosen for a signal made up of 3 sinusoids in a white noise

Figure 6.9 presents the results of Prony modeling on this same signal made up of three noisy sinusoids. Again, we realize that the three “lines” are better and better

estimated. The interest of the Prony modeling is to provide a “physical interpretation” of the model by estimating the modal parameters of the analyzed signal in terms of frequencies, amplitudes, phases, and dampings.

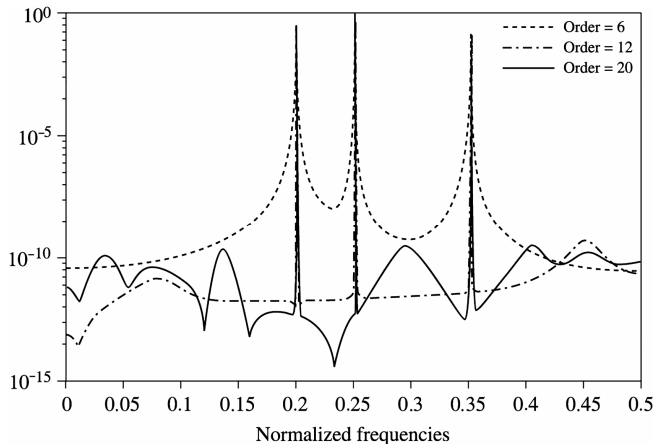


Figure 6.9. Prony spectra at orders 6, 12, and 20 of the three noisy sinusoids

The same type of illustration is performed on a real signal resulting from a vibrating structure. The MDL and AIC criteria applied on this signal indicate an AR modeling order between 17 and 21. The signal is short (of the order of 140 samples). An AR analysis (Figure 6.10) makes it possible to highlight a mode at the normalized frequency around 0.12 that the specialists of the field confirm.

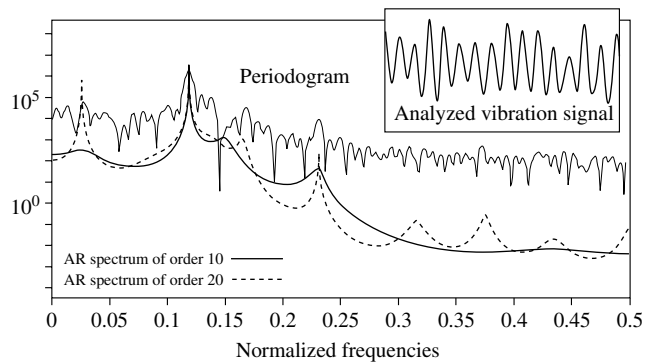


Figure 6.10. AR modeling of a vibration signal

This same mode is again better characterized using a Prony analysis (Figure 6.11), then making it possible to give all the physical quantities linked to this vibration node: frequency and amplitude, in particular.

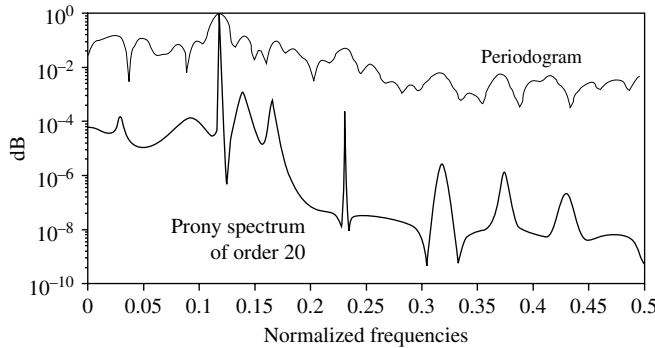


Figure 6.11. Prony spectrum of the vibration signal

6.7. Bibliography

- [AKA 70] AKAIKE H., “Statistical predictor identification”, *Annals of the Institute of Statistical Mathematics*, vol. 22, pp. 203–217, 1970.
- [AKA 74] AKAIKE H., “A new look at the statistical model identification”, *IEEE Transactions on Automatic Control*, vol. 19, pp. 716–723, 1974.
- [BRO 85] BROERSEN P., “Selecting the order of autoregressive models from small samples”, *IEEE Transactions on Acoustics, Speech and Signal Processing*, vol. 33, no. 4, pp. 874–879, 1985.
- [BUR 75] BURG J., Maximum entropy spectral analysis, PhD Thesis, Stanford University, Stanford, USA, 1975.
- [BUR 85] BURSHTEIN D., WEINSTEIN E., “Some relations between the various criteria for autoregressive model order determination”, *IEEE Transactions on Acoustics, Speech and Signal Processing*, vol. 33, no. 4, pp. 1017–1019, 1985.
- [CHA 82] CHAN Y., LANGFORD R., “Spectral estimation via the HOYW equations”, *IEEE Transactions on Acoustics, Speech and Signal Processing*, vol. 30, no. 5, pp. 689–698, 1982.
- [DUC 95] DUCASSE A., MAILHES C., CASTANIÉ F., “Amplitude and phase estimator study in Prony method for noisy exponential data”, *Proceedings of IEEE International Conference on Acoustics, Speech and Signal Processing-95*, Detroit, USA, May, pp. 1796–1799, 1995.
- [DUC 97] DUCASSE A., Estimation de sous-harmoniques à l'aide de méthodes paramétriques, PhD Thesis, INP Toulouse, 1997.

- [DUC 98] DUCASSE A., MAILHES C., CASTANIE F., “Estimation de fréquences: panorama des méthodes paramétriques”, *Traitemet du Signal*, vol. 15, no. 2, pp. 149–162, 1998.
- [FUC 88] FUCHS J.J., “Estimating the number of sinusoids in additive white noise”, *IEEE Transactions on Acoustics, Speech and Signal Processing*, vol. 36, no. 12, pp. 1846–1853, 1988.
- [GIN 85] GINGRAS D., “Asymptotic properties of HOYW estimates of the AR parameters of a time series”, *IEEE Transactions on Acoustics, Speech and Signal Processing*, vol. 33, no. 4, pp. 1095–1101, 1985.
- [GOL 89] GOLUB G., VAN LOAN C., *Matrix Computations*, John Hopkins University Press, 1989.
- [HAY 89] HAYKIN S., *Modern Filters*, Macmillan Publishing Company, 1989.
- [KAS 80] KASHYAP R., “Inconsistency of the AIC rule for estimating the order of autoregressive models”, *IEEE Transactions on Automatic Control*, vol. 25, no. 10, pp. 996–998, 1980.
- [KAY 80] KAY S.M., “Noise compensation for autoregressive spectral estimates”, *IEEE Transactions on Acoustics, Speech and Signal Processing*, vol. 28, no. 3, pp. 292–303, 1980.
- [KAY 88] KAY S.M., *Modern Spectral Estimation: Theory and Applications*, Prentice Hall, Englewood Cliffs, NJ, 1988.
- [KON 88] KONSTANTINIDES K., YAO K., “Statistical analysis of effective singular values in matrix rank determination”, *IEEE Transactions on Acoustics, Speech and Signal Processing*, vol. 36, no. 5, pp. 757–763, 1988.
- [LAC 84] LACOUME J., GHARBI M., LATOMBE C., NICOLAS J., “Close frequency resolution by maximum entropy spectral estimators”, *IEEE Transactions on Acoustics, Speech and Signal Processing*, vol. 32, no. 5, pp. 977–983, 1984.
- [LAN 80] LANG S., MC CLELLAN J., “Frequency estimation with maximum entropy spectral estimators”, *IEEE Transactions on Acoustics, Speech and Signal Processing*, vol. 28, no. 6, pp. 720–789, 1980.
- [LEV 47] LEVINSON N., “The Wiener RMS error criterion in filter design and prediction”, *Journal of Mathematics and Physics*, vol. 25, pp. 261–278, 1947.
- [MAK 77] MAKHOUL J., “Stable and efficient Lattice methods for linear prediction”, *IEEE Transactions on Acoustics, Speech and Signal Processing*, vol. 25, no. 5, pp. 423–428, 1977.
- [MAR 87] MARPLE S., *Digital Spectral Analysis with Applications*, Prentice Hall, Englewood Cliffs, NJ, 1987.
- [MOR 77] MORF M., DICKINSON B., KAILATH T., VIEIRA A., “Efficient solution of covariance equations for linear prediction”, *IEEE Transactions on Acoustics, Speech and Signal Processing*, vol. 25, no. 5, pp. 429–433, 1977.

- [PRO 92] PROAKIS J., RADER C., LING F., NIKIAS C., *Advanced Digital Signal Processing*, Macmillan Publishing Company, 1992.
- [PUK 88] PUKKILA T., KRISHNAIAH P., “On the use of autoregressive order determination criteria in univariate white noise tests”, *IEEE Transactions on Acoustics, Speech and Signal Processing*, vol. 36, no. 5, pp. 764–774, 1988.
- [RIS 83] RISSANEN J., “A universal prior for the integers and estimation by minimum description length”, *Annals of Statistics*, vol. 11, pp. 417–431, 1983.
- [SAK 79] SAKAI H., ARASE M., “Recursive parameter estimation of an autoregressive process disturbed by white noise”, *International Journal of Control*, vol. 30, pp. 949–966, 1979.
- [SÖD 91] SÖDERSTROM T., STOICA P., “On accuracy of HOYW methods for cisoids”, *Proceedings of IEEE International Conference on Acoustics, Speech and Signal Processing-91*, pp. 3573–3576, 1991.
- [SÖD 93] SÖDERSTROM T., STOICA P., “Accuracy of High-Order Yule-Walker methods for frequency estimation of complex sine waves”, *IEE Proceedings F, Radar, Sonar and Navigation*, vol. 140, no. 1, pp. 71–80, 1993.
- [STO 89] STOICA P., SÖDERSTROM T., T1 F., “Asymptotic properties of the high-order Yule-Walker estimates of sinusoidal frequencies”, *IEEE Transactions on Acoustics, Speech and Signal Processing*, vol. 37, no. 11, pp. 1721–1734, 1989.
- [STO 92] STOICA P., SÖDERSTROM T., VAN HUFFEL S., “On SVD-based and TLS-based high-order Yule-Walker methods of frequency estimation”, *Signal Processing*, vol. 29, pp. 309–317, 1992.
- [SWI 80] SWINGLER D., “Frequency errors in MEM processing”, *IEEE Transactions on Acoustics, Speech and Signal Processing*, vol. 28, no. 2, pp. 257–259, 1980.
- [VAN 91] VAN HUFFEL S., VANDEWALLE J., *The Total Least Squares Problem*, SIAM, 1991.
- [WAX 85] WAX M., KAILATH T., “Detection of signals by information theoretic criteria”, *IEEE Transactions on Acoustics, Speech and Signal Processing*, vol. 33, no. 2, pp. 387–392, 1985.
- [WAX 88] WAX M., “Order selection for AR models by predictive least squares”, *IEEE Transactions on Acoustics, Speech and Signal Processing*, vol. 36, no. 4, pp. 581–588, 1988.
- [WIL 93] WILKES D., CADZOW J., “The effects of phase on high-resolution frequency estimators”, *IEEE Transactions on Signal Processing*, vol. 41, no. 3, pp. 1319–1330, 1993.
- [YIN 87] YIN Y., KRISHNAIAH P., “On some nonparametric methods for detection of the number of signals”, *IEEE Transactions on Acoustics, Speech and Signal Processing*, vol. 35, no. 11, pp. 1533–1538, 1987.

Chapter 7

Minimum Variance

In 1969, J. Capon proposed the following method that bears his name in the array processing domain:

A high-resolution method of estimation is introduced which employs a wavenumber window whose shape changes and is a function of the wavenumber at which an estimate is obtained. It is shown that the wavenumber resolution of this method is considerably better than that of the conventional method [CAP 69].

Actually, he had already presented this approach in a publication dating back to 1967 [CAP 67], in which he mentioned Levin's previous publication [LEV 64]. In 1971, two years after Capon's publication, Lacoss adapted it to the time-series spectral analysis:

The maximum likelihood method [...], which has been used previously (Capon, 1969) for wavenumber analysis with arrays, can be adapted to single time-series spectral analysis. One derivation of this is given below in terms of minimum variance unbiased estimators of the spectral components [LAC 71].

The method was initially called maximum likelihood. We will see why this name is not properly adapted (see section 7.4). The approach is actually based on a variance minimization, hence its current name.

Chapter written by Nadine MARTIN.

Since then, the method has been used both in spectral and in spatial processing, the spatial processing being nevertheless privileged. Its interest is clearly expressed in J. Capon's introductory sentence, "the window is adapted at each frequency". This adaptation faculty enables the Capon method to reach higher performance than the Fourier-based methods. Let us illustrate it in one example. Figure 7.1 represents the spectral analysis of a noisy sinusoid by two approaches, the periodogram and the Capon method or minimum variance (MV).

Figure 7.1 shows that the spectrum estimated by the MV method has a narrower main lobe and fewer secondary lobes, and this points out a gain in resolution and a weaker variance compared with the periodogram. This gain is not without consequence. The computational complexity of the MV method is higher. But this point is not an obstacle nowadays and it will be less and less so in the future.

The MV method has an additional degree of freedom compared with methods based on Fourier transform, the choice of a parameter called the order. This choice can be seen as a handicap. Actually, it is not. Contrary to methods based on models such as the autoregressive (AR) model, the choice of this order does not have any link to the number of searched frequencies (see section 6.2.4). The higher the order is, the higher the resolution of the method will be. Moreover, while preserving high performances, it is possible to estimate a spectrum with a relatively weak order compared with the necessary window lengths in Fourier methods. An order 6 for the MV analysis of a 16-sample simulated signal (bottom right of Figure 7.1) is enough to estimate the spectrum correctly.

The spectral analysis of a real-world signal, a hydraulic noise measured with an accelerometer in an oil station, is represented in Figure 7.2. This signal with duration of 16.6 s, sampled at a frequency of 3,000 Hz over 50,000 samples, is made up of a large number of sine waves as well as of other components with a wider spectral bandwidth. The MV method (top curve of Figure 7.2) estimates the total of these components with an order of 300, which means the inverse of a matrix 300×300 . The interest of this approach, in spite of the calculation time, is then a drop-off in variance, which makes the extraction of various spectral structures easier. The periodogram (bottom curve of Figure 7.2) also estimates the component set but a high variance requires the use of more complex techniques to extract the various spectral structures from it [DUR 99, MAI 06a, MAI 06b].

Figure 7.3 shows another advantage of the MV approach when analyzing a shorter signal duration of 43 ms (128 samples) instead of 16.6 s. A higher resolution makes possible the estimation of more spectral components than with the periodogram. An order of 80 is then enough.

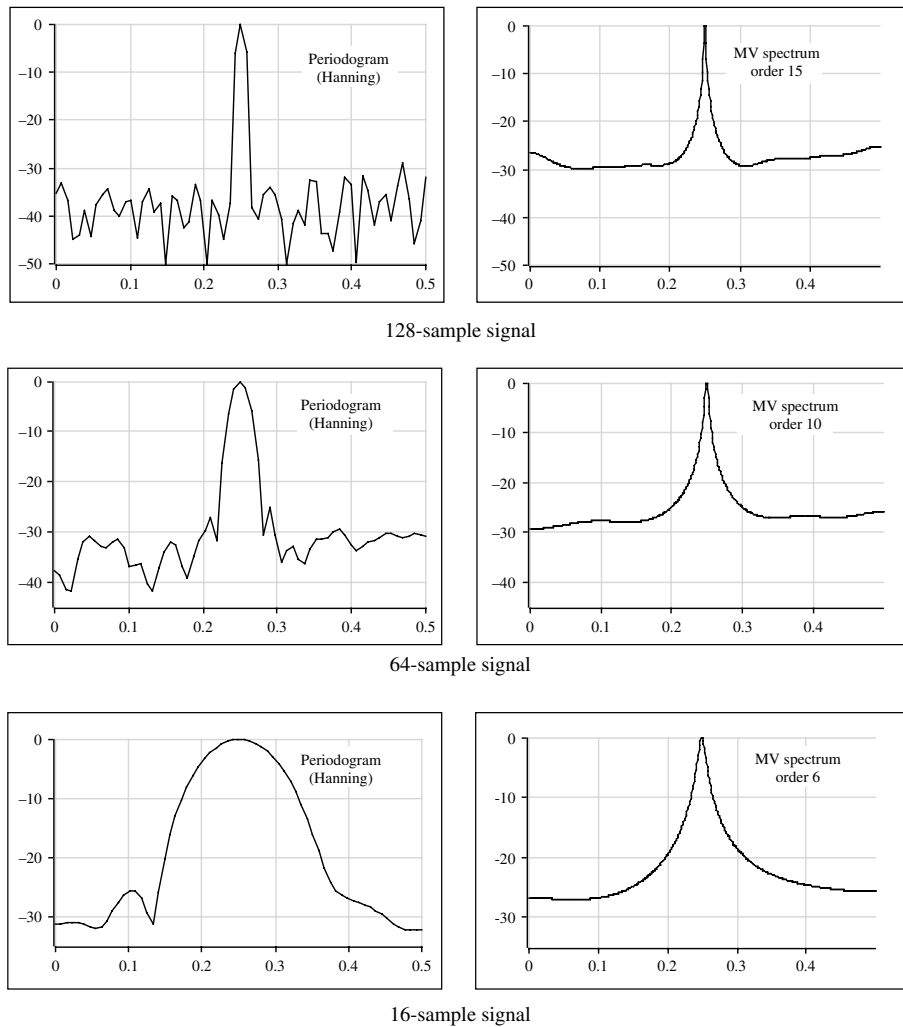


Figure 7.1. Comparison of a simple periodogram weighted by a Hanning window (left column) and the MV method (right column) for the estimation of the power spectral density of a sine wave (0.25 Hz, sampling frequency 1 Hz), not very noisy (20 dB), on a time support of 128 samples (top curves), 64 samples (middle curves), and 16 samples (below curves). Horizontal axes: frequency. Vertical axes: spectrum in dB

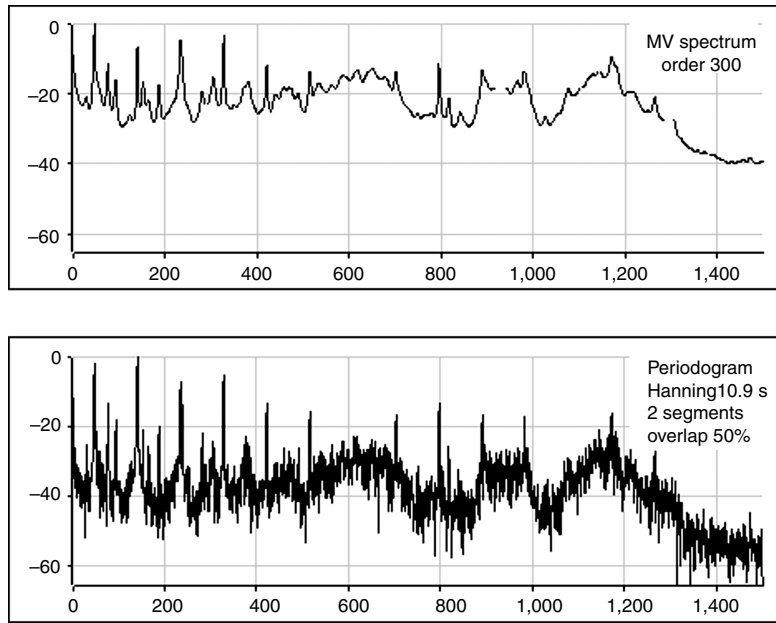


Figure 7.2. Spectral analysis of a real-world signal – a hydraulic noise measured with an accelerometer in an oil station (duration 16.6 s, 50,000 samples, sampling frequency 3,000 Hz) by the MV method (top) and by the averaged periodogram method (bottom). Horizontal axes: frequency in Hz. Vertical axes: spectrum in dB

Experimental comparisons with other algorithms are developed on non-stationary signals in [BON 90, LAT 87]. Synthesis sheets were drawn up to briefly present a set of time-frequency approaches for the MV estimator [BAS 92] (see also [FER 86] for an adaptive MV estimator). As regards the applications, the reader will be able to consult [PAD 95, PAD 96] for an application in mechanics, [LEP 98] in seismics on the characterization of avalanche signals, [PAD 09] in non-destructive testing of ferromagnetic steel with Barkhausen noises, and [MAR 95] in room acoustics for an original adaptation in the time-octave domain.

Section 7.1 presents the MV method as a finite impulse response (FIR) filter bank. The order, as we have just seen in Figures 7.1 and 7.2, corresponds to the number of coefficients of the filter impulse response, a filter being designed at each frequency channel. This concept of FIR filter bank places the MV method as an intermediate method between those based on Fourier and those based on models. The MV method designs a filter according to the analyzed signal while the Fourier methods are decomposed on a base of exponential functions, which are identical whatever the signal (see section 7.3).

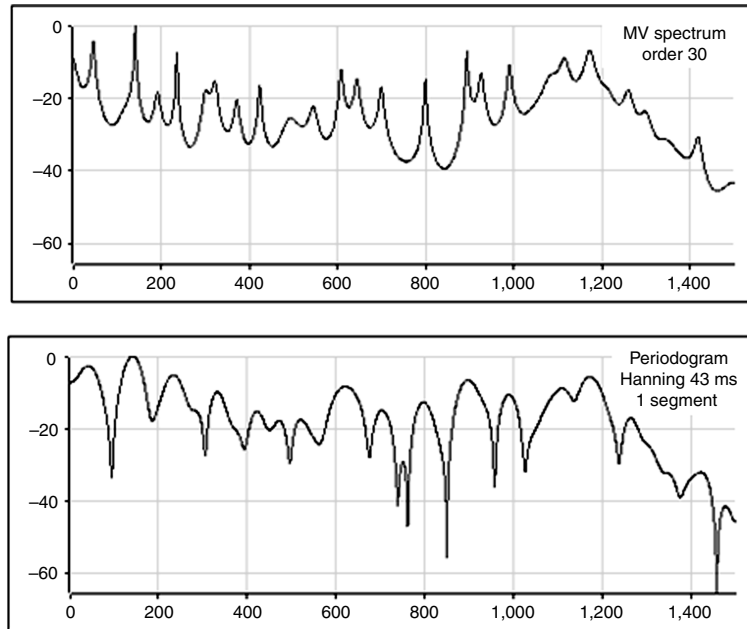


Figure 7.3. Spectral analysis of a real-world signal – a hydraulic noise measured with an accelerometer in an oil station (duration 43 ms, 128 samples, sampling frequency 3,000 Hz) by the MV method (top) and by the periodogram method (bottom). Horizontal axes: frequency in Hz. Vertical axes: spectrum in decibels

The “parametric” term is often attributed to the MV method because the filter parameters need to be estimated (see section 7.1). However, it is important to note that these parameters do not contain all the spectral information contrary to the model-based methods. The MV method is considered as a high-resolution method that does not perform as well as the model-based method. Thus, this intermediate situation is due not only to the concept, but also to the properties obtained. In section 7.2, we insist on the particular structure of the filters designed this way, which lead to properties closely linked to the type of the analyzed signal. In the same section, we illustrate how the MV method performs by considering simulated signals of a relatively short time duration on which the theoretical results established in an asymptotic context are not applicable.

Initiated by Lagunas, modifications were proposed and led to estimators called normalized MV. All these modifications are presented in section 7.5. More recently, the study of MV filter properties led to a new estimator more adapted to the analysis of mixed signals. This estimator, called CAPNORM, is described in section 7.6.

7.1. Principle of the MV method

Let $x[k]$ be a discrete, random, stationary signal sampled at frequency $f_s = 1/T_s$ and of power spectral density $S_x(f)$. The concept of the MV method, schematized in Figure 7.4, is based on the construction of an FIR filter at a frequency f_c , applied to signal $x[k]$ according to the following two constraints:

- 1) At frequency f_c , the filter transfers the input signal without modification.
- 2) At frequencies other than frequency f_c , the filter output power is minimized.

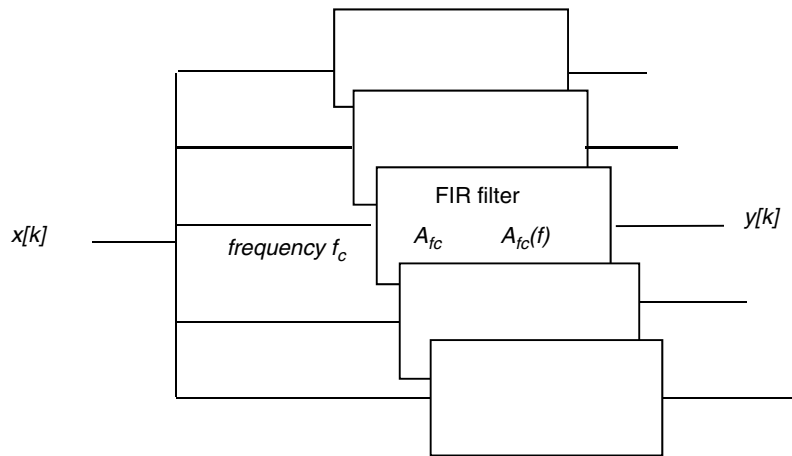


Figure 7.4. Construction of an FIR filter bank for the analysis of a signal $x[k]$ at all frequencies f_c within the range $[0, f_c/2]$

The first constraint implies that the filter frequency response, referred to as $A_{f_c}(f_c)$, is equal to 1 at frequency f_c :

$$A_{f_c}(f_c) = 1 \quad [7.1]$$

To take the second constraint into account, the power P of the filter output $y[k]$ is expressed as the spectral density of the input:

$$P = E(y(k)^2) = \int_{-f_c/2}^{+f_c/2} |A_{f_c}(f)|^2 S_x(f) df \quad [7.2]$$

To set apart the frequency f_c in which we take interest, the power spectral density of $x[k]$ is decomposed into two parts:

$$S_x(f) = S_x^o(f) + S_x^i(f)$$

with

$$S_x^o(f) = \begin{cases} S_x(f) & \text{for } f_c - \varepsilon \leq f \leq f_c + \varepsilon \\ 0 & \text{otherwise} \end{cases}$$

$$S_x^i(f) = \begin{cases} S_x(f) & \text{for } f < f_c - \varepsilon \text{ and } f > f_c + \varepsilon \\ 0 & \text{otherwise} \end{cases}$$

knowing that $\varepsilon \ll f_c$.

The aim of this decomposition is to set apart the spectral information at frequency f_c . As ε approaches 0, the limit of the integral of the spectrum $S_x^o(f)$ is the searched quantity $P(f_c)$. By applying the first constraint defined by [7.1], as ε approaches 0, [7.2] is:

$$P = \int_{-f_c/2}^{+f_c/2} |A_{f_c}(f)|^2 S_x^i(f) df + P(f_c) \quad [7.3]$$

with:

$$P(f_c) = \lim_{\varepsilon \rightarrow 0} \int_{-f_c/2}^{+f_c/2} S_x^o(f) df$$

The second constraint consists of minimizing integral [7.3]. Given the fact that the added term $P(f_c)$ is a constant, it is equivalent to minimizing the total output power P . By applying the Parseval relation, the dual expression is expressed according to the covariance matrix \mathbf{R}_x of the input signal $x[k]$ and of the vector \mathbf{A}_{f_c} of the coefficients of an FIR filter impulse response at frequency f_c :

$$P = \mathbf{A}_{f_c}^H \mathbf{R}_x \mathbf{A}_{f_c} \quad [7.4]$$

with

$$\mathbf{A}_{f_c}(f) = \mathbf{E}_{f_c}^H \mathbf{A}_{f_c}$$

$$\mathbf{E}_f^T = \left(1, e^{2\pi j f T_c}, \dots, e^{2\pi j (M-1) f T_c} \right)$$

$$\mathbf{R}_x = E(\mathbf{X} \cdot \mathbf{X}^H) \in \mathbb{R}^{M \times M}$$

and

$$\mathbf{X}^T = (x(k-M), \dots, x(k-1))$$

$(\cdot)^T$ and $(\cdot)^H$ denote transpose and hermitic transpose, respectively.

The minimization of [7.4] under constraint [7.1] is achieved by the technique of Lagrange multipliers [CAP 70]. It makes it possible to obtain the filter impulse response at frequency f_c :

$$\mathbf{A}_{f_c} = \frac{\mathbf{R}_x^{-1} \mathbf{E}_{f_c}}{\mathbf{E}_{f_c}^H \mathbf{R}_x^{-1} \mathbf{E}_{f_c}} \quad [7.5]$$

and the output power P by:

$$P_{MV}(f_c) = \frac{1}{\mathbf{E}_{f_c}^H \mathbf{R}_x^{-1} \mathbf{E}_{f_c}} \quad [7.6]$$

$P_{MV}(f_c)$ is the Capon estimator, also called the MV estimator. The estimated quantity is linked to the searched power, the power $P(f_c)$ of the signal at frequency f_c , by [7.3]. Thus, it is clear that the more efficient the minimization is, the better the estimation is, i.e. the integral of [7.3] approaches 0.

Such a filter is built at frequencies ranged between 0 and $f_c/2$. The FIR bank filter defined this way does not require any particular hypothesis on the signal apart from the stationarity property and the existence of its power spectral density. The signal can be real or complex. No model is applied. The filter coefficients are automatically adapted from the signal autocorrelation matrix.

Indeed, to calculate [7.6], the autocorrelation matrix should be estimated. To this end, the reader will be able to refer to [GUE 85] and to Chapter 3 of this book. In addition, [HON 98b] and [JAN 99] consider for the Capon method the case of the progressive covariance matrices, estimated as in [7.4] from the data vector

$\mathbf{X}^T = (x[k-M], \dots, x[k-1])$, or retrograde, from $\mathbf{X}^T = (x[k+M], \dots, x[k+1])$, or both progressive and retrograde. In this latter case, the statistic precision is increased, the signal being stationary.

It is interesting to note that the Capon estimator can be used as a covariance estimator for any other estimator of power spectral density simply by an inverse Fourier transform. Hongbin has demonstrated the good statistic properties of this estimator [HON 98a].

7.2. Properties of the MV estimator

7.2.1. Expressions of the MV filter

To understand the internal mechanism of the MV estimator, it is very instructive to study the behavior of the designed filter by setting the constraints as explained in section 7.1. Given that the shape of the filter depends on the signal, a theoretical study should be derived according to the signal. We chose one simple model and a comprehensive conclusion can then be drawn as a result of an experimental study on more complex signals. In this section we present the main elements of such a study [DUR 00].

Let us consider the simple case where $x[k]$ is a complex exponential function at frequency f_{exp} embedded in an additive, complex, centered white noise $w[k]$ of variance σ^2 . Let $Ce^{j\phi}$ be the complex amplitude of this exponential, for which the signal is written in the following vector form:

$$\mathbf{X} = Ce^{j\phi} \mathbf{E}_{f_{\text{exp}}} + \mathbf{W} \quad [7.7]$$

where \mathbf{X} and $\mathbf{E}_{f_{\text{exp}}}$ are defined as in [7.4] and:

$$\mathbf{W}^T = (w[k-M], \dots, w[k-1])$$

The signal covariance matrix is:

$$\mathbf{R}_x = C^2 \mathbf{E}_{f_{\text{exp}}} \mathbf{E}_{f_{\text{exp}}}^H + \sigma^2 \mathbf{I} \quad [7.8]$$

with \mathbf{I} being the identity matrix of dimension $M \times M$.

Using the Sherman–Morrison formula [GOL 85], we deduce the inverse of autocorrelation matrix:

$$\mathbf{R}_x^{-1} = \frac{1}{\sigma^2} \begin{pmatrix} \frac{C^2}{\sigma^2} \\ \mathbf{I} - \frac{C^2}{1+M\frac{C^2}{\sigma^2}} \mathbf{E}_{f_{\text{exp}}} \mathbf{E}_{f_{\text{exp}}}^H \end{pmatrix} \quad [7.9]$$

Let us assume:

$$Q = \frac{\frac{C^2}{\sigma^2}}{1+M\frac{C^2}{\sigma^2}} \quad [7.10]$$

Let us note that $\frac{C^2}{\sigma^2}$ represents the signal-to-noise ratio. By substituting [7.9] and [7.10] into [7.5], the MV filter impulse response is expressed as:

$$\mathbf{A}_{f_c} = \frac{\mathbf{E}_{f_c} - Q \mathbf{E}_{f_{\text{exp}}} \mathbf{E}_{f_{\text{exp}}}^H \mathbf{E}_{f_c}}{M - Q \left| \mathbf{E}_{f_c}^H \mathbf{E}_{f_{\text{exp}}} \right|^2} \quad [7.11]$$

We can deduce from this the frequency response of the filter adapted to the signal $x[k]$ at the frequency f_c :

$$A_{f_c}(f) = \frac{D(f_c - f) - Q M D(f_{\text{exp}} - f) D(f_c - f_{\text{exp}})}{1 - Q M \left| D(f_c - f_{\text{exp}}) \right|^2} \quad [7.12]$$

with $D(f_k - f_i)$ the Dirichlet's kernel defined by:

$$D(f_k - f_i) = \frac{1}{M} \mathbf{E}_{f_i}^H \mathbf{E}_{f_k} = e^{\pi j(f_k - f_i)(M-1)T_s} \frac{\sin(\pi(f_k - f_i)MT_s)}{M \sin(\pi(f_k - f_i)T_s)} \quad [7.13]$$

By substituting [7.9] into [7.6], the MV estimator is expressed as:

$$P_{\text{MV}}(f_c) = \frac{\sigma^2}{M \left(1 - Q M \left| D(f_c - f_{\text{exp}}) \right|^2 \right)} \quad [7.14]$$

Function [7.12] is a relatively complex function that we will study for noticeable frequency values and for extreme signal-to-noise ratios.

If the filter frequency f_c is equal to the exponential frequency f_{exp} , [7.12] and [7.14] are written as:

$$A_{f_{\text{exp}}}(f) = D(f_{\text{exp}} - f) \quad [7.15]$$

and:

$$P_{\text{MV}}(f_c) = \frac{\sigma^2}{M(1-QM)} = \frac{\sigma^2}{M} + C^2 \quad [7.16]$$

The signal is filtered by a narrow band filter centered on the exponential frequency with a maximum equal to 1. In this particular case, the MV estimator is reduced to a Fourier estimator, a simple periodogram, non-weighted and non-averaged. The frequency response is a Dirichlet's kernel (see [7.15]). The output power given by [7.16] is dependent on the order M [LAC 71, SHE 91]. This dependence in $1/M$ is responsible for a bias, which diminishes when the order increases (see section 7.2.2).

For the other cases, it is necessary to make approximations. If the signal-to-noise ratio is weak ($C^2/\sigma^2 \ll 1$), Q approaches 0 and [7.12] and [7.14] are:

$$A_{f_c}(f) \approx D(f_c - f) \quad [7.17]$$

and:

$$P_{\text{MV}}(f_c) = \frac{\sigma^2}{M} \quad [7.18]$$

This drastic approximation also leads to a simple periodogram, non-weighted and non-averaged with a frequency response equals to a Dirichlet's kernel centered on the MV filter frequency.

The other case is more interesting. It is about studying the case of a signal-to-noise ratio bigger than $1(C^2/\sigma^2 \gg 1)$. In this case, the product QM approaches 1 and the frequency response is no longer a Dirichlet's kernel. Equation [7.12] highlights the basic principle of the MV estimator. While the denominator is constant, the numerator is the difference between two Dirichlet's kernels. The first is

centered on the filter frequency f_c and the second is centered on the exponential frequency f_{exp} . This second kernel is also smoothed by a kernel that depends on the difference $(f_c - f_{\text{exp}})$ between these two frequencies. Let us examine the behavior of this impulse response according to the relative position of these two frequencies.

The filter frequency f_c is far from the exponential frequency f_{exp}

The smoothing factor $D(f_c - f_{\text{exp}})$ approaches 0. Then, [7.12] reduces to:

$$A_{f_c}(f) \approx \begin{cases} D(f_c - f) & \text{if } f \neq f_{\text{exp}} \\ 0 & \text{if } f \rightarrow f_{\text{exp}} \end{cases} \quad [7.19]$$

In this case, the response is a Dirichlet's kernel except at the exponential frequency. This latter point is the fundamental difference with a Fourier estimator.

The filter frequency f_c is close to the exponential frequency f_{exp}

Given the fact that the term $(f_c - f_{\text{exp}})$ is weak, contrary to the preceding case, the smoothing factor $D(f_c - f_{\text{exp}})$ plays a predominant role. The impulse response [7.12] generally has two predominant lobes. This response has a maximum that is greater than 1 and is no longer at the filter frequency but at a frequency ranged between f_{exp} and f_c [DUR 00]. The filter is no longer a narrow band filter.

The preceding approximations were validated with simulations [DUR 00]. They lead to a key conclusion. The filter generated by the MV method does not lead to narrow band filters, which was often claimed in the literature [KAY 88, LAG 86]. Actually, the constraints imposed by the MV are not those of a narrow band filter. This characteristic has important consequences when an equivalent bandwidth should be calculated (see section 7.5.1).

Figure 7.5 illustrates the MV filters calculated when analyzing a mixed signal, sum of a narrow band filter and of a wideband filter. It also represents the signal power estimated by the MV method at order 12. It was necessary to calculate a frequency response at all frequencies of this spectrum. The other five curves are some examples of responses at specific frequencies in relation to the studied signal. It is clear that only the frequency response calculated at the sinusoid frequency (Figure 7.5(f)) is similar to that of a narrow band filter. All the others (Figures 7.5(b) to 7.5(e)) have lobes whose maximal amplitude can reach 25, which is greatly superior to 1. Figures 7.5(c) and 7.5(e) are examples where, at the filter frequency, the lobe is not at its maximum.

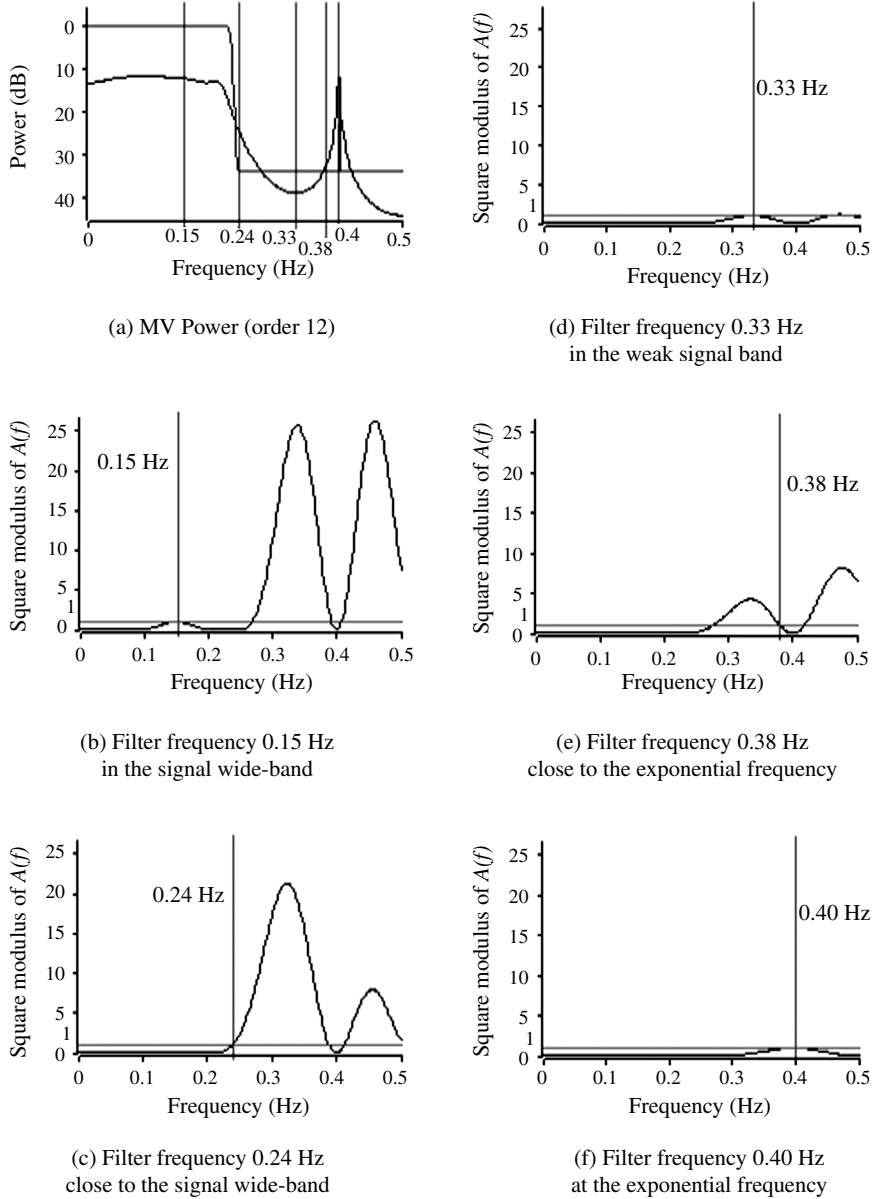


Figure 7.5. Square modulus of the frequency responses of MV filters at frequencies $f_c = 0.15$ Hz (b), $f_c = 0.24$ Hz (c), $f_c = 0.33$ Hz (d), $f_c = 0.38$ Hz (e), $f_c = 0.4$ Hz (f). (a) MV power at order $M = 12$. Signal = sum of a sinusoid (0.4 Hz, amplitude 0.5, signal-to-noise ratio 25 dB) and of a white noise of variance 1 filtered by an elliptic low-pass filter (order 12, attenuation 80 dB from 0.22 to 0.25 Hz), sampling frequency 1 Hz, 256 samples

7.2.2. Probability density of the MV estimator

Knowing the probability density of the MV estimator is the best way for accessing all the estimator moments. We will consider a more general signal than in the preceding paragraph. Let a complex signal $x[k]$ be the sum of an ordinary deterministic signal $d[k]$ and of a Gaussian centered random noise $w[k]$. The vector $\mathbf{W}^T = (w[k-1], \dots, w[k-M])$ is normally distributed $\mathbf{N}(0, \mathbf{R}_w)$ where $\mathbf{R}_w = E(\mathbf{W} \cdot \mathbf{W}^H)$ represents the covariance matrix $M \times M$ of the noise $w[k]$. The vector \mathbf{X} defined by $\mathbf{X}^T = (x[k-1], \dots, x[k-M])$ is therefore normally distributed $\mathbf{N}(\mathbf{D}, \mathbf{R}_w)$, where $\mathbf{D}^T = (d[k-1], \dots, d[k-M])$.

If $x[k]$ is filtered by an MV filter defined by its impulse response coefficients \mathbf{A}_{f_c} (see [7.5]), the complex filter output $y[k]$ is:

$$y[k] = \mathbf{A}_{f_c}^T \mathbf{X} \quad [7.20]$$

The filtering operation being linear, $y[k]$ is normally distributed:

$$y[k] \sim \mathbf{N}\left(\mathbf{A}_{f_c}^T m_x, \mathbf{A}_{f_c}^H \mathbf{R}_w \mathbf{A}_{f_c}\right)$$

The square modulus of $y[k]y^*[k]$ is Capon estimator according to [7.4] and [7.6] and is a non-central χ^2 with two degrees of freedom, of proportionality parameter $\mathbf{A}_{f_c}^H \mathbf{R}_d \mathbf{A}_{f_c}$ and of non-central parameter $\mathbf{A}_{f_c}^H \mathbf{R}_d \mathbf{A}_{f_c}$. This distribution is the probability density of the MV estimator in a relatively general context without any particular hypothesis, either on the additive noise except for its Gaussianity or on the deterministic signal, which can be made up of several components. The correlation matrices are assumed to be known.

From this distribution, the mean and the variance of the MV estimator are deduced:

$$\begin{aligned} E(P_{\text{MV}}(f_c)) &= \mathbf{A}_{f_c}^H \mathbf{R}_w \mathbf{A}_{f_c} + \mathbf{A}_{f_c}^H \mathbf{R}_d \mathbf{A}_{f_c} \\ \text{Var}(P_{\text{MV}}(f_c)) &= \left(\mathbf{A}_{f_c}^H \mathbf{R}_w \mathbf{A}_{f_c}\right)^2 + 2 \cdot \mathbf{A}_{f_c}^H \mathbf{R}_w \mathbf{A}_{f_c} \cdot \mathbf{A}_{f_c}^H \mathbf{R}_d \mathbf{A}_{f_c} \end{aligned} \quad [7.21]$$

It is interesting to note that these expressions are expressed in terms of $\mathbf{A}_{f_c}^H \mathbf{R}_w \mathbf{A}_{f_c}$ and $\mathbf{A}_{f_c}^H \mathbf{R}_d \mathbf{A}_{f_c}$, which represent the output powers of the MV filter

driving by the noise $w[k]$ only or by the deterministic signal $d[k]$ only, the filter being designed from the sum $x[k] = d[k] + w[k]$. These expressions are to be compared to those calculated for a periodogram (see section 7.3).

If the additive noise $w[k]$ is white of variance σ^2 , then $\mathbf{R}_w = \sigma^2 \mathbf{I}$, \mathbf{I} being the identity matrix of dimension $M \times M$. The mean and the variance of $P_{MV}(f_c)$ are:

$$\begin{aligned} E(P_{MV}(f_c)) &= \sigma^2 \mathbf{A}_{f_c}^H \mathbf{A}_{f_c} + \mathbf{A}_{f_c}^H \mathbf{R}_d \mathbf{A}_{f_c} \\ Var(P_{MV}(f_c)) &= \sigma^4 (\mathbf{A}_{f_c}^H \mathbf{A}_{f_c})^2 + 2\sigma^2 \cdot \mathbf{A}_{f_c}^H \mathbf{A}_{f_c} \cdot \mathbf{A}_{f_c}^H \mathbf{R}_d \mathbf{A}_{f_c} \end{aligned} \quad [7.22]$$

The mean expression, whether the noise is white or not, shows that the MV estimator is biased. The basic definition of the MV estimator summed up by [7.3] brings us to an identical conclusion from the frequency domain:

$$\text{Bias}(P_{MV}(f_c)) = \int_{-f_c/2}^{+f_c/2} |A_{f_c}(f)|^2 S_x^i(f) df \quad [7.23]$$

with $S_x^i(f)$ as defined in [7.2].

The MV estimator is built on the minimization of this integral; as derived in [7.3], this integral approaches 0 but is never equal to 0. Then, due to their design, MV estimator can be only a biased estimator of the signal power. If we consider again the case of the noisy exponential function (see [7.7]), at the frequency of the exponential, the impulse response, i.e. the inverse Fourier transform of the frequency response given by [7.15], is equal to the vector $\mathbf{E}_{f_{\text{exp}}}$, hence from [7.21] the MV estimator mean is:

$$E(P_{MV}(f_c)) = \frac{\sigma^2}{M} + C^2 \text{ for } f_c = f_{\text{exp}} \quad [7.24]$$

and the bias is:

$$\text{Bias}(P_{MV}(f_c)) = \frac{\sigma^2}{M} \text{ for } f_c = f_{\text{exp}} \quad [7.25]$$

This expression is actually directly visible in [7.16]. This bias depends on the noise variance and on the order M . This formula illustrates the fact that the bias is not null, but it especially clearly shows the interest of a high order to reduce the bias

influence. These results are illustrated in Figure 7.6 for different orders of magnitude of the order M . It is about the spectral analysis of a sinusoid embedded in a low-level noise (signal-to-noise ratio of 20 dB) at orders varying from 3 to 70. The figure is zoomed in the sinusoid frequency and the amplitudes are linearly represented to better picture the bias. The minimum amplitude increases when M diminishes.

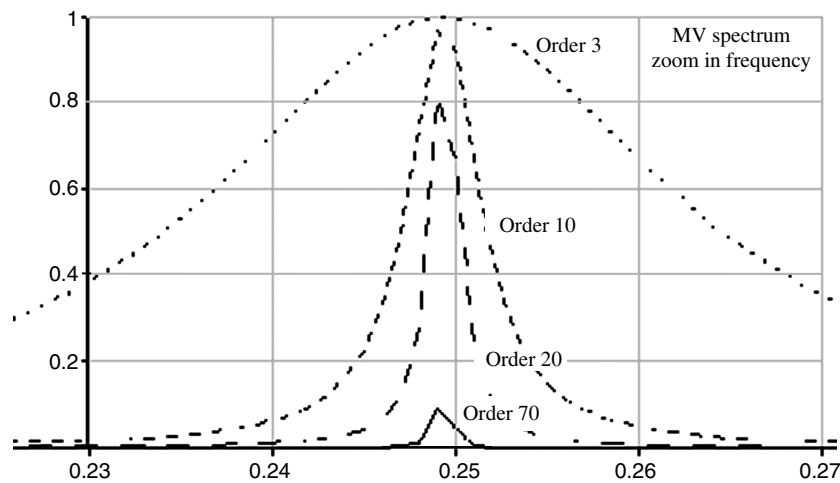


Figure 7.6. Illustration of the bias and resolution of the MV estimator for a noisy sinusoid (0.25 Hz, amplitude 1, sampling frequency 1 Hz, signal-to-noise ratio of 20 dB, 128 time samples). Spectra estimated by the MV method at orders 3, 10, 20, and 70. Horizontal axis: zoom in sinusoid frequency. Vertical axis: linear spectrum

We will see in section 7.4 that, to have a non-biased estimator, it is necessary to take account of *a priori* knowledge stronger than the covariance matrix of the analyzed signal.

As regards the variance given by [7.21] and [7.22], in the particular case of an exponential embedded in an additive white noise (see [7.7]), at the exponential frequency the variance is:

$$\text{var}(P_{\text{MV}}(f_c)) = \frac{\sigma^4}{M^2} + 2 \cdot \frac{\sigma^2 C^2}{M} \text{ for } f_c = f_{\text{exp}} \quad [7.26]$$

This equation shows again dependency of the variance compared to the order M . Actually, it will be more interesting to calculate this variance at another frequency than the exponential frequency, from the frequency response given by [7.12]. The calculations would be more complex, so we will do with experimental observations only.

[CAP 70] and [CAP 71] presented an experimental study in the array processing domain to argue the fact that the MV estimator has a weaker variance than a periodogram and an AR estimator for long duration signals. This study was extended to spectral analysis [LAC 71] and taken back in [KAY 88].

This weak variance is an important property of the MV estimator property that we have already illustrated in Figures 7.1–7.3. Figure 7.7 illustrates the variance diminution according to the order for a sinusoid at a high signal-to-noise ratio of 20 dB. This figure clearly shows that for a high order relative to the signal size (order of 70 for 128 samples), the variance is of the same magnitude order as that of the periodogram. In Figure 7.2 showing the analysis of a real signal with a high order (order of 300), the variance is still weak compared to that of the periodogram because the signal size is of 50,000 samples. The effects of the estimation of the signal autocorrelation matrix are thus sensitive when the ratio of the order to the signal sample number is of the order of half or more than half.

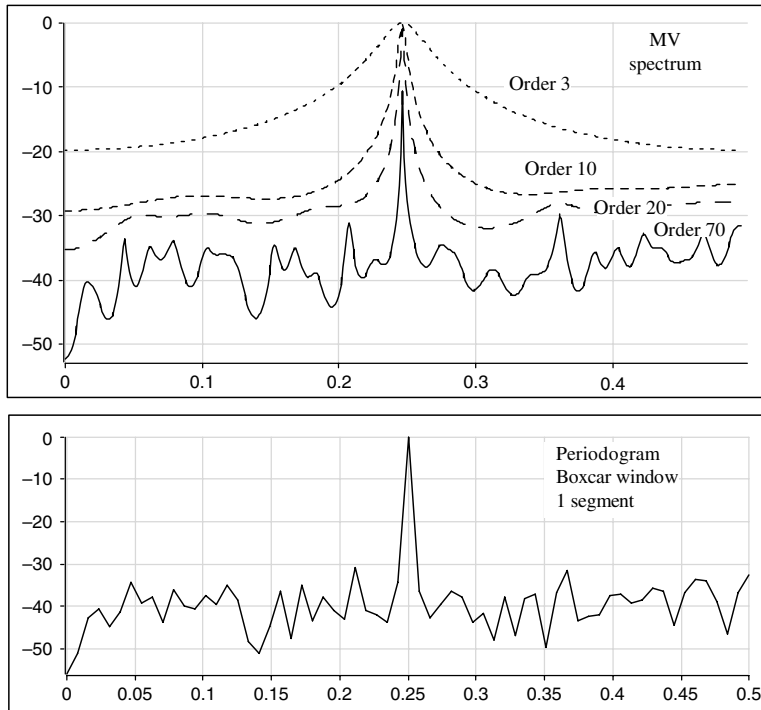


Figure 7.7. Variance and resolution of the MV estimator for the analysis of a signal made up of a noisy sinusoid (0.25 Hz, sampling frequency 1 Hz, signal-to-noise ratio of 20 dB, time support 128 samples). Top: superposition of spectra estimated by the MV method at the orders 3, 10, 20, and 70. Bottom: periodogram. Horizontal axes: frequency. Vertical axes: spectrum in dB

For a complete asymptotic statistic study, the reader can refer to the works of Liu and Sherman [LIU 98a] and to those of Ioannidis [IOA 94].

7.2.3. Frequency resolution of the MV estimator

A partially analytical and partially numerical study is suggested in [LAC 71]. Lacoss qualifies the frequency resolution of a spectral estimator $S(f)$ with the -3 dB bandwidth, denoted by ΔB_{-3dB} , and defined as the frequency bandwidth at half-maximum of the peak:

$$\Delta B_{-3dB} = f_+ - f_- \quad [7.27]$$

with $10 \log(S(f_+)/S(f)) = 10 \log(S(f_-)/S(f)) = -3$ for a peak at frequency f .

From this definition, Lacoss calculates an approximate expression of this bandwidth when the signal is defined as in [7.7] and made up of one exponential embedded in white noise with variance $\sigma^2 = 1$, and for an exact covariance matrix as defined in [7.8]. This study is concurrently performed with a non-weighted and non-averaged periodogram (parameters that induce the higher resolution), an MV estimator, and an AR estimator. Lacoss obtains the following approximate expressions:

$$(\Delta B_{-3dB})_{FOU} = \frac{\sqrt{6}}{\pi T_s M} \quad [7.28]$$

$$(\Delta B_{-3dB})_{MV} = \left(\frac{3}{C^2 M} \right)^{1/2} \cdot \frac{2}{\pi T_s M} \quad [7.29]$$

$$(\Delta B_{-3dB})_{AR} = \frac{2}{\pi T_s M^2 C^2} \quad [7.30]$$

with $(\Delta B_{-3dB})_{FOU}$, the -3 dB bandwidth of a simple periodogram (see [7.31] in section 7.3), $(\Delta B_{-3dB})_{MV}$, that of the MV estimator (see [7.14]), and $(\Delta B_{-3dB})_{AR}$, that of the AR estimator [LAC 71].

From these equations, at a given M , an MV estimator has a better resolution than a periodogram but does not perform as well as an AR estimator. Lacoss also highlights an essential difference between these estimators: the MV estimator is a power estimator whereas the others are a power spectral density estimator.

This property, which we will mention again in section 7.5, is fundamental for the comparison of the estimators.

Figure 7.7 shows the evolution of the MV method resolution with the filter order for a not very noisy sinusoid (signal-to-noise ratio of 20 dB); Figure 7.6 shows a zoom at the central frequency. It is clearly evident that the quantity $\Delta B_{-3\text{dB}}$ of the estimated peak diminishes with the order, hence an improvement of the frequency resolution with the order of the MV estimator.

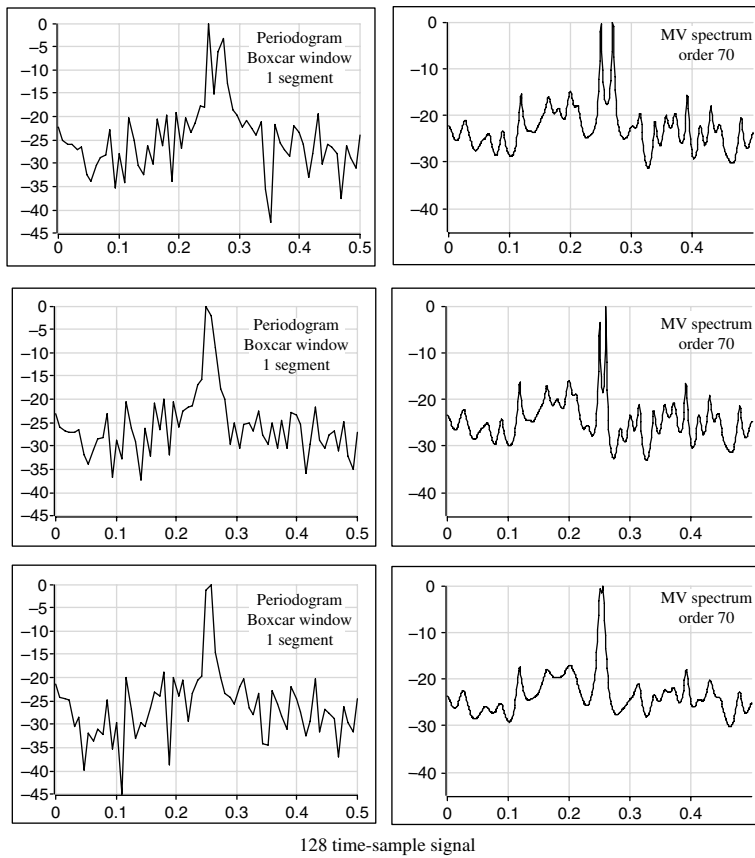


Figure 7.8. Spectral analysis of the sum of two sinusoids of the same amplitude 1, of sampling frequency 1 Hz, of signal-to-noise ratio of 10 dB, on a time support of 128 samples by the MV estimator (order 70) (right column) comparatively to the periodogram (non-averaged and non-weighted) (left column). Frequencies of the sinusoids 0.25 and 0.27 Hz (at the top), 0.25 and 0.26 Hz (in the middle), 0.25 and 0.256 Hz (at the bottom).
Horizontal axes: frequency. Vertical axes: spectrum in dB

It is interesting to know the capacity of a spectral estimator to separate two close frequencies. At a signal-to-noise ratio of 10 dB, Figure 7.8 shows this capacity for three values of frequency difference and comparatively with the periodogram in its more resolute version, i.e. non-averaged and non-weighted. Two peaks are separated if the amplitudes of the emerging peaks are higher than the estimator standard deviation. Thus, in the top part of Figure 7.8, the difference between the two frequencies is 0.02 Hz in reduced frequency and the MV estimator as well as the periodogram separate the two peaks. In the middle of Figure 7.8, the difference between the two frequencies is only 0.01 Hz. The MV estimator still separates the two peaks while the periodogram presents only one peak. However, a more detailed study of the periodogram could conclude on the possible presence of two non-resolved peaks by comparing the obtained peak with the spectral window of the estimator. Actually, the peak obtained by the periodogram has a bandwidth greater than the frequency resolution of the periodogram (bandwidth at -3 dB for 128 samples equal to 0.008 Hz) [DUR 99]. In Figure 7.8 at the bottom, where the frequency difference is only of 0.006 Hz, the estimators do not separate the peaks even if two maxima are observed on the MV estimator. These maxima do not emerge relatively to the estimator's standard deviation.

7.3. Link with the Fourier estimators

The comparison with the Fourier-based methods is immediate if the estimator is written in the form of a filtering. A periodogram or a non-averaged correlogram $S_{FOU}(f)$ can be written as:

$$S_{FOU}(f) = \frac{1}{M} \mathbf{E}_f^H \mathbf{R}_x \mathbf{E}_f \quad [7.31]$$

This result is well known. The Fourier estimator is the output power of a filter bank whose impulse response of each filter at the frequency f is an exponential function at this frequency, a function limited in time by a rectangular window of M samples, the length of the vector \mathbf{E}_f . This vector is the counterpart of \mathbf{A}_{f_c} for the Capon method (see [7.4]) but is totally independent of the signal. The power is divided by M so that the result is homogeneous to a spectrum (see section 7.5.1).

The statistical performances of a periodogram are well known. In this section we transcribe them with the same notations as that of the statistical study of the MV estimator in section 7.2.2. The periodogram $S_{FOU}(f)$ is a non-central χ^2 , with two degrees of freedom, having the proportionality parameter $\mathbf{E}_{f_c}^H \mathbf{R}_w \mathbf{E}_{f_c}$ and

non-central parameter $\mathbf{E}_{f_c}^H \mathbf{R}_d \mathbf{E}_{f_c}$, hence the expressions of the mean and of the variance:

$$\begin{aligned} E(S_{\text{FOU}}(f)) &= \frac{1}{M} (\mathbf{E}_f^H \mathbf{R}_w \mathbf{E}_f + \mathbf{E}_f^H \mathbf{R}_d \mathbf{E}_f) \\ \text{Var}(S_{\text{FOU}}(f)) &= \frac{1}{M^2} \left((\mathbf{E}_f^H \mathbf{R}_w \mathbf{E}_f)^2 + 2 \cdot \mathbf{E}_f^H \mathbf{R}_w \mathbf{E}_f \cdot \mathbf{E}_f^H \mathbf{R}_d \mathbf{E}_f \right) \end{aligned}$$

which should be directly compared with [7.21].

To make the link with more typical scalar expressions, we should note that $\frac{1}{M} \mathbf{E}_f^H \mathbf{R}_d \mathbf{E}_f$ represents the periodogram of the deterministic signal, which is function of $\mathbf{E}_f^H \mathbf{E}_f = M$ in the case of a white noise.

Let us continue with a smoothed periodogram $\tilde{S}_{\text{FOU}}(f)$:

$$\tilde{S}_{\text{FOU}}(f) = \frac{1}{M} \mathbf{E}_f^H \tilde{\mathbf{R}}_x \mathbf{E}_f \quad [7.32]$$

where the covariance matrix $\tilde{\mathbf{R}}_x$ is calculated from the signal $x(k)$ weighted by a window. Let \mathbf{G}_{FOU} be a diagonal matrix $M \times M$ whose elements are the samples of this weighting window; the matrix $\tilde{\mathbf{R}}_x$ is:

$$\tilde{\mathbf{R}}_x = E((\mathbf{G}_{\text{FOU}} \mathbf{X})(\mathbf{G}_{\text{FOU}} \mathbf{X})^H) (\mathbf{G}_{\text{FOU}} \mathbf{X})(\mathbf{G}_{\text{FOU}} \mathbf{X})^H \quad [7.33]$$

Thus, [7.32] becomes:

$$\tilde{S}_{\text{FOU}}(f) = \frac{1}{M} (\mathbf{E}_f^H \mathbf{G}_{\text{FOU}}) \mathbf{R}_x (\mathbf{G}_{\text{FOU}}^H \mathbf{E}_f) \quad [7.34]$$

If this latest expression is compared to the equation of the MV method obtained by combining [7.4] and [7.5], we note that the MV method consists of applying on the signal a particular weighting window induced by the method and defined by the matrix \mathbf{G}_{MV} :

$$\mathbf{G}_{\text{MV}} = \frac{\mathbf{R}_x^{-1}}{\mathbf{E}_f^H \mathbf{R}_x^{-1} \mathbf{E}_f} \quad [7.35]$$

No longer diagonal as in the Fourier estimators, \mathbf{G}_{MV} is a function of the signal and of the frequency. It is equal to \mathbf{R}_x^{-1} , the inverse of the covariance matrix of the analyzed signal, weighted by a quadratic form function of the frequency. This quadratic form $\mathbf{E}_f^H \mathbf{R}_x^{-1} \mathbf{E}_f$ is actually the power of a signal, which would have \mathbf{R}_x^{-1} as covariance matrix; this factor can thus be seen as a power normalization factor.

7.4. Link with a maximum likelihood estimator

By comparing the form of the equations, Capon [CAP 69] and Lacoss [LAC 71] concluded that the MV method was equivalent to a maximum likelihood method. In 1977, Lacoss recognized the “strange” meaning of this terminology, but he wrote that it is “too late” to change it [LAC 77]. Eleven years later, Kay examined the difference between these two estimators again [KAY 88].

Let us consider the simple case where the signal $x[k]$ is a complex exponential function at the frequency f_{exp} embedded in an additive complex white, Gaussian, centered noise $w[k]$ of variance σ^2 . Let C_c be the complex amplitude of this exponential, the signal is described in the following vector form:

$$\mathbf{X} = C_c \mathbf{E}_{f_{\text{exp}}} + \mathbf{W} \quad [7.36]$$

where \mathbf{X} , $\mathbf{E}_{f_{\text{exp}}}$, and \mathbf{W} are defined in [7.7].

If the frequency f_{exp} is supposed to be known, it is possible to calculate an estimation \hat{C}_c of the complex amplitude C_c by a maximum likelihood method. Because the noise $w[k]$ is Gaussian, maximizing the probability density of $(\mathbf{X} - C_c \mathbf{E}_{f_{\text{exp}}})$ means minimizing the quantity $(\mathbf{X} - C_c \mathbf{E}_{f_{\text{exp}}})^H \mathbf{R}_w^{-1} (\mathbf{X} - C_c \mathbf{E}_{f_{\text{exp}}})$ with \mathbf{R}_w the noise correlation matrix. The minimization leads to [KAY 88]:

$$\hat{C}_c = \mathbf{H}_{f_{\text{exp}}}^H \mathbf{X} \text{ with } \mathbf{H}_{f_{\text{exp}}} = \frac{\mathbf{R}_w^{-1} \mathbf{E}_{f_{\text{exp}}}}{\mathbf{E}_{f_{\text{exp}}}^H \mathbf{R}_w^{-1} \mathbf{E}_{f_{\text{exp}}}} \quad [7.37]$$

The bias and the variance of \hat{C}_c are:

$$E\{\hat{C}_c\} = \mathbf{H}_{f_{\text{exp}}}^H C_c \mathbf{E}_{f_{\text{exp}}} = C_c, \quad [7.38]$$

and:

$$\text{var}\{\hat{C}_c\} = E\left\{\left(\hat{C}_c - E(\hat{C}_c)\right)^2\right\} = \mathbf{H}_{f_{\text{exp}}}^H \mathbf{R}_w \mathbf{H}_{f_{\text{exp}}} = \frac{1}{\mathbf{E}_{f_{\text{exp}}}^H \mathbf{R}_w^{-1} \mathbf{E}_{f_{\text{exp}}}} \quad [7.39]$$

The maximum likelihood estimator can be interpreted as the output of a filter whose input is the signal $x[k]$ and of impulse response $\mathbf{H}_{f_{\text{exp}}}$. Another way of proceeding leads to the same expression of the estimator \hat{C}_c . It is about minimizing the filter output variance given by the first part of [7.39] by constraining the bias to be 0. The bias expression in [7.38] makes it possible to express the constraint in the form:

$$\mathbf{H}_{f_{\text{exp}}}^H \mathbf{E}_{f_{\text{exp}}} = 1 \quad [7.40]$$

Thus, the maximum likelihood estimator is also an MV estimator but this estimator is non-biased.

Comparing this approach with that of the Capon method results in the following conclusions. The constraint imposed on the two filters is the same (see [7.1] and [7.40]), but the similarity stops there. Figure 7.9 illustrates the fact that the maximum likelihood estimator is the output of a filtering, while the Capon estimator is the squared output of a filtering. The nature of estimations is thus very different. Capon is homogeneous to power or variance, while the maximum likelihood estimator is homogeneous to amplitude.

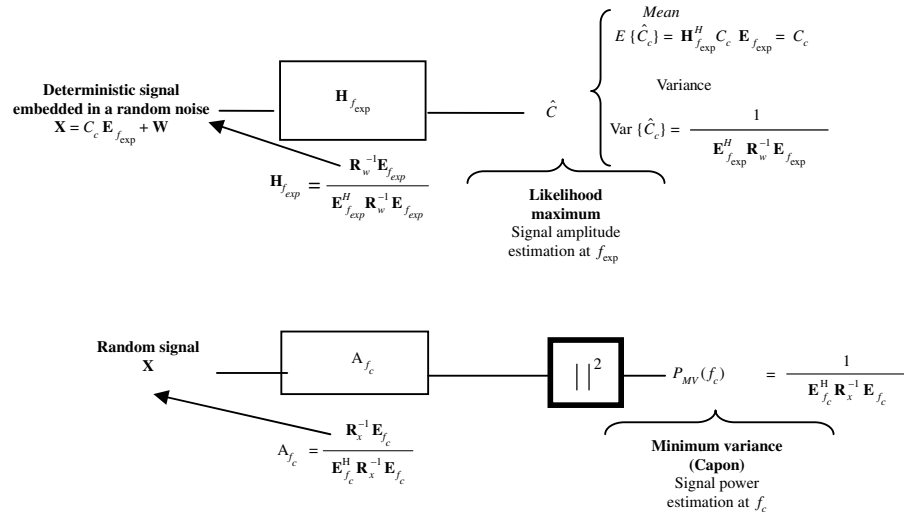


Figure 7.9. MV and maximum likelihood

As the maximum likelihood estimator has a maximal variance, the filter output variance is minimized in both cases. But this minimization is not put in the same terms, which leads to different impulse responses: that of the Capon method depends on the signal covariance matrix (see [7.4]) while that of the maximum likelihood estimator depends on the noise covariance matrix (see [7.37]).

When the analyzed signal has more than one exponential, the maximum likelihood estimator of the amplitude of one of the exponentials requires knowledge of the covariance matrix of the other exponentials embedded in the noise.

These filter structures imply that the bias of the maximum likelihood estimator is null while the Capon estimator is biased (see section 7.2.2).

Thus, the maximum likelihood estimator is more efficient because of its null bias, but it requires a strong *a priori* knowledge, which is not always available. Regarding the approximated maximum likelihood estimators, the reader can refer to the methods developed by Stoica called MAFI for “MAtched FIltter bank” and APES for “Amplitude and Phase Estimation of a Sinusoid” [LI 98, LIU 98b, STO 98, 99]. Another approach combines the APES estimator and the Capon estimator to compensate the bias of the first estimator in frequency and of the second estimator in amplitude [JAK 00].

The Capon estimator is thus more general. It applies to any random signal. The Capon method does not estimate the exponential amplitude, but the signal power at a given frequency. The filter impulse response is calculated from the signal covariance matrix that can always be estimated from the data. The price to pay is a bias that is no longer null.

7.5. Lagunas methods: normalized MV and generalized MV

7.5.1. Principle of the normalized MV

The output power $P_{\text{MV}}(f_c)$ of an MV filter is homogeneous to a power and not to a power spectral density. Lagunas [LAG 84, LAG 86] proposed a modification of the method so that the area under the modified estimator represents the total power of the analyzed signal.

Using the hypothesis that the true spectral density $S_x(f)$ of the signal $x[k]$ is constant around frequency f_c and equal to $S_x(f_c)$, $P_{\text{MV}}(f_c)$ given by [7.2] is:

$$P_{\text{MV}}(f_c) \approx S_x(f_c) \int_{-f_c/2}^{+f_c/2} |A_{f_c}(f)|^2 df \quad [7.41]$$

Constraint [7.1] being verified, the power $P_{\text{MV}}(f_c)$ is linked to the density $S_x(f_c)$ by a factor that we will note as $\beta_{\text{NMV}}(f_c)$. Applying the Parseval relation, this factor is:

$$\beta_{\text{NMV}}(f_c) = \int_{-f_c/2}^{+f_c/2} |A_{f_c}(f)|^2 df = \frac{1}{T_s} \mathbf{A}_{f_c}^H \mathbf{A}_{f_c} \quad [7.42]$$

By normalizing [7.41] by [7.42], Lagunas proposed a normalized estimator denoted as:

$$S_{\text{NMV}}(f_c) = \frac{P_{\text{MV}}(f_c)}{\beta_{\text{NMV}}} \quad [7.43]$$

By considering [7.4] and [7.42], estimator [7.43] can be expressed as the impulse response of the Capon filter; hence:

$$S_{\text{NMV}}(f_c) = T_s \frac{\mathbf{A}_{f_c}^H \mathbf{R}_x \mathbf{A}_{f_c}}{\mathbf{A}_{f_c}^H \mathbf{A}_{f_c}} \quad [7.44]$$

Substituting for \mathbf{A}_{f_c} from [7.5] into [7.44] gives the expression of the nonlinear minimum variance (NMV) estimator:

$$S_{\text{NMV}}(f_c) = T_s \frac{\mathbf{E}_{f_c}^H \mathbf{R}_x^{-1} \mathbf{E}_{f_c}}{\mathbf{E}_{f_c}^H \mathbf{R}_x^{-2} \mathbf{E}_{f_c}} \quad [7.45]$$

According to the definition of $\beta_{\text{NMV}}(f_c)$ (see [7.42]) and knowing that the filter frequency response equals 1 at the frequency f_c , the coefficient $\beta_{\text{NMV}}(f_c)$ has wrongly been assimilated to the equivalent bandwidth of Capon filters [LAG 86]. Actually, this name makes the implicit hypothesis that the frequency responses of the MV filters are null outside the vicinity of f_c . The MV filter study presented in section 7.2.3 shows that these filters are not narrow bandpass filters. Other very important lobes are generally present. Thus, for most filters, the maximum of the frequency response is not at frequency f_c and is much greater than 1. Therefore, the

definition of [7.42] does not correspond to that of an equivalent filter bandwidth, even in magnitude order.

Moreover, this implicit hypothesis of narrowband filters, necessary to write [7.41], is damageable to the properties of this estimator. These consequences are discussed in section 7.5.2.

Most frequently, the proposed normalization [IOA 94, KAY 88] consists of dividing the power $P_{\text{MV}}(f_c)$ by the quantity:

$$B_e = \frac{1}{T_s} \mathbf{E}_{f_c}^H \mathbf{E}_{f_c} = \frac{1}{T_s M} \quad [7.46]$$

This quantity B_e is the equivalent bandwidth of the impulse response \mathbf{E}_{f_c} of a Fourier estimator and not that of the response \mathbf{A}_{f_c} of an MV filter. It is thus about an approximation. The statistical performances of this estimator are studied in [IOA 94].

An alternative normalization is proposed in section 7.6.

7.5.2. Spectral refinement of the NMV estimator

The NMV method is not designed to have a higher resolution than the MV method. Its objective is to estimate a quantity homogeneous to a power spectral density and not to a power. The frequency resolution is not improved, but the visualization makes it possible to better separate close frequencies. Figure 7.10 shows the improvement brought by the NMV estimator compared to the MV estimator for two close frequencies. At a finite order M , the peaks sharpen, but still remain centered on the same frequency.

This outcome is due to the normalization by the factor $\beta_{\text{NMV}}(f_c)$ and it can be explained from the MV filter study presented in section 7.2 [DUR 00]. Let us calculate the ratio $\frac{P_{\text{MV}}(f)}{S_{\text{NMV}}(f)}$ at the exponential frequency f_{exp} and at a close frequency $(f_{\text{exp}} + \varepsilon)$ with ε tending to 0.

When the filter frequency f_c is equal to the frequency f_{exp} , the frequency response is given by [7.15]. In this case, the normalization factor defined by [7.42] and denoted as $\beta_{\text{NMV exp}}(f_c)$ is:

$$\beta_{\text{NMV exp}}(f_c) \approx \int_{-f_c/2}^{+f_c/2} |D(f_{\text{exp}} - f)|^2 df \quad [7.47]$$

When the filter frequency f_c is equal to the frequency $(f_{\text{exp}} + \varepsilon)$, the frequency response is given by [7.12] that we can approximate at order 2 [DUR 00]. The normalization factor, denoted as $\beta_{\text{NMV}\varepsilon}(f_c)$ in this case, becomes:

$$\beta_{\text{NMV}\varepsilon}(f_c) = \int_{-f_c/2}^{+f_c/2} \frac{|D(f_{\text{exp}} + \varepsilon - f) - D(f_{\text{exp}} - f)(1 - (\pi M T_s)^2 \varepsilon^2 / 6)|^2}{(\pi M T_s)^2 \varepsilon^2 / 3} df \quad [7.48]$$

When ε tends to 0, we have:

$$\beta_{\text{NMV exp}}(f_c) \ll \beta_{\text{NMV}\varepsilon}(f_c) \quad [7.49]$$

This important relation shows that the factor $\beta_{\text{NMV}}(f_c)$ considerably increases as soon as the frequency moves away from the peak maximum. This relation makes it possible to obtain the following order relation between the amplitude ratios:

$$\frac{S_{\text{NMV}}(f + \varepsilon)}{P_{\text{MV}}(f + \varepsilon)} \ll \frac{S_{\text{NMV}}(f)}{P_{\text{MV}}(f)} \quad [7.50]$$

Close to a spectrum maximum, the NMV estimator sharpens its peak without keeping the amplitudes. The spectrum is thus subjected to a transformation that accentuates each spectral variation and that, with a finite order M , does not correctly estimate the spectrum amplitudes. This property is illustrated in Figure 7.11, which presents the NMV spectrum of the same signal as in Figure 7.5. In the wideband part, the spectrum is estimated with amplitudes much lower than the true spectrum and with unrealistic oscillations. On the contrary, the brutal variation of the normalization factor around the pure frequency explains the improvement of this estimator at this frequency compared to the MV estimator (see Figure 7.5).

7.5.3. Convergence of the NMV estimator

It is of interest to study the asymptotic properties of the NMV estimator to give reasons for its use. Let us consider the intermediate expression of the estimator given by [7.44], which can be put in the following form:

$$\mathbf{R}_x \mathbf{A}_{f_c} = \left(\frac{1}{T_s} S_{\text{NMV}}(f_c) \right) \mathbf{A}_{f_c} \quad [7.51]$$

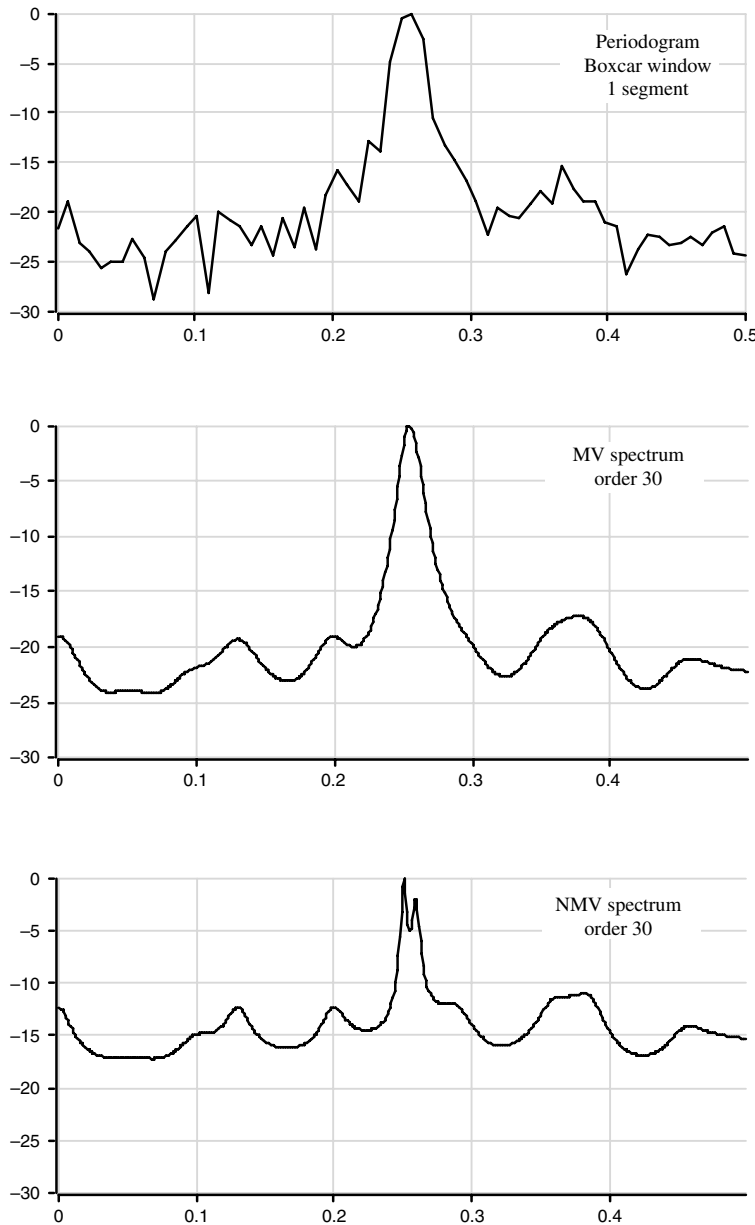


Figure 7.10. NMV estimator compared to the MV estimator and to the periodogram for the power spectral density estimation of the sum of two sinusoids at close frequencies (0.25 and 0.26 Hz, sampling frequency 1 Hz, 128 time samples) of same amplitude 1 with a signal-to-noise ratio of 10 dB. Horizontal axes: frequency

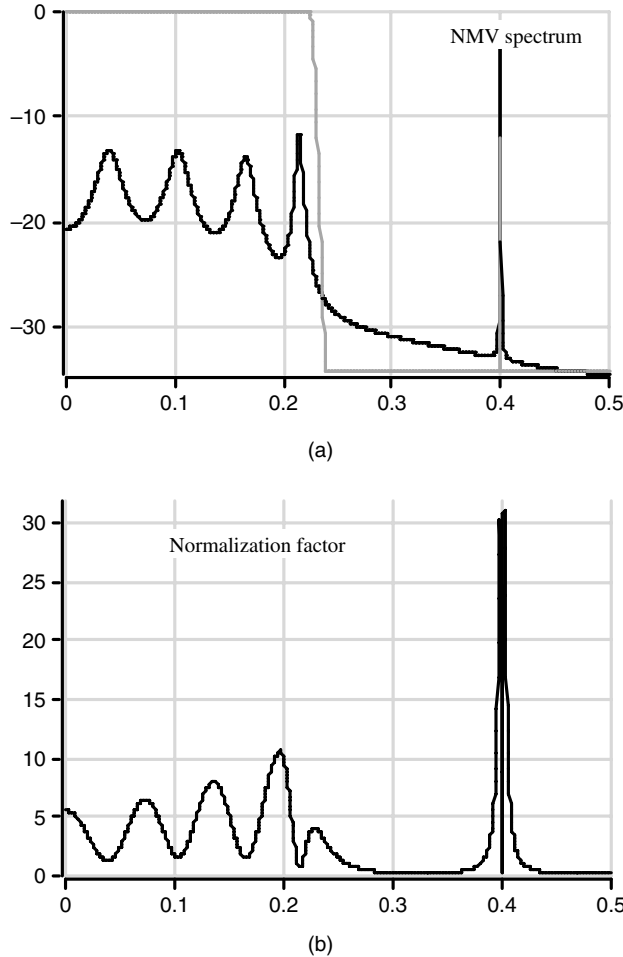


Figure 7.11. Spectral analysis by the NMV estimator of the same signal as that used for Figure 7.5. (a) Superimposition of the true spectrum (gray curve) and of the NMV estimation at order 12 (black curve). (b) Normalization factor in Hz. Vertical axes: spectra in dB. Horizontal axes: frequency in Hz

Equation [7.51] is an eigenvalue equation. At each frequency f_c , the impulse response calculated by the Capon estimator is an eigenvector of the signal covariance matrix. The associated eigenvalue is the spectrum value estimated by the normalized NMV estimator at frequency f_c . This link with the eigenvalue theory [LAG 86] indicates that the NMV method is essentially a pure frequency estimation method because the method comes back to the calculation of eigenvalues of the signal covariance matrix. Figure 7.11 illustrates this point of view.

Equation [7.51] has a second point of interest. It makes it possible to study the convergence of the NMV estimator. Let us consider the following theorem [GRE 58]:

Let $\{\lambda_0, \lambda_1, \dots, \lambda_{M-1}\}$ be the set of eigenvalues and $\{v_0, v_1, \dots, v_{M-1}\}$ the set of eigenvectors of the autocorrelation matrix \mathbf{R}_x . This matrix being Toeplitz, if $M \rightarrow \infty$, then we have the following convergence property:

$$\lambda_i \rightarrow S_x(i / MT_s) \quad [7.52]$$

$$\mathbf{v}_i \rightarrow \frac{1}{\sqrt{M}} \left(1, e^{2\pi ji/MT_s}, \dots, e^{2\pi j(M-1)i/MT_s} \right) \quad [7.53]$$

Thus, we can deduce the convergence property of the NMV estimator when considering eigenvalue equation [7.51] and applying theorem [7.53]. If $M \rightarrow \infty$, then for any frequency f_c multiple of $1/MT_s$:

$$\begin{aligned} \lambda_{f_c} &= \frac{1}{T_s} S_{\text{NMV}}(f_c) \rightarrow S_x(f_c) \\ \mathbf{v}_{f_c} &= \mathbf{A}_{f_c} \rightarrow \frac{1}{\sqrt{M}} \mathbf{E}_{f_c} \end{aligned} \quad [7.54]$$

This theorem implies consequential results for it points out that when the filter order M tends to the infinite, the NMV estimator converges toward the true value of the spectrum for all the frequencies multiple of $1/MT_s$ wideband part.

As a conclusion, at a finite order M , the NMV estimator is adapted to the estimation of pure frequencies without giving a correct estimation in amplitude. It brings a spectral refinement in relation to the MV estimator, which makes it possible to separate close frequencies. To improve the estimation, it is necessary to increase the order given that the NMV estimator converges toward the true spectrum at an infinite order.

7.5.4. Generalized MV estimator

To improve the convergence of the NMV estimator, Lagunas [LAG 86] proposed a generalization of this estimator referred to as $S_{\text{GMV}}(f)$:

$$S_{\text{GMV}}(f_c) = T_s \frac{\mathbf{E}_{f_c}^H \mathbf{R}_x^{-q+1} \mathbf{E}_{f_c}}{\mathbf{E}_{f_c}^H \mathbf{R}_x^{-q} \mathbf{E}_{f_c}} \quad [7.55]$$

q being a positive integer. The justification of this generalized estimator comes from the fact that when a positive defined matrix is raised to a power higher than 1, the contrast between the eigenvalues is increased. This estimator is also defined as data filtering [MAR 95]. The impulse response, denoted as $\mathbf{A}_{f_{c,q}}$, does not apply directly on the signal to be analyzed but on the preprocessed signal so that the signal correlation matrix should be raised to the power q at the end of the preprocessing. Instead of [7.4], the filter output power denoted as P_q is:

$$P_q = \mathbf{A}_{f_{c,q}}^H \mathbf{R}_x^q \mathbf{A}_{f_{c,q}} \quad [7.56]$$

The minimization of this equation with the same constraint as for the MV estimator [7.1] leads to the following expression of $\mathbf{A}_{f_{c,q}}$:

$$\mathbf{A}_{f_{c,q}} = \frac{\mathbf{R}_x^{-q} \mathbf{E}_{f_c}}{\mathbf{E}_{f_c}^H \mathbf{R}_x^{-q} \mathbf{E}_{f_c}} \quad [7.57]$$

This estimator is a generalization of the MV estimators. Actually, if the filter is designed this way, it is directly applied on the signal, the output power is the generalized estimator denoted as $P_{q,G}(f_c)$:

$$P_{q,G}(f_c) = \mathbf{A}_{f_{c,q}}^H \mathbf{R}_x \mathbf{A}_{f_{c,q}} \quad [7.58]$$

According to the value of q , we find all the different estimators:

$$- q = 0$$

$$P_{0,G}(f_c) = \frac{\mathbf{E}_{f_c} \mathbf{R}_x \mathbf{E}_{f_c}}{M^2}, \text{ i.e. the periodogram estimator;}$$

$$- q = 1 \quad P_{1,G}(f_c) = P_{\text{MV}}(f_c), \text{ the Capon estimator;}$$

$$- q = 2 \quad P_{2,G}(f_c) = S_{\text{NMV}}(f_c), \text{ the normalized Capon or Lagunas estimator;}$$

$$- q \geq 2 \quad P_{q,G}(f_c) = S_{\text{GMV}}(f_c), \text{ the generalized estimator.}$$

For an increasing value of q and at a finite order M , the generalized estimator provides a correct value of the position of the peaks in frequency. Experimentally, the generalized estimator converges quite quickly and sometimes it is not necessary to use an order q higher than 5. However, the higher q is, the more disturbed the amplitude of the peaks will be. This generalization is also supported by the constrained minimization techniques, which can include other estimators than those presented in this section [MAR 88, MAR 95].

It can be interesting to couple this frequency estimation with a power estimator, such as the Capon estimator. This leads to hybrid estimators. The hybrid methods couple the Capon estimator with frequency estimators, either the NMV (LAGCAP estimator) or the AR estimator (ARCAP). These estimators are presented in [DON 04] as well as in [LEP 98, PAD 96].

7.6. A new estimator: the CAPNORM estimator

The strong idea of the normalized MV estimator presented in section 7.5 is to define a spectral density estimator from the power estimator given by the MV. This idea is based on [7.41]. However, this equation makes the implicit hypothesis that the MV filters are narrow band, a hypothesis that is not verified. It is of interest to propose another writing of this equation.

A solution consists of adapting the integration support in [7.41] to the filter shape. [DUR 00] has proposed such an adaptation, which leads to a new estimator called CAPNORM.

The main part of the frequency response is located around the filter frequency f_c . Let ΔB be the width of the lobe containing f_c , the contribution to the integral of [7.2] is close to 0 outside this band, either $S_x(f) \approx 0$ or $|A_{f_c}(f)| \approx 0$, then:

$$P_{\text{MV}}(f_c) \approx \int_{\Delta B} |A_{f_c}(f)|^2 S_x(f) df \quad [7.59]$$

If $S_x(f)$ is assumed to be constant in the band ΔB , such that $S_x(f) \approx S_x(f_c)$, then [7.41] is:

$$P_{\text{MV}}(f_c) \approx S_x(f_c) \int_{\Delta B} |A_{f_c}(f)|^2 df \quad [7.60]$$

By substituting [7.6] into [7.60], a new estimator denoted as $S_{\text{CNorm}}(f_c)$ is defined as [DUR 00]:

$$S_{\text{CNorm}}(f_c) = \frac{1}{\mathbf{E}_{f_c}^H \mathbf{R}_x^{-1} \mathbf{E}_{f_c} \beta_{\text{CNorm}}(f_c)} \quad [7.61]$$

where $\beta_{\text{CNorm}}(f_c)$ is:

$$\beta_{\text{CNorm}}(f_c) \approx \int_{\Delta B} |A_{f_c}(f)|^2 df \quad [7.62]$$

This local integral should be evaluated. Owing to its nonlinearity, we will numerically approximate [7.62] by:

$$\beta_{\text{CNorm}}(f_c) \approx \Delta B \sup_{f \in \Delta B} |A_{f_c}(f)|^2 \quad [7.63]$$

within the band $\Delta B = [f_-, f_+]$, which can be called the equivalent filter band at frequency f_c , defined by:

$$|A_{f_c}(f_-)|^2 = |A_{f_c}(f_+)|^2 = \frac{1}{2} |A_{f_c}(f)|^2 \quad [7.64]$$

The quantity $\beta_{\text{CNorm}}(f_c)$ should be considered as an integration support, which adapts to the shape of the frequency response around the frequency f_c of the filter, the band ΔB being the local equivalent band of the lobe containing this frequency.

Figure 7.12 illustrates the CAPNORM estimator on the same signal as that used for Figures 7.5 and 7.11. The peak of the exponential frequency is sharpened. The amplitude is always underestimated but with a weaker bias. The strong improvement is especially on the signal wideband. The estimation is close to the true spectrum, the oscillations being almost completely suppressed. The amplitude of the wideband spectrum is around the theoretical value, which is a considerable gain even compared to the MV estimator (see Figure 7.13). The factor $\beta_{\text{CNorm}}(f_c)$ is weaker and more stable than the normalization factor $\beta_{\text{NMV}}(f_c)$. An experimental statistical study of this estimator is presented in [DUR 00].

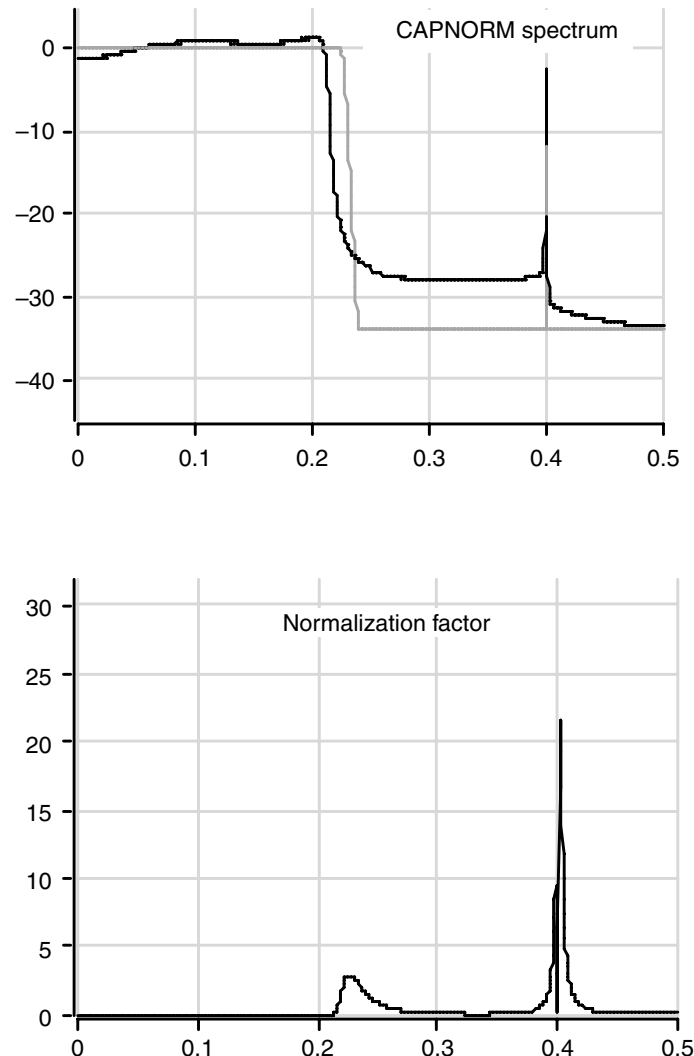


Figure 7.12. Spectral analysis by the CAPNORM estimator of the same signal as that used for Figure 7.5. (a) Superimposition of the true spectrum (gray curve) and of the CAPNORM estimation at order 12 (black curve). (b) Normalization factor in Hz. Vertical axis: spectra in dB. Horizontal axes: frequency in Hz

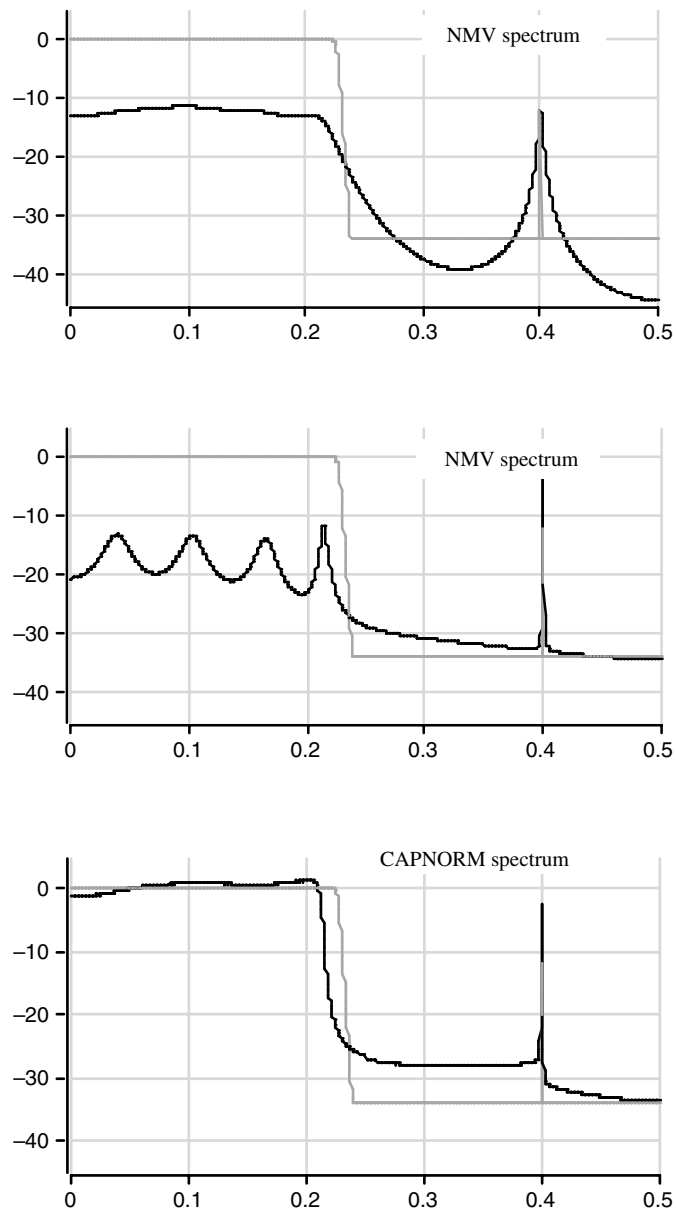


Figure 7.13. Comparison of the MV, NMV, and CAPNORM estimators, all at order 12 (black curves) and the true spectrum (gray curves) for the spectral analysis of the same signal as that used for Figure 7.5. Horizontal axes: frequency in Hz. Vertical axes: spectra in dB

7.7. Bibliography

- [BAS 92] BASSEVILLE M., FLANDRIN P., MARTIN N., "Signaux non-stationnaires. Analyse temps-fréquence et segmentation", *Traitemennt du Signal*, vol. 9, no. 1, 1992, Supplément.
- [BON 90] BONDANT L., MARS J., MARTIN N., "Analyse spectrale de signaux non-stationnaires par des méthodes temps-fréquence: Fourier, Wigner-Ville lissée, AR et Lagunas évolutifs, méthodes hybrides", *French Acoustics Congress*, SFA, Lyon, 1990.
- [CAP 67] CAPON J., GREENFIELD R.J., KOLKER R.J., "Multidimensional maximum-likelihood processing of a large aperture seismic array", *Proceedings of the IEEE*, vol. 55, pp. 192–211, February 1967.
- [CAP 69] CAPON J., "High-resolution frequency-wavenumber spectrum analysis", *Proceedings of the IEEE*, vol. 57, pp. 1408–1418, August 1969.
- [CAP 70] CAPON J., GOODMAN N.R., "Probability distributions for estimates of the frequency-wavenumber spectrum", *Proceedings of the IEEE*, vol. 58, pp. 1785–1786, 1970.
- [CAP 71] CAPON J., "Correction to probability distributions for estimates of the frequency-wavenumber spectrum", *Proceedings of the IEEE*, vol. 59, p. 112, January 1971.
- [DON 04] DONCARLI C., MARTIN N. (eds), *Décision dans le plan temps-fréquence*, Hermès Science, Paris, 2004.
- [DUR 99] DURNERIN M., Une stratégie pour l'interprétation en analyse spectrale. Détection et caractérisation des composantes d'un spectre, PhD Thesis, Grenoble-INP, September 1999.
- [DUR 00] DURNERIN M., MARTIN N., "Minimum variance filters and mixed spectrum estimation", *Signal Processing*, vol. 80, no. 12, pp. 2597–2608, December 2000.
- [FER 86] FERNANDEZ J., MARTIN N., "Adaptive spectral estimation by ML filtering", *Proceedings of EUSIPCO 86*, pp. 323–326, 1986.
- [GOL 85] GOLUB G.H., LOAN C.F.V., *Matrix Computations*, Johns Hopkins University Press, US, Maryland, 1985.
- [GRE 58] GRENDANDER U., SZEGO G., *Toeplitz Forms and Their Applications*, University of California Press, Berkeley, 1958.
- [GUE 85] GUEGUEN C., "Analyse de la parole par les méthodes de modélisation paramétrique", *Annales des Télécommunications*, vol. 40, no. 5–6, pp. 253–269, 1985.
- [HON 98a] HONGBIN L., STOICA P., JIAN L., "Capon estimation of covariance sequence", *Circuits Systems and Signal Processing*, vol. 17, no. 1, pp. 29–49, 1998.
- [HON 98b] HONGBIN L., STOICA P., JIAN L., JAKOBSSON A., "On the performance analysis of forward-only and forward-backward matched filterbank spectral estimators", *Conference Record of the Thirty-First Asilomar Conference on Signals, Systems and Computers*, Los Alamitos, CA, IEEE Computer Society, 1998.

- [IOA 94] IOANNIDIS E., "On the behaviour of a Capon-type spectral density estimator", *The Annals of Statistics*, vol. 22, no. 4, pp. 2089–2114, 1994.
- [JAK 00] JAKOBSSON A., STOICA P., "Combining Capon and APES for estimation of spectral lines", *Circuits, Systems, and Signal Processing*, vol. 19, no. 2, pp. 159–169, 2000.
- [JAN 99] JANSSON M., STOICA P., "Forward-only and forward-backward sample covariances – a comparative study", *Signal Processing*, vol. 77, no. 3, pp. 235–245, September 1999.
- [KAY 88] KAY S.M., *Modern Spectral Estimation Theory and Applications*, Prentice-Hall, Englewood Cliffs, NJ, 1988.
- [LAC 71] LACOSS R.T., "Data adaptive spectral analysis methods", *Geophysics*, vol. 36, no. 4, pp. 661–675, August 1971.
- [LAC 77] LACOSS R.T., "Autoregressive and maximum likelihood spectral analysis methods", in TACCONI G. (ed.) *Aspects of Signal Processing*, part 2, D. Reidel Publishing Company, Dordrecht-Holland, pp. 591–615, 1977.
- [LAG 84] LAGUNAS M.A., GASULL A., "An improved maximum likelihood method for power spectral density estimation", *IEEE Transactions on Acoustics Speech and Signal Processing*, vol. 32, pp. 170–172, February 1984.
- [LAG 86] LAGUNAS M.A., SANTAMARIA M.E., GASULL A., MORENO A., "Maximum likelihood filters in spectral estimation problems", *Signal Processing*, vol. 10, no. 1, pp. 19–34, January 1986.
- [LAT 87] LATOMBE C., "Analyse spectrale évolutive – Comparaison de plusieurs algorithmes sur l'ensemble de plusieurs signaux tests du GRECO SARTA", *GRETSI*, June 1987.
- [LEP 98] LEPRETTRE B., MARTIN N., GLANGEAUD R., NAVARRE J.P., "Three-component signal characterization in the time, time-frequency, and polarization domains using the arcap method: Application to seismic detection of avalanches", *IEEE Transactions on Signal Processing*, vol. 46, no. 1, January 1998.
- [LEV 64] LEVIN M.J., Maximum likelihood array processing, Semi annual Tech. Summary Report on Seismic Discrimination, Massachusetts Institute of Technology, Lincoln Laboratories, Lexington, MA., December 1964.
- [LI 98] LI H., LI J., STOICA P., "Performance analysis of forward-backward matched-filterbank spectral estimators", *IEEE Transactions on Signal Processing*, vol. 46, no. 7, pp. 1954–1966, July 1998.
- [LIU 98a] LIU X., SHERMAN P.J., "Asymptotic statistical properties of the Capon MV spectral estimator for mixed spectrum processes", *Ninth IEEE Signal Processing Workshop on Statistical Signal and Array Processing*, New York, pp. 328–331, 1998.
- [LIU 98b] LIU Z.S., LI H., LI J., "Efficient implementation of Capon and APES for spectral estimation", *IEEE Transactions on Aerospace and Electronic Systems*, vol. 34, no. 4, pp. 1314–1319, October 1998.

- [MAI 06a] MAILHES C., MARTIN N., SAHLI K., LEJEUNE G., Invited conference, “Condition monitoring using automatic spectral analysis”, Special session on “Condition monitoring of machinery”, *Third European Workshop on Structural Health Monitoring, SHM 2006*, Granada, Spain, pp. 1316–1323, July 5–7, 2006.
- [MAI 06b] MAILHES C., MARTIN N., SAHLI K., LEJEUNE G., “A spectral identity card”, *European Signal Processing Conference, EUSIPCO 06*, Florence, Italy, September 4–8, 2006.
- [MAR 88] MARTIN N., LACOUME J.L., SANTAMARIA M.E., “Unified spectral analysis”, *EUSIPCO*, pp. 179–182, 1988.
- [MAR 95] MARTIN N., MARS J., MARTIN J., CHORIER C., “A Capon’s time-octave representation: application in room acoustics”, *IEEE Transaction on Signal Processing*, vol. 43, no. 8, pp. 1842–1854, August 1995.
- [PAD 95] PADOVESE L., TERRIEZ J.M., MARTIN N., “Etude des Phénomènes Dynamiques dans les Pylônes Compression des Téléphériques Monocâble”, *Mécanique Industrielle et Matériaux*, vol. 48, no. 4, December 1995.
- [PAD 96] PADOVESE L., MARTIN N., TERRIEZ J.M., “Méthode temps-fréquence hybride ARCAP pour l’identification des caractéristiques dynamiques d’un pylône compression d’un téléphérique monocâble”, *Traitemet du Signal*, vol. 13, no. 3, September 1996.
- [PAD 09] PADOVESE L., MILLIOZ F., MARTIN N., “Time-frequency and time-scale analysis of Barkhausen noise signals”, *Proceedings of the Institution of Mechanical Engineers, Part G, Journal of Aerospace Engineering for the Structure and Machine Monitoring*, special issue, 223 (G5), pp. 577–588, 2009.
- [SHE 91] SHERMAN P.J., “On the family of ML spectral estimates for mixed spectrum identification”, *IEEE Transactions on Signal Processing*, vol. 39, no. 3, March 1991.
- [STO 98] STOICA P., JAKOBSSON A., LI J., “Matched-filter-bank interpretation of some spectral estimators”, *Signal Processing*, vol. 66, no. 1, pp. 45–59, April 1998.
- [STO 99] STOICA P., HONGBIN L., JIAN L., “A new derivation of the APES filter”, *IEEE Signal Processing Letters*, vol. 6, pp. 205–206, August 1999.

Chapter 8

Subspace-Based Estimators and Application to Partially Known Signal Subspaces

8.1. Model, concept of subspace, definition of high resolution

8.1.1. *Model of signals*

Let $x_a(t)$ be an analogic signal made up of P complex sine waves in an additive noise:

$$x_a(t) = \sum_{i=1}^P \alpha_i e^{j2\pi f_i t} + b_a(t) \quad [8.1]$$

where the α_i are centered complex random and independent variables of variances $\sigma_{\alpha_i}^2$, where $b_a(t)$ is a centered, complex, white noise of variance $E(|b_a(t)|^2) = \sigma^2$ independent from α_i . We suppose the noise and the signals to be circular so that the methods presented here will be based only on the first correlation functions of the different signals. Moreover, we will further work on the sampled signals $x(k) = x_a(kT_e)$ and $b(k) = b_a(kT_e)$ where T_e is a sampling period verifying the Shannon theorem for the complex sine waves. Using the non-correlation hypotheses of the sine waves and of the noise we can write the autocorrelation function of the observations as:

$$\gamma_{xx}(k, m, m') = \sum_{i=1}^P \sum_{l=1}^P E(\alpha_i \alpha_l^*) e^{j2\pi(f_i - f_l)kT_e} e^{j2\pi(mf_i - m'f_l)T_e} + \sigma^2 \delta_{m-m'} \quad [8.2]$$

Chapter written by Sylvie MARCOS and Rémy BOYER.

where $\delta_{m-m'}$ is the Kronecker symbol. If the α_i are non-correlated (e.g. if $\alpha_i = A_i e^{j\phi_i}$ with the deterministic A_i and the random ϕ_i uniformly distributed on $[0, 2\pi]$ and independent each of the others) then $x(k)$ is stationary and its correlation coefficients are:

$$\gamma_{xx}(m - m') = \sum_{i=1}^P \sigma_{\alpha_i}^2 e^{j2\pi f_i(m - m')T_e} + \sigma^2 \delta_{m-m'} \quad [8.3]$$

and the M order correlation matrix Γ_{xx} is written:

$$\Gamma_{xx} = \begin{bmatrix} \gamma_{xx}(0) & \dots & \gamma_{xx}(M-1) \\ \vdots & \ddots & \vdots \\ \gamma_{xx}(M-1)^* & \dots & \gamma_{xx}(0) \end{bmatrix} \quad [8.4]$$

($*$ denotes the conjugate of a complex number). We will consider this case in the following.

In practice, it is not Γ_{xx} that will be used but its estimate:

$$\hat{\Gamma}_{xx} = \begin{bmatrix} \hat{\gamma}_{xx}(0) & \dots & \hat{\gamma}_{xx}(M-1) \\ \vdots & \ddots & \vdots \\ \hat{\gamma}_{xx}(M-1)^* & \dots & \hat{\gamma}_{xx}(0) \end{bmatrix} \quad [8.5]$$

where:

$$\hat{\gamma}_{xx}(m) = \frac{1}{N} \sum_{n=-(N-1)/2}^{(N-1)/2} x(n+m)x^*(n) \quad [8.6]$$

and N is supposed to be odd. This estimation of Γ_{xx} relies on the assumption that $x(k)$ is ergodic.

8.1.2. Concept of subspaces

The methods that will be presented below are based on the decomposition of the observation space in two subspaces, the signal subspace and the noise subspace. Actually, by introducing the vector $\mathbf{x}(k)$ of the M snapshots $\{x(k), x(k+1), \dots, x(k+M-1)\}$, we easily verify that:

$$\mathbf{x}(k) = \begin{bmatrix} x(k) \\ x(k+1) \\ \vdots \\ x(k+M-1) \end{bmatrix} = \mathbf{A}\mathbf{s}(k) + \mathbf{b}(k) \quad [8.7]$$

with

$$\begin{aligned}\mathbf{A} &= [\mathbf{a}_1, \dots, \mathbf{a}_P] \\ \mathbf{s}(k) &= [\alpha_1 e^{j2\pi f_1 k T_e}, \dots, \alpha_P e^{j2\pi f_P k T_e}]^T \\ \mathbf{b}(k) &= [b(k), \dots, b(k+M-1)]^T\end{aligned}\quad [8.8]$$

where:

$$\mathbf{a}_i = \mathbf{a}(f_i) = [1, e^{j2\pi f_i T_e}, e^{2j2\pi f_i T_e}, \dots, e^{j(M-1)2\pi f_i T_e}]^T \quad [8.9]$$

$\mathbf{a}(f_i)$ is the complex sinusoid vector at frequency f_i , \mathbf{A} is the matrix of dimension (M, P) the columns of which are the complex sinusoid vectors, and $\mathbf{s}(k)$ contains the amplitudes of the sine waves (T and H indicate the transpose and the transconjugate of a vector or a matrix, respectively).

According to the model [8.7], we can see that in the absence of noise, the M -dimensional complex vector of the observations $\mathbf{x}(k)$ in \mathbb{C}_M belongs to the P -dimensional subspace, $\text{esp}\{\mathbf{A}\}$ spanned by the complex sinusoid vectors $\mathbf{a}(f_i)$ that are supposed to be linearly independent. When noise is present, it is no longer the case. However, the information of interest concerning the frequencies of the sine waves remains limited to this subspace called the signal subspace (the complex sinusoid space). We call noise subspace the subspace complementary to $\text{esp}\{\mathbf{A}\}$ in \mathbb{C}_M .

The subspaces-based methods rely on the two fundamental hypotheses that follow: $P < M$ and *matrix \mathbf{A} of dimension (M, P) is full rank*. This implies that the vectors $\mathbf{a}(f_i)$, for $i = 1, \dots, P$, are not linearly dependent. It is easy to see, \mathbf{A} being a Vandermonde matrix (see [8.8], [8.9]), that this property is verified as soon as the f_i are all different. This is not the case in a large number of array processing problems where the source vectors \mathbf{a}_i may have a very different form from that given in [8.9] according to the antenna geometry, the sensor gains, the wavefronts, etc. (see [FLI 98]).

The methods based on this decomposition of the observation space are often called eigendecomposition-based methods because the first of them actually proceeded this way. However, the subspace noise and the subspace signal concepts exist independently of any decomposition in eigenelements. Indeed, there are methods that do not use this procedure. It is the case of the “linear” methods as for example the propagator method that will be presented later.

8.1.3. Definition of high resolution

The methods based on the decomposition of the observation space into signal and noise subspaces have, in most cases, the high-resolution property. We say that a method has a high resolution when its asymptotic resolution is theoretically infinite

in the sense that two signals, however close their frequencies may be, can be separated (estimated or detected) whatever the signal-to-noise ratio (SNR) may be, provided that the number of samples N used for the estimation of the correlation matrix [8.5], [8.6] tends to infinity and that the model [8.4] is verified.

To better illustrate this concept of high resolution in relation to the classic Fourier analysis, we here rewrite the spectral estimators of the periodogram and of the correlogram, making the same sizes of observations M and N , which were introduced in the preceding sub-sections, appear. Given N observations of the signal $x(k)$ partitioned in L adjacent sequences of M successive observations of $x(k)$, the Bartlett periodogram is given by [MAR 87]:

$$\begin{aligned}\widehat{S}_{xx}^{per}(f) &= \frac{1}{L} \sum_{l=0}^{L-1} \widehat{S}_{xx}^{(l)}(f) \\ \widehat{S}_{xx}^{(l)}(f) &= \frac{1}{M} \left| \sum_{m=0}^{M-1} x(lM+m) \exp \{-j2\pi fmT_e\} \right|^2\end{aligned}\quad [8.10]$$

In the same way, the correlogram is written ([MAR 87]; see also section 5.2):

$$\widehat{S}_{xx}^{corr}(f) = \sum_{m=-(M-1)/2}^{(M-1)/2} \widehat{\gamma}_{xx}(m) \exp \{-j2\pi fmT_e\} \quad [8.11]$$

where $\widehat{\gamma}_{xx}(m)$ is given in [8.6]. The high-resolution property of the subspace-based methods comes from the fact that at fixed M , it is enough to increase N indefinitely so that the method distinguishes two sine waves, however close to each other they may be. This is not the case for the periodogram and for the correlogram methods since not only N but also M should increase indefinitely to have this result.

8.1.4. Connection with spatial analysis or array processing

It is important to know that the subspace-based methods have been first introduced in array processing where the problem is to extract, from information simultaneously measured on a network of M sensors, information, particularly spatial information, concerning P sources emitting or reflecting waves that propagate in a given physical environment. It is easy to make a parallel between the problem of detection and estimation of P frequencies contained in a time series and the problem of detection and estimation of the directions of arrival (DOA) of P waves coming from dispersed sources in a given space. This parallelism is exact in the so-called uniform linear antenna (ULA) consisting of an array of omnidirectional sensors, aligned and equally spaced with equal gains. Conversely, all the spectral analysis methods have been extended to the case of array processing [JOH 82].

In array processing, the vectors \mathbf{a}_i are called source steering vectors and they take into account the propagation parameters of the waves, the localization parameters of the sources in relation to the antenna (therefore of the antenna geometry), and the reception parameters of the antenna sensors.

8.2. MUSIC

8.2.1. Principle of the MUSIC method

The MUSIC method (MULTiple SIgnal Characterization) was introduced at the same time in [SCH 79] and in [BIE 83] in array processing and it is a geometric approach to the problem. It can be seen as an extension of the Pisarenko method [PIS 73] in the case of time series.

Let us take again the model [8.4] of the covariance matrix, which is a definite, non-negative and Hermitian matrix, and let us consider its eigendecomposition:

$$\boldsymbol{\Gamma}_{xx} = \sum_{m=1}^M \lambda_m \mathbf{v}_m \mathbf{v}_m^H = \mathbf{V} \boldsymbol{\Lambda} \mathbf{V}^H \quad [8.12]$$

where $\boldsymbol{\Lambda} = \text{diag}\{\lambda_1, \dots, \lambda_M\}$ and $\mathbf{V} = [\mathbf{v}_1, \dots, \mathbf{v}_M]$. The eigenvalues λ_m are real and positive, arranged in descending order and the corresponding eigenvectors \mathbf{v}_m are orthonormal. The following theorem determines the foundation of the MUSIC method.

THEOREM 8.1.— Let the following partition be

$$\mathbf{V} = [\mathbf{V}_s, \mathbf{V}_b], \quad \boldsymbol{\Lambda}_s = \text{diag}[\lambda_1, \dots, \lambda_P], \quad \boldsymbol{\Lambda}_b = \text{diag}[\lambda_{P+1}, \dots, \lambda_M]$$

where \mathbf{V}_s and \mathbf{V}_b are of dimensions $M \times P$ and $M \times (M - P)$ with $P < M$, respectively. Using the hypothesis that the covariance matrix $\boldsymbol{\Gamma}_{ss}$ of the amplitudes of the complex sine waves is of full rank P , the minimum eigenvalue of $\boldsymbol{\Gamma}_{xx}$ is σ^2 and is of multiplicity $M - P$ and the columns of \mathbf{V}_s span the same subspace as \mathbf{A} , i.e.:

$$\begin{aligned} \boldsymbol{\Lambda}_b &= \sigma^2 \mathbf{I} \\ \text{esp}\{\mathbf{V}_s\} &= \text{esp}\{\mathbf{A}\} \\ \text{esp}\{\mathbf{V}_b\} &\perp \text{esp}\{\mathbf{A}\} \end{aligned} \quad [8.13]$$

where \perp indicates the orthogonality.

PROOF.— In the absence of noise, the covariance matrix $\boldsymbol{\Gamma}_{xx}$ is written:

$$\boldsymbol{\Gamma}_{xx} = \mathbf{A} \boldsymbol{\Gamma}_{ss} \mathbf{A}^H \quad [8.14]$$

The matrices \mathbf{A} and Γ_{ss} being of dimensions (M, P) and (P, P) , with $P < M$, respectively, matrix Γ_{xx} of dimension (M, M) is of rank at most equal to P . In theorem 8.1 we suppose that \mathbf{A} and Γ_{ss} are full rank, therefore Γ_{xx} is of rank P . On the other hand, Γ_{xx} , being a covariance matrix, is Hermitian, definite, non-negative, and its eigenvalues are consequently real and positive or null. The hypothesis $P < M$ implies that Γ_{xx} has $M - P$ eigenvalues equal to zero and P strictly positive eigenvalues.

Let \mathbf{v} be an eigenvector of Γ_{xx} associated with the null eigenvalue; then:

$$\Gamma_{xx}\mathbf{v} = \mathbf{A}\Gamma_{ss}\mathbf{A}^H\mathbf{v} = 0 \quad [8.15]$$

The matrices \mathbf{A} and Γ_{ss} being of full rank, we obtain:

$$\mathbf{A}^H\mathbf{v} = 0$$

implying that \mathbf{v} belongs to the kernel of the application associated with the matrix \mathbf{A}^H , that is to say $\text{esp}\{\mathbf{A}\}^\perp$, the subspace orthogonal to the subspace spanned by the columns of \mathbf{A} . If we denote $\text{esp}\{\mathbf{V}_b\}$ the set of the eigenvectors associated with the zero eigenvalue, then it immediately comes $\text{esp}\{\mathbf{V}_b\} \subset \text{esp}\{\mathbf{A}\}^\perp$. Conversely, any vector of $\text{esp}\{\mathbf{A}\}^\perp$ is an eigenvector of Γ_{xx} associated with the zero eigenvalue. Hence $\text{esp}\{\mathbf{V}_b\} = \text{esp}\{\mathbf{A}\}^\perp$. This implies that the other eigenvectors of Γ_{xx} associated with strictly positive eigenvalues and spanning $\text{esp}\{\mathbf{V}_s\}$ are in $\text{esp}\{\mathbf{A}\}$. Then we have $\text{esp}\{\mathbf{V}_s\} \subset \text{esp}\{\mathbf{A}\}$. Now, Γ_{xx} being Hermitian, we know that there is an orthonormal basis of eigenvectors, which implies that the dimension of $\text{esp}\{\mathbf{V}_s\}$ is P . Hence $\text{esp}\{\mathbf{V}_s\} = \text{esp}\{\mathbf{A}\}$.

In the presence of white noise, the eigenvalues of:

$$\Gamma_{xx} = \mathbf{A}\Gamma_{ss}\mathbf{A}^H + \sigma^2\mathbf{I}$$

are those of $\mathbf{A}\Gamma_{ss}\mathbf{A}^H$ increased by σ^2 and the eigenvectors are unchanged, hence the results of Theorem 8.1.

It follows that the subspace $\text{esp}\{\mathbf{V}_s\}$ spanned by the eigenvectors associated with the biggest P eigenvalues of Γ_{xx} is the signal subspace and that the subspace $\text{esp}\{\mathbf{V}_b\}$ spanned by the $M - P$ eigenvectors associated with the smallest eigenvalue σ^2 is the noise subspace. Thus, it immediately results that the complex sinusoid vectors $\mathbf{a}(f_i)$ are orthogonal to the noise subspace, i.e.:

$$\mathbf{V}_b^H\mathbf{a}(f_i) = 0, \quad i = 1, \dots, P \quad [8.16]$$

Consequently, the signal vectors corresponding to the searched frequencies are the vectors $\mathbf{a}(f)$ of the form given in [8.9] which are orthogonal to \mathbf{V}_b .

In order that the resolution of the nonlinear system [8.16] gives the searched frequencies in a unique way, there should be at the most P linearly independent vectors of the form [8.9] in a subspace of dimension P in \mathbb{C}_M . This is true provided $P + 1 < M$. \square

THEOREM 8.2.—*If $P + 1 < M$, any set of P vectors of the form $\mathbf{a}(f)$ given in [8.9], for different P values of f , forms a free family (set of linearly independent vectors) of \mathbb{C}_M .*

PROOF.—In \mathbb{C}_M , an infinity of vectors of the form $\mathbf{a}(f)$ [8.9] exist when f scans the set of real numbers. However, any family of $I < M$ vectors $\{\mathbf{a}(f_1), \dots, \mathbf{a}(f_I)\}$, where the parameters f_i are different, is free because it is easy to verify that the matrix formed by these vectors is of the Vandermonde type. Thus, in a subspace of dimension $I < M$, only I vectors of this type exist. Actually, if another one existed, noted $\mathbf{a}(f_{I+1})$ with $f_{I+1} \neq f_i$ for $i = 1, \dots, I$ in this subspace of dimension I , it would be written as a linear combination of these I vectors and the system $\{\mathbf{a}(f_1), \dots, \mathbf{a}(f_{I+1})\}$ would not be free, which is impossible if $I+1 < M$. Therefore, in $\text{esp}\{\mathbf{A}\}$, subspace of dimension P , if $P + 1 < M$, only P vectors of the form $\mathbf{a}(f)$ exist, which are the complex sinusoid vectors \mathbf{a}_i , for $i = 1, \dots, P$, columns of \mathbf{A} .

In the case of array processing, because of the particular form of the source vectors \mathbf{a}_i , we generally cannot conclude on the uniqueness of the set of solutions [FLI 98], and we make the hypothesis that only the source vectors are solutions of [8.16]. \square

8.2.2. Pseudo-spectral version of MUSIC

The MUSIC algorithm is thus as follows. First, the minimum eigenvalue of the covariance matrix [8.4] of the snapshots has to be determined as well as the number of eigenvalues equal to this value. Next we construct a noise subspace basis \mathbf{V}_b of the eigenvectors associated with this minimum eigenvalue, and then we form the following estimator:

$$S_{\text{MUSIC}}(f) = \frac{1}{\mathbf{a}^H(f)\mathbf{V}_b\mathbf{V}_b^H\mathbf{a}(f)} \quad [8.17]$$

This estimator takes maximum values (theoretically infinite because its denominator measures the orthogonality between the noise subspace and the candidate vector of the form [8.9]) for the true values of the frequencies present in the signal. It is often called pseudo-spectrum by analogy with the spectral estimators introduced in the preceding chapters, although it is not an energy spectrum.

In practice, the covariance matrix is replaced by its estimate $\widehat{\Gamma}_{xx}$ [8.5] so that the estimator [8.17] becomes:

$$S_{\text{MUSIC}}(f) = \frac{1}{\mathbf{a}^H(f)\widehat{\mathbf{V}}_b\widehat{\mathbf{V}}_b^H\mathbf{a}(f)} \quad [8.18]$$

where $\widehat{\mathbf{V}} = [\widehat{\mathbf{V}}_s, \widehat{\mathbf{V}}_b]$ is a partition of the eigenvectors of $\widehat{\mathbf{T}}_{xx}$. Because $\widehat{\mathbf{V}}_b$ differs from its value \mathbf{V}_b , the estimator [8.18] will not make infinite peaks appear. However, the arguments of the maxima of [8.18] yield an estimation of the searched frequencies. Actually, we could have directly chosen the denominator of [8.18] as estimator because it measures the orthogonality of a vector of analysis $\mathbf{a}(f)$ and of the noise subspace. We have taken its inverse for comparing this pseudo-spectrum to the other spectra.

Let us note that the set of the eigenvectors of the covariance matrix [8.4] forming an orthonormal basis of \mathbb{C}_M , $\mathbf{V}_s \mathbf{V}_s^H$, and $\mathbf{V}_b \mathbf{V}_b^H$ represent the orthogonal projectors on the signal and noise subspaces, respectively, and they are such that:

$$\mathbf{V}_s \mathbf{V}_s^H = \mathbf{I} - \mathbf{V}_b \mathbf{V}_b^H \quad [8.19]$$

It follows that maximizing [8.17] means maximizing:

$$\mathbf{a}^H(f) \mathbf{V}_s \mathbf{V}_s^H \mathbf{a}(f) \quad [8.20]$$

which, in an equivalent manner, also constitutes an estimator of the searched frequencies.

8.2.3. Polynomial version of MUSIC

Ideally, the P frequencies contained in the signal to be analyzed, f_1, \dots, f_P make to zero the following function:

$$(S_{\text{MUSIC}}(f))^{-1} = \mathbf{a}^H(f) \mathbf{V}_b \mathbf{V}_b^H \mathbf{a}(f) \quad [8.21]$$

which measures the orthogonality between an analysis vector $\mathbf{a}(f)$ and the noise subspace. By introducing the vector:

$$\mathbf{u}(z) = [1, z, z^2, \dots, z^{M-1}]^T \quad [8.22]$$

we have:

$$\mathbf{a}(f) = \mathbf{u}(e^{j2\pi f}) \quad [8.23]$$

The searched frequencies are then the solution of $(S_{\text{MUSIC}}(f))^{-1}(f_i) = 0$ which is rewritten:

$$\mathbf{u}^T(1/z_i) \mathbf{V}_b \mathbf{V}_b^H \mathbf{u}(z_i) = 0 \quad \text{for } z_i = e^{j2\pi f_i} \quad [8.24]$$

In other words, the frequencies contained in the signal to be analyzed are theoretically the arguments of the P roots situated on the unit circle of:

$$P(z) = \mathbf{u}^T(1/z) \mathbf{V}_b \mathbf{V}_b^H \mathbf{u}(z) \quad [8.25]$$

The uniqueness of the P roots on the unit circle for determining the P frequencies results from Theorem 8.2. It is important to note that $P(z)$ possesses $2M - 2$ symmetric roots in relation to the unit circle, i.e. if z_i is the solution, then $1/z_i$ is also the solution. Thus, there are $M - 1$ roots of module less than or equal to 1 (inside the unit circle) and the searched frequencies thus correspond to the P roots which are on the unit circle. In the practical case, we have only $\widehat{\Gamma}_{xx}$ and we thus choose as estimate the P roots which are closest to the unit circle.

The relation between the polynomial version of MUSIC and the pseudo-spectral version is established by noting that:

$$P(e^{j2\pi f}) = a \prod_{i=1}^{M-1} |e^{j2\pi f} - z_i|^2 \quad [8.26]$$

where a is a constant. $P(e^{j2\pi f})$ is thus the sum of the squares of the distances of $e^{j2\pi f}$ with the roots of $P(z)$; it is minimal when $e^{j2\pi f}$ is aligned with a root close to the unit circle. We show that the performance of the pseudo-spectral and polynomial versions of MUSIC is the same [FOR 98]. The interest of this version resides in the complexity. Searching the zeros of a polynomial is much less costly in calculation than searching the peaks in a pseudo-spectrum.

The MUSIC method is known for its superior performance, especially in resolution, compared to the other methods. In particular, contrary to the methods presented before, the estimates of the pure frequencies obtained by the MUSIC method converge to their true values while the number of samples N used in the estimation of the covariance [8.5] and [8.6] tends to infinity. The MUSIC method is thus a high-resolution method.

However, the limitations of the MUSIC method are important. First, the MUSIC method is based on a precise modeling of the noise by supposing that the covariance matrix of the noise is known with a multiplying factor. In the case of array processing, the MUSIC method is also less robust with a poor knowledge of the propagation model (i.e. the form \mathbf{a} of the source vectors) than the beamforming method (equivalent to the periodogram method) or the minimum variance method. The MUSIC method also requires a determination of the number of complex sine waves before building the estimator of the frequencies. The computational complexity of the MUSIC method, particularly for the search of the eigenelements of the covariance matrix, of the order of M^3 is an important constraint, which pushes the searchers to conceive less complex algorithms (see the section on linear methods). Finally, we will refer to [FOR 98] and [MAR 98c] for the study of the performance and of the robustness of the MUSIC method.

8.3. Determination criteria of the number of complex sine waves

The theory tells us that the number of complex sine waves, given the order of the model, is equal to the number of eigenvalues strictly higher than the smallest eigenvalue of the covariance matrix of the observed signals. However, because we have only a finite number of samples of the signal to analyze and thus only an estimate of the covariance and also because the computer programs of eigenelement research introduce numeric errors, the order of the model is difficult to determine. It seems delicate to choose a threshold without risking not to detecting a frequency contained in the signal. Actually, the performance of the MUSIC method is conditioned by the determination of the number of estimated complex sine waves.

To remedy this limitation, criteria resulted from the information theory were proposed to determine the order of a model [RIS 78, SCH 78]. We simply give here the two most well known criteria (Akaike, MDL). They are based on the likelihood function of the observations.¹

8.3.1. AIC criterion (Akaike information criterion)

Akaike [AKA 73] proposed this criterion to determine the order of an AR model. It consists in minimizing the following quantity in relation to the supposed number p of complex sine waves:

$$\text{AIC}(p) = -N \log \frac{\prod_{i=p+1}^M \hat{\lambda}_i}{\left(\frac{1}{M-p} \sum_{i=p+1}^M \hat{\lambda}_i\right)^{M-p}} + p(2M - p) \quad [8.27]$$

where p is an estimation of P , N the number of observations, and $\hat{\lambda}_i$ the eigenvalues of $\hat{\Gamma}_{xx}$ arranged in descending order. For this criterion, the estimation of the noise variance is given by the average of the $M - p$ smallest eigenvalues of the covariance matrix, that is to say:

$$\hat{\sigma}^2(p) = \frac{1}{M-p} \sum_{i=p+1}^M \hat{\lambda}_i$$

8.3.2. Minimum description length criterion

Minimum description length (MDL) criterion is inspired from [RIS 78, SCH 78] to determine the order of a model. The MDL criterion differs from the AIC criterion

¹ For more details see Chapter 6.

by the second term, which is introduced:

$$\text{MDL}(p) = -N \log \frac{\prod_{i=p+1}^M \hat{\lambda}_i}{\left(\frac{1}{M-p} \sum_{i=p+1}^M \hat{\lambda}_i \right)^{M-p}} + \frac{1}{2} p(2M-p) \log N \quad [8.28]$$

The MDL criterion is consistent, i.e. it converges to the true value of P when N tends to infinity. Comparisons of this criterion exist in [ZHA 89] and in [GRO 98], for example. It is known that the AIC criterion tends to overestimate the number of complex sine waves, even at strong SNR, while the MDL criterion tends to underestimate this number at weak or average SNR and at a finite number of observations N .

Numerous improvements of these criteria were proposed [GRO 98]. We can mention the works in the array processing domain [CHO 93], which make a joint estimation of the number of sources and of their DOA. There are also works that are concerned with determining the number of sources when the noise is colored [CAD 89, ZHA 89].

However, let us note that, philosophically speaking, the problem of determining a threshold to discriminate a sine wave from noise is delicate. Indeed, if we consider that the noise term includes everything that it is not a useful signal, the noise can then be made up of many weak-power sine waves. That is why even if, theoretically, the MUSIC method separates what is white noise from what is pure sine wave, in practice, it will always be difficult to decide on the exact number of sine waves. In other words, a weak-power sine wave (compared to the others) risks not being detected.

8.4. The *MinNorm* method

This method is a variant of the MUSIC method. Indeed, estimator [8.17] tests the orthogonality of an analysis vector supposed to be a complex sinusoid vector, with respect to all the vectors of \mathbf{V}_b which forms a basis of the noise subspace. The *MinNorm* method consists in using only one vector \mathbf{d} of this noise subspace. Thus, let us consider the following spectral estimator:

$$S_{\text{MN}}(f) = \frac{1}{\mathbf{a}^H(f)\mathbf{d}\mathbf{d}^H\mathbf{a}(f)} = \frac{1}{|\mathbf{a}^H(f)\mathbf{d}|^2} \quad [8.29]$$

and, in the same way as for MUSIC, the associated polynomial estimator:

$$P_{\text{MN}}(z) = \sum_{m=1}^M d_m z^{m-1} \quad [8.30]$$

where the d_m are the coefficients of vector \mathbf{d} and with:

$$(S_{MN}(f))^{-1} = |P_{MN}(e^{j2\pi f})|^2 \quad [8.31]$$

It was shown in [KUM 83] that, by choosing the vector \mathbf{d} of minimum norm, with 1 as first component, the zeros of the estimating polynomial [8.30] associated with the noise were reduced inside the unit circle.

Searching the vector \mathbf{d} of minimum norm which belongs to $\text{esp}(\mathbf{V}_b)$, means searching the vector \mathbf{w} so that:

$$\begin{aligned} \mathbf{d} &= \mathbf{V}_b \mathbf{w} \\ J(\mathbf{w}) &= \| \mathbf{d} \|^2 + \lambda(\mathbf{d}^H \mathbf{e}_1 - 1) \quad \text{minimum} \end{aligned} \quad [8.32]$$

where \mathbf{e}_1 is a vector of first component equal to 1 with all the other components equal to zero. Minimizing:

$$J(\mathbf{w}) = \mathbf{w}^H \mathbf{V}_b^H \mathbf{V}_b \mathbf{w} + \lambda(\mathbf{w}^H \mathbf{V}_b^H \mathbf{e}_1 - 1) \quad [8.33]$$

with respect to \mathbf{w} , by noting that the vectors of \mathbf{V}_b being orthonormal, $\mathbf{V}_b^H \mathbf{V}_b = \mathbf{I}$, leads to:

$$\mathbf{w} = -\frac{\lambda}{2} \mathbf{V}_b^H \mathbf{e}_1 \quad [8.34]$$

The condition of first component equal to 1 gives:

$$\lambda = -\frac{2}{\mathbf{e}_1^H \mathbf{V}_b \mathbf{V}_b^H \mathbf{e}_1} \quad [8.35]$$

Finally, we obtain:

$$\mathbf{d} = \frac{\mathbf{V}_b \mathbf{V}_b^H \mathbf{e}_1}{\mathbf{e}_1^H \mathbf{V}_b \mathbf{V}_b^H \mathbf{e}_1} \quad [8.36]$$

Thus, the frequencies included in the signal can be directly obtained by searching the zeros of the polynomial of degree $M - 1$, $P_{MN}(z)$. It is shown in [KUM 83] that the P zeros corresponding to the peaks in [8.29] are situated on the unit circle and that the $M - P$ other zeros remain limited inside the unit circle.

The MinNorm method is more sensitive than the MUSIC method to a small number of snapshots for the estimation of the covariance matrix. It is also shown that MinNorm has a better separating power than MUSIC, but a larger estimation variance (see [FOR 98]).

8.5. “Linear” subspace methods

8.5.1. The linear methods

The methods called linear are an alternative to the MUSIC method, as far as they are based on the orthogonal subspaces but they do not require any eigendecomposition. They use only linear operations on the covariance matrix and have a smaller computational complexity than the MUSIC method. Moreover, they can be made adaptive for real-time applications or so as to follow a non-stationary context.

Among these methods that were developed in array processing, we mainly distinguish the propagator method [MUN 91, MAR 90a, MAR 95], BEWE (bearing estimation without eigendecomposition) [YEH 86], and SWEDE (subspace method without eigendecomposition) [ERI 94] which were unified and compared in [MAR 97]. Only the propagator method is presented here because it has been shown to have the best performance.

8.5.2. The propagator method

This method is based on the partition of the matrix of the complex sinusoid vectors [8.8] in accordance with:

$$\mathbf{A} = \begin{bmatrix} \mathbf{A}_1 \\ \mathbf{A}_2 \end{bmatrix} \quad [8.37]$$

where \mathbf{A}_1 and \mathbf{A}_2 are the matrices of dimension $P \times P$ and $(M - P) \times P$, respectively.

8.5.2.1. Definition of the propagator

Using the hypothesis that \mathbf{A}_1 is non-singular, the propagator \mathbf{P} is the unique operator from \mathbb{C}_{M-P} to \mathbb{C}_P defined by the equivalent relations:

$$\mathbf{P}^H \mathbf{A}_1 = \mathbf{A}_2 \quad [8.38]$$

or

$$\mathbf{Q}^H \mathbf{A} = \mathbf{0} \quad \text{with} \quad \mathbf{Q} = \begin{bmatrix} \mathbf{P} \\ -\mathbf{I}_{M-P} \end{bmatrix} \quad [8.39]$$

where \mathbf{I}_{M-P} and $\mathbf{0}$ are the identity matrix of dimension $M - P$ and the null matrix of dimension $(M - P) \times P$, respectively.

In spectral analysis, \mathbf{A} and \mathbf{A}_1 are Vandermonde matrices. This implies that \mathbf{A} and \mathbf{A}_1 are full rank as soon as the pure frequencies are different. In array processing, given the more general form of the matrices \mathbf{A} and \mathbf{A}_1 , this definition suggests points which will not be discussed further here (see [MAR 97]).

We easily notice that relation [8.39] is similar to [8.16]. It means that the subspace spanned by the columns of matrix \mathbf{Q} , esp $\{\mathbf{Q}\}$, is included in the noise subspace esp $\{\mathbf{V}_b\}$. Moreover, because \mathbf{Q} contains the block \mathbf{I}_{M-P} , its $M - P$ columns are linearly independent. It results that:

$$\text{esp } \{\mathbf{Q}\} = \text{esp } \{\mathbf{V}_b\} = \text{esp } \{\mathbf{A}\}^\perp \quad [8.40]$$

On the other hand, if we introduce the matrix of dimension (M, P) :

$$\mathbf{Q}^\perp = \begin{bmatrix} \mathbf{I}_P \\ \mathbf{P}^H \end{bmatrix} \quad [8.41]$$

we have:

$$\text{esp } \{\mathbf{Q}^\perp\} = \text{esp } \{\mathbf{V}_s\} = \text{esp } \{\mathbf{A}\} \quad [8.42]$$

Therefore, the propagator makes it possible to define the noise and the signal subspaces using matrices \mathbf{Q} et \mathbf{Q}^\perp .

An important difference in defining the noise and the signal subspaces with vectors of \mathbf{V}_b and of \mathbf{V}_s is that the vectors of \mathbf{Q} and of \mathbf{Q}^\perp are not orthonormal and that the matrices $\mathbf{Q}\mathbf{Q}^H$ and $\mathbf{Q}^\perp\mathbf{Q}^{\perp H}$ do not represent projection operators on the noise and the signal subspaces, respectively, as is the case for $\mathbf{V}_b\mathbf{V}_b^H$ and $\mathbf{V}_s\mathbf{V}_s^H$. It was shown in [MAR 97] that an orthonormalization of the matrices \mathbf{Q} and \mathbf{Q}^\perp in \mathbf{Q}_O and \mathbf{Q}_O^\perp , respectively, gives better performance of estimation.

When the noise subspace is determined using the propagator, the pseudo-spectrum:

$$S_{\text{propa}}(f) = \frac{1}{\mathbf{a}^H(f)\mathbf{Q}_O\mathbf{Q}_O^H\mathbf{a}(f)} \quad [8.43]$$

yields an estimator of the frequencies. The solutions are the arguments of the maxima of [8.43].

8.5.2.2. Propagator estimation via a least square technique

The advantage of the propagator is the simple way in which we can obtain it starting from the covariance matrix.

In the no noise case, the covariance matrix of the data Γ_{xx} [8.4] becomes:

$$\Gamma_{xx} = \mathbf{A}\Gamma_{ss}\mathbf{A}^H \quad [8.44]$$

By using partition [8.37] of the matrix of the complex sinusoid vectors and by decomposing the covariance matrix:

$$\Gamma_{xx} = [\mathbf{A}\Gamma_{ss}\mathbf{A}_1^H, \mathbf{A}\Gamma_{ss}\mathbf{A}_2^H] = [\mathbf{G}, \mathbf{H}] \quad [8.45]$$

where \mathbf{G} and \mathbf{H} are the matrices of dimension $M \times P$ and $M \times (M - P)$, respectively, definition [8.38] thus implies:

$$\mathbf{H} = \mathbf{GP} \quad [8.46]$$

This important relation means that the last $M - P$ columns of the covariance matrix without the noise belong to the subspace spanned by the first P columns. The propagator \mathbf{P} is thus the solution of the overdetermined linear system [8.46].

Using the hypothesis that the sine waves are not totally correlated, a hypothesis that is also necessary for MUSIC, matrix \mathbf{G} is of full rank and the propagator is obtained by the least-squares solution:

$$\mathbf{P} = (\mathbf{G}^H \mathbf{G})^{-1} \mathbf{G}^H \mathbf{H} \quad [8.47]$$

In the *noisy case*, the decomposition [8.45] of matrix [8.4] is still possible, but relation [8.46] is no longer valid. An estimation $\hat{\mathbf{P}}$ of the propagator can however be obtained by minimizing the following cost function:

$$J(\hat{\mathbf{P}}) = \| \mathbf{H} - \mathbf{GP} \|^2 \quad [8.48]$$

where $\| . \|$ is the Frobenius norm. The minimization of [8.48] yields:

$$\hat{\mathbf{P}} = (\mathbf{G}^H \mathbf{G})^{-1} \mathbf{G}^H \mathbf{H} \quad [8.49]$$

Thus, obtaining the propagator and therefore determining the matrix \mathbf{Q} , which leads to the noise subspace and to the pseudo-spectrum [8.43], requires the inversion of a matrix of dimension P , which is less complex in calculations than the eigendecomposition of a matrix of dimension M . The reduction of the calculations compared to the MUSIC method is in $O(P/M)$ [MAR 95]. The higher the number of observations, compared to the number of frequencies to estimate, the bigger this gain. Moreover, an adaptive version, capable of tracking possible variations in time of the noise subspace, was given in [MAR 96], limiting again the computation complexity. The reduction of complexity is then in $O(P^2/M^2)$ compared to MUSIC. Let us finally note that this estimation of the propagator does not require that the noise is white. However, if the noise is white, we can find a joint estimation of the variance of the noise and of the propagator, as indicated in the following section.

8.5.2.3. Estimation of the propagator in the presence of white noise

Under the hypothesis that the noise is spatially and temporally white of variance σ^2 , \mathbf{P} can be extracted from Γ_{xx} by introducing the following partition of the modified covariance matrix:

$$\Gamma_{xx}(\delta) = \Gamma_{xx} - \delta \mathbf{I}_M = [\mathbf{G}(\delta), \mathbf{H}(\delta)] \quad [8.50]$$

where δ is a positive scalar number and where $\mathbf{G}(\delta)$ and $\mathbf{H}(\delta)$ are sub-matrices of the respective dimensions $M \times P$ and $M \times (M - P)$. It is shown in [MAR 90a] that $(\hat{\mathbf{P}} = \mathbf{P}, \delta = \sigma^2)$ is the unique solution of:

$$\mathbf{H}(\delta) = \mathbf{G}(\delta)\hat{\mathbf{P}} \quad [8.51]$$

The following proposition was established in [MAR 90a].

PROPOSITION.— Under the hypothesis that matrix \mathbf{A}_2 , of dimension $(M - P) \times P$, is of rank P , $(\hat{\mathbf{P}} = \mathbf{P}, \delta = \sigma^2)$ is the unique solution of [8.51] if and only if $M - P > P$. \square

Let us note that the bigger $M - P$ compared to P , the less constraining this additional hypothesis on \mathbf{A}_2 , i.e. when the number of observations is bigger than the number of frequencies to estimate.

The estimation of the noise variance is obtained using the following comments. By partitioning Γ_{xx} of [8.4] in accordance with:

$$\Gamma_{xx} = \begin{bmatrix} \mathbf{G}_1 \mathbf{H}_1 \\ \mathbf{G}_2 \mathbf{H}_2 \end{bmatrix} \begin{array}{l} \}P \\ \}M - P \end{array} \quad [8.52]$$

where \mathbf{G}_1 , \mathbf{G}_2 , \mathbf{H}_1 , and \mathbf{H}_2 are matrices of dimensions $P \times P$, $(M - P) \times P$, $P \times (M - P)$, and $(M - P) \times (M - P)$, respectively, we have:

$$\begin{cases} \mathbf{G}_1 = \mathbf{A}_1 \Gamma_{ss} \mathbf{A}_1^H + \sigma^2 \mathbf{I}_P \\ \mathbf{G}_2 = \mathbf{A}_2 \Gamma_{ss} \mathbf{A}_1^H \\ \mathbf{H}_1 = \mathbf{A}_1 \Gamma_{ss} \mathbf{A}_2^H \\ \mathbf{H}_2 = \mathbf{A}_2 \Gamma_{ss} \mathbf{A}_2^H + \sigma^2 \mathbf{I}_{M-P} \end{cases} \quad [8.53]$$

It is then easy to see that:

$$\sigma^2 = \frac{\text{tr}\{\mathbf{H}_2 \Pi\}}{\text{tr}\{\Pi\}} \quad [8.54]$$

where $\Pi = \mathbf{I}_{M-P} - \mathbf{G}_2 \mathbf{G}_2^\dagger = \mathbf{I}_{M-P} - \mathbf{A}_2 \mathbf{A}_2^\dagger$ and where $\text{tr}\{\cdot\}$ denotes the trace operator and \dagger the pseudo-inverse of a matrix.

A possible estimation of σ^2 is thus the following [MAR 90b, MAR 97]:

$$\hat{\sigma}^2 = \text{R\'e} \left\{ \frac{\text{tr}\{\hat{\mathbf{H}}_2 \hat{\Pi}\}}{\text{tr}\{\hat{\Pi}\}} \right\} \quad [8.55]$$

where $\widehat{\boldsymbol{\Pi}} = \mathbf{I} - \widehat{\mathbf{G}}_2 \widehat{\mathbf{G}}_2^\dagger$ and where $\widehat{\mathbf{H}}_2, \widehat{\mathbf{G}}_2$ enter the partition of $\widehat{\boldsymbol{\Gamma}}_{xx}$:

$$\widehat{\boldsymbol{\Gamma}}_{xx} = \begin{bmatrix} \widehat{\mathbf{G}}_1 & \widehat{\mathbf{H}}_1 \\ \widehat{\mathbf{G}}_2 & \widehat{\mathbf{H}}_2 \end{bmatrix} \quad [8.56]$$

When the noise is estimated, it can then be removed from the covariance matrix $\boldsymbol{\Gamma}_{xx}$ so that the propagator is then extracted from [8.51] according to:

$$\widehat{\mathbf{P}} = \mathbf{G}(\widehat{\sigma}^2)^\dagger \mathbf{H}(\widehat{\sigma}^2) \quad [8.57]$$

Let us note that this estimation of the noise variance was taken again in [STO 92] and the authors have especially shown that this method was less complex than the search of the smallest eigenvalue of $\boldsymbol{\Gamma}_{xx}$. Actually, we here evaluate at $(M - P)P^2 + P^3/3$ and $(M - P)^2$ the number of multiplications necessary to the computation of $\boldsymbol{\Pi}$ and then of $\widehat{\sigma}^2$, respectively.

Along the same line, a joint estimation of $(P, \sigma^2, \mathbf{P})$ was obtained in [MAR 90a]. It should be noted that the joint determination of the number of complex sine waves, of the noise variance, and of the propagator (and therefore of the noise and signal subspaces) remains less computationally complex than the search of the eigenvalues of a matrix of dimension $M \times M$, and this being all the more so as the number of observations is larger compared to the number of frequencies to estimate. The asymptotic performance of the propagator method was analyzed and compared to those of MUSIC and of the other linear methods in [MAR 98b]. It is shown that the propagator method's performance is superior to the other linear methods and is equivalent to MUSIC.

8.6. The ESPRIT method

The ESPRIT method (Estimation of Signal Parameters via Rotational Invariance Techniques) [ROY 86] initially designed for array processing can be applied to spectral analysis. Its main advantage is that it considerably reduces the computational cost involved by the estimation of the frequencies. Actually, this technique, rather than requiring the search of minima or maxima in a pseudo-spectrum, uses the search of the eigenvalues of a matrix of dimension $P \times P$ from which we can directly extract the estimates of the P pure frequencies contained in the signal. In array processing, this complexity reduction is obtained with the constraint that the antenna array possesses an invariant form by translation (*translational displacement invariance*). In other words, the antenna array is made up of doublets of sensors obtained by the same translation. This is the case particularly when the antenna array is uniform linear (ULA model). We will directly give the application of the ESPRIT method to the spectral analysis and for the more general case of the array processing we recommend the reader to refer to [MAR 98].

Let us consider two vectors, each of $M - 1$ observations:

$$\bar{\mathbf{x}}(k) = \begin{bmatrix} x(k) \\ x(k+1) \\ \vdots \\ x(k+M-2) \end{bmatrix} \quad \text{and} \quad \bar{\mathbf{x}}(k+1) = \begin{bmatrix} x(k+1) \\ x(k+2) \\ \vdots \\ x(k+M-1) \end{bmatrix} \quad [8.58]$$

According to [8.7], it is easy to see that we have:

$$\begin{aligned} \bar{\mathbf{x}}(k) &= \bar{\mathbf{A}}\mathbf{s}(k) + \bar{\mathbf{b}}(k) \\ \bar{\mathbf{x}}(k+1) &= \bar{\mathbf{A}}\mathbf{s}(k+1) + \bar{\mathbf{b}}(k+1) \end{aligned} \quad [8.59]$$

where:

$$\begin{aligned} \bar{\mathbf{A}} &= [\bar{\mathbf{a}}_1, \dots, \bar{\mathbf{a}}_P] \\ \mathbf{s}(k) &= [\alpha_1 e^{j2\pi f_1 k T_e}, \dots, \alpha_P e^{j2\pi f_P k T_e}]^T \\ \bar{\mathbf{b}}(k) &= [b(k), \dots, b(k+M-2)]^T \end{aligned} \quad [8.60]$$

and:

$$\bar{\mathbf{a}}_i = \bar{\mathbf{a}}(f_i) = [1, e^{j2\pi f_i T_e}, e^{2j2\pi f_i T_e}, \dots, e^{j(M-2)2\pi f_i T_e}]^T \quad [8.61]$$

We note that:

$$\mathbf{s}(k+1) = \Phi \mathbf{s}(k) \quad [8.62]$$

where:

$$\Phi = \text{diag}\{e^{j2\pi f_1 T_e}, \dots, e^{j2\pi f_P T_e}\} \quad [8.63]$$

is a unitary matrix of dimension $P \times P$. Thus we see that matrix Φ , which is often associated with a rotation operator, contains all the information about the frequencies to estimate.

We then introduce:

$$\mathbf{z}(k) = \begin{bmatrix} \bar{\mathbf{x}}(k) \\ \bar{\mathbf{x}}(k+1) \end{bmatrix} = \tilde{\mathbf{A}}\mathbf{s}(k) + \mathbf{n}(k) \quad [8.64]$$

where:

$$\tilde{\mathbf{A}} = \begin{bmatrix} \bar{\mathbf{A}} \\ \bar{\mathbf{A}}\Phi \end{bmatrix} \quad \text{and} \quad \mathbf{n}(k) = \begin{bmatrix} \bar{\mathbf{b}}(k) \\ \bar{\mathbf{b}}(k+1) \end{bmatrix} \quad [8.65]$$

It is thus the structure of the matrix $\tilde{\mathbf{A}}$ of dimension $2M \times P$, which will be exploited to estimate Φ without having to know $\bar{\mathbf{A}}$.

It is easy to see that the covariance matrix Γ_{zz} of all the observations contained in $\mathbf{z}(k)$ is of dimension $2M \times 2M$ and is written:

$$\Gamma_{zz} = E[\mathbf{z}(k)\mathbf{z}(k)^H] = \tilde{\mathbf{A}}\Gamma_{ss}\tilde{\mathbf{A}}^H + \sigma^2\mathbf{I} \quad [8.66]$$

where Γ_{ss} is the covariance matrix of dimension $P \times P$ of the amplitudes of the complex sine waves and \mathbf{I} is the identity matrix of dimension $2M \times 2M$. Thus, the structure of the covariance matrix is identical to that of the observation [8.4] and we can then apply the theorem of the eigendecomposition and the definition of the signal and noise subspaces. In particular, let \mathbf{V}_s be the matrix of dimension $2M \times P$ of the eigenvectors of the covariance matrix Γ_{zz} associated with the eigenvalues which are strictly larger than the variance of the noise σ^2 , it results that the columns of \mathbf{V}_s and the columns of $\tilde{\mathbf{A}}$ span the same signal subspace. There is thus a unique operator \mathbf{T} as:

$$\mathbf{V}_s = \tilde{\mathbf{A}}\mathbf{T} \quad [8.67]$$

By decomposing \mathbf{V}_s as:

$$\mathbf{V}_s = \begin{bmatrix} \mathbf{V}_x \\ \mathbf{V}_y \end{bmatrix} = \begin{bmatrix} \bar{\mathbf{A}}\mathbf{T} \\ \bar{\mathbf{A}}\Phi\mathbf{T} \end{bmatrix} \quad [8.68]$$

where the matrices \mathbf{V}_x and \mathbf{V}_y are of dimension $M \times P$, we can see that the subspaces $\text{esp}\mathbf{V}_x = \text{esp}\mathbf{V}_y = \text{esp}\bar{\mathbf{A}}$ are the same. Let Ψ be the unique matrix $P \times P$ of transition from the basis of the columns of \mathbf{V}_x to that of the columns of \mathbf{V}_y , we have:

$$\mathbf{V}_y = \mathbf{V}_x\Psi \quad [8.69]$$

Because \mathbf{V}_x is of dimension $M \times P$ and of full rank P , it then results:

$$\Psi = (\mathbf{V}_x^H\mathbf{V}_x)^{-1}\mathbf{V}_x^H\mathbf{V}_y \quad [8.70]$$

On the other hand, by using relation [8.69] and partition [8.68] it results:

$$\bar{\mathbf{A}}\mathbf{T}\Psi = \bar{\mathbf{A}}\Phi\mathbf{T} \implies \bar{\mathbf{A}}\mathbf{T}\Psi\mathbf{T}^{-1} = \bar{\mathbf{A}}\Phi \quad [8.71]$$

Because we have supposed that $\bar{\mathbf{A}}$ is of full rank, it results:

$$\mathbf{T}\Psi\mathbf{T}^{-1} = \Phi \quad [8.72]$$

Therefore, the eigenvalues of Ψ are equal to the diagonal elements of matrix Φ , and the columns of \mathbf{T} are the eigenvectors of Ψ .

It is on this latter relation that the ESPRIT method is based on. After having decomposed matrix Γ_{zz} in eigenelements, relation [8.70] makes it possible to obtain the operator Ψ whose eigenvalues are the diagonal elements of Φ where the frequencies can be extracted from. In practice, only an estimation of matrix Γ_{zz} as

well as of its eigenvectors is available and the estimation of Ψ is obtained by replacing relation [8.70] by the minimization of $\| \widehat{\mathbf{V}}_y - \widehat{\mathbf{V}}_x \Psi \| ^2$. The solution is again given by [8.70] where \mathbf{V}_x and \mathbf{V}_y are replaced by their estimates.

This least-squares process [GOL 80] consists in supposing that the estimation of \mathbf{V}_x is perfect and that only $\widehat{\mathbf{V}}_y$ has errors. The least-squares process thus aims to minimize these errors. The total least-squares method [GOL 80] makes it possible to take errors on the estimation of \mathbf{V}_x and of \mathbf{V}_y into account at the same time. The solution of the total least-squares criterion is given using the matrix of dimension $M \times 2P$, $\mathbf{V}_{xy} = [\mathbf{V}_x, \mathbf{V}_y]$. We then search the eigendecomposition of the matrix of dimension $M \times M$:

$$\mathbf{V}_{xy}^H \mathbf{V}_{xy} = \mathbf{V} \Lambda \mathbf{V}^H \quad [8.73]$$

We then partition the matrix of dimension $M \times M$ of the eigenvectors \mathbf{V} in accordance with:

$$\mathbf{V} = \begin{bmatrix} \mathbf{V}_{11} & \mathbf{V}_{12} \\ \mathbf{V}_{21} & \mathbf{V}_{22} \end{bmatrix} \quad [8.74]$$

It finally results:

$$\Psi = -\mathbf{V}_{12} \mathbf{V}_{22}^{-1} \quad [8.75]$$

Finally, let us note that a method of array processing, also applicable to spectral analysis, using at the same time the technique of the propagator to obtain the signal subspace and the ESPRIT technique for the search of the pure frequencies starting from the signal subspace, was successfully proposed in [MAR 94b]. The joint use of these two techniques involves a reduction in the overall computational complexity.

8.7. Illustration of the subspace-based methods performance

Here it is not about making a compared study of the performance of various spectral analysis methods but simply about illustrating the behavior of the main subspace-based methods with respect to the more conventional methods on a simple example.

Indeed, it is known that the methods of the periodogram and of the correlogram are limited by the parameter M (size of the window on which we make the Fourier transform [8.10], [8.11]). The minimum variance method or Capon method [CAP 69] is limited by the SNR. It is actually proved that for an infinite SNR, the minimum variance method is identical to the MUSIC method [UNN 89]. Finally, it is demonstrated that the inverse of the minimum variance spectral estimator is an average of the inverses of the spectral estimators obtained by linear prediction of various orders

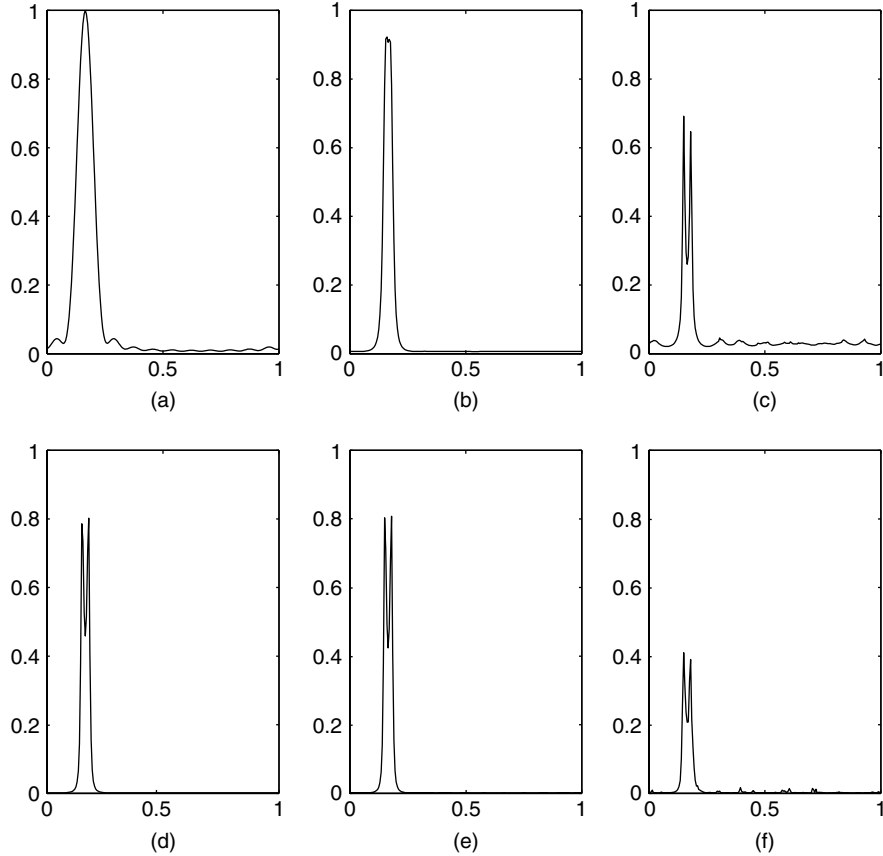


Figure 8.1. Average of the pseudo-spectra over 100 Monte-Carlo simulations:
 (a) periodogram, (b) minimum variance, (c) linear prediction, (d) propagator,
 (e) MUSIC, (f) MinNorm. $M = 12$, $N = 50$, $f_1/Fe = 0.15$, $f_2/Fe = 0.18$,
 $RSB = 10 \text{ dB}$

[BUR 72]. This explains that the minimum variance method is more smoothed than the linear prediction method. These results are illustrated in the following paragraph.²

The simulations concern a signal having two complex sine waves whose frequencies are equal to $f_1 = 0.15F_e$ and $f_2 = 0.18F_e$, respectively, where F_e is the sampling frequency. The observed signal is that of [8.1] and [8.7] where the noise is characterized by its SNR. Only the techniques using the pseudo-spectra

² A more detailed comparison of the performance of the periodogram and the minimum variance methods is presented in Chapter 7.

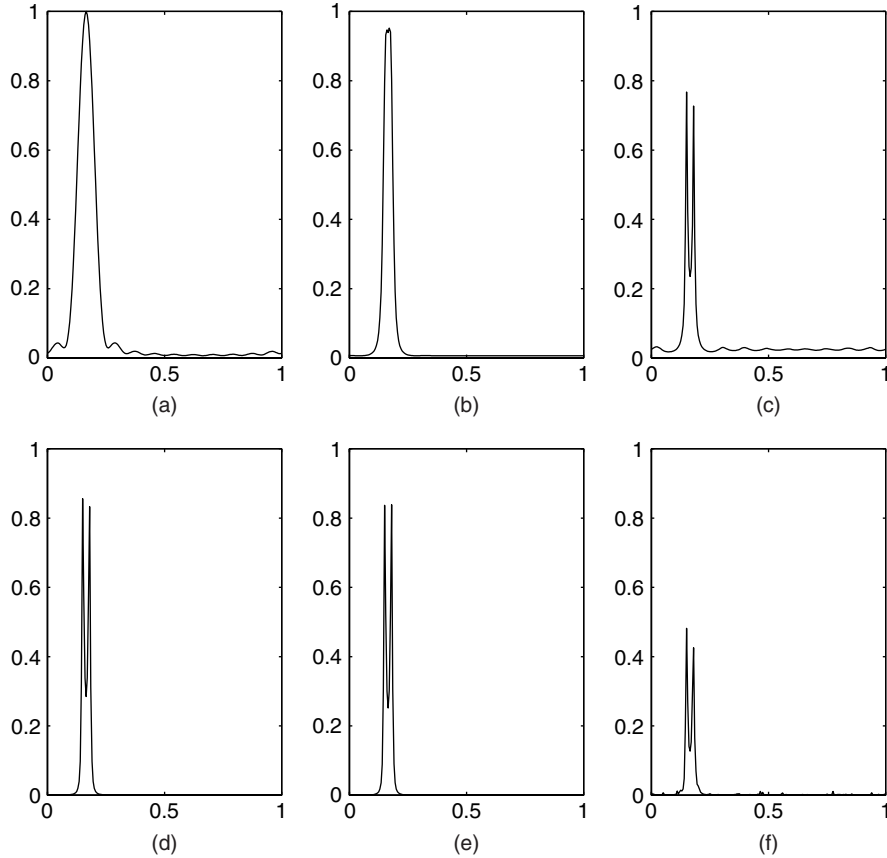


Figure 8.2. Average of the pseudo-spectra over 100 Monte-Carlo simulations:
 (a) periodogram, (b) minimum variance, (c) linear prediction, (d) propagator;
 (e) MUSIC, (f) MinNorm. $M = 12$, $N = 100$, $f_1/Fe = 0.15$, $f_2/Fe = 0.18$,
 $RSB = 10 \text{ dB}$

are represented here. Figures 8.1–8.4 represent the average of the pseudo-spectra on 100 Monte-Carlo simulations obtained for the periodogram, minimum variance, linear prediction, propagator, MUSIC, and MinNorm methods for different values of parameters M , SNR , P . We notice the superiority of the subspace-based methods compared to the conventional methods even if the linear prediction method offers here a satisfactory behavior apart from the oscillations. In Tables 8.1–8.4, the different results of resolution, average and standard deviations of the estimates, are put together. In these tables, the resolution at $\pm\Delta$ for $\Delta = 0.01, 0.005, 0.002$ indicates the number of times (over 100 simulations) where two pure frequencies have been detected at

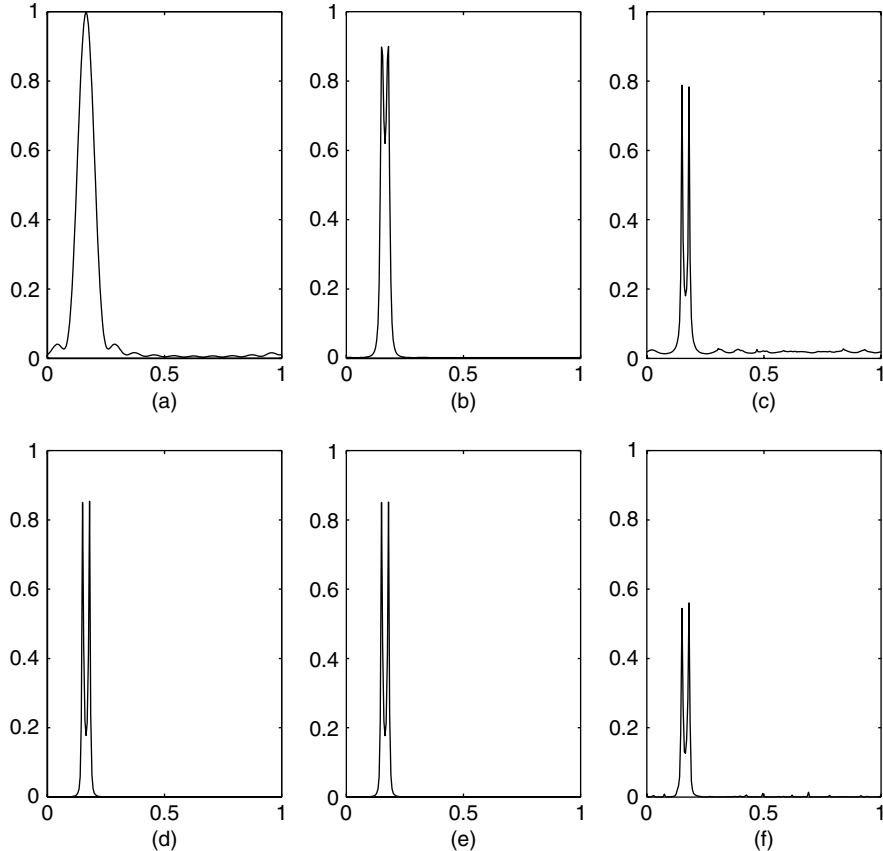


Figure 8.3. Average of the pseudo-spectra over 100 Monte-Carlo simulations:
 (a) periodogram, (b) minimum variance, (c) linear prediction, (d) propagator,
 (e) MUSIC, (f) MinNorm. $M = 12$, $N = 50$, $f_1/Fe = 0.15$, $f_2/Fe = 0.18$,
 $RSB = 15 \text{ dB}$

the same time, each in an interval of $\pm\Delta$ around the true values. The averages and standard deviations are calculated on each of the detected sine waves.

8.8. Adaptive research of subspaces

Two essential calculation steps are necessary for the implementation of the subspace-based methods. The first consists in searching the signal or noise subspaces. The second consists in estimating the frequencies of the signal from the signal subspace or from the noise subspace. That can amount, as we have seen above, to searching either the minima or the maxima of a function called pseudo-spectrum, or

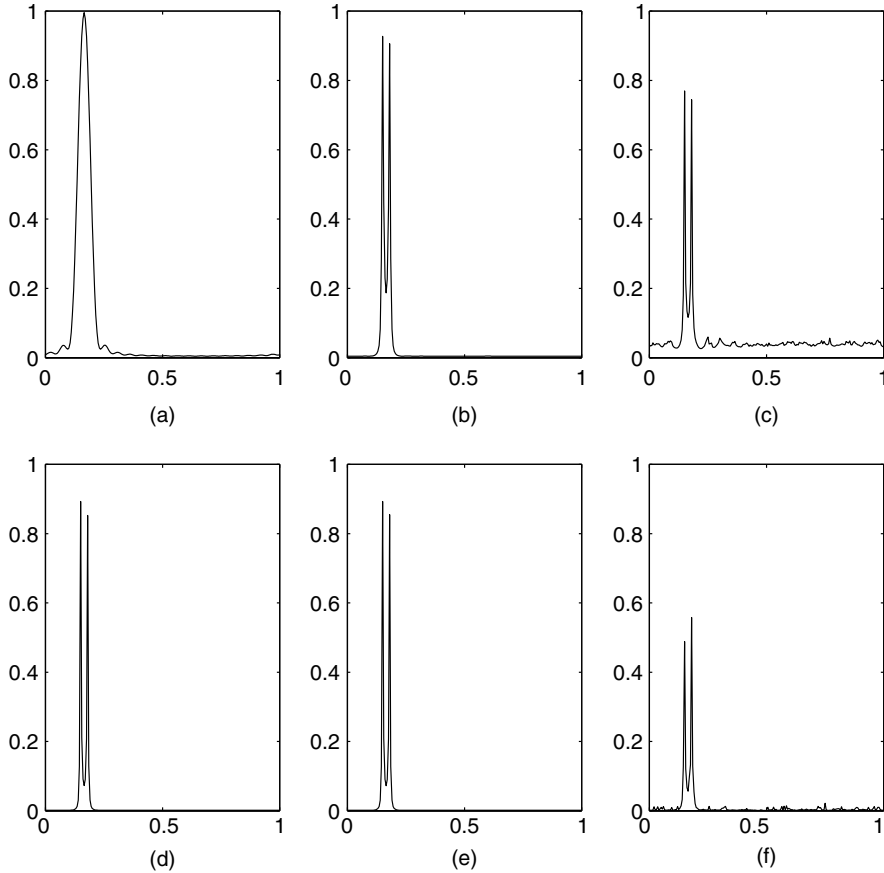


Figure 8.4. Average of the pseudo-spectra over 100 Monte-Carlo simulations:
 (a) periodogram, (b) minimum variance, (c) linear prediction,
 (d) propagator, (e) MUSIC, (f) MinNorm. $M = 20$, $N = 50$, $f_1/Fe = 0.15$,
 $f_2/Fe = 0.18$, $RSB = 10 \text{ dB}$

the roots of a polynomial, or the eigenvalues of a matrix built with the help of a basis of the signal subspace.

Despite the different variants, we should keep in mind that this second calculation stage remains costly. However, this stage is also necessary for the more classical methods of spectral analysis.

The first calculation step mentioned above is specific to the subspace-based methods.

Method	(a)	(b)	(c)	(d)	(e)	(f)
resolution of ± 0.01	0	28	95	97	98	65
resolution of ± 0.005	0	2	59	72	73	42
resolution of ± 0.002	0	1	43	56	57	19
mean value 1	—	0.1548	0.1505	0.1514	0.1513	0.15
mean value 2	—	0.1739	0.1804	0.1787	0.1786	0.1795
standard deviation 1	—	0.1546	0.0964	0.0818	0.0812	0.1265
standard deviation 2	—	0.2095	0.0900	0.0831	0.0825	0.1118

Table 8.1. Performance of the different methods (over 100 Monte-Carlo simulations): (a) periodogram, (b) minimum variance, (c) linear prediction, (d) propagator, (e) MUSIC, (f) MinNorm. $M = 12$, $N = 50$, $f_1/Fe = 0.15$, $f_2/Fe = 0.18$, $RSB = 10 \text{ dB}$

Method	(a)	(b)	(c)	(d)	(e)	(f)
resolution of ± 0.01	0	20	99	100	100	82
resolution of ± 0.005	0	0	85	94	94	59
resolution of ± 0.002	0	0	72	88	88	35
mean value 1	—	0.1550	0.1502	0.1503	0.1503	0.1498
mean value 2	—	0.1731	0.1799	0.1797	0.1797	0.1787
standard deviation 1	—	0.1581	0.0224	0.0412	0.0412	0.0943
standard deviation 2	—	0.2319	0.0574	0.0387	0.0387	0.1192

Table 8.2. Performance of the different methods (over 100 Monte-Carlo simulations): (a) periodogram, (b) minimum variance, (c) linear prediction, (d) propagator, (e) MUSIC, (f) MinNorm. $M = 12$, $N = 100$, $f_1/Fe = 0.15$, $f_2/Fe = 0.18$, $RSB = 10 \text{ dB}$

Method	(a)	(b)	(c)	(d)	(e)	(f)
resolution of ± 0.01	0	100	100	100	100	89
resolution of ± 0.005	0	64	91	96	96	61
resolution of ± 0.002	0	47	87	93	93	48
mean value 1	—	0.1518	0.1502	0.1502	0.1502	0.1501
mean value 2	—	0.1781	0.1801	0.1798	0.1798	0.1795
standard deviation 1	—	0.0949	0.0412	0.0316	0.0316	0.1034
standard deviation 2	—	0.0975	0.0424	0.0283	0.0283	0.1063

Table 8.3. Performance of the different methods (over 100 Monte-Carlo simulations): (a) periodogram, (b) minimum variance, (c) linear prediction, (d) propagator, (e) MUSIC, (f) MinNorm. $M = 12$, $N = 50$, $f_1/Fe = 0.15$, $f_2/Fe = 0.18$, $RSB = 15 \text{ dB}$

Method	(a)	(b)	(c)	(d)	(e)	(f)
resolution of ± 0.01	0	100	100	100	100	92
resolution of ± 0.005	0	100	95	100	100	72
resolution of ± 0.002	0	100	91	100	100	63
mean value 1	—	0.1500	0.1499	0.1500	0.1500	0.1500
mean value 2	—	0.1800	0.1801	0.1800	0.1800	0.1799
standard deviation 1	—	0.0000	0.0316	0.0000	0.0000	0.0728
standard deviation 2	—	0.0000	0.0360	0.0000	0.0000	0.0916

Table 8.4. Performance of the different methods (over 100 Monte-Carlo simulations): (a) periodogram, (b) minimum variance, (c) linear prediction, (d) propagator, (e) MUSIC, (f) MinNorm. $M = 20$, $N = 50$, $f_1/Fe = 0.15$, $f_2/Fe = 0.18$, $RSB = 10 \text{ dB}$

The search of the eigenvalues and eigenvectors of a matrix is complex from a computational point of view and it is all the more so as the dimension of the space of the observations increases. Moreover in a non-stationary environment, this research should be repeated at each new observation. In practice, $\widehat{\Gamma}_{xx}$ is updated in an adaptive way by introducing the time variable k and by adopting the recursive relation:

$$\widehat{\Gamma}_{xx}(k) = \beta \widehat{\Gamma}_{xx}(k-1) + \alpha \mathbf{x}(k) \mathbf{x}^H(k) \quad [8.76]$$

where β and α are weighting coefficients (forgotten factors).

A large number of adaptive algorithms have been developed in the literature to estimate the matrix whose columns span the signal subspace in a recursive way (i.e. by using the calculations of the preceding moment each time a new data is observed). Some classifications of these algorithms have been given in the following works: [YAN 95, COM 90, SCH 89, BIS 92]. Actually, it is possible to regroup them in three large families.

First, we find the algorithms that are inspired from the classical techniques of eigenvalue/singular value decompositions (EVD/SVD) as the QR iteration, the Jacobi algorithm, and the Lanczos algorithm [COM 90, FUH 88]. In this family, we also find the algorithms derived from the power method [GOL 89, COM 90, OWS 78, KAR 84].

In the second family, we include the algorithms whose principle is based on the works of Bunch *et al.* [BUN 78a] that analyze the updating of a Hermitian matrix which was modified by the addition of a matrix of rank one [KAR 86, SCH 89, DEG 92].

The last family puts together the algorithms that consider the EVD/SVD as an optimization problem with or without the constraints of the gradient method [OWS 78,

KAR 84, YAN 95], the conjugate gradient method [YAN 89], and the Gauss-Newton method [RED 82, BAN 92].

We should add to this classification a fourth family of “linear” methods that were presented above (see the propagator method) which does not require any eigendecomposition and which can be made adaptive with a noticeable reduction of the complexity [MAR 96, ERI 94, YEH 87].

Another classification of the adaptive algorithms according to their complexity measured in number of complex operations, given the set of two multiplications and one addition, was proposed in [SAN 98], to which the interested reader is invited to refer. We distinguish the algorithms of complexity $O(M^2)$ (of the order of M^2 operations) and those of complexity $O(MP^2)$ and $O(MP)$. These rough estimates are to be compared to a complexity in $O(M^3)$ necessary for the eigendecomposition. This classification was also made in [COM 90].

However, it is necessary to keep in mind that the complexity alone is not the unique criterion to take into account to choose an algorithm. We should also consider the convergence capacity (rate and precision), its capacity of tracking a non-stationary environment, its stability regarding the numerical errors, as well as the hypothesis necessary to establish this algorithm. A comparison of these algorithms was made in [SAN 98].

8.9. Integrating *a priori* known frequencies into the MUSIC criterion

In this section, we present two ways to integrate *a priori* known frequencies into the MUSIC criterion.³ The first one is called Prior-MUSIC (P-MUSIC) [BOY 08]. This scheme is based on the spectral MUSIC algorithm [SCH 79] and thus can deal with irregular as well as regular sampling. On the other hand, the P-MUSIC needs to assume uncorrelated known and unknown complex amplitudes. In addition, like all the algorithms based on the spectral MUSIC, the P-MUSIC needs a costly enumerative optimization of its spectral criterion. The second one, called Projected Companion Matrix-MUSIC (PCM-MUSIC) [KOR 09], exploits the regularity of the sampling process, like the root-MUSIC algorithm [BAR 83], and in this way decreases the computational cost. In addition, no assumption is made on the complex amplitudes.

8.9.1. A spectral approach: The Prior-MUSIC algorithm

Assume that we know s frequencies among p with $s < p$. Without loss of generality, matrix \mathbf{A} can be partitioned into $\mathbf{A}_{\mathcal{K}} = [\mathbf{a}_1, \dots, \mathbf{a}_s]$ composed by the

³ The interested reader can see the more recent publication [BOU 09] dealing with the prior version of the MODE algorithm.

known vectors and $\mathbf{A}_{\mathcal{U}} = [\mathbf{a}_{s+1}, \dots, \mathbf{a}_p]$ composed by the unknown vectors⁴. In this scenario, the linear model of the observation is given by:

$$\mathbf{x}(k) = \mathbf{As}(k) + \mathbf{b}(k) = [\mathbf{A}_{\mathcal{K}} \quad \mathbf{A}_{\mathcal{U}}] \begin{bmatrix} \mathbf{s}_{\mathcal{K}}(k) \\ \mathbf{s}_{\mathcal{U}}(k) \end{bmatrix} + \mathbf{b}(k) \quad [8.77]$$

where $\mathbf{s}_{\mathcal{K}}(k)$ and $\mathbf{s}_{\mathcal{U}}(k)$ are accordingly defined.

The question is how jointly to remove the known parameters and estimate the unknown ones.

8.9.1.1. The Prior-MUSIC cost function

The Prior-MUSIC tackles this problem and is based on the following optimization problem:

$$\arg \min_{\mathbf{s}, f} C(\mathbf{s}, f) \quad [8.78]$$

where the cost function of the P-MUSIC is given by:

$$C(\mathbf{s}, f) = \sum_{k=1}^K \|\mathbf{a}(f) - \mathbf{E}\mathbf{As}(k)\|^2 \quad [8.79]$$

where \mathbf{E} is the oblique projector along $\text{esp}\{\mathbf{A}_{\mathcal{K}}\}$ on $\text{esp}\{\mathbf{A}_{\mathcal{U}}\}$. This oblique projector [BEH 94] is defined by:

$$\mathbf{E} = \mathbf{A}_{\mathcal{U}} (\mathbf{A}_{\mathcal{U}}^H \mathbf{P}_{\mathcal{K}}^\perp \mathbf{A}_{\mathcal{U}})^{-1} \mathbf{A}_{\mathcal{U}}^H \mathbf{P}_{\mathcal{K}}^\perp \quad [8.80]$$

where $\mathbf{P}_{\mathcal{K}}^\perp = \mathbf{I} - \mathbf{A}_{\mathcal{K}} (\mathbf{A}_{\mathcal{K}}^H \mathbf{A}_{\mathcal{K}})^{-1} \mathbf{A}_{\mathcal{K}}^H$, satisfying the two conditions: $\mathbf{E}\mathbf{A}_{\mathcal{K}} = \mathbf{0}$ and $\mathbf{E}\mathbf{A}_{\mathcal{U}} = \mathbf{A}_{\mathcal{U}}$. In addition, as orthogonal projectors, oblique projectors are idempotent, meaning that $\mathbf{E}^2 = \mathbf{E}$. Assuming that $\mathbf{A}_{\mathcal{U}}$ has been estimated without error, the cost function of the P-MUSIC becomes:

$$C(\mathbf{s}, f) = \sum_{k=1}^K \|\mathbf{a}(f) - \mathbf{E}\mathbf{A}_{\mathcal{K}}\mathbf{s}_{\mathcal{K}}(k) - \mathbf{E}\mathbf{A}_{\mathcal{U}}\mathbf{s}_{\mathcal{U}}(k)\|^2 \quad [8.81]$$

$$= \sum_{k=1}^K \|\mathbf{a}(f) - \mathbf{A}_{\mathcal{U}}\mathbf{s}_{\mathcal{U}}(k)\|^2 \quad [8.82]$$

So, it is clear that we look for a vector $\mathbf{a}(f)$ which belongs to $\text{esp}\{\mathbf{A}_{\mathcal{U}}\}$ while the other contributions in $\text{esp}\{\mathbf{A}_{\mathcal{K}}\}$ have been removed.

⁴ Here, we can assume irregular sampling. In the case of regular sampling, \mathbf{A} is a Vandermonde matrix.

8.9.1.2. Minimization of the cost function with respect to the complex amplitude parameters

Minimizing $C(\mathbf{s}, f)$ is equivalent to minimizing each positive term $\|\mathbf{a}(f) - \mathbf{EAs}(k)\|^2$ in sum [8.79]. In this case, it is easy to see that the complex amplitude parameters given by $\bar{\mathbf{s}}(k) = (\mathbf{A}^H \mathbf{E}^H \mathbf{EA})^{-1} \mathbf{A}^H \mathbf{E}^H \mathbf{a}(f)$ verify the nullity of the first-order partial derivative of the cost function according to

$$\frac{\partial C(\mathbf{s}, f)}{\partial \mathbf{s}(k)} \Big|_{\mathbf{s}(k)=\bar{\mathbf{s}}(k)} = \frac{\partial \|\mathbf{a}(f) - \mathbf{EAs}(k)\|^2}{\partial \mathbf{s}(k)} \Big|_{\mathbf{s}(k)=\bar{\mathbf{s}}(k)} = \mathbf{0}$$

So, the cost function with respect to the frequency parameter becomes:

$$C(\bar{\mathbf{s}}, f) = K \|\mathbf{P}_{\mathcal{U}}^\perp \mathbf{a}(f)\|^2 \quad [8.83]$$

where $\mathbf{P}_{\mathcal{U}}^\perp = \mathbf{I} - \mathbf{A}_{\mathcal{U}}(\mathbf{A}_{\mathcal{U}}^H \mathbf{A}_{\mathcal{U}})^{-1} \mathbf{A}_{\mathcal{U}}^H$ is the unknown orthogonal projector on subspace $\text{esp}\{\mathbf{A}_{\mathcal{U}}^\perp\}$. Consequently, we need to estimate a basis of this subspace to completely determine the cost function $C(\bar{\mathbf{s}}, f)$. To reach this goal, we proceed in the following manner.

8.9.1.3. Estimation of $\text{esp}\{\mathbf{A}_{\mathcal{U}}^\perp\}$ and final criterion

First consider the correlation matrix of the complex amplitudes defined in [8.4] partitioned accordingly:

$$\boldsymbol{\Gamma}_{ss} = \begin{bmatrix} \boldsymbol{\Gamma}_{\mathcal{K}, \mathcal{K}} & \boldsymbol{\Gamma}_{\mathcal{K}, \mathcal{U}} \\ \boldsymbol{\Gamma}_{\mathcal{K}, \mathcal{U}}^H & \boldsymbol{\Gamma}_{\mathcal{U}, \mathcal{U}} \end{bmatrix} \quad [8.84]$$

The correlation matrix is given by:

$$\begin{aligned} \boldsymbol{\Gamma}_{xx} &= \mathbf{A} \boldsymbol{\Gamma}_{ss} \mathbf{A}^H + \sigma^2 \mathbf{I} \\ &= \mathbf{A}_{\mathcal{K}} \boldsymbol{\Gamma}_{\mathcal{K}, \mathcal{K}} \mathbf{A}_{\mathcal{K}}^H + \mathbf{A}_{\mathcal{U}} \boldsymbol{\Gamma}_{\mathcal{U}, \mathcal{U}} \mathbf{A}_{\mathcal{U}}^H + \mathbf{A}_{\mathcal{K}} \boldsymbol{\Gamma}_{\mathcal{K}, \mathcal{U}} \mathbf{A}_{\mathcal{U}}^H + \mathbf{A}_{\mathcal{U}} \boldsymbol{\Gamma}_{\mathcal{K}, \mathcal{U}}^H \mathbf{A}_{\mathcal{K}}^H + \sigma^2 \mathbf{I} \end{aligned}$$

After removing⁵ the contribution of the noise, the projected correlation matrix is given by:

$$\bar{\boldsymbol{\Gamma}}_{xx} = \mathbf{P}_{\mathcal{K}}^\perp (\boldsymbol{\Gamma}_{xx} - \sigma^2 \mathbf{I}) \quad [8.85]$$

$$= \mathbf{P}_{\mathcal{K}}^\perp \mathbf{A}_{\mathcal{U}} \boldsymbol{\Gamma}_{\mathcal{U}, \mathcal{U}} \mathbf{A}_{\mathcal{U}}^H + \mathbf{P}_{\mathcal{K}}^\perp \mathbf{A}_{\mathcal{U}} \boldsymbol{\Gamma}_{\mathcal{K}, \mathcal{U}}^H \mathbf{A}_{\mathcal{K}}^H \quad [8.86]$$

where $\mathbf{P}_{\mathcal{K}}^\perp = \mathbf{I} - \mathbf{A}_{\mathcal{K}}(\mathbf{A}_{\mathcal{K}}^H \mathbf{A}_{\mathcal{K}})^{-1} \mathbf{A}_{\mathcal{K}}^H$ is the known projector. To extract a basis of subspace $\text{esp}\{\mathbf{A}_{\mathcal{U}}^\perp\}$, we need to assume that the known and the unknown

⁵ In practice, the noise variance is estimated.

complex amplitudes are uncorrelated,⁶ meaning $\mathbf{\Gamma}_{\mathcal{K},\mathcal{U}} = \mathbf{0}$. Taking into account this assumption, we obtain:

$$\bar{\mathbf{\Gamma}}_{xx} = \mathbf{P}_{\mathcal{K}}^{\perp} \mathbf{A}_{\mathcal{U}} \mathbf{\Gamma}_{\mathcal{U},\mathcal{U}} \mathbf{A}_{\mathcal{U}}^H \quad [8.87]$$

The Hermitian character of the correlation matrix is now destroyed but the right basis of the projected correlation matrix $\bar{\mathbf{\Gamma}}_{xx}$ is not affected by the projection operation and it remains only the desired subspace. So, consider the SVD of the projected correlation matrix $\bar{\mathbf{\Gamma}}_{xx}$ according to:

$$\bar{\mathbf{\Gamma}}_{xx} = \mathbf{U} \mathbf{Q} [\mathbf{V} | \bar{\mathbf{V}}]^H \quad [8.88]$$

where \mathbf{V} (respectively $\bar{\mathbf{V}}$) is $M \times (p - s)$ (respectively $M \times s$). As $\text{esp}\{\mathbf{A}_{\mathcal{U}}^{\perp}\} = \text{esp}\{\bar{\mathbf{V}}\}$, the final criterion of the P-MUSIC is given by:

$$\arg \min_f S_{\text{P-MUSIC}}(f) \quad \text{where} \quad S_{\text{P-MUSIC}}(f) = \mathbf{a}(f)^H \bar{\mathbf{V}} \bar{\mathbf{V}}^H \mathbf{a}(f) \quad [8.89]$$

where we have omitted the constant K^{-1} . On Figure 8.5, it is reported the pseudo-spectra of the MUSIC and the P-MUSIC algorithms where a single frequency is known. As we can see, two minima exist for the MUSIC algorithm but for the P-MUSIC, one of the two minima has been removed.

8.9.1.4. Large sample regime

First note that criterion [8.83] of the P-MUSIC is formally identical to the one for the MUSIC approach in case of estimating s frequencies. Nevertheless, the way to obtain projector $\bar{\mathbf{V}} \bar{\mathbf{V}}^H$ is not the same as for the standard MUSIC since the known frequencies are taken into account. But for a large number of samples, we know that:

$$\mathbf{A}_{\mathcal{K}}^H \mathbf{A}_{\mathcal{U}} \xrightarrow{M \rightarrow \infty} \mathbf{0} \iff \mathbf{P}_{\mathcal{K}}^{\perp} \mathbf{A}_{\mathcal{U}} \xrightarrow{M \rightarrow \infty} \mathbf{A}_{\mathcal{U}} \quad [8.90]$$

since $\frac{1}{M} \mathbf{a}(f_p)^H \mathbf{a}(f_q) \xrightarrow{M \rightarrow \infty} \delta_{p-q}$. This means that $\text{esp}\{\mathbf{A}_{\mathcal{U}}\}$ and $\text{esp}\{\mathbf{A}_{\mathcal{K}}\}$ are mutually orthogonal subspaces for a large number of samples. In this scenario, the projected correlation becomes:

$$\bar{\mathbf{\Gamma}}_{xx} \xrightarrow{M \rightarrow \infty} \mathbf{A}_{\mathcal{U}} \mathbf{\Gamma}_{\mathcal{U},\mathcal{U}} \mathbf{A}_{\mathcal{U}}^H \quad [8.91]$$

which coincides with the correlation matrix for the unknown subspace $\text{esp}\{\mathbf{A}_{\mathcal{U}}\}$. So, the (asymptotic) accuracy of the P-MUSIC algorithm is the same as the MUSIC for estimating s frequencies.

⁶ Notice that the unknown complex amplitudes may be correlated.

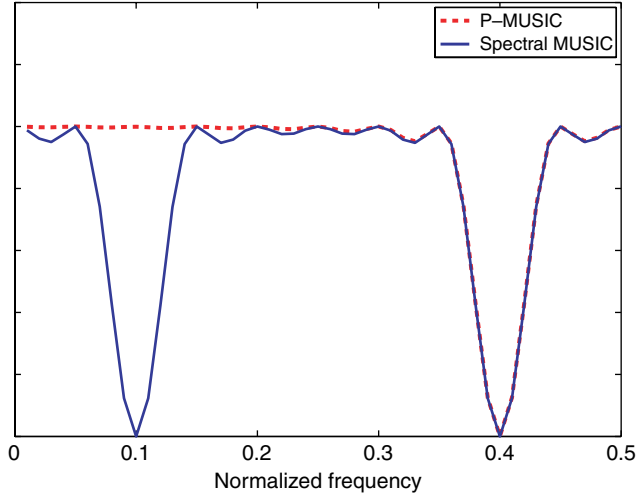


Figure 8.5. $S_{P\text{-MUSIC}}(f)$ and $S_{\text{MUSIC}}(f)$ vs. the normalized frequency with $p = 2$, $s = 1$, $M = 20$, $K = 100$. The known frequency is 0.1 and the unknown one is equal to 0.4

8.9.2. A polynomial-based rooting approach: The projected companion matrix-MUSIC algorithm

The Prior-MUSIC approach assumes that the unknown and known complex amplitudes are uncorrelated. In this section, we present a polynomial-based rooting MUSIC approach with no assumption on the complex amplitude parameters. This algorithm is not based on the projection of the correlation matrix but on the projection of the companion matrix.

8.9.2.1. Companion matrix and associated characteristic polynomial

Let explicitly introduce polynomial $P(z)$, defined in [8.25], according to:

$$P(z) = q_{M-1}^* \frac{1}{z^{M-1}} + \dots + q_0 + \dots + q_{M-1} z^{M-1} \quad [8.92]$$

The coefficients of polynomial $P(z)$ are computed by summing the entries along the diagonal of the noise projector $\mathbf{V}_b \mathbf{V}_b^H$ introduced in [8.19]. More precisely, we have:

$$q_m = \sum_{m+1}^M [\mathbf{V}_b \mathbf{V}_b^H]_{n,n-m} \quad [8.93]$$

where $m \in [0 : M - 1]$ and $[\mathbf{V}_b \mathbf{V}_b^H]_{a,b}$ denotes entry (a,b) of matrix $\mathbf{V}_b \mathbf{V}_b^H$. Toward the definition of the Companion matrix, remark that $P(z)$ can be factorized according to:

$$P(z) = \frac{q_{M-1}}{z^{M-1}} G(z) \quad [8.94]$$

where we have assumed $z \neq 0$ and $q_{M-1} \neq 0$ and we have defined the monic⁷ polynomial:

$$G(z) = \frac{q_{M-1}^*}{q_{M-1}} + \dots + \frac{q_0}{q_{M-1}} z^{M-1} + \dots + \frac{q_{M-2}}{q_{M-1}} z^{2M-3} + z^{2M-2} \quad [8.95]$$

Notice that solving $G(z)$ is equivalent to solving $P(z)$. Then the $(2M - 2) \times (2M - 2)$ associated companion matrix is defined according to:

$$\mathbf{C} = \begin{bmatrix} 0 & 1 & & \\ & \ddots & \ddots & \\ & & 0 & 1 \\ -\frac{q_{M-1}^*}{q_{M-1}} & \dots & -\frac{q_{M-3}}{q_{M-1}} & -\frac{q_{M-2}}{q_{M-1}} \end{bmatrix} \quad [8.96]$$

The characteristic polynomial of \mathbf{C} is given by:

$$G(z) = \det(z\mathbf{I} - \mathbf{C})$$

where $\det(\cdot)$ denotes the determinant. So, $\lambda_1, \dots, \lambda_{2M-2}$ denoting the eigenvalues of matrix \mathbf{C} coincide with the roots of $G(z)$ and thus $P(z)$. Due to the fact $P(z)$ is a conjugate centro-symmetric polynomial, the $2M - 2$ roots occur in reciprocal conjugate pairs, meaning that there are $M - 1$ roots, denoted by λ , and $M - 1$ roots, denoted by $1/\lambda^*$. The complex eigenvalues of the companion matrix can be written according to $\lambda = rz$, where $r = |\lambda|$ and $z = e^{j2\pi f}$. Obviously, we have $f = \text{angle}\{\lambda\}/(2\pi)$. So, keeping in mind that the roots of $P(z)$ occur in reciprocal conjugate pairs, the eigenvalues are given by rz or $\frac{1}{r}z$. As we look for only the roots belonging to the unit circle (unit modulus), we must have:

$$r = 1 \Rightarrow r = \frac{1}{r}$$

⁷ Its leading (i.e. highest power) coefficient is 1.

This implies that the desired eigenvalues have a multiplicity of two, i.e. they appear two times in the spectrum of the companion matrix. The other ones, called the extraneous solutions, are symmetrically distributed with respect to the unit circle since $r \neq 1/r$. Without loss of generality, suppose that the p desired solutions are associated with the first eigenvalues (each of multiplicity two), i.e.:

$$z_1 \longleftrightarrow \lambda_1 = \lambda_2$$

$$z_2 \longleftrightarrow \lambda_3 = \lambda_4$$

$$z_3 \longleftrightarrow \lambda_5 = \lambda_6$$

$$\vdots$$

and the other ones (i.e. $\lambda_{2p+1}, \dots, \lambda_{2M-2}$) are the eigenvalues of multiplicity one associated with the extraneous solutions.

8.9.2.2. Jordan decomposition of the companion matrix

In this case, the Jordan decomposition of the companion matrix is as follows [BAZ 06]:

$$\mathbf{C} = \mathbf{W} \Delta \mathbf{W}^{-1}$$

in which the square $(2M - 2)$ -rank Confluent Vandermonde⁸ structured matrix is given by:

$$\mathbf{W} = [\mathbf{P}(z_1) \, \dots, \, \mathbf{P}(z_p) \mid \mathbf{u}(\lambda_{2p+1}) \, \dots, \, \mathbf{u}(\lambda_{2M-2})]$$

where:

$$\mathbf{P}(z_m) = [\mathbf{u}(z_m) \mid \mathbf{u}'(z_m)] = \left[\begin{array}{c|c} 1 & 0 \\ z_m & 1 \\ z_m^2 & 2z_m \\ \vdots & \vdots \\ z_m^{2p-2} & (2p-3)z_m^{2p-4} \end{array} \right]$$

⁸ The Confluent Vandermonde matrix can be viewed as an extended Vandermonde matrix in the sense that the confluent rows are the derivatives of the original Vandermonde rows.

In the above expression, we have introduced the first-order partial derivative of vector $\mathbf{u}(z_m)$ according to:

$$\mathbf{u}'(z_m) = \left. \frac{\partial \mathbf{u}(z)}{\partial z} \right|_{z=z_m}$$

Note that $\text{rank}(\mathbf{P}(z_m)) = 2 < 2p - 2$ since $\mathbf{u}(z_m)$ and $\mathbf{u}'(z_m)$ cannot be collinear. This implies that $\text{rank}(\mathbf{W}) = 2M - 2$ and thus justifies the non-singularity of \mathbf{W} . In addition, we have:

$$\Delta = \left[\begin{array}{c|c} \mathbf{J}(z_1) & \mathbf{0} \\ \ddots & \\ \hline & \mathbf{J}(z_p) \\ \hline & \lambda_{2p+1} \\ & \ddots \\ \mathbf{0} & \lambda_{2M-2} \end{array} \right]$$

where:

$$\mathbf{J}(z_m) = \begin{bmatrix} z_m & 1 \\ 0 & z_m \end{bmatrix}$$

is a 2×2 Jordan matrix parameterized by z_m . We can remark that this decomposition is a straightforward generalization of the well-known property that the companion matrix can be diagonalized in a Vandermonde structured basis in case of single multiplicity of the eigenvalues. The particular structure of the Jordan decomposition of \mathbf{C} is a consequence of the fact that the eigenvalues corresponding to the desired solutions are of multiplicity two.

8.9.2.3. Projected companion matrix

Knowing s frequencies or equivalently z_1, \dots, z_s , we consider the following projector:

$$\mathbf{P}_{\bar{\mathbf{A}}}^\perp = \mathbf{I} - \bar{\mathbf{A}}(\bar{\mathbf{A}}^H \bar{\mathbf{A}})^{-1} \bar{\mathbf{A}}^H$$

onto $\text{esp}(\bar{\mathbf{A}}^\perp)$ where:

$$\bar{\mathbf{A}} = [\mathbf{P}(z_1) \mathbf{P}(z_2) \dots \mathbf{P}(z_s)]$$

The aim is now to solve the following polynomial:

$$\tilde{G}(z) = \det(z\mathbf{I} - \mathbf{P}_{\bar{\mathbf{A}}}^{\perp} \mathbf{C}) \quad [8.97]$$

Notice that:

$$\begin{aligned} \mathbf{P}_{\bar{\mathbf{A}}}^{\perp} \mathbf{C} &= (\mathbf{P}_{\bar{\mathbf{A}}}^{\perp} \mathbf{W}) \Delta \mathbf{W}^{-1} \\ &= \sum_{m=1}^s \underbrace{\mathbf{P}_{\bar{\mathbf{A}}}^{\perp} \mathbf{P}(z_m)}_0 \mathbf{J}(z_m) \begin{bmatrix} \tilde{\mathbf{v}}_{2m-1}^T \\ \tilde{\mathbf{v}}_{2m}^T \end{bmatrix} + \sum_{m=s+1}^p \mathbf{P}_{\bar{\mathbf{A}}}^{\perp} \mathbf{P}(z_m) \mathbf{J}(z_m) \begin{bmatrix} \tilde{\mathbf{v}}_{2m-1}^T \\ \tilde{\mathbf{v}}_{2m}^T \end{bmatrix} \\ &\quad + \sum_{m=2p+1}^{2M-2} \lambda_m \mathbf{P}_{\bar{\mathbf{A}}}^{\perp} \mathbf{u}(\lambda_m) \tilde{\mathbf{v}}_m^T \end{aligned}$$

where matrix \mathbf{W}^{-1} has been partitioned according to:

$$\mathbf{W}^{-1} = \begin{bmatrix} \tilde{\mathbf{v}}_1^T \\ \hline \tilde{\mathbf{v}}_2^T \\ \vdots \\ \hline \tilde{\mathbf{v}}_{2M-2}^T \end{bmatrix}$$

Since we suppose that the frequencies are all distinct, we have $\text{rank}(\bar{\mathbf{A}}) = 2s$. It follows that $\text{rank}(\mathbf{P}_{\bar{\mathbf{A}}}^{\perp}) = 2(M - s - 1)$. Using the rank property of the matrix multiplication [STO 05, Appendix A], we obtain:

$$\begin{aligned} \text{rank}(\mathbf{P}_{\bar{\mathbf{A}}}^{\perp} \mathbf{C}) &= \min(\text{rank}(\mathbf{P}_{\bar{\mathbf{A}}}^{\perp}), \text{rank}(\mathbf{C})) \\ &= \min(2(M - s - 1), 2(M - 1)) \\ &= 2(M - s - 1) \end{aligned}$$

Thus, the effect of this projection is to decrease the rank of the companion matrix to $2(M - s - 1)$ by canceling the previously estimated solutions.

8.9.2.4. Case of a large number of samples

We know that:

$$\frac{1}{M} \mathbf{u}(z_p)^H \mathbf{u}(z_q) \xrightarrow{M \rightarrow \infty} \delta_{p-q} \quad [8.98]$$

$$\frac{2}{M^2} \mathbf{u}'(z_p)^H \mathbf{u}(z_q) \xrightarrow{M \rightarrow \infty} \delta_{p-q} \quad [8.99]$$

$$\frac{3}{M^3} \mathbf{u}'(z_p)^H \mathbf{u}'(z_q) \xrightarrow{M \rightarrow \infty} \delta_{p-q} \quad [8.100]$$

thus, we have:

$$\mathbf{P}_{\bar{\mathbf{A}}}^\perp \mathbf{P}(z_m) = \mathbf{P}(z_m) - \bar{\mathbf{A}} (\bar{\mathbf{A}}^H \bar{\mathbf{A}})^{-1} \bar{\mathbf{A}}^H \mathbf{P}(z_m)$$

where:

$$\bar{\mathbf{A}}^H \mathbf{P}(z_m) = \begin{bmatrix} \mathbf{P}(z_1)^H \mathbf{P}(z_m) \\ \vdots \\ \mathbf{P}(z_s)^H \mathbf{P}(z_m) \end{bmatrix}$$

with:

$$\mathbf{P}(z_s)^H \mathbf{P}(z_m) = \begin{bmatrix} \mathbf{u}(z_s)^H \mathbf{u}(z_m) & | & \mathbf{u}(z_s)^H \mathbf{u}'(z_m) \\ \mathbf{u}'(z_s)^H \mathbf{u}(z_m) & | & \mathbf{u}'(z_s)^H \mathbf{u}'(z_m) \end{bmatrix}$$

Using the above asymptotic properties, we have $\mathbf{P}(z_s)^H \mathbf{P}(z_m) \xrightarrow{M \rightarrow \infty} \mathbf{0}$ as long as $m \neq s$. In conclusion, we have:

$$\mathbf{P}_{\bar{\mathbf{A}}}^\perp \mathbf{P}(z_m) \xrightarrow{M \rightarrow \infty} \mathbf{P}(z_m)$$

A similar methodology can be adopted to show that $\mathbf{P}_{\bar{\mathbf{A}}}^\perp \mathbf{u}(\lambda_m) \xrightarrow{M \rightarrow \infty} \mathbf{u}(\lambda_m)$ as long as $z_s \neq \lambda_m$. Thus,

$$\mathbf{P}_{\bar{\mathbf{A}}}^\perp \mathbf{C} \xrightarrow{M \rightarrow \infty} \sum_{m=s+1}^p \mathbf{P}(z_m) \mathbf{J}(z_m) \begin{bmatrix} \tilde{\mathbf{v}}_{2m-1}^T \\ \tilde{\mathbf{v}}_{2m}^T \end{bmatrix} + \sum_{m=2p+1}^{2M-2} \lambda_m \mathbf{u}(\lambda_m) \tilde{\mathbf{v}}_m^T$$

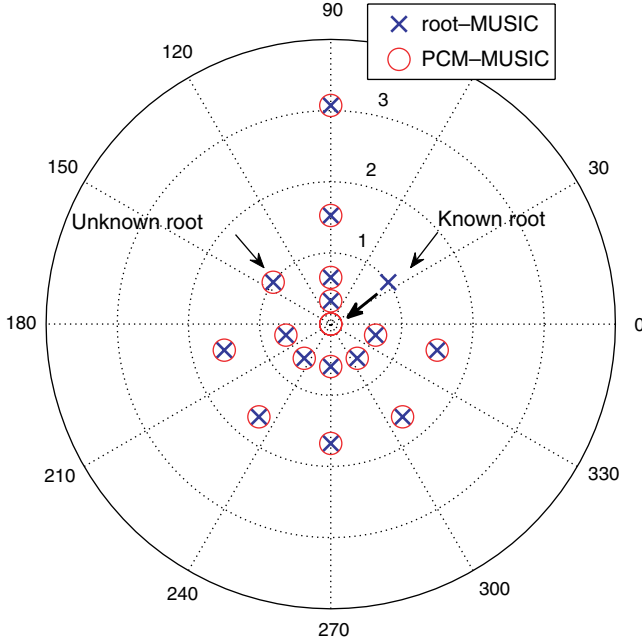


Figure 8.6. Polar representation of the eigenvalues of the companion matrix (root-MUSIC) and of projected companion matrix (PCM-MUSIC) with $p = 2$, $s = 1$, $M = 10$, $K = 50$. The known angular-frequency is 0.1 and the unknown one is equal to 0.4

It follows that, for a large number of samples, the PCM-MUSIC method eliminates only the roots associated with known frequencies without affecting the roots associated with unknown/desired ones. Remark that due to the fact that the number of samples (the dimension of the companion matrix) is virtually $2M - 2$ instead of M , we are rapidly close to the asymptotic conditions of working. In Figure 8.6, the polar coordinate plot of the eigenvalues of the companion matrix and of the projected companion matrix is given. We can see that the known solution is removed while the other eigenvalues are not/weakly affected. The effect of the projection is clearly visible on the figure since the known eigenvalue is pushed toward the origin of the unit circle.

8.10. Bibliography

[AKA 73] AKAIKE H., “Maximum likelihood identification of Gaussian autoregressive moving average models”, *Biometrika*, vol. 60, pp. 255–265, 1973.

- [BAN 92] BANNOUR S., AZIMI-SADJADI M.R., "An adaptive approach for optimal data reduction using recursive least squares learning method", *Proceedings of IEEE ICASSP*, San Francisco, CA, II297-II300, March 1992.
- [BAR 83] BARABELL A., "Improving the resolution performance of eigenstructure-based direction-finding algorithms", *IEEE International Conference on Acoustics, Speech and Signal Processing'83*, vol. 8, pp. 336–339, April 1983.
- [BAZ 06] BAZAN F.S.V., GRATTON S., "An explicit Jordan decomposition of companion matrices", *TEMA Tendencias em Matematica Aplicada e Computacional*, vol. 7, pp. 209–218, 2006.
- [BEH 94] BEHRENS R.T., SCHAFER L.L., "Signal processing applications of oblique projection operators", *IEEE Transactions on Signal Processing*, vol. 42, no. 6, June 1994.
- [BIE 83] BIENVENU G., KOPP L., "Optimality of high resolution array processing using the eigensystem approach", *IEEE Transactions on Acoustics, Speech and Signal Processing*, vol. ASSP-31, pp. 1235–1247, October 1983.
- [BIS 92] BISCHOF C.H., SHROFF G.M., "On updating signal subspaces", *IEEE Transactions on Signal Processing*, vol. 40, pp. 96–105, 1992.
- [BOH 85] BOHME J.F., "Array processing", in LACOUME J.L., DURRANI T.S., STORA R. (eds), *NATO Advanced Study Institute*, Session XLV, Signal Processing, Les Houches, France, North-Holland, 1985.
- [BOH 86] BOHME J.F., "Estimation of spectral parameters of correlated signals in wavefields", *Signal Processing*, vol. 10, pp. 329–337, 1986.
- [BOU 09] BOULEUX G., STOICA P., BOYER R., "An optimal prior knowledge-based DOA estimation method", *17th European Signal Processing Conference (EUSIPCO 2009)*, Glasgow, UK, 2009.
- [BOU 92] BOUVET M., *Traitemen des signaux pour les systèmes SONAR*, Masson, Paris, 1992.
- [BOY 08] BOYER R., BOULEUX G., "Oblique projections for direction-of-arrival estimation with prior knowledge", *IEEE Transactions on Signal Processing*, vol. 56, no. 4, pp. 1374–1387, 2008.
- [BRE 86] BRESLER Y., MACOVSKI A., "Exact maximum likelihood parameter estimation of superimposed exponential signals in noise", *IEEE Transactions on Acoustics, Speech and Signal Processing*, vol. ASSP-34, no. 5, pp. 1081–1089, October 1986.
- [BUN 78a] BUNCH J.R., NIELSEN C.P., SORENSEN D., "Rank-one modification of the symmetric eigenproblem", *Numerische Mathematik*, vol. 31, pp. 31–48, 1978.
- [BUN 78b] BUNCH J.R., NIELSEN C.P., "Updating the singular value decomposition", *Numerische Mathematik*, vol. 31, pp. 111–129, 1978.
- [BUR 72] BURG J.P., "The relationship between maximum entropy spectra and maximum likelihood spectra", *Geophysics*, vol. 37, pp. 375–376, April 1972.
- [CAD 88] CADZOW J.A., "A high resolution direction of arrival algorithm for narrow-band coherent and incoherent sources", *IEEE Transactions Acoustics, Speech and Signal Processing*, vol. ASSP-36, no. 7, pp. 965–979, July 1988.

- [CAD 89] LE CADRE J.P., "Parametric methods for spatial signal processing in the presence of unknown colored noise fields", *IEEE Transactions on Acoustics, Speech and Signal Processing*, vol. 37, no. 7, pp. 965–983, 1989.
- [CAP 69] CAPON J., "High-resolution frequency-wavenumber spectrum analysis", *Proceedings of IEEE*, vol. 57, pp. 1408–1418, February 1969.
- [CHE 89] LE CHEVALIER F., *Principes de Traitement des Signaux Radar et Sonar*, Masson, Collection technique et scientifique des télécoms, 1989.
- [CHO 93] CHOI J., SONG I., KIM S., KIM S.Y., "A combined determination-estimation method for direction of arrival estimation", *Signal Processing*, vol. 30, pp. 123–131, 1993.
- [COM 90] COMON P., GOLUB G.H., "Tracking a few extreme singular values and vectors in signal processing", *Proceedings of IEEE*, vol. 78, no. 8, pp. 1327–1343, August 1990.
- [DEG 92] DEGROAT R.D., "Noniterative subspace tracking", *IEEE Transactions on Signal Processing*, vol. 40, pp. 571–577, 1992.
- [DUD 84] DUDGEON D.E., MERSEREAU R.M., *Multidimensional Digital Signal Processing*, Prentice Hall, Englewood Cliffs, NJ, 1984.
- [EDW 73] EDWARD J.A., FITELSON M.M., "Notes on max-entropy processing", *IEEE Transactions on Information Theory*, vol. IT-19, pp. 232–234, 1973.
- [ERI 94] ERIKSSON A., STOICA P., SÖDERSTRÖM T., "On-line subspace algorithms for tracking moving sources", *IEEE Transactions on Signal Processing*, vol. 42, no. 9, pp. 2319–2330, September 1994.
- [EVA 81] EVANS J.E., JOHNSON J.R., SUN D.F., "High resolution angular spectrum estimation techniques for terrain scattering analysis and angle of arrival estimation", *Proceedings of 1st Acoustics, Speech and Signal Processing Workshop on Spectral Estimation*, Hamilton, Ontario, Canada, pp. 134–139, 1981.
- [FLI 98] FLIELLER A., LARZABAL P., MARCOS S., CLERGEOT H., "Autocalibration d'antenne: modélisation, identifiabilité et traitement", Chapter 23 in *Méthodes à Haute résolution. Traitement d'Antenne et Analyse spectrale*, MARCOS S. (ed.), Hermès, 1998.
- [FOR 98] FORSTER P., VILLIER E., "Performances asymptotiques des méthodes HR", Chapter 9 in *Méthodes à Haute résolution. Traitement d'Antenne et Analyse spectrale*, MARCOS S. (ed.), Hermès, 1998.
- [FUH 88] FUHRMANN D.R., "An algorithm for subspace computation with applications in signal processing", *SIAM Journal on Matrix Analysis and Applications*, vol. 9, no. 2, pp. 213–220, 1988.
- [GOL 80] GOLUB G.H., VAN LOAN C.F., "An analysis of the total least square problem", *SIAM Journal of Numerical Analysis*, vol. 17, no. 6, 1980.
- [GOL 89] GOLUB G.H., VAN LOAN C.F., *Matrix Computations*, 2nd edition, Johns Hopkins University Press, Baltimore, MD, 1989.

- [GRO 98] GROUFFAUD J., LARZABAL P., CLERGEOT H., “Sélection d’ordre de modèle pour les méthodes HR”, Chapter 6 in *Méthodes à Haute résolution. Traitement d’Antenne et Analyse spectrale*, MARCOS S. (ed.), Hermès, 1998.
- [HAY 91a] HAYKIN S., *Adaptive Filter Theory*, 2nd edition, Prentice Hall, International Editors, 1991.
- [HAY 91b] HAYKIN S., *Advances in Spectrum Analysis and Array Processing*. Vol. II, HAYKIN S. (ed.), Advanced Reference Series, Prentice Hall, 1991.
- [HAY 92] HAYKIN S., REILLY J.P., KEZYS V., VERTATSCHISCH E., “Some aspects of array signal processing”, *IEE Proceedings-F*, vol. 139, no. 1, pp. 1–26, February 1992.
- [JAF 88] JAFFER A.G., “Maximum likelihood direction finding of stochastic sources: a separable solution”, *Proceedings of the IEEE International Conference on Acoustics, Speech and Signal Processing*, ICASSP-88, New York, pp. 2893–2896, 1988.
- [JOH 82] JOHNSON D.H., “The application of spectral analysis methods to bearing estimation problems”, *Proceedings of IEEE*, vol. 70, pp. 1018–1028, 1982.
- [JOH 93] JOHNSON D.H., DUDGEON D.E., *Array Signal Processing*, OPPENHEIM A.V. (ed.), Signal Processing Series, Prentice Hall, 1993.
- [KAR 86] KARASALO I., “Estimating the covariance matrix by signal subspace averaging”, *IEEE Transactions on Acoustics, Speech and Signal Processing*, vol. ASSP-34, pp. 8–12, 1986.
- [KAR 84] KARHUNEN J., “Adaptive algorithms for estimating eigenvectors of correlation type matrices”, *Proceedings of IEEE ICASSP*, San Diego, CA, 14.6.1–14.6.4, March 1984.
- [KAV 86] KAVEH M., BARABELL A.J., “The statistical performance of the MUSIC and the minimum-norm algorithms in resolving plane waves in noise”, *IEEE Transactions on Acoustics, Speech and Signal Processing*, vol. ASSP-34, N 412, pp. 331–341, April 1986.
- [KOR 09] EL KORSO M.N., BOYER R., MARCOS S., “Fast sequential source localization using the projected companion matrix approach”, *Third International Workshop on Computational Advances in Multi-Sensor Adaptive Processing (CAMSAP-09)*, 2009.
- [KUM 83] KUMARESAN R., TUFTS D.W., “Estimating the angles of arrival of multiple plane waves”, *IEEE Transactions on Aerospace and Electronic Systems*, vol. AES-19, pp. 134–139, January 1983.
- [MAR 90a] MARCOS S., BENIDIR M., “On a high resolution array processing method non-based on the eigenanalysis approach”, *Proceedings of ICASSP*, Albuquerque, New Mexico, pp. 2955–2958, 1990.
- [MAR 90b] MARCOS S., BENIDIR M., “Source bearing estimation and sensor positioning with the Propagator method”, *Advanced Signal Processing Algorithms, Architectures and Implementations*, LUK F.T. (ed.), SPIE-90, San Diego, CA, pp. 312–323, 1990.
- [MAR 93] MARCOS S., “Calibration of a distorted towed array using a propagation operator”, *Journal of Acoustical Society of America*, vol. 93, no. 4, pp. 1987–1994, 1993.
- [MAR 94a] MARCOS S., MARSAL A., BENIDIR M., “Performances analysis of the Propagator method for source bearing estimation”, *Proceedings of ICASSP*, Adelaide, Australia, pp. IV.237–IV.240, 1994.

- [MAR 95] MARCOS S., MARSAL A., BENIDIR M., “The Propagator method for source bearing estimation”, *Signal Processing*, vol. 42, no. 2, pp.121–138, 1995.
- [MAR 96] MARCOS S., BENIDIR M., “An adaptive tracking algorithm for direction finding and array shape estimation in a nonstationary environment”, special edition in “Array optimization and adaptive tracking algorithms”, *Journal of VLSI Signal Processing*, vol. 14, pp. 107–118, October 1996.
- [MAR 97] MARCOS S., SANCHEZ-ARAUJO J., “Méthodes linéaires haute résolution pour l'estimation de directions d'arrivée de sources. Performances asymptotiques et complexité”, *Traitemennt du Signal*, vol. 14, no. 2, 1997.
- [MAR 98a] MARCOS S., SANCHEZ-ARAUJO J., “Méthodes linéaires HR pour l'estimation de directions d'arrivée de sources”, Chapter 5 in *Méthodes à Haute résolution. Traitement d'Antenne et Analyse spectrale*, MARCOS S. (ed.), Hermes, 1998.
- [MAR 98b] MARCOS S., SANCHEZ-ARAUJO J., “Performances asymptotiques des méthodes linéaires HR”, Chapter 10 in *Méthodes à Haute résolution. Traitement d'Antenne et Analyse spectrale*, MARCOS S. (ed.), Hermes, 1998.
- [MAR 98c] MARCOS S., “Sensibilité des méthodes HR aux perturbations de modèle”, Chapter 11 in *Méthodes à Haute résolution. Traitement d'Antenne et Analyse spectrale*, MARCOS S. (ed.), Hermes, 1998.
- [MAR 87] MARPLE S.L., JR., *Digital Spectral Analysis with Applications*, OPPENHEIM A.V. (ed.), Signal Processing series, Prentice Hall, 1987.
- [MAR 94b] MARSAL A., MARCOS S., “A reduced complexity ESPRIT method and its generalization to an antenna of partially unknown shape”, *Proceedings of ICASSP 94*, Adelaide, Australia, pp. IV.29–IV.32, 1994.
- [MAR 98] MARTINERIE F., LE CADRE J.P., VILLIER E., RAVAZZOLA P., “Quelques variantes des méthodes HR”, Chapter 3 in *Méthodes à Haute résolution. Traitement d'Antenne et Analyse spectrale*, MARCOS S. (ed.), Hermes, 1998.
- [MUN 91] MUNIER J., DELISLE G.Y., “Spatial analysis using new properties of the cross-spectral matrix”, *Transactions on Signal Processing*, vol. 39, no. 3, pp. 746–749, 1991.
- [NIC 89] NICOLAU E., ZAHARIA D., *Adaptive Arrays*, Studies in Electrical and Electronic Engineering, Elsevier, 1989.
- [OWS 78] OWSLEY N.L., “Adaptive data orthogonalization”, *Proceedings of IEEE ICASSP*, pp. 109–112, 1978.
- [PIL 89] PILLAI S.U., *Array Signal Processing*, Springer-Verlag, 1989.
- [PIS 73] PISARENKO V.F., “The retrieval of harmonics from a covariance function”, *Geophysical Journal of the Royal Astronomical Society*, vol. 33, pp. 347–366, 1973.
- [POR 88] PORAT B., FRIEDLANDER B., “Analysis of the asymptotic relative efficiency of the MUSIC algorithm”, *IEEE Transactions on Acoustics, Speech and Signal Processing*, vol. ASSP-36, pp. 532–544, April 1988.

- [RED 82] REDDY V.U., EGARDT B., KAILATH T., "Last squares type algorithm for adaptive implementation of Pisarenko's harmonic retrieval method", *IEEE Transactions on Acoustics, Speech and Signal Processing*, vol. ASSP-30, pp. 241–251, 1982.
- [RIS 78] RISSANEN J., "Modelling by shortest data description", *IEE Automatica*, vol. 14, pp. 465–471, February 1978.
- [ROY 86] ROY R., PAULRAJ A., KAILATH T., "ESPRIT—a subspace rotation approach to estimation of parameters of cisoids in noise", *IEEE Transactions on Acoustics, Speech and Signal Processing*, vol. ASSP-34, pp. 1340–1342, October 1986.
- [ROY 89] ROY R., KAILATH T., "ESPRIT—estimation of signal parameters via rotational invariance techniques", *IEEE Transactions on Acoustics, Speech and Signal Processing*, vol. ASSP-37, pp. 984–995, July 1989.
- [SAN 98] SANCHEZ-ARAUJO J., MARCOS S., BENIDIR M., COMON P., "Algorithmes adaptatifs pour la poursuite du sous-espace source", Chapter 14 in *Méthodes à Haute résolution. Traitement d'Antenne et Analyse spectrale*, MARCOS S. (ed.), Hermès, 1998.
- [SCH 79] SCHMIDT R.O., "Multiple emitter location and signal parameter estimation", *RADC Spectral Estimation Workshop*, Rome, NY, pp. 243–258, 1979.
- [SCH 78] SCHWARTZ G., "Estimating the dimension of a model", *The Annals of Statistics*, vol. 6, pp. 461–464, February 1978.
- [SHA 85] SHAN T.J., WAX M., KAILATH T., "On spatial smoothing for direction of arrival estimation of coherent signals", *IEEE Transactions on Acoustics, Speech and Signal Processing*, vol. ASSP-33, N 4, pp. 806–811, August 1985.
- [SHA 88] SHARMAN K.C., "Maximum likelihood estimation by simulated annealing", *Proceedings of the IEEE International Conference on Acoustics, Speech and Signal Processing*, ICASSP-88, New York City, pp. 2241–2244, April 1988.
- [SCH 89] SCHREIBER R., "Implementation of adaptive array algorithms", *IEEE Transactions on Acoustics, Speech and Signal Processing*, vol. 34, no. 5, pp. 1550–1556, October 1989.
- [SHA 89] SHARMAN K.C., MCCLURKIN G.D., "Genetic algorithms for maximum likelihood parameter estimation", *Proceedings of the IEEE International Conference on Acoustics, Speech and Signal Processing*, ICASSP-89, Glasgow, Scotland, pp. 2716–2719, May 1989.
- [STO 05] STOICA P., MOSES R.L., *Spectral Analysis of Signals*, Prentice Hall, 2005.
- [STO 89] STOÏCA P., NEHORAI A., "MUSIC, maximum likelihood and Cramer-Rao bound", *IEEE International Conference on Acoustics, Speech and Signal Processing*, vol. ASSP-37, N 12, pp. 720–741, May 1989.
- [STO 90a] STOÏCA P., NEHORAI A., "MUSIC, maximum likelihood and Cramer-Rao bound: further results and comparisons", *IEEE International Conference on Acoustics, Speech and Signal Processing*, vol. ASSP-38, N 12, pp. 2140–2150, December 1990.
- [STO 90b] STOÏCA P., SHARMAN K.C., "Novel eigen analysis method for direction estimation", *IEE Proceedings-F*, vol. 137, no. 1, February 1990.

- [STO 92] STOÏCA P., SODERSTROM T., SIMONYTE V., “On estimating the noise power in array processing”, *Signal Processing*, vol. 26, pp. 205–220, 1992.
- [UNN 89] UNNIKRISHNA PILLAI S., *Array Signal Processing*, Springer-Verlag, 1989.
- [VIB 91] VIBERG M., OTTERSTEN B., “Sensor array processing based on subspace fitting”, *Transactions on Signal Processing*, vol. 39, no. 5, pp. 1110–1121, 1991.
- [WAX 85] WAX M., KAILATH T., “Detection of signals by information theoretic criteria”, *IEEE Transactions on Acoustics, Speech and Signal Processing*, vol. ASSP-33, pp. 387–392, February 1985.
- [WAX 89] WAX M., ZISKIND I., “Detection of the number of coherent signals by the MDL principle”, *IEEE Transactions on Acoustics, Speech and Signal Processing*, vol. ASSP-37, pp. 1190–1196, February 1989.
- [WIR 11] WIRFALT P., JANSSON M., BOULEUX G., STOICA P., “Prior knowledge-based direction of arrival estimation”, *36th International Conference on Acoustics, Speech and Signal Processing (ICASSP2011)*, Prague, Czech Republic, 2011.
- [ZHA 89] ZHANG Q.T., WONG K.M., YIP P.C., REILLY J.P., “Statistical analysis of the performance of information theoretic criteria in the detection of the number of signals in array processing”, *IEEE Transactions on Acoustics, Speech and Signal Processing*, vol. ASSP-37, pp. 1557–1567, October 1989.
- [YAN 89] YANG X., SARKAR T.K., ARVAS E., “A survey of conjugate gradient algorithms for solution of extreme eigen-problem of a symmetric matrix”, *IEEE Transactions on Acoustics, Speech and Signal Processing*, vol. 37, pp. 1550–1556, 1989.
- [YAN 95] YANG B., “Projection approximation subspace tracking” *IEEE Transactions on Signal Processing*, vol. 43, pp. 95–107, 1995.
- [YEH 86] YEH C.C., “Projection approach for bearing estimations”, *IEEE Transactions on Acoustics, Speech and Signal Processing*, vol. ASSP-34, no. 5, pp. 1347–1349, 1986.
- [YEH 87] YEH C.C., “Simple computation of projection matrix for bearing estimations”, *IEE Part F*, vol. 134, no. 2, pp. 146–150, April 1987.

PART 4

Advanced Concepts

Chapter 9

Multidimensional Harmonic Retrieval: Exact, Asymptotic, and Modified Cramér-Rao Bounds

9.1. Introduction

The one-dimensional harmonic model is very useful in many fields such as signal processing, audio compression, digital communications, biomedical signal processing, electromagnetic analysis, and others. A generalization of this model to $P > 1$ dimensions can be encountered in several domains (see [MCC 82] and references therein) such as multiple-input multiple-output (MIMO) channel modeling from channel sounder measurements [PES 04, HAA 04], wireless communications [HAA 98, GER 05, BOE 06], passive localization and radar processing [CHE 08, CHE 10, JIA 08, JIN 09], etc. In addition, we can find in [TAO 01, XIA 02] an analysis of the identification problem and in [KOR 11], the study of the statistical resolution limit associated with this model.

For many practical estimation problems, optimal estimators such as the maximum likelihood (ML) estimator, the maximum *a posteriori* estimator, or the minimum mean-squared error estimator are infeasible. Therefore, one often needs to resort to suboptimal techniques such as expectation maximization, gradient-based algorithms, Markov chain Monte-Carlo methods, particle filters, and in particular the popular subspace-based estimation methods [HAA 98, GER 05, PES 04, ROE 06, TAO 01, LIU 06, BOY 08b], or combinations of these methods. These techniques are usually evaluated by computing the mean square error (MSE) through extensive Monte-Carlo simulations and comparing it to theoretical performance.

Chapter written by Rémy BOYER. Part of this chapter has been published in [BOY 08a].

In signal processing, many lower bounds of the MSE exist such as, for instance, the Weiss-Weinstein or Ziv-Zakai bounds (see [TRE 07] and references therein). But one of the most popular bounds is the deterministic Cramér-Rao bound (CRB) [STO 89]. It is important to notice that we know that for sufficient signal-to-noise ratio (SNR) the ML estimator meets this bound [REN 06].

More precisely, in this chapter, we propose closed-form (non-matrix) expressions of the deterministic CRB for the M -order harmonic model (sum of M waveforms) of dimension P , viewed as an $N_1 \times \dots \times N_P$ tensor, contaminated by an additive white complex Gaussian noise. This work is an extension of the seminal work of Stoica and Nehorai [STO 89] for the one-dimensional ($P = 1$) harmonic model. Obviously, many works have been carried out on the determination of the deterministic CRB for small P , i.e. for $P = 2$ (two-dimensional harmonic model) [FRA 02, HUA 92] or for $P = 3$ and $P = 4$ in the context of sensor array [XIA 01]. Other contributions provide matrix-based expressions of the CRB for any P [LIU 06], but to the best of our knowledge, we cannot find closed-form expressions of the deterministic CRB for any dimension P . Closed-form expressions [DIL 98, DEL 08] are important for at least two reasons: (i) they provide useful insight into the behavior of the bound, and (ii) for large analysis duration ($N_p \gg 1, \forall p \in [1 : P]$) and/or dimension P , computing the CRB in a brute force manner becomes an impracticable task.¹

An alternative scenario is investigated in the second part of this chapter. More precisely, sometimes, we are interested in estimating deterministic angular-frequency parameters in each dimension while the complex amplitudes are viewed as random time-varying nuisance parameters [GER 05, PES 05]. In such cases, the statistics of the observation depend not only on the vector parameter to be estimated, but also on a nuisance parameters we do not want to estimate. The presence of a time-varying nuisance parameters makes the numerical computation of the CRB a costly operation since it is necessary to inverse a very large (growing with time) Fisher information matrix (FIM). This is particularly true for multidimensional data as considered here. In addition, as the nuisance parameters are time varying, the number of these parameters is not bounded while the number of parameter of interest is. To avoid these problems, a modified CRB (MCRB) has been derived in [DAN 94]. This bound is based on the expectation with respect to (w.r.t.) the nuisance parameters of the reduced-size FIM, called modified FIM (MFIM), as computed for fixed nuisance parameters. The scalar version of this bound has been presented in [MOE 98] and its vector formulation in [GIN 00]. In this chapter, we derive closed-form (non-matrix) expressions of this bound for the multidimensional harmonic retrieval problem with time-varying complex amplitudes in the case of asymptotic (large but not infinite) analysis duration in each dimension. As a by-product, (i) we also extend the

¹ The computation of the CRB for the considered model is of $O(N_1 N_2 \dots N_P)$.

asymptotic CRB (ACRB) to the important case of multiple snapshots (i.e. for time-varying complex amplitudes) and (ii) we study the modified ACRB to precisely characterize what we lose or not w.r.t. the ACRB.

This chapter is organized as follows. Section 9.2 presents the multidimensional harmonic model and the associated CanDecomp (CANonical DECOMPosition)/Parafac (PARAllel FACctor) decomposition. Section 9.3 introduces and analyzes a closed-form expression of the deterministic CRB for asymptotic analysis duration. Section 9.4 presents the analysis of the modified ACRB. Section 9.5 is dedicated to the conclusion. The derivation of the ACRB is given in Appendix A and we present in Appendix B, the exact (non-asymptotic) CRB for a first-order harmonic model of dimension P . Appendix C extends the ACRB to the important case of multiple snapshots and finally, Appendix D applies the results proposed in this chapter to the bistatic MIMO radar.

9.2. CanDecomp/Parafac decomposition of the multidimensional harmonic model

The multidimensional harmonic model assumes that the observation can be modeled as the superposition of M undamped exponentials sampled on a P -dimensional grid. More specifically, we define a noisy M -order harmonic model of dimension P according to:

$$[\mathcal{Y}]_{n_1 \dots n_P} = [\mathcal{X}]_{n_1 \dots n_P} + \sigma [\mathcal{E}]_{n_1 \dots n_P} \quad [9.1]$$

where $[\mathcal{Y}]_{n_1 \dots n_P}$ denotes the (n_1, \dots, n_P) -th entry of the $(N_1 \times \dots \times N_P)$ tensor (multiway array) \mathcal{Y} associated with the noisy M -order harmonic model of dimension P . Let $N_p > 1$ be the analysis duration along the p th dimension and define $n_p \in [0 : N_p - 1]$. Tensor \mathcal{X} in model [9.1] is the $(N_1 \times \dots \times N_P)$ tensor associated with the noise-free M -order harmonic model of dimension P defined by:

$$[\mathcal{X}]_{n_1 \dots n_P} = \sum_{m=1}^M \alpha_m \prod_{p=1}^P e^{i\omega_m^{(p)} n_p} \quad [9.2]$$

in which the m th complex amplitude is denoted by $\alpha_m = a_m e^{i\phi_m}$ where $a_m > 0$ is the m th real amplitude, ϕ_m the m th initial phase, and $\omega_m^{(p)}$ the m th angular frequency along the p th dimension.² Let $d(\omega_m^{(p)}) = [1 \ e^{i\omega_m^{(p)}} \dots e^{i\omega_m^{(p)}(N_p-1)}]^T$ be

² In this chapter, the angular frequencies are assumed to be all distinct. The case of identical parameters is tackled in [LIU 07] where a dedicated estimation scheme is proposed. The corresponding asymptotic CRB is studied in [SAJ 07].

the Vandermonde vector containing the angular-frequency parameters. As:

$$\underbrace{[\mathbf{d}(\omega_m^{(1)}) \circ \mathbf{d}(\omega_m^{(2)}) \circ \dots \circ \mathbf{d}(\omega_m^{(P)})]_{n_1 \dots n_P}}_{\mathcal{D}_m} = \prod_{p=1}^P e^{i\omega_m^{(p)} n_p} \quad [9.3]$$

in definition [9.2] and in which \circ denotes the outer product, it is straightforward to see that the tensor, \mathcal{X} , associated with the noise-free M -order harmonic model of dimension P can be expressed as the linear combining of M rank-1 tensors: $\mathcal{D}_1, \dots, \mathcal{D}_M$, each of size $N_1 \times \dots \times N_P$, according to:

$$\mathcal{X} = \sum_{m=1}^M \alpha_m \mathcal{D}_m \in \mathbb{C}^{N_1 \times \dots \times N_P} \quad [9.4]$$

Consequently, the noise-free M -order harmonic model of dimension P follows a CanDecomp/Parafac model [HAR 70, TAO 01, XIA 02] and its vectorized expression is:

$$\begin{aligned} x &= \text{vec}(\mathcal{X}) \\ &= [[\mathcal{X}]_{000} \dots [\mathcal{X}]_{N_1-1 \ N_2-1 \ 0} \ [\mathcal{X}]_{001} \dots \dots \ [\mathcal{X}]_{N_1-1 \ N_2-1 \ N_3-2} \ [\mathcal{X}]_{00 \ N_3-1} \dots]^T \\ &= \sum_{m=1}^M \alpha_m \text{vec}(\mathcal{D}_m) \end{aligned} \quad [9.5]$$

where:

$$\text{vec}(\mathcal{D}_m) = \mathbf{d}(\omega_m^{(1)}) \otimes \mathbf{d}(\omega_m^{(2)}) \otimes \dots \otimes \mathbf{d}(\omega_m^{(P)}) \quad [9.6]$$

in which \otimes denotes the Kronecker product. Tensor $\sigma \mathcal{E}$ in model [9.1] is the noise tensor where σ is a positive real scalar and each entry $[\mathcal{E}]_{n_1 \dots n_P}$ follows a complex Gaussian distribution $\mathcal{CN}(0, 1)$. In addition, we assume the decorrelation of (i) the noise-free signal and the noise and (ii) the noise in each dimension, i.e.

$$E\{[\mathcal{X}]_{n_1 \dots n_P} [\mathcal{E}]_{n'_1 \dots n'_P}^*\} = 0 \quad [9.7]$$

$$E\{[\mathcal{E}]_{n_1 \dots n_P} [\mathcal{E}]_{n'_1 \dots n'_P}^*\} = \prod_{p=1}^P \delta_{n_p n'_p} \quad [9.8]$$

where $E\{\cdot\}$ is the mathematical expectation and δ_{ij} the Kronecker delta. So, based on expressions [9.5], [9.7], and [9.8], the final expression of the vectorized noisy model is:

$$y = \text{vec}(\mathcal{Y}) = x + \sigma e \quad [9.9]$$

where $e = \text{vec}(\mathcal{E}) \sim \mathcal{CN}(0, I_{N_1 \dots N_P})$.

9.3. CRB for the multidimensional harmonic model

The noisy observation y in expression [9.9] follows a complex Gaussian distribution, i.e. $y \sim \mathcal{CN}(x, \sigma^2 I_{N_1 \dots N_P})$ and is a function of the real parameter vector θ given by:

$$\theta = [\theta'^T \ \sigma^2]^T$$

in which:

$$\theta' = [\underline{\omega}^T \ \underline{a}^T \ \underline{\phi}^T]^T$$

where:

$$\underline{a} = [a_1 \dots a_M]^T, \quad [9.10]$$

$$\underline{\phi} = [\phi_1 \dots \phi_M]^T, \quad [9.11]$$

$$\underline{\omega} = [\underline{\omega}^{(1)T} \dots \underline{\omega}^{(P)T}]^T \text{ with } \underline{\omega}^{(p)} = [\omega_1^{(p)} \dots \omega_M^{(p)}]^T \quad [9.12]$$

9.3.1. Deterministic CRB

A fundamental result [RAO 45, CRA 46] often called “covariance inequality principle” is the following. Let $\Gamma = E\{(\hat{\theta} - \theta)(\hat{\theta} - \theta)^T\}$ be the covariance matrix of an unbiased estimate of θ , denoted by $\hat{\theta}$ and define the CRB associated with the M -order harmonic model of dimension P , denoted by $\text{CRB}_{(P)}$. The covariance inequality principle states that under quite general/weak conditions, $\Gamma - \text{CRB}_{(P)}(\theta)$ is a positive semi-definite matrix or equivalently in terms of the MSE, we have:

$$\text{MSE}([\hat{\theta}]_i) = E\left\{\left([\hat{\theta}]_i - [\theta]_i\right)^2\right\} \geq \text{CRB}_{(P)}([\theta]_i) \quad [9.13]$$

In other words, the variance of any unbiased estimate is always bounded below by the CRB. In addition, if the MSE for a given unbiased estimator is equal to the CRB, we say that the considered estimator is statistically efficient. More specifically, the CRB w.r.t. the signal parameters is given by:

$$\text{CRB}_{(P)}([\theta']_i) = \frac{\sigma^2}{2} [F_{\theta'\theta'}^{-1}]_{ii}, \text{ for } i \in [1 : (P+2)M] \quad [9.14]$$

where:

$$F_{\theta'\theta'} = \begin{bmatrix} J_{\underline{\omega}\underline{\omega}} & J_{\underline{\omega}\underline{a}} & J_{\underline{\omega}\underline{\phi}} \\ J_{\underline{\omega}\underline{a}}^T & J_{\underline{a}\underline{a}} & J_{\underline{a}\underline{\phi}} \\ J_{\underline{\omega}\underline{\phi}}^T & J_{\underline{a}\underline{\phi}}^T & J_{\underline{\phi}\underline{\phi}} \end{bmatrix} \quad [9.15]$$

is the FIM w.r.t. the signal parameter θ' . In addition, in equation [9.15], we have defined each block of the FIM by:

$$J_{pq} = \Re \left\{ \left(\frac{\partial x}{\partial p} \right)^H \frac{\partial x}{\partial q} \right\} \quad [9.16]$$

with $\Re\{\cdot\}$ being the real part of a complex number and x the noise-free M -order harmonic model of dimension P introduced in expression [9.5]. Note that to obtain equation [9.14], we have exploited the property that the signal and the nuisance (noise) parameters are decoupled. So, the CRB for the i th signal parameter, denoted by $[\theta']_i$, is given by the (i, i) th term of the FIM inverse weighed by $\sigma^2/2$.

9.3.2. Deterministic asymptotic CRB for the M -order harmonic model of dimension P

In the following, we consider a large analysis duration ($N_p \gg 1, \forall p$) where analytic inversion of the FIM is feasible and thus closed-form expressions of the deterministic CRB_(P) can be obtained.

THEOREM 9.1.– *The deterministic asymptotic CRB_(P) (ACRB_(P)) for the M -order harmonic model of dimension P defined in equation [9.1] w.r.t. the model parameter θ' , i.e. ACRB_(P)(θ'), is given by:*

$$\text{ACRB}_{(P)}(\omega_m^{(p)}) = \frac{6}{N_p^2 \mathcal{N}_P \text{SNR}_m} \quad [9.17]$$

$$\text{ACRB}_{(P)}(a_m) = \frac{a_m^2}{2 \mathcal{N}_P \text{SNR}_m} \quad [9.18]$$

$$\text{ACRB}_{(P)}(\phi_m) = \frac{3P + 1}{2 \mathcal{N}_P \text{SNR}_m} \quad [9.19]$$

where $\text{SNR}_m = a_m^2/\sigma^2$ is the local SNR for $m \in [1 : M]$ and:

$$\mathcal{N}_P = \prod_{p=1}^P N_p$$

PROOF.– see Appendix A. □

The deterministic $\text{ACRB}_{(P)}$ is fully characterized by the tensor size, (and thus dimension P), and the local SNR. In the sequel, we list some important properties of the ACRB .

- P1. The deterministic $\text{ACRB}_{(P)}$ is invariant to the specific value of the initial phase.
- P2. The deterministic $\text{ACRB}_{(P)}$ is invariant to the specific value of the angular frequency.
- P3. According to expression [9.17], the ACRB for the p th angular frequency depends of the cube of the corresponding dimension, N_p , and is only linear in the other ones.
- P4. As expected at an intuitive level, the ACRB for the real amplitude and for the initial phase are invariant to the specific dimension p .

9.3.2.1. Convergence with respect to dimension P

In this part, the $\text{ACRB}_{(P+1)}$ is associated with the tensor of size $N_1 \times \dots \times N_P \times N_{P+1}$, i.e. the first P dimensions, N_1, \dots, N_P , remains identical as for the tensor associated with the $\text{ACRB}_{(P)}$ and the last one, i.e. the $(P+1)$ th, is added. In addition, it makes sense to consider the ACRB for the same waveform m and dimension p . In this case, we study the behavior of the $\text{ACRB}_{(P)}$ w.r.t. dimension P .

THEOREM 9.2.– *The $\text{ACRB}_{(P)}$ is a strictly monotonically decreasing sequence w.r.t. dimension P , i.e. $\text{ACRB}_{(P)}([\theta']_i) < \text{ACRB}_{(P-1)}([\theta']_i) < \dots < \text{ACRB}_{(1)}([\theta']_i)$.*

PROOF.– Using equations [9.17], [9.18], and [9.19], the quotient of two consecutive ACRB is given by:

$$\frac{\text{ACRB}_{(P+1)}(\omega_m^{(p)})}{\text{ACRB}_{(P)}(\omega_m^{(p)})} = \frac{\text{ACRB}_{(P+1)}(a_m)}{\text{ACRB}_{(P)}(a_m)} = \frac{1}{N_{P+1}} \quad [9.20]$$

$$\frac{\text{ACRB}_{(P+1)}(\phi_m)}{\text{ACRB}_{(P)}(\phi_m)} = \left(\frac{3P+4}{3P+1} \right) \frac{1}{N_{P+1}} \quad [9.21]$$

As N_{P+1} in expressions [9.20] and [9.21] is large, meaning $\frac{1}{N_{P+1}} \ll 1$, and as $1 < \frac{3P+4}{3P+1} < 2$ in equation [9.21], we have $\text{ACRB}_{(P+1)}([\theta']_m) < \text{ACRB}_{(P)}([\theta']_m)$. Consequently, the $\text{ACRB}_{(P)}$ is a strictly monotonically decreasing sequence w.r.t. dimension P . □

We can say:

– Increasing the dimension of the harmonic model decreases the $\text{ACRB}_{(P)}$. We explain that, at an intuitive level, according to the following argumentation. When dimension P increases, i.e. $P \rightarrow P + 1$, we have to estimate more parameters so

the degree of freedom decreases but at the same time the $\text{ACRB}_{(P+1)}$ benefitiates from N_{P+1} additional samples. These two facts together explain why the $\text{ACRB}_{(P)}$ is decreased by a factor $1/N_{P+1}$.

We have:

$$\text{ACRB}_{(P)}(\omega_m^{(p)}) = \frac{1}{\prod_{p=2}^P N_p} \text{ACRB}_{(1)}(\omega_m) \quad [9.22]$$

$$\text{ACRB}_{(P)}(a_m) = \frac{1}{\prod_{p=2}^P N_p} \text{ACRB}_{(1)}(a_m) \quad [9.23]$$

$$\text{ACRB}_{(P)}(\phi_m) = \frac{3P+1}{4 \prod_{p=2}^P N_p} \text{ACRB}_{(1)}(\phi_m) \quad [9.24]$$

where $\text{ACRB}_{(1)}$ is the bound derived by Stoica and Nehorai [STO 89] for $P = 1$.

9.3.2.2. The cubic tensor case

A cubic or balanced tensor is a tensor with identical sizes, i.e. $N_p = N, \forall p$. According to the previous theorem, the $\text{ACRB}_{(P)}$ are:

$$\text{ACRB}_{(P)}(\omega_m^{(p)}) = \frac{6}{N^{P+2} \text{SNR}_m} = \frac{1}{N^{P-1}} \text{ACRB}_{(1)}(\omega_m) \quad [9.25]$$

$$\text{ACRB}_{(P)}(a_m) = \frac{a_m^2}{2N^P \text{SNR}_m} = \frac{1}{N^{P-1}} \text{ACRB}_{(1)}(a_m) \quad [9.26]$$

$$\text{ACRB}_{(P)}(\phi_m) = \frac{3P+1}{2N^P \text{SNR}_m} = \frac{3P+1}{4N^{P-1}} \text{ACRB}_{(1)}(\phi_m) \quad [9.27]$$

For cubic tensors, we can say:

- The “order of magnitude” of the $\text{ACRB}_{(P)}$ for the real amplitude and the initial phase is $O(N^{-P})$ and $O(N^{-P+2})$ for the angular frequency.
- The rate of convergence [SCH 02], i.e. the “speed” at which the $\text{ACRB}_{(P)}$ approaches its limit, for the angular frequency and for the real amplitude is geometric. For the initial phase parameter, the convergence is also geometric for large dimension P .

9.3.2.3. Illustration of the ACRB

In this part, we choose to illustrate the derived bounds for small and large cubic tensors of size $N = 3$ and $N = 1000$, respectively. The dimension of the multidimensional harmonic model is $P = 3$ and its “vectorized” form is $x = 2e^{i\frac{\pi}{3}} (d(1) \otimes d(0.5) \otimes d(0.2))$. We illustrate in Figure 9.1, the behavior of the derived bounds w.r.t. the SNR in linear scale. More precisely, we have reported:

- The numerical CRB that is the bound based on brute force computation of expression [9.14]. Its complexity is $O(N^3)$.
- The ACRB defined in expressions [9.17], [9.18], and [9.19].
- The exact CRB defined in expressions [9.57], [9.58], and [9.59] for a first-order multidimensional harmonic model of dimension three.

As expected for a very short duration, the ACRB is not accurate for the angular frequency (see Figure 9.1a) and in particular for the initial phase parameter (see Figure 9.1c). In addition, we can observe that the exact CRB and the numerical CRB are merged. In Figure 9.2, we have drawn the $\text{ACRB}_{(P)}$ for P in range $[1 : 5]$ and for long analysis duration ($N = 1000$). Note that if the complexity is very high ($O(10^9)$), then the numerical CRB or matrix-based derivation of this bound is impracticable. As we can see increasing the dimension P decreases the ACRB.

9.3.3. Asymptotic CRB for a constant amount of data

In given contexts/applications, we have a constant amount of data, \mathcal{D} , for every dimension, P . In this section, we investigate the derived bound that integrates this constraint. Let $N_p^{(P)}$ be the number of samples in the p th dimension among P . So, we have:

$$\prod_{p=1}^P N_p^{(P)} = \mathcal{D} \quad [9.28]$$

Constraint [9.28] implies that we have no assurance that the $\text{ACRB}_{(P)}$ exists for fixed N and P . In other terms, it is not always possible to find integers, $N_p^{(P)}$, that satisfy constraint [9.28] for all P and N . For instance, assume that $\mathcal{D} = 9$, the $\text{ACRB}_{(3)}$ does not exist since the integer 9 cannot be decomposed into the product of three integers strictly greater than one. But, if the ACRB exists, then its expression is:

$$\text{ACRB}_{(P)}(\omega_m^{(p)}) = \frac{6}{N_p^{(P)} \mathcal{DSNR}_m} \quad [9.29]$$

$$\text{ACRB}_{(P)}(a_m) = \frac{a_m^2}{2\mathcal{DSNR}_m} \quad [9.30]$$

$$\text{ACRB}_{(P)}(\phi_m) = \frac{3P + 1}{2\mathcal{DSNR}_m} \quad [9.31]$$

The main difference to the ACRB without constraint [9.28] is that the dependence w.r.t. dimension P is only though the square of term $N_p^{(P)}$ for the angular-frequency parameter and term $3P + 1$ for the initial phase. Remark the important point that the ACRB for the real amplitude parameter becomes invariant to parameter P .

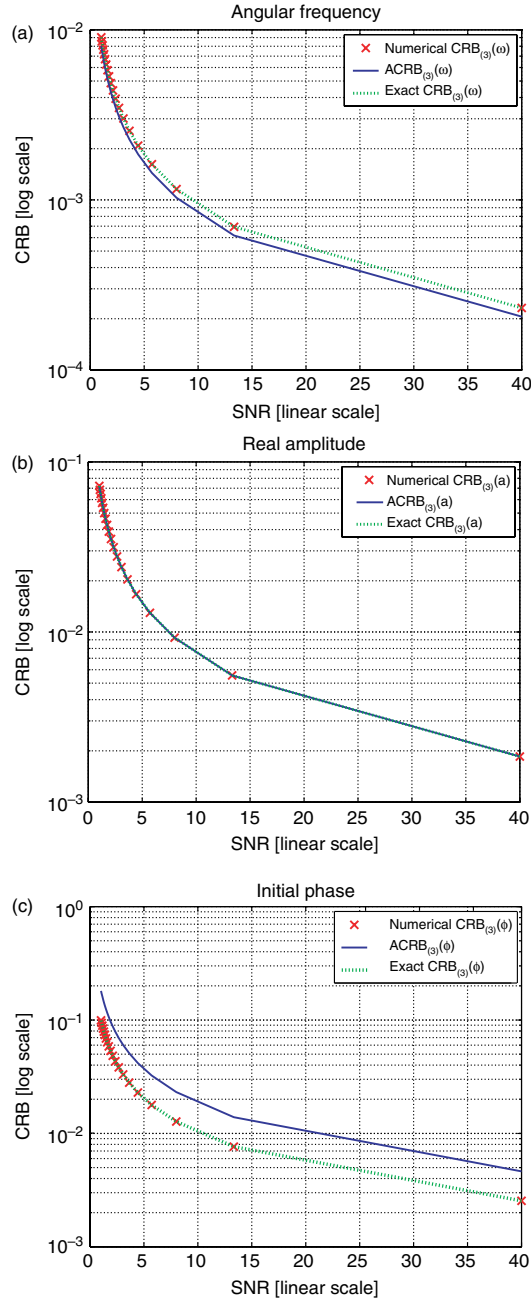


Figure 9.1. CRB versus SNR for a first-order harmonic model of dimension 3 for very short analysis duration ($N = 3$)

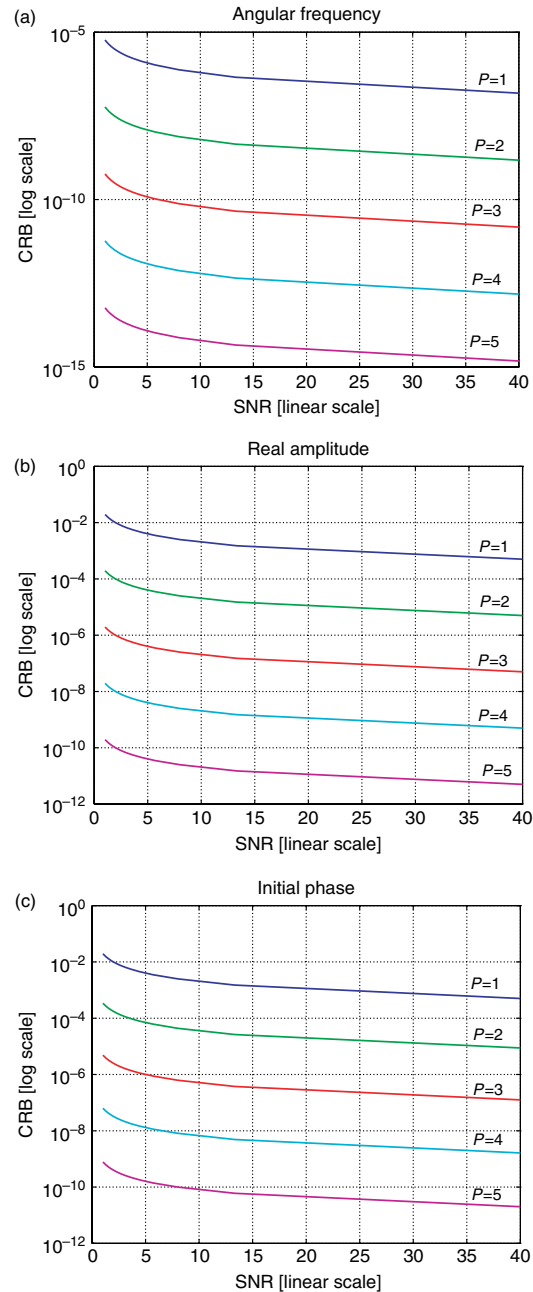


Figure 9.2. ACRB versus SNR for a first-order harmonic model of dimension 3 for large analysis duration ($N = 1000$)

9.3.3.1. Real amplitude and Initial phase

The $\text{ACRB}_{(P)}$ for the real amplitude is constant w.r.t. dimension P and is equal to the $\text{ACRB}_{(1)}$, i.e.

$$\text{ACRB}_{(P)}(a_m) = \text{ACRB}_{(P-1)}(a_m) = \dots = \text{ACRB}_{(1)}(a_m) \quad [9.32]$$

So, the accuracy for real amplitude is not affected by considering multidimensional harmonic model. Contrary to the real amplitude parameters, the rate for the initial phase is not constant (w.r.t. P) and is given by:

$$\frac{\text{ACRB}_{(P+1)}(\phi_m)}{\text{ACRB}_{(P)}(\phi_m)} = \frac{P + \frac{4}{3}}{P + \frac{1}{3}} = \lambda(P)$$

As the rate is higher than 1, the $\text{ACRB}_{(P)}(\phi_m)$ strictly monotonically increases with P and we have:

$$\text{ACRB}_{(P)}(\phi_m) > \text{ACRB}_{(P-1)}(\phi_m) > \dots > \text{ACRB}_{(1)}(\phi_m) \quad [9.33]$$

As rate $\lambda(P)$ is a strictly monotonically decreasing sequence in the following interval:

$$\lambda(1) = \frac{7}{4} \leq \lambda(P) < 1 = \lim_{P \rightarrow \infty} \lambda(P) \quad [9.34]$$

the increasing of the bound remains relatively low for small and moderate P and becomes almost constant for large P . In conclusion, the estimation accuracy of this parameter is degraded but not seriously.

9.3.3.2. Angular-frequency parameter

For the p th angular-frequency parameter, the number of samples into the p th dimension, $N_p^{(P)}$, plays an important role since the quotient of two consecutive ACRB is given by:

$$\frac{\text{ACRB}_{(P+1)}(\omega_m^{(p)})}{\text{ACRB}_{(P)}(\omega_m^{(p)})} = \left(\frac{N_p^{(P)}}{N_p^{(P+1)}} \right)^2 \quad \text{for } p \in [1 : P] \quad [9.35]$$

– For cubic tensors and according to constraint [9.28], we have $N^{(P)} > N^{(P+1)}$ and thus the ACRB is a monotonically increasing sequence.

– For unbalanced tensors, the ACRB can be locally, i.e. for a given dimension p , a constant, a strictly monotonically increasing or decreasing sequences, depending on the specific distribution of the tensor sizes. But, if the accuracy is improved in a given dimension, this means that the accuracy decreases in another one.

9.3.3.3. Illustration of the ACRB for constant amount of data

Consider a total amount of data equal to $\mathcal{D} = 1.2 \times 10^{10}$. For instance, there exist tensors of sizes:

Dim. 1	1.2×10^{10}
Dim. 2	$(4 \times 10^7) \times (3 \times 10^2)$
Dim. 3	$10^5 \times (4 \times 10^2) \times (3 \times 10^2)$
Dim. 4	$(2.5 \times 10^2) \times (4 \times 10^2) \times (3 \times 10^2) \times (4 \times 10^2)$

Obviously, other distributions of parameter $N_p^{(P)}$ are possible. In Figure 9.3, we have illustrated the ACRB for a first-order ($M = 1$) harmonic model of dimension 3 under constraint [9.28]. These figures confirm the conclusions given in the previous sections. In particular,

– In Figure 9.3a, we can see that for increasing parameter P , the bound increases. But locally, we can have other behaviors as we can see in Figure 9.3b since for

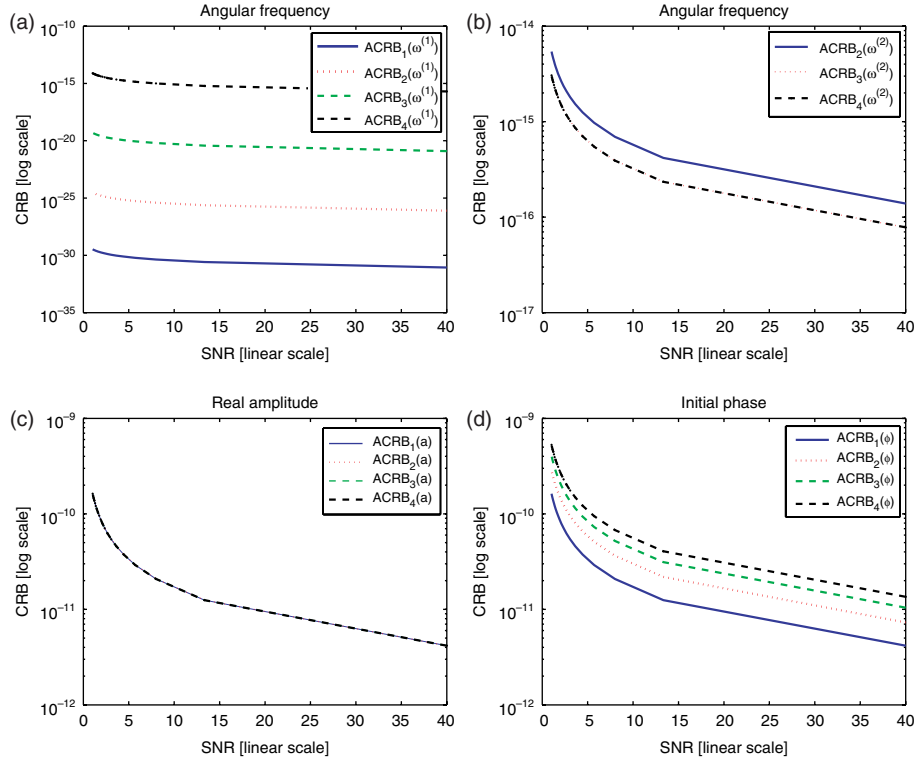


Figure 9.3. ACRB versus SNR for a first-order harmonic model of dimension 3 under constraint [9.28]

parameter $\omega^{(2)}$, the ACRB for dimension three and four are lower than the ACRB for dimension two.

– In Figure 9.3c, we can check that the ACRB for the real amplitude is invariant to parameter P .

– Finally, Figure 9.3d indicates that the ACRB for the initial phase increases with parameter P .

So, constraint [9.28] modifies drastically the behavior of the ACRB.

9.4. Modified CRB for the multidimensional harmonic model

We first study the case of a single snapshot ($T = 1$) and after that we show that the proposed analysis can be easily extended to the case of time-varying complex amplitudes i.e. to the multiple snapshots case where $T > 1$. So,

$$\theta' = [\underline{\omega}^T \underline{a}^T]^T$$

is a real deterministic vector of model parameters to be estimated in the presence of the random nuisance vector $\underline{\phi} = [\phi_1, \dots, \phi_M]^T$.

9.4.1. Definition of the modified CRB for $T = 1$

The MCRB associated with the MD-harmonic model of dimension P , denoted by $\text{MCRB}_{(P)}$, verifies the covariance inequality principle under general/weak conditions. Thus,

$$\text{MSE}([\hat{\theta}']_i) = E \left\{ \left([\hat{\theta}']_i - [\theta']_i \right)^2 \right\} \geq \text{MCRB}_{(P)}([\theta']_i)$$

where the MCRB [DAN 94, MOE 98, GIN 00] is defined according to:

$$\text{MCRB}_{(P)}(\theta') = \frac{\sigma^2}{2} \left[E_{\underline{\phi}} \{ F_{\theta' \theta'}(\underline{\phi}) \} \right]^{-1} \quad [9.36]$$

The above expression means that the MFIM is averaged w.r.t. the nuisance parameters (i.e. initial phase parameters). The former w.r.t. the signal parameter θ' is defined according to:

$$F_{\theta' \theta'}(\underline{\phi}) = \begin{bmatrix} J_{\underline{\omega}\underline{\omega}} & J_{\underline{\omega}\underline{a}} \\ J_{\underline{\omega}\underline{a}}^T & J_{\underline{a}\underline{a}} \end{bmatrix} \quad [9.37]$$

where in equation [9.37], the (i, j) th entry of each block of the MFIM is defined as for the FIM in equation [9.15]. So, the MCRB for the i th signal parameter, denoted by $[\theta']_i$, is given by the (i, i) th term of the MFIM inverse weighted by $\sigma^2/2$.

9.4.2. Modified CRB in the case of a large number of samples

9.4.2.1. Definition of the asymptotic bound

The modified asymptotic CRB (MACRB) is defined according to:

$$\text{MACRB}_{(P)}(\theta') \stackrel{\text{def}}{=} \{\text{MCRB}_{(P)}(\theta') \text{ subject to } N_p \gg 1, p \in [1 : P]\}$$

where the $\text{MCRB}_{(P)}(\theta')$ is the MCRB defined in equation [9.36]. As the MACRB is essentially an MCRB, this bound also satisfies the covariance inequality principle under the constraint that $N_p \gg 1, \forall p$.

9.4.2.2. Derivation of the modified asymptotic CRB

Two important properties of the MACRB are given here.

P1. The MFIM is asymptotically block-diagonal meaning that the angular frequency and the real amplitude are asymptotically decoupled parameters.

P2. The MFIM is asymptotically phase-invariant, i.e. $E_{\underline{\phi}}\{F_{\theta'\theta'}(\underline{\phi})\} = F_{\theta'\theta'}$.

PROOF.– The MFIM w.r.t. θ' can be extracted from the FIM defined in equation [9.55]. So, the MFIM is block-diagonal and is given by:

$$F_{\theta'\theta'} \xrightarrow{N_p \gg 1} \mathcal{N}_P \begin{bmatrix} \Upsilon_P \otimes \Delta^2 & 0 \\ 0 & I_M \end{bmatrix} \quad [9.38]$$

□

At this point, we can note that the MACRB for the considered model is identical to the ACRB when the initial phase parameters are known. In addition, the computational cost of the ACRB depends largely on the number of samples. On the other hand, the computation of the MACRB is independent of this parameter.

THEOREM 9.3.– *The deterministic $\text{MACRB}_{(P)}$ for the M -order harmonic model of dimension P defined in equation [9.1] w.r.t. the model parameter θ' , i.e. $\text{MACRB}_{(P)}(\theta')$, is given by:*

$$\text{MACRB}_{(P)}(\omega_m^{(p)}) = \frac{6}{N_p^2 \mathcal{N}_P \text{SNR}_m} \underbrace{\frac{P - 2/3}{P + 1/3}}_{r(P)} \quad [9.39]$$

$$\text{MACRB}_{(P)}(a_m) = \frac{a_m^2}{2 \mathcal{N}_P \text{SNR}_m} \quad [9.40]$$

PROOF.– To obtain a closed-form (non-matrix) expression of the MACRB, we have to find an analytic expression of $F_{\theta'\theta'}^{-1}$ in equation [9.38]. As the MFIM is block-diagonal, we need to derive $\Upsilon_P^{-1} \otimes \Delta^{-2}$. The key point is the inversion of the full

matrix Υ_P . First of all, this matrix can be decomposed as a diagonal matrix plus a rank one matrix according to $\Upsilon_P = \frac{1}{4}\gamma_P\gamma_P^T + \Sigma_P$ where $\gamma_P = [N_1 \dots N_P]^T$ and $\Sigma_P = \text{diag} \left\{ \frac{N_1^2}{12}, \dots, \frac{N_P^2}{12} \right\}$. Using the inversion lemma [STO 05], the inverse of the above matrix is given by:

$$\Upsilon_P^{-1} = \Sigma_P^{-1} - \frac{36}{1+3P}\Omega_P \quad [9.41]$$

where:

$$\Omega_P = \begin{bmatrix} \frac{1}{N_1^2} & \frac{1}{N_1 N_2} & \cdots & \frac{1}{N_1 N_P} \\ \frac{1}{N_1 N_2} & \frac{1}{N_2^2} & \cdots & \frac{1}{N_2 N_P} \\ \vdots & \vdots & \ddots & \vdots \\ \frac{1}{N_1 N_P} & \frac{1}{N_2 N_P} & \cdots & \frac{1}{N_P^2} \end{bmatrix}$$

and $\Sigma_P^{-1} = \text{diag} \left\{ \frac{12}{N_1^2}, \dots, \frac{12}{N_P^2} \right\}$. Now considering the diagonal terms of the inverse of the MFIM up to $\sigma^2/2$, we obtain expressions [9.39] and [9.40]. \square

9.4.3. Generalization to time-varying initial phase

Assume now that the initial phases are time-varying according to:

$$\phi_m(1), \dots, \phi_m(T)$$

They are random variables and a_m is a deterministic quantity. So, the time-varying complex amplitudes are now given by $\alpha_m(t) = a_m e^{i\phi_m(t)}$ in model [9.2]. The parameters of interest, θ' , are defined as before and the random nuisance parameters are collected in the $(TM) \times 1$ vector $\underline{\phi} = [\underline{\phi}(1)^T \dots \underline{\phi}(T)^T]^T$ where $\underline{\phi}(t) = [\phi_1(t), \dots, \phi_M(t)]^T$. Let us define the MACRB for T snapshots according to:

$$\text{MACRB}_{(P)}^{(T)}(\theta') = \frac{\sigma^2}{2} \left[E_{\underline{\phi}} \left\{ F_{\theta', \theta'}^{(T)} \right\} \right]^{-1}$$

where the MFIM is now considered as the $(T\mathcal{N}_P) \times 1$ noise-free observation vector $\dot{x}_T = [x(1)^T \dots x(T)^T]^T = (I_T \otimes Z) [\alpha(1)^T \dots \alpha(T)^T]^T$. It is easy to show $F_{\theta', \theta'}^{(T)} = T F_{\theta', \theta'}$ and this leads to the following simple result:

$$\text{MACRB}_{(P)}^{(T)}(\theta') = \frac{1}{T} \text{MACRB}_{(P)}(\theta') \quad [9.42]$$

For a fixed number of snapshots, T , the $\text{MACRB}_{(P)}^{(T)}$ is strictly proportional to the $\text{MACRB}_{(P)}$. Consequently, the closed-form expressions derived in equations [9.39] and [9.40] are valid up to the constant $1/T$.

9.4.4. Analysis of the MACRB

9.4.4.1. Remarks

R1. The angular frequency and the real amplitude parameters are asymptotically decoupled. This is a consequence of the block-diagonal structure of the MFIM.

R2. The $\text{MACRB}_{(P)}^{(T)}$ is asymptotically invariant w.r.t. the initial phase. This property and the considered time-varying model of the complex amplitudes explain why we obtain the simple relation [9.42].

R3. The $\text{MACRB}_{(P)}^{(T)}$ is invariant w.r.t. the angular frequency.

R4. The $\text{MACRB}_{(P)}^{(T)}$ is a function of the product of the data-tensor sizes.

R5. The $\text{MACRB}_{(P)}^{(T)}$ for the m th angular frequency depends on the cube of the corresponding dimension, N_p , and is only linear in the other one.

R6. The $\text{MACRB}_{(P)}^{(T)}$ for the real amplitude is constant w.r.t. the model parameter.

9.4.4.2. Comparison to the $\text{ACRB}_{(P)}^{(T)}$

Generalizing the derivation proposed in Theorem 1, we have the following result.

THEOREM 9.4.– *The deterministic $\text{ACRB}_{(P)}^{(T)}$ for the M -order harmonic model of dimension P and for T snapshots w.r.t. the model parameter θ' , i.e. $\text{ACRB}_{(P)}^{(T)}(\theta')$, is given by:*

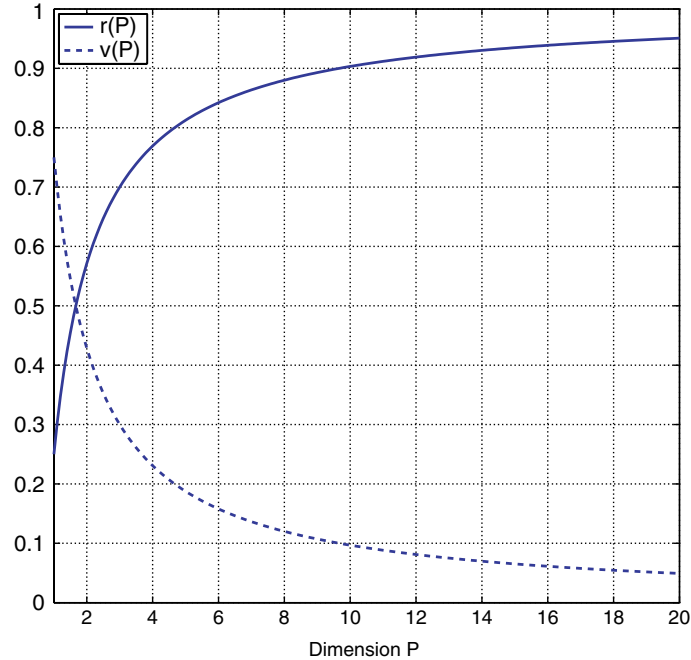
$$\text{ACRB}_{(P)}^{(T)}(\omega_m^{(\ell)}) = \frac{6}{T\mathcal{N}_P N_\ell^2 \text{SNR}_m} \quad [9.43]$$

$$\text{ACRB}_{(P)}^{(T)}(a_m) = \frac{a_m^2}{2T\mathcal{N}_P \text{SNR}_m} \quad [9.44]$$

PROOF.– See Appendix C. Comparing expressions [9.39] and [9.40] up to $1/T$ to the one below, we can say: \square

– The MACRB for the real amplitude parameter is equal to the ACRB, i.e. $\text{MACRB}_{(P)}^{(T)}(a_m) = \text{ACRB}_{(P)}^{(T)}(a_m)$, $m \in [1 : M]$.

– For a fixed dimension P , the MACRB for the angular-frequency parameter is directly proportional to the ACRB, i.e. $\text{MACRB}_{(P)}^{(T)}(\omega_m^{(p)}) \propto \text{ACRB}_{(P)}^{(T)}(\omega_m^{(p)})$, $m \in [1 : M]$, $p \in [1 : P]$ and the proportionality constant is $r(P)$ defined in equation [9.39]. As $r(P)$ is a strictly monotonically increasing sequence w.r.t. dimension P (see Figure 9.4) according to $\frac{1}{4} \leq r(P) < 1 \xrightarrow{P \rightarrow \infty} r(P)$, it is easy to conclude the following:

**Figure 9.4.** Relative distance $v(P)$ and ratio $r(P)$

- The well-known fact that the MACRB for the angular-frequency parameter is lower than the ACRB is confirmed. It is standard to call the MACRB a losing bound. More precisely, the MACRB for the single-dimensional harmonic model is four times higher than the ACRB.

- If the dimension P increases, the MACRB tends to be equal to the ACRB. This is an unexpected new result.

- The losing character of the MACRB is not true for the real amplitude parameters. This is not a well-known fact.

Let $d(P) = \text{ACRB}_{(P)}^{(T)}(\omega_m^{(\ell)}) - \text{MACRB}_{(P)}^{(T)}(\omega_m^{(\ell)}) > 0$ be the distance between the two bounds and $v(P) = \frac{d(P)}{\text{ACRB}_{(P)}^{(T)}(\omega_m^{(\ell)})}$ be the associated relative distance (RD). We have:

$$v(P) = 1 - r(P) < 1 \iff d(P) < \text{ACRB}_{(P)}^{(T)}(\omega_m^{(\ell)})$$

So, the distance $d(P)$ is upper-bounded by the $\text{ACRB}_{(P)}^{(T)}(\omega_m^{(\ell)})$. At high SNR, we know that the $\text{ACRB}_{(P)}^{(T)}(\omega_m^{(\ell)})$ is a small quantity and the two bounds are close. In conclusion, the two bounds can be considered close under the following situations:

- For large dimension P and for any SNR.
- For all dimension P at high SNR.

9.4.5. Numerical illustrations

In this section, we present numerical and analytical illustrations of the ACRB and the MACRB associated with a three-dimensional harmonic model with $M = 2$ sources and $T = 50$ snapshots. The real amplitudes are equal to 1 and the initial phases are a given realization of a normal distribution. The tensor \mathcal{X} is of size $10 \times 10 \times 10$ with $\omega_1^{(1)} = 0.4$, $\omega_2^{(1)} = 2.2$, $\omega_1^{(2)} = 0.7$, $\omega_2^{(2)} = 1.7$, $\omega_1^{(3)} = 0.1$ and $\omega_2^{(3)} = 1.3$. As we can see in Figure 9.5, the MACRB coincides with the MCRB (computed numerically) even if the dimensions of the tensor are moderately large. This is also true for the ACRB and the CRB. This observation suggests that the asymptotic regime is rapidly reached or in other words, the MACRB (resp. ACRB) is rapidly close to the MCRB (respectively CRB). From a practical point of view, this is of great importance.

In addition, we illustrate in Figure 9.6 the closeness between the bounds and their corresponding asymptotic version w.r.t. the number of samples in each dimension.

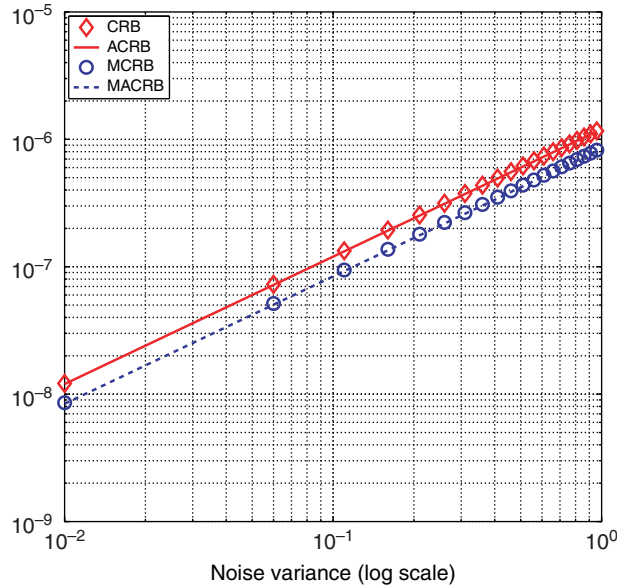


Figure 9.5. $CRB(\omega_1^{(1)})$, $ACRB(\omega_1^{(1)})$, $MCRB(\omega_1^{(1)})$, and $MACRB(\omega_1^{(1)})$ w.r.t. the noise variance for a three-dimensional harmonic model with $M=2$ sources and $T=50$ snapshots. The size of the associated cubic tensor is $10 \times 10 \times 10$

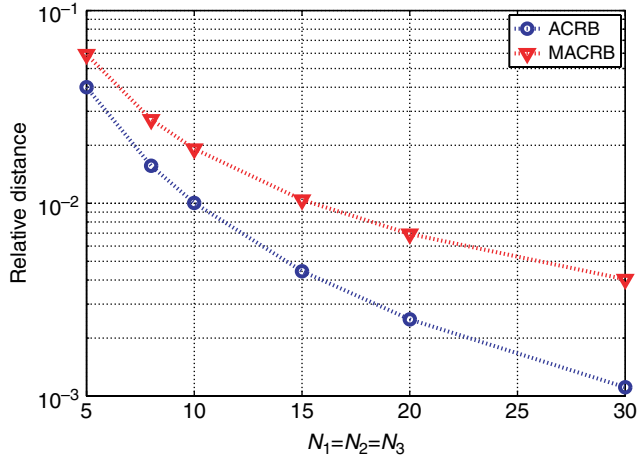


Figure 9.6. $RD(\omega_1^{(1)})$ and $RD_M(\omega_1^{(1)})$ defined in equations [9.45] and [9.46], respectively w.r.t. $N_1 = N_2 = N_3 = 10$ for with $T = 420$ and $\sigma^2 = 0.1$

The criterion is the RD for parameter ω defined by:

$$RD(\omega) = \frac{|\text{ACRB}_{(P)}^{(T)}(\omega) - \text{CRB}_{(P)}^{(T)}(\omega)|}{\text{CRB}_{(P)}^{(T)}(\omega)} \quad [9.45]$$

$$RD_M(\omega) = \frac{|\text{MACRB}_{(P)}^{(T)}(\omega) - \text{MCRB}_{(P)}^{(T)}(\omega)|}{\text{MCRB}_{(P)}^{(T)}(\omega)} \quad [9.46]$$

9.5. Conclusion

This chapter deals with the asymptotic estimation performance on the model parameters (angular frequency, initial phase, and real amplitude) for an M -order multidimensional harmonic model of dimension P . We have shown that increasing the dimension of the harmonic model decreases the ACRB and thus improves the minimal theoretical variance of the estimation of the model parameters. For P -order cubic tensors of size $N \times \dots \times N$, the “order of magnitude” of the ACRB for the real amplitude and the initial phase is $O(N^{-P})$ and $O(N^{-P+2})$ for the angular frequency. The last conclusion is that if the amount of data is constant for all dimensions (i.e. $\mathcal{N}_P = cst$), the ACRB for the angular frequency is a strictly monotonically increasing sequence for cubic tensors but can be locally (for a given dimension) a constant or a strictly monotonically decreasing sequence for unbalanced tensors. Regarding the

real amplitude parameter, the ACRB becomes invariant to parameter P . Finally, we show that the estimation accuracy for the initial phase is degraded for increasing P but not seriously. In the context of the multidimensional harmonic retrieval with time-varying complex amplitudes, we have extended the ACRB and derived closed-form (non-matrix) expressions of the MACRB for the angular frequencies and the real amplitudes. The MACRB takes into account that the time-varying initial phase parameters are considered random *nuisance* parameters. We have shown that asymptotically the MFIM is phase-invariant, so there is no need to average w.r.t. the nuisance parameter the MFIM to compute the MACRB. We finally have identified two scenarios where the ACRB and the MACRB are close: (1) for large dimension P and for any SNR and (2) for all dimension P at high SNR.

9.6. Appendices

9.6.1. Appendix A: ACRB for the MD-harmonic model of dimension P

The partial derivatives of the noise-free signal w.r.t. the angular frequency, the real amplitude, and the initial phase are given by:

$$\begin{aligned}\frac{\partial x}{\partial \omega_m^{(p)}} &= i\alpha_m \left(\mathbf{d}(\omega_m^{(1)}) \otimes \dots \otimes \mathbf{d}'(\omega_m^{(p)}) \otimes \dots \otimes \mathbf{d}(\omega_m^{(P)}) \right) \\ \frac{\partial x}{\partial a_m} &= e^{i\phi_m} \left(\mathbf{d}(\omega_m^{(1)}) \otimes \dots \otimes \mathbf{d}(\omega_m^{(P)}) \right) \\ \frac{\partial x}{\partial \phi_m} &= i\alpha_m \left(\mathbf{d}(\omega_m^{(1)}) \otimes \dots \otimes \mathbf{d}(\omega_m^{(P)}) \right)\end{aligned}$$

$$\text{for } m \in [1 : M], \text{ and } \mathbf{d}'(\omega_m^{(p)}) = [0, e^{i\omega_m^{(p)}}, 2e^{2i\omega_m^{(p)}} \dots (N_p - 1) e^{(N_p-1)i\omega_m^{(p)} }]^T.$$

Using the asymptotic properties of the harmonic model [STO 89], $\frac{1}{N_p^3} \mathbf{d}'(\omega_k^{(p)})^H \mathbf{d}'(\omega_m^{(p)}) \xrightarrow{N_p \gg 1} \frac{1}{3} \delta_{k-m}$, $\frac{1}{N_p^2} \mathbf{d}'(\omega_k^{(p)})^H \mathbf{d}(\omega_m^{(p)}) \xrightarrow{N_p \gg 1} \frac{1}{2} \delta_{k-m}$, $\frac{1}{N_p} \mathbf{d}(\omega_k^{(p)})^H \mathbf{d}(\omega_m^{(p)}) \xrightarrow{N_p \gg 1} \delta_{k-m}$, a straightforward derivation leads to:

$$\begin{aligned}J_{\omega_k^{(j)} \omega_m^{(u)}} &= \Re \left\{ \left(\frac{\partial x}{\partial \omega_k^{(j)}} \right)^H \frac{\partial x}{\partial \omega_m^{(u)}} \right\} \\ &= \begin{cases} a_k^2 \frac{N_u^3}{3} \prod_{p=1, p \neq j}^P N_p, & \text{for } j = u \text{ and } k = m, \\ a_k^2 \frac{N_u^2}{2} \frac{N_j^2}{2} \prod_{p=1, p \neq j, u}^P N_p, & \text{for } j \neq u \text{ and } k = m, \\ 0, & \text{otherwise.} \end{cases} \quad [9.47]\end{aligned}$$

So, we have:

$$\begin{aligned} J_{\underline{\omega}^{(j)} \underline{\omega}^{(u)}} &= \begin{bmatrix} J_{\omega_1^{(j)} \omega_1^{(u)}} & \dots & J_{\omega_1^{(j)} \omega_M^{(u)}} \\ \vdots & & \vdots \\ J_{\omega_M^{(j)} \omega_1^{(u)}} & \dots & J_{\omega_M^{(j)} \omega_M^{(u)}} \end{bmatrix}_{M \times M} \\ &= \begin{cases} \frac{N_j^2}{3} \mathcal{N}_P \Delta^2, & \text{for } j = u, \\ \frac{N_u N_j}{4} \mathcal{N}_P \Delta^2, & \text{for } j \neq u, \end{cases} \end{aligned} \quad [9.48]$$

where $\Delta = \text{diag}\{a_1, \dots, a_M\}$ and thus:

$$J_{\underline{\omega} \underline{\omega}} = \begin{bmatrix} J_{\underline{\omega}^{(1)} \underline{\omega}^{(1)}} & \dots & J_{\underline{\omega}^{(1)} \underline{\omega}^{(P)}} \\ \vdots & & \vdots \\ J_{\underline{\omega}^{(P)} \underline{\omega}^{(1)}} & \dots & J_{\underline{\omega}^{(P)} \underline{\omega}^{(P)}} \end{bmatrix}_{PM \times PM} = \mathcal{N}_P (\Upsilon_P \otimes \Delta^2) \quad [9.49]$$

where we have defined the following $(P \times P)$ symmetric matrix:

$$\Upsilon_P = \begin{bmatrix} \frac{N_1^2}{3} & \frac{N_1 N_2}{4} & \dots & \frac{N_1 N_P}{4} \\ \frac{N_1 N_2}{4} & \frac{N_2^2}{3} & \dots & \frac{N_2 N_P}{4} \\ \vdots & \vdots & & \vdots \\ \frac{N_1 N_P}{4} & \frac{N_2 N_P}{4} & \dots & \frac{N_P^2}{3} \end{bmatrix} \quad [9.50]$$

Next, we have $J_{\omega_k^{(j)} \phi_m} \xrightarrow{N_j \gg 1} \Re \left\{ \alpha_k^* \alpha_m \frac{N_j}{2} \mathcal{N}_P \delta_{k-m} \right\}$ and thus $J_{\underline{\omega}^{(j)} \underline{\phi}} \xrightarrow{N_j \gg 1} \frac{1}{2} N_j \mathcal{N}_P \Delta^2$. Finally, we find the following compact expression for the $PM \times M$ matrix $J_{\underline{\omega} \underline{\phi}} = \frac{N_P}{2} (\gamma_P \otimes \Delta^2)$ where $\gamma_P = [N_1 \dots N_P]^T$. In addition, the other blocks of the FIM are:

$$[J_{\underline{a} \underline{a}}]_{km} \xrightarrow{N_p \gg 1} \Re \left\{ e^{i(\phi_m - \phi_k)} \mathcal{N}_P \delta_{k-m} \right\} = \begin{cases} \mathcal{N}_P, & \text{for } k = m, \\ 0, & \text{otherwise,} \end{cases} \quad [9.51]$$

$$[J_{\underline{\phi} \underline{\phi}}]_{km} \xrightarrow{N_p \gg 1} \Re \left\{ i^* \alpha_k^* i \alpha_m \mathcal{N}_P \delta_{k-m} \right\} = \begin{cases} a_k^2 \mathcal{N}_P, & \text{for } k = m, \\ 0, & \text{otherwise,} \end{cases} \quad [9.52]$$

$$[J_{\underline{a} \underline{\phi}}]_{km} \xrightarrow{N_p \gg 1} 0, \quad \forall k, m, \quad [9.53]$$

$$[J_{\underline{\omega} \underline{a}}]_{km} \xrightarrow{N_p \gg 1} 0, \quad \forall k, m. \quad [9.54]$$

For $k = m$, expressions [9.53] and [9.54] are purely imaginary numbers. This explains why $J_{\underline{a}\underline{\phi}}$ and $J_{\underline{\omega}\underline{a}}$ are null matrices. Consequently, the blocks of the FIM are asymptotically diagonal or null and we obtain:

$$J_{\underline{a}\underline{a}} = \mathcal{N}_P I_M, \quad J_{\underline{\phi}\underline{\phi}} = \mathcal{N}_P \Delta^2, \quad J_{\underline{a}\underline{\phi}} = 0_{M \times M}, \quad J_{\underline{\omega}\underline{a}} = 0_{PM \times M}$$

Finally, the FIM w.r.t. θ' is given by:

$$F_{\theta'\theta'} \xrightarrow{N_p \gg 1} \mathcal{N}_P \begin{bmatrix} \Upsilon_P \otimes \Delta^2 & 0 & \frac{1}{2}(\gamma_P \otimes \Delta^2) \\ 0 & I_M & 0 \\ \frac{1}{2}(\gamma_P^T \otimes \Delta^2) & 0 & \Delta^2 \end{bmatrix} \quad [9.55]$$

Thanks to the standard inverse of a partitioned matrix [STO 89], analytic expression of $F_{\theta'\theta'}^{-1}$ is possible. We obtain:

$$F_{\theta'\theta'}^{-1} \xrightarrow{N_p \gg 1} \begin{bmatrix} \Lambda & 0 & \times \\ 0 & J_{\underline{a}\underline{a}}^{-1} & 0 \\ \times & 0 & \Theta \Lambda \Theta^T + J_{\underline{\phi}\underline{\phi}}^{-1} \end{bmatrix} \quad [9.56]$$

where:

$$\begin{aligned} \Lambda &= (J_{\underline{\omega}\underline{\omega}} - J_{\underline{\omega}\underline{\phi}} J_{\underline{\phi}\underline{\phi}}^{-1} J_{\underline{\phi}\underline{\omega}})^{-1} = \frac{1}{\mathcal{N}_P} \left[\left(\Upsilon_P - \frac{1}{4} \gamma_P \gamma_P^T \right)^{-1} \otimes \Delta^{-2} \right] \\ &= \frac{12}{\mathcal{N}_P} (\text{diag}(\gamma_P)^{-2} \otimes \Delta^{-2}) \end{aligned}$$

and $\Theta = J_{\underline{\phi}\underline{\phi}}^{-1} J_{\underline{\omega}\underline{\phi}} = \frac{1}{2} (\gamma_P^T \otimes I_M)$. So, the (3, 3)-block of matrix $F_{\theta'\theta'}^{-1}$ is given by:

$$\begin{aligned} \Theta \Lambda \Theta^T + J_{\underline{\phi}\underline{\phi}}^{-1} &= \frac{3}{\mathcal{N}_P} \left(\underbrace{\gamma_P^T \text{diag}(\gamma_P)^{-2} \gamma_P}_{P} \otimes \Delta^{-2} \right) + \frac{1}{\mathcal{N}_P} \Delta^{-2} \\ &= \frac{3P+1}{\mathcal{N}_P} \Delta^{-2} \end{aligned}$$

Hence, the inverse of the FIM is:

$$F_{\theta'\theta'}^{-1} \xrightarrow{N_p \gg 1} \frac{1}{\mathcal{N}_P} \begin{bmatrix} 12 (\text{diag}(\gamma_P)^{-2} \otimes \Delta^{-2}) & 0 & \times \\ 0 & I_M & 0 \\ \times & 0 & (3P+1) \Delta^{-2} \end{bmatrix}$$

So, the CRB associated with the M -order harmonic model of dimension P is given by the diagonal terms of the FIM inverse, which proves the theorem.

9.6.2. Appendix B: Exact CRB for the first-order harmonic model of dimension P

Using the same formalism as before, we derive in the following theorem the exact (non-asymptotic) closed-form of the CRB for the first-order harmonic model of dimension P .

THEOREM 9.5.— *The exact $CRB_{(P)}$ for the first-order harmonic model of dimension P defined in equation [9.1] where $M = 1$ w.r.t. the model parameter $\theta' = [\omega^{(1)}, \dots, \omega^{(P)}, a, \phi]^T$, i.e. $CRB_{(P)}(\theta')$, is given by:*

$$CRB_{(P)}(\omega^{(p)}) = \frac{6}{\mathcal{N}_P(N_p^2 - 1) SNR} \quad [9.57]$$

$$CRB_{(P)}(a) = \frac{a^2}{2\mathcal{N}_P SNR}, \quad [9.58]$$

$$CRB_{(P)}(\phi) = \frac{3 \sum_{p=1}^P \frac{N_p-1}{N_p+1} + 1}{2\mathcal{N}_P SNR} \quad [9.59]$$

where $SNR = a^2/\sigma^2$.

PROOF.— To prove this result, we consider the first-order harmonic model of dimension P given by $x = ae^{i\phi}(d(\omega^{(1)}) \otimes \dots \otimes d(\omega^{(P)}))$ where the model parameters are the following triplet: $\{\omega^{(1)}, \dots, \omega^{(P)}, a, \phi\}$. Recalling some standard results on power sums, we have:

$$\mathbf{d}'(\omega^{(p)})^H \mathbf{d}'(\omega^{(p)}) = \sum_{n=0}^{N_p-1} n^2 = \frac{1}{6}(N_p - 1)N_p(2N_p - 1) \quad [9.60]$$

$$\mathbf{d}'(\omega^{(p)})^H \mathbf{d}(\omega^{(p)}) = \sum_{n=0}^{N_p-1} n = \frac{1}{2}(N_p - 1)N_p \quad [9.61]$$

$$\mathbf{d}(\omega^{(p)})^H \mathbf{d}(\omega^{(p)}) = \sum_{n=0}^{N_p-1} 1 = N_p \quad [9.62]$$

□

Using equations [9.60]–[9.62], we have $J_{\underline{\omega}\underline{\omega}} = \frac{a^2}{2}\mathcal{N}_P\Psi_P$, where we have defined the following $(P \times P)$ symmetric matrix:

$$\Psi_P = \begin{bmatrix} \frac{(N_1-1)(2N_1-1)}{2} & \frac{(N_1-1)(N_2-1)}{3} & \dots & \frac{(N_1-1)(N_P-1)}{2} \\ \frac{(N_1-1)(N_2-1)}{3} & \frac{(N_2-1)(2N_2-1)}{3} & \dots & \frac{(N_2-1)(N_P-1)}{2} \\ \vdots & \vdots & & \vdots \\ \frac{(N_1-1)(N_P-1)}{2} & \frac{(N_2-1)(N_P-1)}{2} & \dots & \frac{(N_P-1)(2N_P-1)}{3} \end{bmatrix} \quad [9.63]$$

and:

$$J_{\underline{aa}} = \mathcal{N}_P, J_{\underline{\phi}\underline{\phi}} = a^2 \mathcal{N}_P, J_{\underline{a}\underline{\phi}} = J_{\underline{\omega}\underline{a}} = 0, J_{\underline{\omega}\underline{\phi}} = \frac{a^2}{2} \mathcal{N}_P \nu_P$$

where $\nu_P = [N_1 - 1, N_2 - 1, \dots, N_P - 1]^T$.

Consequently, the FIM inverse has a similar structure as [9.56] where:

$$\Lambda = \frac{2}{a^2} \frac{1}{\mathcal{N}_P} \left(\Psi_P - \frac{\nu_P \nu_P^T}{2} \right)^{-1} = \frac{2}{a^2} \frac{1}{\mathcal{N}_P} D_P \quad [9.64]$$

where $D_P = \text{diag} \left\{ \frac{6}{N_1^2 - 1}, \dots, \frac{6}{N_P^2 - 1} \right\}$ with $\Theta = \frac{\nu_P^T}{2}$ and $\Theta \Lambda \Theta^T + J_{\underline{\phi}\underline{\phi}}^{-1} = \frac{1}{a^2 \mathcal{N}_P} \left(3 \sum_{p=1}^P \frac{N_p - 1}{N_p + 1} + 1 \right)$. More precisely, the inverse of the FIM is:

$$F_{\theta'\theta'}^{-1} = \frac{1}{\mathcal{N}_P} \begin{bmatrix} \frac{2}{a^2} D_P & 0 & \times \\ 0 & 1 & 0 \\ \times & 0 & \frac{1}{a^2} \left(3 \sum_{p=1}^P \frac{N_p - 1}{N_p + 1} + 1 \right) \end{bmatrix}$$

Considering the diagonal terms of the above matrix weighed by $\sigma^2/2$, we obtain expressions [9.57], [9.58] and [9.59].

For cubic tensors, we have:

$$\text{CRB}_{(P)}(\omega^{(p)}) = \frac{6}{N^P (N^2 - 1) \text{SNR}} \quad [9.65]$$

$$\text{CRB}_{(P)}(a) = \frac{a^2}{2N^P \text{SNR}} \quad [9.66]$$

$$\text{CRB}_{(P)}(\phi) = \frac{3P \frac{N-1}{N+1} + 1}{2N^P \text{SNR}} \quad [9.67]$$

Note that as expected if $N_p \gg 1$ for all p , the exact CRB becomes the ACRB. The exact CRB for a first-order harmonic of dimension P is quite similar to the asymptotic analysis derived in the previous sections. In particular, the exact $\text{CRB}_{(P)}$ for the first-order case shares the same properties as the $\text{ACRB}_{(P)}$.

9.6.3. Appendix C: ACRB for the MD-harmonic model with multiple snapshots

In this section, we generalize the analysis presented in Appendix A where the ACRB has been derived for a single snapshot. Here, we consider multiple snapshots ($T > 1$). The model parameters are collected in the following $((P + T + 1)M) \times 1$ vector:

$$\bar{\theta}' = [\underline{\omega}^T \underline{\phi}^T \underline{a}^T]^T$$

We define the ACRB for T snapshots according to:

$$\text{ACRB}_{(P)}^{(T)}([\theta']_i) = \frac{\sigma^2}{2} [\bar{F}_{\bar{\theta}' \bar{\theta}'}^{-1}]_{ii}, \quad \text{for } i \in [1 : (P + T + 3)M] \quad [9.68]$$

where the FIM, denoted by $\bar{F}_{\bar{\theta}' \bar{\theta}'}$, is considered in equation [9.68] under the constraint $N_p \gg 1, \forall p$. After some straightforward derivations, the FIM is expressed as:

$$\bar{F}_{\bar{\theta}' \bar{\theta}'} \xrightarrow{N_p \gg 1} \mathcal{N}_P \begin{bmatrix} B & 0 \\ 0 & TI_M \end{bmatrix} \quad [9.69]$$

where:

$$B = \left[\begin{array}{c|cc} T \Upsilon_P \otimes \Delta^2 & \gamma_P \otimes \frac{\Delta^2}{2} & \dots \gamma_P \otimes \frac{\Delta^2}{2} \\ \hline \gamma_P^T \otimes \frac{\Delta^2}{2} & \Delta^2 & 0 \\ \vdots & & \ddots \\ \gamma_P^T \otimes \frac{\Delta^2}{2} & 0 & \Delta^2 \end{array} \right] \quad [9.70]$$

The block structure of the FIM indicates that the angular frequency and the time-varying initial phase are asymptotically decoupled to the real amplitude. According to the above FIM, we can see that the ACRB for the real amplitude is given by equation [9.44]. The analytic inverse of matrix B based on the determination of the inverse of the Schur complement [STO 05] is given by:

$$B^{-1} = \begin{bmatrix} \frac{1}{T} \Sigma_P \otimes \Delta^{-2} & \times \\ \times & \left(1 + \frac{3P}{T}\right) \Delta^{-2} \end{bmatrix} \quad [9.71]$$

Considering the diagonal term of the above expression, we obtain expression [9.43].

9.6.4. Appendix D: Application to the bistatic MIMO radar with widely separated arrays

To illustrate the proposed results in the context of a up-to-date signal processing application, we study in this appendix the bistatic multiple-input multiple-output (MIMO) radar with widely separated arrays. More precisely, based on the attractive MIMO communication theory [GER 05, BOE 06], the MIMO radar has been receiving increasing attention. The MIMO radar uses multiple antennas to simultaneously transmit several non-coherent known waveforms and exploits multiple antennas to receive the reflected signals (echoes). This diversity in term of waveform coding allows us to transmit orthogonal waveforms [HAI 08, CHE 08]. We assume that the range of the target presented in the range-bin of interest is much larger than the aperture of the transmit and receive arrays. A target is modeled as a narrowband point source in the far-field, which is commonly used in standard MIMO radar systems [LI 08]. The MIMO radar can be subdivided into two classes:

- 1) The co-located radar where the transmitter and the receiver are close enough so that they share the same angle variable [LI 08, BOY 11].
- 2) The radar with widely separated arrays [HAI 08, TRA 11].

In this appendix, we focus our analysis on the second case. More precisely, the optimal estimation performance is derived for the bistatic MIMO radar system with N_T -element transmitting uniform linear array (ULA) and N_R -element receiving ULA. The considered scheme utilizes widely separated transmitters and receivers such that the target is observed from many different aspects simultaneously, resulting in spatial diversity. We are interested in the localization and estimation of the normalized Doppler frequency of:

- M targets for a large number of pulses, i.e. $L \gg 1$, and sensors, i.e. $N_T \gg 1$, $N_R \gg 1$.
- A single target for any number of pulses and sensors.

9.6.4.1. The space-time model

According to references [CHE 10, JIN 09], the bistatic MIMO radar is described for the ℓ th pulse by the following $N_R \times T$ matrix:

$$X_\ell = \sum_{m=1}^M \rho_m e^{2i\pi f_m \ell} a_R(\gamma_m) a_T(\psi_m)^T S + W_\ell, \quad \ell \in [0 : L - 1] \quad [9.72]$$

in which:

- the number of samples per pulse period is denoted by T ,

- the radar cross section of the m th target is denoted by ρ_m ,
- the normalized Doppler frequency of the m th target is denoted by f_m ,
- the $N_T \times T$ source matrix is defined as:

$$S = \begin{bmatrix} s_0^T \\ \vdots \\ s_{N_T-1}^T \end{bmatrix} = \begin{bmatrix} s_0(1) & \dots & s_0(T) \\ \vdots & & \vdots \\ s_{N_T-1}(1) & \dots & s_{N_T-1}(T) \end{bmatrix} \quad [9.73]$$

The sources are assumed to be known mutually orthogonal transmitted pulse waveforms, i.e.

$$SS^H = S^*S^T = TI, \quad [9.74]$$

- the noise matrix³ defined by W_ℓ follows an independent, zero-mean complex Gaussian distribution with a covariance given by:

$$E\{w_\ell w_{\ell'}^H\} = \begin{cases} \sigma^2 I_{TN_R} & \text{for } \ell = \ell' \\ 0 & \text{otherwise} \end{cases} \quad [9.75]$$

where $w_\ell = \text{vec}(W_\ell)$ defines the vectorized noise,

- the steering vectors are given by:

$$a_R(\gamma_m) = [1 e^{2i\pi \frac{d_R}{\lambda} \sin(\gamma_m)} \dots e^{2i\pi \frac{d_R}{\lambda} \sin(\gamma_m)(N_R-1)}]^T \quad [9.76]$$

$$a_T(\psi_m) = [1 e^{2i\pi \frac{d_T}{\lambda} \sin(\psi_m)} \dots e^{2i\pi \frac{d_T}{\lambda} \sin(\psi_m)(N_T-1)}]^T \quad [9.77]$$

where ψ_m is the angle of the target w.r.t. the transmit array (i.e. DOD), γ_m the angle of the target w.r.t. the reception array (i.e. DOA), λ the wavelength and d_T and d_R the interelement space in the transmission and reception arrays, respectively.

After matched filtering [WOO 80], we obtain:

$$Y_\ell = \frac{1}{\sqrt{T}} X_\ell S^H = \sum_{m=1}^M \alpha_m e^{2i\pi f_m \ell} a_R(\gamma_m) a_T(\psi_m)^T + Z_\ell \quad [9.78]$$

where $\alpha_m = \sqrt{T} \rho_m$ and $Z_\ell = \frac{1}{\sqrt{T}} W_\ell S^H$ denotes the noise matrix after matched filter. It is straightforward to rewrite the above matrix-based expression as a vectorized CanDecomp/Parafac model of dimension $P = 3$ according to:

$$y = [\text{vec}(Y_0)^T \dots \text{vec}(Y_{L-1})^T]^T = x + z \quad [9.79]$$

³ The clutter and jammer echoes are not considered in this work.

where $z = [z_0^T \dots z_{L-1}^T]^T$ with $z_\ell = \text{vec}(Z_\ell)$ and:

$$x = \sum_{m=1}^M \alpha_m (c(f_m) \otimes a_T(\psi_m) \otimes a_R(\gamma_m)) \quad [9.80]$$

in which:

$$c(f_m) = [1 \ e^{2i\pi f_m} \ \dots \ e^{2i\pi f_m(L-1)}]^T \quad [9.81]$$

The equivalence between the space-time MIMO radar model (after the matched filter) and the CanDecomp/Parafac decomposition has been noticed recently in references [NIO 10, BOY 11].

It is straightforward to prove that the observation follows a complex Gaussian distribution according to $y \sim \mathcal{CN}(x, \sigma^2 I_{LN_T N_R})$. Thanks to the orthogonality of the sources, given by relation [9.74], and the statistical property [9.75] of the vectorized noise, the vectorized noise after the matched filter follows an independent, zero-mean complex Gaussian distribution with a covariance given by:

$$E\{z_\ell z_{\ell'}^H\} = \frac{1}{T} (S^* \otimes I_{N_R}) E\{w_\ell w_{\ell'}^H\} (S^T \otimes I_{N_R}) = \begin{cases} \sigma^2 I_{N_T N_R} & \text{for } \ell = \ell' \\ 0, & \text{otherwise} \end{cases}$$

and thus $E\{(y - x)(y - x)^H\} = E\{zz^H\} = \sigma^2 I_{LN_T N_R}$.

9.6.4.2. ACRB and CRB for the non-physical parameters

Let $N_1 = L$, $N_2 = N_T$, $N_3 = N_R$ and:

$$\omega_m^{(1)} = 2\pi f_m \quad [9.82]$$

$$\omega_m^{(2)} = 2\pi \frac{d_T}{\lambda} \sin(\psi_m) \quad [9.83]$$

$$\omega_m^{(3)} = 2\pi \frac{d_R}{\lambda} \sin(\gamma_m) \quad [9.84]$$

define the non-physical parameters. In this case, model [9.80] is similar to equation [9.5] because $d(\omega_m^{(1)}) = c(f_m)$, $d(\omega_m^{(2)}) = a_T(\phi_m)$ and $d(\omega_m^{(3)}) = a_R(\gamma_m)$. The main results of this appendix are:

– For a large number of pulses and sensors and for M targets belonging to the radar field of view, we can apply Theorem 1 to model [9.79] and we obtain:

$$\text{ACRB}_{(3)}(\omega_m^{(1)}) = \frac{6}{L^3 N_T N_R T \text{SNR}_m} \quad [9.85]$$

$$\text{ACRB}_{(3)}(\omega_m^{(2)}) = \frac{6}{LN_T^3 N_R T \text{SNR}_m} \quad [9.86]$$

$$\text{ACRB}_{(3)}(\omega_m^{(3)}) = \frac{6}{LN_T N_R^3 T \text{SNR}_m} \quad [9.87]$$

where $\text{SNR}_m = |\rho_m|^2 / \sigma^2$.

– For a single target belonging to the radar field of view, we can apply Theorem 5 to equation [9.79] with $M = 1$ and we obtain:

$$\text{CRB}_{(3)}(\omega^{(1)}) = \frac{6}{LN_T N_R (L^2 - 1) T \text{SNR}} \quad [9.88]$$

$$\text{CRB}_{(3)}(\omega^{(2)}) = \frac{6}{LN_T N_R (N_T^2 - 1) T \text{SNR}} \quad [9.89]$$

$$\text{CRB}_{(3)}(\omega^{(3)}) = \frac{6}{LN_T N_R (N_R^2 - 1) T \text{SNR}} \quad [9.90]$$

where $\text{SNR} = |\rho|^2 / \sigma^2$.

9.6.4.3. ACRB and CRB for the physical parameters

Let κ be the vector containing the physical parameters such as:

$$\kappa = \left[\underline{f}^T \underline{\psi}^T \underline{\gamma}^T |\underline{\rho}^T| e^{i\arg(\underline{\rho}^T)} \sigma^2 \right]^T$$

where $\underline{f} = [f_1 \dots f_M]^T$, $\underline{\psi} = [\psi_1 \dots \psi_M]^T$, $\underline{\gamma} = [\gamma_1 \dots \gamma_M]^T$, $\underline{\psi} = [\psi_1 \dots \psi_M]^T$, and $\underline{\rho} = [\rho_1 \dots \rho_M]^T$. It makes sense to obtain the ACRB for the physical parameters of interest, namely the normalized Doppler frequency, the DOA and the DOD. This can be done by a re-parametrization technique according to [KAY 93]:

$$\text{ACRB}_{(3)}(\theta) = J \text{ACRB}_{(3)}(\kappa) J^T \quad [9.91]$$

meaning that the non-physical parameter vector, θ , and the physical parameters vector, κ , are implicitly linked according to $g(\kappa) = \theta$ and the Jacobian matrix is defined as $[J]_{ij} = \frac{\partial g([\kappa]_i)}{\partial [\kappa]_j}$. It is straightforward to see that the Jacobian matrix is

diagonal according to:

$$J = \begin{bmatrix} J_1 & & & 0 \\ & J_2 & & \\ & & J_3 & \\ & & & J_4 \\ 0 & & & & I_M \\ & & & & & 1 \end{bmatrix} \quad [9.92]$$

where $J_1 = 2\pi I_M$, $J_4 = \sqrt{T}I_M$, $J_2 = 2\pi \frac{d_T}{\lambda} C_\psi$, and $J_3 = 2\pi \frac{d_R}{\lambda} C_\gamma$ where $C_\psi = \text{diag}\{\cos(\psi_1), \dots, \cos(\psi_M)\}$ and $C_\gamma = \text{diag}\{\cos(\gamma_1), \dots, \cos(\gamma_M)\}$. So thanks to the simple structure of the Jacobian matrix, expression [9.91] for the parameters of interest becomes:

$$\text{ACRB}_{(3)}(\underline{f}) = J_1^{-1} \text{ACRB}_{(3)}(\underline{\omega}^{(1)}) J_1^{-1} \quad [9.93]$$

$$\text{ACRB}_{(3)}(\underline{\psi}) = J_2^{-1} \text{ACRB}_{(3)}(\underline{\omega}^{(2)}) J_2^{-1} \quad [9.94]$$

$$\text{ACRB}_{(3)}(\underline{\gamma}) = J_3^{-1} \text{ACRB}_{(3)}(\underline{\omega}^{(3)}) J_3^{-1} \quad [9.95]$$

where J_1^{-1} , J_2^{-1} , and J_3^{-1} are easily derived. Finally, the ACRBs w.r.t. the physical parameters are given by:

$$\begin{aligned} \text{ACRB}_{(3)}(f_m) &= \frac{\text{ACRB}_{(3)}(\omega_m^{(1)})}{[J_1^2]_{mm}} = \frac{3}{2\pi^2 L^3 N_T N_R T \text{SNR}_m} \\ \text{ACRB}_{(3)}(\psi_m) &= \frac{\text{ACRB}_{(3)}(\omega_m^{(2)})}{[J_2^2]_{mm}} = \frac{3\lambda^2}{2\pi^2 d_T^2 \cos^2(\psi_m) L N_T^3 N_R T \text{SNR}_m} \\ \text{ACRB}_{(3)}(\gamma_m) &= \frac{\text{ACRB}_{(3)}(\omega_m^{(3)})}{[J_3^2]_{mm}} = \frac{3\lambda^2}{2\pi^2 d_R^2 \cos^2(\gamma_m) L N_T N_R^3 T \text{SNR}_m} \end{aligned}$$

Using the same methodology for $M = 1$, we can derive the CRBs w.r.t. the physical parameters according to:

$$\begin{aligned} \text{CRB}_{(3)}(f) &= \left(\frac{\partial g(f)}{\partial f} \right)^{-2} \text{CRB}_{(3)}(\omega^{(1)}) = \frac{3}{2\pi^2 L N_T N_R (L^2 - 1) T \text{SNR}} \\ \text{CRB}_{(3)}(\psi) &= \left(\frac{\partial g(\psi)}{\partial \psi} \right)^{-2} \text{CRB}_{(3)}(\omega^{(2)}) = \frac{3\lambda^2}{2\pi^2 d_T^2 \cos^2(\psi) L N_T N_R (N_T^2 - 1) T \text{SNR}} \\ \text{CRB}_{(3)}(\gamma) &= \left(\frac{\partial g(\gamma)}{\partial \gamma} \right)^{-2} \text{CRB}_{(3)}(\omega^{(3)}) = \frac{3\lambda^2}{2\pi^2 d_R^2 \cos^2(\gamma) L N_T N_R (N_R^2 - 1) T \text{SNR}} \end{aligned}$$

9.7. Bibliography

- [BOE 06] BOELCSKEI H., GESBERT D., PAPADIAS C., VAN DER VEEN A.J., *Space-Time Wireless Systems: From Array Processing to MIMO Communications*, Cambridge University Press, Spring 2006.
- [BOY 08a] BOYER R., “Deterministic asymptotic Cramer-Rao bound for the multidimensional harmonic model”, *Signal Processing*, vol. 88, no. 12, pp. 2869–2877, December 2008.
- [BOY 08b] BOYER R., “Decoupled root-MUSIC algorithm for multidimensional harmonic retrieval”, *9th IEEE International Workshop on Signal Processing Advances in Wireless Communications (SPAWC'08)*, 2008.
- [BOY 11] BOYER R., “Performance bounds and angular resolution limit for the moving colocated MIMO radar”, *IEEE Transactions on Signal Processing*, vol. 59, no. 4, April 2011.
- [CHE 08] CHEN C.-Y., VAIDYANATHAN P.P., “MIMO radar space-time adaptive processing using prolate spheroidal wave functions”, *IEEE Transactions on Signal Processing*, vol. 56, no. 2, pp. 623–635, February 2008.
- [CHE 10] CHEN J., GU H., SU W., “A new method for joint DOD and DOA estimation in bistatic MIMO radar”, *Signal Processing*, vol. 90, no. 2, pp. 714–718, February 2010.
- [CRA 46] CRAMER H., *Mathematical Methods of Statistics*, Princeton University Press, Princeton, NJ, 1946.
- [DAN 94] D’ANDREA A.N., MENGALI U., REGGIANINI R., “The modified Cramér-Rao bound and its application to synchronization problems”, *IEEE Transactions on Communications*, vol. 42, no. 2/3/4, pp. 1391–1399, Feb/March/Apr 1994.
- [DEL 08] DELMAS J.-P., “Closed-form expressions of the exact Cramér-Rao bound for parameter estimation of BPSK, MSK, or QPSK waveforms”, *IEEE Signal Processing Letters*, vol. 15, pp. 405–408, 2008.
- [DIL 98] DILAVEROGLU E., “Nonmatrix Cramér-Rao bound expressions for high-resolution frequency estimators”, *IEEE Transactions on Signal Processing*, vol. 46, no. 2, pp. 463–474, 1998.
- [FRA 02] FRANCOS J.M., “Cramér-Rao bound on the estimation accuracy of complex-valued homogeneous Gaussian random fields” *IEEE Transactions on Signal Processing*, vol. 50, no. 3, pp. 710–724, March 2002.
- [GER 05] GERSHMAN A.B., SIDIROPOULOS N.D., *Space-Time Processing for MIMO Communications*, pp. 41(75), Wiley Press, 2005.
- [GIN 00] GINI F., REGGIANINI R., “On the use of Cramér-Rao-like bounds in the presence of random nuisance parameters”, *IEEE Transactions on Communications*, vol. 48, no. 12, pp. 2120–2126, December 2000.
- [HAA 98] HAARDT M., NOSSEK J.A., “Simultaneous Schur decomposition of several nonsymmetric matrices to achieve automatic pairing in multidimensional harmonic retrieval problems”, *IEEE Transactions on Signal Processing*, vol. 46, no. 1, pp. 161–169, January 1998.

- [HAA 04] HAARDT M., THOMA R.S., RICHTER A., “Multidimensional high-resolution parameter estimation with application to channel sounding”, Chapter 5 in *High-Resolution and Robust Signal Processing*, Marcel Dekker, New York, NY, pp. 255–338, 2004.
- [HAI 08] HAIMOVICH A.M., BLUM R.S., CIMINI L.J., “MIMO radar with widely separated antennas”, *IEEE Signal Processing Magazine*, vol. 25, no. 1, pp. 116–129, 2008.
- [HAR 70] HARSHMAN R.A., “Foundations of the PARAFAC procedure: model and conditions for an “explanatory” multi-mode factor analysis”, *UCLA Working Papers in Phonetics*, vol. 16, pp. 1–84, 1970.
- [HUA 92] HUA Y., “Estimating two-dimensional frequencies by matrix enhancement and matrix pencil” *IEEE Transactions on Signal Processing*, vol. 40, no. 9, pp. 2267–2280, September 1992.
- [JIA 08] JIAN L., Xu L., STOICA P., FORSYTHE K.W., BLISS D.W., “Range compression and waveform optimization for MIMO radar: a Cramer-Rao bound based study” *IEEE Transactions on Signal Processing*, vol. 56, no. 1, pp. 218–232, January 2008.
- [JIN 09] JIN M., LIAO G., LI J., “Joint DOD and DOA estimation for bistatic MIMO radar” *Signal Processing*, vol. 89, no. 2, pp. 244–251, February 2009.
- [KAY 93] KAY S.M., *Fundamentals of Statistical Signal Processing*, vol. 1, Prentice Hall, 1993.
- [KOR 11] EL KORSO M.N., BOYER R., RENAUD X., MARCOS S., “Statistical resolution limit for the multidimensional harmonic retrieval model: Hypothesis test and Cramer-Rao bound approaches”, *EURASIP Journal on Advances in Signal Processing*, special issue, 2011, In press.
- [LI 08] LI J., STOICA P., *MIMO Radar Signal Processing*, Wiley-Interscience, p. 448, October 2008.
- [LIU 06] LIU J., LIU X., “An eigenvector-based algebraic approach for multidimensional frequency estimation with improved identifiability”, *IEEE Transactions on Signal Processing*, vol. 54, no. 12, pp. 4543–4556, December 2006.
- [LIU 07] LIU J., LIU X., MA X., “Multidimensional frequency estimation from finite snapshots in the presence of identical frequencies,” *IEEE Transactions on Signal Processing*, vol. 55, no. 11, pp. 5179–5194, November 2007.
- [MCC 82] MCCLELLAN J.H., “Multidimensional spectral estimation”, *Proceedings of IEEE*, vol. 70, pp. 1029–1037, September 1982.
- [MOE 98] MOENECLAEG M., “On the true and the modified Cramér-Rao bounds for the estimation of a scalar parameter in the presence of nuisance parameters”, *IEEE Transactions on Communications*, vol. 46, no. 11, pp. 1536–1544, November 1998.
- [NIO 10] NION D., SIDIROPOULOS N.D., “Tensor algebra and multi-Dimensional harmonic retrieval in signal processing for MIMO radar”, *IEEE Transactions on Signal Processing*, vol. 58, no. 11, pp. 5693–5705, November 2010.
- [PES 04] PESAVENTO M., MECKLENBREUKER C.F., BOHME J.F., “Multidimensional rank reduction estimator for parametric MIMO channel models”, *EURASIP Journal on Applied Signal Processing*, vol. 2004, no. 9, pp. 1354–1363, 2004.

- [PES 05] PESAVENTO M., Fast Algorithms for Multidimensional Harmonic Retrieval, PhD thesis, Ruhr-Universitt Bochum (Department of Electrical Engineering), 2005.
- [RAO 45] RAO C.R., “Information and accuracy attainable in the estimation of statistical parameters”, *Bulletin of the Calcutta Mathematical Society*, vol. 37, pp. 81–91, 1945.
- [REN 06] RENAUD A., FORSTER P., CHAUMETTE E., LARZABAL P., “On the high-SNR conditional maximum-likelihood estimator full statistical characterization”, *IEEE Transactions on Signal Processing*, vol. 54, no. 12, pp. 4840–4843, 2006.
- [ROE 06] ROEMER F., HAARDT M., DEL GALDO G., “Higher order SVD based subspace estimation to improve multi-dimensional parameter estimation algorithms”, *Proceedings of Asilomar Conference*, pp. 961–965, October–November 2006.
- [SAJ 07] SAJJAD N., BOYER R., “Asymptotic Cramer-Rao bound for multi-dimensional harmonic models”, *Proceedings of IEEE International Conference on Acoustics, Speech and Signal Processing (ICASSP07)*, 2007.
- [SCH 02] SCHATZMAN M., *Numerical Analysis: A Mathematical Introduction*, Clarendon Press, Oxford, 2002.
- [STO 89] STOICA P., NEHORAI A., “MUSIC, maximum likelihood, and Cramér-Rao bound”, *IEEE Transactions on Signal Processing*, vol. 37, no. 5, pp. 720–741, May 1989.
- [STO 05] STOICA P., MOSES R.L., *Spectral Analysis of Signals*, Prentice Hall, 2005.
- [TAO 01] TAO J., SIDIROPOULOS N.D., TEN BERGE J.M.F., “Almost-sure identifiability of multidimensional harmonic retrieval”, *IEEE Transactions on Signal Processing*, vol. 49, no. 9, pp. 1849–1859, September 2001.
- [TRA 11] TRAN N.D., RENAUD A., BOYER R., MARCOS S., LARZABAL P., “MIMO radar in the presence of modelling error: a Cramér-Rao bound investigation”, *Proceedings of IEEE International Conference on Acoustics, Speech and Signal Processing (ICASSP11)*, 2011.
- [TRE 07] VAN TREES H.L., BELL K.L., *Bayesian Bounds for Parameter Estimation and Nonlinear Filtering/Tracking*, Wiley-IEEE Press, 2007.
- [WOO 80] WOODWARD P.M., *Probability and Information Theory with Applications to Radar*, Artech House, Norwood, MA, 1980.
- [XIA 01] XIANGQIAN L., SIDIROPOULOS N.D., “Cramér-Rao lower bounds for low-rank decomposition of multidimensional arrays”, *IEEE Transactions on Signal Processing*, vol. 49, no. 9, pp. 2074–2086, September 2001.
- [XIA 02] XIANGQIAN L., SIDIROPOULOS N.D., “Almost sure identifiability of constant modulus Multidimensional harmonic retrieval”, *IEEE Transactions on Signal Processing*, vol. 50, no. 9, pp. 2366–2368, September 2002.

Chapter 10

Introduction to Spectral Analysis of Non-Stationary Random Signals

The spectral analysis of non-stationary random signals can be made, *as in the stationary case*, using two large categories of methods:

- 1) Non-parametric methods;
- 2) Parametric methods.

In each of these categories, we find two types of methods specific to the non-stationary case. Actually, in non-stationary context, the spectral analysis can be made:

- either by using the stationary tools and adapting them to the non-stationary nature of signals;
- or by introducing new techniques.

Thus, the reader will find three parts in this chapter: the first part that makes it possible to set out the problem of defining the “evolutive spectrum”, the second part that tackles the non-parametric techniques, and the third part that creates a panorama of the parametric methods used in a non-stationary context.

A more complete panorama of the tools for spectral analysis of non-stationary random signals can be found in [HLA 08].

Chapter written by Corinne MAILHES and Francis CASTANIÉ.

10.1. Evolutive spectra

10.1.1. Definition of the “evolutive spectrum”

The problem of the spectral representation of a random process is a difficult problem which deserves our attention. Loynes [LOY 68] formulates a set of properties that should be those of any spectral representation, with all these properties being verified in the stationary case. These properties are listed in section 10.1.2. He also reviews five different definitions of spectral representations. Among these, Priestley's [PRI 65, PRI 91] is based on oscillatory random processes. The definition is only valid for a reduced and badly defined class of random processes since linear combination of oscillatory processes is not necessarily oscillatory. Instead of this definition, Grenier [GRE 81a, GRE 81b] prefers that of Mélard [MEL 78] and Tjøstheim [TJØ 76], which is built based on the (unique) canonical decomposition of any random process $x(t)$ [LAC 00]:

$$x(t) = \sum_{u=-\infty}^t h(t,u) \varepsilon(u) + v(t) \quad [10.1]$$

$\varepsilon(t)$ represents the process of innovation of $x(t)$ such that $E[\varepsilon(t)\varepsilon(u)] = \delta(t-u)$ and $v(t)$ corresponds to the process part referred to as “singular”.

Starting from this canonical decomposition, Mélard and Tjøstheim propose to define the evolutive spectrum as:

$$s(t,f) = \sum_{u=0}^{+\infty} h(t,t-u) e^{-j2\pi fu} \quad [10.2]$$

This definition meets a large number of the properties listed by Loynes.

However, a paradox can be highlighted with this definition of evolutive spectrum [10.2]. Actually, using very precise hypotheses, we can show that identical innovations for $t > p$ (p being a parameter that intervenes in the hypotheses) lead to evolutive spectra which become identical only for $t \rightarrow \infty$. Within the framework of parametric modeling in a stationary context, this problem causes Grenier [GRE 81a, GRE 81b] to replace [10.1] by a status space model in an observable canonical form:

$$\mathbf{x}(t) = \mathbf{A}(t)\mathbf{x}(t-1) + \mathbf{b}(t)\varepsilon(t)$$

$$x(t) = (1 \ 0 \ 0 \ \cdots \ 0)\mathbf{x}(t)$$

with:

$$\mathbf{A}(t) = \begin{pmatrix} -a_1(t) & -a_2(t) & \cdots & -a_p(t) \\ 1 & 0 & \cdots & 0 \\ \vdots & \vdots & \ddots & \vdots \\ 0 & \cdots & 1 & 0 \end{pmatrix} \text{ and } \mathbf{b}(t) = [b_0(t) b_1(t) \cdots b_{p-1}(t)]^T$$

Thus, the evolutive spectrum is rational and defined by:

$$s(t, f) \triangleq \left| \frac{\bar{b}(t, z)\bar{b}(t, 1/z^*)}{\bar{a}(t, z)\bar{a}(t, 1/z^*)} \right|_{z=e^{j2\pi f}} \quad [10.3]$$

where $\bar{a}(t, z)$ and $\bar{b}(t, z)$ are written as:

$$\begin{aligned} \bar{a}(t, z) &= 1 + a_1(t)z^{-1} + \cdots + a_p(t)z^{-p} \\ \bar{b}(t, z) &= b_0(t) + b_1(t)z^{-1} + \cdots + b_{p-1}(t)z^{-p+1} \end{aligned}$$

Grenier [GRE 81a, GRE 81b] shows that the rational evolutive spectrum behaves in a more satisfactory way than the evolutive spectrum of equation [10.2].

10.1.2. Evolutive spectrum properties

The evolutive spectrum defined this way observes a large number of properties desired by Loynes [LOY 68]:

- the variance of the process can be written as:

$$E[x(t)^2] = \sigma_x^2(t) = \int_{-\infty}^{+\infty} s(t, f) df$$

- $s(t, f)$ coincides in the stationary case with the power spectral density of the process;

- the evolutive spectrum is a real and positive function of t and f ;

- if the process is real, $s(t, f) = s(t, -f)$;

- to multiply the process by a complex exponential $\exp(-j2\pi f_0 t)$ means shifting (modulo 1) its evolutive spectrum by f_0 : the corresponding evolutive spectrum is $s(t, f + f_0)$;

- if $x_2(t) = x_1(t+h)$ then $s_2(t,f) = s_1(t+h,f)$;
- if the non-stationary process $x(t)$ is identical to the rational process $x_1(t)$ for the negative times and to the purely autoregressive process $x_2(t)$ of order p for the strictly positive times, then:

$$\begin{aligned}s(t,f) &= s_1(t,f) \quad t \leq 0 \\ s(t,f) &= s_2(t,f) \quad t > p\end{aligned}$$

when the processes $x_1(t)$ and $x_2(t)$ are non-correlated, whether they are stationary or non-stationary.

10.2. Non-parametric spectral estimation

The major interest of the non-parametric spectral estimation is of not making an *a priori* hypothesis on the signal (as the parametric methods do) and of providing a “blind” analysis tool which is applicable to any type of signal.

Among the non-parametric methods used in non-stationary context, the oldest is the sliding Fourier transform (also called “the short-term” Fourier transform). The Fourier transform was adapted with the introduction of a time window of sufficiently small size so that the analyzed signal is quasi-stationary along this window. The spectrogram that results from this is defined as:

$$S_{TF}(t,f) = |X(t,f)|^2$$

where $X(t,f)$ designates the Fourier transform of the weighted signal by an analysis time window $w(t)$ that we move in time:

$$X(t,f) = \int_{\mathbb{R}} x(u) w(u-t) \exp(-j2\pi fu) du$$

The major obstacle of this technique is the compulsory compromise to be made between the time resolution and the spectral resolution that we wish to obtain. With the shortening of the size of the analysis window, the time localization improves to the detriment of the spectral localization and vice versa.

For signals with rapid variations, this solution is thus not very satisfactory. Historically, the Wigner–Ville distribution then appeared. This time–frequency tool verifies a large number of desired properties of the time–frequency representations, which explains its success. It is defined in the following way:

$$W(t, f) = \int_{\mathbb{R}} x\left(t + \frac{u}{2}\right) x^*\left(t - \frac{u}{2}\right) \exp(-j2\pi fu) du$$

It preserves the localizations in time and frequency and allows an exact description of the modulations of linear frequencies. However, it can take negative values and its bilinear structure generates interferences between the different components of a signal, sometimes making its interpretation difficult. To reduce the inferential terms, smoothing is introduced. We obtain then the smoothed pseudo-Wigner–Ville distribution:

$$W(t, f) = \iint_{\mathbb{R}^2} \left| w_f\left(\frac{u}{2}\right) \right|^2 w_t(v-t) x\left(v + \frac{u}{2}\right) x^*\left(v - \frac{u}{2}\right) \exp(-j2\pi fu) dv du$$

We can generalize this time–frequency representation by the formulation of a class known as Cohen’s class:

$$C(t, f) = \frac{1}{2\pi} \iiint_{\mathbb{R}^3} \Phi(\theta, \tau) x\left(u + \frac{\tau}{2}\right) x^*\left(u - \frac{\tau}{2}\right) \exp(-j(\theta t - 2\pi\tau f - \theta u)) du d\tau d\theta$$

Φ is an arbitrary kernel. The definition of the kernel is sufficient to determine a representation. The desired properties of a time–frequency representation induce certain conditions on the kernel. Based on this, the Wigner–Ville transform can be derived but we can also introduce the distributions of Choi–Williams, Zao–Atlas–Marx, Page, Rihaczek, etc. Thus, the user finds a set of time–frequency representations at his disposal, each one having its own characteristics and favoring a part of the desirable properties according to the case of interest. For example, if the time localization of a frequency jump is a primordial criterion, the Zao–Atlas–Marx distribution is without any doubt the most interesting to use.

Further details on these time–frequency representations can be found in [HLA 08] and [FLA 93].

10.3. Parametric spectral estimation

Applying parametric models in a non-stationary context is interesting in so far as that makes it possible to take advantage of the good frequency resolution of these methods on relatively short windows and to have numerous noise reduction algorithms available.

The use of a parametric method puts the problem of *a priori* knowledge on the signal because the model should be chosen so that it is the closest possible to the

signal type studied. In a non-stationary context, the parametric modeling is used by modifying the different kinds of models known in the stationary case to adapt them to the context. A complete chapter of [HLA 08] is dedicated to the use of the parametric models in the case of non-stationary signals.

There are chiefly two ways of using the parametric modeling methods in a non-stationary context. The first way consists of supposing a local stationarity and of using a method of stationary parametric modeling on short observation windows. The second way consists of using these parametric models to modify these models by suppressing a stationarity condition and by making them adequate for modeling a non-stationary phenomenon.

10.3.1. Local stationary postulate

We can discriminate two categories among the parametric modeling methods postulating the local stationarity: (1) the *sliding* methods and (2) the *adaptive* and *recursive* methods.

The *sliding* methods use the stationary parametric models on a short observation window which is shifted step-by-step along the time axis. The model parameters noted $\theta(k)$ are thus estimated at time k according to an *a priori* observation window of fixed size, which is progressively shifted along the time axis:

$$\hat{\theta}(k) = \hat{\theta}(x(k), x(k-1), \dots, x(k-N))$$

The time increment corresponds to the step of the window displacement and that chosen by the user. It can be of a sample yielding a high computational cost for an interest, which sometimes can be minimal. If the signal evolution is slow, there is no need to shift this observation window (which corresponds also to the parameter estimation window) with a one sample increment. Rather, an M sample increment should be used. The successive spectral analyses will be thus made on every M sample. The size of the analysis window is an important parameter of this kind of method. On the one hand, it should be short enough to make it possible to postulate the local stationarity, but on the other hand, it conditions the maximum order of the model and thus of the spectral resolution.

In the *adaptive* and *recursive* methods, the parameters are enriched in a recursive way over time, which often gives them the property to “adapt” themselves to a non-stationary context. The modeling is called adaptive if its parameters are modified using a given criterion as soon as a new signal value is known. These techniques are

often used for real-time applications. Essentially, there are two types of stationary modeling that are made adaptive:

- the state space model the autoregressive moving average (ARMA) modeling via the state space model and Kalman modeling, with the particular case of adaptive AR [FAR 80]; and
- Prony modeling [CAS 88, LAM 88]. The framework of the adaptive ARMA is based more particularly on the framework on a stochastic approach using its state space model and the Kalman filtering [NAJ 88]; these aspects are not tackled in this book.

In the context of non-stationary parametric modeling, the classic adaptive methods have memories with exponential forgetting strategies and can be regrouped into two families of algorithms: the gradient methods and the least-squares methods. For more information on adaptive algorithms, see [BEL 89, HAY 90].

10.3.2. Elimination of a stationary condition

To build a usable parametric model in a non-stationary context, we can modify the parametric models known and used in a stationary context by eliminating one of the stationarity condition. The model then becomes intrinsically non-stationary and can be applied in the framework of a spectral analysis.

The unstable models and the models with variable or evolutive parameters can be mentioned among all the models built this way.

In unstable models, a part of the poles is on the unit circle, making them unstable and likely to model certain classes of particular non-stationarities. The ARIMA (autoregressive integrated moving average) models and the seasonal models [BOX 70] are among the most well known. Box and Jenkins [BOX 70] have largely contributed to the popularization of the ARIMA models (p, d, q) . This is a category of non-stationary models which make it possible to describe only one type of non-stationarity of the “polynomial” type. The ARIMA model can be seen as a particular case of ARMA model $(p + d, q)$ in which the polynomial of the autoregressive part is of the form:

$$\tilde{a}(z) = \left(1 - z^{-1}\right)^d \tilde{a}_p(z)$$

with d an integer and:

$$\check{a}_p(z) = 1 + \sum_{n=1}^p a_n z^{-n} \quad [10.4]$$

a polynomial whose roots are inside the unit circle.

The models with variable or evolutive parameters correspond to the parametric models in which the parameters vary in time. The evolutive models that are most well known and most used are the evolutive ARMA and more particularly the evolutive AR. Actually, the ARMA models can be used for modeling non-stationary signals by supposing that the parameters of the model progress over time. The first problem is to define the evolution of the coefficients of the model. A retained solution is the projection of these coefficients on a finite basis of functions: the parameters of the model are expressed in the form of linear combinations of functions $f_m(k)$ of a predefined basis. This class of models was introduced by [LIP 75, MEN 91, RAO 70] and popularized by [GRE 86]. The process $x(k)$ is thus modeled as being the output of a recursive linear filter with coefficients that vary with time, excited by an entry of the Gaussian white noise type $n(k)$:

$$x(k) = \sum_{l=1}^p a_l(k-l)x(k-l) + \sum_{l=0}^q b_l(k-l)n(k-l) \quad [10.5]$$

with:

$$a_l(k) = \sum_{m=1}^M a_{lm} f_m(k)$$

$$b_l(k) = \sum_{m=1}^M b_{lm} f_m(k)$$

To make the writing easier, the degree of the basis M is chosen as identical for the AR part and for the MA part, but in practice it will be natural to consider different degrees.

The evolutive AR model is a particular case of the evolutive ARMA model in which the MA part is reduced to an order zero.

The choice of the basis of functions is an important step of the modeling process. Choosing an orthogonal basis is not necessary for the identification of the model but improves the estimation by a better numerical conditioning of the systems to solve. According to the non-stationarity type, the optimal base is that which will make it possible to represent in the best possible way (lowest possibility of

approximation error) the AR and MA coefficients with a minimum number of base functions. The bases of the functions usually used are the time powers, the Legendre basis, and the Fourier basis.

The concept of evolutive parameters is also found in the definition of the Kamen evolutive poles [KAM 88] or through the evolutive Prony model [MOL 95], extensions of the stationary Prony model in which the poles have a trajectory which varies over time.

For the models with non-stationary inputs, among which the multi-pulse model is without any doubt the most popular, the multi-pulse modeling was proposed for the speech coding by Atal and Remde [ATA 82]. This consists of determining the impulse input (series of excitation pulses) which, by feeding a linear translation invariant system (of impulse response $h(k)$), will make it possible to describe the signal $x(k)$ by:

$$x(k) = \sum_{m=1}^L a_m h(k - k_m) + e(k)$$

The epochs of the excitation pulses $\{k_m\}$ are not necessarily regularly distributed. Thus, starting from a determined waveform $h(k)$, either by *a priori* knowledge or by preliminary modeling (AR modeling in general), we search the indicating pulses $\{k_m, a_m\}$ which minimize a quadratic error criterion.

This type of approach makes it possible to model signals presenting transients, echoes, or multi-paths. In addition to speech coding (under Atal “pulse” [ATA 82]), this type of modeling was used in seismics [COO 90, GUE 86, HAM 88], in electromyography [GAS 88], etc. A summary of multi-pulse modeling as well as a thorough analysis of the method and of its different variations can be found in [GAS 93]. In particular, there we will find models associating the Prony modeling and the multi-pulse. The “multi-model multi-pulse” approach and the link existing between AR modeling and Prony modeling leads to the visualization of the generalization of the multi-pulse modeling by systematically associating a Prony modeling to each waveform. Thus, the analysis of multi-pulse Prony means considering the following model:

$$\hat{x}(k) = \sum_{n=1}^N \sum_{m=1}^{P_n} B_{mn} z_{mn}^{k-k_n} U(k - k_n)$$

in which $U(k)$ designates the heavyside function.

10.3.3. Application to spectral analysis

The sliding and adaptive methods make it possible to estimate a vector parameter according to time. The time–frequency analysis naturally results from this estimation by defining an evolutive spectrum identical to the spectral estimator of the corresponding stationary model in which we replace the stationary parameters by the estimated time-varying parameters.

Thus, the AR sliding or AR adaptive modeling lead to the estimation of the vector of the time-varying autoregressive coefficients $a(t)$. The time–frequency analysis resulting from the sliding or adaptive AR modeling consists of plotting the following spectral estimator in the time–frequency plane:

$$s(t, f) = \frac{1}{2\pi} \frac{\sigma_e^2(t)}{|\bar{a}(t, z)\bar{a}(t, 1/z^*)|_{z=e^{j2\pi f}}}$$

$\sigma_e^2(t)$ representing the power of the excitatory white noise at each moment (or at each adaptation step).

We will note the similarity of this AR sliding or adaptive spectrum with the definition of the evolutive spectrum of equation [10.3].

Also, the sliding or adaptive Prony modeling leads to estimating time-varying complex amplitudes $\{b_n(t)\}_{n=1,p}$ and poles $\{z_n(t)\}_{n=1,p}$. This type of modeling makes it possible to plot a spectral estimator in the time–frequency plane; this estimator is defined by:

$$s(t, f) = \left| \sum_{n=1}^P b_n(t) \frac{1-z_n^2(t)}{(1-z_n(t)1/z^*)(1-z_n(t)z)} \right|_{z=e^{j2\pi f}}$$

It is also possible to use these sliding or adaptive methods in a different way. In the context of mode tracking, the final product of the time–frequency analysis can be the plot of the modes (i.e. the poles) estimated over time. Actually, the AR sliding or adaptive modeling makes it possible to estimate the poles by solving at each moment of:

$$\bar{a}(t, z) = 0$$

The sliding or adaptive Prony modeling directly provides the estimation of these time-varying poles according to time.

By selecting only the poles whose module is close enough to the unit circle, we can thus follow the evolution in time of the frequencies characterizing the signal of interest, as well as their amplitudes in the case of Prony modeling.

The unstable models, the evolutive models and the multi-pulse models make up the class of non-stationary parametric models built starting from stationary models by eliminating one or several stationarity conditions. These models can have multiple applications, among which the time–frequency analysis has an important place.

For the unstable models or evolutive ARMA, the expression of a transmittance in z leads to the definition of an evolutive spectrum according to equation [10.3], which allows a time–frequency analysis of the process.

The multi-pulse methods authorize a time–frequency analysis particularly well adapted to the case of non-stationary signals made up of a sum of modes appearing at different moments. In a time–frequency analysis context, this type of modeling allows the definition of a rational spectrum for the case of determinist signals.

The monomodel case leads to:

$$\check{x}(z) = \frac{\sum_{m=1}^L a_m z^{-k_m}}{\sum_{m=1}^P b_m z^{-m}}$$

where the $\{b_m\}_{m=1,P}$ correspond to the coefficients of the AR model used for modeling the waveform $h(k)$. We thus get to the expression of an ARMA rational spectrum of a very high degree in MA (of the order of the length N of the observation window).

10.4. Bibliography

- [ATA 82] ATAL B.S., REMDE J.M., “A new model of LPC excitation for producing natural speech at low bit rates”, *Proceedings of IEEE ICASSP-82*, pp. 614–618, 1982.
- [BEL 89] BELLANGER M., *Analyse des signaux et filtrage numérique adaptatif*, Masson, 1989.
- [BOX 70] BOX G., JENKINS G., *Time Series Analysis, Forecasting and Control*, Holden-Day, San Francisco, 1970.
- [CAS 88] CASTANIÉ F., LAMBERT-NEBOUT C., “A fast and parallel algorithm to solve the Vandermonde system in Prony modeling”, *Proceedings of EUSIPCO 88*, Grenoble, pp. 571–574, September 1988.

- [COO 90] COOKEY M., TRUSSELL H., WON I., "Seismic deconvolution by multi-pulse methods", *IEEE Transactions On Acoustics, Speech and Signal Processing*, vol. 38, no. 1, pp. 156–159, 1990.
- [FAR 80] FARGETTON H., GENDRIN R., LACOUME J.-L., "Adaptive methods for spectral analysis of time varying signals", *Proceedings of EUSIPCO 80*, Lausanne, Switzerland, pp. 777–792, September 1980.
- [FLA 93] FLANDRIN P., *Temps-fréquence*, Hermès, 1993.
- [GAS 88] GASMI F., SLTBON S., CASTANIÉ F., "Multi-pulse excitation modeling applied to EMG signals", *Proceedings of EUSIPCO 88*, pp. 1271–1274, May 1988.
- [GAS 93] GASMI F., La modélisation multi-impulsionnelle, PhD Thesis, INP Toulouse, 1993.
- [GRE 81a] GRENIER Y., "Estimation de spectres rationnels non-stationnaires", *Proceedings of GRETSI 1981*, Nice, France, pp. 185–192, 1981.
- [GRE 81b] GRENIER Y., "Rational non-stationary spectra and their estimation", *1st ASSP Workshop on Spectral Estimation*, Hamilton, Ontario, pp. 6.8.1–6.8.8, 1981.
- [GRE 86] GRENIER Y., "Modèles ARMA à coefficients dépendant du temps: estimateurs et applications", *Traitemet du Signal*, vol. 3, no. 4, pp. 219–233, 1986.
- [GUE 86] GUEGUEN C., MOREAU N., "Determining MA models as salvos of pulses", *Proceedings of ICASSP 86*, pp. 12.4.1–12.4.4, 1986.
- [HAM 88] HAMIDI R., BOUCHER J.-M., BOELLE J.-L., "Combined used of homomorphic filtering and multi-pulse modeling for the deconvolution of seismic reflection signals", *Proceedings of EUSIPCO 88*, pp. 975–978, 1988.
- [HAY 90] Haykin S., *Adaptive Filter Theory*, Prentice Hall, 1990.
- [HLA 08] HLAWATSCH F., AUGER F. (eds), *Time-Frequency Analysis*, ISTE Ltd, and John Wiley & Sons, New York, 2008.
- [KAM 88] KAMEN E., "The poles and zeros of a linear time-varying system", *Linear Algebra and its Application*, vol. 98, pp. 263–289, 1988.
- [LAC 00] LACAZE B., *Processus aléatoires pour les communications numériques*, Hermès, Paris, 2000.
- [LAM 88] LAMBERT-NEBOUT C., CASTANIÉ R., "An adaptive Prony algorithm", *Proceedings of EUSIPCO 88*, pp. 403–406, September 1988.
- [LIP 75] LLPORACE L., "Linear estimation of non-stationary signals", *Journal of Acoustics Society of America*, vol. 58, no. 6, pp. 1288–1295, 1975.
- [LOY 68] LOYNES R., "On the concept of the spectrum for non-stationary processes", *Journal of the Royal Statistical Society, Series B*, vol. 30, no. 1, pp. 1–30, 1968.
- [MEL 78] MELARD G., "Propriétés du spectre évolutif d'un processus non-stationnaire", *Annales de l'Institut Henri Poincaré*, Section B, vol. 14, no. 4, pp. 411–424, 1978.

- [MEN 91] MENDEL J., “Tutorial on high-order statistics in signal processing and system theory: theoretical results and some applications”, *Proceedings of the IEEE*, vol. 79, no. 3, pp. 277–305, 1991.
- [MOL 95] MOLINARO R., CASTANIÉ R., “Modèle de Prony à pôles dépendant du temps”, *Traitemennt du Signal*, vol. 12, no. 5, pp. 421–431, 1995.
- [NAJ 88] NAJIM M., *Modélisation et identification en traitement du signal*, Masson, 1988.
- [PRI 65] PRIESTLEY M., “Evolutionary spectra and non-stationary processes”, *Journal of the Royal Statistical Society, Series B*, vol. 27, no. 2, pp. 204–237, 1965.
- [PRI 91] PRIESTLEY M., *Non-linear and Non-stationary Time Series Analysis*, Academic Press, 1991.
- [RAO 70] RAO T., “The fitting of non-stationary time-series models with time-dependent parameters”, *Journal of the Royal Statistical Society, Series B*, vol. 32, no. 2, pp. 312–322, 1970.
- [TJØ 76] TJØSTHEIM D., “Spectral generating operators for non-stationary processes”, *Advances in Applied Probability*, vol. 8, pp. 831–846, 1976.

Chapter 11

Spectral Analysis of Non-uniformly Sampled Signals

11.1. Applicative context

The most common assumption in the field of spectral analysis is that the sampling rate is constant. Sometimes it is also considered that some samples might be randomly lost, but the idea that the sampling times could be random remains unconventional. However, there are various applications where observations occur on an irregular basis. This is especially true for passive detection systems. Events such as the arrival of a car to a tollbooth and the occurrence of a call to a telephone exchange arise at unpredictable times.

The case of laser velocimetry is interesting in two aspects. First, because it belongs to the category of passive detection systems: the velocity measurement is indeed triggered by the passage of an oil particle into the interferometric area, which is an intrinsically random event. Second, because there is a deep motive to estimate the spectrum of the velocity field, the frequency distribution of its power gives information on some key features of the fluid (dissipative, inertial phenomena, etc.).

Analysis tools are required to study such systems. The objective of this chapter is to give a short overview of them.

Chapter written by Arnaud RIVOIRA and Gilles FLEURY.

11.2. Theoretical framework

11.2.1. Signal model

Henceforth, it will be assumed that the observed signal, $X(t)$, is a centered one-dimensional stationary Gaussian random process. Furthermore, it will also be assumed that correlations between samples decay fast enough over time:

$$\int_0^\infty \tau^2 |\gamma(\tau)| d\tau < \infty$$

This assumption can be seen as a certain spectral smoothness. More accurately, it means that the second-order derivative of the spectrum is bounded. This is useful for two reasons:

- ensuring a finite value of the spectral estimator variance;
- identifying the relevant information as the smooth part of the spectral estimate, the fluctuating part being considered as related to the estimation noise.

The objective of this chapter is to extract from the data, e.g. either from the vector series $(t_k, x(t_k))$ when sampling are available or from the scalar series $(x(t_k))$ otherwise, the most meaningful information on either γ or equivalently Γ , both functions being related to each other by an invertible transformation.

11.2.2. Sampling process

The sampling process is supposed to be of Poisson type with a constant density ρ . The parameter ρ should be thought of as a mean sampling rate.

11.3. Generation of a randomly sampled stochastic process

11.3.1. Objective

The objective of this section is to detail how to sample a reliable stochastic process with a given spectrum. This fundamentally arduous issue will lead us to introduce a parametric class of processes named CARMA.

11.3.2. Generation of the sampling times

A simple way to generate a set of Poisson times consists of taking advantage of the fact that the length between two consecutive times defines a series of “exponential” independent random variables. In other words, it is sufficient to generate a series of

independent random variables uniformly distributed on $]0, 1[$, (u_n) , and to compute recursively the successive times as follows:

$$\begin{cases} t_0 = 0 \\ t_{n+1} = t_n - \frac{1}{\rho} \log(u_n) \end{cases}$$

11.3.3. CARMA processes

Söderström was the first to introduce this class, named CARMA, with reference to the usual ARMA processes, to simulate properly the random sampling of a stochastic process. The CARMA processes are indeed the transposed version of the ARMA processes to the domain of time continuous signal. The idea of this transposition is to replace the rational discrete filter with a continuous one, in other terms to replace the finite difference equation with a differential equation.

In state space form, the signal x is defined by:

$$\begin{cases} dz = Azdt + dW e_p \\ x = b^T z \end{cases}$$

with:

$$A = \begin{bmatrix} 0 & 1 & 0 & \cdots & 0 \\ 0 & 0 & 1 & \ddots & \vdots \\ \vdots & \vdots & \ddots & \ddots & 0 \\ 0 & 0 & \cdots & 0 & 1 \\ -a_0 & -a_1 & \cdots & -a_{p-2} & -a_{p-1} \end{bmatrix}$$

$$z = \begin{bmatrix} \phi \\ \phi^{(1)} \\ \vdots \\ \phi^{(p-2)} \\ \phi^{(p-1)} \end{bmatrix} \quad b = \begin{bmatrix} b_0 \\ \vdots \\ b_q \\ 0 \\ \vdots \\ 0 \end{bmatrix} \quad e_p = \begin{bmatrix} 0 \\ \vdots \\ \vdots \\ 0 \\ 1 \end{bmatrix}$$

dW being the Brownian motion increment.

The roots of the characteristic polynomial of matrix A are the eigenvalues of the dynamic system driven by the Brownian motion W , e.g. the time continuous rational filter. These roots will be noted λ_i . To guarantee the stability of the system, the following assumption should be added: $\Re(\lambda_i) > 0$.

Integrating the previous differential equation between two consecutive sampling times gives:

$$\mathbf{z}(t_{n+1}) = \exp(A(t_{n+1} - t_n)) \mathbf{z}(t_n) + \mathbf{r}_n$$

where \mathbf{r}_n is a centered p -sized Gaussian vector with a covariance matrix Σ_n given by:

$$\Sigma_n = \int_0^{t_{n+1}-t_n} \exp(sA) \mathbf{e}_p \mathbf{e}_p^* \exp(sA)^* ds = U \Phi M(t_{n+1} - t_n) \Phi^* U^*$$

with:

$$U = \begin{bmatrix} 1 & 1 & \cdots & 1 \\ \lambda_1 & \lambda_2 & \cdots & \lambda_p \\ \vdots & \vdots & & \vdots \\ \lambda_1^{p-1} & \lambda_2^{p-1} & \cdots & \lambda_p^{p-1} \end{bmatrix}$$

$$\Phi = \begin{bmatrix} \frac{1}{\prod_{i \neq 1} (\lambda_1 - \lambda_i)} & 0 & \cdots & 0 \\ 0 & \frac{1}{\prod_{i \neq 2} (\lambda_2 - \lambda_i)} & \ddots & 0 \\ \vdots & \ddots & \ddots & 0 \\ 0 & \cdots & 0 & \frac{1}{\prod_{i \neq p} (\lambda_p - \lambda_i)} \end{bmatrix}$$

$$M(\Delta) = \sigma^2 \begin{bmatrix} \frac{e^{\Delta(\lambda_1 + \lambda_1^*)} - 1}{\lambda_1 + \lambda_1^*} & \frac{e^{\Delta(\lambda_2 + \lambda_1^*)} - 1}{\lambda_2 + \lambda_1^*} & \cdots & \frac{e^{\Delta(\lambda_p + \lambda_1^*)} - 1}{\lambda_p + \lambda_1^*} \\ \frac{e^{\Delta(\lambda_1 + \lambda_2^*)} - 1}{\lambda_1 + \lambda_2^*} & \frac{e^{\Delta(\lambda_2 + \lambda_2^*)} - 1}{\lambda_2 + \lambda_2^*} & \ddots & \vdots \\ \vdots & \ddots & \ddots & \frac{e^{\Delta(\lambda_p + \lambda_{p-1}^*)} - 1}{\lambda_p + \lambda_{p-1}^*} \\ \frac{e^{\Delta(\lambda_1 + \lambda_p^*)} - 1}{\lambda_1 + \lambda_p^*} & \cdots & \frac{e^{\Delta(\lambda_{p-1} + \lambda_p^*)} - 1}{\lambda_{p-1} + \lambda_p^*} & \frac{e^{\Delta(\lambda_p + \lambda_p^*)} - 1}{\lambda_p + \lambda_p^*} \end{bmatrix}$$

Thus $X(t)$ could be considered as a stationary process provided that $z(0)$ follows the Gaussian law $N(0, \Sigma_\infty)$ with the asymptotical covariance matrix:

$$N(0, \Sigma_\infty) = \lim_{\Delta \rightarrow \infty} U \Phi M(\Delta) \Phi^* U^* = U \Phi M(\infty) \Phi^* U^*$$

where:

$$M(\infty) = \sigma^2 \begin{bmatrix} -1 & -1 & \cdots & -1 \\ \overline{\lambda_1 + \lambda_1^*} & \overline{\lambda_2 + \lambda_1^*} & \ddots & \overline{\lambda_p + \lambda_1^*} \\ -1 & -1 & \ddots & \vdots \\ \overline{\lambda_1 + \lambda_2^*} & \overline{\lambda_2 + \lambda_2^*} & \ddots & -1 \\ \vdots & \ddots & \ddots & \overline{\lambda_p + \lambda_{p-1}^*} \\ -1 & \cdots & -1 & \overline{-1} \\ \overline{\lambda_1 + \lambda_p^*} & \cdots & \overline{\lambda_{p-1} + \lambda_p^*} & \overline{\lambda_p + \lambda_p^*} \end{bmatrix}$$

The samples of the process X are then determined recursively from the above relation with the following data as input:

- $z = 0$;
- sampling times t_n ;
- Gaussian vector r_n paths.

11.4. Spectral analysis using undated samples

When sampling times are lost, severely altered by noise, or simply when they have not been stored for cost-saving purpose, some specific tools should be used. The objective of this section is precisely to show how the spectrum could be estimated based on the list of samples sorted in the chronological order and the value of the mean sampling rate ρ .

11.4.1. Non-parametric estimation

Shapiro and Silverman have been the pioneers in this field. They have notably established that Poisson sampling enables us to get rid of spectral aliasing no matter what the value of the mean sampling rate ρ is. The starting point of their work is what we called pseudo-correlation coefficients, namely, the series made up of the correlation coefficients computed along the whole path:

$$\hat{c}(k) = \frac{1}{N} \sum_{n=1}^N x(t_n)x(t_{n+k})$$

In the random sampling case, these coefficients cannot be derived from the correlation function γ by a simple sampling operation. That is the reason why we chose to call them pseudo-correlation. The relation with γ is the following:

$$c(k) = \mathcal{E}\{\hat{c}(k)\} = \int_0^\infty \gamma(s) \wp_{k-1}(s) ds = \frac{1}{(k-1)!} \rho^k \int_0^\infty \gamma(s) s^{k-1} e^{-\rho s} ds$$

where:

$$\wp_{k-1}(s) = \frac{1}{(k-1)!} \rho^k s^{k-1} e^{-\rho s}$$

is the probability function of $t_{n+k} - t_n$.

This expression can be recast using the spectrum Γ :

$$c(k) = 2\pi \int_{-\infty}^{\infty} \Gamma(\nu) \phi(2\pi\nu)^{k+1} d\nu$$

where ϕ is the characteristic function of the time length:

$$\phi(z) = \int_0^{\infty} \wp_0(s) e^{isz} ds = \frac{1}{1 - i\frac{z}{\rho}}$$

The principle of this method is to estimate the spectrum Γ from the pseudo-correlation coefficients. Given that those coefficients $\widehat{c}(k)$ converge to $c(k)$, it makes sense to try to find a way to inverse the previous relation between $c(k)$ and Γ . This inversion is not only possible, but can even be calculated explicitly:

$$\begin{cases} \Gamma(\nu) = \sum_{k=0}^{\infty} d(k) (\psi_k(2\pi\nu) + \psi_k(-2\pi\nu)) \\ d(k) = \sqrt{\frac{2}{\rho}} \sum_{\ell=0}^k (-2)^{\ell} \frac{k!}{\ell!(k-\ell)!} c(\ell) \end{cases}$$

where:

$$\psi_k(2\pi\nu) = -\sqrt{2\rho} \frac{(2\pi i\nu + \rho)^k}{(2\pi i\nu - \rho)^{k+1}}$$

The family of functions ψ_k is derived from that of $\phi(2\pi\nu)^{k+1}$ by orthonormalization to make the inversion easier. Unfortunately, the coefficients are not perfectly known: They are estimated through $\widehat{c}(k)$ up to an estimation noise and the inversion formula is not stable. To fix this issue, Masry introduced a weighting sequence $\Upsilon(k)$ to apply to the $d(k)$ coefficients:

$$\widehat{\Gamma}(\nu) = \sum_{k=0}^{\infty} \widehat{d}(k) \Upsilon(k) (\psi_k(2\pi\nu) + \psi_k(-2\pi\nu))$$

with:

$$\Upsilon(k) = h \left(\frac{1}{N} e^{\alpha k} \right)$$

where $\alpha > \ln(3)$ and h is a function verifying:

$$\begin{cases} |h(u)| \leq h(0) = 1 \\ |uh(u)| \leq K_1 \\ 1 - h(u) \leq K_2 |u| \end{cases}$$

When there exists an integer $r > 2$ so that γ meets the following conditions of smoothness and decrease:

$$t^{r/2}\gamma^{(k)}(t) \in L^2[0, \infty[\quad \text{for } k \in \{0, \dots, r\}$$

Then the estimator is consistent and there exists a ν -independent positive number B_2 so that:

$$\mathcal{E} \left\{ \left| \Gamma(\nu) - \widehat{\Gamma}(\nu) \right|^2 \right\} < B_2 \frac{1}{\ln(N)^{r-2}}$$

Hence, even with those restrictive conditions on the smoothness and decrease of the function, the convergence rate is excessively low. The consequence of this is that such estimators are seldom used in real-life applications. It is somehow the counterpart of putting aside the knowledge of the sample times.

11.4.2. Parametric estimation

The idea is to restrict the size of the estimation set to boost the convergence rate. The starting point remains the same, e.g. the computation of the pseudo-correlation coefficients. Those coefficients are stored into a K -sized vector named pseudo-correlation vector:

$$\widehat{\mathbf{V}}_N = \frac{1}{N} \sum_{n=1}^N x(t_n) \mathbf{X}_n$$

where:

$$\mathbf{X}_n = [x(t_n) \cdots x(t_{n-K})]^\top$$

When the number of samples goes to infinity, this vector tends to its expected value:

$$\begin{aligned} \lim_{N \rightarrow \infty} \widehat{\mathbf{V}}_N &= \mathcal{E} \{ x(t_n) \mathbf{X}_n \} \\ &= \mathbf{V}(\sigma, \lambda, b) \\ &= [v_0(\sigma, \lambda, b) \quad v_1(\sigma, \lambda, b) \quad \cdots \quad v_K(\sigma, \lambda, b)]^\top \end{aligned}$$

with:

$$\begin{aligned} v_k(\sigma, \lambda, b) &= U \Phi \mathcal{E} \{ M(t_{n+k} - t_n) \} \Phi^* U^* \\ &= U D_k \Phi M(\infty) \Phi^* U^* \end{aligned}$$

where:

$$D_k = \begin{bmatrix} \frac{1}{\left(1 - \frac{\lambda_1}{\rho}\right)^k} & 0 & \cdots & 0 \\ 0 & \frac{1}{\left(1 - \frac{\lambda_2}{\rho}\right)^k} & \ddots & \vdots \\ \vdots & \ddots & \ddots & 0 \\ 0 & \cdots & 0 & \frac{1}{\left(1 - \frac{\lambda_p}{\rho}\right)^k} \end{bmatrix}$$

Thus it is possible to estimate the parameters minimizing the distance between the pseudo-correlation vector and its expected value:

$$\begin{bmatrix} \hat{\sigma} & \hat{\lambda} & \hat{b} \end{bmatrix} = \arg \min \delta \left(\mathbf{V}(\sigma, \lambda, b), \hat{\mathbf{V}}_N \right)$$

where δ is a relevant metric on the vector space, for instance, that of the Euclidean Norm. To find a solution, the size of the pseudo-correlation vector should at least be equal to the number of degrees of freedom of the CARMA process, namely, p for the poles of the CAR part, $p - 1$ for the zeros of the numerator, and 1 other degree for the variance of the input noise. The size K of the pseudo-correlation vector should then be greater than $2p$. Besides, it is advised to go beyond this minimal size when the mean sampling rate is high. Indeed, in this case, the first pseudo-correlation coefficients will provide information on short-time correlation and, therefore, will not be suitable to capture the low-frequency information. An instance of sensible choice for application would be $K = 2 \max(p, \rho)$.

When the order of the CARMA process increases, the estimation issue becomes similar to the non-parametric one and consequently gets more and more touchy (multimodality of the distance criterion, noisy estimation, and so on). Hence, it is reasonable to focus on the low-dimension models. Because of their popularity, the order 2 systems deserve special attention and some detailed development. The parameters can be calculated from the pseudo-correlation vector of size 3. The estimation process is given thereafter:

- 1) Estimate ν_0 , ν_1 , and ν_2 through empirical means.
- 2) Compute the following intermediate variables:

$$\begin{aligned} \hat{R} &= \sqrt{\frac{\hat{\nu}_0(\hat{\nu}_1 - \hat{\nu}_0)}{\hat{\nu}_0\hat{\nu}_2 - \hat{\nu}_1^2}} \\ \hat{\theta} &= \cos^{-1} \left(\frac{1}{2} \sqrt{\frac{\hat{\nu}_0(\hat{\nu}_2 - \hat{\nu}_1)^2}{(\hat{\nu}_0\hat{\nu}_2 - \hat{\nu}_1^2)(\hat{\nu}_1 - \hat{\nu}_0)}} \right) \end{aligned}$$

3) Derive the corresponding poles:

$$\begin{cases} \hat{\lambda}_1 = \rho \left(1 - \hat{R} \cdot e^{-i\hat{\theta}} \right) \\ \hat{\lambda}_2 = \rho \left(1 - \hat{R} \cdot e^{+i\hat{\theta}} \right) \end{cases}$$

4) Compute the input noise standard deviation:

$$\hat{\sigma} = |\hat{\lambda}_1| \sqrt{-4\hat{\nu}_0 \cdot \Re(\hat{\lambda}_1)}$$

11.5. Spectral analysis using dated samples

In most applications, the practitioner knows both the sample values and the corresponding sampling times. Hence, he is able to estimate many more features than only the pseudo-correlation coefficients. The objective of this part is to show that this extra information could be exploited to improve substantially the quality of the spectral estimation.

11.5.1. Masry's work

Masry's work is still the reference in terms of theoretical and mathematical content. The scope of his study goes significantly beyond the scope of this chapter (Gaussian processes with Poisson sampling). For clarity's sake, it has been decided to stick to the framework introduced at the beginning of the chapter and to give only a simplified version of his results.

Define first some extended periodogram:

$$I_N(\nu) = \frac{1}{N} \left| \sum_{n=1}^N x(t_n) e^{-i2\pi t_n \nu} \right|^2$$

The spectral estimator suggested by Masry is a convolution product of that extended periodogram by a window function $W_N(\nu) = 1/b_N \cdot W(\nu/b_N)$:

$$\hat{\Gamma}_N(\nu) = \int_{-\infty}^{\infty} W_N(f) I_N(\nu - f) df$$

where W is an even-bounded real function such that $\int_{-\infty}^{\infty} W = 1$ and b_N is a series verifying:

$$\begin{cases} \lim_{N \rightarrow \infty} b_N = 0 \\ \lim_{N \rightarrow \infty} N b_N = \infty \end{cases}$$

The first condition ensures that $\hat{\Gamma}_N$ is asymptotically unbiased:

$$\lim_{N \rightarrow \infty} \hat{\Gamma}_N(\nu) = \Gamma(\nu)$$

The second ensures that the estimation variance is asymptotically zero:

$$\lim_{N \rightarrow \infty} Nb_N \text{cov} \left(\widehat{\Gamma}_N(\nu_1), \widehat{\Gamma}_N(\nu_2) \right) = \frac{1}{\rho} \delta_{\nu_1, \nu_2} \int_{-\infty}^{\infty} |W|^2 (\gamma(0) + \rho \Gamma(\nu))^2$$

The window function $W_N(\nu)$ is concentrating around zero to remove progressively the blurring effect from the estimates, but slow enough to keep the variance increase under control. This result could unfortunately not be used as it is. Indeed, the convolution product $\int_{-\infty}^{\infty} W_N(f) I_N(\nu - f) df$ cannot be calculated exactly from a finite collection of $I_N(\nu_i)$ values. Moreover, to produce good-quality estimates the window width parameter b_N should be a function of ν . The rationale behind that is that a 1 Hz loss in resolution has a much more dramatic impact at 10 Hz than at 1 MHz.

11.5.2. Slotted technique

This method, introduced by Mayo, is probably the most popular in the field of laser velocimetry. It is also one of the most simple and intuitive methods. The idea is to estimate the value of the correlation function γ on time intervals $E_k = [(k - 1/2)\Delta\tau, (k + 1/2)\Delta\tau]$. To do that, pairs of samples $(x(t_i), x(t_j))$ are sorted with respect to their underlying time length $|t_j - t_i|$ and put into the corresponding bin B_k defined by:

$$(i, j) \in B_k \Leftrightarrow |t_j - t_i| \in E_k$$

The correlation function is then estimated by empirical correlation on each bin:

$$\widehat{\chi}_k = \frac{\sum_{i,j \in B_k} x(t_i)x(t_j)}{\text{card}(B_k)}$$

This version gives rise to a very noisy spectral estimator in the high-frequency domain. Van Maanen and Tummers suggest replacing this numerator expression with another, which would be less sensitive to the input noise:

$$\widehat{\chi}_k = \frac{\sum_{i,j \in B_k} x(t_i)x(t_j)}{\sum_{i,j \in B_k} x(t_i)^2}$$

The estimated spectrum is then given by:

$$\widehat{\Gamma}_N(\nu_j) = \widehat{\sigma}^2 \Delta\tau \left(1 + \sum_{k=1}^K \chi_k \omega_k(\nu_j) \cos(2\pi k \nu_j \Delta\tau) \right)$$

with:

$$\omega_k(\nu_j) = \begin{cases} 1 + \cos\left(\frac{k\pi\Delta\tau\nu_j}{6}\right) & \text{if } \frac{k\Delta\tau\nu_j}{6} < \pi \\ 0 & \text{otherwise} \end{cases}$$

and:

$$\hat{\sigma}^2 = \frac{1}{N} \sum_{n=1}^N x(t_n)^2$$

The window function ω_k allows lowering significantly the contribution of the correlation coefficients corresponding to very distant samples to the high-frequency estimation. The idea is to swap the estimation noise in high frequency for a resolution loss. Another enhancement, introduced by Nobach *et al.*, consists of using overlapping bins to reduce the singularities of the estimated correlation functions and by the way high-frequency noise on the spectrum. In this case, the coefficients χ_k are computed as follows:

$$\hat{\chi}_k = \frac{\sum_{i,j \in B_k} x(t_i)x(t_j)\kappa\left(\frac{t_i - t_j}{\Delta\tau} - k\right)}{\sum_{i,j \in B_k} x(t_i)^2\kappa\left(\frac{t_i - t_j}{\Delta\tau} - k\right)}$$

where κ is the triangle function:

$$\kappa(t) = \begin{cases} 1 - |t| & \text{if } |t| < 1 \\ 0 & \text{otherwise} \end{cases}$$

11.5.3. IRINCORREL: A consistent spectral estimator

11.5.3.1. Principles

The IRINCORREL estimator can be seen as an enhancement of that introduced by Masry. The idea is to replace the continuous convolution product $\int_{-\infty}^{\infty} W_N(f)I_N(\nu - f)df$ by a more tractable expression:

$$\hat{\Gamma}_N(\nu) = \frac{1}{N} \sum_{n=1}^N \sum_{\ell=1}^{L_N} x(t_n)x(t_{n+\ell}) \cos(2\pi\nu(t_{n+\ell} - t_n)) w_N(t_{n+\ell} - t_n)$$

where w_N is the inverse Fourier transform of W_N , for example, $w_N(s) = w(b_N s)$.

The whole issue is to find a relevant way to choose the weighting function $w_N(s)$. In [RIV 02a], it is shown that unbiased estimators suffer from a high level

of variability. Therefore, it is necessary to take into account both bias and variance. It is then judicious to demand that the function $w_N(s)$ minimizes the mean square estimation error function ε_N (indeed ε_N is a function of ν , as Γ and $\widehat{\Gamma}_N$ are):

$$\varepsilon_N = \sqrt{E \left\{ \left(\widehat{\Gamma}_N - \Gamma \right)^2 \right\}} \quad [11.1]$$

The maximal correlation length L_N should be at least equal to 1 and should be defined such that the expected contribution of $w_N(t_{n+\ell} - t_n)$ to the previous sum remains significant. Since the random variables $t_{n+\ell} - t_n$ are distributed around $1/\rho$ with standard deviation, they are defined by the following law:

$$\wp_{\ell-1}(s) = \frac{1}{(\ell-1)!} \rho^\ell s^{\ell-1} e^{-\rho s}$$

The mean value of the IRINCORREL estimator is therefore:

$$\mathcal{E} \left\{ \widehat{\Gamma}_N(\nu) \right\} = \int_0^\infty \gamma(\tau) \cos(2\pi\nu\tau) \left[w(\tau b_N) \sum_{\ell=1}^{L_N} \wp_\ell(\tau) \right] d\tau$$

The mean square estimation error function ε_N has been presented in [RIV 02b]. It leads to an optimal expression of the window width b_N .

$$b_N = \left(\frac{\int_{-\infty}^\infty w^2}{N\rho} \right)^{1/5} \left(\frac{\gamma(0) + \rho\Gamma(\nu)}{\Gamma''(\nu) \int_{-\infty}^\infty \nu^2 W(\nu) d\nu} \right)^{2/5}$$

where $\Gamma''(\nu)$ is the second-order derivative of $\Gamma(\nu)$.

It appears that the optimal window width requires the value of the second-order derivative of the spectrum. Hence, the idea is to follow a two-step approach:

- 1) Estimate both the spectrum value $\Gamma(\nu)$ and its second-order derivative $\Gamma''(\nu)$ using a non-optimal method.
- 2) Estimate the spectrum value using the optimal window width computed from those estimated values of $\Gamma(\nu)$ and $\Gamma''(\nu)$.

To estimate $\Gamma''(\nu)$, the same kind of sum can be used:

$$\begin{aligned} \widehat{\Gamma}''(\nu) &= -4\pi^2 \nu^2 \frac{1}{N} \sum_{n=1}^N \sum_{\ell=1}^{L_N} x(t_n)x(t_{n+\ell})(t_{n+\ell} - t_n)^2 \cos(2\pi\nu(t_{n+\ell} - t_n)) \\ &\quad \times w(b_N''(t_{n+\ell} - t_n)) \end{aligned}$$

The optimal window width b_N'' for the second-order derivatives should decay with a power of $1/7$ of N . For convenience sake, this window width b_N'' would be derived

from b_N assuming that they both are related to each other by a simple multiplicative factor, which depends only on the size of the sample set N :

$$b''_N = b_N N^{2/35}$$

Last but not the least, the maximal correlation length L_N should be greater or equal to 1 and should be defined such that the expected contribution of $w_N(t_{n+\ell} - t_n)$ to the previous sum remains significant. Since the random variables $(t_{n+\ell} - t_n)$ are distributed around ℓ/ρ with a standard deviation of $\sqrt{\ell}/\rho$, this condition will be considered as approximately met when most of the time lengths lie beyond the width of the w_N window, namely:

$$\ell/\rho - 2\sqrt{\ell}/\rho > \frac{D}{b_N}$$

where D is the width of the w window, which depends on the shape of the window. Hence:

$$L_N = \left\lfloor \left(1 + \sqrt{1 + \frac{\rho D}{b_N}} \right)^2 \right\rfloor$$

with $\lfloor \cdot \rfloor$ being the floor function.

11.5.3.2. Algorithm

The algorithm can be summed up as follows:

- Step 1

$$\text{Compute } \begin{cases} b_N(\nu) = \frac{\nu}{\sqrt{\int_{-\infty}^{\infty} f^2 W(f) df}} \frac{1}{(N\rho)^{1/5}} \\ b''_N(\nu) = b_N(\nu) N^{2/35} \end{cases}$$

$$\text{Determine } L_N(\nu) = \left\lfloor \left(1 + \sqrt{1 + \frac{\rho D}{b_N(\nu)}} \right)^2 \right\rfloor$$

set $\widehat{\Gamma}_0(\nu) = 0, \widehat{\Gamma}''_0(\nu) = 0$

for $n = 1 \dots N$

$X = 0, Y = 0$

for $\ell = 1 \dots L_N$

$$\begin{cases} \delta t = 2\pi(t_{n+\ell} - t_n) \\ dX = x(t_{n+\ell}) \cos(\delta t \cdot \nu) \\ X = X + dX \cdot w(b_N(t_{n+\ell} - t_n)) \\ Y = Y + dX \cdot w(b''_N(t_{n+\ell} - t_n))(\delta t)^2 \end{cases}$$

endfor

```


$$\begin{cases} \widehat{\Gamma}_n(\nu) = \widehat{\Gamma}_{n-1}(\nu) + x(t_n) \cdot X \\ \widehat{\Gamma''}_n(\nu) = \widehat{\Gamma''}_{n-1}(\nu) + x(t_n) \cdot Y \end{cases}$$

endfor

$$\begin{cases} \widehat{\Gamma}_N(\nu) = \frac{2}{N} \widehat{\Gamma}_N(\nu) \\ \widehat{\Gamma''}_N(\nu) = -\frac{2}{N} \widehat{\Gamma''}_N(\nu) \end{cases}$$

- Step 2
Compute  $b_N(\nu) = \left( \frac{\int_{-\infty}^{\infty} w^2}{N\rho} \right)^{1/5} \left( \frac{\gamma(0) + \rho\Gamma(\nu)}{\Gamma''(\nu) \int_{-\infty}^{\infty} \nu^2 W(\nu) d\nu} \right)^{2/5}$ 
Determine  $L_N(\nu) = \left[ \left( 1 + \sqrt{1 + \frac{\rho D}{b_N(\nu)}} \right)^2 \right]$ 
set  $\widehat{\Gamma}_0(\nu) = 0$ 
for  $n = 1 \dots N$ 
 $X = 0$ 
for  $\ell = 1 \dots L_N$ 

$$\begin{cases} \delta t = 2\pi(t_{n+\ell} - t_n) \\ dX = x(t_{n+\ell}) \cos(\delta t \cdot \nu) \\ X = X + dX \cdot w(b_N(t_{n+\ell} - t_n)) \end{cases}$$

endfor
 $\widehat{\Gamma}_n(\nu) = \widehat{\Gamma}_{n-1}(\nu) + x(t_n) \cdot X$ 
endfor
 $\widehat{\Gamma}_N(\nu) = \frac{2}{N} \widehat{\Gamma}_N(\nu)$ 

```

Let N_f denote the number of spectral samples and N_{slot} the number of slots for the “slotting technique”. The resulting computational effort is $O(N^{6/5}N_f)$ multiplications, whereas the slotting technique requires $O(N^2N_{\text{slot}})$. In general, N_f is comparable to N_{slot} and negligible compared with N . In most cases, 30–100 logarithmically distributed estimates are enough to characterize a signal, whereas N amounts to 10,000–100,000. Then, the computational complexity is reduced by a factor of 1,000–10,000.

11.6. Perspectives

A new non-parametric spectral estimator based on the Masry’s work has been proposed. This spectral estimator called IRINCORREL requires that knowledge of the sampling times, the samples, the sampling law, and the high-frequency decay of

the spectrum be at least roughly known. It takes only $O(N^{\frac{6}{5}}N_f)$ multiplications to compute recursively N_f IRINCORREL spectral estimates (compared to $O(N^2N_{\text{slot}})$ for the slotting estimator). Besides, unlike the slotting estimator, its consistency has been established for a wide class of signals and sampling processes, including Gaussian signals and Poisson sampling processes. Its convergence rate is $O(N^{-\frac{2}{5}})$, which is rather satisfactory since the empirical mean converges at the $O(N^{-\frac{1}{2}})$ rate in ideal cases.

11.7. Bibliography

- [ADR 87] ADRIAN R.J., YAO C.S., “Power spectra of fluid velocities measured by laser Doppler velocimetry”, *Experiments in Fluids*, vol. 5, pp. 17–28, 1987.
- [BEN 00] BENEDICT L.H., NOBACH H., TROPEA C., “Estimation of turbulent velocity spectra from laser Doppler data”, *Measurement Science and Technology*, vol. 11, no. 8, pp. 1089–1104, 2000.
- [BOS 02] BOS R., DE WAELE S., BROERSEN P.M.T., “AR spectral estimation by application of the burg algorithm to irregularly sampled data”, *Proceedings of IEEE Instrumentation and Measurement Technology Conference*, vol. 2, pp. 1208–1213, 2002.
- [GAS 75] GASTER M., ROBERT J.B., “Spectral analysis of randomly sampled signals”, *Journal of the Institute of Mathematics and its Applications*, vol. 15, no. 2, pp. 195–216, 1975.
- [JON 81] JONES R.H., “Fitting a continuous time autoregression to discrete data”, *Applied Time Analysis*, Academic Press, New York, vol. 2, pp. 651–682, 1981.
- [LOM 76] LOMB N.R., “Least squares frequency analysis unequally spaced data”, *Astrophysics and Space Science*, vol. 39, no. 2, pp. 447–462, 1976.
- [MAS 83] MASRY E., “Spectral and probability density estimation from irregularly observed data”, in PARZEN E. (ed.), *The Statistical Analysis of Irregularly Observed Time Series in Statistics, Lecture Notes in Statistics*, Springer-Verlag, New York, pp. 224–250, 1983.
- [NIT 97] NITA L., OKSMAN J., “Fast generation of synthetic nonuniformly sampled signals: from quantized to continuous sampling intervals”, *Proceedings of IEEE International Conference on Digital Signal Processing*, NY, vol. 2, pp. 1059–1062, 1997.
- [RIV 02a] RIVOIRA A., FLEURY G., “Recursive non parametric spectral estimation from irregularly sampled observations”, *Proceedings of International Conference on Digital Signal Processing*, vol. 2, pp. 799–802, 2002.
- [RIV 02b] RIVOIRA A., MOUDDEN Y., FLEURY G., “Real time continuous AR parameter estimation from randomly sampled observations”, *Proceedings of IEEE International Conference on Acoustics Speech and Signal Processing*, vol. 2, pp. 1725–1728, 2002.
- [RIV 04] RIVOIRA A., FLEURY G., “A consistent non parametric spectral estimator for randomly sampled signals”, *IEEE Transactions on Signal Processing*, vol. 52, no. 9, pp. 2383–2395, 2004.

- [SCA 82] SCARGLE J.D., "Studies in astronomical time series analysis II. Statistical aspects of spectral analysis of unevenly spaced data", *Astrophysical Journal*, vol. 263, no. 2, pp. 835–853, 1982.
- [SCO 76] SCOTT P.F., Distorsion and estimation of the autocorrelation function and spectrum of a randomly sampled signal, PhD thesis, Rensselaer Polytechnic Institute, Troy, NY, 1976.
- [SHA 60] SHAPIRO L.S., SILVERMAN R.A., "Alias-free sampling of random noise", *Journals of the Society for Industrial and Applied Mathematics*, vol. 8, pp. 225–248, 1960.
- [SHA 76] SHAY M.T., Digital estimation of autocovariance funtions and power spectra from randomly sampled data using a lag product technique, PhD thesis, Texas A&M University, College Station, TX, 1976.
- [SÖD 91] SÖDERSTRÖM T., "Computing stochastic continuous-time models from ARMA models", *International Journal of Control*, vol. 53, no. 6, pp. 1311–1326, 1991.

Chapter 12

Space–Time Adaptive Processing

By considering a typical space–time processing problem for radar applications, this chapter extends the problematic of spectral estimation in two directions:

- 1) Extension to two-dimensional estimation – space and time (slow time) – for signal processing of radar signals.
- 2) Extension to the discrimination targets vs. (noise + clutter) problem – one step beyond the estimation problem.

It will be seen that this extension leads to different architectures – pre- and post-Doppler architectures – which have specific properties for side antenna radars and forward antenna radars.

Space–time adaptive processing (STAP) makes use jointly of the spatial and temporal dimension of the received signals on sub-array antenna, whereas classical antenna processing exploits only the spatial dimension for filtering/separation. STAP then take benefits from specific 2D properties of the received signals in the joint space–time domain or in the joint dual angle–frequency domain. This approach is of particular interest when received signals exhibit a coupling between angle and frequency. Then, although the signals may be spread in both 1D domains and non-separable with 1D processing, they also fill only one dimension in the joint 2D domain, leading to possible separation.

This situation is observed for ground clutter signal filtering on airborne radars, where a direct relation exists between the Doppler frequency and the angle of arrival

of the clutter echoes. These clutter echoes are classically filtered by a spatial filter (angular filtering by the antenna lobe), followed by a time filter (Doppler frequency analysis). Clutter, which is spread in both angular and frequency domains, is then not totally eliminated and clutter residues strongly limit detection performances.

In this context, STAP is of great interest, and its implementation in operational radars now becomes available due to the maturity of multi-channel active array antennas associated with ever-increasing computational capacity of onboard processing. The main applications on short and middle terms are slow-moving target detection in air-to-ground operations (targets embedded in main lobe clutter), and improved detection of air targets in air-to-air operations (targets embedded in side lobe clutter). These two applications will be used throughout this chapter as operational guidelines.

However, the selection of a STAP architecture, and especially the choice between pre- and post-Doppler architectures remains complex because it relies on very different and partially contradicting arguments, combined with operational constraints.

This chapter is dedicated to engineers who are not specialists in STAP, but familiar with radar and signal processing. The goal is to point out the main principles of major STAP architectures and to derive criteria of selection for airborne radar. Indeed, there is no globally optimal architecture whatever the application, but several architectures are more or less suited to the operational context.

In addition, numerous questions are still quite open and have to be answered with experimentation on real data. The aim of this chapter is not to answer all these pending questions, but rather to give viewpoints that have to be considered.

In the first section, the chapter will present in detail the STAP issue for airborne radars. Two canonical configurations will be studied, pointing out the benefits of STAP: the side antenna configuration (e.g. slow-moving ground targets detection on business aircraft) and the forward antenna configuration (e.g. air target detection on combat aircraft). Special emphasis will be put on clutter location in the range-angle-Doppler domain, motivations for STAP application and specificities in relation to the application.

In the second section, the general principles of STAP processing will be presented and their relation with spectral estimation will be examined.

The major pre- and post-Doppler STAP architectures will then be described in the third section.

The fourth section will analyze the advantages and drawbacks of the two macro architectures (pre- or post-Doppler), and a synthesis will be given in the final section.

It is hoped that this analysis, emphasizing the important consequences of the architecture selection, will help the spectral analysis engineer to clarify his objectives when applying the different spectral analysis techniques described in this book to multidimensional situations.

12.1. STAP, spectral analysis, and radar signal processing

12.1.1. *Generalities*

Standard radar signal processing involves both detection and location (range, Doppler, angles) of the targets. The majority of the computational power is devoted to detection, since location is estimated only for the detected targets, which are much less than the total number of range-Doppler-angle bins to be processed.

The overall objective of radar signal processing is to maximize the detection probability, while ensuring a pre-requisite level of false alarm probability.

Most constant false alarm rate (CFAR) detectors compare the level in the cell under test (CUT) to a statistic based on adjacent cell data. For instance, the standard cell-averaging CFAR compares the power in the CUT with the average power in a given environment of neighboring cells. If the difference between the power in the CUT and the average power in the neighboring cells exceeds a given threshold, a detection is declared. This threshold is determined for a required probability of false alarm, and thus provides a certain probability of detection. Of course, these probabilities of detection and false alarm are affected by clutter echoes, and the challenge for radar signal processing is to provide sufficient robustness in those varying situations – and primarily not to increase the false alarm probability. Furthermore, signal processing must provide the location parameters – range, Doppler, angles – for the detected targets.

Without entering into too many details, it is important to note that most modern radars use active antennas, which provide multiple channels on receive, thus opening the way to space-time processing of the received signals, exploiting the specific bi-dimensional or multi-dimensional properties of the disturbances: noise, jamming, and clutter. Better exploitation of these intrinsic properties of noise will in turn improve the overall performance, compared to the classical mono-channel system.

Two different canonical architectures for STAP processing will be analyzed, to outline the benefits of STAP processing, and the direct relation between clutter

localization in range-Doppler-angle and the appropriate processing architecture. Studying these two simple configurations will allow simple analytical formulations of deterministic space-time processing to be derived, and two macro-architectures – pre-Doppler STAP and post-Doppler – to be derived, emphasizing the duality of these main techniques.

In actual practice, though, STAP filtering can only be adaptive, for the following reasons:

- non-identical sub-arrays, and poor knowledge of their diagrams;
- incomplete knowledge of the configuration (platform movement and orientation);
- non-perfect calibration between reception channels;
- high level of noisy signals to be canceled (typically two to four orders of magnitude higher than the useful signal).

Architectures for this adaptive processing will be described in section 12.3.

12.1.2. Radar configuration with side antenna

12.1.2.1. Necessity of space-time processing

This configuration, presented in Figure 12.1, is typical of an air-ground surveillance system on-board a fast business jet. The antenna is in a side-looking position, and the waveform is a low-repetition frequency waveform, to avoid range ambiguities. The problem consists in detecting slow-moving targets, competing with clutter echoes coming through the main lobe of the antenna, exhibiting velocities comparable to those of possible targets.

In this configuration, Doppler frequency, F_d , of a clutter echo is directly related to its angle of arrival through the following relation – fundamental for side antennas (Figure 12.2):

$$F_d = \frac{2V}{\lambda} \sin \theta \quad [12.1]$$

producing Doppler spreading of the ground echoes, as seen through the main lobe:

$$\Delta F_d = \pm \frac{2V}{\lambda} \theta_{3dB}$$

where θ_{3dB} is the 3 dB width of the antenna diagram main lobe.

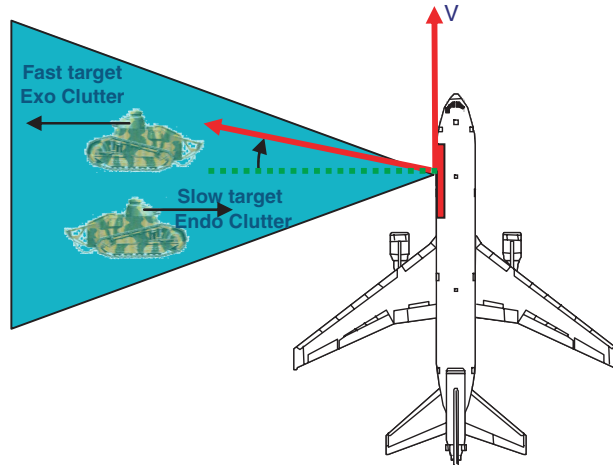


Figure 12.1. Side-looking radar configuration

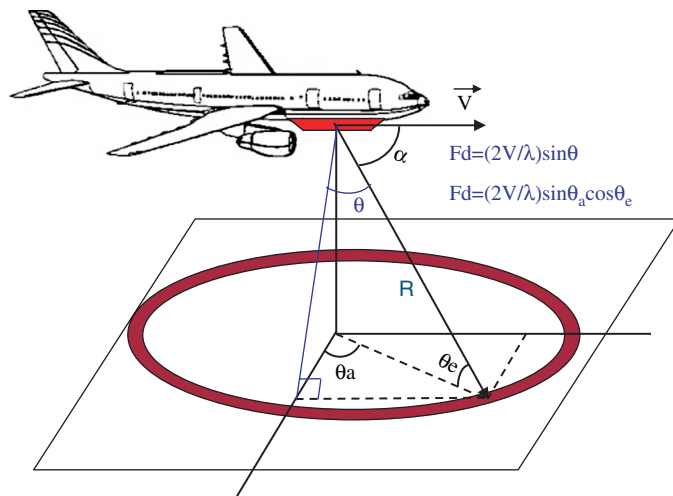


Figure 12.2. Geometry for side-looking radar configuration

Bi-dimensional space-time processing can then benefit from relation [12.1], showing that in the Doppler-angle plane clutter echoes are concentrated along a straight line, the “clutter edge”, occupying only a 1D domain in the 2D plane.

A bi-dimensional filter, operating along the clutter edge, as shown in Figure 12.3, allows rejection of clutter echoes while still preserving endo-clutter

targets, whereas no mono-dimensional processing, either temporal or spatial, would be able to simultaneously reject clutter and preserve target signals.

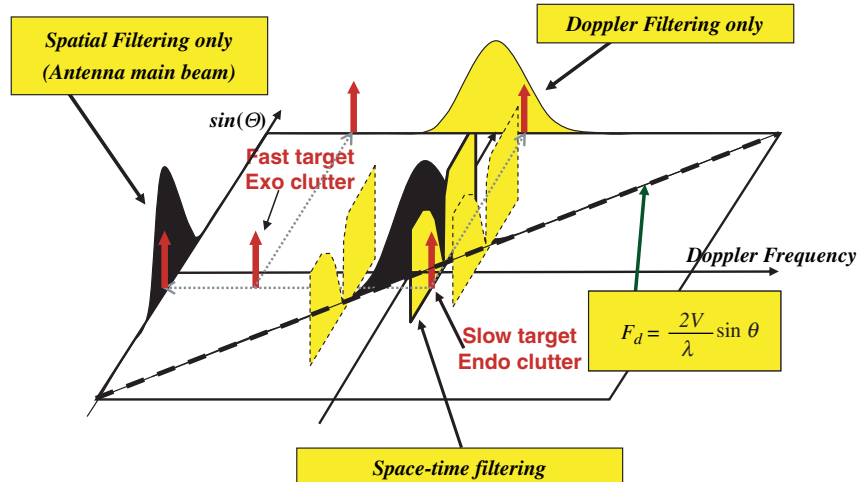


Figure 12.3. STAP filtering in the angle-Doppler plane, for side-looking configuration

12.1.2.2. STAP – Post-Doppler view

The previous analysis naturally leads to post-Doppler STAP processing: it is clear from Figure 12.3 that clutter cancelation can be obtained by a filter operating along the clutter edge, i.e. a Doppler stop-band filter whose null depends on the clutter angle of arrival. In the literature, this approach is referred to as factored STAP. For simplicity, we will assume in the following that the antenna is perfectly aligned along the velocity vector, and made of two identical sub-arrays receiving signals $s_0(t)$ and $s_1(t)$ (Figure 12.4), the distance between the two phase centers being D .

Under these hypotheses, an analytical expression can be derived for post-Doppler STAP processing. For a point echo incoming from angle of arrival θ at Doppler frequency F_d , the relation between signals on sub-arrays # 0 and 1 is:

$$\tilde{s}_1(F_d) = \tilde{s}_0(F_d) \cdot e^{-j2\pi \frac{D}{\lambda} \sin \theta} = A \cdot e^{-j2\pi \frac{D}{\lambda} \sin \theta}$$

with $\tilde{s}_0(F_d)$ and $\tilde{s}_1(F_d)$ as the Doppler spectra on sub-arrays # 0 and 1, θ the angle of arrival of echo at Doppler frequency F_d , D the distance between the phase centers of the two sub-arrays, and λ the wavelength.

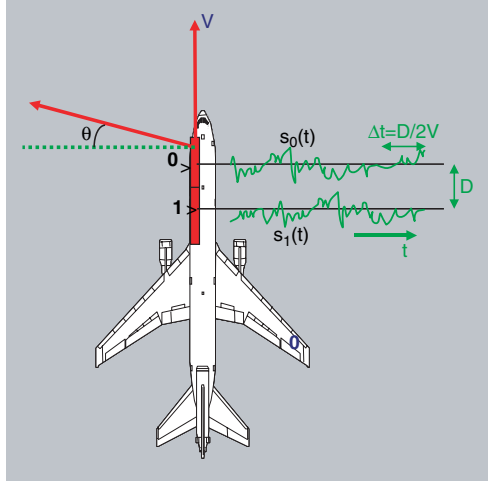


Figure 12.4. Antenna with two sub-arrays in side looking configuration

For clutter echo: $\sin \theta = F_d \cdot \frac{\lambda}{2V}$, and the clutter cancellation filter then calculates X_{post} :

$$X_{\text{post}} = \tilde{s}_1(F_d) e^{j2\pi F_d \frac{D}{2V}} - \tilde{s}_0(F_d) \quad [12.2]$$

This expression describes a spatial filter whose coefficient depends on frequency. It allows easy derivation of the filter velocity response, by noting that, for a target at the same Doppler frequency F_d and of radial velocity v_r :

$$\begin{aligned} F_d &= \frac{2V}{\lambda} \sin \theta + \frac{2v_r}{\lambda} \\ \Rightarrow \frac{D}{\lambda} \sin \theta &= F_d \frac{D}{2V} - \frac{v_r}{V} \frac{D}{\lambda} \\ \Rightarrow \tilde{s}_1(F_d) &= \tilde{s}_0(F_d) \cdot e^{-j2\pi \left(\frac{F_d D}{2V} - \frac{v_r D}{V \lambda} \right)} = A \cdot e^{-j2\pi \left(\frac{F_d D}{2V} - \frac{v_r D}{V \lambda} \right)} \end{aligned}$$

Then equation [12.2] becomes, with $\frac{D}{\lambda} = \frac{1}{2\theta_{3dB}}$:

$$X_{\text{post}} = A \cdot e^{j\pi \frac{v_r D}{V \lambda}} \cdot 2j \sin \left(\pi \frac{v_r D}{V \lambda} \right) = A \cdot e^{j\pi \frac{v_r D}{V \lambda}} \cdot 2j \sin \left(\frac{\pi}{4} \frac{v_r}{V} \frac{D}{\theta_{3dB}} \right)$$

leading to the following aspect for filter response (Figure 12.5):

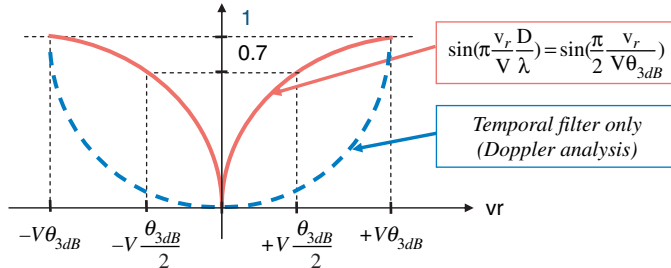


Figure 12.5. STAP filter velocity response for side-looking configuration

This kind of analysis allows fast estimation of the benefits to be expected from STAP, at the design phases of the system.

12.1.2.3. STAP – pre-Doppler view

Pre-Doppler STAP is dual from the previous post-Doppler processing, and can be derived in a straightforward manner through the Fourier transform of expression [BRE 76]:

$$X_{\text{pré}} = s_1 \left(t + \frac{D}{2V} \right) - s_0(t) = A e^{j2\pi F_d t} e^{j\pi \frac{v_r D}{V \lambda}} 2j \sin \left(\pi \frac{v_r}{V \lambda} \frac{D}{\lambda} \right)$$

In this canonical configuration, pre-Doppler STAP then consists in subtracting the signals coming through both sub-arrays, at instants shifted from $D/2V$ (Figure 12.6). This processing, ancestor of STAP, is known as DPCA (Displaced Phase Center Antenna). It may also be derived in an intuitive manner, noting that the phase center of the system transmitter-receiver #1 will take the place of the system transmitter-receiver #2, $D/2V$ later – and will then see exactly the same clutter echoes at that time.

12.1.3. Radar configuration with forward antenna

This configuration is encountered for airborne meteo or fighter radars. The waveform is typically medium repetition frequency, with ambiguities in range. In this situation, air targets must be detected against clutter echoes coming through side lobes as well as main lobes of the antenna.

The frontal implantation of the antenna leads to a distribution of clutter more complex than previously, in the angle Doppler plane. For one range cell (without taking into account possible ambiguities in range), it is concentrated on an ellipse, as shown in Figure 12.7.

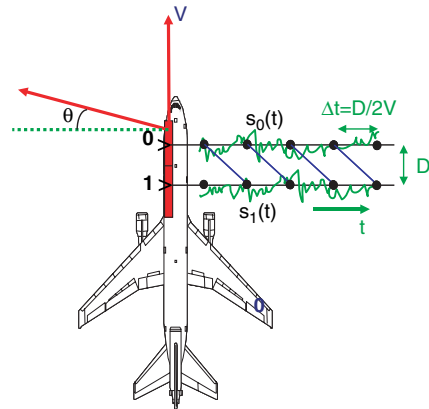


Figure 12.6. Pre-Doppler STAP for side-looking configuration

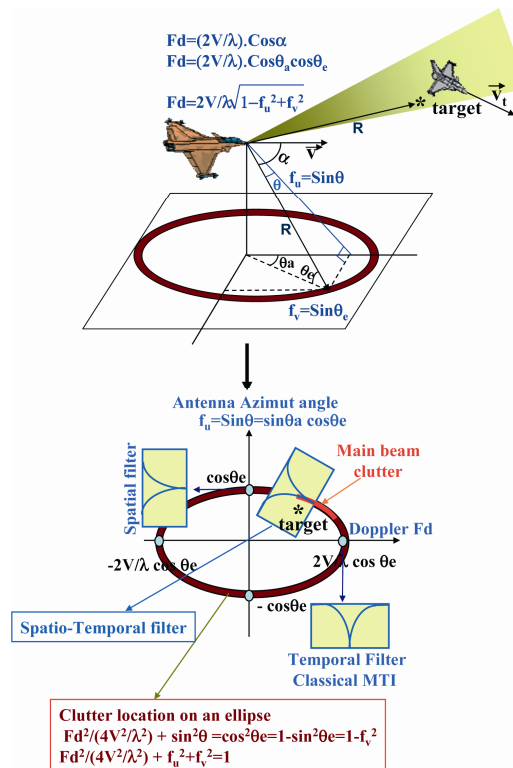


Figure 12.7. Clutter distribution in the azimuth-Doppler plane, for front radar configuration

The dimensions of this ellipse depend on the elevation angle, θ_e in Figure 12.7, under which the clutter is seen, and thus on the considered range. It becomes necessary, for clear understanding of STAP issue in this configuration (and more generally in every configuration different from side-looking), to consider not only the azimuth-Doppler plane, but the 3D azimuth-elevation-Doppler space, or more simply the cosines-Doppler volume (f_u, f_v, F_d).

Clutter is localized in this volume along the half-bowl shown in Figure 12.8.

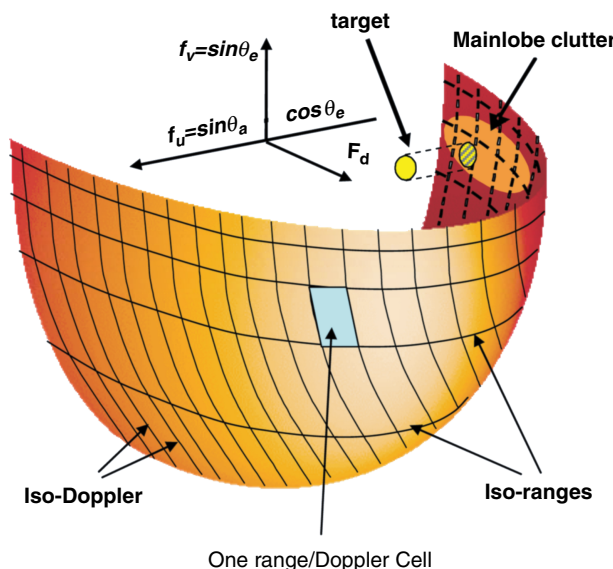


Figure 12.8. Three-dimensional localization of clutter – forward antenna configuration

For intermediate configuration between forward antenna configuration and side antenna configuration (and in particular side-looking with crab angle), the clutter is localized on the ellipsoid shown in Figure 12.9, left. The limit form for pure side looking is the half-plane (Figure 12.9, right). The cut for a given elevation angle (i.e. a given range) in Figure 12.9, right, corresponds to the straight line in Figure 12.3 in the azimuth-Doppler plane.

The intermediate and forward antenna configurations thus create a dependence with range for the clutter echoes angle-Doppler representation. To this non-stationarity of clutter in range is generally added the presence of range ambiguities, and of course the natural heterogeneity of physical clutter, as described in section 12.4.3. This will have direct consequences on the adaptive learning of STAP filter coefficients, which will have to be limited to a small extent in range.

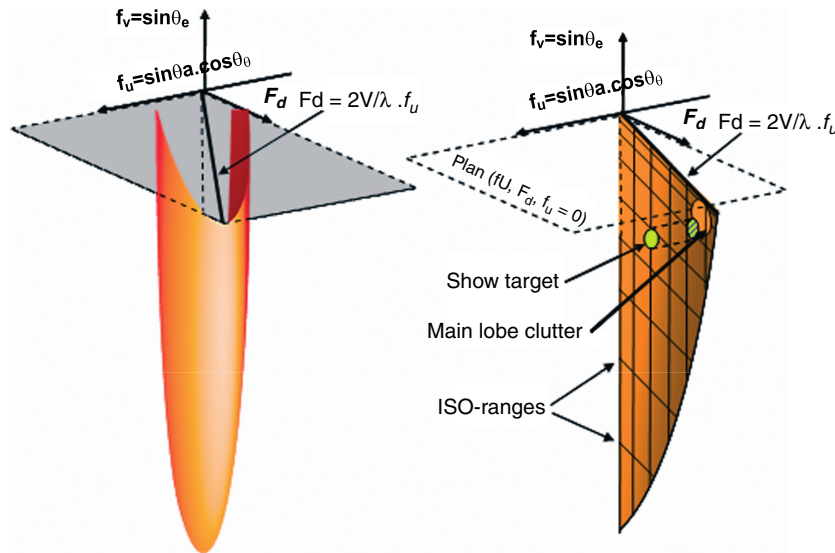


Figure 12.9. Three-dimensional localization of clutter – intermediate antenna configuration (left), side-looking antenna configuration (right)

Moreover, it can be seen that, strictly speaking, a 3D STAP filter is required to cancel clutter echoes coming from ambiguous range cells. Indeed, in the range cell of a possible target, different rings from Figure 12.8 will be superposed, corresponding to ambiguous range cells (folding of Figure 12.8 parallel to the vertical axis, for horizontal flight, flat terrain scenarios): these clutter echoes will be canceled by a space-time filter taking advantage of the elevation angle.

12.2. Space-time processing as a spectral estimation problem

In this section, space-time processing principles are described for a radar with several sub-arrays and associated receiving channels. For the sake of simplicity, an antenna made of identical adjacent sub-arrays is considered, but the theory can be extended to a more general antenna structure, and to different sub-arrays distributed on a plane, by changing the expression of the “expected signal” or “replica”, and of the associated replicas.

12.2.1. Overview of space-time processing

Consider the situation shown in Figure 12.12. The antenna transmits successive periodic pulses with repetition period T_r , whose envelope is shown in Figure 12.10,

right. On receive, an array of antennas, assumed to be linear and regular, receives the signals, whose envelopes are shown in Figure 12.10, left. Without noise, these samples are characterized by a phase shift φ_v from pulse to pulse, and φ_0 from channel to channel, as illustrated.

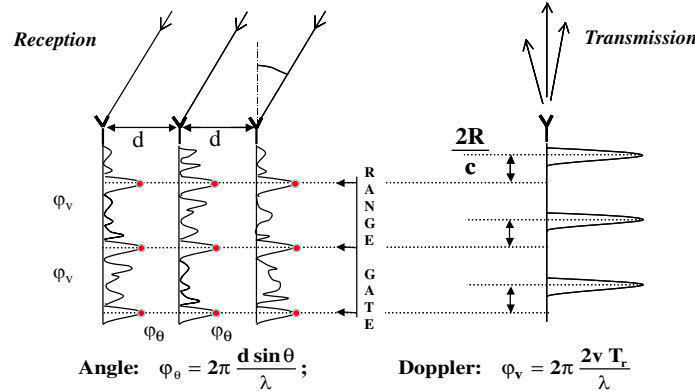


Figure 12.10. Multi-channel reception

The principle of standard coherent processing consists in summing these samples, after compensating for the phase shifts for a velocity-angle hypothesis (v, θ) – and performing that compensation/summation in parallel for every possible hypothesis.

12.2.2. Processing in additive white noise

To describe this processing more precisely, consider a receiving array with N channels corresponding to regularly spaced sub-arrays, receiving a burst of M pulses. D being the distance between the phase centers of adjacent sub-arrays, G_n the antenna diagram of the sub-array # n , T_r the repetition period. The vector $a(v, \theta)$ of the signals received from a target of unit amplitude in direction θ with velocity v is written:

$$a(v, \theta) = s_{t,M}(v) \otimes s_s(\theta)$$

where $s_s(\theta)$ and $s_{t,M}(v)$ are, respectively, the steering vectors, for space with dimension N and time with dimension M . More precisely, for the receiving channel # n and time sample # m , the corresponding component of vector a is written:

$$a_{nm}(v, \theta) = G_n^{1/2}(\theta) \cdot e^{\frac{2j\pi}{\lambda} n D \sin \theta} \cdot e^{\frac{2j\pi}{\lambda} m 2v T_r}$$

If α is the complex amplitude of the target, and n the vector of additive noise samples, the received vector z , made of the received samples marked with a point in Figure 12.10, is written:

$$z = \alpha a(\nu, \theta) + n \quad \text{with} \quad E[n n^H] = \sigma^2 Id \quad (.)^H \text{ for conjugate transpose}$$

In these conditions, the optimal processing can be written as a spectral estimation problem consisting in finding parameters $\hat{\alpha}$ that minimize:

$$\hat{\alpha} = \underset{\alpha}{\operatorname{Argmin}} \left\{ E \left[(z - \alpha a(\nu, \theta))^H (z - \alpha a(\nu, \theta)) \right] \right\}$$

Minimization of the previous quantity, with respect to α , leads to:

$$\hat{\alpha} = \frac{a^H(\nu, \theta)z}{a^H(\nu, \theta)a(\nu, \theta)} \quad \text{spectral estimation of amplitude}$$

$\hat{\alpha}$ is an unbiased estimate of α , and its variance is:

$$Var[\hat{\alpha}] = \frac{\sigma^2}{a^H(\nu, \theta)a(\nu, \theta)}$$

The detection test then comes naturally to compare for each hypothesis (ν, θ) the quantity $|y(\nu, \theta)|^2 = \frac{|\hat{\alpha}|^2}{Var[\hat{\alpha}]}$ to a detection threshold depending on the required false alarm rate:

$$|y(\nu, \theta)|^2 = \frac{1}{\sigma^2} \frac{|a^H(\nu, \theta)z|^2}{a^H(\nu, \theta)a(\nu, \theta)} \stackrel{\text{target present}}{>} \eta$$

This external product of the received vector signal z with the replica vector $a(\nu, \theta)$ performs the summation in phase of the received samples for hypothesis (ν, θ) .

This processing would also have been found directly by inserting $\hat{\alpha}$ in place of α in the expression $E \{ (z - \alpha a(\nu, \theta))^H (z - \alpha a(\nu, \theta)) \}$. The detection consists then in a test on the residual output error after estimating parameters α .

Finally, a more flexible and general formulation which will be useful in the following can be established by stating the detection problem as an estimation problem of the amplitude with an imposed linear structure of the estimator:

$$\hat{\alpha} = w^H z$$

The estimator (or filter) w^H is chosen classically so that $\hat{\alpha}$ is a non-biased estimate of α with minimal variance, which results in the following linearity constrained minimization:

$$\underset{w}{\text{Min}} \left\{ w^H E[nn^H]w \right\} \quad \text{s.t.} \quad w^H a(\nu, \theta) = 1$$

In white noise, $E[nn^H] = \sigma^2 Id$, the solution of the minimization is:

$$w^H = \frac{a^H(\nu, \theta)}{a^H(\nu, \theta)a(\nu, \theta)} \quad \text{and} \quad \hat{\alpha} = \frac{a^H(\nu, \theta)z}{a^H(\nu, \theta)a(\nu, \theta)}$$

12.2.3. Processing in additive colored noise

When the additive noise is not white (i.e. when it is not evenly distributed on the (ν, θ) plane, which is indeed the case for clutter echoes described in the previous section), it can be characterized by its correlation matrix Γ : $\Gamma = E[n n^H]$, matrix measuring the correlation between all possible couples of space-time samples. The structure of Γ is Hermitian block toeplitz in case of space-time data:

$$\Gamma = \begin{bmatrix} \Gamma_s(\mathbf{0}) & \Gamma_s(T_r) & \cdots & \Gamma_s((M-1)T_r) \\ \Gamma_s^H(T_r) & \Gamma_s(\mathbf{0}) & \cdots & \Gamma_s((M-2)T_r) \\ \vdots & \vdots & \ddots & \vdots \\ \Gamma_s^H((M-1)T_r) & \cdots & \cdots & \Gamma_s(\mathbf{0}) \end{bmatrix}$$

where $\Gamma_s(0)$ is the classical spatial correlation between channels at the same time and $\Gamma_s(mT_r)$ is correlation between channels with time lag mT_r .

It is worth noting that while $\Gamma_s(0)$ is Hermitian, it is not the case for $\Gamma_s(mT_r)$ (correlation between sensor #n1 and sensor #n2 shifted m time lags is not the complex conjugate of correlation between sensor #n2 shifted m time lags and sensor n2).

In these colored noise conditions, assuming Γ to be known, it can be shown [CHE 02] that the optimal processing on receive, under Gaussian assumptions on n ,

consists in coming back to the previous situation by introducing a whitening filter F on the signal channel, and copying this filter on the replica channel.

The whitened signal is then the vector $z_w = Fz$, the whitened replica is $a_w(v, \theta) = Fa(v, \theta)$. This whitening matrix F is defined by the whitening condition:

$$\mathbb{E}[Fn n^H F^H] = Id, \text{ identity matrix}$$

The filter F performs the whitening and the normalization of noise. As $\mathbb{E}[n n^H] = \Gamma$ by definition, this condition is also written: $F^H F = \Gamma^{-1}$.

The optimal processing then consists in evaluating the following expression, as shown in Figure 12.11:

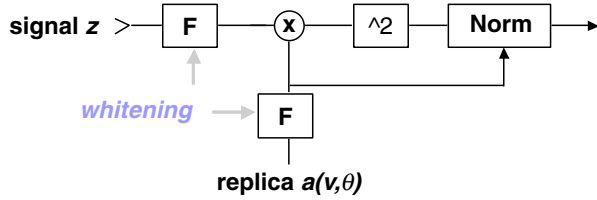


Figure 12.11. Processing in additive colored noise

$$y(v, \theta) = \frac{a_w^H(v, \theta) z_w}{\sqrt{a_w^H(v, \theta) a_w(v, \theta)}} = \frac{a^H(v, \theta) F^H F z}{\sqrt{a^H(v, \theta) F^H F a(v, \theta)}}$$

The normalization (denominator) is necessary since after whitening the whitened replicas $a_w(v, \theta)$ do not have the same energy – especially those corresponding to directions and Doppler near the clutter edge.

Finally, the optimal processing consists in evaluating, for each possible couple (v, θ) , the filtered output $y(v, \theta)$:

$$y(v, \theta) = \frac{\mathbf{a}^H(v, \theta) \Gamma^{-1} z}{\sqrt{a^H(v, \theta) \Gamma^{-1} a(v, \theta)}}$$

and comparing $|y(v, \theta)|^2$ to a detection threshold depending on the required false alarm rate.

In this expression, as indicated in Figure 12.11, the numerator represents the correlation (scalar product) of vector z of received signals with replicas $a(v, \theta)$ of

the expected signals, after whitening of these two vectors by a whitening matrix F . Similarly, the denominator represents the normalization by the energy of the whitened replica.

As shown in section 12.2.2, the previous processing (optimal for Gaussian noise) could have also been obtained via the estimation problem, on the whitened signals and replicas:

$$\hat{\alpha} = \underset{\alpha}{\operatorname{Argmin}} \left\{ E \left[(z_w - \alpha a_w(v, \theta))^H (z_w - \alpha a_w(v, \theta)) \right] \right\}$$

or as $z_w = Fz$, $a_w(v, \theta) = Fa(v, \theta)$, and $F^H F = \Gamma^{-1}$

$$\hat{\alpha} = \underset{\alpha}{\operatorname{Argmin}} \left\{ E \left[(z - \alpha a(v, \theta))^H \Gamma^{-1} (z - \alpha a(v, \theta)) \right] \right\}$$

Minimization of the previous quantity, with respect to α , leads to:

$$\hat{\alpha} = \frac{a^H(v, \theta) \Gamma^{-1} z}{a^H(v, \theta) \Gamma^{-1} a(v, \theta)}$$

$\hat{\alpha}$ is an unbiased estimate of α , and its variance is:

$$\operatorname{Var}[\hat{\alpha}] = \frac{1}{a^H(v, \theta) \Gamma^{-1} a(v, \theta)}$$

Then the detection test will operate on:

$$|y(v, \theta)|^2 = \frac{|\hat{\alpha}|^2}{\operatorname{Var}[\hat{\alpha}]} = \frac{\mathbf{a}^H(v, \theta) \Gamma^{-1} z}{\sqrt{a^H(v, \theta) \Gamma^{-1} a(v, \theta)}} \stackrel{\text{target present}}{>} \eta$$

Finally, as before, a more flexible and general formulation which will be useful in the following can be established by stating the detection problem as an estimation problem of the amplitude with an imposed linear structure of the estimator:

$$\hat{\alpha} = w^H z$$

The estimator (or filter) w^H is chosen classically so that $\hat{\alpha}$ is a non-biased estimate of α with minimal variance, which results in the following linearly constrained minimization:

$$\begin{aligned}
& \underset{w}{\operatorname{Min}} \left\{ w^H E[n n^H] w - w^H \Gamma w \right\} \quad \text{s.t.} \quad w^H a(\nu, \theta) = 1 \\
& \Rightarrow \hat{\alpha} = w^H z = \frac{a^H(\nu, \theta) \Gamma^{-1} z}{a^H(\nu, \theta) \Gamma^{-1} a(\nu, \theta)} \\
& \operatorname{Var}[\hat{\alpha}] = w^H \Gamma w = \frac{1}{a^H(\nu, \theta) \Gamma^{-1} a(\nu, \theta)} \\
& |y(\nu, \theta)|^2 = \frac{|\hat{\alpha}|^2}{\operatorname{Var}[\hat{\alpha}]} = \frac{\mathbf{a}^H(\nu, \theta) \Gamma^{-1} z}{\sqrt{a^H(\nu, \theta) \Gamma^{-1} a(\nu, \theta)}} = |y(\nu, \theta)|^2 \stackrel{\text{target present}}{>} \eta
\end{aligned}$$

It is worth noting that the variance of $\hat{\alpha}$ is also the output noise power after applying filter w .

In actual practice, the noise correlation matrix Γ is not known *a priori*. When these noises are essentially constituted by clutter echoes, it is often legitimate to assume that clutter echoes statistics vary slowly with range. If z_k is the vector of received signals in the range cell # k , and if K signal free range cells are supposed available to train the processor. Then the minimization problem can be reformulated as a minimization of the averaged output noise power over the K range cells:

$$\underset{w}{\operatorname{Min}} \left\{ \frac{1}{K} \sum_{k=1}^K w^H z_k z_k^H w \right\} \quad \text{s.t.} \quad w^H a(\nu, \theta) = 1$$

The solution is:

$$w^H = \frac{\mathbf{a}^H(\nu, \theta) \hat{\Gamma}^{-1}}{\mathbf{a}^H(\nu, \theta) \hat{\Gamma}^{-1} \mathbf{a}(\nu, \theta)}$$

where:

$$\hat{\Gamma} = \frac{1}{K} \sum_k [z_k \ z_k^H] \text{ is the estimated covariance matrix.}$$

Finally, the processing consists in evaluating:

$$y(\nu, \theta) = \frac{a^H(\nu, \theta) \hat{\Gamma}^{-1} z_0}{\sqrt{a^H(\nu, \theta) \hat{\Gamma}^{-1} a(\nu, \theta)}}$$

and comparing $|y(\nu, \theta)|^2$ to a threshold depending on the required false alarm rate.

In the literature, this processing is referred to as the AMF detector (adaptive matched filter detector). It is optimal under Gaussian interference assumptions, and does make sense only if the statistics of the training data z_k are representative of the interference statistics in the CUT z_0 (i.e. for Gaussian interference $E[z_k z_k^H] = \Gamma$).

The choice of the training data will be analyzed in the following section.

12.3. STAP architectures

12.3.1. Generalities and notations

As already mentioned, STAP is an adaptive bi-dimensional filtering, where different spatial channels are combined at different instants (digital time signals from the different sub-arrays), through different filtering coefficients, estimated from training data obtained from range cells, in the neighborhood of the CUT. These coefficients are generally obtained – in a more or less straightforward manner – from the correlation matrix of the signals received from clutter, which is a key element in the adaptation. Furthermore, the implementation of STAP processing must keep in-line with the objectives of radar processing: obtaining a high probability of detection while maintaining a low false alarm rate. For these reasons, the STAP technique should always guarantee the following:

- 1) Selection of training data with same statistics as the CUT;
- 2) Exploitation of the training data to cancel the clutter, while still preserving potential targets in the CUT;
- 3) Detection by comparison of the residual level in the CUT after filtering and comparison (if needed) to the average level in secondary data, obtained from filtering of the surrounding range-Doppler cells.

In the following, the standard conventions will be:

- N : number of spatial channels (sub-arrays);
- M : number of time samples per channel (number of pulses, or number of time lags);
- M_p : number of pulses in a coherent radar burst;
- K : number of range cells.

The data used in the STAP filter can be represented as a “data cube” (Figure 12.12):

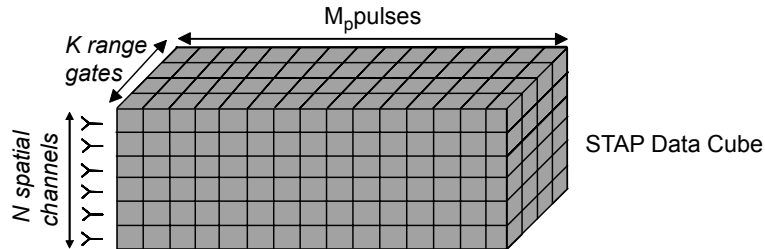


Figure 12.12. STAP data cube

Training data will refer to the data used for estimating the filter coefficients, and secondary data will refer to the data used for estimating the local residual noise for CFAR operation. Training data are a reference for the filtering, and secondary data are a reference for the thresholding.

12.3.2. Pre-Doppler STAP

Optimal detection theory, under stationary hypothesis, leads to an architecture where STAP filtering and CFAR detection are simultaneously performed, with M (number of pulses used in the filter) equal to M_p [BRE 73, BRE 76, KLE 02]. Radar bursts, however, are typically made of ~ 100 pulses in medium repetition frequency modes, and ~ 1000 pulses in high repetition frequency modes, which makes it difficult to implement such optimal architectures (large dataset required for training, and huge computing power requirement). It then becomes necessary to define sub-optimal architectures leading to more affordable complexities.

The first approach – and the most direct one – consists in partitioning the data cube with dimension KNM_p , into smaller blocks with dimension KNM , and implementing STAP filtering in a sliding way to such sub-blocks. This approach makes sense because interference cancelation generally requires a limited order for the filter (typically between 3 and 12). This leads to several pre-Doppler architectures, which are sub-optimal implementations of the STAP filtering for a whole burst.

12.3.2.1. PRI staggered pre-Doppler STAP architecture

The PRI staggered pre-Doppler architecture is the sub-optimal implementation of the AMF detector of section 12.2.3. It is obtained naturally while trying to implement the AMF detector in a sliding way to time sub-blocks.

To derive the PRI-staggered pre-Doppler STAP architecture, the model of received space-time signal on a whole burst for one range cell is modified as follows:

$$Z = \alpha a(\nu, \theta) s_{t, M_p - M}^T(\nu) + N$$

where the received signals have been arranged into a $(MN \times (M_p - M + 1))$ matrix Z and $s_{t, M_p - M}^T = \left[1, e^{\frac{2j\pi}{\lambda} m_1 2\nu T_r}, \dots, e^{\frac{2j\pi}{\lambda} (M_p - M) 2\nu T_r} \right]$. In this expression, the j th column of Z represents the (sliding) vector signal starting from time lag j , with MN components (from time lag j , sensor 0, to time lag $j + M - 1$, sensor $N - 1$)

In the following, subscripts $\nu, \theta, M_p - M$ will be omitted for simplicity.

12.3.2.1.1. PRI staggered pre-Doppler STAP architecture with clutter only reference data sets – the sub-block AMF STAP filter

If $\{Z_k\}$ are the matrix of received data in $k = \{1, 2, \dots, K\}$ clutter only range cells, and Z_0 the matrix signal for the CUT, then the minimization problem can be formulated in a similar way as previously, but in a two step procedure:

1. Find filter w such as:

$$w = \underset{w}{\operatorname{Min}} \left\{ \frac{1}{K(M_p - M + 1)} \sum_{k=1}^K w^H Z_k Z_k^H w \right\} \quad \text{s.t.} \quad w^H a(\nu, \theta) = 1$$

2. Estimate the amplitude with w obtained in step 1:

$$\hat{\alpha} = \underset{\alpha}{\operatorname{Min}} \left\{ (w^H Z_0 - \alpha s_t^T)(w^H Z_0 - \alpha s_t^T)^H \right\}$$

Step 1 gives:

$$w^H = \frac{a^H \hat{\Gamma}^{-1}}{a^H \hat{\Gamma}^{-1} a}$$

$$\hat{\Gamma} = \frac{1}{K(M_p - M + 1)} \sum_{k=1}^K Z_k Z_k^H$$

$\hat{\Gamma}$ is the estimated covariance matrix

Step 2 then gives:

$$\hat{\alpha} = w^H g = \frac{a^H \hat{\Gamma}^{-1} g}{a^H \hat{\Gamma}^{-1} a} \quad \text{where} \quad g = \frac{Z_0 s_t^*}{s_t^T s_t}$$

The detection test will be, as $w^H \hat{\Gamma} w = \frac{1}{a^H \hat{\Gamma}^{-1} a}$ is the estimated residual output power after STAP filtering:

$$\frac{|a^H \hat{\Gamma}^{-1} g|^2}{a^H \hat{\Gamma}^{-1} a} > \eta$$

The vector \mathbf{g} of size MN can be recognized as being simply the Fourier transform of each line of the matrix Z which involves staggered FFT in time to be computed; hence the name of PRI staggered pre-Doppler STAP. Although the STAP filter is applied after Doppler analysis, it is obviously a pre-Doppler architecture because the covariance matrix involved for STAP filtering is the space-time covariance matrix. This approach presented in detail in [SAV 06] is also called by the author pre-Doppler trained post-Doppler STAP. Staggered Doppler analysis is needed before STAP filtering because the space-time steering vector \mathbf{a} depends on the velocity hypothesis versus Doppler analysis and also ensures to retrieve the overall coherent gain of the whole burst. The PRI staggered pre-Doppler STAP architecture is presented in Figure 12.13 for $M = 3$ taps and $N = 6$ spatial channels.

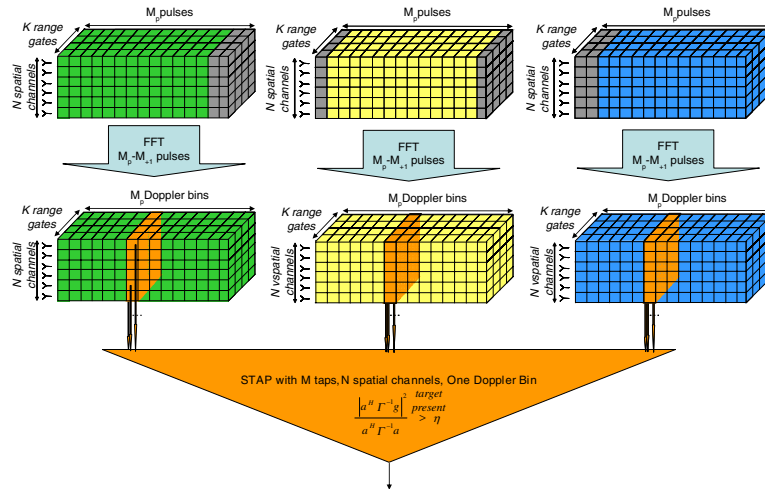


Figure 12.13. AMF PRI staggered pre-Doppler STAP architecture

The computing load associated with the computation of the adaptive coefficients is typically of the order $O(N^3M^3)$ (inversion of an NM matrix). However, if the coefficients do not require frequent updating in range and time (air-ground configuration with clutter stationary in range, non-maneuvering platform), the total computational load will be dominated by the filtering operation, $O(KNM^*M_p)$, and the staggered FFTs, $O(KMN^*4M_p\log_2 M_p)$, which have to be performed at the radar coherent burst rhythm (typically tens of ms). This architecture is known as “range independent pre-Doppler STAP”.

12.3.2.1.2. PRI staggered pre-Doppler STAP architecture with no clutter only reference data sets – the maximum likelihood estimation detector (MLED)

When clutter is highly heterogeneous and/or in case of high target densities, the previous assumption of available representative clutter only reference data $\{Z_k\}$ is no longer valid. In this case, a STAP algorithm that avoids the need for training data is required. In a similar way as before, the problem is now stated in terms of *combined* filtering/amplitude estimation as follows:

$$\underset{w, \alpha}{\text{Min}} \left\{ (w^H Z_0 - \alpha s_t^T)(w^H Z_0 - \alpha s_t^T)^H \right\} \quad \text{s.t.} \quad w^H a(\nu, \theta) = 1$$

The solution is:

$$\hat{\alpha} = w^H g = \frac{a^H \hat{Q}^{-1} g}{a^H \hat{Q}^{-1} a} \quad \text{where} \quad g = \frac{Z_0 s_t^*}{s_t^T s_t^*}$$

$$w^H = \frac{a^H \hat{Q}^{-1}}{a^H \hat{Q}^{-1} a}$$

$$\hat{Q} = \frac{Z_0 Z_0^H}{s_t^T s_t^*} - gg^H = \frac{Z_0 Z_0^H}{M_p - M + 1} - gg^H$$

\hat{Q} is the estimated signal free covariance matrix

The above expression of $\hat{\alpha}$ and \hat{Q} has been shown to be the maximum likelihood estimator for amplitude α (\hat{Q} is the estimation of the signal free clutter only covariance matrix). This estimator is also called APES in the literature [LI 96].

The detection test will be:

$$\frac{\left| a^H \hat{Q}^{-1} g \right|^2}{a^H \hat{Q}^{-1} a} \stackrel{\text{target present}}{>} \eta$$

as $w^H \hat{Q} w = \frac{1}{a^H \hat{Q}^{-1} a}$ is the estimated residual output power after STAP filtering.

This test is called the maximum likelihood estimation detector in [ABO 05]. The architecture of the processing is the same as Figure 12.13, except for the final test where matrix $\hat{\mathbf{F}}^{-1}$ is replaced by $\hat{\mathbf{Q}}^{-1}$.

The estimation of the covariance matrix $\hat{\mathbf{Q}}$ is a key factor of performance, and the MLED will be used only when sufficiently long bursts are available to make this estimation correctly.

12.3.2.1.3. PRI staggered pre-Doppler STAP architecture with no clutter only reference datasets – the minimum variance method (MVM)

This method has already been presented in Chapter 7. Its extension to STAP can be found in [CHE 06]. It is derived here in a formulation similar to the MLED of previous section for comparison. As the MLED, the MVM avoids the need for clutter-only training data. The problem for MVM can be stated as follows, in a two-step procedure identical to that of the AMF STAP filter of section 12.3.2.1.1:

1. Find filter w such as:

$$\underset{w}{\operatorname{Min}} \left\{ \frac{(w^H Z_0)(w^H Z_0)^H}{(M_p - M + 1)} \right\} \quad \text{s.t.} \quad w^H a(\nu, \theta) = 1$$

2. Estimate the amplitude for w obtained in step 1:

$$\underset{\alpha}{\operatorname{Min}} \left\{ (w^H Z_0 - \alpha s_t^T)(w^H Z_0 - \alpha s_t^T)^H \right\}$$

Step 1 gives:

$$w^H = \frac{a^H \hat{\mathbf{R}}^{-1}}{a^H \hat{\mathbf{R}}^{-1} a}$$

with $\hat{\mathbf{R}} = \frac{Z_0 Z_0^H}{M_p - M + 1}$

$\hat{\mathbf{R}}$ is the estimated signal +clutter covariance matrix

Step 2 gives:

$$\hat{\alpha} = w^H g = \frac{a^H \hat{\mathbf{R}}^{-1} g}{a^H \hat{\mathbf{R}}^{-1} a} \quad \text{where} \quad g = \frac{Z_0 s_t^*}{s_t^T s_t^*}$$

The architecture of the processing is again the same as Figure 12.13, except for the final test which can be done only on the estimated amplitude as there is here no estimation of the clutter only covariance matrix:

$$\frac{|a^H \hat{\mathbf{R}}^{-1} g|^2}{|a^H \hat{\mathbf{R}}^{-1} a|^2} > \eta(\nu, \theta)$$

It is important to notice that this is just a Doppler-angle representation of the clutter + noise situation in the CUT and no longer a joint clutter suppression and CFAR detection procedure as for the previous methods. The thresholding should therefore also guarantee clutter suppression, for instance by defining, in the Doppler-angle representation, a contour inside which every return is assumed to be a clutter return, and/or by defining a detection threshold locally adapted on secondary data obtained from filtering of the surrounding range-Doppler cells (hence the dependence of the threshold on target position in the angle-Doppler plane).

Compared with the MLED, the MVM exhibits better resolution but a higher variance on amplitude estimate (it is not the maximum likelihood for amplitude estimation). It shows less sensitivity compared with the MLED and has to be reserved for high SNR situation, where what matters is spectral resolution, or for scenarios where the clutter is very non-stationary (urban clutter, for instance), or where there are too many targets – and therefore a high probability to include targets in the training data.

Finally, as for the MLED, the estimation of the covariance matrix is a key factor of performance, and the MVM will be used only when sufficiently long bursts are available to make this estimation correctly.

12.3.2.2. Space-time FIR filter

This approach has been widely discussed [KLE 02] and is sometimes referred simply to as “pre-Doppler STAP” [WAR 94].

The rationale for space-time FIR filtering is to avoid the added computational burden due to staggered FFT’s of the sub-block AMF architecture of Figure 12.13. It can be formulated using the same general scheme as in section 12.3.2.1.1:

1. First step, find filter w such as:

$$w = \underset{w}{\operatorname{Min}} \left\{ \frac{1}{K(M_p - M + 1)} \sum_{k=1}^K w^H Z_k Z_k^H w \right\} \quad \text{s.t.} \quad w^H e = 1$$

$$e = \underbrace{[1 1 \cdots 1]}_{N \text{ times}} \underbrace{[0 0 0 \cdots 0]}_{(NM - N) \text{ times}}^T$$

The constraint vector e in place of $a(v, \theta)$ no longer depend on (v, θ) , and can be viewed as the required filter solution when the interference is only white noise (quiescent solution). Expression of e above is given in the usual case of non-overlapping sub-arrays, with antenna weighting applied at element level.

2. Second step, estimate the amplitude for w obtained in step 1:

$$\hat{\alpha} = \underset{\alpha}{\operatorname{Min}} \left\{ (w^H Z_0 - \alpha s_t^T) (w^H Z_0 - \alpha s_t^T)^H \right\}$$

Step 1 gives:

$$w^H = \frac{e^H \hat{\Gamma}^{-1}}{e^H \hat{\Gamma}^{-1} e}$$

$$\hat{\Gamma} = \frac{1}{K(M_p - M + 1)} \sum_{k=1}^K Z_k Z_k^H$$

$\hat{\Gamma}$ is the estimated covariance matrix

Step 2 gives then:

$$\hat{\alpha} = w^H g = \frac{e^H \hat{\Gamma}^{-1} g}{e^H \hat{\Gamma}^{-1} e} \quad \text{where} \quad g = \frac{Z_0 s_t^*}{s_t^T s_t^*}$$

The detection test will be, as $w^H \hat{\Gamma} w = \frac{1}{e^H \hat{\Gamma}^{-1} e}$ is the estimated residual output power after STAP filtering:

$$\frac{|e^H \hat{\Gamma}^{-1} g|^2}{e^H \hat{\Gamma}^{-1} e} = \frac{|(e^H \hat{\Gamma}^{-1} X) s_t^*|^2}{(e^H \hat{\Gamma}^{-1} e)(s_t^T s_t^*)} \stackrel{\text{target present}}{>} \eta$$

As constraint vector e no longer depends on target Doppler frequency, STAP filtering can be implemented as a pre-processing prior to Doppler analysis, avoiding the necessity of staggered FFT.

This pre-processing is a transverse filter sliding along the data with M adaptive coefficients on each spatial channel (Figure 12.14).

12.3.2.3. Pre-Doppler STAP and side-looking configuration

Pre-Doppler STAP may be a good solution for side-looking configuration, where the simplicity of the angle-Doppler relation for clutter echoes (Figure 12.3) and its invariance with range allow using the same adaptive coefficients for a large number of range cells, and for the whole angle-Doppler plane.

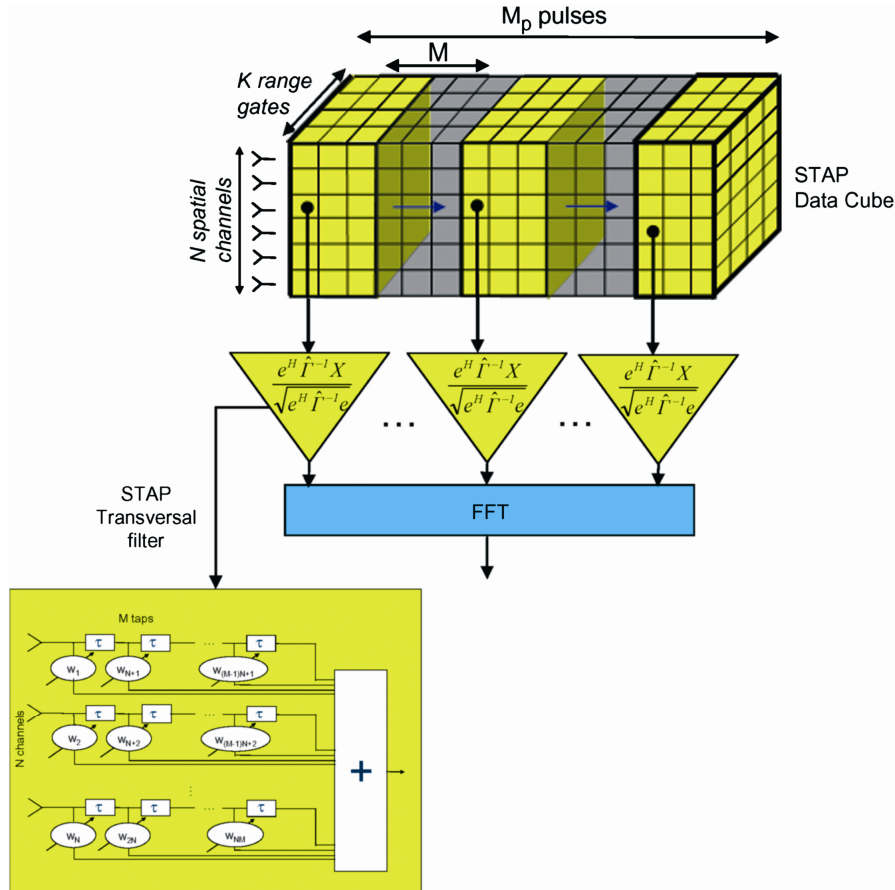


Figure 12.14. Space–time FIR filter pre-Doppler STAP architecture

The order of magnitude of the number of pulses to take into account in a STAP block is directly related to the clutter spectrum extent: roughly speaking, the length of the impulse response of the filter should be at least equal to the inverse of the clutter spectrum extent (see Figure 12.5):

$$M = \frac{\lambda}{2} \frac{1}{V \theta_{3dB} T_r} = \frac{L}{2V T_r}$$

12.3.2.4. Pre-Doppler STAP and front antenna configuration

For more general configurations, and in particular for a front antenna with range ambiguities, the complexity of the angle-Doppler relation for clutter echoes

(Figure 12.8) makes it difficult to cancel with the same filter the echoes incoming through the main lobe and through side lobes, and to use the same filter for different range gates.

12.3.2.4.1. Main lobe clutter filtering

If only main lobe clutter cancellation is required, the issue is very similar to the side-looking configuration. Indeed, in the main lobe, the angle-Doppler relation can be assimilated to a straight line (tangent to the clutter ellipse in Figure 12.7). This relation is also largely stationary with range, excepted for very low elevation configurations – and pre-Doppler STAP is still an adequate solution.

The order of magnitude of the number of pulses M in a STAP block is, as previously, related to the clutter spectral width as was the case for the side-looking configuration:

$$M = \frac{\lambda}{2} \frac{1}{(V \cdot |\sin \theta_a|) \cdot \theta_{3dB} \cdot T_r} = \frac{L}{2V \cdot |\tan \theta_a| \cdot T_r}$$

where θ_a is the azimuth angle (see Figure 12.7) between the main lobe clutter axis and the normal to the antenna.

12.3.2.4.2. Side lobe clutter cancellation

Side lobe clutter cancellation can be largely improved if STAP filtering is performed independently on different regions of the clutter ellipse (Figure 12.8). In the case of pre-Doppler STAP, this is done by partitioning the data in range, and performing STAP filtering independently on these different regions in range. This is known as “range dependent” pre-Doppler STAP.

In principle, this is equivalent to processing differently each clutter ellipse from Figure 12.7 (iso-range of Figure 12.8). If there are ambiguities in range, STAP filtering should indeed involve spatial degrees of freedom in elevation, to be added to the spatial degrees of freedom in azimuth. The number of time samples in the STAP filter is then difficult to determine analytically and depends strongly on the exact configuration, on the clutter spectral extent, and its power level.

The main disadvantage of “range dependent STAP” approach is the difficulty to fulfill requirements as stated at the beginning of this section. Rapid adaptation in range can lead to insufficient training data, and increasing this adaptation zone may involve training data not completely representative of the CUT. Moreover, it is clearly difficult to cancel the clutter on a wide region of the elliptical clutter ring covered by training data.

12.3.3. Post-Doppler STAP

12.3.3.1. Introduction

An obvious alternative to pre-Doppler STAP consists in performing first the standard Doppler analysis on each sub-array channel, and then the spatial adaptive clutter cancelation, *independently* in each Doppler bin. This approach is called post-Doppler STAP. When pulse compression is also performed before STAP filtering, the total coherent integration has been obtained, and STAP can then be combined with CFAR detection [KEL 86]. Anyway, the approach remains sub-optimal, due to the implicit assumption that spatial filtering can be applied independently for each Doppler frequency.

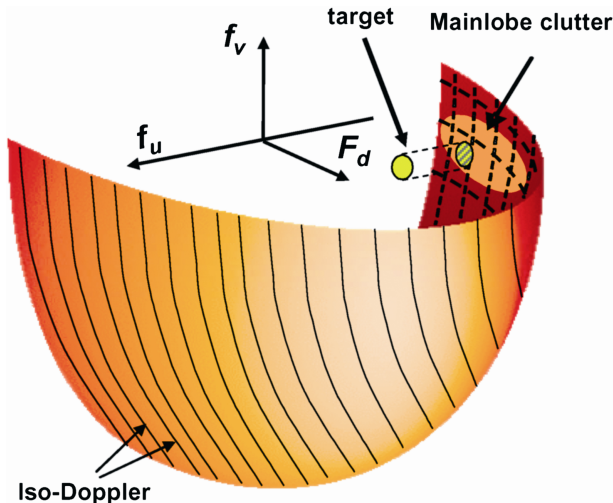


Figure 12.15. Clutter ellipsoid partitioned with iso-Doppler for front antenna configuration

Doppler separation of clutter echoes is another way of discriminating different regions of the clutter ellipsoid, and thus potentially improving cancellation. This point is illustrated in Figure 12.15, for front antenna configuration, where iso-Doppler lines can be seen. Clutter falling in a given Doppler bin corresponds to an elliptical ring in the plane (f_u, f_v). If that ring were infinitely thin (long integration time), and if contamination by adjacent Doppler side lobes were negligible, then a pure spatial adaptive processing would be sufficient for clutter cancellation in a Doppler bin (factored STAP, section 12.3.3.2). This approach can also be combined with the “range dependent” aspect if needed, but there is increasing difficulty in satisfying the steps 1 and 2 mentioned earlier, in comparison with the pre-Doppler approach. Moreover, another difficulty stems from the higher signal-to-noise level in

the training data, compared to the pre-Doppler approach, due to the Doppler integration gain: the target signal will be very easily canceled, if it is also present in these training data.

If these difficulties can be mitigated, post-Doppler STAP, however, provides higher performances than pre-Doppler for complex clutter situations, with a lower computation load.

There are many variants of post-Doppler STAP, and an exhaustive description can be found in [WAR 94]. In the following, only a brief description of the four main approaches will be given. In each case, post-Doppler architecture will be represented as a transformation of the initial STAP data cube.

12.3.3.2. Signal model in the space-Doppler domain

Signal model in the space-Doppler domain can be derived directly from signal model in the space-time model of section 12.2.2, considering the two domains are related via a FFT.

The vector $\tilde{a}(v, \theta)$ of the signals received from a target of unit amplitude in direction θ with velocity v is written:

$$\tilde{a}(v, \theta) = \tilde{s}_{f, M_p}(v) \otimes s(\theta)$$

where $s(\theta)$ and $\tilde{s}_{f, M_p}(v)$ are, respectively, the steering vectors, for space with dimension N and Doppler frequency with dimension M_p . More precisely, for the receiving channel # n and Doppler frequency f , the corresponding component of vector $\tilde{a}(v, \theta)$ is written:

$$\tilde{a}_{nm}(v, \theta) = G_n^{1/2}(\theta) \cdot e^{j\frac{2\pi}{\lambda} n D \sin \theta} \cdot \tilde{s}_{f, M_p}(v)$$

$\tilde{s}_{f, M_p}(v)$ is simply the Fourier transform of the time steering vector $s_{t, M_p}(v)$ and can be written:

$$\tilde{s}_{f, M_p} = H P s_{t, M_p}$$

where H is the $(M_p \times M_p)$ FFT matrix with element $H_{m,l}$ given by $H_{m,l} = e^{-j2\pi \frac{l}{M_p} m}$ and P is a $(M_p \times M_p)$ diagonal matrix with diagonal elements corresponding to the weighting time window used for Doppler analysis.

As $s_{t,M_p}(v)$ is a pure cisoïd, $\tilde{s}_{f,M_p}(v)$ can be written in a more convenient way:

$$\begin{aligned}\tilde{s}_{f,M_p}(v) &= \tilde{p}(f - \frac{2v}{\lambda}) \quad \text{with} \quad f = [f_0 \ f_1 \dots f_{M_p-1}]^T \\ f_l &= \frac{l}{M_p T_r} \quad l = [0 : M_p - 1]^T\end{aligned}$$

with $\tilde{p}(f)$ being the Fourier transform of the weighting function.

Note that for no weighting, P is the identity matrix, and $\tilde{p}(f)$ reduces to:

$$\tilde{p}_{ld}(f) = e^{-j\pi(M_p-1)fT_r} \frac{\sin M_p \pi f T_r}{\sin \pi f T_r}$$

The signal model of section 12.2.3 then becomes:

$$\tilde{z} = \alpha \tilde{a}(v, \theta) + \tilde{n} \quad \text{with} \quad E[\tilde{n}\tilde{n}^H] = \tilde{\Gamma}$$

$\tilde{z} = [\tilde{z}_1 \ \tilde{z}_2 \ \dots \ \tilde{z}_{M_p-1}]^T$ with \tilde{z}_l being the spatial received vector signal in Doppler bin f_l and $\tilde{\Gamma}$ is the space-Doppler covariance matrix.

The space-Doppler covariance matrix is related to the space-time matrix by:

$$\tilde{\Gamma} = (HP \otimes \underline{1})\Gamma(HP \otimes \underline{1})^H \quad \text{as} \quad \tilde{n} = (HP \otimes \underline{1})n$$

with $\underline{1}$ being a vector of size $(N \times 1)$ with all elements equal to unity.

The structure of space-Doppler covariance matrix is:

$$\tilde{\Gamma} = \begin{bmatrix} \tilde{\Gamma}_s(f_0, f_0) & \tilde{\Gamma}_s(f_0, f_1) & \cdots & \tilde{\Gamma}_s(f_0, f_{M_p-1}) \\ \tilde{\Gamma}_s^H(f_0, f_1) & \tilde{\Gamma}_s(f_1, f_1) & \cdots & \tilde{\Gamma}_s(f_1, f_{M_p-1}) \\ \vdots & \vdots & \ddots & \vdots \\ \tilde{\Gamma}_s^H(f_0, f_{M_p-1}) & \cdots & \cdots & \tilde{\Gamma}_s(f_{M_p-1}, f_{M_p-1}) \end{bmatrix}$$

and its inverse is noted:

$$\tilde{\Gamma}^{-1} = \begin{bmatrix} \tilde{\mathbf{G}}_s^{-1}(f_0, f_0) & \tilde{\mathbf{G}}_s^{-1}(f_0, f_1) & \cdots & \tilde{\mathbf{G}}_s^{-1}(f_0, f_{M_p-1}) \\ \tilde{\mathbf{G}}_s^{-1H}(f_0, f_1) & \tilde{\mathbf{G}}_s^{-1}(f_1, f_1) & \cdots & \tilde{\mathbf{G}}_s^{-1}(f_1, f_{M_p-1}) \\ \vdots & \vdots & \ddots & \vdots \\ \tilde{\mathbf{G}}_s^{-1H}(f_0, f_{M_p-1}) & \cdots & \cdots & \tilde{\mathbf{G}}_s^{-1}(f_{M_p-1}, f_{M_p-1}) \end{bmatrix}$$

$$G_s^{-1}(f_l, f_k) \neq \tilde{\Gamma}_s^{-1}(f_l, f_k)$$

$\tilde{\Gamma}_s(f_l, f_l)$ is the classical spatial correlation between channels at the same Doppler frequency f_l .

$\tilde{\Gamma}_s(f_l, f_k)$ is the spatial correlation between channels at two different Doppler frequencies f_l and f_k .

It is worth noting that $\tilde{\Gamma}_s(f_l, f_k)$ is not equal to zero due to finite time sample support that induces Doppler leakage between Doppler bins. With the use of time weighting function P and/or in case of “weak” interference, the leakage is limited to a few Doppler adjacent bins. This will be used by all post-Doppler STAP approaches.

Finally, note also that the signal in the space-Doppler domain is no longer stationary as $\tilde{\Gamma}_s(f_l, f_k) \neq \tilde{\Gamma}_s(f_0, f_{k-l})$. This property is of serious consequence to post-Doppler STAP approaches, as it means that the estimation of covariance matrix $\tilde{\Gamma}$ can only be performed by averaging along the range dimension.

12.3.3.3. Adaptive matched filter in the space-Doppler domain

With the above notations, the expression of the optimal full-dimension post-Doppler matched filter can be derived:

$$\tilde{y}(v, \theta) = \frac{\tilde{a}^H(v, \theta)\tilde{\Gamma}^{-1}\tilde{z}}{\sqrt{\tilde{a}^H(v, \theta)\tilde{\Gamma}^{-1}\tilde{a}(v, \theta)}}$$

As for pre-Doppler STAP (section 12.3.2), this optimal processing leads to joint processing of all Doppler bins, and then to a filter of dimension $M_p \times N$, which is non-tractable in practice. As for pre-Doppler approaches, a reduction in dimension is needed. For post-Doppler approaches, this reduction in dimension is obtained by processing jointly only a few Doppler bins surrounding the Doppler bin under test.

To derive the reduced dimension AMF's for post-Doppler STAP approaches, it is considered first that hypothesis on target velocity are made at Doppler frequency bins, i.e.:

$$\nu = \frac{\lambda}{2} f_l^T$$

Furthermore it is generally assumed that:

$$\tilde{s}_{f,M_p} \left(\frac{\lambda}{2} f_l \right) = \delta(f - f_l) \text{ with } f_l = \frac{l}{M_p T_r}$$

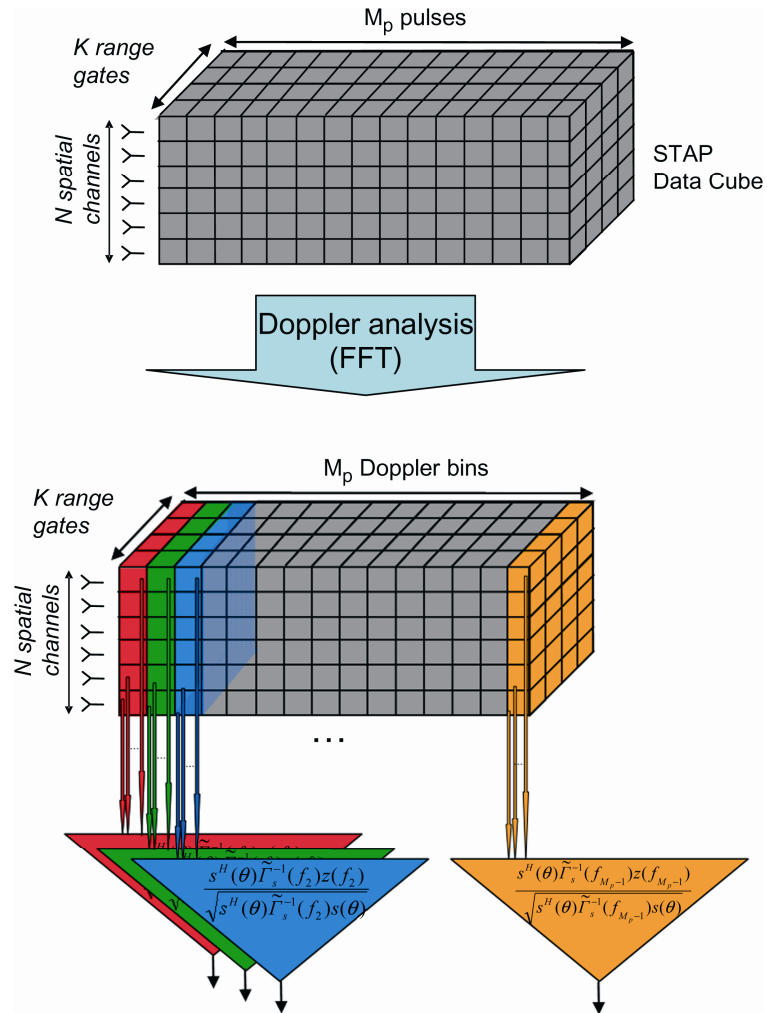
Under these assumptions, the full-dimension AMF can be re-written in a more convenient way for each Doppler bin:

$$\tilde{y}(f_l, \theta) = \frac{s^H(\theta) \sum_{m=0}^{M_p-1} \tilde{G}_s^{-1}(f_l, f_m) \tilde{z}(f_m)}{\sqrt{s^H(\theta) \tilde{G}_s^{-1}(f_l, f_l) s(\theta)}}$$

12.3.3.4. Factored STAP

The synoptic of the “factored STAP” approach is shown in Figure 12.16. In this approach, an FFT Doppler spectral analysis is performed for each range cell, transforming the M_p time (slow-time) samples into M_p Doppler bins. A purely spatial adaptive processing is then performed in each Doppler bin, providing M_p adapted beams. Detection is then performed independently in each Doppler cell, through a CFAR detector.

While being called “factored”, this approach would be better denominated as “post-Doppler spatial adaptive beamforming”. The key assumption there is that Doppler filtering perfectly discriminates clutter echoes in different Doppler filters – which is not true in reality, since Doppler side lobes introduce a “leak” from one Doppler filter to the others, especially when clutter echoes are strong. The approach is then clearly sub-optimal, and gives poor performances against main lobe clutter echoes (air-ground detection of slow targets). For angular side lobe clutter rejection, however, this solution is generally sufficient to provide the required clutter cancelation.

**Figure 12.16.** Factored STAP architecture

Mathematically, the assumptions made for the factored STAP approach is that $\tilde{\Gamma}$ is block diagonal:

$$\tilde{\Gamma} = \begin{bmatrix} \tilde{\Gamma}_s(f_0) & 0 & \cdots & 0 \\ 0 & \tilde{\Gamma}_s(f_1) & \cdots & 0 \\ \vdots & \vdots & \ddots & \vdots \\ 0 & \cdots & \cdots & \tilde{\Gamma}_s(f_{M_p-1}, f_{M_p-1}) \end{bmatrix}$$

and hence in this specific case:

$$\tilde{\Gamma}^{-1} = \begin{bmatrix} \tilde{\Gamma}_s^{-1}(f_0) & 0 & \cdots & 0 \\ 0 & \tilde{\Gamma}_s^{-1}(f_1) & \cdots & 0 \\ \vdots & \vdots & \ddots & \vdots \\ 0 & \cdots & \cdots & \tilde{\Gamma}_s^{-1}(f_{M_p-1}, f_{M_p-1}) \end{bmatrix}$$

The adaptive matched filter of section 12.3.3.2 reduces then in a Doppler-dependent spatial beam forming:

$$\tilde{y}(f_l, \theta) = \frac{s^H(\theta) \hat{\Gamma}_s^{-1}(f_l, f_l) z(f_l)}{\sqrt{s^H(\theta) \hat{\Gamma}_s^{-1}(f_l, f_l) s(\theta)}}$$

12.3.3.5. Adjacent bin post-Doppler STAP

The “adjacent bin post-Doppler STAP” architecture is a generalization of the factored STAP architecture. Adjacent Doppler bins are jointly used for adaptation to mitigate the contamination between Doppler bins, which limited the performances of the factored STAP architecture. Contrary to the factored approach, this is a true bi-dimensional space-frequency processing, and quasi-optimal performances can be obtained with a low number of adjacent Doppler bins (e.g. $M = 3$).

A synoptic of the adjacent bin post-Doppler STAP architecture is presented in Figure 12.17. In this figure, three Doppler bins are jointly processed (the two neighbors of the bin under process). This process must be repeated for each of the M_p Doppler bins (or more exactly for the subset of the Doppler bins contaminated with clutter), thus providing M_p adapted beams.

Mathematically, the assumption made for adjacent bin post-Doppler STAP is that $\tilde{\Gamma}$ is block diagonal. With $M = 3$ adjacent Doppler bins, this gives:

$$\tilde{\Gamma} = \begin{bmatrix} \tilde{\Gamma}_s(f_0, f_0) & \tilde{\Gamma}_s(f_0, f_1) & 0 & 0 & 0 & \cdots & 0 \\ \tilde{\Gamma}_s^H(f_0, f_1) & \tilde{\Gamma}_s(f_1, f_1) & \tilde{\Gamma}_s(f_1, f_2) & 0 & 0 & \cdots & 0 \\ 0 & \tilde{\Gamma}_s^H(f_1, f_2) & \tilde{\Gamma}_s(f_2, f_2) & \tilde{\Gamma}_s(f_2, f_3) & 0 & \cdots & 0 \\ \vdots & \vdots & \vdots & \vdots & \vdots & \vdots & 0 \\ 0 & 0 & 0 & \cdots & 0 & \tilde{\Gamma}_s^H(f_{M_p-2}, f_{M_p-1}) & \tilde{\Gamma}_s(f_{M_p-1}, f_{M_p-1}) \end{bmatrix}$$

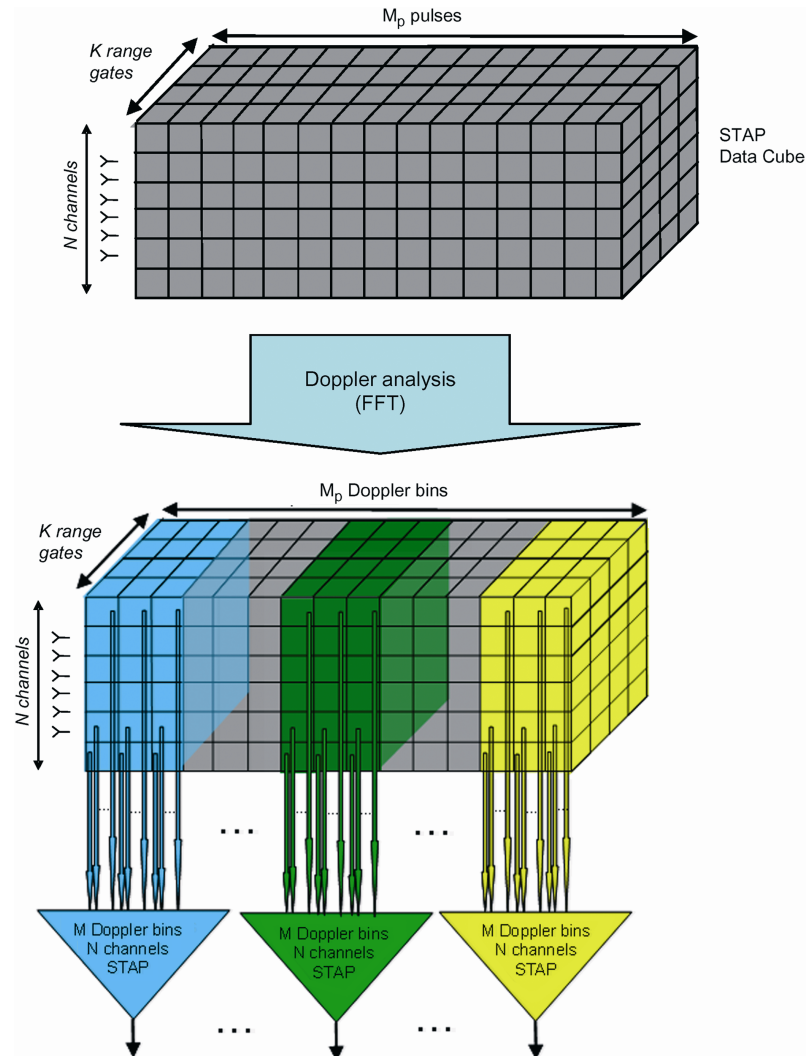


Figure 12.17. Adjacent bin post-Doppler STAP architecture

and hence in this specific case the adaptive matched filter of section 12.3.3.2 reduces then in a joint spatial-Doppler processing of the three adjacent Doppler bins:

$$\tilde{y}(f_l, \theta) = \frac{s^H(\theta) \sum_{m=l-1}^{l+1} \tilde{G}_s^{-1}(f_l, f_m) \tilde{z}(f_m)}{\sqrt{s^H(\theta) \tilde{G}_s^{-1}(f_l, f_l) s(\theta)}}$$

12.3.3.6. Joint domain localized (JDL) STAP

The joint domain localized (JDL) architecture is a generalization of the previous one, where the “adjacent bin” approach is also used on the spatial dimension. A standard digital beam forming is first performed on the sub-array signals, and then adjacent beams are jointly processed with adjacent Doppler bins in the adaptive processing. The whole angle-Doppler domain is thus processed in parallel for each block of angle and Doppler bins. This is in fact an adaptive local angle-Doppler adaptive processing, whose architecture is given in Figure 12.18.

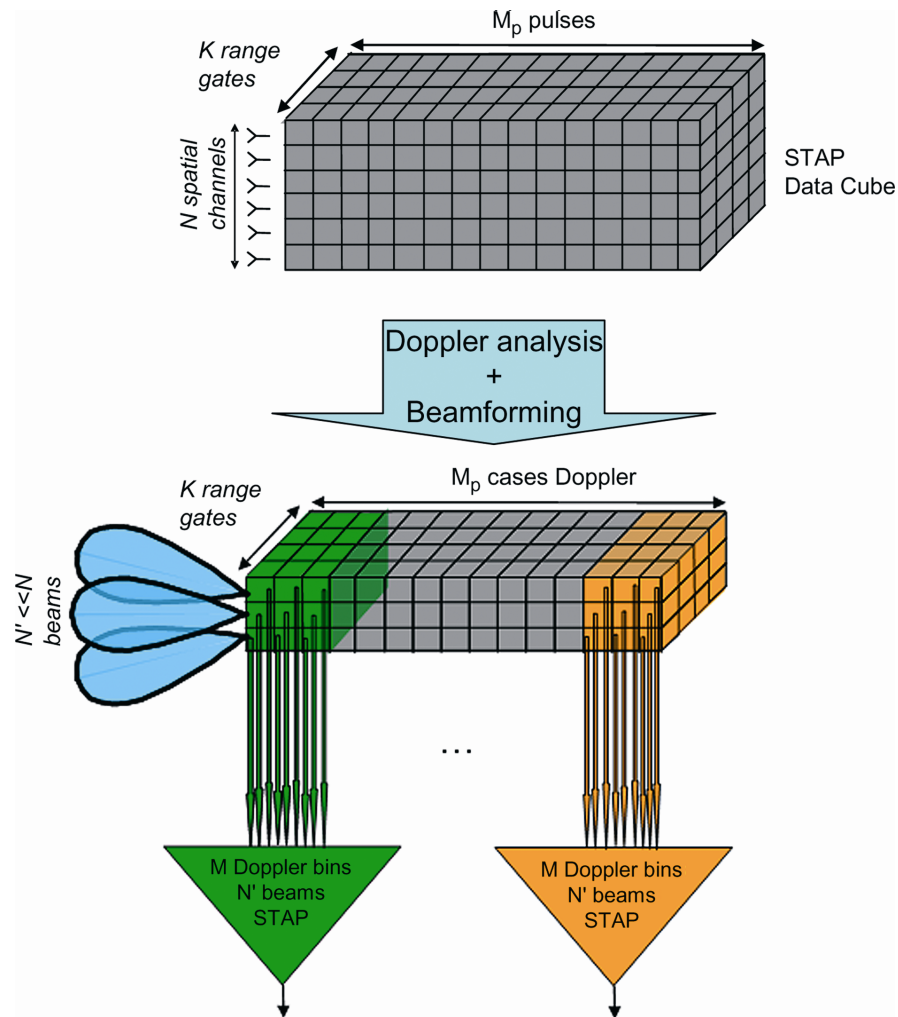


Figure 12.18. STAP joint domain localized architecture

This approach is particularly useful when the number of spatial channels (sub-arrays) is large, whereas only a few channels would be sufficient for clutter cancelation: the processing then comes down to a local STAP – typically 3–5 adjacent Doppler bins \times 3–5 adjacent beams.

A typical application for Joint Domain Localized STAP is the air-ground configuration, when anti-jamming and STAP are both required. Anti-jamming is performed first, taking benefits of all spatial degrees of freedom provided by sub-array partitioning, and the STAP filtering operates then in a second step on a few anti-jammed beams adjacent to the beam under test. Anti-jamming and clutter filtering are thus cascaded, and the computing load is minimized, while still preserving global spatial efficiency for anti-jamming. This will be further analyzed in section 12.4.6.

12.3.3.7. PRI staggered post-Doppler STAP

This architecture has already been presented in section 12.3.2.1 for pre-Doppler STAP. However, in its post-Doppler implementation, *the space-time covariance matrix used for filtering is now depending on the Doppler frequency bin under test*. It is worth noting that the sum of the space-time covariance matrix, in each Doppler bin, over all the Doppler bins, gives the space-time covariance matrix used in pre-Doppler STAP.

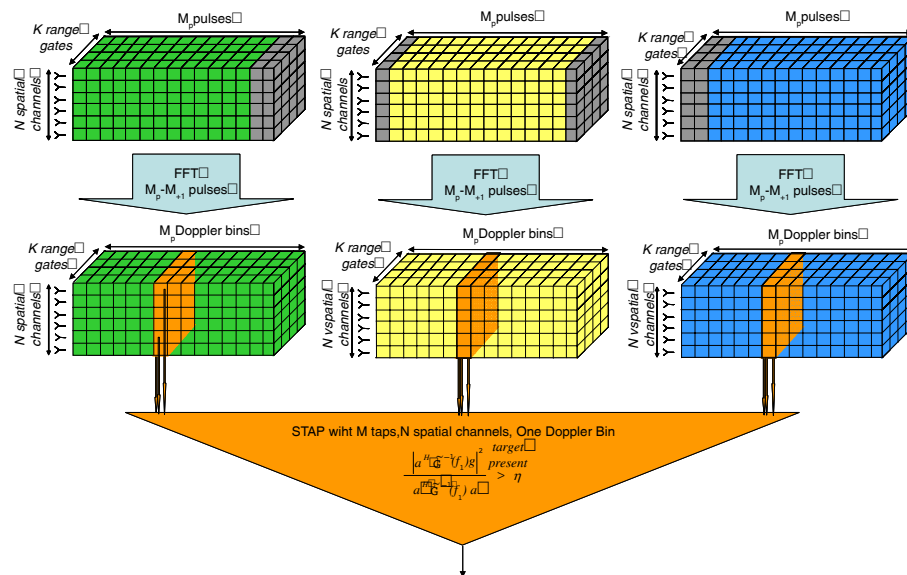


Figure 12.19. AMF PRI staggered post-Doppler STAP architecture

PRI staggered post-Doppler STAP architecture is presented in Figure 12.19, for $M = 3$ taps and $N = 1$ Doppler bins, with the dependency of the covariance matrix on the Doppler bin shown explicitly.

PRI staggered post-Doppler STAP is then the most powerful “hybrid” architecture, able to combine pre-Doppler and post-Doppler characteristics (e.g. adjacent bin post-Doppler STAP with 3 Doppler bins and 5 taps can be implemented).

In comparison with the previous adjacent bin post-Doppler STAP, PRI staggered requires less degrees of freedom if Doppler filtering uses a weighting function, or if the spacing between Doppler bins has been strongly reduced through zero padding [WAR 94].

12.4. Relative advantages of pre-Doppler and post-Doppler STAP

There is no absolute advantage to either pre-Doppler or post-Doppler STAP, but rather specific situations where one approach has to be preferred to the other. The following discussion tries to provide elements and criteria for selection of one approach, examining several points that have to be considered when building a STAP solution. The ultimate choice remains, however, heavily dependent on the specificities of the application such as radar modes, platform characteristics, scenarios, and available computer power.

12.4.1. *Estimation of adaptive filtering coefficients*

High STAP performances are conditioned by compliance to the constraints 1 and 2 given at the beginning of section 12.3.1. Training data and data from the CUT must have similar statistics, and training data must be in sufficient quantity.

For pre-Doppler architectures, training data are generally sufficient, since averaging can be performed in the time domain, which allows a small number of range bins to be used as training data. This is a very attractive characteristic, for instance for air-air modes on fighter aircrafts, where range ambiguities of clutter, in forward antenna configuration, give rise to an important clutter heterogeneity (see section 12.1.3). Of course, the drawback of this “range-dependent” approach is the large computing power required.

For post-Doppler architectures, the only averaging available is in the range domain (and possibly also the Doppler domain if the Doppler resolution provides on clutter a much better resolution than the beamwidth). Fulfilment of conditions 1 and 2 from section 12.3.1 is then more difficult, all the more so when the number of

spatial channels gets larger, in relation to clutter complexity. Air-air modes on fighters can again be taken as examples. This complex clutter configuration also corresponds to situations where post-Doppler processing would seem interesting, for the preliminary Doppler separation of clutter echoes it provides. One way of overcoming that drawback is to use a post-Doppler architecture, taking advantage of adaptive coefficients derived from the space-time covariance matrix. An example of such architecture is given in [SAV 06].

When the number of training data is not sufficient, there are many different techniques for alleviating the problem, for both pre- and post-Doppler processing. The simplest and best known is the so-called diagonal loading, where a small fraction of an identity matrix (3–4 times the noise variance) is added to the estimated clutter covariance matrix \hat{R} . This decreases the number of snapshots necessary to a value much lower than the dimension of the covariance matrix, and further stabilizes the diagram after adaptation – at the cost of a slightly degraded resolution and reduced clutter notch depth.

When the clutter is strong enough, the inverse of the estimated covariance matrix can be replaced by a projection on the subspace orthogonal to clutter. The associated methods are generally referred to as reduced rank STAP. However, all these techniques are very sensitive to the assumed dimension of the clutter subspace, which is often difficult to estimate for complex scenarios or in the presence of calibration errors. To decrease this sensitivity, the orthogonal projection can be replaced by a weighted projection: this technique is called lean matrix inversion [GIE 98].

Another technique allows low side lobes level for the adapted diagram to be obtained: constrained adaptive pattern synthesis only adjusts the components of the weights vector belonging to the subspace orthogonal to the clutter subspace, and adds constraints for obtaining an adapted diagram best approximating the desired diagram [HER 97].

Regardless of the method, decreasing the fluctuations of the estimation of the filtering coefficients (which is a source of increased side lobes for the adapted diagram) always brings a reduction in the clutter cancelation ratio. The exact impact on the residual clutter level – and thus on the detection performance – still has to be analysed on real data.

Finally, an open field of research for mitigating the lack of training data is the “knowledge-aided STAP”, described in [MEL 04a, BER 07, MEL 04b]. The approach is different and complementary to the previous techniques. It consists of exploiting external data, such as maps, and digital terrain models, for improving the selection of the adequate training data – or even for estimating the adaptive coefficients.

12.4.2. Exclusion of target signal from training data

Signals coming from moving targets should not be canceled by the STAP filter, and must therefore be excluded from the training data. Different strategies can be implemented, depending on the radar mode and on the selected STAP architecture. When in a tracking mode, for instance, the CUT can easily be excluded from the training data, when the range-Doppler bins are approximately known. The issue is trickier in search mode, where this information is not available. Moreover, if a post-Doppler architecture is used, the target signal will be enhanced by Doppler integration, and then will more strongly influence the training data. However, a post-Doppler architecture allows easier selection of clutter polluted areas, for using them as training data – if the issue of too few training data does not recur.

For pre- and post-Doppler architectures, range-dependent STAP can be used to exclude the CUT from the training data, at the cost of increased computing complexity.

Generally speaking, finally, this issue will definitely be trickier with post-Doppler architectures.

12.4.3. Clutter heterogeneity

Obtaining representative clutter data is made more difficult by existing heterogeneity of clutter, such as:

- natural presence of point scatterers on the diffuse clutter;
- transitions in the landscape, such as urban, rural, or littoral coasts, or masks and shadows;
- internal movement of the clutter, trees, swell, clouds, rain, etc.

To these natural heterogeneities can be added some “artefacts”, depending on the radar configuration and mode: front antenna and range ambiguities, for instance.

Whatever the source of the heterogeneity, the result is a non-stationarity in range of the observed clutter (level and Doppler spectra). Once again, if post-Doppler architectures may have an edge through their capability of identifying homogenous regions (on the basis of range-Doppler maps), they often provide only limited performances because of the reduced number of representative snapshots. A nice solution could be to use a post-Doppler approach for training data selection, followed by a pre-Doppler processing for STAP filtering.

Concerning point scatterers, which could raise a false alarm rate because they would be poorly canceled (the STAP filter is based on the average clutter level), an efficient approach consists in forming a guard channel as described in [NIC 07].

Finally, as mentioned in the previous section, knowledge-aided approaches provide promising perspectives for future systems.

For extreme situations where the clutter is completely non-stationary in range (e.g. urban clutter + range ambiguities), the spectral estimation approaches from sections 12.3.2.1.2 and 12.3.2.1.3 are good candidates for the exclusion of targets.

12.4.4. Computing load

The computing load of pre- and post-Doppler architectures is highly dependent on the application (e.g. radar modes, platform, scenarios, use of range-dependent STAP or not). Anyway, the following general rules can still be useful:

- When post-Doppler factored STAP provides sufficient clutter cancelation ratio (side lobe clutter, generally speaking), this approach is the most competitive, as far as computing load is concerned.
- Pre-Doppler architectures are to be preferred when a post-Doppler architecture would have required several adjacent Doppler bins, or several time channels (PRI staggered post-Doppler STAP). This is generally true for main lobe clutter cancelation, and even more so for range-dependent STAP, where the cost of coefficient estimation is the largest. The smaller dimension of the filter coefficients vector does not compensate for the numerous estimations of this vector (one per Doppler bin) to be performed.
- Post-Doppler architectures should be preferred in tracking modes, taking advantage of the possibility to define a STAP filter localized, in range and Doppler, around the expected position of the targets.

12.4.5. Angular position estimation

Adaptive monopulse technique [NIC 04] can be used, either in pre- or post-Doppler architectures.

Most often, as noted in [NIC 04], the number of degrees of freedom required for accurate angular location is significantly higher than for detection – with direct impact on system definition (number of spatial channels) and the computational load.

12.4.6. Anti-jamming and STAP compatibility

This issue was already mentioned in section 12.3.3.4. Unlike clutter cancelation, anti-jamming requires only spatial degrees of freedom. For the same reasons as in STAP filtering, the target signal should be excluded from the training data, which leads to implementing the anti-jamming spatial filter in front of pulse compression and Doppler filtering, thus limiting the coherent integration gain on the target signal. Anti-jamming coefficients should also be computed on signal portions non-contaminated by clutter, since its presence would increase the number of required degrees of freedom – and since the clutter will be canceled later.

Because anti-jamming filter implements zeros in the direction of the jammers, the maximum number of jammers which can be canceled is directly related to the number of spatial channels (typically $N/2$ jammers with N sub-arrays, if low side lobes are required for the adapted diagram). STAP filtering generally requires only a few spatial degrees of freedom, especially for main lobe clutter cancelation.

For both improved performance and minimal computational load, it is therefore interesting to cascade anti-jamming and STAP if many spatial channels (sub-arrays) are available. The critical issue in such arrangements is to prevent STAP affecting anti-jamming zeros: a nice solution consists in implementing STAP on the basis of adjacent anti-jammed beams, in a STAP joint domain localized architecture.

12.5. Conclusion

The main architectures for pre- and post-Doppler STAP have been presented, with a discussion of their relative advantages and disadvantages. It is of course difficult to make a definite choice. Post-Doppler STAP is more attractive with its capability to discriminate clutter in the Doppler domain, which should provide good performances on complex clutter, in particular through identification of clutter heterogeneities. However, some significant drawbacks are also incurred:

- Target signal cancellation;
- Insufficient number of training data.

The implications of these advantages and limitations have to be examined in detail, with real signals, for a specific application.

In this context, PRI staggered post-Doppler STAP is certainly a promising architecture, able to combine the most attractive aspects of pre- and post-Doppler STAP for a given application, either in a filtering approach (sections 12.3.2.1.1 and 12.3.2) or in a spectral estimation approach (sections 12.3.2.1.2 and 12.3.2.1.3),

depending both on the expected clutter degree of non-stationarity and on the target density.

12.6. Bibliography

- [ABO 05] ABOUTANIOUS E., MULGREW B., “A STAP algorithm for Radar target detection in heterogeneous environments”, *IEEE Signal Processing Workshop on Statistical Signal and Array Processing*, 17–20 July 2005.
- [BER 07] BERGIN J.S., KIRK D.R., CHANEY G., MCNEIL S., ZULCH P.A., “Evaluation of knowledge-aided STAP using experimental data”, *2007 IEEE Aerospace Conference*, 3–10 March, pp. 1–13, 2007.
- [BRE 73] BRENNAN L.E., REED I.S., “Theory of adaptive Radar”, *IEEE Transactions on Aerospace and Electronic Systems*, vol. 9, no. 2, pp. 237–252, 1973.
- [BRE 76] BRENNAN L.E., MALLET, J.D., REED I.S., “Adaptive arrays in airborne MTI”, *IEEE Transactions on Antennas and Propagation*, vol. AP-24, no. 5, pp. 607–615, 1976.
- [CHE 02] LE CHEVALIER F., *Principles of Radar and Sonar Signal Processing*, Artech House, 2002.
- [CHE 06] LE CHEVALIER F., Maria S., “STAP processing without noise-only reference: requirements and solutions”, *Proceedings of the CIE International Conference of Radar* (IEEE Press), Shanghai, China, October 2006.
- [GIE 98] GIERULL C., “Fast and effective method for low-rank interference suppression in presence of channel errors”, *IEE Electronics Letters*, vol. 34, no. 6, pp. 518–520, 1998.
- [HER 97] HERBERT G., “A new projection based algorithm for low sidelobe pattern synthesis in adaptive arrays”, *Proceedings of the IEE International Conference of Radar 97*, Edinburgh, UK, October, pp. 396–400, 1997.
- [KEL 86] KELLY E.J., “An adaptive detection algorithm”, *IEEE Transactions on Aerospace and Electronic Systems*, vol. 22, no. 1, pp. 115–127, 1986.
- [KLE 02] KLEMM R., “Principles of space-time adaptive processing”, *The Institution of Electrical Engineers*, London, UK, 2002.
- [LI 96] LI J., STOICA P., “An adaptive filtering approach to spectral estimation and SAR imaging”, *IEEE Transactions on Signal Processing*, vol. 44, no. 6, pp. 1469–1483, 1996.
- [MEL 04a] MELVIN W.L., “A STAP overview”, *IEEE Aerospace and Electronic Systems Magazine*, vol. 19, no. 1, Part 2, pp. 19–35, 2004.
- [MEL 04b] MELVIN W.L., SHOWMAN G.A., GUERCI J.R., “A knowledge-aided GMTI detection architecture”, *Proceedings of the IEEE Radar Conference 2004*, 26–29 April, pp. 301–306, 2004.
- [NIC 07] NICKEL U., “Detection with Adaptive Arrays with Irregular Digital Subarrays”, *2007 IEEE Radar Conference*, 17–20 April, pp. 635–640, 2007.

- [NIC 04] NICKEL U., "Performance analysis of space-time adaptive monopulse", *Signal Processing*, vol. 84, no. 9, pp. 1561–1579, 2004.
- [RIC 99] RICHARDSON P.G., "Space-time adaptive processing for manoeuvring airborne radar", *IEE Electronics and Communication Engineering Journal*, February, pp. 57–63, 1999.
- [SAV 06] SAVY L., "Benefits of space-time adaptive processing for air to air operations", *Proceedings of the CIE International Conference of Radar (IEEE Press)*, Shanghai, China, October 2006.
- [WAR 94] WARD J., Space-time adaptive processing for airborne Radar, Lincoln Laboratory MIT, Technical report No. 1015, 13 December 1994.

12.7. Glossary

AMF	Adaptive matched filter
APES	Amplitude phase estimation of a sinusoid
CAPS	Constrained adaptive pattern synthesis
CFAR	Constant false alarm rate
CUT	Cell under test
DPCA	Displaced phase center antenna
DL	Diagonal loading
EVP	Eigenvector projection
FFT	Fast fourier transform
FIR	Finite impulse response
MLED	Maximum likelihood estimator detector
PD	Detection probability
PFA	False alarm probability
PRI	Pulse repetition frequency
STAP	Space time adaptive processing
SMI	Sample matrix inversion

Chapter 13

Particle Filtering and Tracking of Varying Sinusoids

Particle filtering belongs to the class of adaptive processing methods, particularly well suited to the context of non-stationary signals. It allows for real-time estimation (that is to say updated every sample) of the parameters directly related to time-dependent analyzed signal spectrum.

After a general presentation of nonlinear filtering, strategies for efficient particle filtering are discussed: resampling, links with Markov chains with sampling of the state vector size (jump Markov systems, JMSs), auxiliary particle filters (APFs), importance sampling, and efficient proposal distribution, Rao-Blacwellization.

Finally, application to spectral analysis is illustrated through the example of a signal composed of a sum of sinusoids of varying frequencies and amplitudes. The changing number of sinusoids is also tracked over time.

13.1. Particle filtering

Particle filters have the ability to deal with nonlinear models (as is the case with many physical real-world models) and non-Gaussian noises (which is interesting for state model noises, rather than observation noises that are often Gaussian due to central limit theorem).

Chapter written by David BONACCI.

In addition to these interesting properties, particle filtering is also very attractive because of its natural links with Markov chains (for sampling the size of the state vector), allowing easy marriage of the two concepts within a single algorithm (estimation of the size of the state vector jointly with the value of its components).

13.1.1. Generalities

13.1.1.1. A nonlinear filtering

Let us consider the physical system described by the following state and observation equations:

$$x_t = u(x_{t-1}) + \eta_t \quad [13.1]$$

where x_t is a vector representing the actual state of the system at time t , $u(x_{t-1})$ is an operator (nonlinear) expressing the transition of the system from time $t - 1$ to time t , and η_t is the vector of model noise. The observation at time t is:

$$y_t = h(x_t) + \varepsilon_t \quad [13.2]$$

where h is the observation operator (also nonlinear) and ε_t the observation noise. The two noises η_t and ε_t are assumed to be independent, zero mean and with covariance matrix Q_t and R_t , respectively.

Filtering consists in estimating the system state at each observation date t using only observations that are available in real time, i.e. until the date t .

In the linear case, this problem is completely solved by the Kalman filter. However, in the case of strongly nonlinear systems, this filter remains sub-optimal and could observe instabilities and divergences. The best way to deal with nonlinearities is of course to consider the problem of optimal nonlinear filtering. The theoretical solution to this problem is known but, in practice, the implementation remains problematic.

The great feature of the Kalman filter is that the evolution of the filter depends only on the second-order characteristics of the system. In the case of an optimal nonlinear filter, the knowledge of all the moments is required (or more appropriately the probability density function) to determine the evolution of the filter.

So instead of a single analysis vector x_t^a and the covariance matrix associated with the error at time t , we then need to know the analysis conditional probability density function of the state vector $p^a(x_t | x_{0:t-1})$ knowing all states till date t . Similarly, instead of a state vector associated with its predicted error covariance matrix, a predicted density $p^f(x_t | x_{0:t-1})$ of the state vector is needed.

As in the linear case (Kalman), discrete particle filtering can be broken down into two stages:

1) *Prediction stage*: derivation of the analysis pdf (probability density function) (at date t_{k-1}) using the evolution equation [13.1]. Assuming that the noise model has normal (Gaussian) distribution, the conditional pdf of the state vector expressed in z at time t knowing its value in x at date $t-1$ is $\Phi(z|u(x_{t-1}), Q_k)$ where:

$$\Phi(z|m, \Sigma) = \frac{\exp\left[-\frac{1}{2}(z-m)^T \Sigma^{-1} (z-m)\right]}{\sqrt{\det(2\pi\Sigma)}} \text{ is the density of a Gaussian vector of}$$

mean m and covariance matrix Σ . Then:

$$p^f(x_t | x_{0:t-1}) = \int \Phi(\cdot | u(x_{t-1}), Q_k) \cdot p^a(x_t | x_{0:t-1}) dx \quad [13.3]$$

2) *Correction stage* (or analysis): analysis pdf is derived using Bayes rule and observation equation [13.2]. Again assuming that the noise is Gaussian:

$$p^a(x | x_{0:t-1}) = \frac{p^f(x | x_{0:t-1}) \cdot \Phi(y_t | h(x), R_t)}{\int p^f(z | x_{0:t-1}) \cdot \Phi(y_t | h(z), R_t) dz} \quad [13.4]$$

In practice, the two major problems are as follows:

- 1) Integration versus the state vector is difficult to achieve numerically.
- 2) In addition, the integration in [13.3] requires the calculation of $u(x_{t-1})$ for many values of x , which can be costly in computation time.

13.1.1.2. The particle filter

The basic idea is to approximate the analysis pdf at time $t-1$ by a discrete distribution calculated in N states: $x_{t-1}^1, \dots, x_{t-1}^N$ with associated probabilities $\omega_1(t-1), \dots, \omega_N(t-1)$.

That is to say $p^a(\cdot|x_{0:t-1})$ is approximated by a sum of Dirac delta functions.

So if there is no noise model, predicted pdf [13.3] is also a sum of delta functions and corresponds to the discrete distribution based on points $u(x_{t-1}^j)$ with weights ω_j for $j = 1, \dots, N$.

But if the noise model is present, function [13.3] is continuous. We can then use a random Monte-Carlo draw: N realizations η_1, \dots, η_N of a Gaussian vector with zero mean and covariance matrix Q_t are drawn (assuming that the noise model is Gaussian). So the pdf [13.3] can be approximated by the discrete distribution located in:

$$x_j^f(t) = u(x^a(t-1)) + \eta_j, \quad j = 1, \dots, N \quad [13.5]$$

with the same probabilities $\omega_1, \dots, \omega_N$.

The new analysis distribution defined by [13.4] $p^a(x|x_{0:t-1})$ then reduces to the discrete distribution evaluated at the same points but with weights:

$$\omega_j(t) = \frac{\omega_j(t-1) \cdot \Phi(y_t | h(x_t^j), R_t)}{\sum_{l=1}^N \omega_l(t-1) \cdot \Phi(y_t | h(x_t^l), R_t)}, \quad j = 1, \dots, N \quad [13.6]$$

This is the basic particle filter (or “bootstrap filter”). Explicitly, it acts as follows:

Initialization: N initial states (or particles) $x_1^a(t_0), \dots, x_N^a(t_0)$ are chosen according to the fixed initial *a priori* distribution and probabilities $\omega_{1,0}, \dots, \omega_{N,0}$ are set to $1/N$.

Prediction: At time t_k , the particles are moved to $x_j^f(t_k)$ defined by [13.5] maintaining the same probabilities.

Analysis: Having observed y_k^o , probabilities are corrected according to [13.6] and x_j^f becomes x_j^a . The analysis state is obtained by:

$$x^a(t) = \sum_{j=1}^N \omega_j(t) x_t^j$$

And the error covariance matrix:

$$P^a(t) = \sum_{j=1}^N \omega_j(t) [x_t^j - x^a(t)] [x_t^j - x^a(t)]^T$$

13.1.2. Strategies for efficient particle filtering

This section presents all the improvements over the basic particle filter algorithm presented earlier (“bootstrap filter”) to improve performance. These improvements are part of the recent scientific literature and represent emerging nonlinear signal processing methods: resampling, links with Markov chains (JMSs with sampling of the state vector size), APFs, importance sampling, and efficient proposal distribution, Rao-Blacwellization.

13.1.2.1. Resampling

A classical limitation of particle methods is the degeneration of importance weights (when a large majority of the weights tends very rapidly to zero). As the system is chaotic, the problem is that the particles tend to disperse, and many of them eventually receive negligible probability and thus no longer participate really in the filtering operation.

This discrepancy may be limited by introducing a resampling step (or redistribution) of discrete particles under the discrete estimated distribution. The new obtained system of particles is distributed under the target distribution and thus equally weighted:

Redistribution: Before getting $x_j^a(t)$ in $x_j^f(t)$, N particles among the set x_t^1, \dots, x_t^N are drawn according to the discrete probability distribution $\omega_j(t)$, $j = 1, \dots, N$. All the weights are then moved to $1/N$.

Resampling significantly increases the number of particles contributing effectively to the estimation: heavy weight particles are duplicated while the least relevant samples are eliminated. However, it is advisable not to apply resampling systematically because it impoverishes the system of particles. This may lead to filter divergence if the dynamic noise is too low. So the redistribution should be applied only if the variance of the weights becomes too great. The effective size of the particle system introduced by Liu in [LIU 95] is the most commonly used criterion. It is inversely proportional to the variance of the weights:

$$N_{\text{eff}} = \frac{1}{\sum_{j=1}^N (\omega_j(t))^2} \quad [13.7]$$

Possible values of N_{eff} are upper bounded by the total number of particles N . To decide whether a resampling should be applied or not, N_{eff} is compared to a threshold. In the ideal case where the particles are generated directly by the *a posteriori* distribution of the state vector, the weights are all equal to $1/N$. The effective size of the particle system is then N . However, if the particle system has degenerated, all weights are zero except one of them which is one. This unfavorable case corresponds to $N_{\text{eff}} = 1$.

13.1.2.2. Sampling of the state vector size

JMSs are a very important class of models appearing in the signal processing literature (tracking of targets, among others). They are also known as dynamic Bayesian networks (DBNs). Unlike hidden Markov models, they combine hierarchically continuous and discrete state variables.

Consider a stationary, discrete homogeneous first-order Markov chain $\{p_t\}, t \geq 1$, taking values in a set S with the following transition probabilities:

$$\Pi_{ij} = \Pr[p_t = i | p_{t-1} = j], (i, j) \in S \quad [13.8]$$

Let s be the number of elements of S . We then consider a family of s^2 densities $\{f_{ij}(x'|x)\}$, where $x' \in \Re^{nx'}$ and $x \in \Re^{nx}$. The conditional state transition densities of the particle filter are then defined by:

$$p(x_t | x_{0 \rightarrow t-1}, p_{1 \rightarrow t}) = f_{p_{t-1} p_t}(x_t | x_{t-1}) \quad [13.9]$$

where the notation $x_{0 \rightarrow t-1}$ means $\{x_0, x_1, \dots, x_{t-1}\}$. Note that the size or nature of x is a function of p_t , but this dependency is not made explicit to simplify notations.

Neither x_t nor p_t are observed. The observation is $\{y_t\}$ with its conditional observation density knowing all past states and all past observations:

$$p(y_t | x_{0 \rightarrow t}, p_{1 \rightarrow t}, y_{1 \rightarrow t-1}) = g_{p_t}(y_t | y_{1 \rightarrow t-1}, x_t) \quad [13.10]$$

With $y_t \in \Re^{ny_t}$. Note that the above model could be written as a hidden Markov model with a mix of continuous and discrete state variables.

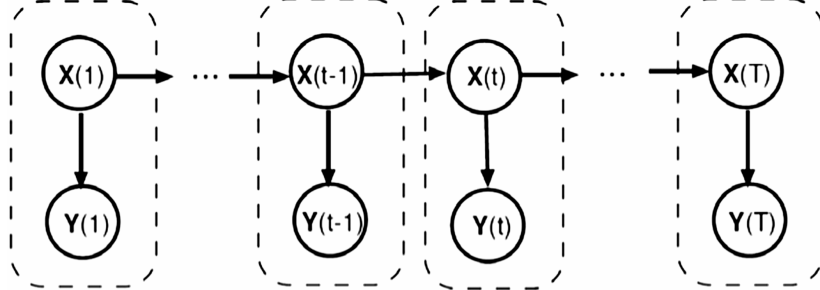


Figure 13.1. Dynamic Bayesian network for the estimation of a sequence of hidden variables

13.1.2.3. Auxiliary particle filter

The idea of the APF is, at time t , to extend the existing paths $\{x_{0 \rightarrow t-1}^j, p_{0 \rightarrow t-1}^j\}$ that are most “promising” in the sense that their predictive likelihoods $p(y_t | y_{1 \rightarrow t-1}, x_{0 \rightarrow t}^j, p_{t-1}^j)$ are high.

However, the analytical calculation of predictive likelihoods is very complicated and approximations are needed. They are calculated as in the following [13.11]:

$$p(y_t | y_{1 \rightarrow t-1}, x_{0 \rightarrow t}^j, p_{t-1}^j) = \sum_{p_t \in S} \prod_{p_{t-1}^j p_t} \int g_{p_t}(y_t | y_{1 \rightarrow t-1}, x_t) f_{p_{t-1}^j p_t}(x_t | x_{t-1}^j) dx_t \quad [13.11]$$

In [PIT 99], the authors propose a simple approximation based on the average of $p(x_t | x_{0:t-1}^j)$. In many applications, especially if $p(y_t | y_{1 \rightarrow t-1}, x_{0 \rightarrow t}^j, p_{t-1}^j)$ varies significantly, the approximation of the predictive likelihood can be insufficient and lead to poor results due to the exploration of state space in uninteresting regions. It is therefore essential to correctly approximate predictive likelihood.

An obvious solution would be to use a second Monte-Carlo approximation method applied to each particle. This solution would generate a lot of extra computational complexity and would introduce even more Monte-Carlo variation.

To resolve this problem, in [AND 03], the authors propose an effective solution based on a deterministic approximation of the integral to calculate the predictive likelihood and on the use of unscented Kalman filter (UKF, see [VAN 00]) to update the parameter of the proposal distribution:

$$\int g_{p_t}(y_t | y_{1 \rightarrow t-1}, x_t) f_{p_{t-1}^j p_t}(x_t | x_{t-1}^j) dx_t = \psi_{p_t}(y_{1 \rightarrow t}, x_{t-1}^j, p_{t-1}^j) \quad [13.12]$$

where ψ_{p_t} is a deterministic integration technique. Note that it is possible to calculate $\psi_{p_t}(y_{1 \rightarrow t}, x_{t-1}^j, p_{t-1}^j)$ during the particle resampling stage without additional computational cost if UKF proposal is used (through the use of UKF approximation).

13.1.2.4. Importance sampling and proposal distribution

In the case the particles can be generated directly following the *a posteriori* distribution $p(x_{0 \rightarrow t} | y_{1 \rightarrow t})$, it is conventionally approximated by the empirical distribution:

$$\hat{p}(x_{0 \rightarrow t} | y_{1 \rightarrow t}) = \sum_{j=1}^N \frac{1}{N} \delta(x_{0 \rightarrow t} - x_{0 \rightarrow t}^j) \quad [13.13]$$

The expectation of any function F of the state variables can then be estimated as follows:

$$\int_{x_{0 \rightarrow t}} F(x_{0 \rightarrow t}) p(x_{0 \rightarrow t} | y_{1 \rightarrow t}) = \frac{1}{N} \sum_{j=1}^N F(x_{0 \rightarrow t}^j) \quad [13.14]$$

This last relationship is very important because it makes the interest of particle methods: this can be applied to the case when F is the state evolution function u , the observation function h , or any quantity depending on the state.

However, it is generally difficult to simulate the target distribution, multivariated and with unknown normalization constant to directly sample particles. A more elaborated sampling method must be used: the importance sampling consists in generating particles according to a proposal $q(x_{0 \rightarrow t} | y_{1 \rightarrow t})$, called importance distribution, whose support includes that of the *a posteriori* distribution $p(x_{0 \rightarrow t} | y_{1 \rightarrow t})$. The weights are then adjusted as follows to reflect the difference between distributions p and q :

$$\omega_j(t) \sim \frac{q(x_{0 \rightarrow t}^j | y_{1 \rightarrow t})}{p(x_{0 \rightarrow t}^j | y_{1 \rightarrow t})} \quad [13.15]$$

Weights are then normalized so that $\sum_{j=1}^N \omega_j(t) = 1$ and the expectation of a function F of the state variables is then estimated by $\int_{x_{0 \rightarrow t}} F(x_{0 \rightarrow t}) p(x_{0 \rightarrow t} | y_{1 \rightarrow t}) = \sum_{j=1}^N \omega_j(t) F(x_{0 \rightarrow t}^j)$.

13.1.2.5. Rao-Blackwellization

When the block decomposition of the filter model is reflecting a conditionally linear Gaussian structure, it is possible to use particle filtering strategies, the so-called Rao-Blackwellized for which the linear model is solved analytically by Kalman filtering.

The “Rao-Blackwellized” particle filter, presented independently by Chen and Liu [CHE 00] and Doucet and Andrieu [DOU 02], significantly reduces estimates variance in the case of such models (conditionally linear Gaussian). This algorithm, treating the linear part of the filter model analytically, thus reduces the size of the vector estimated by particle filtering.

The objective of the algorithm is to compute recursively the joint posterior distribution $p(\lambda_{0 \rightarrow t}, \rho_{0 \rightarrow t} | y_{1 \rightarrow t})$, where $\lambda_{0 \rightarrow t}$ is the portion of the state vector whose variables evolve nonlinearly and $\rho_{0 \rightarrow t}$ designates the variables conditionally linear Gaussian, that is to say those that evolve linearly with the addition of Gaussian noise for a given realization of the vector $\lambda_{0 \rightarrow t}$.

Traditionally, the Bayesian factorization leads to:

$$p(\lambda_{0 \rightarrow t}, \rho_{0 \rightarrow t} | y_{1 \rightarrow t}) = p(\rho_{0 \rightarrow t} | \lambda_{0 \rightarrow t}, y_{1 \rightarrow t}) p(\lambda_{0 \rightarrow t} | y_{1 \rightarrow t}) \quad [13.16]$$

The corresponding filtering problem can then be solved using a Kalman filter that computes a Gaussian approximation of the conditional posterior distribution $p(\rho_t | \lambda_{0 \rightarrow t}, y_{1 \rightarrow t})$. Only the λ_t vector must be estimated by particle filtering:

$$\hat{p}(\lambda_{0 \rightarrow t} | y_{1 \rightarrow t}) = \sum_{j=1}^N \frac{1}{N} \delta(\lambda_{0 \rightarrow t} - \lambda_{0 \rightarrow t}^j) \quad [13.17]$$

The Rao-Blackwellization can also be compared to a multiple model algorithm. The methods traditionally used are based on a bank of filters, each representing one of the possible models. The algorithm then automatically selects a fusion of filter

outputs in view of the received measurement. Particle filtering provides another solution to this problem. In particular, the Rao-Blackwellized algorithm appears as a direct extension of the multiple model algorithms. The difference is that competing hypotheses are explored and selected randomly.

13.2. Application to spectral analysis

The intended application is the spectral analysis of a signal composed of a sum of sinusoids of varying frequencies and amplitudes (sufficiently slowly) over time. The number of sinusoids is also changing over time and tracking their number, together with their estimated parameters, is necessary.

In this case, the parameters to be estimated over time, directly related to the evolutionary spectrum of the signal, are the number of sinusoids, their frequencies, and amplitudes.

The algorithm used in this application is based on the one presented in [AND 03]. This is a SISR (sequential importance sampling and resampling) particle algorithm operating in two steps (sampling and weight). It incorporates some effective strategies for particle filtering (see section 13.1.2) as an UKF proposal and Rao-Blackwellization.

It takes as input a signal composed of a sum of sinusoids corrupted by noise. At each new iteration on time t , it provides and updates estimates of the following physical quantities:

- The number of modes noted p_t ;
- The frequency of each mode $f_k(t)$ for k between 1 and p_t ;
- The amplitude of modes $A_k(t)$ for k between 1 and p_t .

13.2.1. Observation model

Assume that at time t (t being the current sample number), the observed signal consists of sinusoids defined by their frequencies, occurrence dates t_0 and amplitudes.

For a fixed particle j ($1 \leq j \leq N$) where N is the total number of particles, the observation $y(t)$ can be written as a linear combination of p_t^j sinusoidal components:

$$y(t) = \sum_{k=1}^{p_t^j} A_{k,j}(t) \cos(2\pi f_{k,j}(t)(t - t_0_{k,j}(t)) + \phi_{k,j}(t)) \quad [13.18]$$

$$y(t) = \sum_{k=1}^{p_t^j} \left[A_{k,j}(t) \cos(\phi_{k,j}(t)) \cos(2\pi f_{k,j}(t)(t - t_0_{k,j}(t))) \right] \\ - \left[A_{k,j}(t) \sin(\phi_{k,j}(t)) \sin(2\pi f_{k,j}(t)(t - t_0_{k,j}(t))) \right]$$

Defining:

$$\begin{aligned} \alpha_{k,j}(t) &= A_{k,j}(t) \cos(\phi_{k,j}(t)) \\ \beta_{k,j}(t) &= A_{k,j}(t) \sin(\phi_{k,j}(t)) \\ v_{k,j}(t) &= f_{k,j}(t) \cdot (t - t_0_{k,j}(t)) \end{aligned} \quad [13.19]$$

[13.18] can be rewritten as:

$$y(t) = \sum_{k=1}^{p_{j,t}} \alpha_{k,j}(t) \cos(2\pi v_{k,j}(t)) - \beta_{k,j}(t) \sin(2\pi v_{k,j}(t)) \quad [13.20]$$

This allows us to obtain a linear model of observation if the frequencies are assumed (because of the Rao-Blackwellization).

13.2.2. State vector

The state at time t of the overall DBN system is composed of a mixture of discrete and continuous variables. So for a given particle j :

- The order p_t^j is directly related to the size of the state vector. The order represents the number of vibrational modes in the current analyzed signal.
- The state vector x_t^j containing the parameters (continuous) to be estimated.

The state vector x_t^j has dimension $3p_t^j$ and is decomposed as follows:

$$x_t^j = \begin{bmatrix} x_{1,t}^j \\ x_{2,t}^j \end{bmatrix} \quad [13.21]$$

where $x_{1,t}^j$ has dimension $2p_t^j$:

$$x_{1,t}^j = \begin{bmatrix} \alpha_{1,j}(t) \\ \beta_{1,j}(t) \\ \dots \\ \alpha_{k,j}(t) \\ \beta_{k,j}(t) \\ \dots \\ \alpha_{p_t^j,j}(t) \\ \beta_{p_t^j,j}(t) \end{bmatrix} \Downarrow \text{Mode } k \quad [13.22]$$

and $x_{2,t}^j$ has dimension p_t^j :

$$x_{2,t}^j = \begin{bmatrix} f_{1,j}(t) \\ \dots \\ f_{k,j}(t) \\ \dots \\ f_{p_t^j,j}(t) \end{bmatrix} \Downarrow \text{Mode } k \quad [13.23]$$

13.2.3. State evolution model

The proposed state model is as follows:

$$\begin{aligned} x_{1,t} &= A_{1,t}x_{1,t-1} + B_{1,t}v_{1,t} \\ x_{2,t} &= A_{2,t}x_{2,t-1} + B_{2,t}v_{2,t} \\ y(t) &= h(x_{2,t})x_{1,t} + w_t \end{aligned} \quad [13.24]$$

where w_t follows a Gaussian distribution with zero mean and covariance matrix R_t . State noises $v_{1,t}$ and $v_{2,t}$ also follow a Gaussian distribution with zero mean and identity covariance matrices. State matrices $A_{1,t}$ and $A_{2,t}$ are the identity.

The observation function h in turn is a matrix depending nonlinearly on $x_{2,t}$ but applied linearly to the vector $x_{1,t}$: with the proposed partition of the state vector, it appears that $y(t)$ depends linearly on $x_{1,t}$ and nonlinearly on $x_{2,t}$, which allows for the application of Rao-Blackwellization.

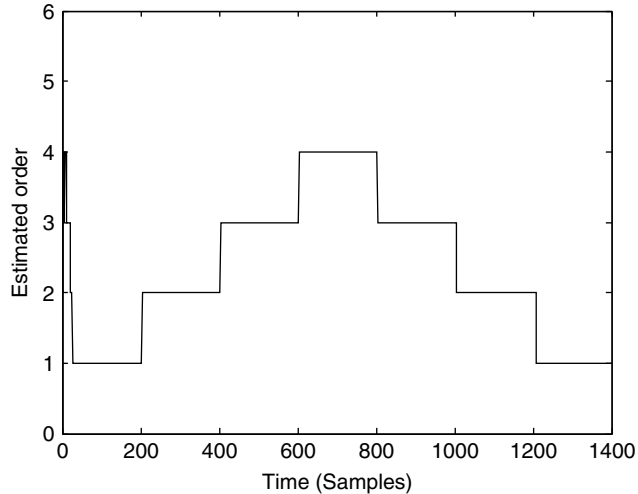


Figure 13.2. Estimated number of oscillating modes versus time

13.2.4. Simulation results

This is a composite signal theoretically composed of the following:

- One mode at normalized frequency 0.0781 is present throughout the total duration of the signal (i.e. 1,400 samples). The associated amplitude is varying slowly in time (t in samples):

$$x_{Amp1} = 0.1 + 0.04 \sin(2\pi 0.0005t)$$

- One mode at normalized frequency 0.1172 is found only between $t = 200$ and $t = 1,200$. The amplitude is still associated with slow sinusoidal variation:

$$x_{Amp2} = 0.07 + 0.02 \sin(2\pi 0.00075t)$$

- One mode at normalized frequency 0.1563 is found between $t = 400$ and $t = 1,000$. The associated theoretical amplitude is:

$$x_{Amp3} = 0.08 + 0.03 \sin(2\pi 0.001t)$$

- One-fourth mode at normalized frequency 0.1953 is found on the central portion of the signal, between $t = 600$ and $t = 800$. The associated amplitude is:

$$x_{Amp4} = 0.09 + 0.01 \sin(2\pi 0.00065t)$$

The other important simulation parameters are:

- $N = 500$ particles.
- measurement noise variance = $10^{-3}/8$.

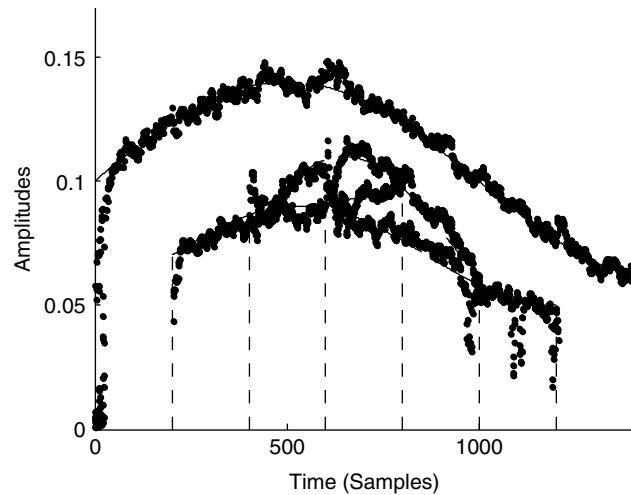


Figure 13.3. Estimated amplitudes versus time

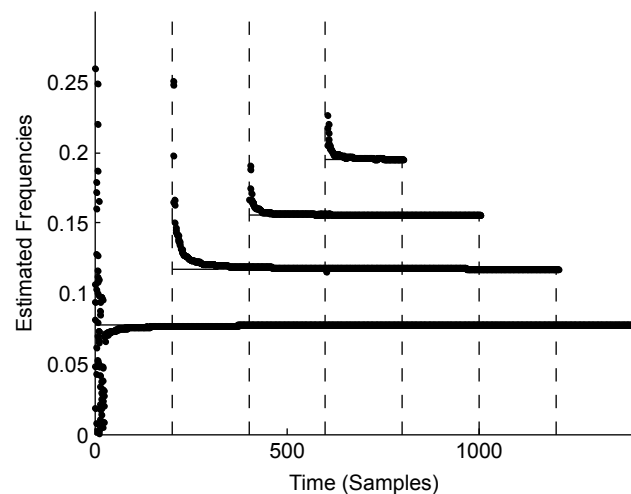


Figure 13.4. Estimated normalized frequencies versus time

13.3. Bibliography

- [AND 03] ANDRIEU C., DAVY M., DOUCET A., “Efficient particle filtering for jump Markov systems. Application to time-varying autoregressions”, *IEEE Transactions on Signal Processing*, vol. 51, no. 7, pp. 1762–1770, 2003.
- [CHE 00] CHEN R., LIU S.J., “Mixture Kalman filters”, *Journal of Royal Statistical Society*, vol. 62, no. 3, pp. 493–508, 2000.
- [DOU 02] DOUCET A., ANDRIEU C., “Particle filtering for partially observed Gaussian state space models”, *Journal of Royal Statistical Society*, vol. 64, no. 4, pp. 827–836, 2002.
- [LIU 95] LIU J.S., CHEN R., “Blind deconvolution via sequential imputation”, *Journal of American Statistical Association*, vol. 90, no. 430, pp. 567–576, 1995.
- [PIT 99] PITT M.K., SHEPHARD N., “Filtering via simulation: Auxiliary particle filter”, *Journal American Statistical Association*, vol. 94, pp. 590–599, 1999.
- [VAN 00] VAN DER MERWE R., DOUCET A., DE FREITAS N., WAN E., The unscented particle filter, Technical Report CUED/F-INFENG/TR 380, Cambridge University Engineering Department, 2000.

List of Authors

Olivier BESSON
ISAE
University of Toulouse
France

David BONACCI
TeSA
Toulouse
France

Rémy BOYER
LSS
CNRS
Gif-sur-Yvette
France

Francis CASTANIÉ
IRIT-TESA
Ecole nationale supérieure d'électrotechnique
d'électronique, d'informatiques
d'hydraulique et des télécommunications
Toulouse
France

André FERRARI
LUAN
University of Nice Sophia-Antiopolis
France

Gilles FLEURY
SUPELEC
Equipe 3S “Supelec Sciences des Systèmes”
Gif-sur-Yvette
France

Éric LE CARPENTIER
IRCCyN
Ecole centrale de Nantes
France

François LE CHEVALIER
Thales Air Operations (Palaiseau) and TU Delft
France

Corinne MAILHES
IRIT
TESA
University of Toulouse
France

Sylvie MARCOS
LSS
CNRS
Gif-sur-Yvette
France

Nadine MARTIN
GIPSA-lab
CNRS
Grenoble
France

Arnaud RIVOIRA
Mysis International Banking Systems S.A.
Paris
France

Laurent SAVY
ONERA
Palaiseau
France

Index

A

Adaptive algorithms, 232, 233, 293
AIC criterion, 162, 216, 217
Akaike Information Criterion (AIC),
159, 160, 162, 165, 216, 217
Analysis vector, 214, 217, 363
Array processing, 94, 169, 185,
209–211, 213, 215, 217, 219,
223, 226
Autocorrelation, 126, 127, 129, 130,
149, 150
function, 13–15, 18, 87, 96, 111,
125–129, 133, 134, 136, 138,
154, 156, 267
covariance matrix, 134, 150, 160,
161, 176, 178, 185, 198
AutoRegressive (AR)
models, 86, 93, 97, 145–147, 149,
154–156, 162, 164, 165, 170, 216,
294–297
Moving Average (ARMA), 74, 79,
110, 113, 114, 116, 145, 146,
152, 154, 156, 157, 159, 162,
293, 294, 297
Auxiliary Particle Filter (APF), 361,
365, 367

C

Capon method, 170, 176, 188, 191,
192, 226
CARMA, 302, 303, 308
Centro-symmetric polynomial,
238
Characteristic polynomial, 237, 238,
303
Cisoid, 24, 25, 28, 29, 33, 38, 40,
41, 49, 54, 60, 101, 126, 130, 134,
135, 346
Cohen’s class, 291
Companion matrix, 233, 237–241,
243
Complex
amplitudes, 117, 118, 158, 233,
235–237, 254, 255, 266, 268, 269,
273, 296
sine waves, 207, 211, 215–217,
223, 225, 227
sinusoid vector, 209, 212, 213, 217,
219, 230
Computational complexity, 154, 170,
215, 219, 226, 314, 367
Confluent Vandermonde structured
matrix, 239

- Convolution sum, 34–36, 43, 49, 54, 59
- Correlation
 - coefficients, 208, 305–309, 311
 - matrix, 159, 160, 190, 199, 208, 210, 235–237, 330, 333, 334
- Correlogram, 138, 141, 188, 210, 226
- Cost function, 221, 234, 235
- Covariance
 - matrix, 68–73, 76–79, 82, 86, 94, 95, 98, 99, 157, 177, 182, 184, 186, 189, 190, 192, 197, 211–216, 218–221, 223, 225, 257, 304, 333, 337–341, 346, 347, 353–355, 362, 363–365, 372
 - method, 148, 156, 157
- Cramér–Rao bounds, 69, 253
- Criterion/criteria, 69, 101, 106, 114, 146, 147, 155, 158–162, 165, 216, 217, 226, 233, 235, 236, 272, 291, 292, 295, 308, 318, 354, 365
- Cumulants, 13, 14, 19, 87, 90, 96, 97, 120

- D**
- Dated samples, 309
- Dirac delta function, 25–27, 39, 49, 58, 364
- Direction of arrival, (DOA) 210, 217, 250, 282
- Dirichlet's kernel, 28, 40, 55, 139, 178–180
- Discrete Fourier transform, 33, 36, 47, 48, 61, 64, 97, 135
- Dynamic Bayesian Network, (DBN) 366, 367, 371

- E**
- Eigendecomposition, 209, 211, 219, 221, 225, 226, 235

- F**
- Fast Fourier Transform, (FFT), 130, 135, 337, 338, 341, 345
- Finite
 - energy signal, 4, 5
 - Impulse Response (FIR), 108, 172, 174–176, 340, 342
 - power signals, 5, 12, 16
- Fisher information, 69, 254
- Fourier series, 17, 30, 36, 38
- Frobenius norm, 221
- Full rank, 209, 211, 212, 219, 221, 225

- G, H**
- Gaussian signals, 14, 15, 70, 315
- Hanning window, 56, 57, 62, 138, 171
- Hermitian, 80, 120, 134, 211, 212, 232, 236, 330
- Hidden Markov models (HMM), 366
- Higher order
 - spectra, 141
 - statistics (HOS), 19
- High-resolution, 169, 173, 209, 210, 215

I, J, K

- Importance sampling, 361, 368, 370
- Infinite Impulse Response (IIR), 109
- Jordan
 - decomposition, 239, 240
 - matrix, 240
- Jump Markov system (JMS), 361, 365, 366
- Kronecker sequence, 29, 40, 58

L

- Large sample, 236
- Laser velocimetry, 301, 310
- Least-squares, 78, 79, 119, 147, 148, 150, 151, 157, 158, 221, 226, 293
- Likelihood function, 70, 77–80, 82, 83, 85, 94, 216
- Line spectrum, 17, 18
- Linear
 - methods, 209, 215, 219, 223, 233
 - prediction, 86, 146, 226–229, 231, 232
- time invariant (LTI) system, 59, 60

M

- Maximum likelihood estimation, 77–86, 158
- Minimum
 - Description Length (MDL) criterion, 159, 160, 161, 216, 217
 - norm, 218
 - variance, 69, 70, 169, 170, 193, 215, 226–229, 231, 232, 339
- MinNorm method, 217, 218, 228
- Moments, 8, 13, 14, 19, 21, 86, 91, 92, 102, 106, 111, 120, 182, 299, 362
- Monte-Carlo simulations, 227–232, 253
- Multiplicity, 211, 239, 240

MUSIC method, 211, 215–217, 219, 221, 226, 243

N

- Narrow band filter, 180
- Noise subspace, 101, 208–209, 212–214, 217, 220–221, 225, 229
- Nonlinear
 - filtering, 286, 361–362, 362–363
 - models, 120, 362
- Non-parametric estimation, 305–307
- Non-stationary context/environment, 219, 232–233, 287, 290–293

O

- Oblique projector, 234
- Observation space, 208–209
- Optimization, 86, 232–234, 247, 285
- Order selection, 158–162, 168
- Orthogonal projector, 214, 234–235
- Orthonormal basis, 212, 214

P

- Parametric estimation, 13, 21, 136, 307–309
- Parseval's theorem, 12, 36–37, 52, 127, 134, 137
- Partition, 211, 214, 219–223, 225–226, 372
- Performance analysis, 204–205, 360
- Periodogram, 79, 81, 95–97, 130, 132, 134–142, 163–164, 170–173, 179, 183, 185–189, 196, 199, 210, 215, 226–232, 309
- Poisson, 302, 305, 309, 315
- Polynomial, 20, 98, 109, 115, 118, 157, 214–215, 217–218, 230, 237–238, 241, 293–294, 303
- based rooting, 237–243
- estimator, 217

Power spectral density (PSD), 11–13, 67, 106
 Prior–MUSIC (P–MUSIC), 233–237
 Projected
 Companion matrix–MUSIC (PCM–MUSIC), 233, 237–243
 correlation, 235, 236
 Prony model, 145–146, 156–158, 162, 164–165, 293, 295–297
 Propagator, 209, 219, 220–221, 223, 226–229, 230–233, 246–247
 Proposal distribution, 363, 365, 367–368
 Pseudo–spectrum, 213–215, 221, 229

R

Rank, 154, 167, 209, 211–212, 219, 221–222, 225, 232, 239–241, 244, 256, 268, 285–286, 355, 359
 Rao–Blackwellization, 361, 365, 369–372
 Rectangular window, 25, 29, 39–40, 47, 49, 53–54, 133, 138, 188
 Root, 20, 94, 98, 115, 118, 153, 157, 214–215, 230, 233, 237–238, 243, 284, 294, 303
 MUSIC, 153, 233, 243, 284
 Rotation operator, 224

S

Sampling process, 233, 302, 315
 Second–order representation, 14, 15, 19
 Sensors, 86, 93, 209–211, 223, 279, 282
 Shannon condition, 41, 43, 45
 Signal
 classes, 3, 106
 subspace, 207–209, 212, 220, 223, 225–226, 229–230, 232, 244, 246

to–noise ratio, (SNR) 73, 145, 178–179, 181, 184–185, 187–188, 210, 254
 Sine cardinal, 27, 39, 49
 Slotting (technique), 310–311, 341–315
 Source vectors, 209, 213, 215
 Sources, 138, 210–211, 217, 244–247, 271, 280–281
 Spectral aliasing, 44–45, 56, 305
 estimator, 21, 95, 119, 146, 154, 156, 167, 186, 188, 204–206, 210, 213, 217, 226, 296, 302, 309–311, 314–315
 MUSIC, 233, 237
 Standard deviation, 188, 228–229, 309, 312–313
 Stationarity, 8, 15–19, 21, 110–111, 115, 176, 292, 297
 Subspace–based methods, 209, 210, 226, 228–230

T

Timescale representation, 10
 Time–frequency representation, 10, 11, 290, 291
 Total least–squares, 150, 151, 157, 158, 226

U, V

Undated samples, 305
 Uniform linear antenna (ULA), 210, 279
 Unit circle, 115, 148, 150, 152, 153, 214, 215, 218, 238, 239, 243, 293, 294, 297
 Unscented Kalman Filter (UKF), 367, 368, 370
 Vandermonde matrix, 209, 234, 239

W, Y

- Waves 41, 49, 54, 119, 139, 140, 170, 207, 209, 210, 211, 215–217, 221, 223, 225, 227, 229
White noise, 79, 84, 107, 110, 113, 114, 139, 140, 146, 151–154, 160, 162, 164, 177, 181, 184, 189, 207, 212, 217, 296, 328, 330, 341

- Wiener–Khintchine’s theorem, 127
Wigner–Ville representation, 20
Window width, 310, 312
Wold’s decomposition, 113
Yule–Walker equations, 99, 100, 113, 149, 159